EUROPEAN PHYSICAL SOCIETY

MESON RESONANCES AND RELATED ELECTROMAGNETIC PHENOMENA

Proceedings of the 1st International Conference organized by the High Energy and Particle Physics Division of the E.P.S. at Bologna, 14-16 April 1971 under the sponsorship of **H.E. Senator Camillo Ripamonti**, *Italian Minister of Scientific and Tecnological Research.*

R. H. DALITZ and A. ZICHICHI

EDITORS

EDITRICE COMPOSITORI Publishers
BOLOGNA - ITALY

International Scientific and Organizing Committee:

R. H. DALITZ - University of Oxford, U. K.
J. LEFRANÇOIS - Lab. de l'Accélérateur Linéaire, France.
M. JACOB - CERN, Geneva, Switzerland.
W. PAUL - University of Bonn, Germany.
A. ZICHICHI - University of Bologna, Italy - **Chairman.**

Session Chairmen:

I. BUTTERWORTH
S. GLASHOW
W. JENTSCHKE
E. LOHRMANN
G. MORPURGO
H. MUIRHEAD
Ch. PEYROU
G. PUPPI
L. RADICATI
R. A. SALMERON
G. SALVINI
G. H. STAFFORD

Scientific Secretariat:

W. BLUM
A. BRODY
P. L. BRUNINI
I. CORBET
P. L. FRABETTI
P. FRAMPTON
P. GENSINI
S. GRAFFI
V. GRECCHI
F. HALZEN
B. JEAN-MARIE
M. JOBES
A. KEMP
P. MAZZANTI
F. NAVACH
F. L. NAVARRIA
F. PALMONARI
J. L. PETERSON
E. REMIDDI
A. ROUGE'
M. SALVINI
G. TURCHETTI
G. VENTURI

Conference Staff:

Executive Secretary — M. ZAINI
Organizing Secretary — S. GABRIELE
Technical Assistance — F. MARTELLI
Treasurer — F. LAUBE

Secretaries:

M. DENZLER
F. MASSERA
O. MASSERA
S. McGARRY
O. POLGROSSI
I. POLI

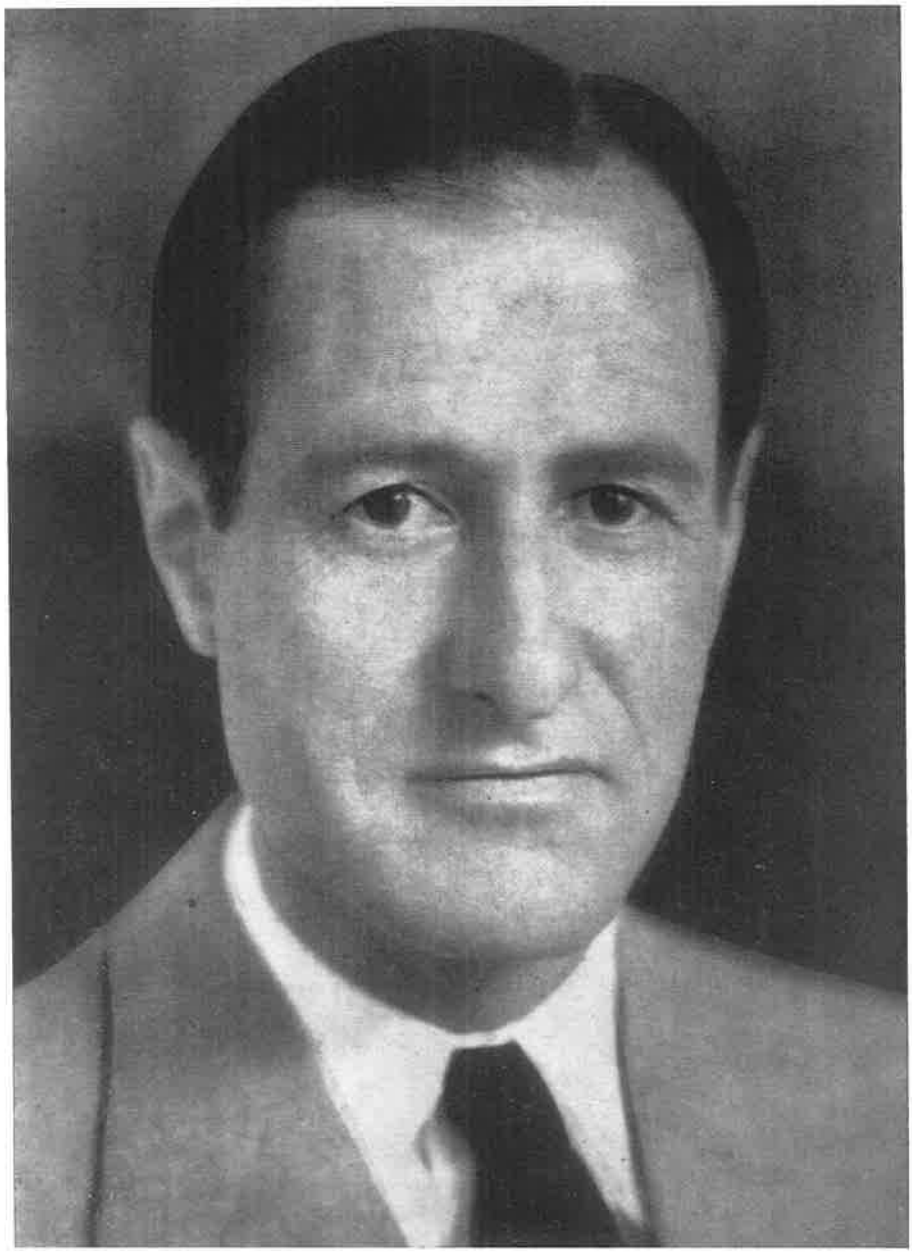

This book is dedicated to the memory of Professor Peter Preiswerk, who was the Chairman of the Board of the High Energy and Particle Physics Division of the European Physical Society at the time of this Conference. Professor Preiswerk was a founder member of the European Physical Society and it was his belief that the European Physical Society could play a vital role in improving and extending international communication between physicists in this field which led to the formation of this Division. He felt particularly that the younger generation of physicists needed more opportunity to express themselves about their situation, and this first Conference of the Division was organised in this spirit, with the inclusion of an evening session for general discussion of the issues before high energy physicists at that time. The very existence of this Division of the European Physical Society may be regarded as one fitting epitaph to his life.

EUROPEAN PHYSICAL SOCIETY
The High Energy and Particle Physics Division

INTERNATIONAL CONFERENCE ON MESON RESONANCES AND RELATED ELECTROMAGNETIC PHENOMENA

Bologna 14-16 April 1971

PROCEEDINGS

R. H. DALITZ and A. ZICHICHI

EDITORS

The symbol on the cover of this volume is number 3 in the Tamil numeration, one or the most ancient languages we know.

TIPOGRAFIA COMPOSITORI - VIALE XII GIUGNO - BOLOGNA

Introduction

This first European Conference on « Meson Resonances and Related Electromagnetic Phenomena » was organized by the High Energy and Particle Physics Division of the European Physical Society, and was held on 14-16 April 1971 at the University of Bologna. The topic of this Conference was one to which a great many European laboratories have made important contributions. It brought specialists together from almost all European countries and from most of the major European laboratories, together with a small number of distinguished research workers from major laboratories beyond.

It was decided to arrange the Conference Sessions according to the following pattern. For each Session, an introductory speaker was selected to give a review of the topic to be covered in that Session, in order to inform and remind the audience about the situation in that field as it was prior to the Conference. From the papers submitted to the Conference by participants, a number of speakers were selected to present their contributions as an invited paper in that Session. The review papers and the invited papers and some contributed papers are contained in this volume of the Proceedings.

The organization of the Conference and the publication of these Proceedings would not have been possible without the financial support provided by the Sponsoring Institutions, which were as follows: The Italian Ministry of Public Education, The National Institute of Nuclear Physics (INFN), The National Committee for Nuclear Energy (CNEN), The University of Bologna, The Camera di Commercio Industria Artigianato e Agricoltura of Bologna.

The editorial work for these Proceedings has depended crucially

upon the efforts of our Scientific Secretary, Dr Maurizio Salvini. We wish to record the debt which we owe him for a most effective collaboration. We owe many thanks also to all of the secretarial and technical staff who assisted in the organization and running of the Conference and whose names are listed on the preceding pages.

Finally we would like to thank most warmly the assistance, the collaboration and the excellent work of the Executive Secretary of the Conference Miss Maria Zaini, whose contribution at all stages of our work has been outstanding.

R. H. DALITZ and A. ZICHICHI

Bologna, May 1972.

Contents

SESSION I-A

Wednesday, 14 April 1971

ππ and Kπ interactions

Chairman: G. H. STAFFORD

Secretaries: G. VENTURI
G. TURCHETTI

$K\pi$ interactions (*)

V. P. HENRI
CERN - Geneva

1. Introduction.

In this introductory talk I will first describe the search for a scalar $K\pi$ resonance by a CERN-Brussels-UCLA Collaboration, which led to a phase shift analysis of the $K\pi$ system. I will then briefly compare these results to the $K\pi$ phase shifts obtained by a group from Johns Hopkins University and to the theoretical phase shifts obtained by Lovelace with the Veneziano model. Finally I will show the results of off-mass shell $K\pi$ scattering phase shifts obtained by a collaboration between Argonne National Laboratory and the University of Chicago.

Let me first recall that the $K\pi$ systems contrary to the $\pi\pi$ states are not subjected to Bose statistics requirement and, therefore, can exist in the $I = \frac{1}{2}$ and $I = \frac{3}{2}$ spin states for any l. Thus for S and P waves there are four possibilities for the $K\pi$ systems $S_{\frac{1}{2}}$, $S_{\frac{3}{2}}$, $P_{\frac{1}{2}}$, $P_{\frac{3}{2}}$: This large number of possibilities complicates the study of the $K\pi$ system. On the other hand the charge exchange reactions are here easier to study than for example the $\pi^0\pi^0$ system in $\pi\pi$ charge exchange.

2. Search for a scalar $K\pi$ resonance.

Recently a search for possible scalar ($J^P = 0^+$), $I = \frac{1}{2}$ resonances in the $K\pi$ system by a CERN-Brussels-UCLA Collaboration has led to a phase shift analysis of $K\pi$ angular distributions observed in the reactions:

$$K^+p \to K^+\pi^-\pi^+p \qquad (77\,300 \text{ events}) \qquad (1)$$

$$K^+p \to K^0\pi^0\pi^+p \qquad (18\,800 \text{ events}) \qquad (2)$$

for beam momenta from 2.5 to 12.7 GeV/c.

(*) Introductory talk

The data, obtained in bubble chamber experiments, come from an International K^+ collaboration ([0]). (See Table I for the list of the contributing laboratories and the cross-sections for (1) and (2).)

TABLE 1. – *Data from international* K^+ *collaboration.*

Laboratory	Momentum	$K^+p \to K^+\pi^-\pi^+p$		$K^+p \to K^0\pi^0\pi^+p$	
		Number of events	Cross-section (mb)	Number of events	Cross-section (mb)
Illinois	2.53	2723	2.18 ± 0.17		
Illinois	2.76	4586	2.27 ± 0.18		
Brussels-CERN K^+ Collaboration	2.95	1108	2.13 ± 0.11	788	2.20 ± 0.19
Illinois	3.2	4823	2.17 ± 0.17		
Brussels-CERN K^+ Collaboration	3.43	1848	2.15 ± 0.11	556	2.19 ± 0.20
Chicago	4.27	1838	1.90 ± 0.20		
Berkeley	4.6	2668	1.80 ± 0.20	759	1.65 ± 0.20
Brussels-CERN K^+ Collaboration	4.97	6241	1.95 ± 0.10	3077	1.68 ± 0.10
Johns Hopkins	5.44	9518	1.58 ± 0.20	900	1.44 ± 0.15
UCLA	7.3	11619	1.75 ± 0.15	2279	1.37 ± 0.15
Brussels-CERN K^+ Collaboration	8.25	4780	1.36 ± 0.08	2721	1.33 ± 0.09
Berkeley	8.92	7559	1.16 ± 0.20	2272	0.66 ± 0.20
Birmingham-Glasgow-Oxford	10	14265	1.19 ± 0.13	4620	0.86 ± 0.16
Rochester	12.6	3691	0.97 ± 0.09	834	0.57 ± 0.07
Total		77267		18806	

Previous studies of reactions (1) and (2) at various beam momenta had shown that the reaction $K^+p \to K^*\Delta$ is dominated by π exchange ([1]). The information on $K\pi$ scattering was, therefore, extracted from the reactions:

$$K^+p \to K^+\pi^-\Delta^{++} \qquad (31\,123 \text{ events}) \tag{3}$$

$$K^+p \to K^0\pi^0\Delta^{++} \qquad (4845 \text{ events}) \tag{4}$$

The present sample of these reactions is about twice as large as in previous analyses ([2]) and the method used is different. In this new study the authors rely mainly on the *shape* of the $K\pi$ angular distribution extrapolated to the pion pole and use the information from the extrapolated cross-section, which from an experimental point of view is less reliable, only to resolve phase shift solution ambiguities.

3. Phase shift analysis.

The method consists of extrapolating to the pion pole the moments of the distribution of the Kπ scattering angle θ (Gottfried-Jackson) for each Kπ mass bin separately and analysing the resulting « on shell » angular distribution in terms of Y_l^m normalized moments.

The four scattering phase shifts δ_l^{2I} ($I = \frac{1}{2}, \frac{3}{2}, l = 0, 1$), *i.e.* δ_0^1, δ_0^3, δ_1^1 and δ_1^3 for a given Kπ mass interval can be obtained from the four measured moments $\langle Y_1^0 \rangle$, $\langle Y_2^0 \rangle$ (for *elastic* and *charge exchange* « CEX ») using the relations:

$$\langle Y_1^0 \rangle = \frac{1}{\sqrt{12\pi}} \frac{6\,\mathrm{Re}(SP^*)}{|S|^2 + 3|P|^2}$$
$$\langle Y_2^0 \rangle = \frac{1}{\sqrt{20\pi}} \frac{6|P|^2}{|S|^2 + 3|P|^2} . \tag{5}$$

where

$$S^{\mathrm{el}} = 2/3\, S_{\frac{1}{2}} + 1/3\, S_{\frac{3}{2}}, \qquad P^{\mathrm{el}} = 2/3\, P_{\frac{1}{2}} + 1/3\, P_{\frac{3}{2}}$$
$$S^{\mathrm{CEX}} = \sqrt{2/3}\,(-S_{\frac{1}{2}} + S_{\frac{3}{2}}), \qquad P^{\mathrm{CEX}} = \sqrt{2/3}\,(-P_{\frac{1}{2}} + P_{\frac{3}{2}}) \tag{6}$$

and

$$L_I = \sin \delta_l^{2I} e^{i\delta_l^{2I}} . \tag{7}$$

For *elastic* scattering:

$$|S|^2 = 1/9\,[4 \sin^2 \delta_0^1 + \sin^2 \delta_0^3 + 4 \sin \delta_0^1 \sin \delta_0^3 \cos(\delta_0^1 - \delta_0^3)]$$
$$|P|^2 = 4/9 \sin^2 \delta_1^1 \tag{8}$$
$$\mathrm{Re}(SP^*) = 2/9 \sin \delta_1^1\,[2 \sin \delta_0^1 \cos(\delta_0^1 - \delta_1^1) + \sin \delta_0^3 \cos(\delta_0^3 - \delta_1^1)]$$

and for *charge exchange* scattering:

$$|S|^2 = 2/9\,[\sin^2 \delta_0^1 + \sin^2 \delta_0^3 - 2 \sin \delta_0^1 \sin \delta_0^3 \cos(\delta_0^1 - \delta_0^3)]$$
$$|P|^2 = 2/9 \sin^2 \delta_1^1 \tag{9}$$
$$\mathrm{Re}(SP^*) = 2/9 \sin \delta_1^1\,[\sin \delta_0^1 \cos(\delta_0^1 - \delta_1^1) - \sin \delta_0^3 \cos(\delta_0^3 - \delta_1^1)] .$$

Thus, if the normalized moments Y_l^m of the elastic and CEX scattering angular distributions are known the four scattering phase shifts can be determined, but several assumptions, justified by experiments, had to be made, *i.e*:

1) Only S and P wave contribute *i.e.* Y_3^m and higher moments are $\simeq 0$.
2) No inelasticity is present for $M(\mathrm{K}\pi) < 1.1$ GeV, *i.e.* no other channels are open (*).
3) The $I = \frac{3}{2}$ P wave amplitude ($P_{\frac{3}{2}}$) is zero for Kπ masses from threshold to ~ 1.1 GeV.

Previous studies ([3]) of the reactions:

$$\mathrm{K}^-\mathrm{n} \to \mathrm{K}^-\pi^-\mathrm{p} \tag{10}$$

$$\mathrm{K}^-\mathrm{p} \to \mathrm{K}^-\pi^-\Delta^{++} \tag{11}$$

have shown that the $P_{\frac{3}{2}}$ amplitude can be neglected for $M(\mathrm{K}\pi) < 1.1$ GeV and also that the $S_{\frac{3}{2}}$ wave amplitude is small in this Kπ mass region, *i.e.*

$$\sigma_0^3 \simeq 1.8 \text{ mb}$$

where

$$\sigma_l^{2I} = 4\pi\lambda^2(2l+1)(\sin^2\delta_l^{2I})|C_I|^2$$

$$\sigma_{\text{elastic}} = \sum_{l,I} \sigma_l^{2I}{}_{\text{elastic}} \tag{12}$$

$$C_{\frac{1}{2}}^{\text{el}} = 2/3, \quad C_{\frac{1}{2}}^{\text{CEX}} = -\sqrt{2/3}, \quad \text{etc.}$$

Equation (12) with $\sigma_0 = 1.8$ mb was then used to further constrain the phase shift solutions after having checked that one of the solutions for δ_0^3 agreed with this result.

(*) The analysis of the reaction $\mathrm{K}^+\mathrm{p} \to \mathrm{K}^0\pi^+\pi^-\pi^+\mathrm{p}$ at 5 and 8.25 GeV/c has shown that the cross-section for $\mathrm{K}^+\pi^- \to \mathrm{K}^0\pi^+\pi^-$ obtained by Chew Low extrapolation is less than 2 mb for Kπ masses < 1.1 GeV and rises to ~ 8 mb at $M(\mathrm{K}\pi) = 1.4$ GeV.

4. Extrapolation procedure.

To obtain the on-mass-shell values of the $\langle Y_1^0 \rangle$ and $\langle Y_2^0 \rangle$, the moments observed as a function of the momentum transfer t are extrapolated to the pion pole at $t = \mu^2 = 0.02$ GeV^2 for each interval of $M(K\pi)$, selecting events with Δ^{++}, *i.e.* with $1.16 < M(p\pi^+) < 1.36$ GeV (reaction (3) or (4)).

The moments extrapolated are *normalized i.e.* the angular distribution is expanded as:

$$\frac{d\sigma}{d\Omega} = \sigma \left[\frac{1}{4\pi} + \langle Y_1^0 \rangle Y_1^0(\cos\theta) + \langle Y_2^0 \rangle Y_2^0(\cos\theta) \right]$$

$$\frac{d\sigma}{d\Omega} = A_0 + A_1 Y_1^0 + A_2 Y_2^0 .$$

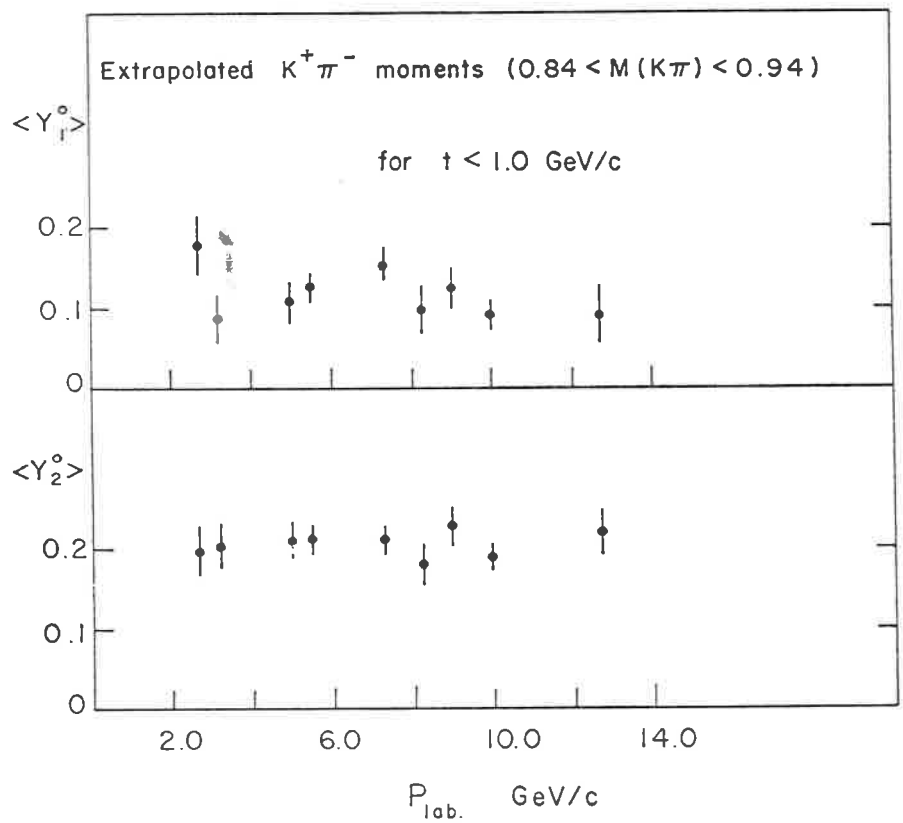

Fig. 1. – $K^+\pi^-$ moments extrapolated to the pion pole *vs.* the K^+ beam momentum.

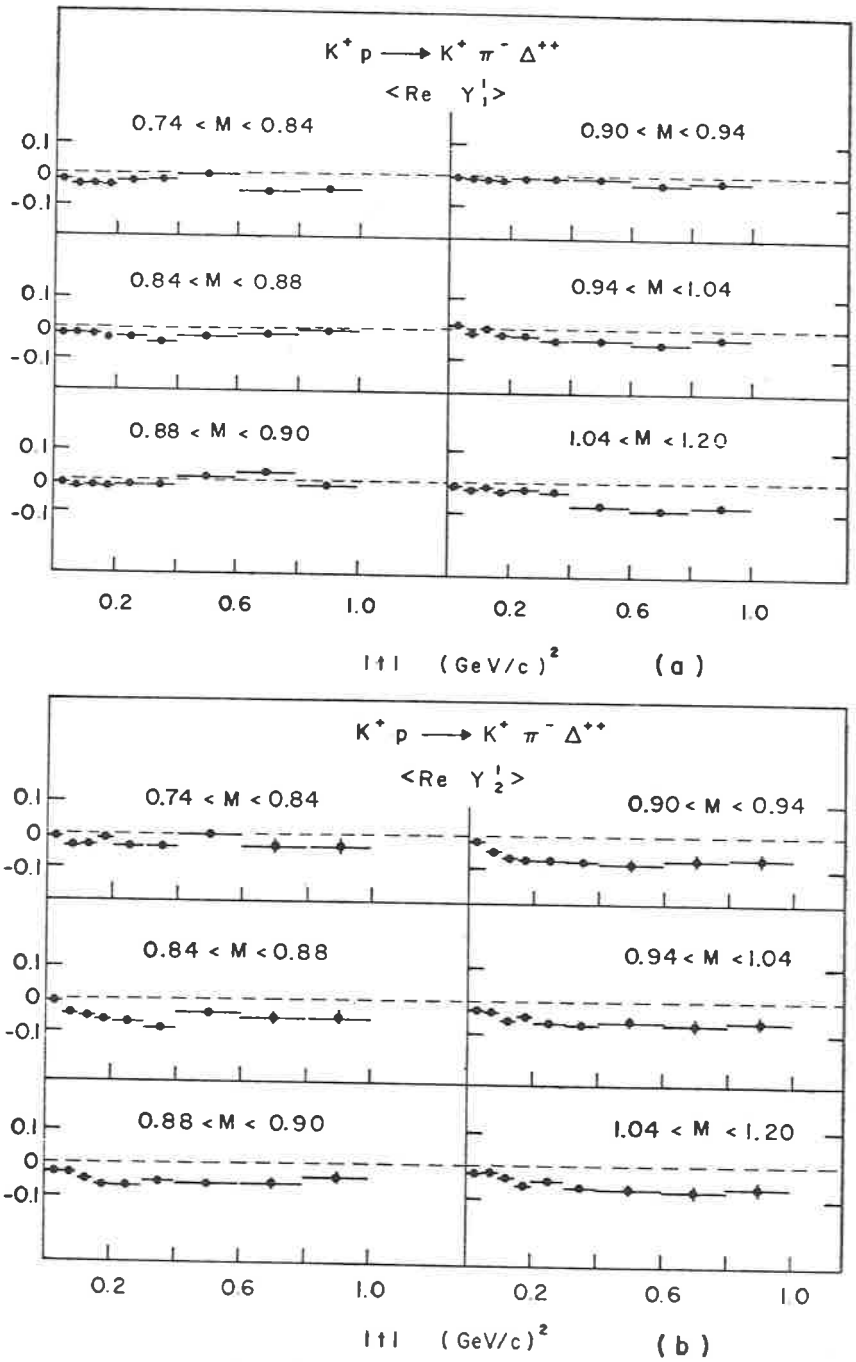

Fig. 2. – Moments $\langle \mathrm{Re}\, Y_1^1 \rangle$ and $\langle \mathrm{Re}\, Y_2^1 \rangle$ for various $M(\mathrm{K}\pi)$ bins as a function of $|t|$.

This method has the following advantages:

1) The normalized moments $\langle Y_1^0 \rangle = A_1/A_0$ are independent of the value of the cross-sections for reactions (1) or (2); the systematic normalization errors are thus suppressed.

2) All t dependent factors as the pion pion propagator and all form factors appearing in the Chew Low formulae for σ and $d\sigma/d\Omega$ cancel out so that the normalized moments are nearly independent of t and can be extrapolated with the use of a low order polynomial in $(t-\mu^2)$.

As a check it was shown that the extrapolated values of $\langle Y_1^1 \rangle$ and $\langle Y_2^0 \rangle$ are independent of beam momentum (fig. 1) as expected if π exchange dominates and that the « illegal » moments $\langle \mathrm{Re}\, Y_l^m \rangle m \neq 0$, which must be 0 if the exchanged system has spin zero, have extrapolated values $\simeq 0$ for $M(K\pi) < 1.1$ GeV, (fig. 2). It was also verified that the Kπ moments are, within errors, insensitive to the $p\pi^+$ mass band chosen.

5. π^+p extrapolated moments.

As an additional check of the method the measured moments (Fig. 3*a*) of the π^+p angular distribution for the events of the reaction

$$K^+p \to K^*\ (892)\ \pi^+p \tag{14}$$

when

$$K^*(892) = 0.84 < M(K\pi) < 0.94\ \mathrm{GeV}$$

have been extrapolated to the pion pole and compared to the on-shell πp scattering data [4] (solid curve Fig. 3*b*). As can be seen the overall agreement between the extrapolated moments and the real π^+p scattering moments is quite good. This result was considered sufficiently encouraging for the extrapolation procedure used to apply it to Kπ scattering.

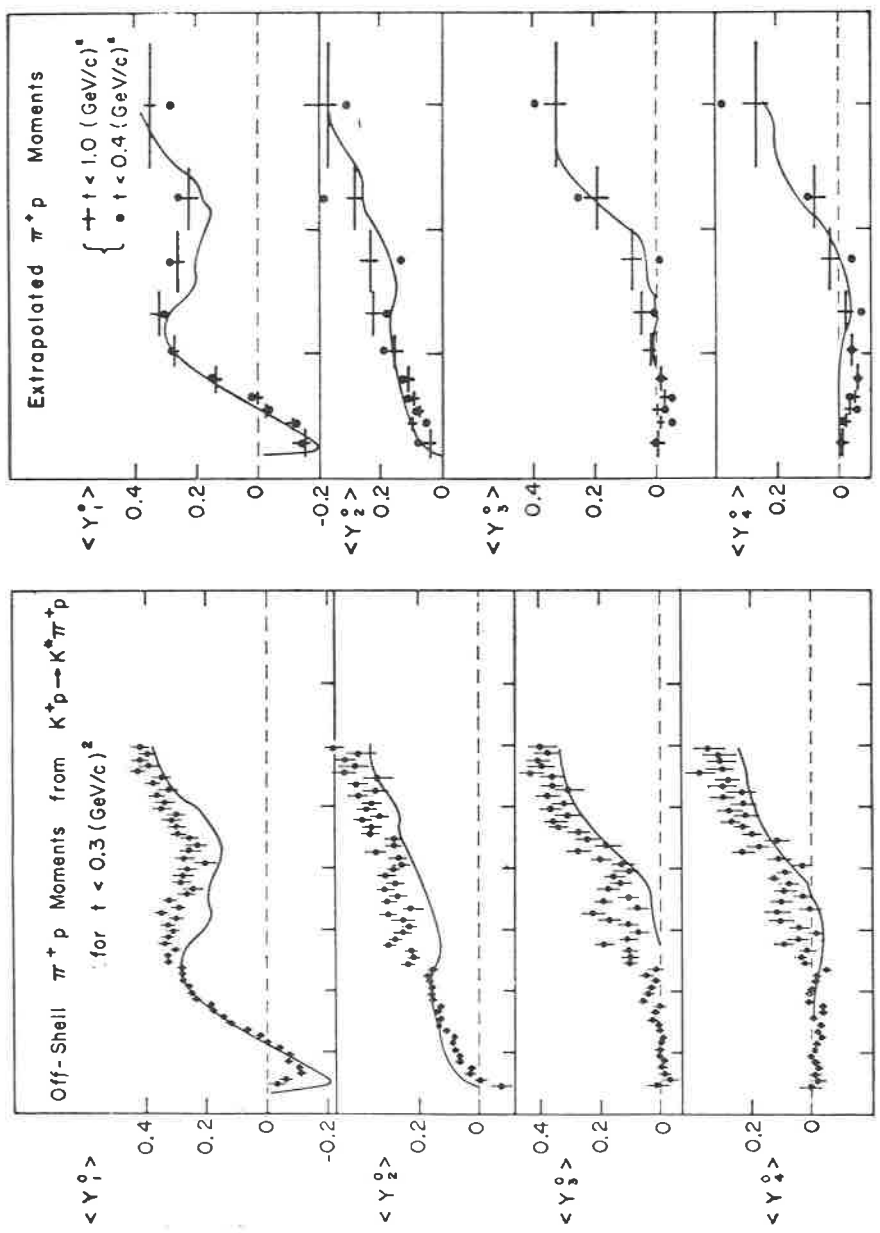

Fig. 3. - *a)* Y_l^m moments of the π^+p system as a function of $M(p\pi^+)$. The curves are the real $\pi^+p \to \pi^+p$ scattering moments calculated from the phase shifts in ref. (4). *b)* Same as for *a)* but for the extrapolated moments.

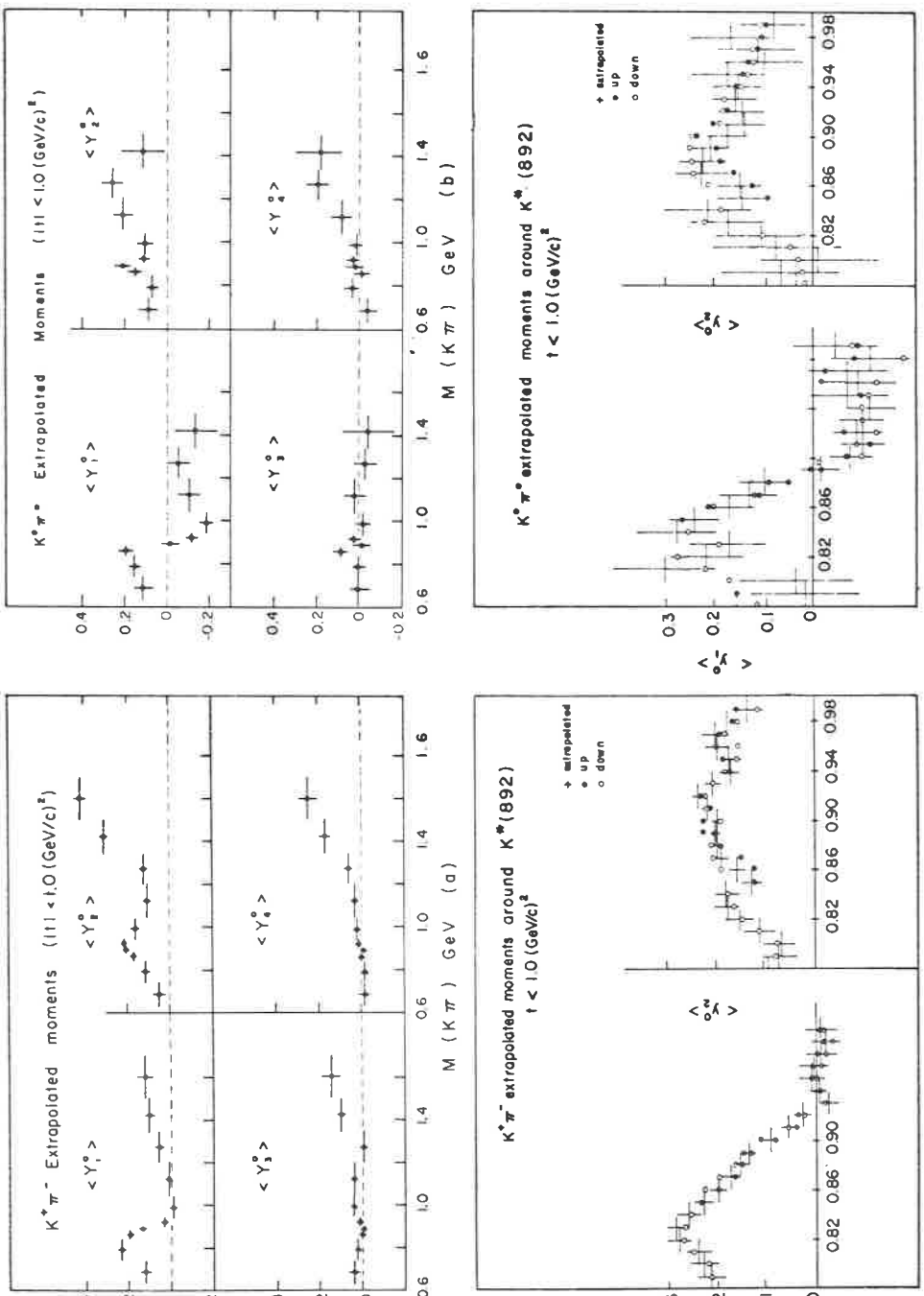

Fig. 4. – *a)* Extrapolated $K^+\pi^-$ moments *vs.* $M(K\pi)$ from the reaction $K^+p \to K^+\pi^-\Delta^{++}$(for all beam momenta combined). *b)* Same as for *a)* but for $K^0\pi^0$ from the reaction $K^+p \to K^0\pi^0\Delta^{++}$. *c)* Same as for *a)* but detail of K*(892) region. The computed moments from the « up » and « down » phase shifts solution are shown. Note the dip in $\langle Y_2^0 \rangle$ for $M(K\pi) = 0.86$ reproduced by the « up » solution. *d)* As for *c)* but for $K^0\pi^0$.

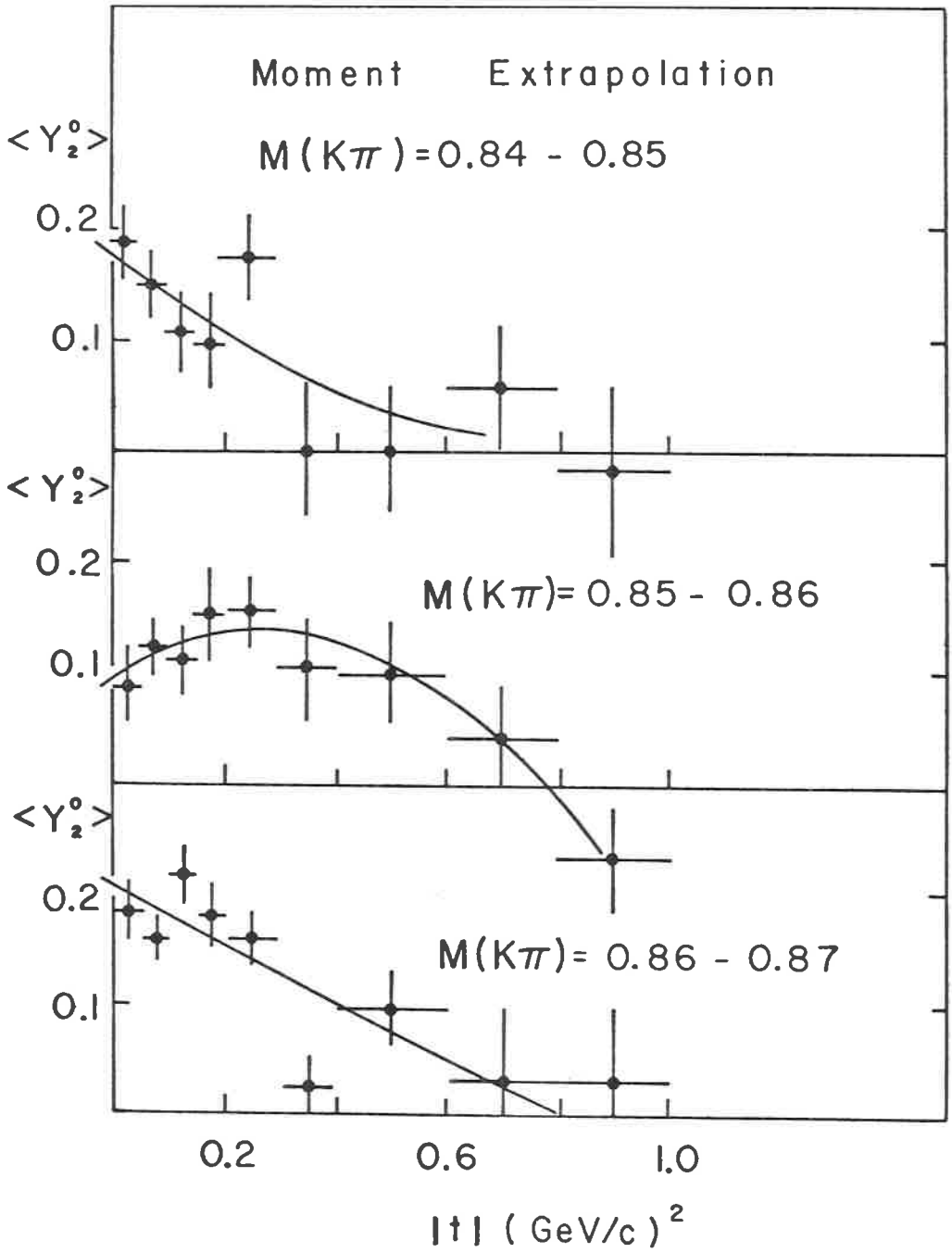

Fig. 4. - Example of $K^+\pi^-$ extrapolation for 3 $M(K\pi)$ mass intervals. A dip in $\langle Y_2^0 \rangle$ for small t is seen in interval $0.85 < M(K\pi) < 0.86$ GeV.

6. Kπ extrapolated moments.

The moments $\langle Y_1^0 \rangle$ and $\langle Y_2^0 \rangle$ extrapolated from $t = -1.0\,(\mathrm{GeV/c})^2$ to the pion pole, using a polynomial of the second degree in $(t-\mu^2)$, *vs.* $M(\mathrm{K}\pi)$ were obtained for the elastic and CEX reactions (Fig. 4*a*), *b*)). It is seen that:

1) Both elastic and CEX $\langle Y_2^0 \rangle$ show a peak in the K*(892) region as expected. [For pure P wave $\langle Y_2^0 \rangle = 2/\sqrt{20\pi} = 0.252$. If S wave is present $\langle Y_2^0 \rangle$ is smaller (see eq. (5)) as seen in Fig. 4].

2) Both elastic and CEX $\langle Y_1^0 \rangle$ are positive below the K*(892) centre (more K forward than backward in the Kπ rest system) due to the interference between the $P_{\frac{1}{2}}$ K* amplitude and a $S_{\frac{1}{2}}$ amplitude.

3) Both $\langle Y_1^0 \rangle$ and $\langle Y_2^0 \rangle$ go to zero above the K* mass.

4) The elastic $\langle Y_1^0 \rangle$ remains small until the K*(1420) region whereas the CEX $\langle Y_1^0 \rangle$ is negative above the K*(892). The difference in behaviour of the two $\langle Y_1^0 \rangle$ indicates the presence of a non zero $S_{\frac{3}{2}}$ wave amplitude, while the compatibility of the two corresponding $\langle Y_2^0 \rangle$ confirms that the $P_{\frac{3}{2}}$ wave amplitude is small.

5) The $\langle Y_3^0 \rangle$ and $\langle Y_4^0 \rangle$ are small below the K*(1420) indicating that the D wave amplitude below ~ 1.1 GeV can be neglected. (There are, therefore, no resonances in D or higher waves for $M(\mathrm{K}\pi) \leqslant 1.1$ GeV and $\Gamma \geqslant 20$ MeV.)

7. Kπ phase shift analysis.

The solutions of eqs. (5)-(9) for the phase shifts δ_1^1, δ_0^3 and δ_0^1 as a function of the Kπ mass are shown in Fig. 5*a*) (*). An arbitrary multiple of π can be added to any phase without changing the solution. If $|S|^2 \leqslant |P|^2$, *i.e.* in the K*(892) region, there is an approximate ambiguity. To each solution δ_0^{2I} corresponds another:

$$\delta_0'^{2I} = \frac{\pi}{2} - (\delta_0^{2I} - \delta_1^1)\,.$$

(*) The phase shifts and their errors are determined independently in each $M(\mathrm{K}\pi)$ bin from the extrapolated moments $\langle Y_1^0 \rangle$ and $\langle Y_2^0 \rangle$ for elastic and CEX scattering by minimizing $\chi^2(\delta_1^1, \delta_0^3, \delta_0^1)$, the sum of four terms of the form

$$\left[\frac{\langle Y_l^0 \rangle_{\mathrm{calc}} - \langle Y_l^0 \rangle_{\mathrm{extrapol}}}{\Delta \langle Y_l^0 \rangle_{\mathrm{extrapol}}}\right]^2 .$$

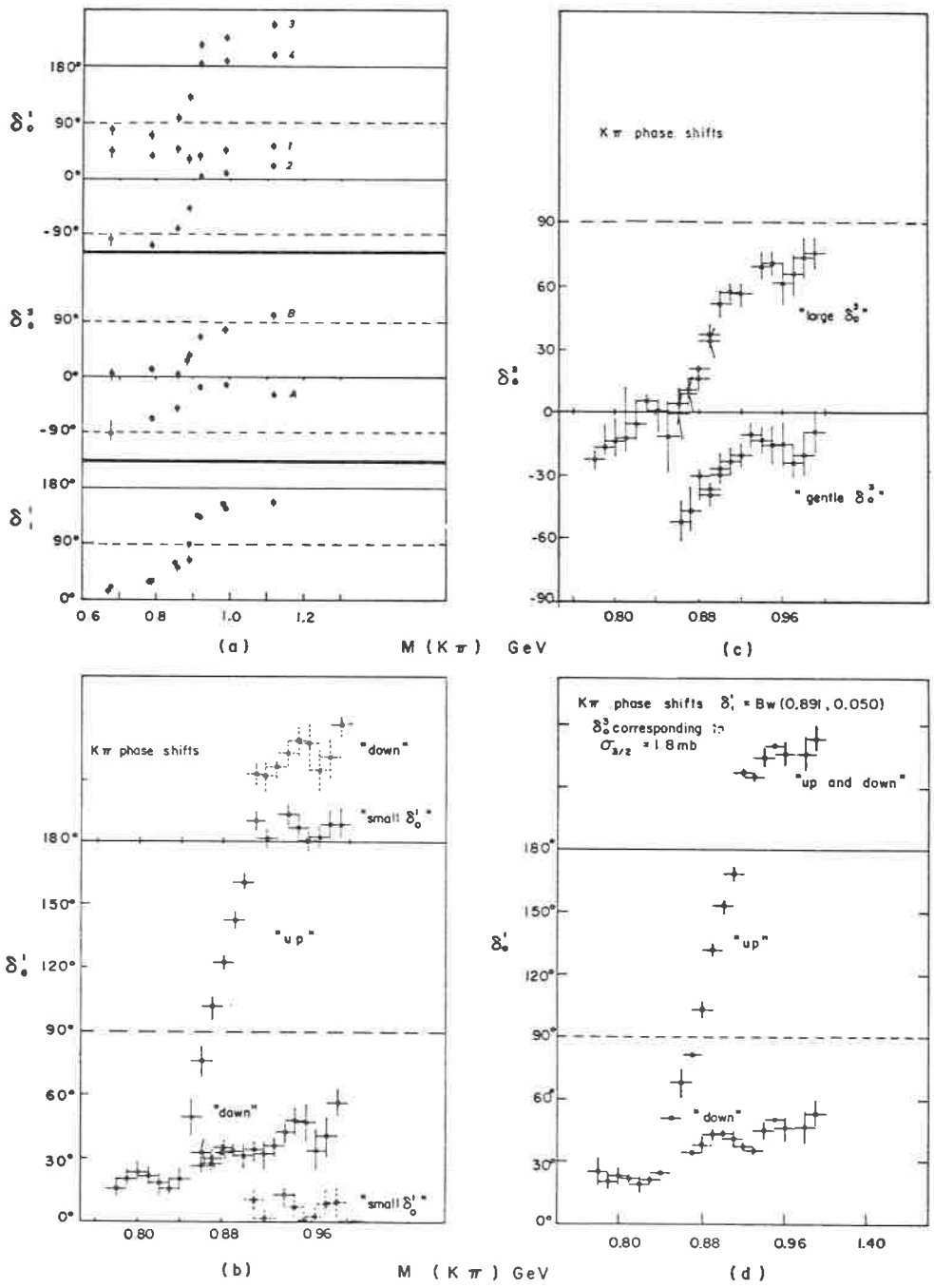

Fig. 5. – Solution of eq. (5) for Kπ scattering phase shifts assuming $\delta_1^3 = 0$. *a*) No other constraints. *b*) Constraining δ_1^1 to a *P* wave Breit Wigner ($M = 0.891$ GeV, $\Gamma = 0.050$ GeV).. Solution for δ_0^1. *c*) Solution for δ_0^3. *d*) Same as for *b*) but with δ_0^3 constraint to correspond to $\sigma_{\frac{3}{2}} = 1.8$ mb and using elastic $K^+\pi^- \to K^+\pi^-$ moments only.

The results show that:

1) δ_1^1 for all solutions follows a K*(892) Breit Wigner distribution.
2) δ_0^3 for small $M(K\pi)$ is either $\simeq 0$ or large negative.
3) δ_0^1 in this same $M(K\pi)$ region is $\sim 40°$ for one solution and $\sim 80°$ or $(80° - \pi)$ for the other.
4) Above $M(K\pi) \sim 0.900$ GeV there are two possibilities to continue δ_0^3 and four to continue δ_0^1.

Additional constraints can be used to try to resolve the ambiguities, *i.e.*:

1) δ_1^1 is constrained to follow a Breit Wigner with mass 0.891 GeV and width 0.050 GeV. (The fit in the K*(892) region is not sensitive to the exact form of Breit Wigner used.)
2) δ_1^3 is still taken to be zero.

The resulting solutions for δ_0^1 and δ_0^3 are shown in Fig. 5*b*), *c*). They present the following characteristics:

1) δ_0^1 has four alternatives:
   i) A « *down* » solution rises $\sim$ linearly from 0° to $\sim 60°$ at ~ 1.0 GeV.
   ii) A « *small* δ_0^1 » solution rises $\sim$ linearly to 30° at ~ 0.900 GeV then drops to $\sim 0°$.
   iii) An « *up-down* » solution resonating at 0.865 GeV with a width $\leqslant 0.035$ GeV passing 180° at 0.900 GeV and joining the «down» solution.
   iv) An « *up-small* δ_0^1 » solution, the same as the previous one for small $M(K\pi)$ but joining the « small $\delta_0^1 + \pi$ » solution after 0.900 GeV.

In the K*(892) region the « up » and « down » solutions are related by formula (14) (*).

(*) Only one solution is found in the bin (0.84÷0.86) GeV with phase $\sim 50°$ suggesting the continuity of the « up » solution (having the best χ^2). This is due to a dip in the $\langle Y_2^0 \rangle$ elastic and CEX moments occurring in this mass band. (Fig. 4 (*c*), (*d*) and (*e*).)

2) δ_0^3 has two alternatives:

i) A « *gentle* δ_0^3 » solution associated with solution « up-down » for δ_0^1 is negative and roughly falls from 0° to — 20° at ~ 1 GeV except for some apparent structure in the neighbourhood of K*(892), (perhaps due to the poorer resolution of the CEX events). This is the favoured solution since it corresponds to a roughly constant $K^+\pi^+$ or $K^-\pi^-$ cross-section of 2 mb in agreement with the quoted results for $K^-\pi^-$ in reactions (10) and (11).

ii) A « *large* δ_0^3 » solution associated with the « small δ_0^1 » solution. It rises to 70° below the K* and would give a $K^+\pi^+$ or $K^-\pi^-$ cross-section of 30 mb. This solution can most likely be ruled out.

If δ_0^3 is now constrained to correspond to $\sigma_0^3 = 1.8$ mb and the δ_0^1 is computed using only the elastic data, the results shown in Fig. 5*d*) are about the same as the previous one.

Two solutions for δ_0^1 remain:

1) The « *up* » solution small for $M(K\pi) < 0.84$ GeV resonating at $M = 0.865$ GeV and with $\Gamma = 0.035$ GeV.
2) The « *down* » solution rising up to $\sim 50°$ at 1.0 GeV.

8. Cross-section extrapolation.

The information on the *magnitude* of the observed Kπ cross-section as a function of Kπ masses for reaction (1) and (2) can also be used in the hope of resolving the remaining δ_0^1 ambiguity. For this an extrapolation to the pion pole of the observed cross-section as a function of t, for each Kπ mass bin needs to be performed.

This cross-section extrapolation depends on various kinematical factors and on badly known normalization factors for the cross-section at each beam momentum. It will depend on the form of the extrapolation function used and in particular on the form factors describing the Kπ or pπ vertices. Examples of extrapolated cross-sections are given in Fig. 6 using P wave Benecke-Dürr ([5]) form factors and linear extrapolation. The result for the $K^+\pi^-$ cross-section show a peak at the K*(892) exceeding the P wave unitarity (80 mb), dropping to ~ 10 mb for $1.0 < M(K\pi) < 1.3$ GeV then rising to ~ 15 mb in the

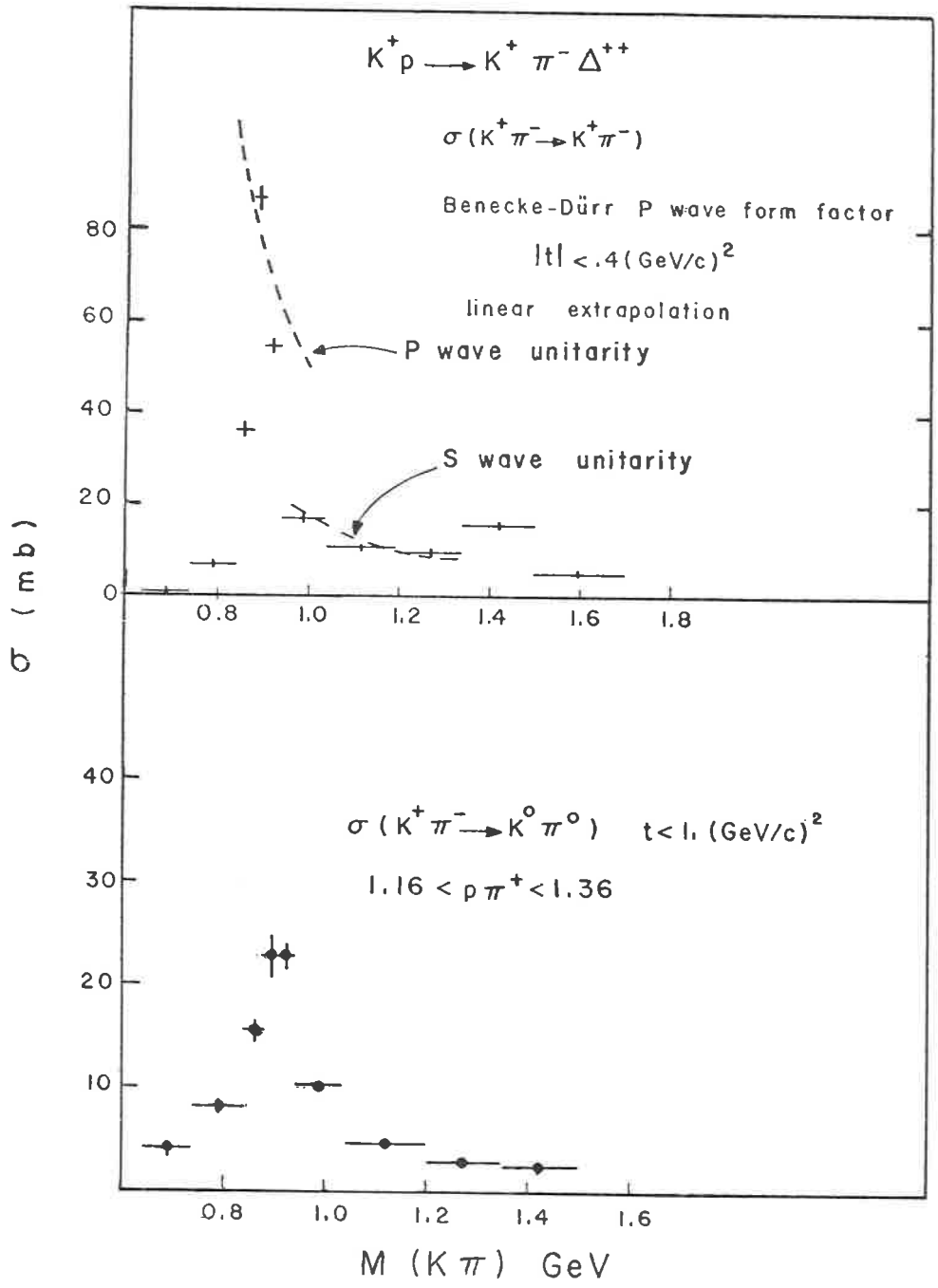

Fig. 6. – Cross-section extrapolation to the pion pole *vs.* $M(K\pi)$ for $K^+\pi^- \to K^+\pi^-$ and for $K^+\pi^- \to K^0\pi^0$.

K*(1420) region and dropping again down to ~ 4 mb for $1.5 < M(K\pi) < 1.7$ GeV. Below 1.1 GeV there are no other resonance broader than ~ 20 MeV.

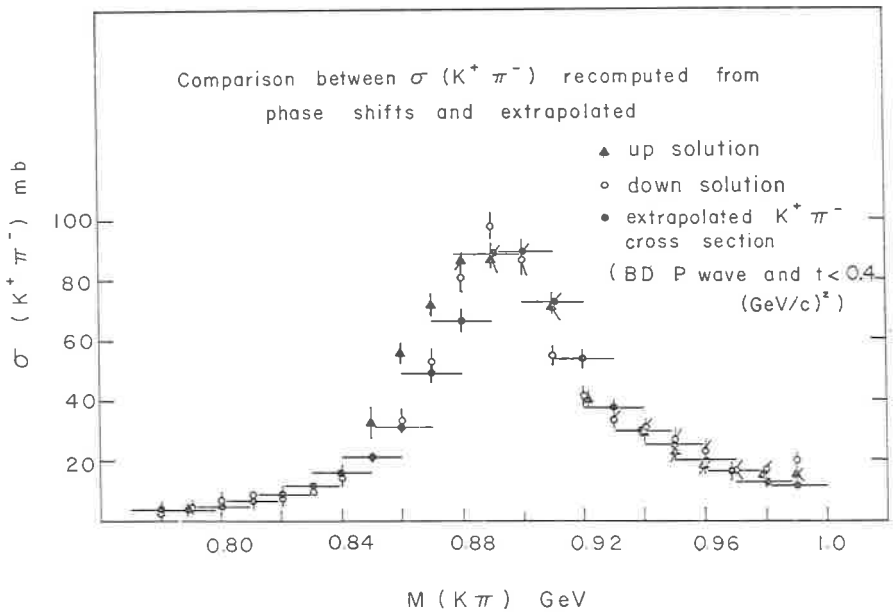

Fig. 7. – Details of Fig. 6 in the K*(892) region for $K^+\pi^- \to K^+\pi^-$. No correction for experimental resolution are made. Points labelled « up » and « down » correspond to the two δ_0^1 solutions.

On Fig. 7 the points labelled « down » and « up » show the predictions uncorrected for the resolution effects for the Kπ cross-section corresponding to the two solutions for δ_0^1 above, (taking $\delta_0^3 = 1.8$ mb and δ_1^1 following a Breit Wigner with $M = 0.891$ GeV, $\Gamma = 0.050$ GeV).

The « up » solution predicts too high a cross-section in the region $0.85 < M(K\pi) < 0.89$ GeV, *i.e.* there is a broad (~ 40 MeV) bump in the low side of the K*(892). Assuming the correctness of the extrapolated cross-section the « down » solution is, therefore, the preferred one. On the other hand, corrections for resolution effects may be sufficiently large to prevent using the Kπ cross-section for rejecting the δ_0^1 « up » solution. A detailed study of the resolution is not feasible at this stage for lack of information on the individual experiments. A more precise knowledge of the Kπ cross-section is, therefore, needed to resolve this ambiguity.

9. Comparison with previous Kπ phase shift analysis.

Let me also quote the results of a previous Kπ scattering analysis done by the Johns Hopkins group (6) on partial samples of the same data reported above. This analysis makes use of *unnormalized* moments which are propor-

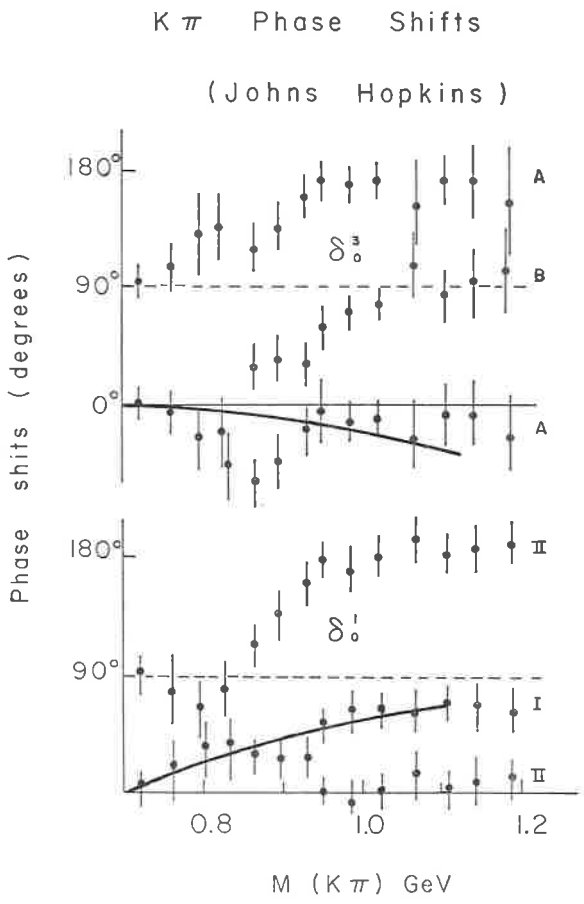

Fig. 8. – Phase shifts solutions for δ_0^1 and δ_0^3 from the analysis of Johns Hopkins University, ref. (6). The curves drawn are a guide to the eye.

tional to the cross-section and, therefore, much more subject to the uncertainties of the cross-sections for reactions (1) and (2).

The results reported by this group for the δ_1^1 and δ_1^3 phase shifts agree with the work described above. Solutions for the δ_0^1 and δ_0^3 phase shifts are obtained from the extrapolated differential cross-sections. A unique set of solution for δ_0^1 and δ_0^3 is obtained by requiring the calculated cross-sections to agree with those extrapolated from $K^+\pi^-$ elastic scattering and with those for $K^-\pi^-$ scattering obtained in other experiments (7). The δ_0^1 solution correspond to the « down » solution and the δ_0^3 to the « gentle δ_0^3 » solution reported above, (Fig. 8). But here again no corrections for resolution effects were taken into account and the reject of the δ_0^1 « up » solution may not be justified.

10. Kπ phase shifts from Veneziano model.

In comparing the results of the Kπ phase shift analysis with the results obtained by Lovelace (8) with a unitarized version of the Veneziano model Fig. 9, we can see that in Lovelace's results δ_1^1 goes through 90° at

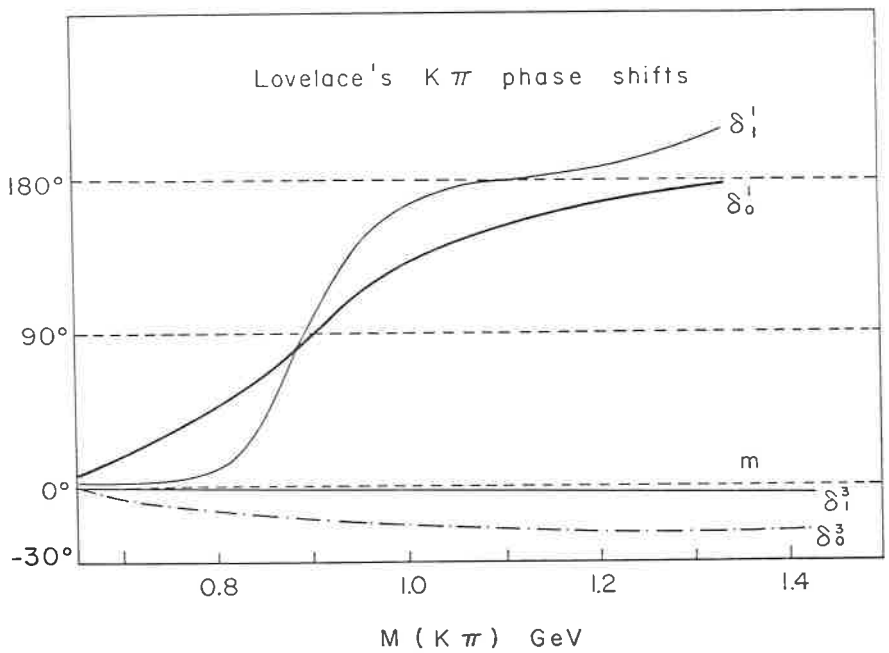

Fig. 9. – Kπ scattering phase shifts calculated by Lovelace with a unitarized version of Veneziano model.

$M(K\pi) = 0.890$ GeV and after levelling off at 180° begins again to increase at $M(K\pi) = 1.1$ GeV. δ_0^1 goes through 90° near 0.900 GeV and shows a broad resonance behaviour with $\Gamma \sim 214$ MeV.

δ_0^3 is small and negative reaching $-30°$.
δ_1^2 is smaller than a few degrees.

Therefore, the $I = \frac{3}{2}$ phase shifts appear to follow the model whereas for the $I = \frac{1}{2}$ phase shifts the S wave resonance of the « up » solution has a width of 35 MeV instead of 214 MeV and the δ_1^1 phase shift does not cross 180°.

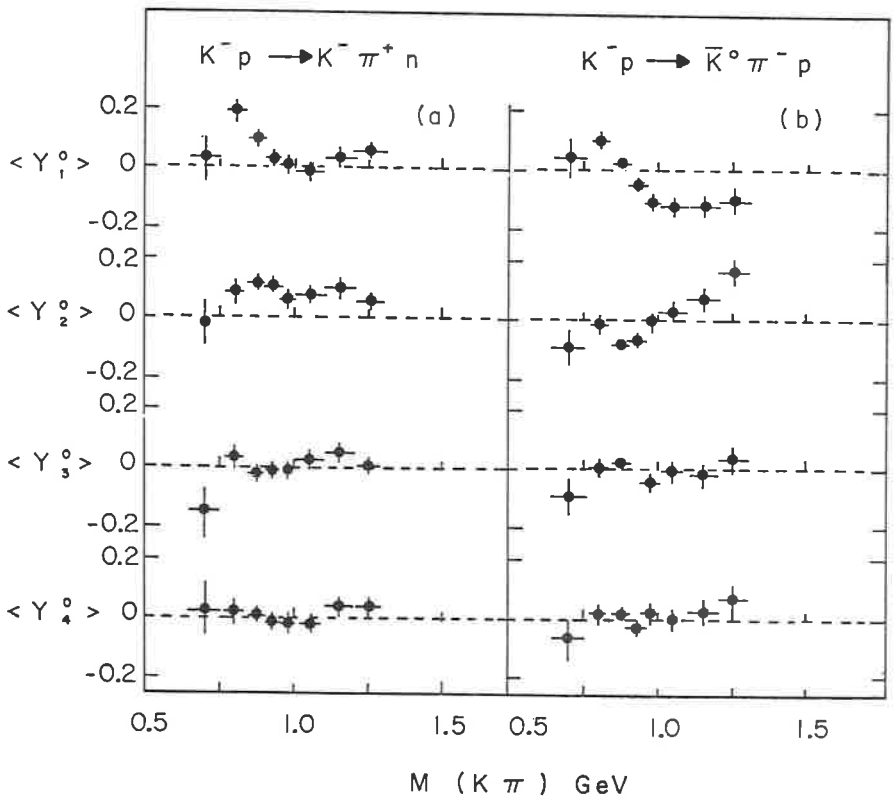

Fig. 10. – *a*) $\langle Y_i^0 \rangle$ moments *vs.* $M(K\pi)$ for reaction $K^+p \to K^-\pi^+n$ and $K^-p \to \bar{K}^0\pi^-p$ at 5.5 GeV/c for $t' < 0.3$ GeV² ref. (9).

11. Off-mass shell Kπ scattering phase shifts.

Finally I would like to say a word on the recent results obtained by a collaboration between Argonne National Laboratory and the University of

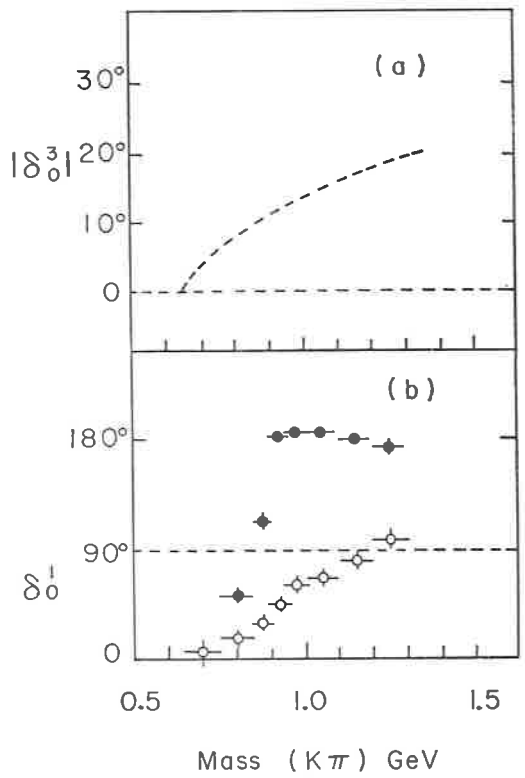

Fig. 10. – *a*) δ_0^1 off mass shell phase shift ref. (9) *b*) δ_0^3 phase shift solution quoted in ref. (9) from ref. (3).

Chicago (8) in the study of the reactions:

$$K^-p \to K^-\pi^+n \qquad 2875 \text{ events} \qquad (15)$$

$$K^-p \to \overline{K}^0\pi^-p \qquad 2086 \text{ events} \qquad (16)$$

at 5.5 GeV/c.

The $\langle Y_l^0 \rangle$ moments of the Kπ system at low momentum transfer were measured ($t' < 0.3$ GeV^2), Fig. 10 (*a*). Strong production of K*(892) and K*(1420) is seen for both reactions. The data is analysed using a simple one particle exchange model including the $I = \frac{1}{2}$ S, P and D waves amplitudes and the $I = \frac{3}{2}$ S wave. The results show that the δ_0^3 phase shift is negative and gives two acceptable solutions for the off mass shell δ_0^1 phase shift which cross 90° at $M(K\pi) \simeq 0.850$ GeV and $M(K\pi) \simeq 1.2$ GeV respectively. Fig. 10 (*b*).

It is interesting to note that although the statistics are limited in this experiment and the model used very simple, the general characteristics of the δ_0^1 phase shift solutions are very close to the one described above.

12. Conclusions.

In the ππ scattering phase shift analysis one possible solution ([10]) has the $J = 0$, $I = 0$ ππ phase shift resonating near the ρ mass. One may speculate that this ππ « resonance » and the « resonant » solution for the $J = 0$, $I = \frac{1}{2}$ Kπ wave may form part of a $J^P = 0^+$ nonet. But so far such conclusions may be premature. Time will tell.

Acknowledgements.

I would like to stress the important contribution of P. Herquet (Brussels) in the preparation of the material contained in this report.

REFERENCES

0) Preliminary results were presented at the 1970 Kiev International Conference on High Energy. P. Herquet and T. Trippe: CERN/D. Ph. II/PHYS 70-29. The new data reported here is included in « search for a Kπ resonance ». CERN-Brussels-UCLA Collaboration: private communication, paper to be published.

1) See for ex.: C. Fu *et al.* (Univ. Cal. Berkeley): UCRL report 18201 (1968); W. De Baere *et al.* (CERN, Brussels): *Nuovo Cimento*, 61 A 397 (1969); C. S. Abrams *et al.* (Univ. Illinois): *Phys. Rev.*, D 1, 2433 (1970); T. Ferbel (Univ. Rochester): *Phys. Rev. Lett.*, **26**, 344 (1971).

2) T. G. Trippe *et al.* (UCLA): *Phys. Lett.*, **28** B, 203 (1968); W. De Baere *et al.* (CERN-Brussels): *Nucl. Phys.*, B **14**, 425 (1969); P. Antich *et al.* (Johns Hopkins Univ.) *Proc. of the Conference on ππ and Kπ interactions.* Argonne National Laboratory, p. 508 (1969) and R. Mercer *et al.*: paper presented at the 1970 Kiev International Conference on High Energy.

3) A. M. BAKKER *et al.* (S.A.B.R.E.): *Nucl. Phys.*, B **24**, 211 (1970) and *Information on the S and P wave* $I = \frac{3}{2}$ $K\pi$ *phase shifts.* Contribution to the International Conference on Mesons Resonances, Bologna, April 1971. Y. CHO *et al.* (Argonne National Laboratory): *Bull. Am. Phys. Soc.*, **15**, 54 (1970); A. R. KIRSHBAUM *et al* (Univ. Cal. Berkeley-UCLA): report UCRL 19426 (1969); P. ANTICH *et al.* (Johns Hopkins Univ.): *Nucl. Phys.*, B **29**, 305 (1971).
4) A. DONNACHIE, R. G. KIRSOPP and C. LOVELACE: *Phys. Lett.*, **26** B, 161 (1968).
5) J. BENECKE and H. P. DÜRR: *Nuovo Cimento*, **56** A, 269 (1968).
6) R. MERCER *et al.* (Johns Hopkins Univ.): $K\pi$ *scattering phase shifts determined for the reaction* $K^+p \to K^+\pi^-\Delta^{++}$ *and* $K^+p \to K^0\pi^0\Delta^{++}$, paper presented at the 1970 Kiev International Conference on High Energy, and *Nucl. Phys.* B **32**, 381 (1971).
7) Y. CHO *et al.* (Argonne National Laboratory): *Phys. Lett.*, **33** B, 409 (1970) and papers of ref. ([3]).
8) C. LOVELACE: *Proc. of the conference on* $\pi\pi$ *and* $K\pi$ *interactions*, Argonne National Laboratory, p. 562 (1969) and *Phys. Lett.*, **28** B, 264 (1968).
9) H. YUTA *et al.* (Argonne National Laboratory; Univ. Chicago): *On mass shell* $K\pi$ *scattering phase shifts. Phys. Rev.* Lett. **26**, 1502 (1971). and private communication.
10) See P. SCHLEIN: *Meson Spectroscopy*, p. 161 (W. A. Benjamin Inc., 1968); E. COLTON and P. SCHLEIN: *Proc. of the conference on* $\pi\pi$ *and* $K\pi$ *interactions*, Argonne National Laboratory, p. 1 (1969); P. SCHLEIN: *Proc. of the conference on* $\pi\pi$ *and* $K\pi$ *interactions*, Argonne National Laboratory, p. 446 (1969); J. P. BATON, G. LAURENS and J. REIGNIER: *Phys. Lett.*, **33** B, 528 (1970).

Study of the dipion system up to the g-meson region in the reaction $\pi^- p \to \pi^+ \pi^- n$ at 17.2 GeV/c with a big magnet spectrometer (*)

G. GRAYER, B. HYAMS, C. JONES and P. SCHLEIN
CERN - Geneva

W. BLUM, H. DIETL, W. KOCH, H. LIPPMANN, E. LORENZ, G. LÜTJENS, W. MÄNNER, J. MEISSBURGER, W. OCHS, U. STIERLIN and P. WEILHAMMER
Max-Planck-Institut für Physik und Astrophysik - Munich

1. Introduction.

The magnet spectrometer of the CERN-Munich-Collaboration using magnetostrictive wire chambers online to a PDP-9 computer is shortly described.

Preliminary results on the mass spectrum and angular distribution of the $\pi^+\pi^-$ system in the mass range $0.280 < m_{\pi^-\pi^+} < 2.0$ GeV/c^2 of the reaction $\pi^- p \to \pi^+ \pi^- n$ at 17.2 GeV/c beam momentum are presented.

This spectrometer which was designed for the study of neutral boson resonances up to masses of 2 GeV/c^2 with high statistics came into operation at CERN in May 1970 and has been working quite satisfactorily for a whole year.

2. Apparatus.

Figure 1*a* shows the layout of the experimental setup. One of the main features of this design is a short distance between the target and the magnet in order to get a reasonable acceptance for the forward going particles even

(*) Invited paper presented by H. Dietl.

at high masses. Figure 1*b* is a sketch out of scale which allow us to distinguish the main components of the apparatus.

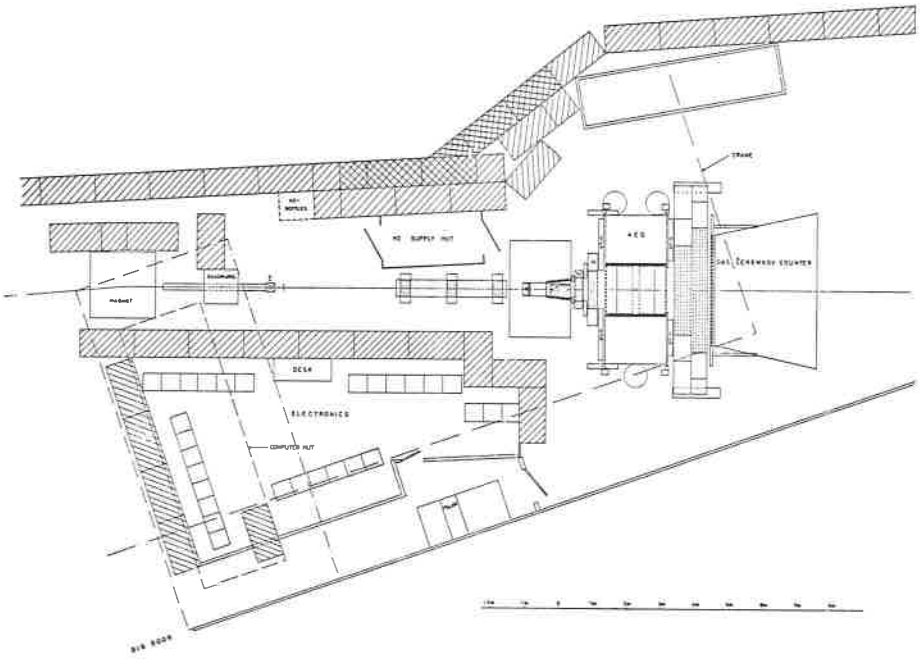

Fig. 1*a*. – Layout of experimental setup.

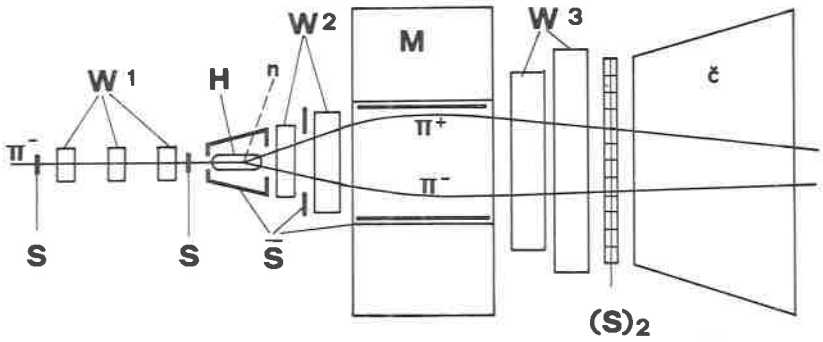

Fig. 1*b*. – Sketch of apparatus out of scale. S) Scintillation counters. $\bar{S}$) Lead-sandwich scintillation counters. H) Liquid hydrogen target. M) Spectrometer magnet. W) Wire spark chambers. $\check{C}$) Gas-Čerenkov.

The track of the incoming π^- is measured with 3 sets of wire-chambers (W1) in front (left) of the 50 cm long liquid hydrogen target, which is surrounded by lead-sandwich scintillation counters ($\bar{S}$). The trajectories of the two outgoing pions are measured with wire chambers in front and behind the magnet (W2, W3). 36 chambers are incorporated into the system, the largest having an active area of (3.60×0.90) m^2. The magnet (M) has an aperture of (1.50×0.50) m^2 and a total length of 2 m including shims, the maximal bending power being 20 k G.m. Two coincident particles are selected by the counter array $(S)_2$, which consists of 32 pairs of 5 mm thick scintillation counters each 10 cm wide and 1 m high.

The threshold gas Čerenkov counter ($\check{C}$) with a volume of 20 m^3 and working at atmospheric pressure distinguishes between pion and kaon-pairs. The K^+K^-n and possibly some $p\bar{p}n$ events form the biggest background and would distort the $\pi^+\pi^-$ spectrum considerably, if interpreted as $\pi^+\pi^-n$ events. We find about 15% of all « good » events not being $\pi^+\pi^-n$.

With the measured 3-momenta of the secondary pions and the known beam momentum plus the information from the gas Čerenkov a complete reconstruction of the reaction is possible. The mass of the recoil nucleon is calculated with an error of ± 140 MeV, which is sufficient to reduce inelastic background (additional π^0) to less than 5%.

The online data collection goes via a system of 30 MHz scalers (SEN SPADAC), and a small computer (DEC PDP-9) on to magnetic tape without any preselection.

3. Preliminary results.

The results shown in Fig. 2 and 3 are preliminary insofar as they represent only part of our total data and also because some corrections, *e.g.* interaction of secondaries in hydrogen, counter inefficiencies, scanning losses of the geometry program, still have to be done.

Figure 2 shows the $\pi^+\pi^-$ mass spectrum of about 100,000 $\pi^+\pi^-n$ events at 17.2 GeV/c from threshold up to 2.0 GeV/c^2 and with $|t| \leqslant 0.2$ (GeV/c)^2.

The lower line is the observed spectrum, the upper points are the data corrected for the acceptance of the apparatus. Clearly visible are the three resonances, the ρ, f and g meson.

In the following Figs. 3*a-i* some normalised moments $\langle Y_l^m \rangle$ of the angular distribution of the dipion system in the Gottfried-Jackson frame are shown.

The $\langle Y_1^0 \rangle$ (Fig. 3*a*), proportional to the *s-p* interference, stays almost constant in the whole ϱ-region and drops rapidly to zero at the KK threshold.

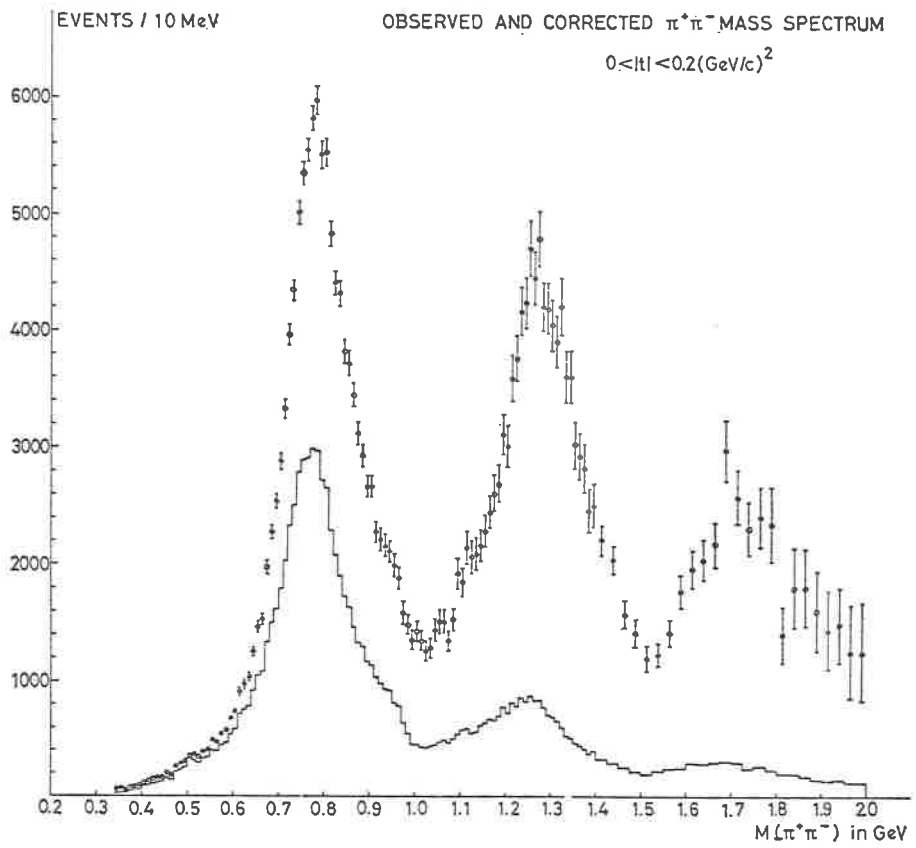

Fig. 2. – Mass spectrum of $\pi^+\pi^-$, observed and corrected.

Since $\langle Y_2^0 \rangle$ (Fig. 3*c*) does not have such a strong fluctuation, we have to assume that the *s*-wave becomes highly inelastic at this mass. A similar result has been presented by us at the Philadelphia meeting on meson spectroscopy in 1970 ([1]).

In the *f* region $\langle Y_3^0 \rangle$ (Fig. 3*f*) displays the classical behaviour of a rapidly varying resonant *d*-wave (Fig. 3*g*) interfering with a relatively small and constant *p*-wave, going through zero before the maximum of the resonance is reached.

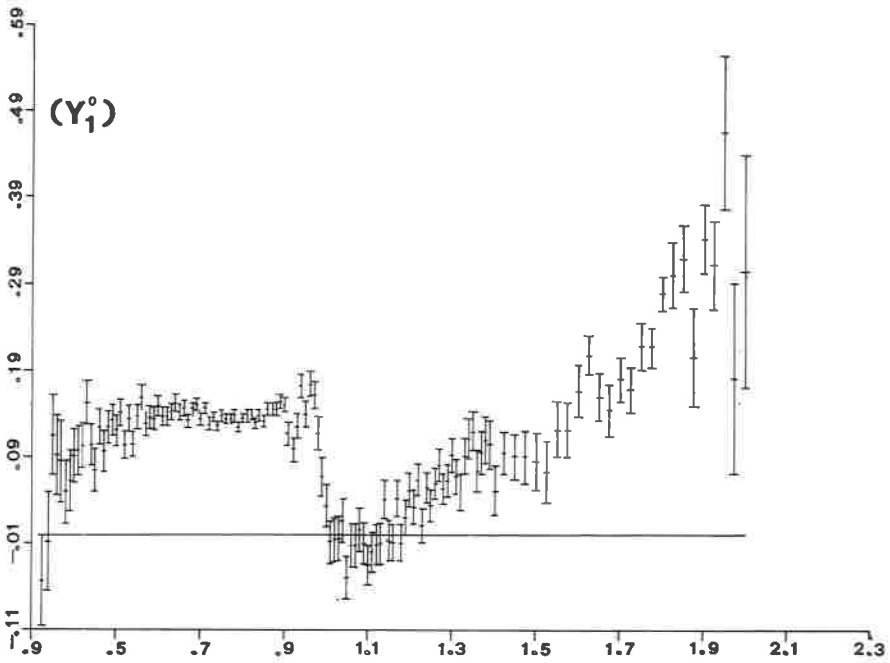
(Y_1^0)
.59
.49
.39
.29
.19
.09
-.01
-.11
.9
.5
.7
.9
1.1
1.3
1.5
1.7
1.9
2.1
2.3
$M(\pi^+\pi^-)$ GeV

FIG, 3a

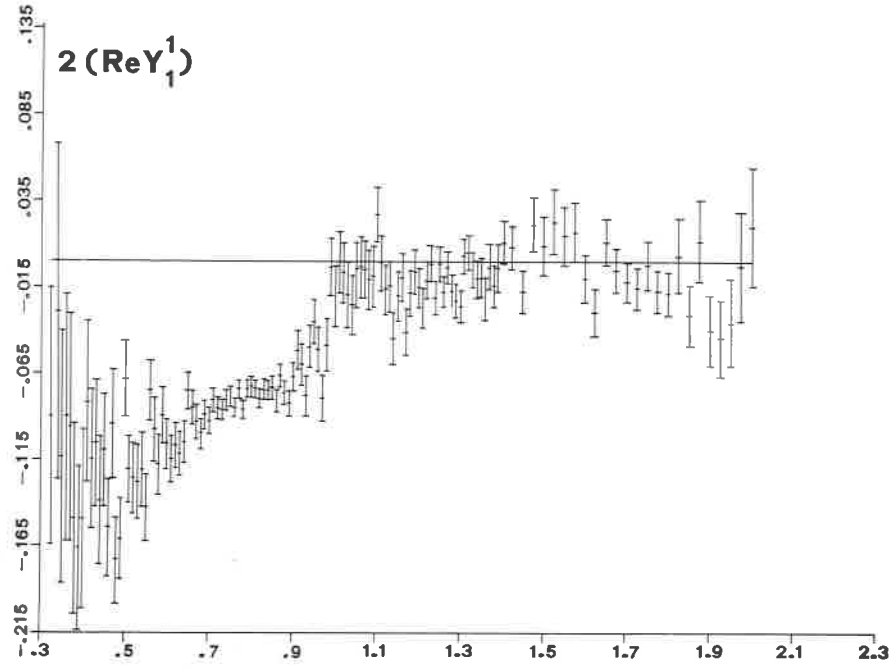
$2(ReY_1^1)$
.135
.085
.035
-.015
-.065
-.115
-.165
-.215
.3
.5
.7
.9
1.1
1.3
1.5
1.7
1.9
2.1
2.3

FIG. 3b

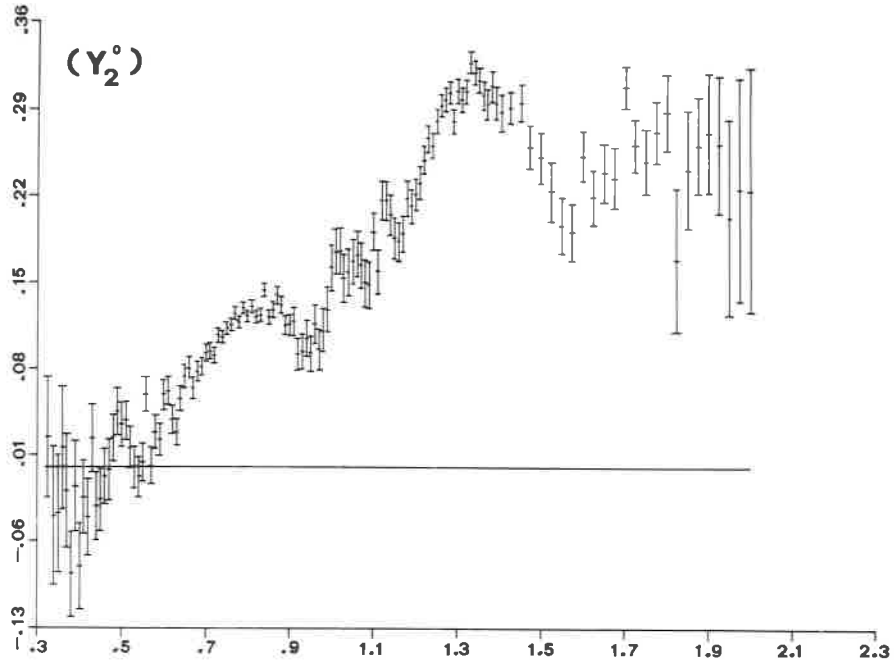
(Y_2^0)
.36
.29
.22
.15
.08
.01
-.06
-.13
.3
.5
.7
.9
1.1
1.3
1.5
1.7
1.9
2.1
2.3

FIG. 3c

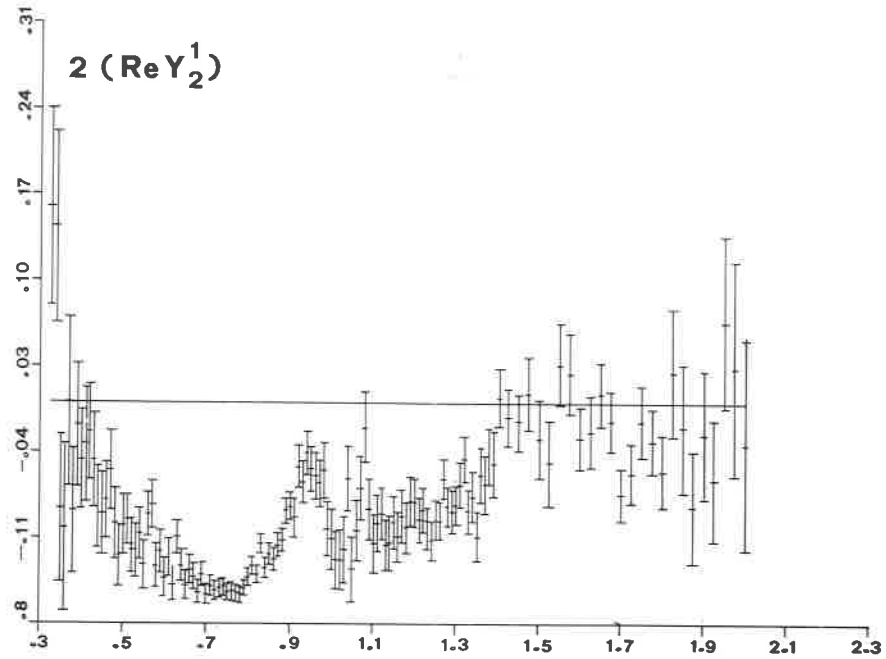
$2\,(\mathrm{Re}\,Y_2^1)$
.31
.24
.17
.10
.03
-.04
-.11
-.18
.3
.5
.7
.9
1.1
1.3
1.5
1.7
1.9
2.1
2.3

FIG. 3d

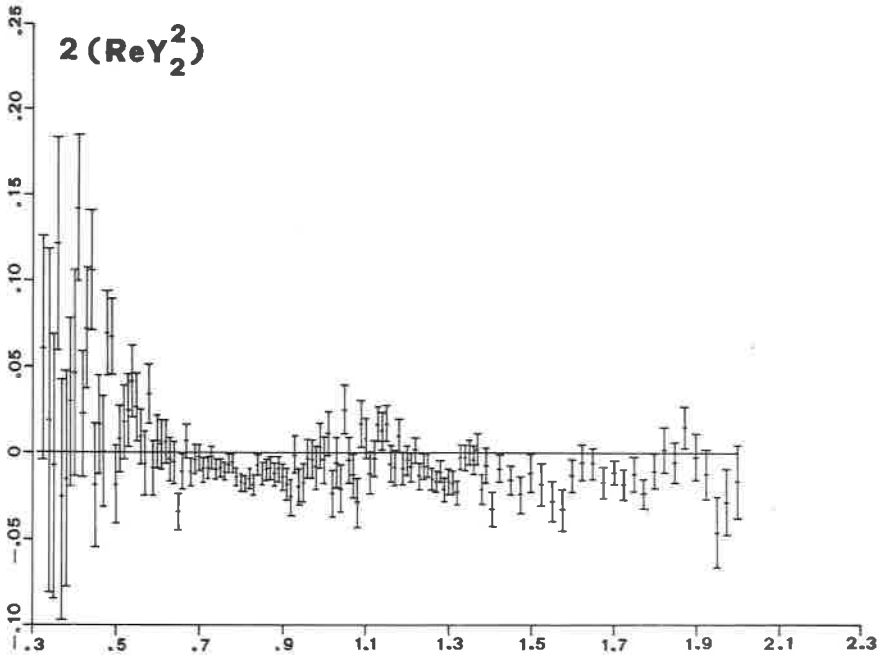
2 (ReY$_2^2$)
.25
.20
.15
.10
.05
0
-.05
-.10
.3
.5
.7
.9
1.1
1.3
1.5
1.7
1.9
2.1
2.3

FIG. 3e

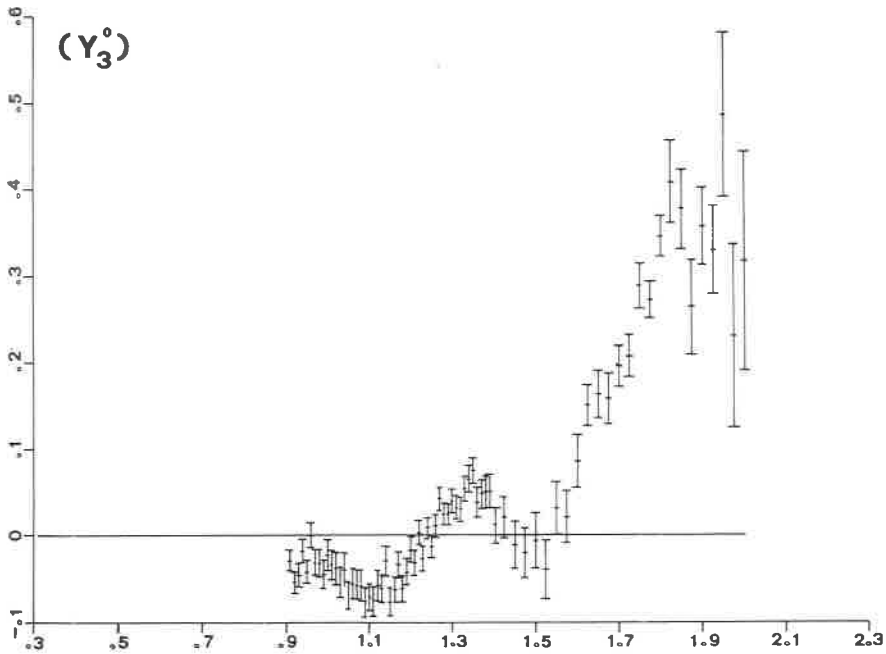
(Y_3^0)
.6
.5
.4
.3
.2
.1
0
-.1
.3
.5
.7
.9
1.1
1.3
1.5
1.7
1.9
2.1
2.3

FIG. 3f

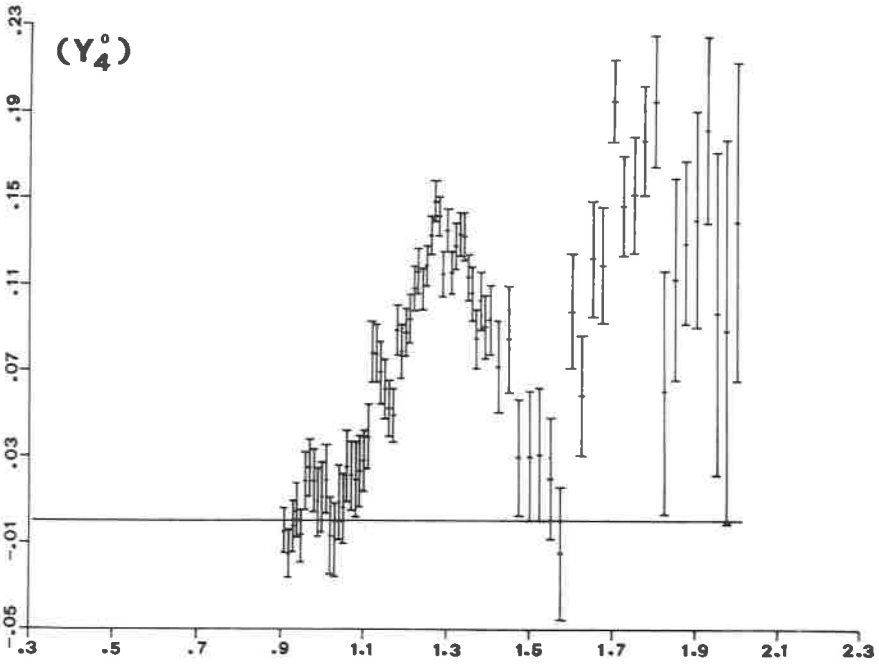
(Y_4^0)
.23
.19
.15
.11
.07
.03
-.01
-.05
.3
.5
.7
.9
1.1
1.3
1.5
1.7
1.9
2.1
2.3

FIG. 3g

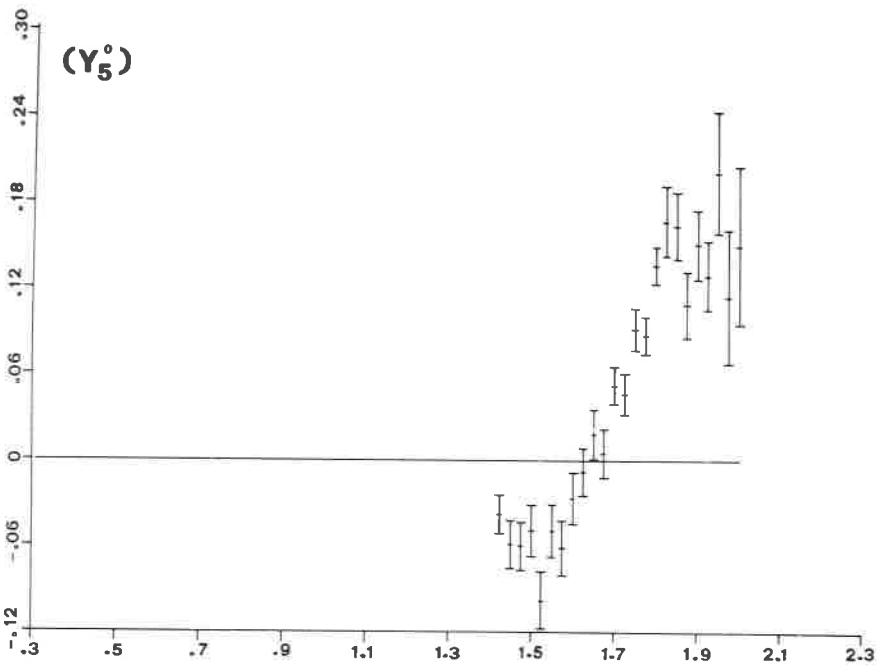
(Y_5^0)
.30
.24
.18
.12
.06
0
-.06
-.12
.3
.5
.7
.9
1.1
1.3
1.5
1.7
1.9
2.1
2.3

FIG. 3h

A very similar behaviour of the $\langle Y_5^0 \rangle$ (Fig. 3*h*) is observed in the *g*-region, where we see a resonant amplitude (Fig. 3*i*) interfering with a small *d*-wave.

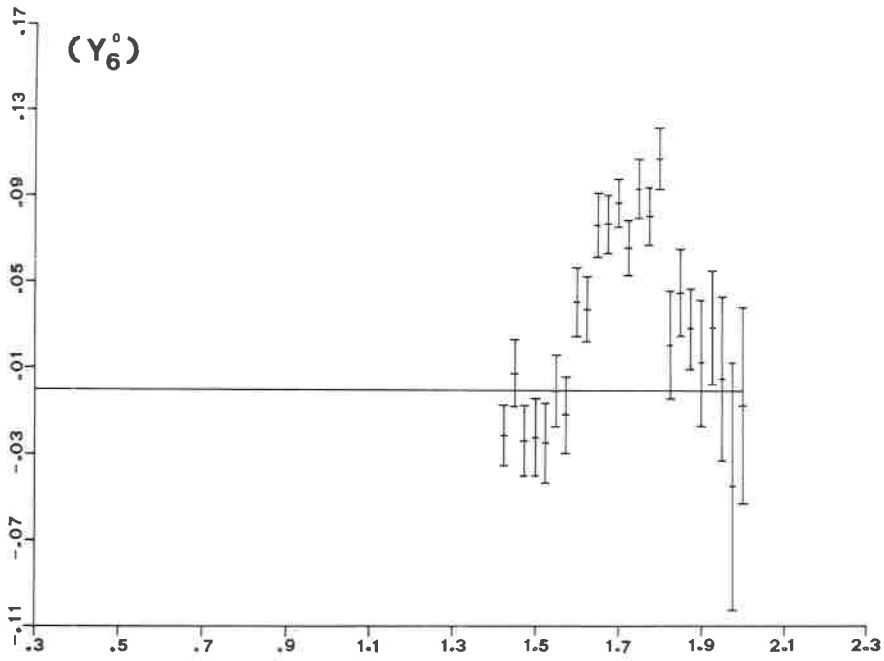

FIG. 3i

Fig. 3. *a)÷i)* Normalised moments $\langle Y_l^m \rangle$ of the angular distribution in Gottfried-Jackson frame. $I(\theta, \varphi) = \sum_l^L t_l^m Y_l^m$; $L \geqslant 2J_{(\pi\pi)}$; $t_0^0 : \frac{1}{\sqrt{4\pi}}$; $t_l^0 = \langle Y_l^0 \rangle$, $t_l^m = 2\langle \mathrm{Re}\, Y_l^m \rangle$, $m \neq 0$.

This together with the fact that the higher moments $\langle Y_7^0 \rangle$ and $\langle Y_8^0 \rangle$ are consistent with zero in this mass region, shows that the spin of the g-meson is 3, as favoured for long (2).

REFERENCES

1) B. D HYAMS *et al.*: *Experimental Meson Spectroscopy* (ed. C. BALTAY and A. H. ROSENFELD), Columbia University Press, New York and London (1970), p. 41.
2) G. GRAYER *et al.*: Determination of the g-Meson Spin, Phys-Letters, **35** B (1971) 160.

Study of $\pi\pi$ scattering from Chew-Low extrapolations of $\pi^-p \to \pi\pi\mathcal{N}$ at 2.77 Gev/c (*)

J. P. Baton, G. Laurens and J. Reignier
Département de Physique des Particules Elémentaires, CEN - Saclay

Part I

$\pi^+\pi^-$ elastic cross-section from Chew-Low extrapolations of $\pi^-p \to \pi^+\pi^-n$ reaction at 2.77 GeV/c

The elastic cross-section for $\pi^+\pi^-$ scattering is determined up to 1.2 GeV by applying the Chew-Low extrapolation method on a high statistics experiment. Different types of extrapolation procedure are used and their results compared.

We present the results of a study of $\pi^+\pi^-$ elastic scattering through the reaction

$$\pi^-p \to \pi^-\pi^+n\,. \tag{1}$$

140 000 pictures were taken in the 2 m CERN HBC with an incident beam of 2.77 GeV/c; they were previously used for a similar study of the $\pi^-\pi^0$ elastic scattering ([1]). Among the 180 000 two prong events scanned, we found 19 500 events fitted by the reaction (1) which after some corrections (**) give a total cross-section of (4.1 ± 0.2) mb.

(*) Invited paper presented by G. Laurens

(**) Reaction (1) is contaminated by $\pi^-p \to \pi^-p + (2\pi^0)$ reaction when the momentum p_+ of the positive track is larger than 1.3 GeV/c (*i.e.* for $\simeq 30\%$ of the events). The magnitude of this contamination is evaluated by comparing the importance of the two reactions for $p_+ < 1.3$ GeV/c and also by studying a similar simulated contamination by fitting $\pi^-p \to \pi^-p(\pi^+\pi^-)$ events to reaction (1); both methods indicate that at most 18% of the ambiguous events (*i.e.* $\simeq 5\%$ of the total) are effectively $\pi^-p \to \pi^-p + (2\pi^0)$ events.

In the determination of the $\pi^+\pi^-$ elastic cross-section, we use the 10 634 events with $|t|<13\,\mu^2$ or the 12 630 events with $|t|<21\,\mu^2$ (t is the squared four momentum transfer to the nucleon); these cuts will be explained below.

The Chew-Low extrapolation method which proved to be so fruitful in our study of the $\pi^-\pi^0$ scattering ([1]) and also in another work on $\pi^+\pi^-$ scattering ([2]) is used again with some improvements however. We define as usual an « off shell $\pi^+\pi^-$ cross-section »:

$$F(\omega, t) = \frac{2\pi}{f^2} \frac{k_{\text{lab}}^2}{\omega\sqrt{\omega^2 - 4\mu^2}} (t-\mu^2)^2 \frac{\partial^2\sigma}{\partial t\,\partial\omega^2} \tag{2}$$

which is analytic in the t-plane cut from $9\mu^2$ to infinity and which is equal at $t=\mu^2$ to the true (on-shell) $\pi^+\pi^-$ elastic cross-section. The notations are the usual ones: $f^2 = 0.081 \pm 0.002$ is the $\pi\mathcal{N}$ coupling constant, ω the dipion mass, k_{lab} the incident pion momentum in the laboratory frame, $\partial^2\sigma/\partial t\,\partial\omega^2$ the experimental differential cross-section for reaction (1). This function is constructed by averaging the experimental values of the right-hand side on small cells of the Chew-Low plot. These cells are chosen in such a way that the number of events in each cell is significant (of the order of 100 events); they are generally of (20÷30) MeV large in ω and $1 \div 3\mu^2$ large in t. We then extrapolate this off-shell cross-section in two essentially different ways:

i) *Simple Chew-Low extrapolation*: we simply represent the functions $F(\omega, t)$ or $F(\omega, t)/|t|$ (pseudo peripheralism) by a polynomial in t with coefficients fitted in the physical region and we compute the value at $t=\mu^2$. This procedure was described in detail in our previous work on $\pi^-\pi^0$ scattering ([1]).

ii) *Extrapolation after a conformal mapping*: following the works of Cutkosky and Deo ([3]) and of Ciulli ([4]), we perform a conformal mapping of the t-plane onto the plane of a « more suitable » variable x. We make the homographic transformation:

$$x = x(t) = \frac{at+b}{t+d} \tag{3}$$

in order to get the mapping represented on Fig. 1; the parameters a, b and d are then uniquely defined and easily computed. We represent the functions $F(\omega, t)$ or $F(\omega, t)/|t|$ by a polynomial in x with coefficients fitted in the physical region and we compute the value at $x = x(t=\mu^2)$. Note that the

authors of refs. ([3,4]) recommend going farther with a mapping that uses elliptic functions and which converts the physical region and cuts of Fig. 1 into two

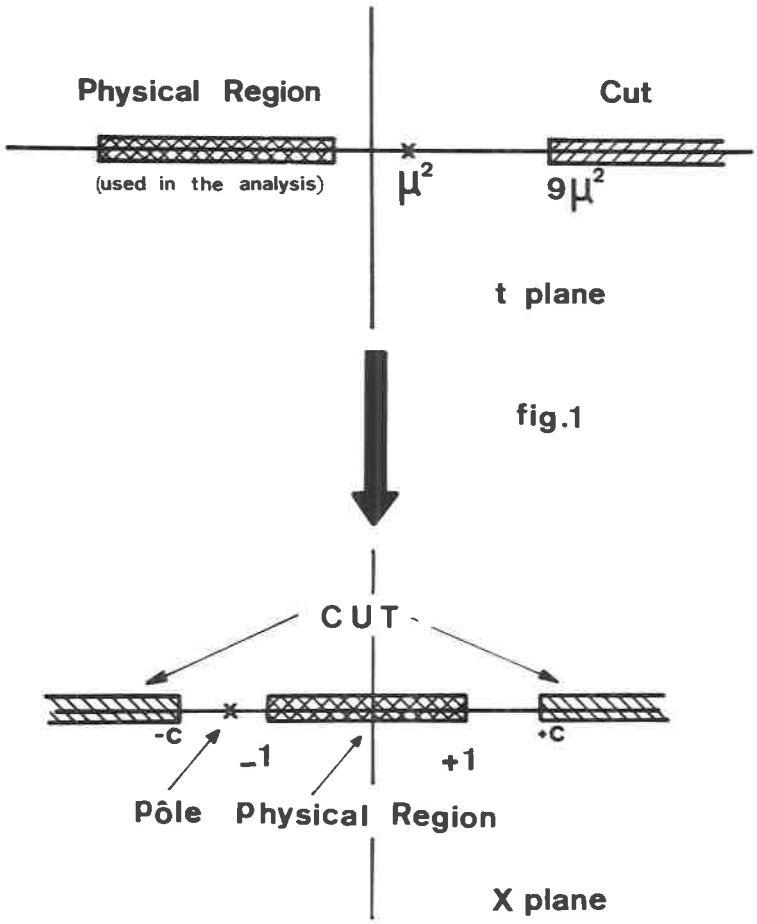

Fig. 1. – Scheme of the conformal mapping used.

concentric circles, followed by a Laurent expansion of the function $F(\omega, t)$ inside the ring to perform the extrapolation at $t = \mu^2$. However, due to the special conditions of our problem, these elliptic functions are very well approximated by the corresponding circular functions and in this approximation both mappings are equivalent. Indeed no further improvement was obtained when carrying on the second mapping.

TABLE I. – *Typical results of different extrapolations.* The first part concerns the extrapolation of $F(\omega, t)$, the second part of the extrapolation of $F(\omega, t)/|t|$ (pseudo peripheralism). Quadratic polynomials in t or x are used except for the extrapolation $F(\omega, t)$ without mapping where a cubic fit is necessary.

ω (MeV)	Extrapolation of $F(\omega, t)$					
	Without mapping			With mapping		
	$\sigma_{\pi\pi}$ (mb)	$F(\omega,0)$ (mb)	χ^2	$\sigma_{\pi\pi}$ (mb)	$F(\omega, 0)$ (mb)	χ^2
540÷600	26±12	0.2± 8	1.7	18±10	3.5± 5	1.6
600÷650	45±13	− 4.8± 8	1.0	42±10	− 3.6± 5	1.0
650÷690	37±17	3.0±10	0.9	61±13	− 5.1± 7	1.0
690÷720	69±22	7.0±14	1.2	57±16	13.0± 9	1.2
720÷750	57±24	18.0±15	0.9	108±17	0.3±10	0.6
750÷780	88±28	17.0±18	0.8	96±20	14.0±11	0.8
780÷810	101±25	− 3.6±18	1.0	85±20	4.2±11	0.9
810÷840	81±24	−15.0±16	1.0	95±18	−16.0±12	0.8
840÷880	−9±23	26.0±17	1.3	24±16	10.0± 9	1.4
880÷920	54±21	−13.0±17	1.1	28±14	1.9± 8	1.3
920÷970	18±15	− 1.0±10	0.4	16±14	2.8± 9	0.8

ω (MeV)	Extrapolation of $F(\omega, t)/\|t\|$			
	Without mapping		With mapping	
	$\sigma_{\pi\pi}$ (mb)	χ^2	$\sigma_{\pi\pi}$ (mb)	χ^2
300÷ 420	22± 6	0.6	18± 6	0.9
420÷ 500	15± 6	2.0	27± 6	0.5
500÷ 580	30± 6	0.4	30± 5	0.5
580÷ 640	34± 5	0.2	36± 6	0.2
640÷ 680	42± 5	1.3	38± 6	1.0
680÷ 710	74± 8	0.4	80± 8	0.8
680÷ 710	74± 8	0.4	80± 8	0.8
710÷ 740	79± 8	1.3	90± 8	1.3
740÷ 770	117± 9	1.0	126±10	1.1
770÷ 800	94± 8	1.3	108± 8	0.6
800÷ 840	70± 5	0.8	68± 6	0.5
840÷ 880	40± 5	0.7	38± 5	0.5
900÷ 950	20± 4	1.1	33± 5	1.2
950÷1000	9± 4	1.2	10± 4	1.2
1000÷1050	13± 3	1.3	11± 4	1.4
1050÷1100	10± 3	1.0	9± 3	1.1
1100÷1150	12± 4	3.0	11± 4	0.4
1150÷1200	21±10	3.2	20± 5	1.6

All the results that we get by these methods, *i.e.* extrapolations i) or ii), with and without the pseudoperipheralism constraints and for several choices of the cells in t and ω) are compatible. Typical results are given in Table I and Fig. 2 and 3. Some general comments are now necessary:

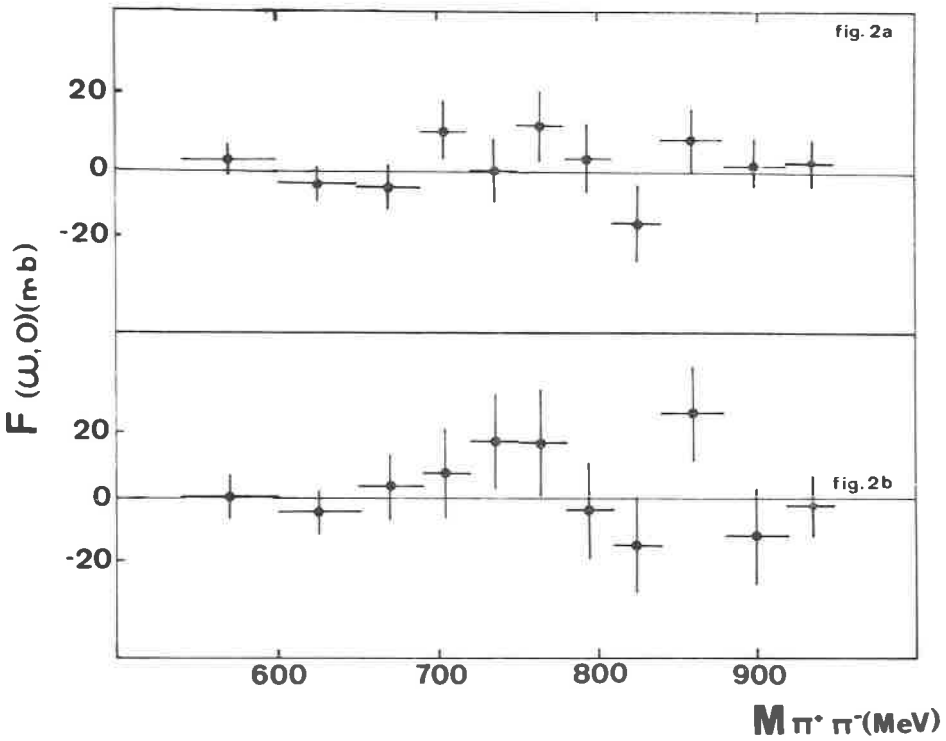

Fig. 2. – $F(\omega, t)$ for $t = 0$, *vs.* dipion mass: *a*) extrapolation with mapping; *b*) extrapolation without mapping.

1) Although all results are compatible, it is apparent that the mapping operation gives rise to definite improvements in the data analysis:

i) For a given degree of the polynomials, the fits of $F(\omega, t)$ are always better when the x-variable is employed. In particular, a quadratic fit in x is as good as a cubic fit in t (see Table I). It is revealing that the use of the x variable reduced appreciably the errors.

ii) Results of the extrapolations with mapping are less sensitive to changes in the t or ω bins and to changes in the range of t values used in the

analysis (the mapping reduces the instability of the extrapolation). This is the origin of our different cuts in t: we use systematically $|t|<13\mu^2$ without mapping and $|t|<21\mu^2$ with mapping.

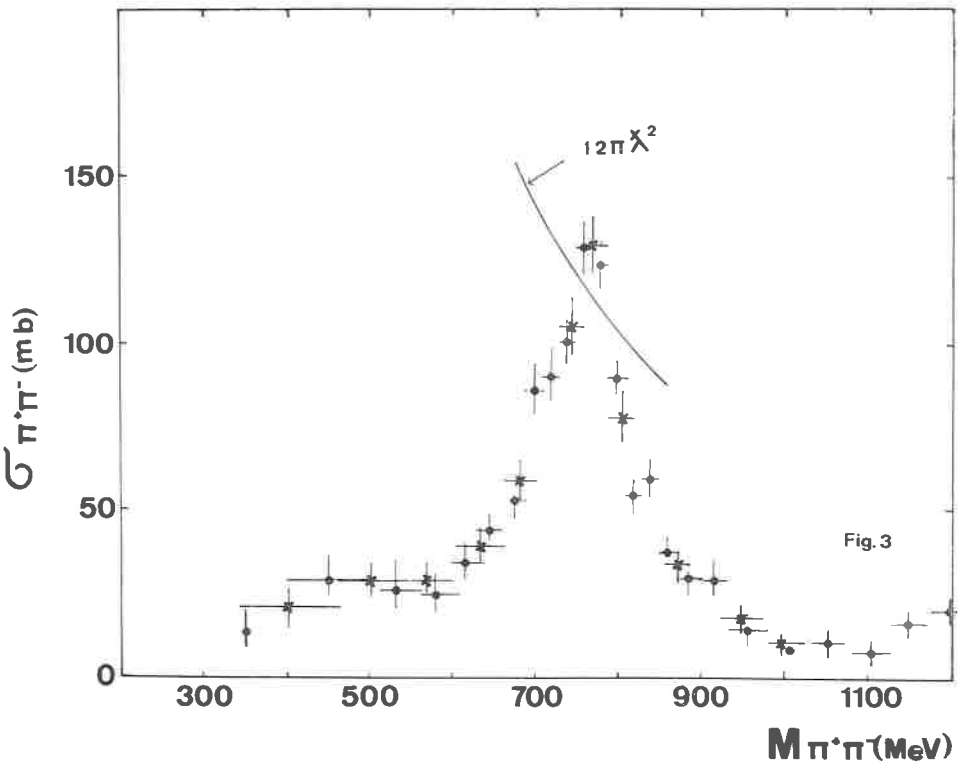

Fig. 3. – Extrapolated $\pi^+\pi^-$ elastic scattering with the constraint at $t=0$ using the conformal mapping and the t values up to $21\mu^2$, *vs.* dipion mass. Crosses and points represent two different choices of the mass intervals.

2) The values of $F(\omega, t)$ at $t=0$ are systematically compatible with zero. These values are quoted in Table I and Fig. 2; the straight line $F(\omega, 0)=0$ has $\chi^2=0.84$ with mapping and $\chi^2=0.89$ without mapping.

3) The extrapolations of $F(\omega, t)/|t|$ (pseudo peripheralism) have another feature which makes the mapping more convenient: the $\pi^+\pi^-$ elastic cross-section exceeds the unitarity limit for a P-wave resonance by a substantial amount compatible with the presence of the large S_0 wave that we find in the

phase-shifts analysis([5]). Without mapping, the cross-section is a little small to account for this large S_0 wave and it would be useful to renormalize it in the phase-shifts analysis ([2]). (Of course, this is a small effect and one could as well say that it falls within the quoted errors).

4) On Fig. 3, we represent the final $\pi^+\pi^-$ elastic cross-section obtained by a quadratic extrapolation of $F(\omega, t)/|t|$ with mapping. Note that as a general rule the $\pi^+\pi^-$ extrapolations require polynomials of degree higher than the $\pi^-\pi^0$ ones (a linear extrapolation is sufficient for the $\pi^-\pi^0$ cross-section) (*) which of course makes the extrapolation problem more delicate (compare refs. ([1]) and ([2])).

Acknowledgements.

We are particularly indebted to Dr. A. Rogozinski for his interest and encouragement in this work. We are also very grateful to J. Bouchez and F. Cadiet for their invaluable assistance in the data acquisition and reduction.

(*) Extrapolation of $\pi^-\pi^0$ elastic cross-section with mapping are in complete agreement with previously published work ([1]) (see also ref. ([5])).

REFERENCES

1) J. P. Baton, G. Laurens and J. Reignier: *Phys. Lett.*, **25** B, 419 (1967); *Nucl. Phys.*, B **3**, 349 (1967).
2) S. Marateck, V. Hagopian, W. Selove, L. Jacobs, F. Oppenheimer, W. Schultz, L. J. Gutay, D. H. Miller, J. Prentice, E. West and W. D. Walker: *Phys. Rev. Lett.*, **21**, 1613 (1968).
3) R. E. Cutkosky and B. B. Deo: *Phys. Rev.*, **174**, 1859 (1968).
4) S. Ciulli: *Nuovo Cimento*, **61** A, 787 (1969); **62** A, 301 (1969).
5) J. P. Baton, G. Laurens and J. Reignier: *Phys. Lett.* **33** B, 528 (1970).

PART II

$\pi\pi$ phase shifts from Chew-Low extrapolations of $\pi^- p \to \pi\pi\mathcal{N}$ at 2.77 GeV/c

A phase shifts analysis is extracted from the $\pi^-\pi^0$ and $\pi^+\pi^-$ elastic scattering data obtained through Chew-Low extrapolation of high statistics $\pi^- p \to \pi^-\pi^0$ and $\pi p \to \pi^+\pi^- n$ reactions at 2.77 GeV/c. The well known up-down ambiguity for the $I = 0$ S-wave is solved in the low energy region where the down solution is the only one compatible with the data. The ambiguity remains at higher energies and it appears furthermore that there the inelasticity starts to play an important role.

We present the results of a phase shifts analysis of $\pi^-\pi^0$ and $\pi^+\pi^-$ elastic scattering data obtained through Chew-Low extrapolation of the reactions:

$$\pi^- p \to \pi^+\pi^- n\,, \tag{1}$$

$$\pi^- p \to \pi^-\pi^0 p\,, \tag{2}$$

at 2.77 GeV/c incident beam momentum. A large part of the experimental material on reaction (2) was already used in our previous work on $\pi^-\pi^0$ scattering (1) but the present analysis which treats both reactions simultaneously and which uses the new extrapolation technique described in ref. (2) improves our knowledge of the $I = 1$ and $I = 2$ states and gives of course new results on the $I = 0$ states. As explained before, the use of conformal mappings in the extrapolations makes it possible to take into account events with rather large momentum transfer to the nucleon and improves furthermore the stability of the extrapolations. In what follows, we always use events with $|t| < 21\mu^2$, *i.e.* 12630 events for reaction (1) and 5860 events for reaction (2); corrections for biases at low t values for reaction (2) or at large momenta of the positive track for reaction (1) are made (see ref. (2) and (3)).

We define as usual « off-shell » differential cross-sections for $\pi\pi$ scattering:

$$F(\omega, t, \cos\theta) = -\frac{2\pi}{f_\beta^2}\,\frac{k_{\text{lab}}^2}{\omega\sqrt{\omega^2/4-\mu^2}}\,\frac{(t-\mu^2)^2}{t}\,\frac{\partial^3\sigma}{\partial t\,\partial\omega^2\,\partial\cos\theta}\,, \tag{3}$$

which are constructed in the physical region of reactions (1) and (2) by averaging the experimental values of the right-hand side of (3) on suitably chosen

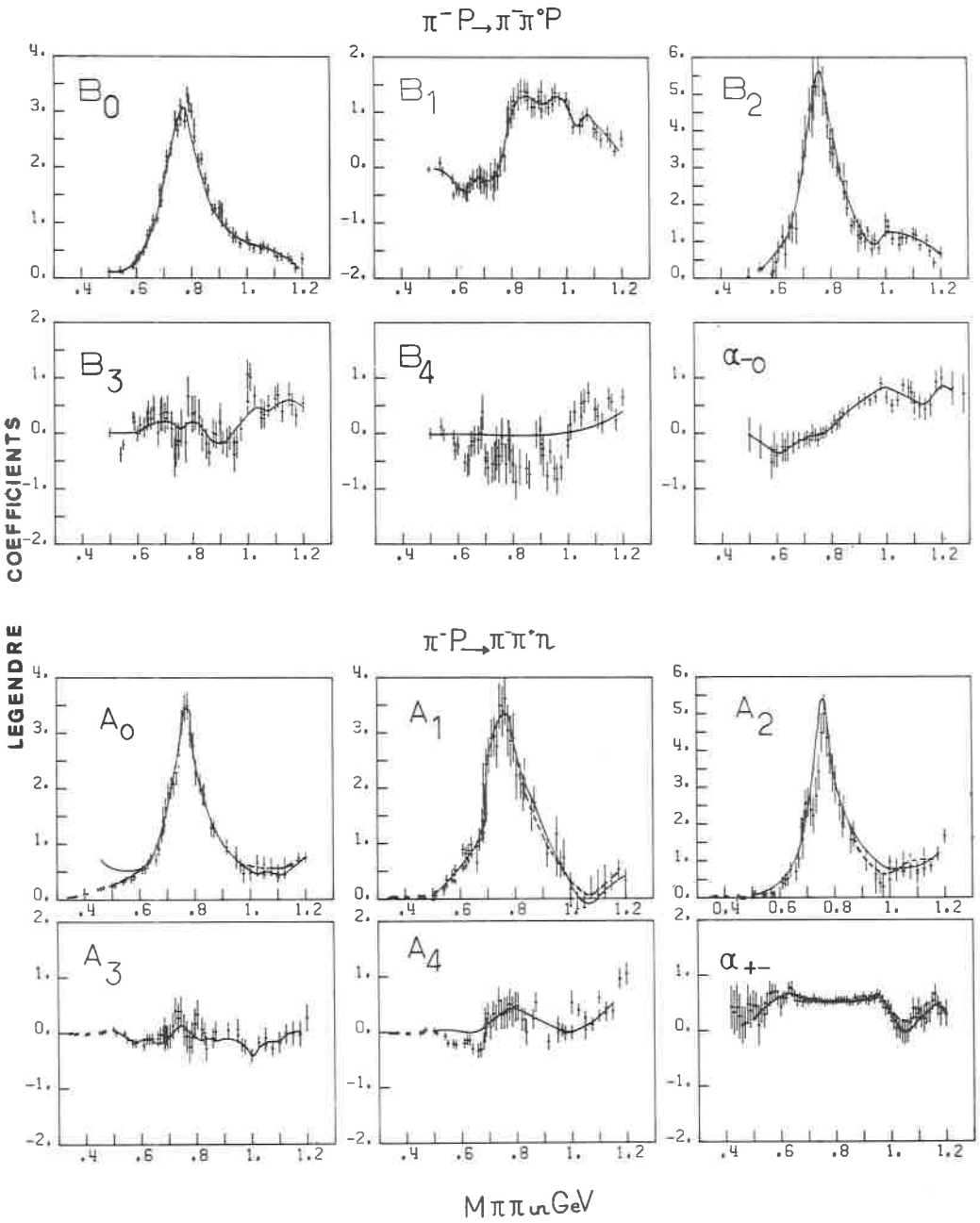

Fig. 1. – Values of the extrapolated Legendre coefficients as functions of the dipion mass. The curves are calculated from the results of the phase shifts analysis (purely elastic phases). For the $\pi^-p \to \pi^+\pi^-n$ case, the dotted curve corresponds to the down solution for the S_0 wave, the full curve to the up solution (whenever they are different). It is clearly seen from the coefficient A_0 that the down solution is the good one at low energy (see text).

small cells in $\cos\theta$, t and ω. The notations are the same as in ref. (2)* for both reactions (1) and (2), θ is the angle between the two negative tracks in the dipion rest frame.

In order to perform the Chew-Low extrapolations, we first expand $F(\omega, t, \cos\theta)$ in Legendre polynomials

$$F(\omega, t, \cos\theta) = \sum_{n=0} A_n(\omega, t) P_n(\cos\theta) , \tag{4}$$

and we extrapolate the coefficients $A_n(\omega, t)$ in $t = \mu^2$ using for each $A_n(\omega, t)$ a polynomial representation in the variable $x(t)$ defined above. Many different extrapolations corresponding to different choices of bins in ω and t were made in this way, the results of which were always nicely compatible. A sample of extrapolated values of the coefficients $A_n(\omega)$ is presented on Figs. 1*a*-1*b*, corresponding to reactions (1) and (2) respectively (we use the letter A for the coefficients of reaction (1), the letter B for reaction (2)). Higher order coefficients are completely negligible. This corresponds to the fact that an S, P, D-waves description of $\pi\pi$ scattering is presumably « safe » below 1.2 GeV. As one can see from formula (3), our extrapolations are made with the pseudoperipheralism constraint in $t = 0$. The validity of this hypothesis has been discussed for the coefficients A_0 and B_0 in our previous works on $\pi\pi$ scattering (refs. (1) and (2)) and found to be very good (recall $A_0 = \frac{1}{2}\sigma_{\pi^-\pi^+}$, $B_0 = \frac{1}{2}\sigma_{\pi^-\pi^0}$). For the other coefficients, the test is rather unconclusive because the errors on the extrapolations without constraint are rather large. Let us mention however that the extrapolations of the forward-backward asymmetry coefficients

$$\alpha(\omega, t) = \left(\frac{F-B}{F+B}\right)_{\omega, t} , \tag{5}$$

which are done without any constraint in $t = 0$ (Figs. 1*a*-1*b*; α_{-0} and α_{+-}) are in complete agreement with the expected values

$$\alpha(\omega) = (A_1 - \tfrac{1}{4}A_3)/2A_0 , \tag{6}$$

computed from the constrained $A_n(\omega)$.

(*) f_β is the appropriate $\pi\mathcal{N}$ coupling constant; $f_0^2 = 0.081 \pm 0.002$ (reaction (2)), $f_\pm^2 = 2f_0^2$ (reaction (1)).

For these phase shifts analysis, we use smooth curves drawn by hand through the values of the coefficients A_n, B_n, α_{-0} and α_{+-}, and we look at each energy ω for a best fit of the 12 values so obtained with the five phase shifts S_0, S_2, P_1, D_0 and D_2 including of course the requirement of continuity of the solutions with respect to ω. In order to estimate the errors, we give at each extrapolated coefficient an error which corresponds to the width of the band of results shown on Figs. 1*a*-1*b*. The phase shifts analysis is made in two ways which correspond to different hypotheses on the absorption parameter η of the amplitudes $S_i^I(\omega) = \eta_i^I(\omega) \exp(2i\delta_i^I(\omega))$.

1. Purely elastic phase shifts ($\eta_i^I = 1$).

This hypothesis is strictly speaking only valid below the four pions threshold ($\omega = 560$ MeV), but it is presumably still reasonable at higher energy, becoming gradually worse when the energy increases. The best fit analysis gives one unique solution for the S, P, D-waves below some 700 MeV and two solutions above, the famous up-down ambiguity for the S_0 wave ([4]) remaining unsolved in this higher energy region. We want to stress that *there is no up-down ambiguity at lower energies where the only existing solution is the so-called down one*. The quality of our phase shifts representation is reflected on Figs. 1*a-b* where the smooth curves drawn through the coefficients A_n, B_n, α_{-0} and α_{+-} are calculated from the results of the phase shifts analysis (*). Coming back to the up-down ambiguity for the S_0 wave, we find that it appears again if one neglects the constraint imposed by the A_0 coefficient (*i.e.* the $\pi^+\pi^-$ elastic cross-section); one gets then a down solution which is very close to the previous one, and an up-solution which finally gives a very bad representation of A_0 as seen on Fig. 1*a* (upper curve at low energy). The phase shifts S_0, S_2, P_1, D_0 and D_2 obtained in this analysis lie along the smooth dotted curves drawn on Fig. 2; errors are not indicated but they are of the order of the width of the bands which are drawn on this Fig. and which will be explained later.

In order to obtain analytical representations of the ππ phase shifts, we

---

(*) The B_4 coefficient which is negative in the lower energy region cannot be reproduced with S,P,D-waves only. We checked that a very small F wave (1 or 2 degree with any sign) could easily account for the difference.

use relativistic effective range formulae (see for instance ([5])):

$$\sqrt{\frac{\nu}{\nu+1}}\,\nu^{l}\,\mathrm{ctg}\,\delta_l^I(\nu)=\sum_{n=0} b_{l,n}^I\left(\log\left(\sqrt{\nu}+\sqrt{\nu+1}\right)\right)^{2n}, \tag{7}$$

where $\nu=\omega^2/4-1$ is the square of the pion momentum in the dipion rest frame. The parameters of the representations were determined by independent best fit adjustments of the different waves, using data between 500 MeV and 900 MeV for the S and P waves and data above 700 MeV for the D waves (imposing furthermore the f^0 mass); they are given in Table I. We want to stress that these representations of the phase shifts should only be used as interpolating formulae inside the energy range used for the fit. In particular, although the coefficient $b_{l,0}^I$ is in principle the inverse of the scattering length, its value is too unstable against small changes in the data or even in the degree of the polynomial used in (7) to really have this physical meaning. Data at much lower energies would be necessary to determine the scattering lengths (see however ([7])). On the other hand, the parametrization (7) can be used in the neighbourhood of a resonance to obtain the parameters of its local Breit-Wigner representation (see ([5])); one gets (*)

$$\begin{aligned}&\rho\text{-resonance:} && m_\varrho=766\ \text{MeV}, && \Gamma_\varrho=133\ \text{MeV},\\ &\varepsilon\text{-resonance } (S_0 \text{ up}): && m_\varepsilon=736\ \text{MeV}, && \Gamma_\varepsilon=181\ \text{MeV}.\end{aligned}$$

TABLE I. – *Parameters of the analytical representation of the purely elastic phase shifts (formula (7)).*

Coeff. / Wave	C_0	C_1	C_2	C_3	χ^2
S_0 down	2.30± 0.17	− 0.69± 0.13	0.02± 0.02	—	0.06
S_0 up	− 2.83± 1.0	4.43± 0.83	− 1.27± 0.17	—	0.9
S_2	− 27.4 ± 9.6	20.8 ± 11.2	− 7.0 ± 4.3	0.9 ±0.00	0.06
P_1	27.0 ± 5.2	−13.4 ± 6.2	6.25± 2.51	−1.77±0.32	0.09
D_0	1538 ± 952	928 ±574	−259 ±161	—	—
D_2	−2000 ±1000	—	—	—	—

(*) Warning! These figures correspond to a definite convention for the resonance parameters, *i.e.*, the resonance energy is the energy for which the phase shift reaches $\pi/2$ and the width is associated with a *local* simple Breit-Wigner representation. One could just as well use other conventions with of course other results; for example: the width of the resonance can be the energy interval between the points where the phase shift goes through $\pi/4$ and $3\pi/4$ (in which case $\Gamma_\rho=127$ MeV), or, the mass and width could be directly related to the position of the corresponding pole in the complex energy plane ($E_{\text{pole}}=m-i\Gamma/2$; for the ρ, $m_\rho=760$ MeV, $\Gamma_\rho=131$ MeV).

TABLE II. – *Values of the purely elastic phase shifts vs. dipion mass.*

ω (MeV)	S_2	P_1	D_2	S_0 (down)	S_0 (up)	D_0
500	− 3± 3	8± 5	—	31±7	—	—
525	− 4± 3	10± 3	—	28±6	—	—
550	− 6± 4	11± 3	—	41±8	—	—
575	− 7± 4	14± 3	—	47±8	—	—
600	−10± 6	18± 3	—	48±4	—	—
625	−10± 6	21± 3	—	50±6	—	—
650	−10± 4	26± 3	—	51±7	—	—
675	− 9± 5	29± 5	—	51±7	—	—
700	− 9±12	42± 5	—	56±5	64±11	—
725	−12± 8	54± 6	—	60±5	72± 6	—
750	−12± 6	69± 8	—	63±6	97± 6	—
775	−10±12	103±12	—	69±4	119± 5	—
800	−15± 4	118± 7	—	75±3	133± 4	1±3
825	−17± 3	131± 6	—	78±3	144± 3	1±3
850	−21± 3	138± 4	—	82±3	149± 3	1±3
875	−22± 4	144± 4	—	87±4	151± 2	2±3
900	−27± 4	149± 4	—	90±4	158± 3	2±3
925	−30± 4	152± 4	—	91±5	161± 4	2±3
950	−31± 4	155± 3	—	86±4	165± 2	3±3
975	−30± 3	156± 3	− 1±3	79±4	168± 2	5±4
1000	−16± 3	157± 3	− 4±3	60±6	172± 2	10±6
1025	− 9± 5	159± 4	− 6±3	61±7	180± 3	9±7
1050	−12± 4	160± 4	− 4±3	66±5	180± 4	14±5
1075	−15± 5	158± 4	− 4±3	72±7	179± 4	13±6
1100	−10± 4	159± 4	− 5±3	84±8	177± 4	18±5
1125	−12± 6	159± 4	− 5±3	72±7	177± 5	19±6
1150	−11± 4	170± 3	−12±4	90±9	170± 6	23±6
1175	−13± 8	173± 3	− 7±5	—	—	—
1200	−12± 6	175± 5	−11±4	—	—	—

TABLE III. – *Values of the different phases in degree and absorption parameters η_l when the inelasticity is taken in account.*

ω (MeV)	S_0 (up)	η_{S_0} (up)	S_0 (down)	η_{S_0} (down)	P_1	η_{P_1}	D_0	η_{D_0}
700	60± 3	—	—	—	43± 5	—	—	—
725	69± 3	—	—	—	54± 6	—	—	—
750	105±15	—	60± 4	—	69± 9	—	—	—
775	118± 3	—	64± 4	1.0 ±0.2	96±18	0.92±0.1	—	—
800	130± 4	0.85±0.1	64± 4	0.70±0.3	111± 8	0.92±0.1	1±3	—
825	140± 3	0.92±0.1	73± 5	0.84±0.2	121± 9	0.82±0.1	1±3	—
850	146± 3	1.0 ±0.1	76± 5	0.76±0.3	129± 8	0.96±0.1	1±3	—
875	153± 3	1.0 ±0.1	76± 1	0.76±0.3	139± 5	0.88±0.1	2±3	—
900	157± 3	1.0 ±0.1	72± 5	0.60±0.4	144± 4	0.86±0.1	2±3	—
925	163± 2	1.0 ±0.1	66±10	0.50±0.3	149± 4	0.88±0.1	2±3	—
950	167± 3	1.0 ±0.1	60± 6	0.32±0.4	152± 4	0.84±0.15	3±3	—
975	170± 3	0.89±0.1	57± 9	0.30±0.4	151± 4	0.80±0.15	5±4	—
1000	176± 2	0.81±0.1	50±10	0.65±0.3	151± 4	0.86±0.1	10±6	0.98±0.1
1025	180± 3	0.93±0.1	32± 6	0.89±0.3	152± 6	0.76±0.2	9±7	1.0 ±0.1
1050	185± 3	0.94±0.1	36± 4	0.98±0.2	151± 5	0.50±0.2	14±8	0.92±0.1
1075	186± 3	0.84±0.1	38± 5	0.90±0.3	151± 5	0.56±0.2	13±6	0.92±0.1
1100	180± 3	0.82±0.1	36± 5	0.85±0.2	154± 5	0.50±0.2	18±5	0.90±0.1
1125	177± 5	0.75±0.1	40±15	0.70±0.2	154± 5	10·42±0.2	21±6	0.80±0.1
1150	174± 5	0.70±0.1	54± 6	0.86±0.2	162± 6	0.40±0.1	22±6	0.84±0.1
1175	—	—	—	—	170± 4	0.76±0.1	—	—
1200	—	—	—	—	170± 7	0.92±0.1	—	—

2. Study of the inelasticity.

Inelastic $\pi\pi$ scattering has recently been shown to exist in different channels at energy of the order of 1 GeV ($\pi\pi \to 4\pi$ refs. ([8,9]), $\pi\pi \to K\bar{K}$ ref. ([10])). Although our purely elastic scattering data cannot give unambiguous answers on inelasticities, we can derive some information if we supplement the data by «reasonable»hypothesis. We consider first the $\pi^-\pi^0$ scattering and we assume that the D_2 wave is not absorbed (invoking the general weakness of the $I = 2$ interaction and some centrifugal barrier effect). It is then possible to determine the four

parameters which correspond to the complex S_2 and P_1 phase shifts. The results of a best fit analysis of the B_n, α_{-0} coefficients indicate that:

i) the inelasticity of the S_2 wave is very poorly determined and can

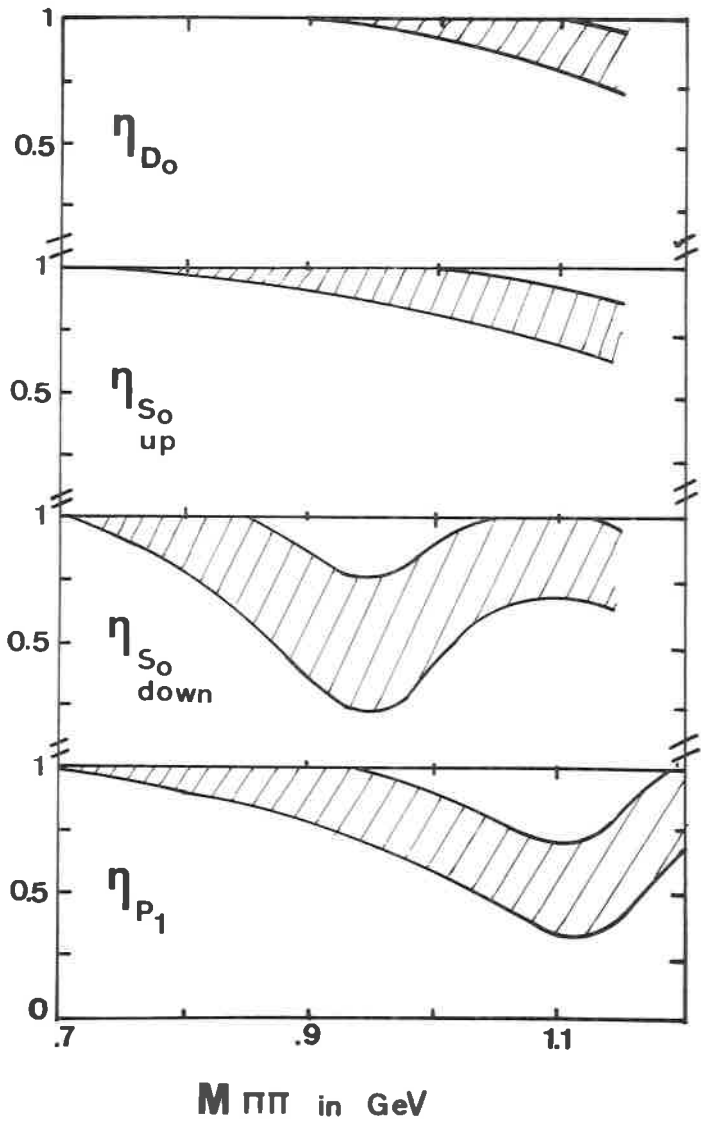

Fig. 2. – Absorption parameters under the assumption that $\eta_{S_2} = \eta_{D_2} = 1$.

always be considered as negligible (*i.e.* $\eta = 1$ is a fair approximation for this wave); the phase remains very close to the purely elastic phase;

ii) the inelasticity of the P_1 wave is better known and clearly not negligible above say 800 MeV (the result for η are compatible with those indicated on Fig. 3); again, the phase remains very close to the purely elastic phase.

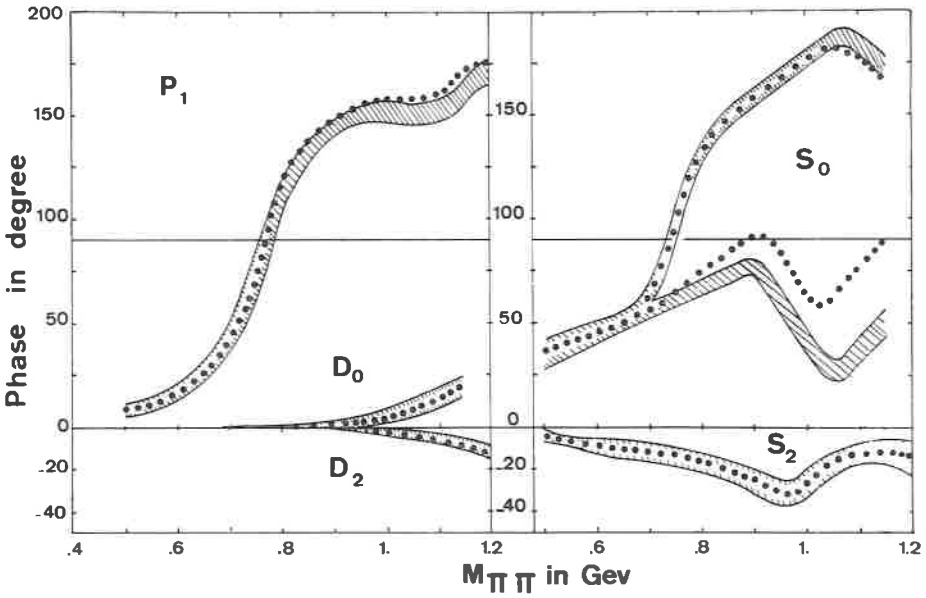

Fig. 3. – Pion-pion phase shifts. The dotted curves correspond to the purely elastic hypothesis; the bands are the results when inelasticity is taken into account. The errors on the purely elastic phases are of the order of the width of these bands.

We then consider all the $\pi^+\pi^-$ and $\pi^-\pi^+$ scattering data together and we assume complex phase shifts for the S_0, P_1 and D_0 waves and, in agreement with our first analysis, real phase shifts for the S_2 and D_2 waves. The best fit at each energy of the coefficients A_n, B_n, α_{-0} and α_{+-} with these eight parameters and the requirement of continuity of the solutions as a function of the energy gives the results represented by bands on Fig. 2 (phases) and Fig. 3 (η-parameters). It is seen that the phases remain very close to the purely elastic ones (curves) with the only exception of the down solution for the S_0 wave at higher energy. Also, the absorption remains small for all the waves up to some 800 MeV and these two facts give us a great confidence

in our purely elastic phases in this energy region. At higher energies, marked departures appear from the purely elastic case and in particular the down solution of the S_0 wave is strongly absorbed. In fact, the behaviour of the up and down solutions is now so different that probably a little amount of information on the inelasticity in the GeV region would be enough to solve the ambiguity (the difference is dramatically exhibited by drawing an Argand diagram).

In conclusion, we can say that this experiment gives definite phase shifts in the three isospin states between 500 MeV and 800 MeV. At lower energies, we conjecture the phases by an extrapolation down to threshold of the analytic representation we get in the intermediate region. At higher energies, the inelasticity becomes rather important and our conclusions on the phase shifts are consequently more ambiguous.

REFERENCES

1) J. P. Baton, G. Laurens and J. Reignier: *Phys. Lett.*, **23** B, 419 (1967); *Nucl. Phys.*, B **3**, 349 (1967).
2) J. P. Baton, G. Laurens and J. Reignier: *Phys. Lett.*, **33** B, 525 (1970).
3) J. P. Baton: *Thesis* (1968); CEA Report R. 3543.
4) J. P. Baton and J. Reignier: *Nuovo Cimento*, **36**, 1149 (1965); E. Malamud and P. E. Schlein: *Phys. Rev. Lett.*, **19**, 1056 (1967); P. B. Johnson *et al.*: *Phys. Rev.*, **163**, 1197 (1967); J. H. Scharenguivel *et al.*: *Phys. Rev.*, **186**, 138 (1969).
5) J. L. Basdevant and J. Reignier: *Herceg Novi Lectures* (1970).
6) S. Weinberg: *Phys. Rev. Lett.*, **17**, 616 (1966).
7) J. H. Scharenguivel *et al.*: *Nucl. Phys.*, B **22**, 16 (1970).
8) G. Ascoli *et al.*: *Phys. Rev. Lett.*, **21**, 1712 (1968).
9) B. Y. Oh *et al.*: *Phys. Rev.*, D **1**, 2494 (1970).
10) W. Beusch *et al.*: *Analysis of the* $K_1^0K_1^0$ *system produced in* $\pi^-p \to K^0\overline{K}^0n$ *at* 4 *and* 6.2 GeV/c, in *Kiev Conference on High-Energy Physics* (1970).

Information on the S- and P-wave $I = {}^3/_2$ $K\pi$ phase shifts (*)

SABRE COLLABORATION

Recently the SABRE-collaboration published a paper in which results on a determination of the $I=\frac{3}{2}$ $K\pi$ elastic scattering cross section by means of the Chew-Low extrapolation method using the reaction

$$K^- + d \to p_s + p + K^- + \pi^- \qquad (1)$$

were presented (1). These data come from a 7 *ev./μ* b exposure of the 81 cm deuterium filled Saclay bubble chamber to a 3 GeV/c K^- beam. The sample of peripheral events of reaction (1), selected by the cut $\Delta^2 < 0.32$ Gev^2, in which Δ^2 is the four momentum transfer from the incoming K^-meson to the final $K^-\pi^-$ system, was subdivided in five $K^-\pi^-$ mass bands up to 1.2 GeV/c^2. In each mass region the $K^-\pi^-$ elastic scattering cross section ($\sigma_{K^-\pi^-}$) was determined and the results are given in Table I. For further details concerning these measurements we refer to ref. (1). In this communication we report on a study of the angular distributions of the outcoming K^- meson in the $K^-\pi^-$ restframe, which together with the $\sigma_{K^-\pi^-}$ values can be used to obtain information on the relevant phase shifts which contribute to the $K^-\pi^-$ scattering in this energy region.

Using the same sample of events as in ref. (1) the spherical harmonic moments $\langle Y_L^m \rangle = 1/N \sum_1^N Y_L^m(\theta_i, \varphi_i)$ of the angular distributions of the K^- meson in the $K^-\pi^-$ restframe, for each of the mass regions have been calculated. The angles θ and φ are defined in Fig. 1 and the moments are given in Fig. 2. We consider only the events for which the $K\pi$ mass is smaller than 1.2 GeV/c^2 as above this value inelastic effects may become important.

(*) Contributed paper submitted by A. M. Bakker, Zeeman-Laboratorium, Amsterdam.

$$K^- + n \rightarrow K^- + \pi^- + p$$

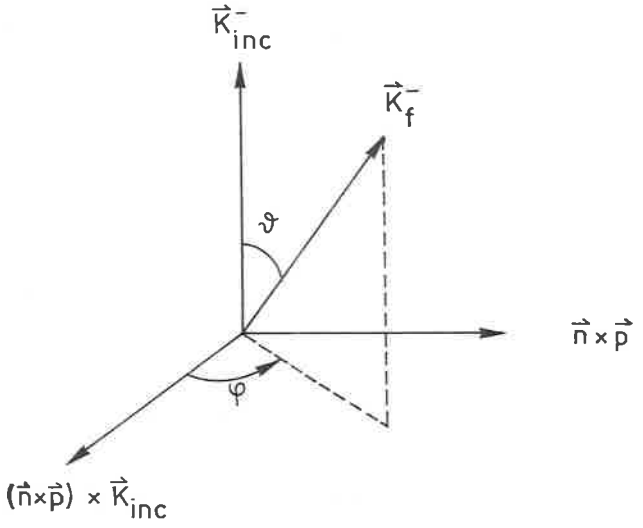

Fig. 1

Before drawing any conclusions we have to consider the following:

1) The limited statistics prohibit meaningful extrapolation of the angular distributions or the moments to the pion pole. In the following analysis we simply use the off-mass-shell moments without applying any corrections for absorption or form factors.

2) As was discussed in ref. ([1]) the $p\pi^-$ effective mass spectrum for the sample of peripheral events indicate the presence of some $\mathcal{N}^*(1236)$ production and possibly other resonances in the low $p\pi^-$ mass region. This low mass enhancement is correlated with forward K^- mesons in the $K^-\pi^-$ rest-frame. The influence of $\mathcal{N}^*$—production on the determination of the cross sections $\sigma_{K^-\pi^-}$ (see ref. ([1])) as well as on the moments was studied in some detail, using the known properties of $\mathcal{N}^*$ production from an analysis of the reaction $K^- + n \rightarrow K^0 + \mathcal{N}^{*-}(1236)$ in the same experiment ([2]). If we

assume a 20% background of $\mathcal{N}^*$ production, the contribution of this background to the moments is indicated in Fig. 2.

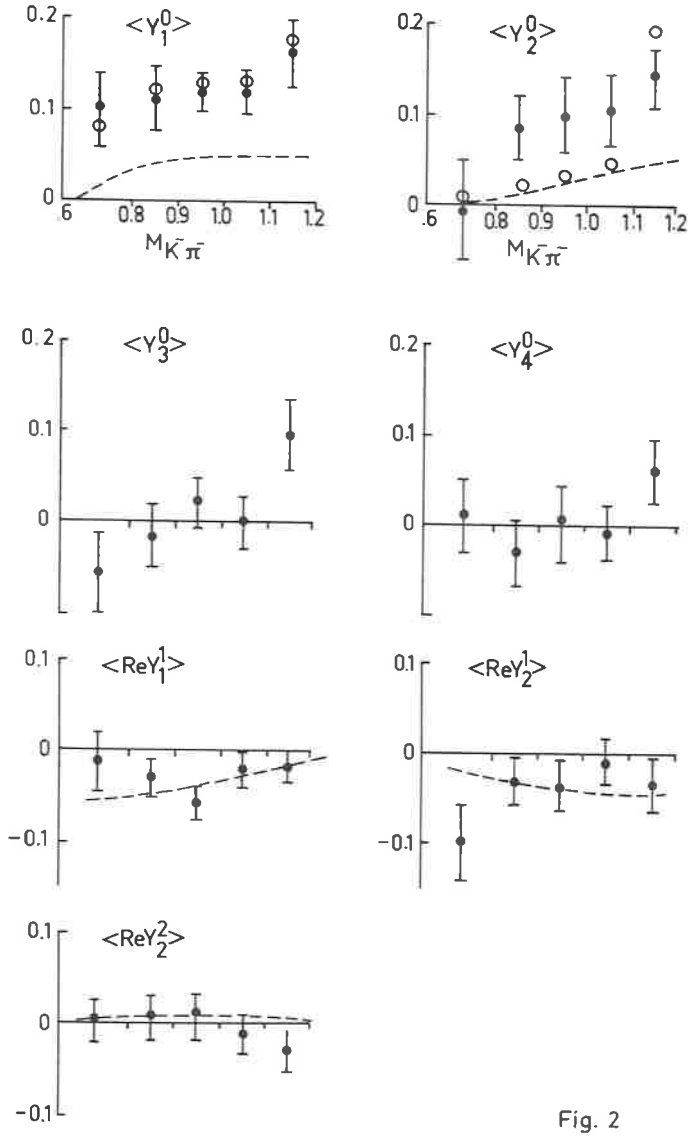

Fig. 2

Assuming that only *S*- and *P*-waves contribute in the Kπ scattering the phase shifts δ_s and δ_p were fitted to the corrected moments and cross-sections

for the five intervals of Table I, using the relations:

$$\sigma_{K^-\pi^-} = \frac{4\pi}{q^2}(\sin^2\delta_s + 3\sin^2\delta_p)$$

$$\langle Y_1^0 \rangle = \sqrt{\frac{3}{\pi}} \frac{\sin\delta_s \sin\delta_p \cos(\delta_s - \delta_p)}{\sin^2\delta_s + 3\sin^2\delta_p}$$

$$\langle Y_2^0 \rangle = \frac{6}{\sqrt{20\pi}} \frac{\sin^2\delta_p}{\sin^2\delta_s + 3\sin^2\delta_p}$$

The results of the fit are indicated in Table I. In order to see if the results were sensitive to the treatment of the background we varied the amount of background as well as some of characteristics of the $\mathcal{N}^*$-production. However the phase shifts did not change significantly. It is to be remarked that the high χ^2 is mainly due to the $\langle Y_2^0 \rangle$ moments as can be seen from Fig. 2.

Concluding we can say that the present data indicate a small δ_s and a negligible δ_p phase shift up to 1.1 GeV/c², however a satisfactory fit could not be obtained, probably due to the neglection of off-mass-shell corrections or incorrect treatment of background.

TABLE 1. – *Results* (*).

$K^-\pi^-$ mass (GeV/c²)	Number of events	$\sigma_{K^-\pi^-}$ (mb) (from ref. [1])	δ_s degrees	δ_p degrees	χ^2 ($ND=1$)
< 0.8	57	1.8±0.5	− 5.4±0.7	− 0.3±0.3	0.27
0.8÷0.9	88	1.4±0.5	− 7.9±3.2	− 0.4±0.7	5.89
0.9÷1.0	111	2.1±0.5	−12.4±5.9	− 0.7±1.9	15.43
1.0÷1.1	166	2.2±0.4	−15.6±5.6	− 0.7±2.4	15.60
1.1÷1.2	188	2.6±0.5	− 4.1±3.6	−10.8±2.9	7.54

(*) The sign of the phase shifts can not be determined with our method. The fit does not change by reversing the sign of δ_s and δ_p simultaneously. The errors in δ_s and δ_p have been multiplied by $\sqrt{\chi^2/ND}$ if $\chi^2/ND > 1$.

REFERENCES

1) A. M. BAKKER, W. HOOGLAND, J. C. KLUYVER, G. GIACOMELLI, P. LUGARESI-SERRA A. M. ROSSI, D. MERRILL, J. C. SCHEUER, G. LAMIDEY, A. ROUGÉ, A. SAPIRA and U. KARSHON: *Nucl. Phys.*, B **24**, 211 (1970).

2) G. BAKKER, W. HOOGLAND, A. G. TENNER, S. A. DE WIT, A. MINGUZZI-RANZI, P. SERRA, D. MERRILL, J. C. SCHEUER, M. LALOUM, A. ROUGÉ, G. ALEXANDER and E. HIRSCH: *Nucl. Phys.*, B **16**, 53 (1970).

On the S- and P-wave phase shifts of the $I = {}^3/_2$ $K^-\pi^-$ elastic scattering (*)

AMSTERDAM-NIJMEGEN COLLABORATION

In a previous analysis of the reaction

$$K^-p \to p\pi^+K^-\pi^- \tag{1}$$

we determined the $K^-\pi^-$ elastic cross section, using a subsample of events of reaction (1), which we classified as

$$K^-p \to \Delta^{++}(1236)K^-\pi^- \tag{2}$$

This means, that we restricted the analysis to the $p\pi^+$ effective mass region $1.14 < M(p\pi^+) < 1.36$ GeV/c². The results were reported at the Kiev Conference, 1970 ([1]). At this moment we report on a sample of 7044 events of type (1). In a further analysis of this reaction we studied the K^- angular distribution in the $K^-\pi^-$ rest system in order to obtain information on the phase shifts. We restricted the analysis to the events for which the $K^-\pi^-$ effective mass is smaller than 1.2 GeV/c², and the four momentum transfer from the initial K^- to the final $K^-\pi^-$ system smaller than 0.4 (GeV/c)². This sample of events was divided in 5 mass regions, indicated in Table I. For each mass region the spherical harmonic moments have been calculated, for the angles θ and φ of the scattering of the K^- in the Jackson frame in the $K^-\pi^-$ rest system. Some of these moments are given in Fig. 1. No extrapolation of these moments to the pion pole has been performed.

(*) Contributed paper submitted by B. Jongejans and H. Voorthuis, Zeeman-Laboratorium, Amsterdam.

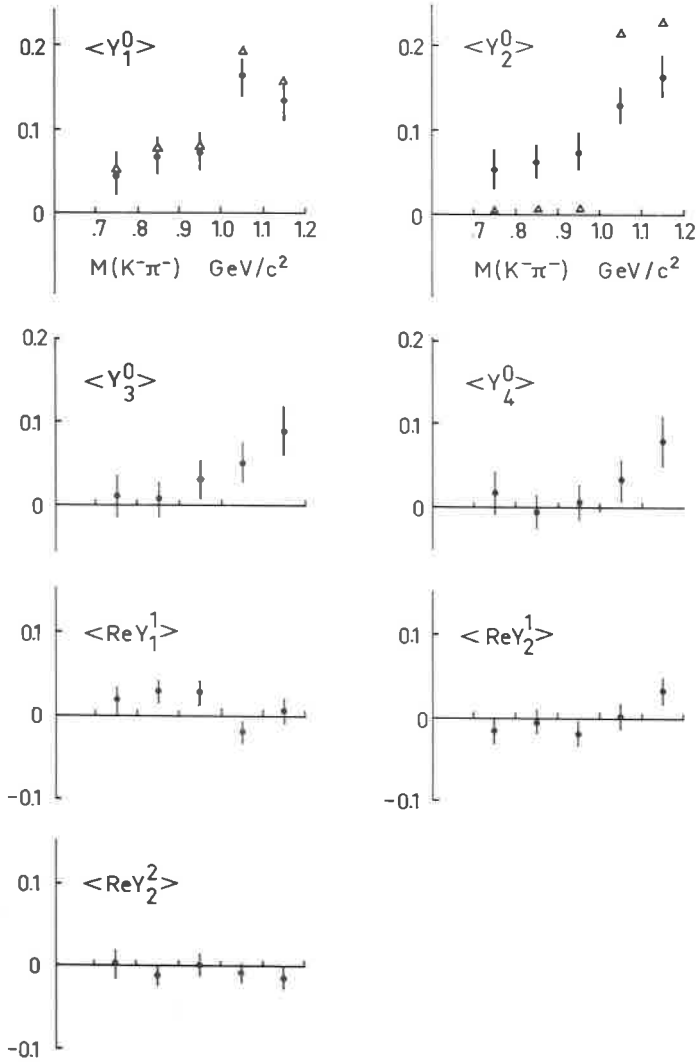

Fig. 1. – Some moments of the θ and φ angles defined in the Jackson frame at the $K^-\pi^-$ vertex for events according the reaction $K^-p \to \Delta^{++}(1236)\, K^-\pi^-$, as a function of $M(K^-\pi^-)$. These moments are averaged over the four momentum transfer $\Delta^2(K^- \to K^-\pi^-) < < 0.4$ (GeV/c)^2. The conditions are $1.14 < M(p\pi^+) < 1.36$ GeV/c^2. The calculated values of $\langle Y_1^0 \rangle$ and $\langle Y_2^0 \rangle$ using the fitted values of the phase shifts δ_0^3 and δ_1^3 are indicated with triangles.

Assuming that only *S*- and *P*-waves contribute to the $K^-\pi^-$ elastic scattering, we fitted the phase shifts δ_0^3 and δ_1^3, with the formulas:

$$\sigma_{K^-\pi^-} = \frac{4\pi}{q^2}(\sin^2\delta_0^3 + 3\sin^2\delta_1^3)$$

$$\langle Y_1^0\rangle = \sqrt{\frac{3}{\pi}}\,\frac{\sin\delta_0^3 \sin\delta_1^3 \cos(\delta_0^3 - \delta_1^3)}{\sin^2\delta_0^3 + 3\sin^2\delta_1^3}$$

$$\langle Y_2^0\rangle = \frac{6}{\sqrt{20\pi}}\,\frac{\sin^2\delta_1^3}{\sin^2\delta_0^3 + 3\sin^2\delta_1^3}$$

where q is the momentum of the final K^- meson in the $K^-\pi^-$ rest system.

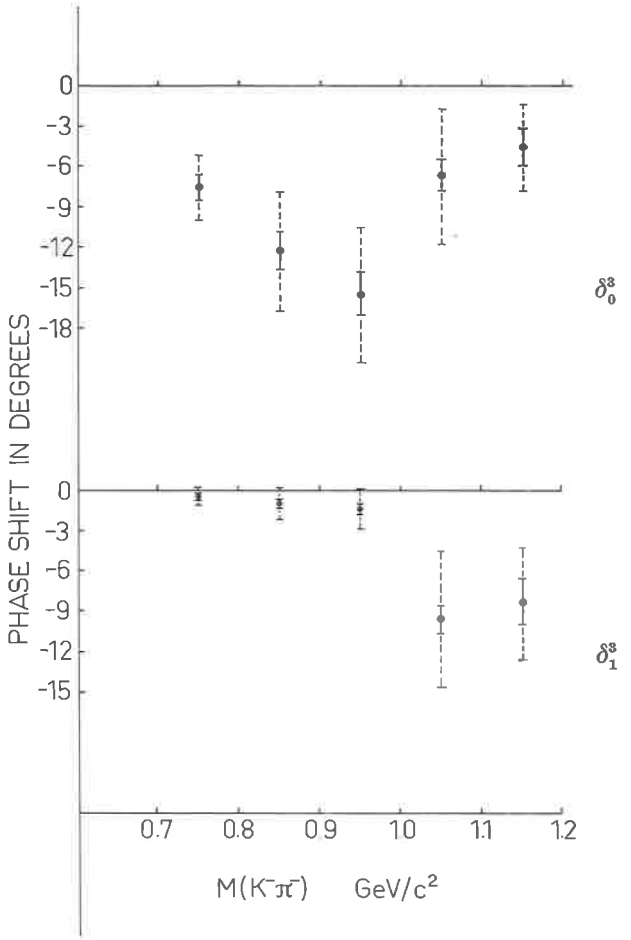

Fig. 2. – The fitted phase shifts δ_0^3 and δ_1^3 as a function of $M(K^-\pi^-)$.

The results are given in Table I and in Fig. 2, as a function of the $K^-\pi^-$ effective mass. The results of a simular analysis using the reaction $K^-d \to p_s pK^-\pi^-$ at 3 GeV/c, reported in the preceding paper (2), are roughly in agreement with our results.

The errors are the statistical ones. To have a more realistic estimate of the physical errors, these errors multiplied by $\sqrt{\chi^2/ND}$ are also shown in Fig. 2.

TABLE I. – *Summary of experimental results for the* $I = \frac{3}{2}$ $K^-\pi^-$ *elastic scattering.*

$K^-\pi^-$ mass (GeV/c²)	Number of events	$\sigma_{K^-\pi^-}$ (mb)	δ_0^3 (degrees)	δ_1^3 (degrees)	χ^2 ($ND = 1$)
0.7÷0.8	142	2.7±0.7	− 7.6±1.0	−0.4±0.2	5.71
0.8÷0.9	199	3.4±0.8	−12.3±1.5	−1.0±0.3	10.68
0.9÷1.0	184	3.3±0.7	−15.5±1.7	−1.3±0.4	14.12
1.0÷1.1	183	3.0±0.7	− 6.7±1.2	−9.5±1.1	22.06
1.1÷1.2	142	1.7±0.7	− 4.7±1.3	−8.5±1.7	5.88

The fit does not change by the simultaneous change in sign for δ_0^3 and δ_1^3

REFERENCES

1) AMSTERDAM-NIJMEGEN COLLABORATION: *Study of* $I = \frac{3}{2}$ $K^-\pi^-$ *elastic scattering in the reaction* $K^-p \to p\pi^+K^-\pi^-$ *at* 4.2 GeV/c *incident* K^- (Contribution to the *Kiev Conference*, August 1970).

2) SABRE COLLABORATION (A. M. BAKKER): *Information on the S- and P-wave phase-shifts in the* $I = \frac{3}{2}$ $K^-\pi^-$ *scattering* (Contribution to the *Bologna Conference*, April 1971).

SESSION I-B

Wednesday, 14 April 1971

δ, S*, $K\overline{K}$ threshold - All non-strange meson of mass around 1000 MeV

Chairman: H. MUIRHEAD

Secretaries: F. NAVACH
A. ROUGÈ

δ, S^*, $K\bar{K}$ threshold. All non-strange mesons of mass around 1000 MeV (*)

W. BEUSCH
CERN - Geneva

1. Introduction.

In the mass region around 1 GeV a remarkable clustering of resonances is observed: $\eta'(958)$, δ, $\pi_{\mathcal{N}}(1016)$, $\varphi(1019)$, $\eta_{0+}(1060)$ and some other bumps have been observed for which the evidence is not yet compelling. This review does not cover the φ and only one « other claim », the M(953), will be mentioned. Not all experimental data on δ and η_{0+} are consistent with each other. I shall review the evidence for the simplifying assumption that all data on δ, $\pi_{\mathcal{N}}$ and η_{0+} can be explained by the existence of an $I=1$ and an $I=0$ resonance, both having $J^P=0^+$.

2. M(953).

A BNL group ([1]) has studied the $\eta'(958)$ in a K^-p HBC exposure at 3.9 and 4.6 GeV/c. They observe a different behaviour of the η' when it is produced in the channel (1)

$$K^-p \to K^-p+\eta' \tag{1}$$

as opposed to the channel (2)

$$K^-p \to \Lambda+\eta' \tag{2}$$

where most bubble chamber data on the η' have been accumulated so far. The data from channel (1) agree with the world average ([2]) as far as the branching ratio $\Gamma(\eta'\to\pi\pi\eta)/\Gamma(\eta'\to\pi^+\pi^-\gamma)$ is concerned; the authors also con-

(*) Introductory talk

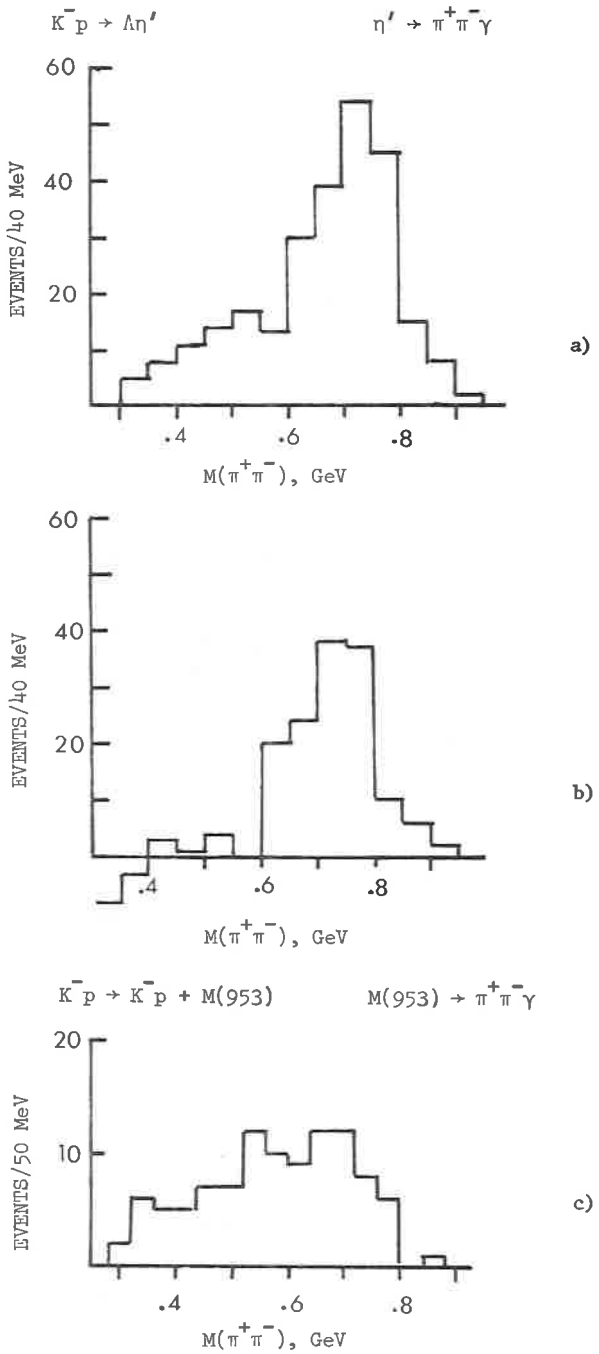

Fig. 1. – Comparison of $K^-p \to \Lambda\eta'$ (ref. (3)) and $K^-p \to K^-p + M(953)$ (ref. (1)) *a)* $\pi^+\pi^-$ mass distribution for $M(\pi^+\pi^- + \text{neutral})$ in the interval $945 \leqslant M(\pi^+\pi^-\gamma) \leqslant 975$ MeV, *b)* same histogram, but $\pi^+\pi^-\pi^0$ background subtracted. *c)* $\pi^+\pi^-$ mass distribution of $M(953) \to \pi^+\pi^-\gamma$, no $\pi^+\pi^-\pi^0$ subtraction is done, this contamination is found negligible (Ref. (1)).

clude that the mass value and width ($m = 953 \pm 2$, $\Gamma \leqslant 10$ MeV) are compatible with previous experiments on the η'. The new feature is the $\pi^+\pi^-$ invariant mass distribution in the $\pi^+\pi^-\gamma$ decay that follows phase space rather than showing an enhancement in the ρ region. In Fig. 1 this result is compared with the data of Rittenberg ([3]). I think that we have to wait for more evidence before we can conclude that there exist two resonances so nearly degenerate as the η' and the M(953).

3. δ, π_N, S*.

The δ was initially observed by the missing-mass spectrometer group at CERN ([4]) as a narrow resonance produced in $\pi^- p \to p + (MM)^-$.

TABLE 1. – *Properties of the δ as observed in different experiments.*

Mass (MeV)	Width (MeV)	Production	Reference
962 ± 5	< 5	$\pi^- p \to p + (MM)^-$	([4]) (1965)
~ 975	$\leqslant 25$	$\bar{p}p \to D^0 +$ pions, $D^0 \to \pi\delta$	([5]) (1968)
970 ± 15	$\leqslant 50$	$K^- p \to Y^*(1385)\delta$	([6]) (1969)
980 ± 10	60 ± 3	$K^- p \to \Lambda\delta$	([7]) (1969)
not seen ([a])		$K^- p \to \Lambda\delta$	([8]) (1969)
980 ± 10	40 ± 15	$\pi^+ n \to pD^0$, $D^0 \to \pi\delta$	([9]) (1969)
980 ± 10	80 ± 30	$K^- p \to Y^*(1385)\delta$	([10]) (1970)

([a]) CRENNELL *et al.* ([8]) point out that the « $\pi\eta$ » enhancement in the Λ« $\pi\eta$ » final state is spurious; it is due to η selection within the $\Lambda\varrho^-\pi^0$ final state. This remark does not apply to the other channels.

It has not been observed in $\pi^- p$ experiments since. In Table 1 some bubble chamber experiments ([5-10]) are listed that refer to a resonance decaying into $\pi\eta$ that is possibly connected with the δ(962) of the MMS ([4]). The δ production in $K^- p$ experiments is of the order of a few μb; even large bubble chamber exposures observe only 20 to 40 events. Higher statistics are available when the δ is observed as the decay product of the D^0. Mass cuts in the D^0 region and the η region and possible reflections make also these observations difficult. In view of these difficulties the agreement among bubble chamber experiments is remarkably good. The average of their values on the mass and the width of the δ are both higher than those found with the missing-mass spectrometer ([4]). More experiments on $\pi p \to \delta p$, sensitive to cross-sections $\leqslant 1$ μb, are needed to resolve this discrepancy.

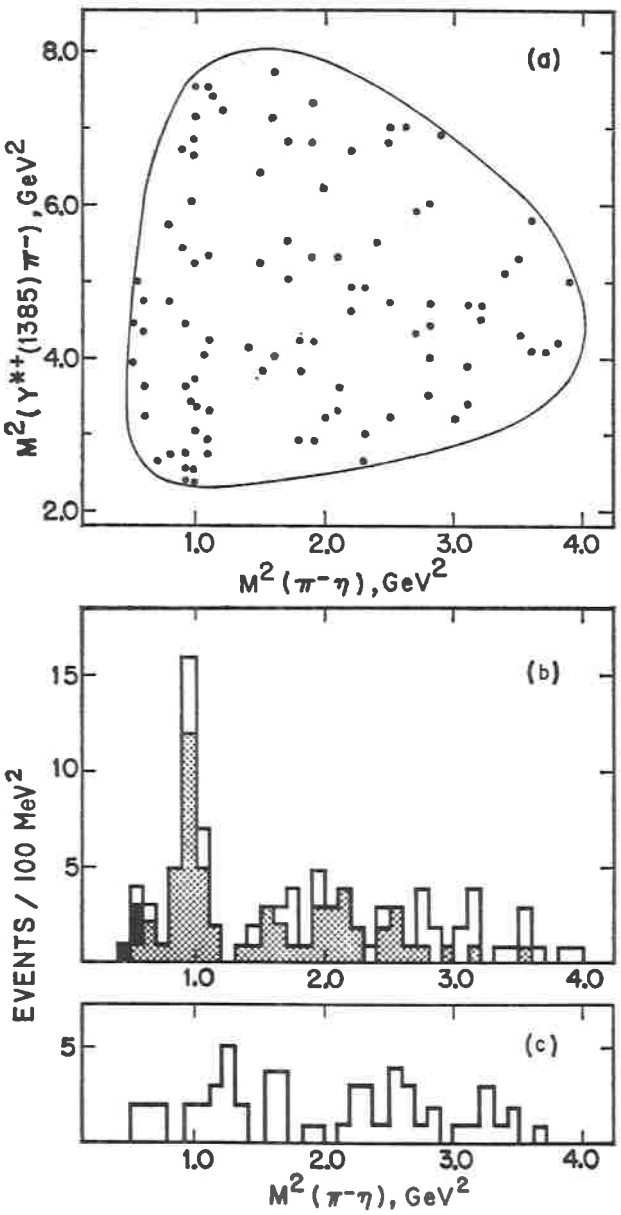

Fig. 2. – Data on $K^-p \to Y^{*+}(1385)\delta^-$ at 5.5 GeV/c (ref. [10]). *a*) Dalitz plot for $Y^{*+}(1385)\pi^-\eta$ final state, *b*) projection on $M^2(\pi^-\eta)$ axis, shaded part is $|t(K^- \to \pi^-\eta)| \leqslant \leqslant 1.5$ (GeV/c)² selection, black part is contribution from $\eta' \to \pi^+\pi^-\eta$ decays, *c*) control histogram with $m(\ll \eta \gg)$ in the mass intervals $450 < m < 500$ MeV and $600 < m < 650$ MeV.

Figure 2 shows an example ([10]) of the recently published experiments on $K^-p \to Y^*(1385)\delta$, where the δ is observed with very little background. The events are selected from the $\Lambda\pi^+\pi^- + M^0$ final state with the missing neutrals M^0 in the η region (500÷600) MeV. This final state is then fitted as $\Lambda\pi^+\pi^-\eta$.

The πη decay of the δ and the absence of the πρ decay suggest that the quantum numbers of the δ are $I^G J^P = 1^-0^+$. These are also the quantum numbers of the $l=0$, $I=1$ $K\bar{K}$ state. In this state, a narrow enhancement near threshold is observed in some experiments: the $\pi_N(1016)$. In their analysis of $\bar{p}p \to K^0_1 K^\pm \pi^\mp$ Astier *et al.* ([11]) have found a fit to this threshold effect corresponding to a virtual bound state below the $K\bar{K}$ threshold, which might be identified with the δ. The low mass and narrow width ([4]) of the δ at this time (1967) seemed to exclude this assignment. The weighted average of the bubble chamber results on $\delta \to \pi\eta$ is now $m = 975 \pm 10$ $\Gamma = 58 \pm 11$ MeV ([12]). With these parameters the assumption that the charged $K\bar{K}$ enhancement at threshold is the $K\bar{K}$ decay mode of the δ looks now like an attractive possibility.

The S* ([13]) or $\eta_{0^+}(1060)$ is observed as an enhancement in the $K^0_1 K^0_1$ system near threshold. The interpretation is still not unambiguous; it could be a resonance or a nonresonant threshold effect. Moreover, the position of the peak and its width are different in different experiments ([14]). We observe some regularities in the production of the charged $K\bar{K}$ system (and in the production of the δ) that may be related to the variation of mass and width of the S*. These regularities can be explained by the production mechanism via meson exchange. A $J^P = 0^+$ resonance with $I=1$ is not coupled to ππ (for Bose statistics) but to $K\bar{K}$. In an experiment with incident pions, δ and

TABLE 2. – *Comparison of* δ *and* π_N *production in* π^-p, K^-p *and* $\bar{p}p$.

Process	Exchange	Observation	Reference
$\pi^-p \to \delta^-p$	η	seen in MMS only	([4])
$K^-p \to \delta^- Y^{*+}$	K	seen	([6,10])
$\bar{p}p \to \delta^\pm +$ pion (*s*)	–	possibly seen ([a])	([15])
$\pi^-p \to \pi_N + p$	η	not seen	([16,17])
$K^-p \to \pi_N + Y$	K	possibly seen ([b])	([18])
$pp \to \pi_N +$ pion (*s*)	–	seen ([a])	([11])

([a]) A direct comparison of $\bar{p}p \to \pi^\pm_N \pi^\mp$ and $\bar{p}p \to \delta^\pm \pi^\mp$ is experimentally very difficult; the data are compatible with both final states being present in the expected ratio ([15]).

([b]) The detection of K^- in multipion final states is very difficult ([18]).

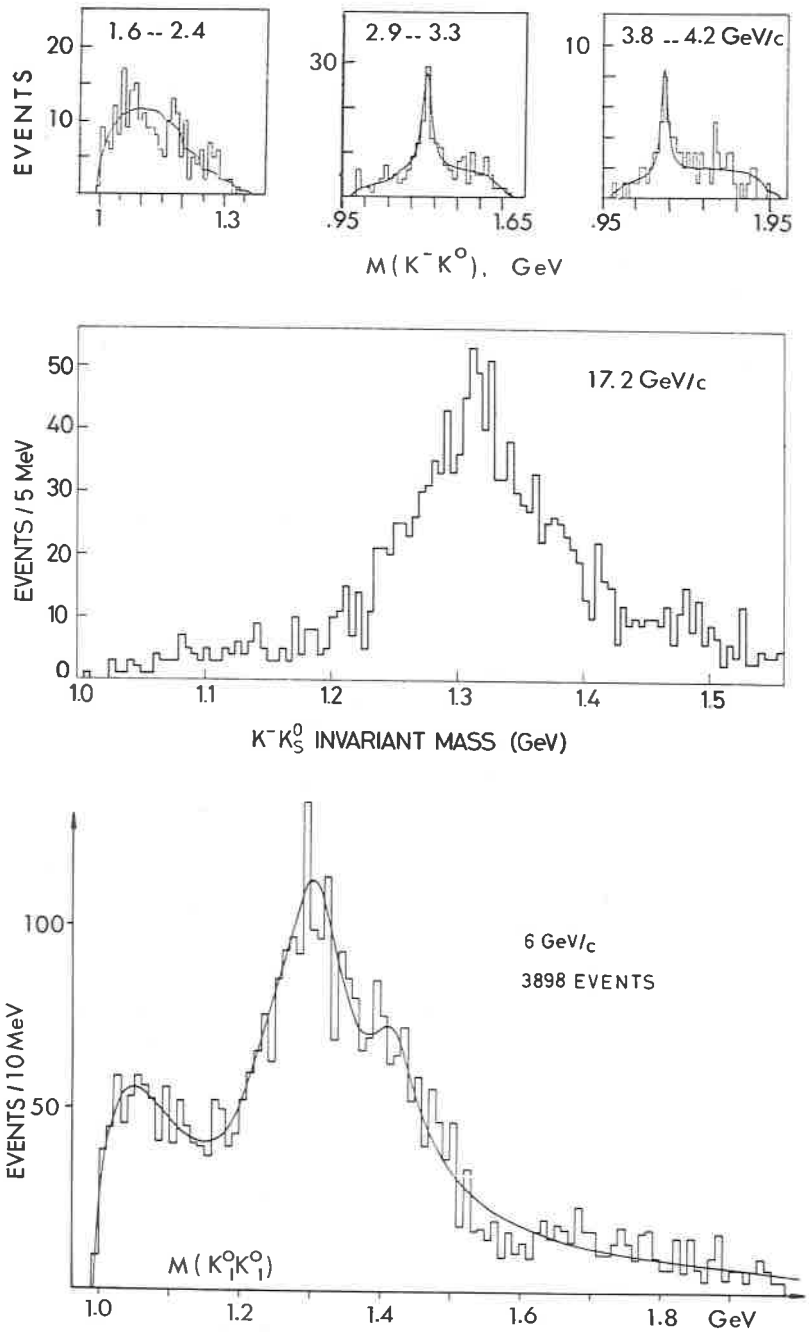

Fig. 3. – Comparison of $\pi^- p \to K^- K^0 p$ and $\pi^- p \to K_1^0 K_1^0 n$. *a*) $K^- K^0$ data at lower energies (ref. [16]). *b*) $K^- K^0$ data at 17.2 GeV/c (Ref. [17]). *c*) $K_1^0 K_1^0$ data at 6 GeV/c (Ref. [20]). Note the absence of any threshold effect in the charged $K\bar{K}$ system at beam momenta above 3 GeV/c.

$\pi_{\mathcal{N}}$ production by π-exchange is therefore forbidden (η or B exchange allowed); with incident kaons, *K*-exchange is allowed. In S* production with incident pions, π-exchange is allowed; *K*-exchange is allowed also here if the incident particles are kaons. In $\bar{p}p$ annihilations both $I=1$ and $I=0$ states can be produced. Table II shows the qualitative features of the production of charged δ and $\pi_{\mathcal{N}}$ ([15-18]).

When η-exchange is expected no $\pi_{\mathcal{N}}$ production is observed and also no δ production (if we disregard the MMS experiment ([4]) in this context).

The $K_1^0K_1^0$ system is not an eigenstate of isospin; $I=0$ and $I=1$ may be present and they may also interfere. Table III gives the qualitative features of $K_1^0K_1^0$ production ([18-20]).

In Fig. 3 $\pi^-p \to K^0K^-p$ and $\pi^-p \to K_1^0K_1^0n$ are compared. The absence of any threshold effect in the charged $K\bar{K}$ is quite striking; it is evidence for the weakness of η (or B) exchange in peripheral production. In $\pi^-p \to$ $\to K_1^0K_1^0n$ the $K\bar{K}$ system near threshold is therefore almost pure $I=0$. This is not true for $K_1^0K_1^0$ produced in $\bar{p}p$ and K^-p interactions where δ and/or $\pi_{\mathcal{N}}$ production is observed. It is quite possible that this difference is responsible for the apparent variation of masses and widths of the $K_1^0K_1^0$ enhancement near threshold as shown in Table III. Some $I=1$ component, the $\pi_{\mathcal{N}}$ (1016), can lower the peak position and sharpen it.

TABLE 3. – *Comparison of* $K_1^0K_1^0$ *production in* $\bar{p}p$, $K^-p(n)$ *and* π^-p.

Production	Meson exchange $K_1^0K_1^0$ state in		Mass (MeV)	width (MeV)	Reference
	$I=0$	$I=1$			
$\bar{p}p \to K_1^0K_1^0$ + pions	–	–	1046 ± 7	40 ± 20	19
$K^-p(n) \to K_1^0K_1^0 + Y$	K	K	1030 ± 10	45^{+35}_{-10}	18
$\pi^-p \to K_1^0K_1^0n$	π	B	~ 1060	$\geqslant 150$	20

Figure 4 shows a $K_1^0K_1^0$ mass distribution observed in $\bar{p}p$ annihilations ([19]). For a quantitative analysis one would have to know the amount of $I=1$ amplitude and its interference with $I=0$. Moreover, the $\bar{p}p$ data may also be influenced by resonances other than $K\bar{K}$ in the final states considered. The argument presented here provides therefore only a qualitative understanding of the observed effect.

The presently available experimental data are compatible with the existence of 0^+ resonances with $I=0$ and $I=1$, both decaying into $K\bar{K}$, but

they do not yet constitute a proof that the $K\overline{K}$ effects in question are decay modes of resonances. Both threshold effects may be due to nonresonant $K\overline{K}$ interactions, parametrized, for example, by a scattering length ([11-20]).

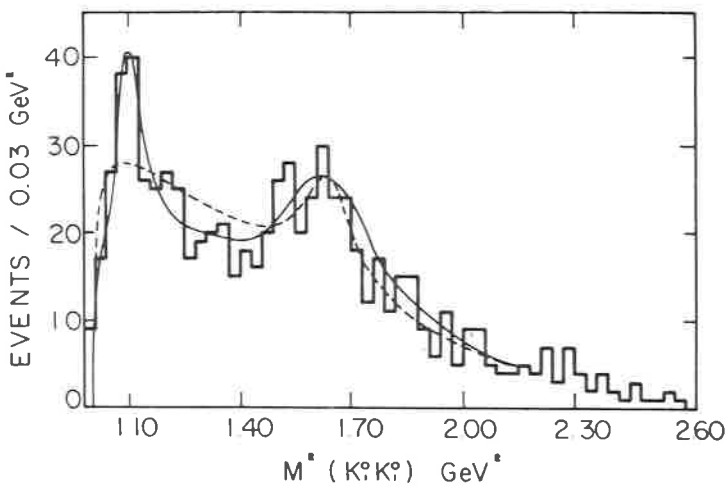

Fig. 4. – Distribution of $M^2(K_1^0K_1^0)$ produced in $\bar{p}p \to K_1^0K_1^0\pi^+\pi^-$ at 0.7 and 1.2 GeV/c (ref. ([19])). Solid line is a fit including a Breit-Wigner for the S* with $m_0 = 1044$ MeV and $\Gamma_0 = 45$ MeV.

With a complex scattering length and effective range this parametrization is flexible enough to fit the mass distribution of a resonance. For a decision, more information is needed, for example, the phase in both decay channels. One is very far from knowing this phase in the case of the δ and π_N; in the case of $S^* \to \pi\pi$ and $\to K\overline{K}$ the situation looks more hopeful.

The analysis of $\pi\pi$ scattering using an extrapolation from the physical region to the pion pole has been discussed in the previous session. No unambiguous solution for the phase shifts has yet been found in the 1 GeV $\pi\pi$ mass region, but new high statistics experiments may soon improve this situation. The same extrapolation can be performed for $\pi^-p \to K^+K^-n$ and $\pi^-p \to K_1^0K_1^0n$ (the $K_1^0K_1^0$ system has the advantage of the absence of any *p*-wave). It has been shown ([21]) that the inelastic channel $\pi\pi \to K\overline{K}$ may reach the unitary limit for *s*-waves in the S* region and that the other inelastic channel $\pi\pi \to 4\pi$ is not very important. Assuming pion exchange dominance and neglecting the 4π final state we can compare $\pi^-p \to (\pi\pi)^0n$ with $\pi^-p \to (K\overline{K})^0n$ and use the constraints of unitarity for this partial wave of

ππ scattering, as expressed in a two-channel formalism. Since the $I=0$ s-wave phase shift δ_0^0 is already large at energies lower than the S* mass and since ππ scattering may become highly inelastic above the KK̄ threshold, a ππ resonance may show up with a shape not yet observed on any other meson resonance. In an extreme case ([20]) a hole in the ππ mass distribution may appear instead of a Breit-Wigner shape. With $\delta_0^0 = 120°$ at 800 MeV ([22]),

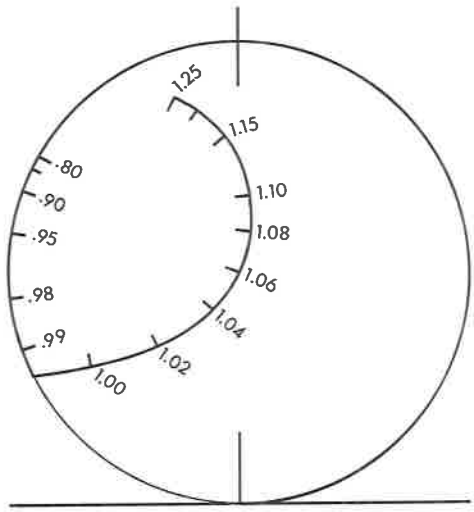

Fig. 5. – Model Argand diagram for the $I=0$ s-wave ππ scattering amplitude assuming a resonance at 1.06 GeV and a branching ratio $\Gamma_{K\bar{K}}/(\Gamma_{\pi\pi}+\Gamma_{K\bar{K}})=\frac{1}{2}$. The phase at 0.8 GeV has been chosen $\delta_0^0 = 125°$; the resonance has $m_0 = 1060$, $\Gamma_0 = 200$ MeV.

mass and width of the S* being $m_0 = 1060$ and $\Gamma_0 = 200$ MeV, respectively and with $\Gamma_{K\bar{K}}/\Gamma_{\text{total}} = \frac{1}{2}$ at m_0, we obtain the model Argand diagram of Fig. 5. The relevant element of the S-matrix is ([20])

$$S_{\pi\pi} = e^{2i\delta} \cdot \frac{m_0^2 - m^2 + i m_0(\Gamma_{\pi\pi} - \Gamma_{K\bar{K}})}{m_0^2 - m^2 - i m_0(\Gamma_{\pi\pi} + \Gamma_{K\bar{K}})},$$

where we have taken

$$\Gamma_{\pi\pi} \pm \Gamma_{K\bar{K}} = \Gamma_0 \left(\frac{1}{2} \frac{q_\pi(m)}{q_\pi(m_0)} \pm \frac{1}{2} \frac{q_K(m)}{q_K(m_0)} \right)$$

and

$$q_K(m \leqslant 2m_K) = +i|q_K(m)|\,,$$

$q_\pi(m)$ and $q_K(m)$ being the c.m.s. π and K momenta at the invariant mass m and δ being a free parameter assumed constant. The mass of $K^\pm$ and K^0 were taken equal (496 MeV) for this model. This Argand diagram is at least compatible with presently available experimental data; however, results from a phase-shift analysis based on future high statistics experiments, including also the $K\overline{K}$ channel, are needed to define the diagram more precisely.

We have seen that the $K\overline{K}$ threshold near the δ and the S* may lead to quite complicated phenomena, such that the traditional bump-hunting method in meson spectroscopy becomes insufficient. On the other hand, these complicated phenomena contain more information than does a simple bump. The presence of the $K\overline{K}$ threshold together with the constraints of unitarity may lead to a better understanding of meson-meson interactions.

REFERENCES

1) M. Aguilar-Benitez, D. Bassano, R. L. Eisner, J. B. Kinson, D. Pandoulas, N. P Samios and V. E. Barnes: *Phys. Rev. Lett.*, **25**, 1635 (1970).
2) Particle Data Group: *Phys. Lett.*, **33 B** (August 1970).
3) A. Rittenberg: *Thesis*, UCRL-18863 (1969).
4) W. Kienzle. B. C. Maglič, B. Levrat, F. Lefebvres, D. Freytag and H. R. Blieden: *Phys. Lett.*, **19**, 438 (1965).
5) C. Defoix, P. Rivet, J. Siaud, B. Conforto, M. Widgoff and F. Shively: *Phys. Lett.*, *39* B, 353 (1968).
6) V. E. Barnes, S. U. Chung, R. L. Eisner, E. Flaminio, P. Guidoni, J. B. Kinson, N. P. Samios, D. Bassano, M. Goldberg and K. Jaeger: *Phys. Rev. Lett.*, **23**, 610 (1969).
7) D. H. Miller, S. L. Kramer, D. D. Carmony, R. L. Eisner, A. F. Garfinkel, L. J. Gutay and W. L. Yen: *Phys. Lett.*, **29** B, 255 (1969).
8) D. J. Crennell, U. Karshon, K. W. Lai, J. S. O'Neall, J. M. Scarr, P. Baumel, R. M. Lea, T. G. Schumann and E. M. Urvater: *Phys. Rev. Lett.*, **22**, 1398 (1969).
9) J. H. Campbell, S. Lichtmann, D. H. Miller, R. J. Miller, W. J. Miller and R. B. Willmann: *Phys. Rev. Lett.*, **22**, 1204 (1969).
10) R. Ammar, W. Kropac, H. Yarger, R. Davis, J. Mott, B. Werner, M. Derrìck, T. Fields and F. Schweingruber: *Phys. Rev.*, **D 2**, 430 (1970).
11) A. Astier, J. Cohen-Ganouna, M. Della Negra, B. Maréchal, L. Montanet, M. Thomas, M. Baubillier and J. Duboc: *Phys. Lett.*, **25** B, 294 (1967).
12) Particle Data Group: *Particle properties tables*, April 1971.
13) D. J. Crennell, G. R. Kalbfleisch, K. W. Lai, J. M. Scarr, T. E. Schumann, I. O. Skillikorn and M. S. Webster: *Phys. Rev. Lett.*, **16**, 1025 (1966).

14) B. MAGLIČ: *Proceedings of the Lund International Conference on Elementary Particles*, Lund, June 25 - July 1, 1969, p. 308.
15) L. MONTANET: CERN, private communication.
16) O. I. DAHL, L. M. HARDY, R. I. HESS, J. KIRZ and D. H. MILLER. *Phys. Rev.*, **163**, 1377 (1967).
17) G. GAYER, B. HYAMS, C. JONES, P. SCHLEIN, W. BLUM, H. DIETL, W. KOCH, H. LIPPMANN, E. LORENZ, G. LÜTJENS, W. MÄNNER, J. MEISSBURGER, U. STIERLIN and P. WEILHAMMER: *Phys. Lett.*, **34** B, 333 (1971).
18) J. ALITTI, V. E. BARNES, D. J. CRENNELL, E. FLAMINIO, M. GOLDBERG, U. KARSHON, K. W. LAI, W. J. METZGER, J. S. O'NEALL, N. P. SAMIOS, J. M. SCARR and T. G. SCHUMANN: *Phys. Rev. Lett.*, **21**, 1705 (1968).
19) M. AGUILAR-BENITEZ, J. BARLOW, L. D. JACOBS, P. MALECKI, L. MONTANET, CH. D'ANDLAU, A. ASTIER, J. COHEN-GANOUNA, M. DELLA NEGRA and B. LÖRSTAD: *Phys. Lett.*, **29** B, 241 (1969).
20) W. BEUSCH: in *Experimental meson spectroscopy*, edited by C. BALTAY and A. H. ROSENFELD (Columbia University Press, New York and London, 1970), p. 185.
21) B. D. HYAMS, W. KOCH, E. LORENZ, G. LÜTJENS, W. OCHS, P. SCHLEIN, U. STIERLIN, P. WEILHAMMER, W. BEUSCH, W. WETZEL, D. JOHNSON, V. STENGER and H. WOHLMUT: in *Experimental meson spectroscopy*, loc. cit., p. 41.
22) $\delta_0^0 \approx 120°$ is the « up » solution as found by J. P. BATON, G. LAURENS and J. REIGNIER: *Phys. Lett.*, **33** B, 528 (1970).

Evidence of S* production in $\bar{p}p$ annihilations at (1.1 ÷ 1.2) GeV/c (*)

J. DUBOC, M. GOLDBERG, B. MAKOWSKI, A. M. TOUCHARD
Institut de Physique Nucléaire - Paris

R. A. DONALD, D. N. EDWARDS, J. GALLETLY, N. WEST
The University of Liverpool - Liverpool

The observation of the S* meson is based on the analysis of the reactions (1):

$$\bar{p}p \to K_1^0 K_1^0 \pi^+\pi^-, \qquad 1258 \text{ events}, \qquad (194 \pm 12)\ \mu b, \tag{1}$$

$$\bar{p}p \to K_1^0 K_1^0 \pi^+\pi^-\pi^0, \qquad 867 \text{ events}, \qquad (134 \pm 10)\ \mu b. \tag{2}$$

The $K_1^0 K_1^0$ effective mass spectra of these two reactions show an enhancement above 1 GeV/c² (Figs. 1 and 2). In order to take proper account of the reflexions of the different resonances produced in these reactions (K*, associated $\bar{K}^*K^*$ production, ϱ or ω, ...), maximum likelihood fits were made, with three different parametrizations for the S*:

a) A simple Breit-Wigner formula: $\dfrac{1}{(M - M_0)^2 + \Gamma^2/4}$.

b) A Jackson's formula taking into account an *s*-wave between the two K_1^0 (2):

$$\frac{M}{q} \frac{\Gamma_0(q/q_0)}{(M^2 - M_0^2)^2 + (M_0\Gamma_0(q/q_0))^2}.$$

c) A scattering length matrix element:

$$\frac{1}{1 + a^2 q^2}.$$

(*) Invited paper presented by B. Makowski

$$\bar{p}p \rightarrow K^0_1 K^0_1 \pi^+ \pi^-$$

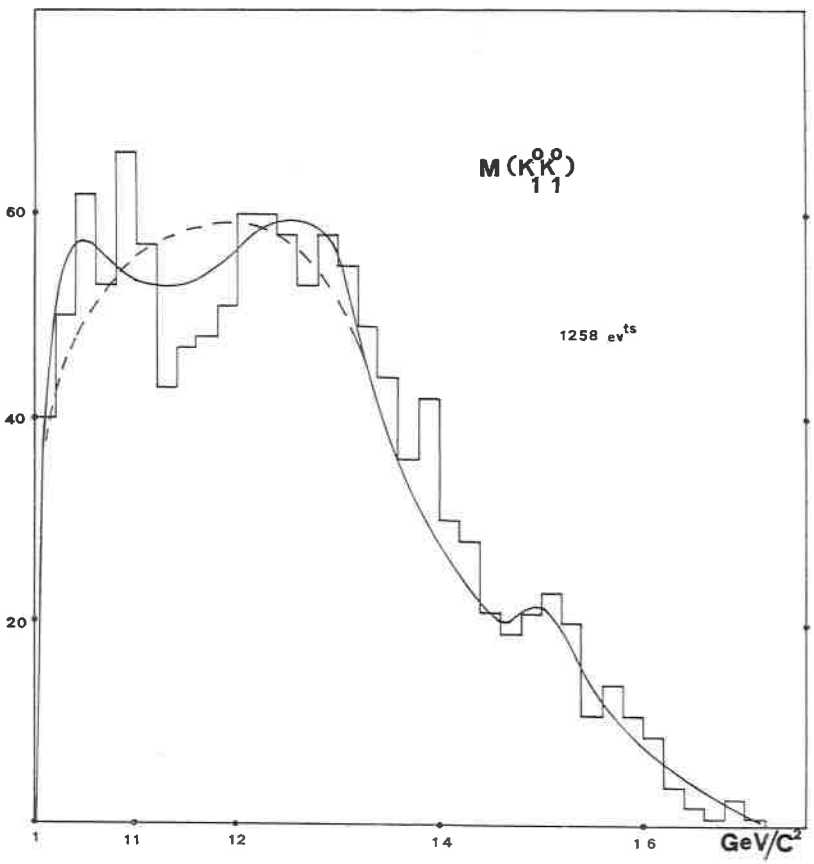

Fig. 1. – $K^0_1K^0_1$ effective mass spectrum in reaction $\bar{p}p \rightarrow K^0_1K^0_1\pi\ \pi^-$. The full curve shows the fit to the data with a Breit-Wigner formula for the S*; the dashed one represents the fit with a scattering length.

The results of these fits are given in Table I and II. These show that the resonance interpretation for this threshold effect is the best.

It will be seen that the values for the mass and width of the S* are smaller than those generally found in $\pi\mathcal{N}$ interactions. Previous annihilations ex-

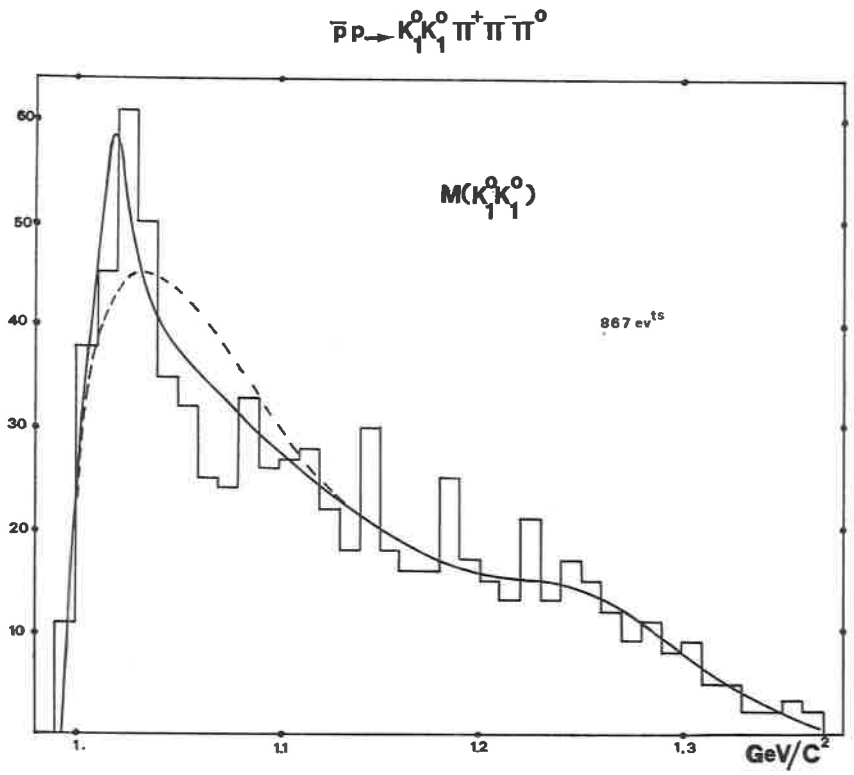

Fig. 2. – $K_1^0K_1^0$ effective mass spectrum in reaction $\bar{p}p \to K_1^0K_1^0\pi^+\pi^-\pi^0$. The full curve shows the fit to the data with a Breit-Wigner formula for the S*; the dashed one represents the fit with a scattering length.

TABLE I. – $\bar{p}p \to K_1^0K_1^0\pi^+\pi^-$.

Hypothesis	%	Mass S* or a_{SL}	Γ (MeV/c^2)	Δ (Loglik) from maximum value
a)	8.9±1.8	1028±12 MeV/c^2	67±23	0
b)	8.9±1.6	1042± 8 MeV/c^2	72±27	0
c) (*)	14.5±3	2± 0.6 fm		−2.7

(*) The introduction of a complex scattering length $A = a + ib$ does not improve the fit.

TABLE II. – $\bar{p}p \to K_1^0 K_1^0 \pi^- \pi^+ \pi^0$.

Hypothesis	%	Mass S* or a_{SL}	Γ (MeV/c²)	Δ (Loglik) from maximum value
a)	10.6±2.6	1018±4 MeV/c²	24±9	0
b)	10.4±2.5	1021±4 MeV/c²	24±9	0
c) (*)	11.5±4	5±1.8 fm		−6.6

(*) The introduction of a complex scattering length $A = a + ib$ does not improve the fit.

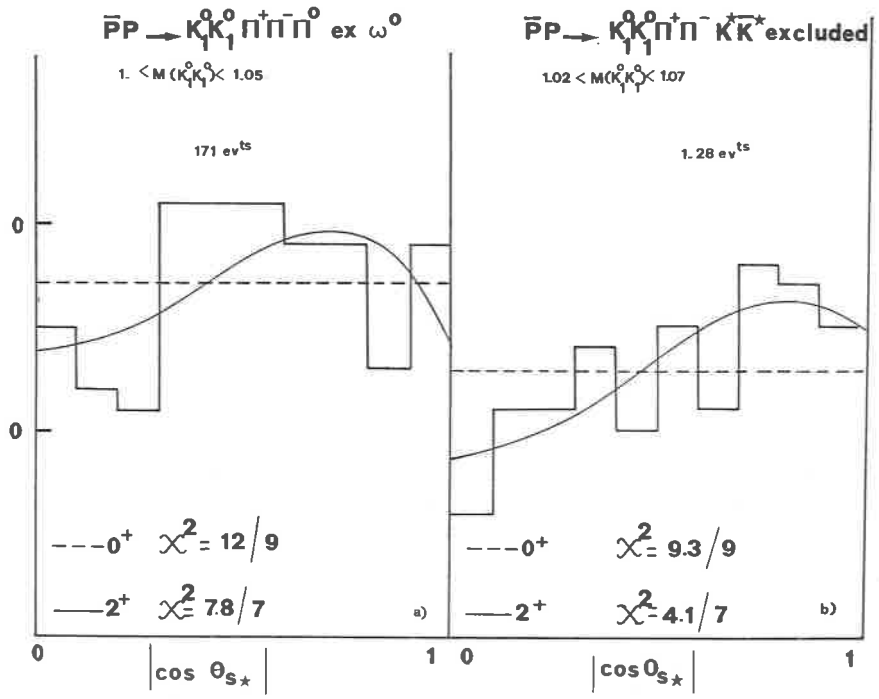

Fig. 3. – Angular distribution of the K_1^0 in the S* region. Curves correspond to a polynomial fit for 0^+ and 2^+ hypothesis in: *a*) $\bar{p}p \to K_1^0 K_1^0 \pi^+ \pi^- \pi^0$, ω^0 excluded; *b*) $\bar{p}p \to K_1^0 K_1^0 \pi^+ \pi^-$, $K^* \bar{K}^*$ excluded.

periments already exhibited this fact (4) which is particularly clearly demonstrated in reaction (2) of the present experiment.

Concerning the spin parity of the S*, originally it was thought to be a $J^P = 0^+$ resonance due to the low Q value. This has been questioned in

some papers ([3,4]) where the angular distributions in $K_1^0K_1^0$ and $\pi^+\pi^-$ were not clearly isotropic. Figure 3 shows for both reactions the distribution of $\cos\theta$ of one K_1^0 with respect to the line of flight of the S* system. There is good agreement with isotropy and no significant improvement is found by using a fourth order polynomial in the fit.

REFERENCES

1) Communication to the *Kiev International Conference of High Energy Physics* (1970); I. P. N. - Liverpool collaboration.
2) J. D. JACKSON: *Nuovo Cimento*, **34**, 1644 (1964).
3) D. H. MILLER *et al.*: *Phys. Lett.*, **28** B, 51 (1968).
4) M. AGUILAR-BENITEZ *et al.*: *Phys. Lett.*, **29** B, 241 (1969).

Observation of narrow 3π peaks in the $\delta^{\pm}$ and $A_1^{\pm}$ region in $\bar{p}p$ annihilations at 5.7 Gev/c (*)

H. W. ATHERTON, B. J. FRANEK, B. R. FRENCH, B. GHIDINI
J. B. KINSON, L. MANDELLI, J. MOEBES, K. MYKLEBOST, B. NELLEN
E. QUERCIGH and V. SIMAK
CERN - Geneva

We report on an analysis of the three charged pion system observed in the annihilation reactions

$\bar{p}p \to K_1^0 K^{\pm}\pi^{\mp}\pi^+\pi^-\pi^0$	1166	events	$(230 \pm 15)\ \mu b$
$\to K_1^0 K_1^0 \pi^+\pi^+\pi^-\pi^-\pi^0$	290	»	$(76 \pm 7)\ \mu b$
$\to K_1^0 K_2^0 \pi^+\pi^+\pi^-\pi^-$	492	»	$(80 \pm 6)\ \mu b$
tot.	1948	»	

at 5.7 GeV/c.

From an analysis of $\sim 200\,000$ pictures of the $2m$ HBC exposed to a $\bar{p}$ beam of 5.7 GeV/c momentum at CERN PS, corresponding to 13 events/μb, we obtained about 12000 events of the type $\bar{p}p \to \bar{K}Km\pi$ ($m \geqslant 1$). All events were required to have at least one K^0 recognised by its charged decay.

The analysis described here was performed using the 1948 events of the three reactions above. Looking at the singly charged (3π) mass spectra for each of the three reactions, we observed that they had similar characteristics: we therefore combined them and treated them together. The resulting distribution is shown in Fig. 1.

One can see two peaks, one around 960 MeV, namely at the position of the δ meson, the other at about 1070 MeV, namely at the A_1 position: their statistical significance is about 4 and 3 st. dev. respectively. Fitting the total distribution with two non relativistic Breit-Wigner's and statistical phase

(*) Invited paper presented by B. Ghidini

space and folding in the experimental resolution (±10 MeV) we obtain the following parameters:

	M (MeV)	Γ (MeV)	Intensity (events)	Cross section (μb)
« δ »	956±7	46±22	180±47	36±9
« A_1 »	1076±5	35^{+20}_{-15}	110±36	22±7

($P(\chi^2) = 40\%$ on total spectrum, 70% in the region (800÷1400) MeV)

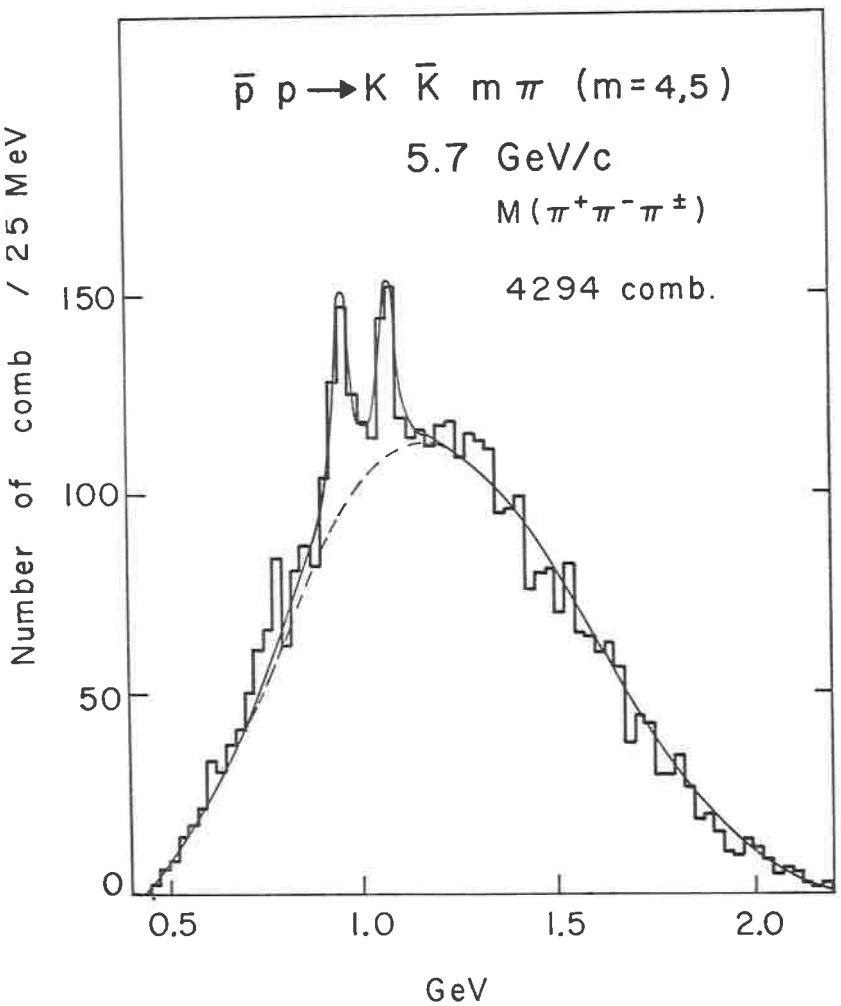

Fig. 1.

The first peak might, at first sight, be identified with the so-called δ meson, but one has to observe that up to now contradictory evidence has been found of a 3π decay of δ: most of the experiments, in which a resonance is observed in this region, show a dominant ηπ decay. Whether the peak observed here represents an alternative decay mode of δ or is a different object will be discussed below in connection with the spin-parity analysis.

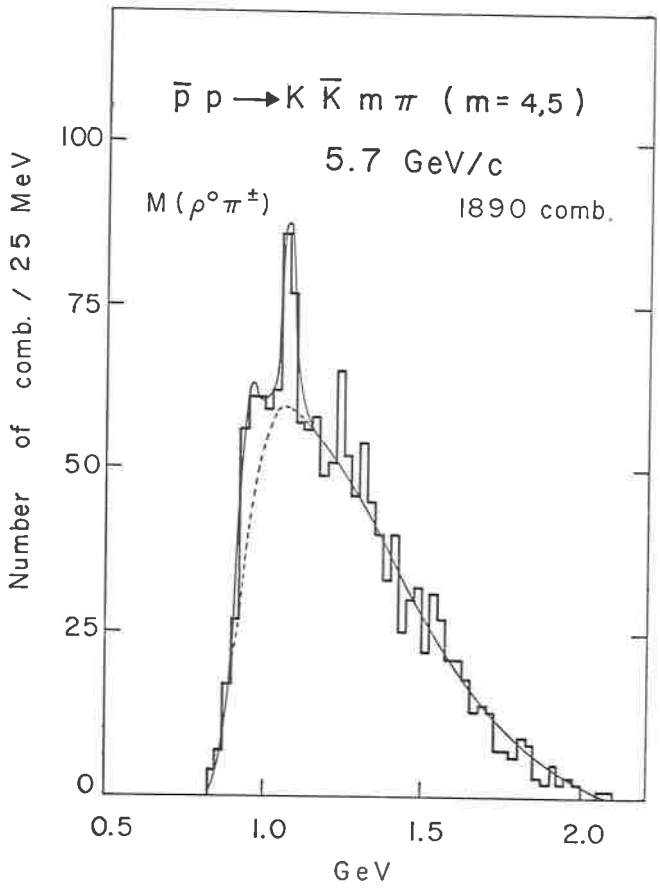

Fig. 2. – $\bar{p}p \to \bar{K}Km\pi$ ($m = 4,5$), 5.7 GeV/c, 1890 comb.

As for the second peak, it seems most natural to identify it with the A_1: the first thing to look at is whether it has a ρπ structure or not. Figure 2 shows the $\rho^0\pi^{\pm}$ mass distribution (ρ definition: (675 ÷ 825) MeV): the A_1

signal is still present and its intensity, as given by the fit, after corrections for ρ tails, is equal, within errors, to the intensity obtained from the total spectrum.

Two more remarks can be made on the « A_1 » peak:

1) the above reactions in which « A_1 » production is observed are of a non-diffractive type;

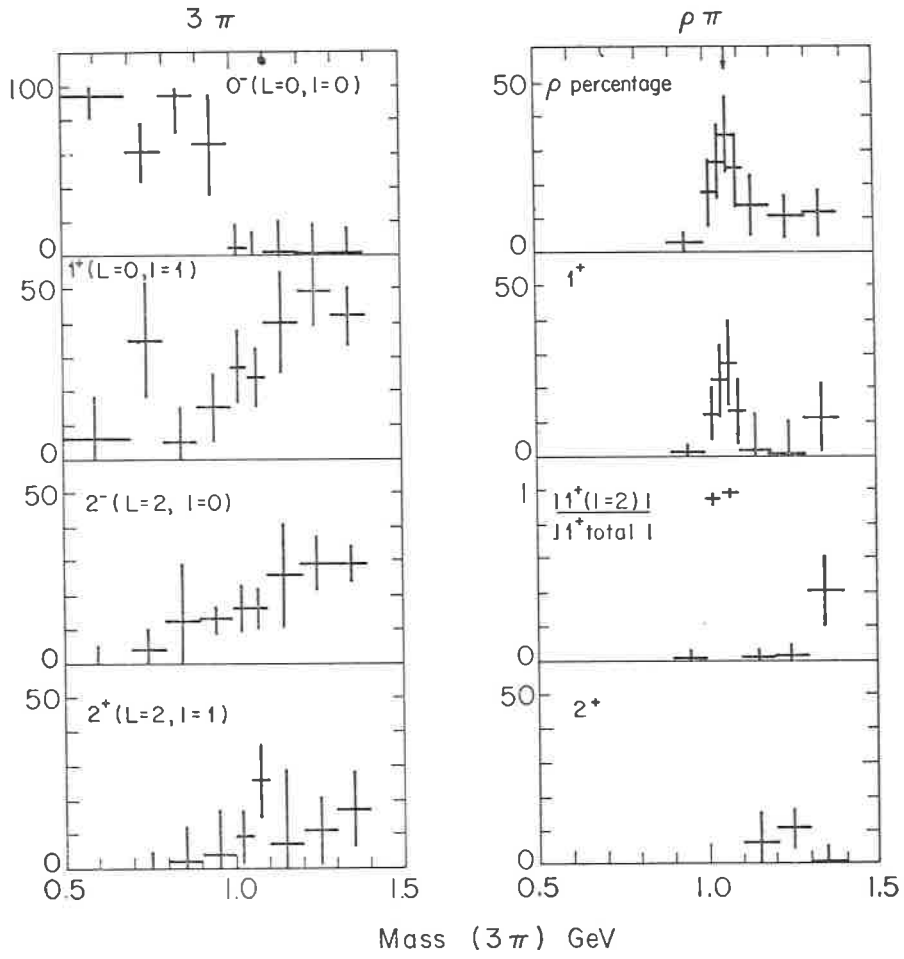

Fig. 3. – $\bar{p}p \to \bar{K}Km\pi\pi$ ($m = 4,5$), 5.7 GeV/c, fractions of some J^P amplitudes *vs.* $M(\pi^{\pm}\pi^{+}\pi^{-})$.

2) it has a narrow width, in contrast to the wide bump usually observed in diffractive production reactions *viz.* $\pi p \to A_1 p$.

As a next step, we tried to perform a spin-parity analysis of both peaks.

Using the Zemach amplitudes for various J^P states up to 2 for both 3π and $\rho\pi$, we built up a matrix element of the type:

$$M^2 = \alpha|\sum A_{\rho\pi}|^2 + (1-\alpha)|\sum A_{3\pi}|^2 ,$$

where α is the fraction of $\rho\pi$ events and $A_{\rho\pi}$, $A_{3\pi}$ represent the different amplitudes for $\rho\pi$ and 3π states respectively.

With this matrix element a maximum likelihood fit was performed on the entire 3π Dalitz-plot for various bands of $M(3\pi)$: in this way, if some amplitude has any particular behaviour, one can hope to pick it up. The results of the fit are displayed on Fig. 3: as some of the J^P come out from the fit to be everywhere negligibly small, these are not plotted here.

Firstly we observe that the ρ fraction (free parameter in the fit) has a maximum in the A_1 region and it drops to smaller values outside; secondly, most of the ρ percentage comes from the 1^+ state which also has a definite and narrow peak in the A_1 region, (the fit was repeated in overlapping regions in order to determine the shape). No such structure is visible in the 3π amplitudes, neither in the δ nor in the A_1 region. Thus, we are unable to draw any definite conclusion about the J^P of the 960 peak. The only thing we can say is that is seems improbable the 3π peaks is the same object as the $\eta\pi$ observed in other experiments: in fact the spin-parity of an $\eta\pi$ resonance belongs to the series 0^+, 1^-, 2^+ while for a 3π resonance 0^+ is forbidden and in our case 1^- and 2^+ are not favoured by the fit: 2^+ is quite small and 1^- has not even been plotted because its fraction is much smaller than 1% in all explored range. So we are left with the series 0^-, 1^+, 2^- but none of them clearly dominates over the others. In conclusion, if this result is confirmed, we will have in the δ region at least two objects of $I \geqslant 1$ and $G = -1$ but with different spin-parity.

Coming again to the A_1; having seen that the $1^+(\rho\pi)$ has a structure in this region we can ask how much the different partial waves (*s* and *d*) contribute to the 1^+ state. The third graph from the top on the right hand side of Fig. 3 shows the fraction of 1^+ (*d*-wave) over the total 1^+; it is nearly 1 in the A_1, indicating dominance of the *d*-wave.

To be a bit more quantitative, starting from the above percentage we calculated the number of events corresponding to each spin state; the cor-

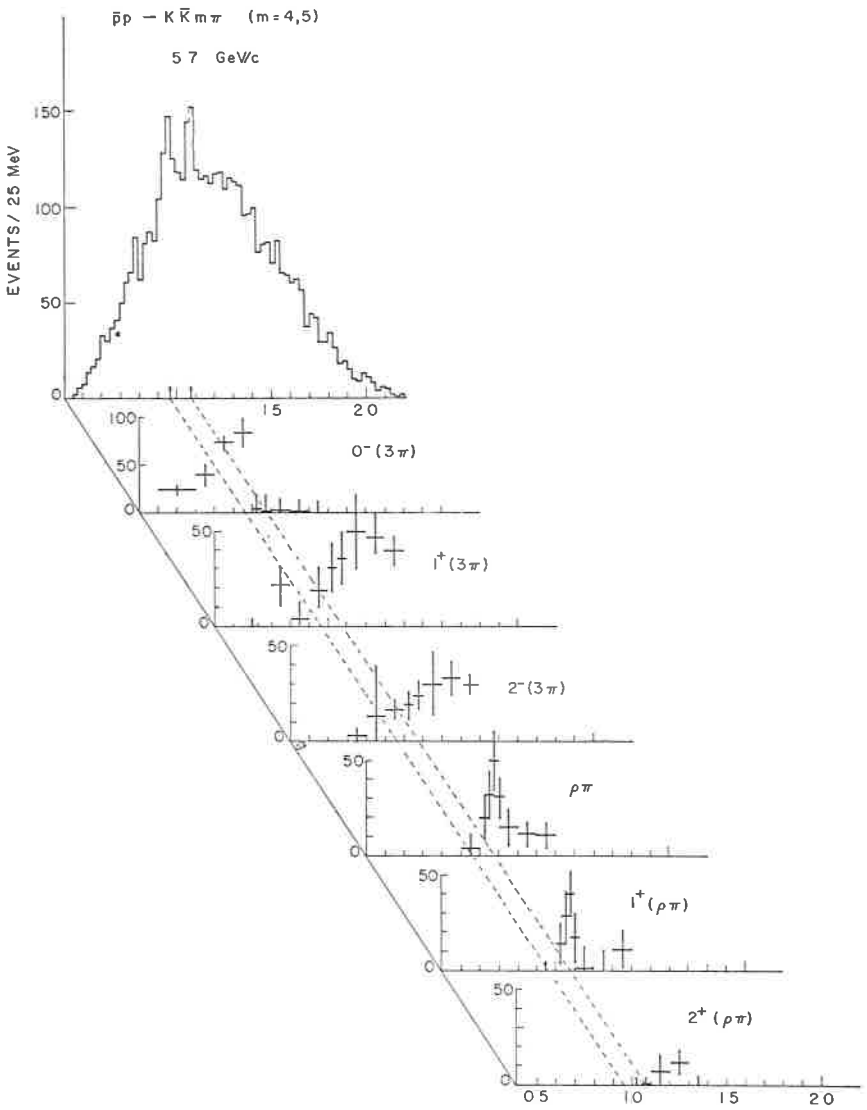

Fig. 4. – $\bar{p}p \to \bar{K}Km\pi$ ($m = 4,5$), 5.7 GeV/c. 3π mass distribution for various spin-parity states

responding mass spectra, together with the total one, are displayed in Fig. 4. From the peaks in the $\rho\pi$ and the $1^+(\rho\pi)$ distributions in the A_1 region one can estimate respectively

$$\rho\pi \text{ (total)} = (114 \pm 34) \text{ events},$$

$$1^+(\rho\pi) \quad = (108 \pm 33) \text{ events}.$$

These numbers have to be compared to the total A_1 intensity found on the total 3π mass spectrum, namely

$$A_1(3\pi) \quad = 110 \pm 36$$

In conclusion, we find three essentially independent observations which, taken together, favour the existence in our data of a narrow « A_1 » resonance of spin and parity 1^+ decaying essentially into $\rho\pi$ with *d*-wave relative orbital angular momentum.

Evidence for the δ meson in decays of the D and E mesons (*)

C. DEFOIX, A. DO NASCIMENTO, J. S. O'NEALL and J. SIAUD
College de France - Paris

R. R. BIZZARRI, L. DOBRZYNSKI, S. N. GANGULI, L. MONTANET
S. REUCROFT and T. YAMAGATA
CERN - Geneva

1. Introduction.

This paper concerns recent results from a study of η^0 production in the reaction $\bar{p}p \to 3\pi^+3\pi^-\pi^0$ at 700 MeV/c. A total of 8600 such events were found in photos taken of the Saclay 81-cm HBC. More details of the fitting can be found in ref. 1.

2. Existence of $\bar{p}p \to \eta^0 4\pi$.

The distribution of the $\pi^+\pi^-\pi^0$-mass combinations is presented in Fig. 1*a*. The dominant feature of the reaction is the production of ω^0 ($\sim 68\%$). However, a selection can be made on the square of the decay matrix element of the ω^0, $\lambda = \frac{4}{3}(|p_+ \times p_-|^2)/(M^2/9 - m_\pi^2)^2$, for all events with a $\pi^+\pi^-\pi^0$-mass combination in the ω^0 region, so as to reduce the number of background events in the η^0 region which are due to ω^0 production. The result of such a selection, $\lambda < 0.5$, is shown in Fig. 2*a*. There is a clear (5—6) s.d. peak at the mass of the η^0. There is evidence of X^0 production in the $\eta^0\pi^+\pi^-$ spectrum (not shown), but such production ($\sim 1\%$) is insufficient to account for all the η^0 produced ($\sim 4\%$). This is shown by Fig. 2*b*, in which the number of η^0 is plotted as a function of T^0/Q for events with no X^0 signal, T^0 being the π^0 kinetic energy in the η^0 system, and Q the Q-value of the decay. The

(*) Invited paper presented by C. Defoix

decay matrix element of the η^0 is proportional to $1 + \alpha\ (T^0/Q - 1)$, with $\alpha = -0.540 \pm 0.017$ ([2]). The curves on Fig. 2*b* show the expected distributions for 200 and 220 η^0 outside the X^0, respectively. The experimental points,

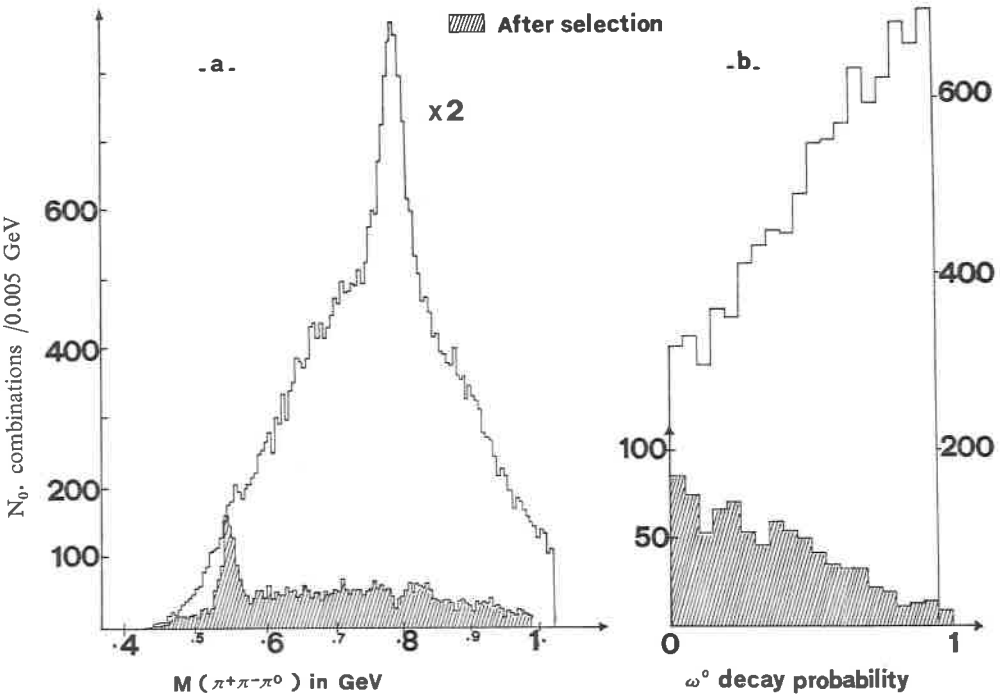

Fig. 1. – *a)* Distribution of $\pi^+\pi^-\pi^0$-mass combinations. Shaded portion is after selections described in text to eliminate ω^0. *b)* Distribution of λ, decay matrix element of ω^0, for $\pi^+\pi^-\pi^0$ combinations in ω^0 mass region. Shaded portion is after selections against ω^0.

derived from the data by fitting a gaussian form plus a polynominal background, are in good agreement with the curves, demonstrating clearly the existence of η^0 which are not associated with the X^0.

3. Separation of states $\eta^0 4\pi$ and $\omega^0 4\pi$.

In order to study further the $\eta^0 4\pi$ events outside the X^0, it is necessary to make selections in order to minimize reflections resulting from the channel $\omega^0 4\pi$. For this purpose, each event is assigned two numbers, these being

estimators that the event is an example of $\eta^0 4\pi$ or $\omega^0 4\pi$. The estimators are functions of the $\pi^+\pi^-\pi^0$ mass and the decay matrix element for the particle in question ([3]). A series of selections based on these estimators has been

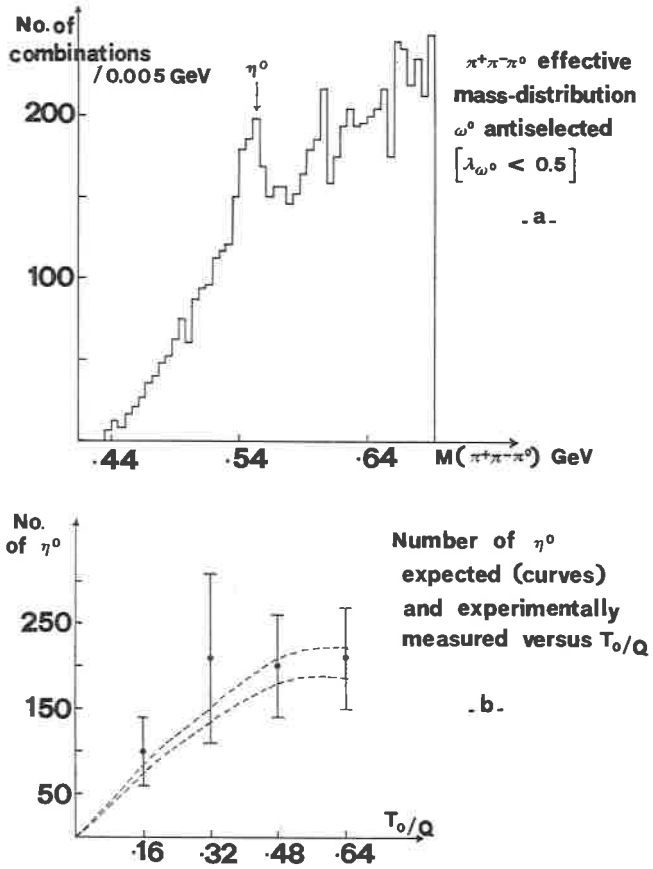

Fig. 2. – *a*) Distribution of $\pi^+\pi^-\pi^0$-mass combinations in η^0 region after elimination of events with $\pi^+\pi^-\pi^0$-mass combinations in ω^0 region and $\lambda > 0.5$. *b*) Number of η^0 as a function of T_0/Q for events with no X^0 signal. Theoretical curves explained in text.

studied, the goal having been to minimize the number of ω^0 while retaining the maximum number of η^0. An essential criterion was that the peak of the ω^0 should disappear from the $\pi^+\pi^-\pi^0$-mass distribution ([4]). A particular selection has been chosen, and the $\pi^+\pi^-\pi^0$ combinations for events retained after the selection are shown shaded on Fig. 1*a*: The ω^0 signal is effectively depressed. Fig. 1*b* contains the distribution of the decay probability, λ, of

$\pi^+\pi^-\pi^0$ combinations in the ω^0 region, with the retained events shaded. The distribution before selection agrees with theory; that after selection is completely different and agrees with the results of Monte-Carlo studies, giving further evidence for the suppression of ω^0.

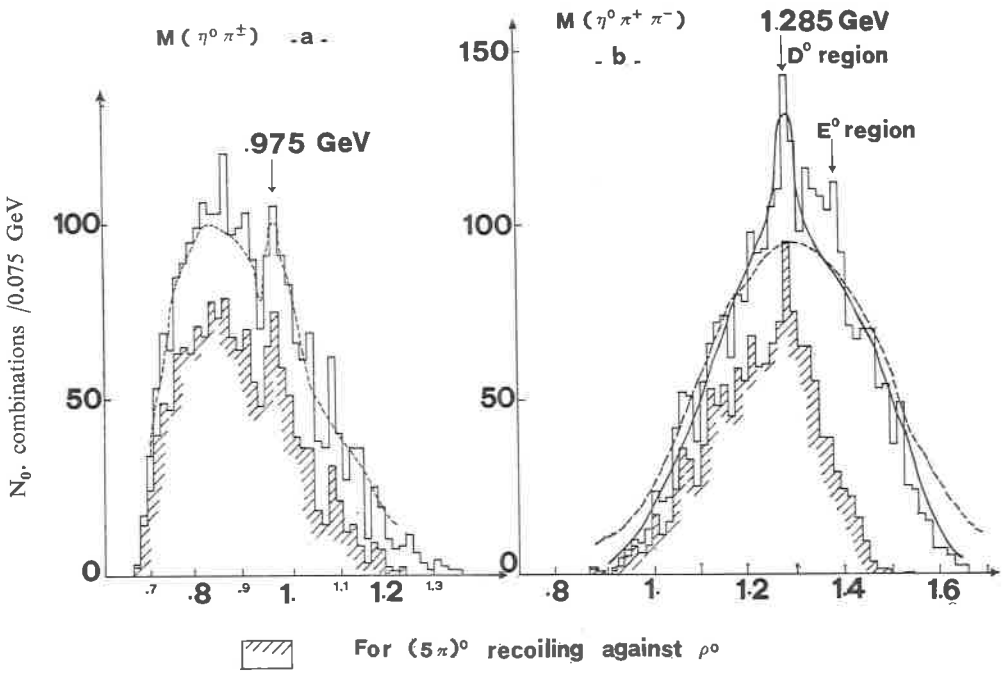

Fig. 3. – Distributions of $\pi^+\pi^-\pi^0\pi^\pm$ (*a*) and $\pi^+\pi^-\pi^0\pi^+\pi^-$ (*b*) masses for retained events having at least one $\pi^+\pi^-\pi^0$ combination in η^0 region ((548 ± 20) MeV). Shaded events are for $\eta^0\pi^+\pi^-$ recoiling against a ρ^0 ($M(\pi^+\pi^-) > 550$ MeV). Curves explained in text.

4. Evidence for $\delta\pi$ decay of D^0 and E^0.

The resulting $(4\pi)^\pm$ and $(5\pi)^0$ masses with at least one $\pi^+\pi^-\pi^0$ combination in the η^0 region ((548 ± 20) MeV) are shown in Figs. 3*a* and 3*b*, respectively. There is a narrow, (5—6) s.d. peak in the $\eta^0\pi^\pm$-mass distribution at 975 MeV. Since the peak cannot be explained as a reflection of the ω^0, it is assumed to be the $\delta^\pm$ meson. The $\eta^0\pi^+\pi^-$ distribution shows two peaks, one at 1285 MeV with a width of ~ 40 MeV, one at about 1400 MeV; these peaks are at such masses as to possibly be the D^0 and E^0 mesons, respectively. The shaded regions

in Fig. 3 are for $\eta^0\pi^+\pi^-$ combinations which recoil against a ρ^0 ($M(\pi^+\pi^-) > > 550$ MeV), indicating the production of $\delta^\pm\pi^\mp\rho^0$ and $D^0\rho^0$ final states.

In order to investigate the correlation between the $\delta^\pm$ and the D^0 mesons, Fig. 4*a* shows the distribution $\eta^0\pi^\pm$ from D^0, *i.e.*, of $(4\pi)^\pm$ mass combinations

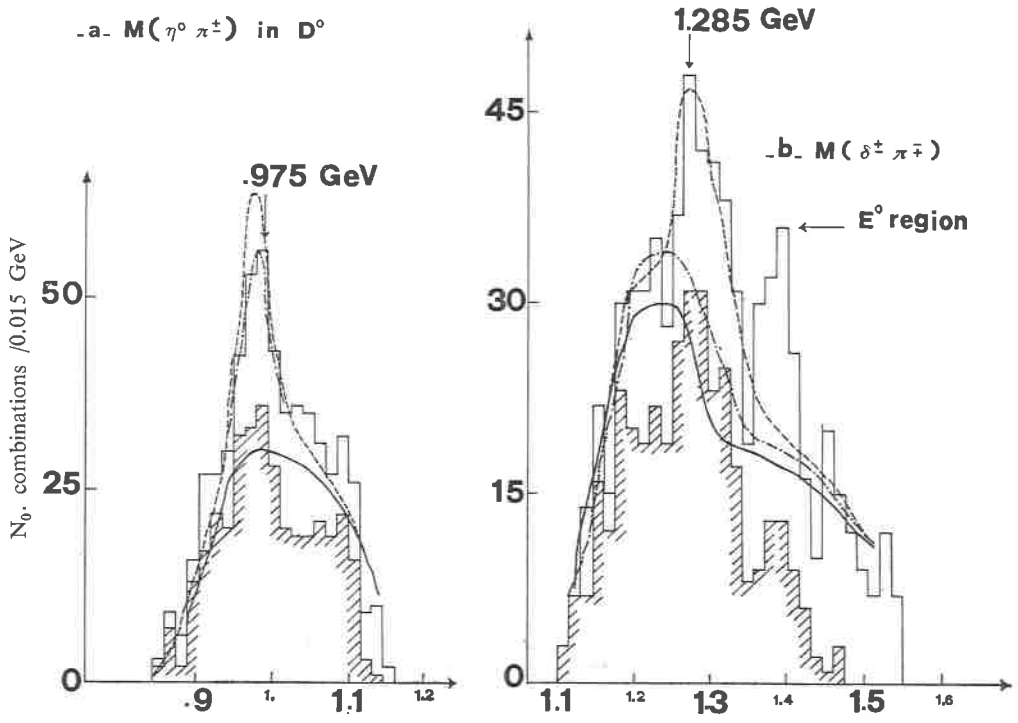

Fig. 4. – *a*) Distribution of $\pi^+\pi^-\pi^0\pi^\pm$ masses associated with $\pi^+\pi^-\pi^0\pi^+\pi^-$ combinations in the D^0 region ((1285 ± 30) MeV) and with at least one $\pi^+\pi^-\pi^0$ combination in the η^0. Shaded events as in Fig. 3. *b*) Distribution of $(5\pi)^0$ masses having at least one $(4\pi)^\pm$ combination in the $\delta^\pm$ region ((975 ± 25) MeV), for which at least one $(3\pi)^0$ combination is in the η^0 region. Shaded events as in Fig. 3.

associated with $(5\pi)^0$ combinations in the D^0 region ((1285 ± 30) MeV) and at least one $(3\pi)^0$ in the η^0. The signal-to-noise ratio for the $\delta^\pm$ is visibly enhanced by this selection. Furthermore, the $\delta^\pm\pi^\mp$ ($M(\delta) = (975\pm25)$ MeV) combinations, shown in Fig. 4*b*, show enhancements at the D^0 and E^0 positions. Their significance is increased over Fig. 3*b*, being (6—7) s.d. for the D^0 and

5 s.d. for the E^0. Finally, Fig. 5 shows the distribution of $(4\pi)^{\pm}$ as in Fig. 4*a*, but associated with the E^0 region ((1360—1410) MeV), again indicating a signal compatible with the $\delta^{\pm}$ effect. As in Fig. 3, the shaded events in Figs. 4 are for $(5\pi)^0$ combinations recoiling against a ρ^0.

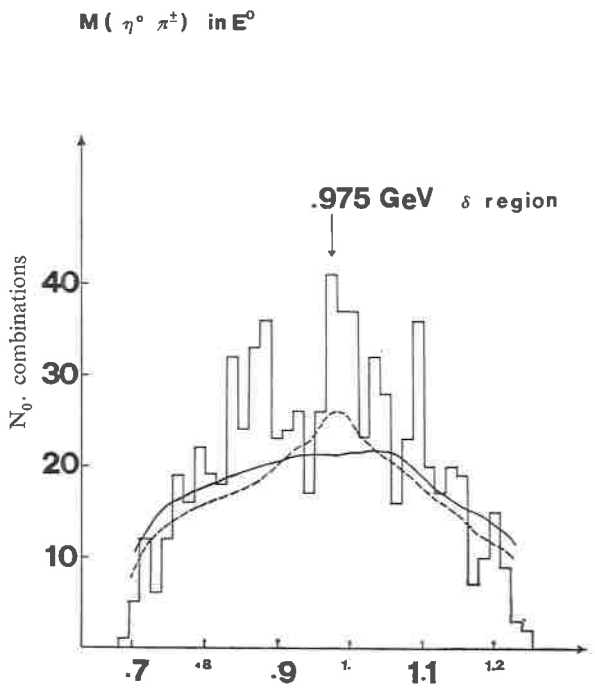

Fig. 5. – Distribution of $\pi^+\pi^-\pi^0\pi^{\pm}$ masses associated with $\pi^+\pi^-\pi^0\pi^+\pi^-$ combinations in the E^0 region ((1360÷1410) MeV) and with at least one $\pi^+\pi^-\pi^0$ in the η^0. Shaded events as in Fig. 3. Curves explained in text.

In order to understand Figs. 3-5, curves have been generated by means of Monte-Carlo events on which the same cuts have been applied as on the data. A background, including ω^0 production, is generated according to previous studies of the $\omega^0 4\pi$ state ([5]). Background plus $\eta^0 4\pi$ are unable to account for the 1285 MeV peak in the $\eta^0\pi^+\pi^-$ distribution of Fig. 3*b* (dashed curve). Background plus 3 %D^0 (solid curve) fit this bump well and also show that the bump at $\sim$ 1400 MeV, the E^0, is not a reflection of the D^0. However, in order to understand the distribution of $\eta^0\pi^{\pm}$ in the D^0, Fig. 4*a*, it is necessary to include $D^0 \to \delta\pi$ (middle curve). This hypothesis fits well most of the

$\delta^{\pm}\pi^{\mp}$ distribution of Fig. 4*b* (top curve), but not in the E^0 region. Neither does it fit well the distribution of $\eta^0\pi^{\pm}$ in the E^0 region, as evidenced by the upper curve of Fig. 5. So it is necessary also to introduce E^0 decaying into $\delta\pi$, which then fits well the $\eta^0\pi^{\pm}$ distribution of Fig. 3*a*. Due to large errors

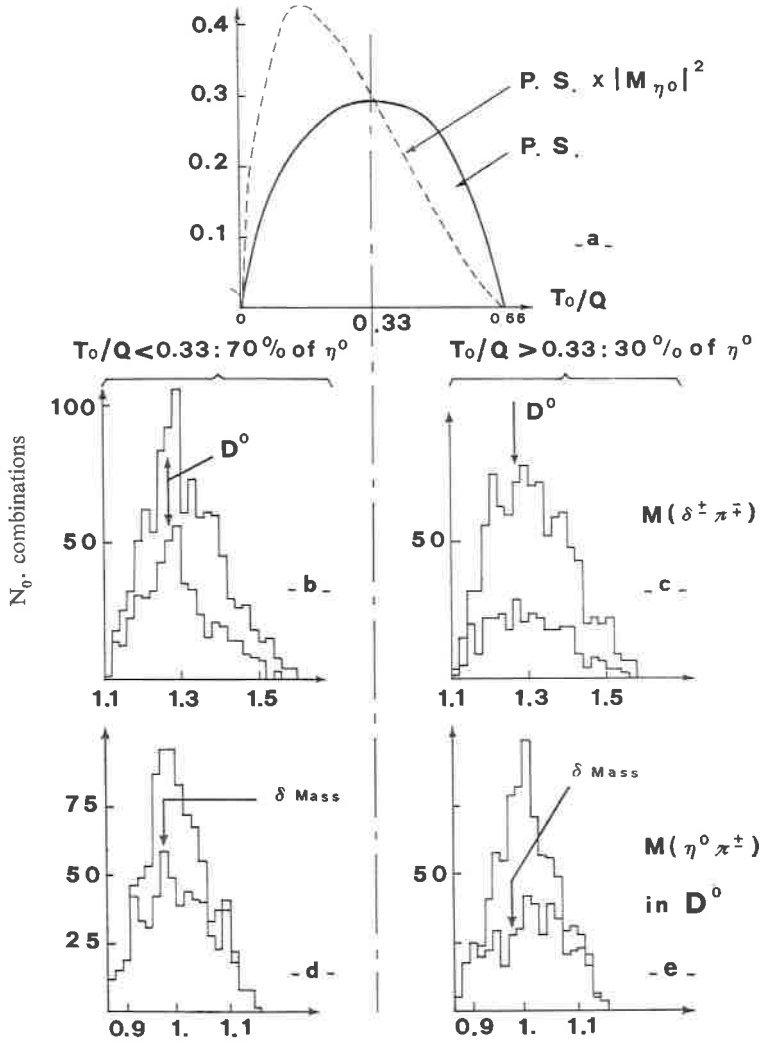

Fig. 6. – *a*) Theoretical distribution of T_0/Q for phase space (solid curve) and η^0 (dotted curve) events. *b-c*) Distribution of $\delta^{\pm}\pi^{\mp}$ masses for $T_0/Q < 0.33$ (*b*) and $T_0/Q > 0.33$ (*c*). Lower curve is for all $\pi^+\pi^-\pi^0$ combinations in ω^0 rejected. *d-e*) Distribution of $\eta^0\pi^{\pm}$ masses in D^0 region for $T_0/Q < 0.33$ (*d*) and $T_0/Q > 0.33$. Lower curves are for all $\pi^+\pi^-\pi^0$ in ω^0 rejected.

in the number of η^0 produced, results are not yet available on the proportions of background, $D^0 \to \eta^0\pi^+\pi^-$, $D^0 \to \delta^\pm\pi^\mp$, $E^0 \to \eta^0\pi^+\pi^-$ and $E^0 \to \delta^\pm\pi^\mp$: Clearly, however, a semi-quantitative understanding of the data has been reached.

5. Other mode of observation of $\delta\pi$ decay of D^0.

Further evidence for a $\delta^\pm\pi^\mp$ decay mode of the D^0, independent of the above method of ω^0 rejection, is shown in Fig. 6. Figure 6*a* demonstrates the theoretical distributions of T^0/Q for phase space (solid line) and for genuine η^0 events multiplied by phase space (dotted line). Selection of events with $T_0/Q < 0.33$ (> 0.33) enhances (reduces) the proportion of η^0 over background, choosing 70% (30%) of the η^0. Figure 6 also shows the distribution of $\delta^\pm\pi^\mp$ masses (*b* and *c*) and of $\eta^0\pi^\pm$ (*d* and *e*) masses in the D^0 region. The distributions on the left (right) are for $T^0/Q < 0.33$ (> 0.33), thus containing the greater (smaller) proportion of η^0. Whereas the distributions with the larger proportion of η^0 (*b* and *c*) show evidence for the D^0 meson and a rather wide peak at the δ mass (distorted by the presence of ω^0), these bumps are less clear in the distributions containing less η^0 (*c* and *e*). In all four cases, the lower curve is the same distribution with all combinations containing a $\pi^+\pi^-\pi^0$ in the ω^0 region rejected. The D^0 signal in the η^0-richer sample (*b*) remains even after the rejection of ω^0. The peak in the δ region, which is seen in both samples, is strongly attenuated in both by the ω^0 rejection. However in the η^0-richer sample (*d*), there remains a signal which is consistent with the δ even after the ω^0 rejection ((3—5) s.d.). Thus, the results of Fig. 6, while demonstrating the problem of the ω^0 reflection, are consistent with the conclusions drawn above from the more complicated method of selection.

6. Conclusion.

In summary, evidence has been seen for the reactions

$$\begin{aligned} \bar{p}p &\to D^0\pi^+\pi^-, \\ &\to D^0\rho^0, \\ &\to E^0\pi^+\pi^-, \end{aligned}$$

followed by the decays

$$\begin{aligned} D^0, E^0 &\to \delta^{\pm}\pi^{\mp} \\ &\hookrightarrow \eta^0\pi^{\pm} \\ &\hookrightarrow \pi^+\pi^-\pi^0 \end{aligned}$$

at 700 MeV/c. Precise quantitative fits of the data and, hence, branching ratios for D^0 and E^0 have yet to be concluded. No spin-parity studies have yet been made, these being extremely complicated in view of the strong ω^0 signal seen in the reaction.

REFERENCES

1) R. R. Bizzarri, *et al.*: CERN/D. Ph. II/70-38, August 1970 (unpublished).
2) C. Baltay: *Procedings of the Philadelphia Conference on Meson Spectroscopy*, New York (1968), p. 107.
3) The estimator that an event represents production of η^0 4π (or ω^0 4π) takes into account the difference between, the $\pi^+\pi^-\pi^0$ mass and the mass of the resonance, due to the resonance width, the experimental resolution, the decay properties (matrix element) of the resonance and the statistical frequency of the resonance (number of 3π combinations in the resonance mass region). The probability, P_i, that the i^{th} $\pi^+\pi^-\pi^0$ combination of an event is an η^0 (ω^0) is a function of the $\pi^+\pi^-\pi^0$ mass and the square of the decay matrix e'ement, described in the text. Experimentally, one knows the form of the surface in a space where x = decay probability, $y = \pi^+\pi^-\pi^0$ mass and z = number of events. For this purpose, the xy—plane is divided into cells and $\langle z\rangle$ calculated for each cell. Also, by extrapolation, one can calculate the background, $\langle z_0\rangle$, in each cell. Then

$$P_i = \frac{\text{signal}}{\text{signal} + \text{background}} = \frac{\langle z\rangle - \langle z_0\rangle}{\langle z\rangle}$$

for each combination. The total estimator that an event be η^0 4π (ω^0 4π) is simply

$$P = \sum_{i=1}^{9} P_i \,.$$

The resulting range for $P(\eta^0)$ is (0.0, 0.5); for ω^0, (0.0, 2.2).
4) Several selections giving equivalent rejections of the ω^0 were found. The one used in this paper corresponds to $P(\omega^0) < 0.7$, $P(\eta^0) > 0.1$. All cuts were tested with Monte-Carlo simulated events, and the above found to give maximal ω^0 rejection (85%) and minimal η^0 rejection (15%).
5) C. Defoix, *et al.*: paper submitted to *Kiev International Conference* (1970) unpublished.

SESSION I-C

Wednesday, 14 April 1971

ω-ρ interference

Chairman: S. GLASHOW

Secretaries: M. SALVINI
B. JEAN MARIE

ω-ρ interference (*)

R. MARSHALL
Daresbury Nuclear Physics Laboratory

1. Introduction.

The situation concerning ω-ρ interference has undergone a radical change during the last 2 or 3 years. During the period 1961-8 we had the case where the theoretical situation was quite thoroughly explored and the experimental situation lagged somewhat behind. There had been a series of experiments mainly involving dipion production by hadronic beams where the ω appeared, disappeared or sometimes hinted at existence. There was nothing conclusive. Overnight the position has changed completely and we now have a series of good experiments which not only firmly establish the apparently G violating decay $\omega \to 2\pi$ and ω-ρ interference but also provide us with reasonably accurate determinations of the parameters involved.

The new era began with the now well known experiment of Goldhaber *et al* [1] who saw evidence for ω-ρ interference in the reaction $\pi^+ p \to \pi^+\pi^-\Delta^{++}$, and has been continued with a series of photoproduction experiments with both high statistics and good resolution.

2. Mass mixing formalism.

The theory used to describe the phenomenon is mass mixing and has been developed by several authors [2-6] from 1961 onwards.

The overall production amplitude S for the final state of interest 2π, 3π or $2e$ is written:

$$S(2\pi, 3\pi, 2e) = (A_\rho A_\omega) \frac{1}{mI - M} \left(\frac{T_\rho}{T_\omega}\right) \qquad (1)$$

(*) Introductory talk.

A_v is the production amplitude for the pure G conserving vector meson states ρ^0 and ω^0. T_v is the corresponding decay amplitude.

The mass matrix is

$$M = \begin{pmatrix} m_\rho - i\Gamma_\rho & -\delta \\ -\delta & m_\omega - i\Gamma_\omega \end{pmatrix}$$

or alternatively one can use

$$\frac{1}{M_2 - m^2 I}$$

with

$$M_2 = \begin{pmatrix} m_\rho^2 - i m_\rho \Gamma_\rho & -\delta(m_\rho + m_\omega) \\ -\delta(m_\rho + m_\omega) & m_\omega^2 - i m_\omega \Gamma_\omega \end{pmatrix}$$

The strength of the mixing is given by δ.

For convenience put $q_v = m_v^2 - m^2 - i m_v \Gamma_v$. Now evaluating eq. (1) with the help of a partial fraction decomposition and neglecting $\delta^2 m_v^2$ compared to $q_\rho q_\omega$, one gets:

$$S = \frac{T_\rho A_\rho}{q_\rho}\left[1 + \frac{\delta(m_\rho + m_\omega)}{q_\omega - q_\rho}\left(\frac{T_\omega}{T_\rho} + \frac{A_\omega}{A_\rho}\right)\right] + \frac{T_\omega A_\omega}{q_\omega}\left[1 + \frac{\delta(m_\rho + m_\omega)}{q_\rho - q_\omega}\left(\frac{T_\rho}{T_\omega} + \frac{A_\rho}{A_\omega}\right)\right] \tag{2}$$

i.e. in the absence of mixing the amplitude would be given simply by $T_\rho A_\rho / q_\rho + T_\omega A_\omega / q_\omega$, a sum of the pure I-spin states.

The ρ and ω states observed experimentally can be written as a superposition of the pure states ρ^0 and ω^0:

$$|\varrho\rangle = |\varrho_0\rangle - \varepsilon|\omega_0\rangle$$

$$|\omega\rangle = |\omega_0\rangle + \varepsilon|\varrho_0\rangle$$

where

$$\varepsilon = \frac{\delta(m_\rho + m_\omega)}{q_\rho - q_\omega} \text{ (complex)} \tag{3}$$

I shall consider only those final states which have been the subject of experimental investigation, namely 2π and 2e.

3. $\pi^+\pi^-$ final state.

Taking the vector dominance picture, one can calculate Γ_ω according to the scheme (7),

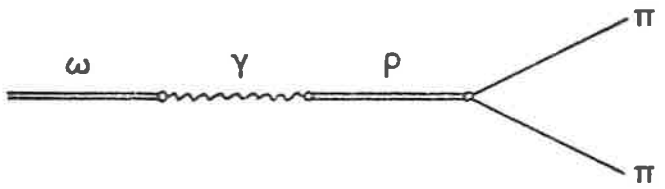

then $\Gamma_{\omega\to 2\pi} \simeq 10^{-2}$ MeV. If this were the only effect then $\omega \to 2\pi$ would not have been observed experimentally to date. The effect observed corresponds to a partial width a factor 10 larger. So neglecting $T_{\omega\to 2\pi}$ in eq. (2) and dropping the bracket ($\simeq 1$) multiplying $T_\rho A_\rho / q_\rho$ then:

$$S_{2\pi} = \frac{T_\rho A_\rho}{q_\rho}\left(1 + \frac{\delta(m_\rho + m_\omega)}{q_\rho - q_\omega}\frac{A_\omega}{A_\rho}\frac{q_\rho}{q_\omega}\right) \tag{4}$$

One sees a conventional ρ term modulated by a function F, the term in the brackets. Now experiments are usually analysed in terms of the phenomenological form

$$S_{2\pi} = \frac{T_\rho A_\rho}{q_\rho}\left(1 + \xi e^{i\varphi}\frac{q_\rho}{q_\omega}\right); \tag{5}$$

i.e. given some data one can always get out (with errors) values for the real number ξ and the phase φ. The question then is whether or not one can get at the physics which is contained in δ and A_ω/A_ρ.

Comparison of eqs. (4) and (5) gives

$$\xi = \frac{|\delta|}{|q_\rho - q_\omega|} \left| \frac{A_\omega}{A_\rho} \right| (m_\rho + m_\omega) \tag{6}$$

and

$$\varphi = \operatorname{Arg} \frac{A_\omega}{A_\rho} + \operatorname{Arg} \delta + \operatorname{Arg} \left(\frac{1}{q_\rho - q_\omega} \right)$$

$$= \varphi_{\omega\rho} + \varphi_\delta + \tan^{-1} \left(\frac{m_\rho \Gamma_\rho - m_\omega \Gamma_\omega}{m_\rho^2 - m_\omega^2} \right) \tag{7}$$

Further we have

$$\Gamma_{\omega \to 2\pi} = |\varepsilon|^2 \Gamma_{\rho \to 2\pi}$$

which gives, using eqs. (3) and (6)

$$\text{B. R. } (\omega \to 2\pi) = \xi^2 \left| \frac{A_\rho}{A_\omega} \right|^2 \frac{\Gamma_\rho}{\Gamma_\omega} \tag{8}$$

The phase φ coming from experiment is the combined phase of A_ω/A_ρ (the relative production phase), $1/(q_\rho - q_\omega)$ and δ. Since the phase is essentially determined by the data in the vicinity of the ω, we can ignore any mass dependence in Γ_ρ and calculate $\operatorname{Arg}\left(1/(q_\rho - q_\omega)\right) \simeq 106°$.

The effect of the phase φ on the modulating function F is shown in Fig. 1 where F is plotted for $\xi = 0.01$ (arbitrary) and $\varphi = 0°$ to $270°$.

To predict the phase for a particular reaction we need to know the phase of δ and A_ω/A_ρ.

Coleman and Glashow ([6]) originally calculated $\operatorname{Re}\delta \simeq 2.5$ MeV in terms of the medium strong SU_3 breaking mass splitting of baryons and mesons. Subsequent calculations by various authors ([8]) gave $\operatorname{Re}\delta = (2.5—5.0)$ MeV. Gourdin ([8]) has calculated on the basis of real physical intermediate states (2π, 3π, $\pi\gamma$ etc.) that $\operatorname{Im}\delta < 0.8$ MeV and similarly Allcock ([9]) calculated $\operatorname{Im}\delta \simeq 0.15$ MeV. The phase of δ is thus expected to be small (and positive). In discussing the data we shall take the starting point that δ is purely real.

The phase of A_ω/A_ρ depends on the production mechanism and hence the reaction.

A comparison between theoretical expectations and the results of specific experiments can now be made. To demonstrate the situation with hadronic beams I have selected only two reactions. For a more thorough consideration of all reactions, the reviews of Goldhaber ([10]) and Roos ([11]) should be consulted.

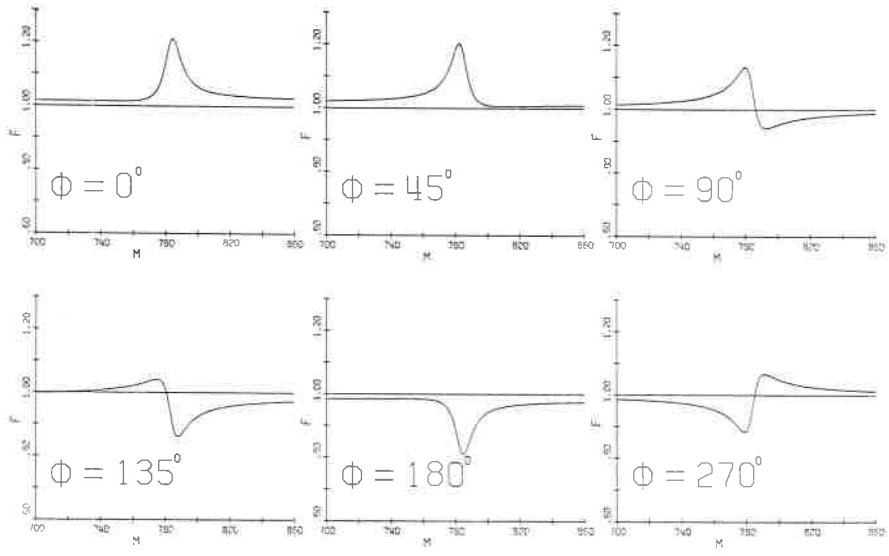

Fig. 1. – The modulating function $F = 1 + \xi e^{i\varphi}(q_\rho/q_\omega)$ for $\xi = 0.01$ and various values of φ.

The reaction $\pi^+ p \to \pi^+\pi^-\Delta^{++}$ has been studied by Goldhaber *et al.*([1]) at 3.7 GeV/c (see Fig. 2) and by a group from Toronto ([12]) at 5.5 GeV/c. The phase of A_ω/A_ρ based on π, B exchange ([3]) is expected to be 90°, so the total phase for this reaction is thus $\sim 196°$. The two groups above have determined $(192 \pm 17)°$ and $(163 \pm 23)°$ respectively, although the final result from Toronto has not yet been published. There is thus reasonable agreement with the prediction. In order to derive a branching ratio it is necessary to have a value for $|A_\rho/A_\omega|$ (eq. (8)) where A_ρ and A_ω are the coherently interfering amplitudes. In the case of production by pion beams, A_ρ/A_ω cannot simply be obtained from the measured cross-section due to the existence of non interfering or incoherent amplitudes. When the degree of coherence « c » is not known, eq. (8) does not lead to a useful determination of the branching ratio, merely a lower limit. The effect of « c » on the phase φ is small provided

$c \geqslant 0.4$ ([13]). Clearly one cannot distinguish between $c \simeq 0$ and a large value of φ and $c \simeq 1$ with $\varphi \simeq 0$.

The reaction $\pi^- p \to \pi^+ \pi^- n$ provides a different example since the phase of A_ρ / A_ω is expected to be $-90°$ leading to an expected value of $\varphi = 16°$.

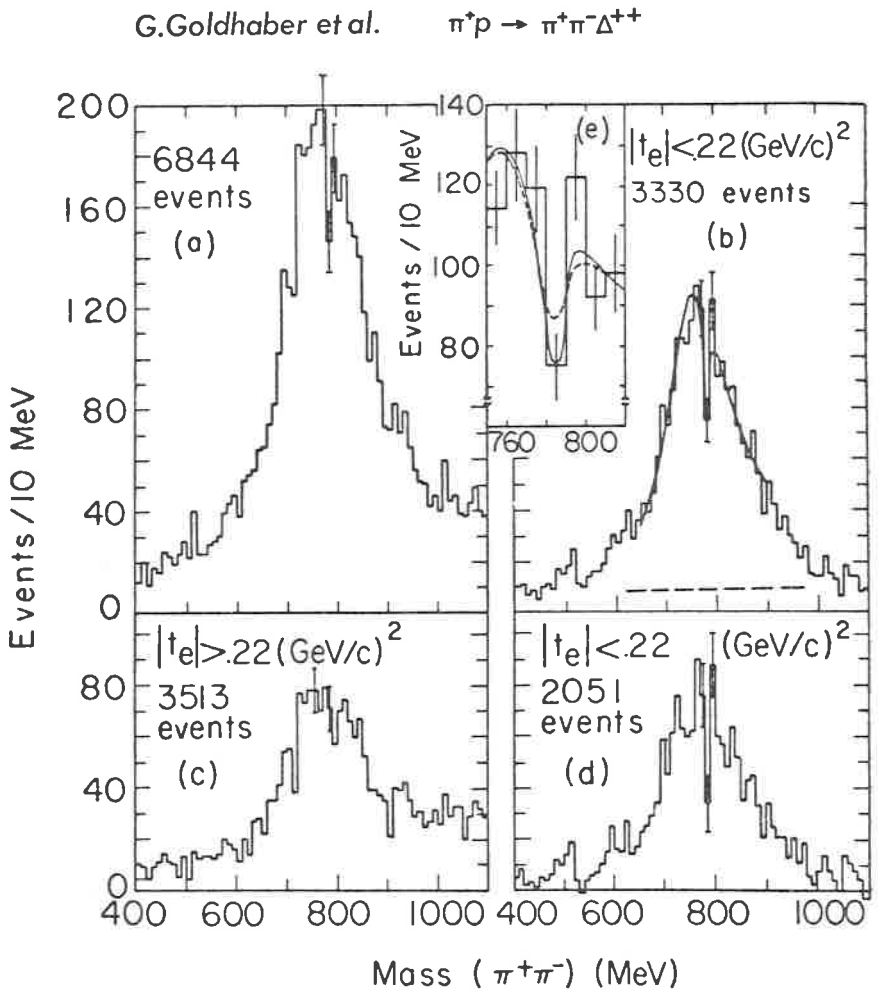

Fig. 2. – The $\pi^+\pi^-$ invariant mass spectrum for the reaction $\pi^+ p \to \pi^+\pi^-\Delta^{++}$ measured by G. GOLDHABER *et al.* *a*) The entire data. *b*) For $|t| < 0.22$ (GeV/c)^2. The dashed curve represents an incoherent background contribution. *c*) For $|t| > 0.22$ (GeV/c)^2. *d*) For $|t| < 0.22$ (GeV/c)^2 with background subtraction from both sides of the Δ^{++} band. *e*) Enlargement of *b*).

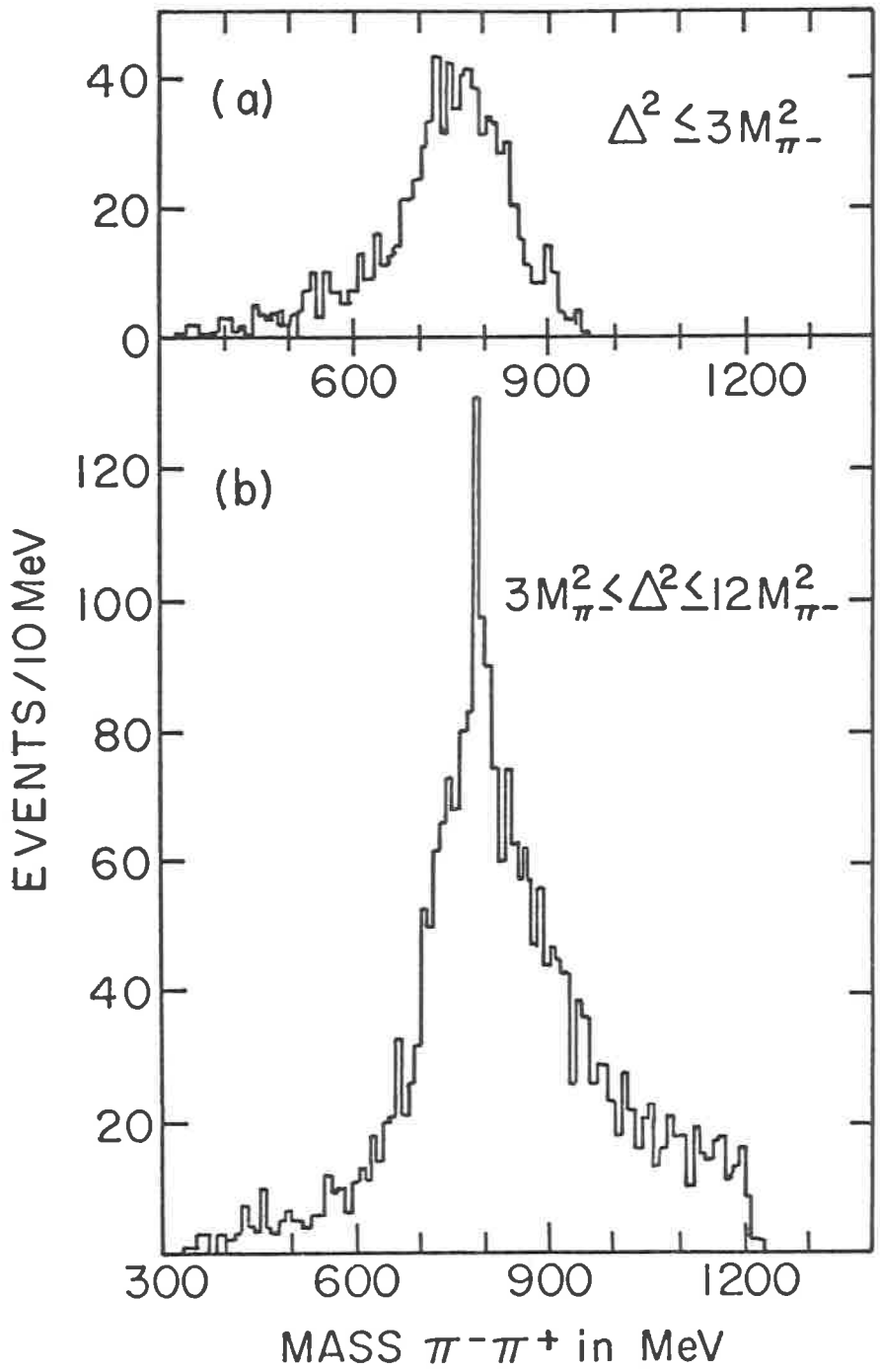

Fig. 3. – The $\pi^+\pi^-$ mass spectrum for the reaction $\pi^- p \to \pi^+\pi^- n$ measured by HAGOPIAN *et al.* *a)* $|t| \leqslant 3m_\pi^2$ *b)* $3m_\pi^2 < |t| < 12m_\pi^2$.

Hagopian *et al* ([13]) investigated this reaction at 2.3 GeV/c (see Fig. 3) and obtained a phase $\varphi = -(15 \pm 30)°$. Again there is good agreement.

TABLE 1.

$\pi^+p \to \pi^+\pi^-\Delta^{++}$	δ MeV	φ
G. GOLDHABER *et al.* ([1]), 3.7 GeV/c	2.7 ± 0.9	$192° \pm 17°$
JACKSON *et al.* Toronto ([12]), 5.5 GeV/c	2.6 ± 0.9	$163° \pm 23°$
LRL Group A (Flatté) et al., 7 GeV/c		$\sim 90°$
π, B exchange gives $\mathrm{Arg}\, A_\omega/A_\rho = 90° \Rightarrow \varphi \approx 196°$		
$\pi^-p \to \pi^+\pi^-n$	δ MeV	φ
S. HAGOPIAN *et al.* ([13]), 2.3 GeV/c		$-15° \pm 30°$
P. Dalpiaz et al. ([23]), 1.67 GeV		$-4° \pm 20°$
π, B exchange gives $\mathrm{Arg}\, A_\omega/A_\rho = -90° \Rightarrow \varphi \approx 16°$		

The results of these two reactions are summarized in Table I (*). I also present in Fig. 4 and 5 the results of the experiments by Allison *et al.* ([14]) on $\bar{p}p \to \pi^+\pi^-\pi^+\pi^-$ and by Abramovich *et al* ([15]) on $\pi^-p \to \pi^-p\pi^+\pi^-$. Although analysis of the data from these reactions is somewhat complicated, the effect of the ω is clearly seen in the data.

There is now a lot of data on photoproduction experiments from the Daresbury ([16]) and DESY-MIT groups ([17]) who have used bremsstrahlung beams and mainly complex nuclear targets. There is also the data from the 82″ hydrogen bubble chamber at SLAC ([18]).

In the case of photoproduction experiments we believe we understand the production mechanism and that $|A_\rho/A_\omega|$ is given by the ratio of the coupling constants $\gamma_\omega/\gamma_\rho$. In the case of coherent production on a nucleus, there remains a (small) correction to be made for incoherent production and ω production by one pion exchange.

Pomeron exchange leads to a A_ω/A_ρ phase of $\sim 0°$ and we thus have the prediction that the total phase should be $\sim 100°$.

(*) I have also included in Table 1 two experiments subsequently presented in this session. They are listed in *italics*.

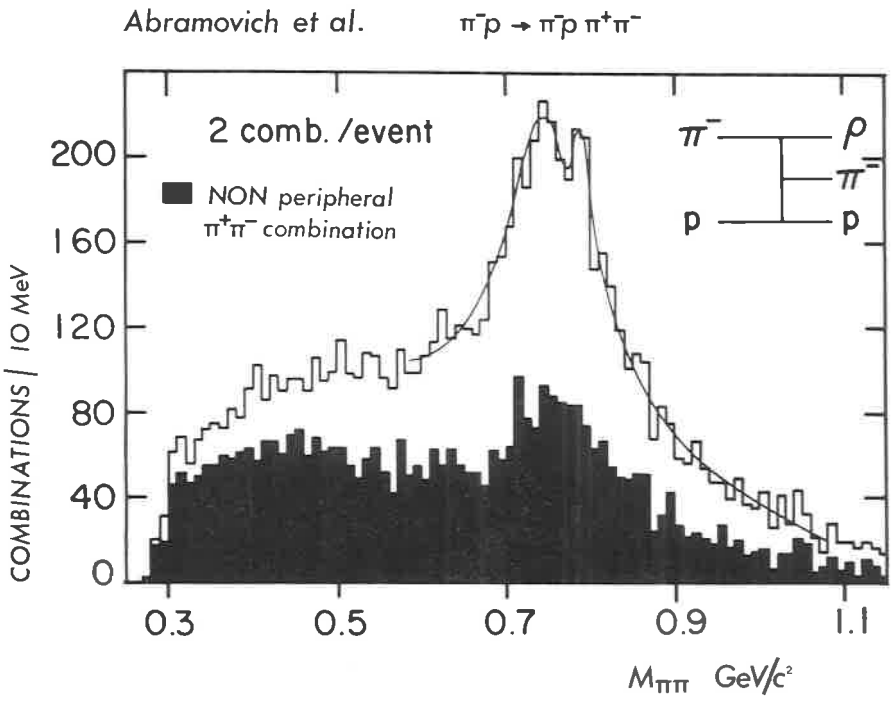

Fig. 4. – The $\pi^+\pi^-$ mass spectrum for the reaction $\pi^- p \to \pi^- p \pi^+\pi^-$ measured by ABRAMOVICH *et al.* There are two $\pi^+\pi^-$ combinations per event. The unshaded histogram is all events, both combinations. The shaded histogram selects that combination where the alternative combination would give a peripheral $\pi^+\pi^-$.

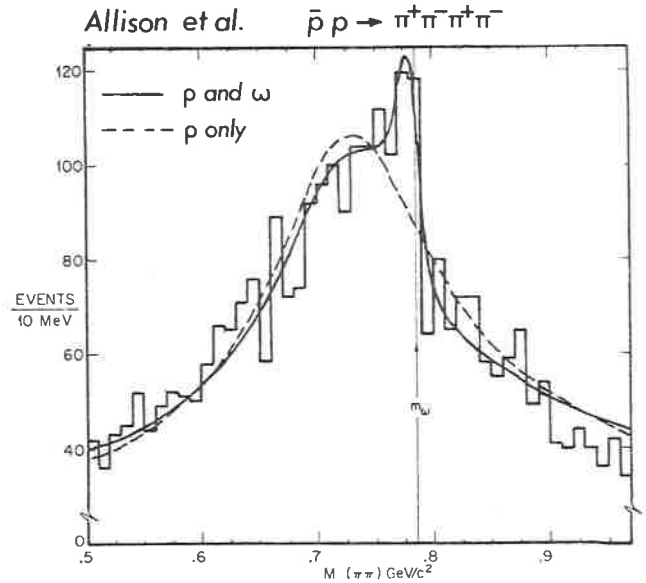

Fig. 5. – The $\pi^+\pi^-$ mass spectrum for the reaction $\bar{p}p \to 2\pi^+ 2\pi^-$ measured by ALLISON *et al.*

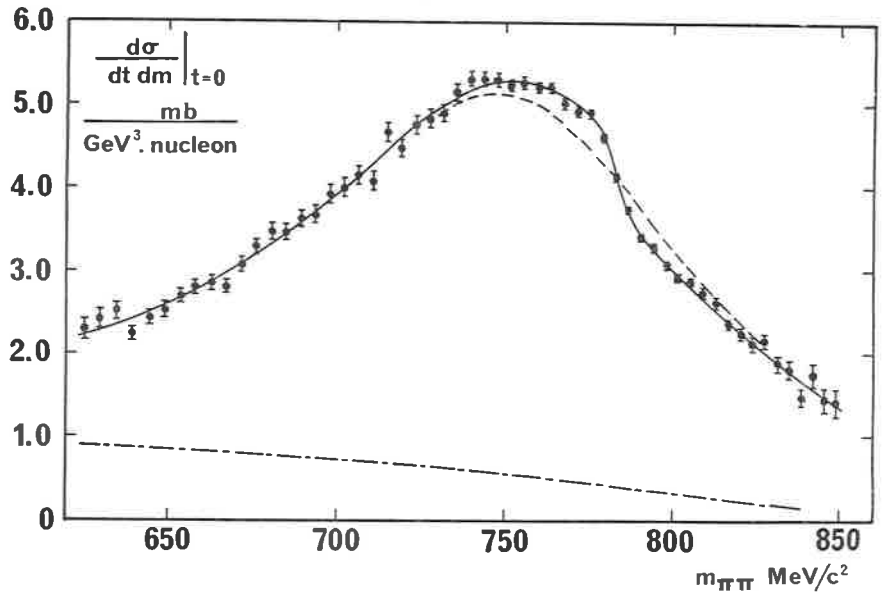

Fig. 6. – The differential cross-section $d\sigma/dt\,dm|_{t=0}$ for the reaction $\gamma C \to C\pi^+\pi^-$ measured by BIGGS *et al.* The solid curve is a fit with ω, ρ terms; the dashed line is a fit with $\xi = 0$. The dot-dashed line shows the incoherent background.

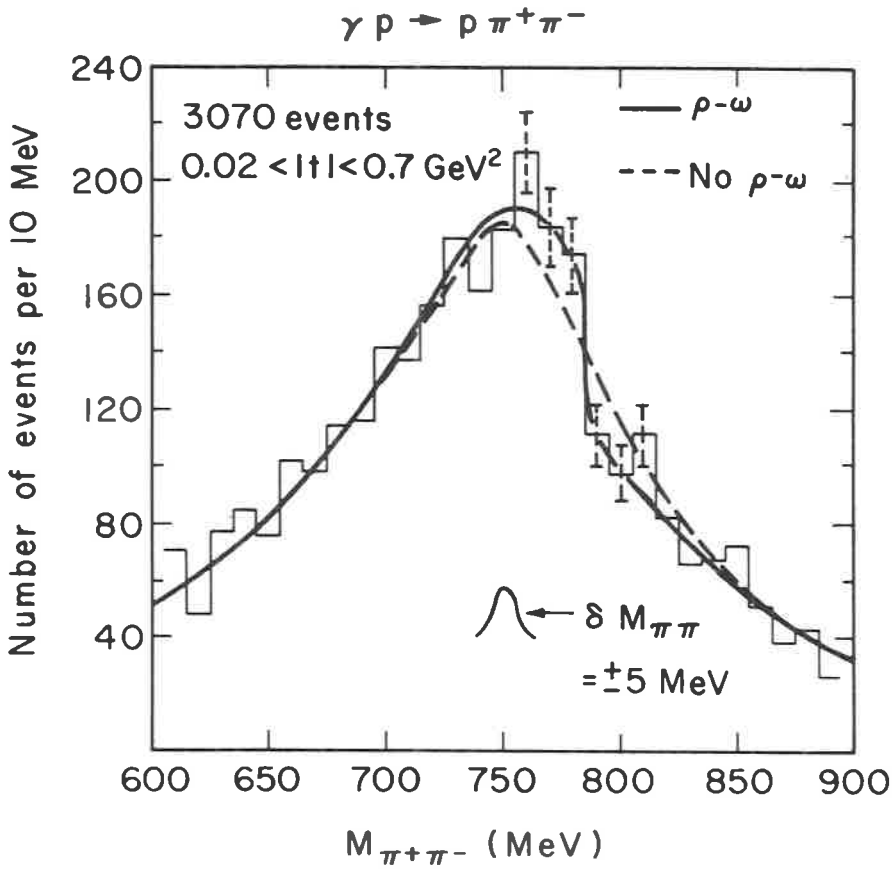

Fig. 7. – The $\pi^+\pi^-$ mass distribution for the reaction $\gamma p \to p\pi^+\pi^-$, measured by MOFFEIT *et al.* at SLAC.

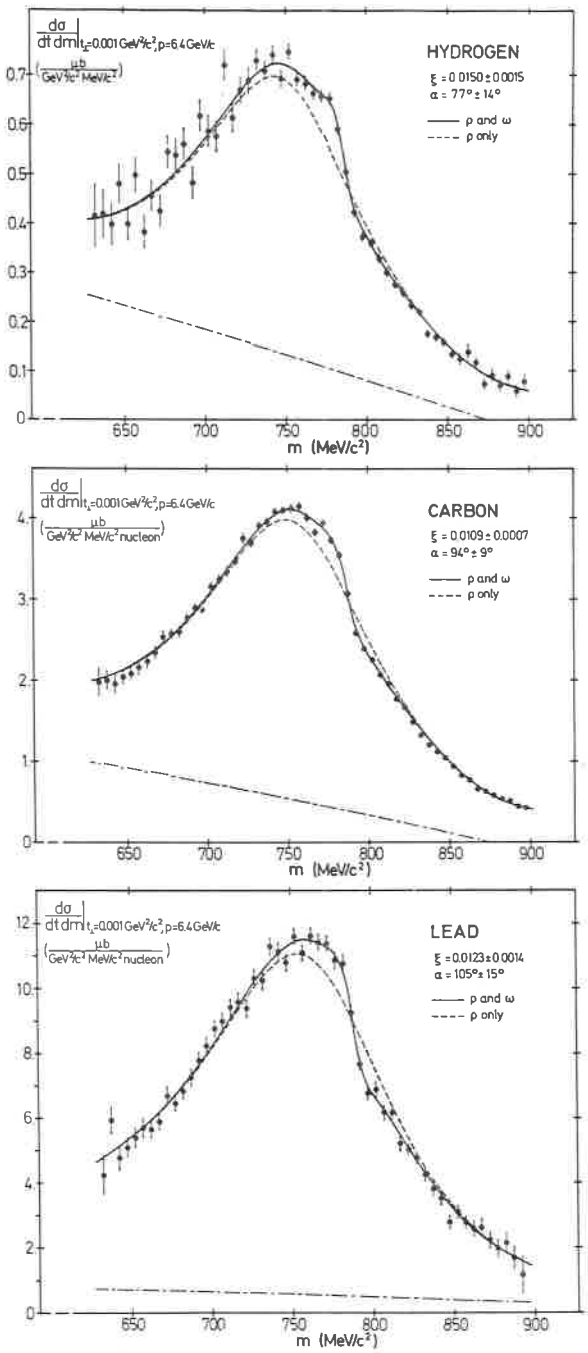

Fig. 8. – The cross-section $d\sigma/dt\,dm(t_\perp = 0.001,\ p = 6.4\ \text{GeV/c})$ for the reaction $\gamma A \to A\pi^+\pi^-$ where A = p, C and Pb. The data is from ALVENSLEBEN *et al.*

The photoproduction data is shown in Fig. 6, 7 and 8. The high statistics of these experiments makes the interference effect clear to see. For comparison and interpretation the total photoproduction data has been redrawn in Fig. 9.

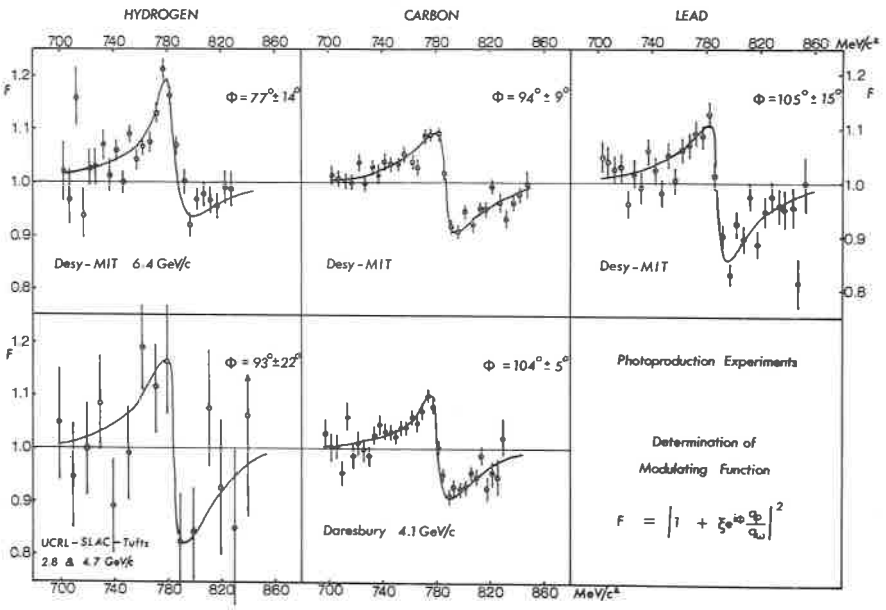

Fig. 9. – The modulating function F as measured by BIGGS *et al*, MOFFEIT *et al.* and ALVENSLEBEN *et al.* for the reaction $\gamma A \rightarrow A\pi^+\pi^-$.

TABLE 2.

	Initial state	ξ	δ (MeV)	B.R. ($\omega \rightarrow 2\pi$) (%)	φ
BIGGS *et al.* [16] Daresbury	γC	0.0097±0.0008	1.7 ±0.18	$0.8^{+0.28}_{-0.22}$	(104± 5)°
MOFFEIT *et al.* [18] SLAC-UCRL-Tufts	γp		2.3 ±0.9	$1.3^{+1.2}_{-0.9}$	(93±22)°
ALVENSLEBEN *et al.* [17] DESY-MIT	γp	0.0150±0.0015	2.45±0.18	1.49±0.22	(77±14)°
	γC	0.0109±0.0007			(94± 9)°
	γPb	0.0123±0.0014			(105±15)°
AUGUSTIN *et al.* [19]	e^+e^-			$3.3^{+2.8}_{-2.0}$	(164±28)°

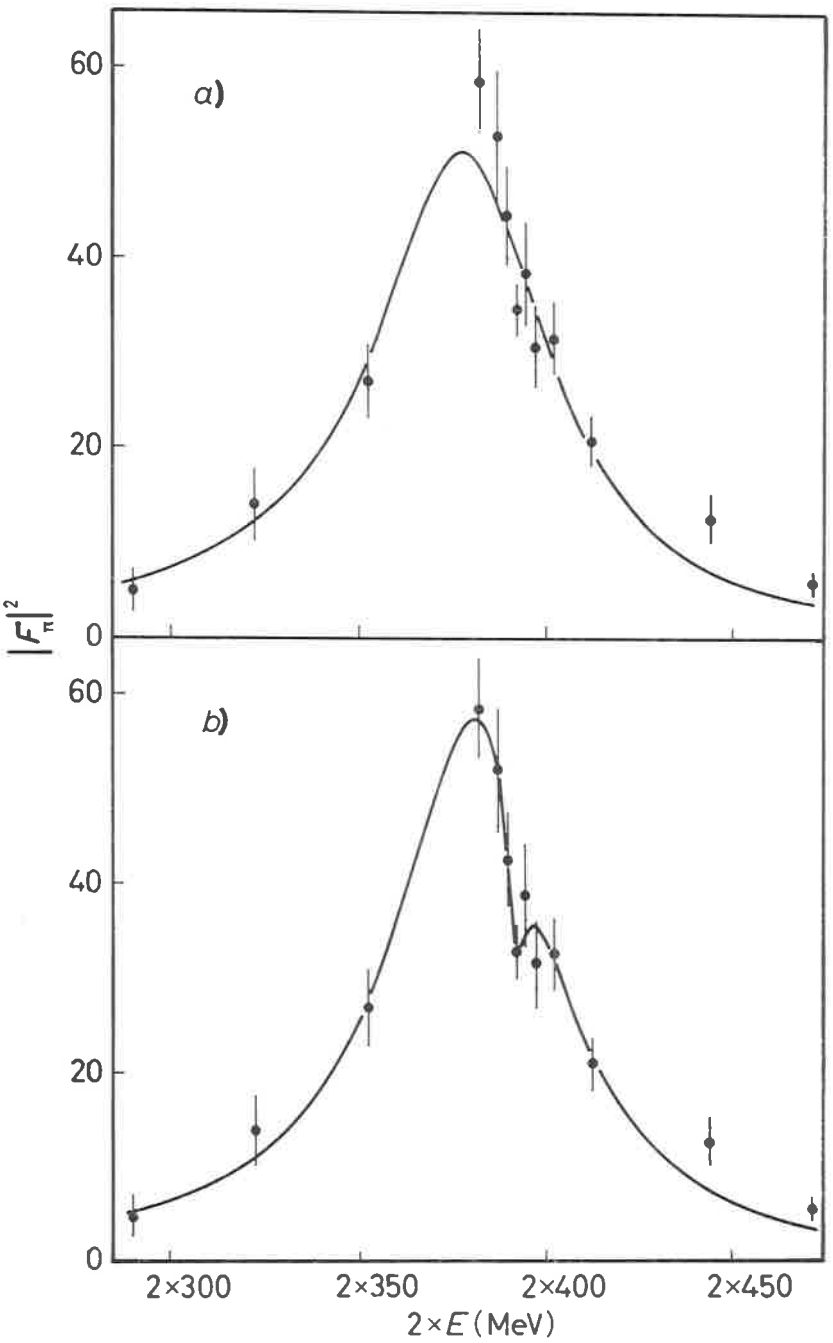

Fig. 10. – The pion form factor $|F_\pi|^2$ as a function of energy as measured by AUGUSTIN *et al.* *a*) ρ only *b*) ω-ρ interference term included.

In this case the ϱ term $A_\varrho T_\varrho / q_\varrho$ has been divided out leaving the modulating function F (eqs. (4) and (5)). There is broad agreement between the groups and comparison with Fig. 1 shows that a phase of $\sim 90°$ is being measured. Table II is a detailed summary of the results showing the values of φ obtained by each experiment. Also listed are the values of ξ, δ and B.R. published by the groups concerned. For comparison the storage ring experiment ([19]) $e^+e^- \to \pi^+\pi^-$ which should measure the same phase, obtained $(164 \pm 28)°$, differing by some $2\frac{1}{2}$ standard deviations. The difference is probably not significant in view of the lower statistics of the Orsay result (see Fig. 10).

It seems that we have reasonable agreement and consistency in the case of the $\pi^+\pi^-$ final state and that the data can be explained without requiring δ to have a phase significantly different from zero.

The values of δ determined by the various groups, in the range (1.7—2.5) MeV, are in reasonable agreement with the predictions.

4. e^+e^- final state.

The e^+e^- final state has been investigated in detail by the Daresbury and DESY-MIT groups, again studying photoproduction on complex nuclei.

For this reaction we can no longer ignore $T_{\omega \to 2e}$ since the two graphs are of comparable strengths;

$$\frac{1}{\gamma_\omega} : \frac{1}{\gamma_\varrho} \approx 1 : 3$$

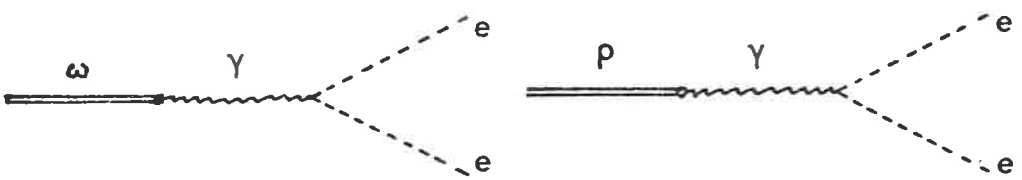

We have the simplification however, in the framework of vector dominance

$$\left|\frac{A_\varrho}{A_\omega}\right| = \frac{\gamma_\omega}{\gamma_\varrho} \quad \text{and} \quad \left|\frac{T_\varrho}{T_\omega}\right| = \frac{\gamma_\omega}{\gamma_\varrho}$$

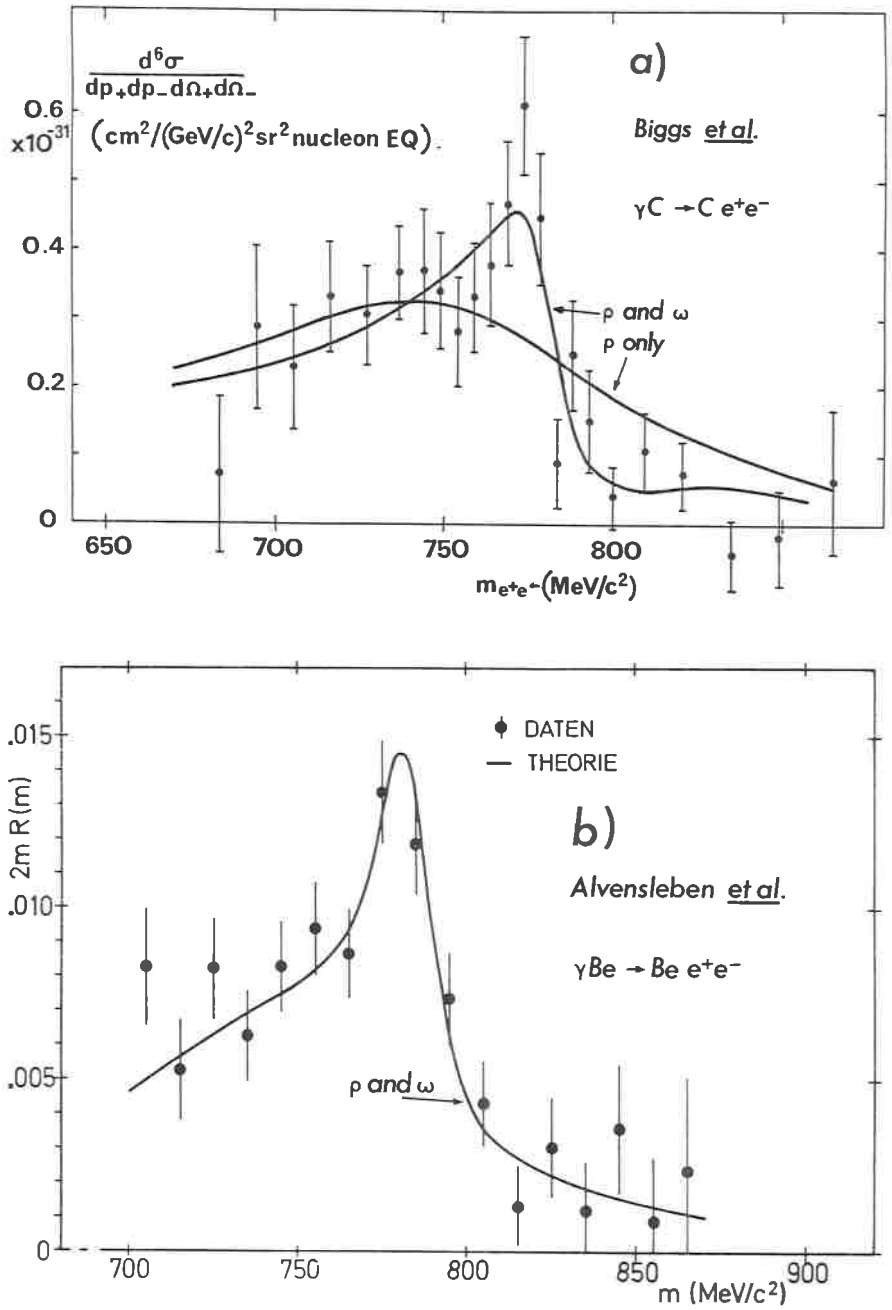

Fig. 11. – *a*) The e^+e^- mass spectrum for the reaction $\gamma C \to C e^+e^-$ measured by BIGGS *et al.* at 3.5 GeV. *b*) The e^+e^- mass spectrum for the reaction $\gamma Be \to Be\, e^+e^-$ measured by ALVENSLEBEN *et al.* at 5.1 GeV.

i.e.

$$S_{e^+e^-} = \frac{T_\varrho A_\varrho}{q_\varrho}\left[1 + \frac{\delta(m_\varrho + m_\omega)}{q_\omega - q_\varrho}\,2\frac{\gamma_\varrho}{\gamma_\omega}\right] + \frac{T_\omega A_\omega}{q_\omega}\left[1 + \frac{\delta(m_\varrho + m_\omega)}{q_\varrho - q_\omega}\,2\frac{\gamma_\omega}{\gamma_\varrho}\right] \qquad (9)$$

It has been customary when analysing the data to ignore the terms in the square brackets and to consider two interfering ϱ and ω amplitudes $S_{e^+e^-} = T_\varrho A_\varrho/q_\varrho + T_\omega A_\omega/q_\omega$ when fitting the data and hence to extract the relative phase of A_ϱ and A_ω. Before comparing this phase with the results from the $\pi\pi$ experiments one should correct for the phase due to the square brackets in eq. (9). Using the value for δ from $\pi\pi$ data, this phase is $\sim 18°$. The mass spectra from Biggs *et al.* ([20]) (Daresbury) for $\gamma C \to Ce^+e^-$ is shown together with the data of Alvensleben *et al.* ([21]) (DESY-MIT) for $\gamma Be \to Be\, e^+e^-$ in Fig. 11. If one believes that the reaction proceeds by Pomeron exchange (Arg $A_\omega/A_\varrho = 0$) then this experiment should just measure the angle due to the mixing terms, *i.e.* 18°.

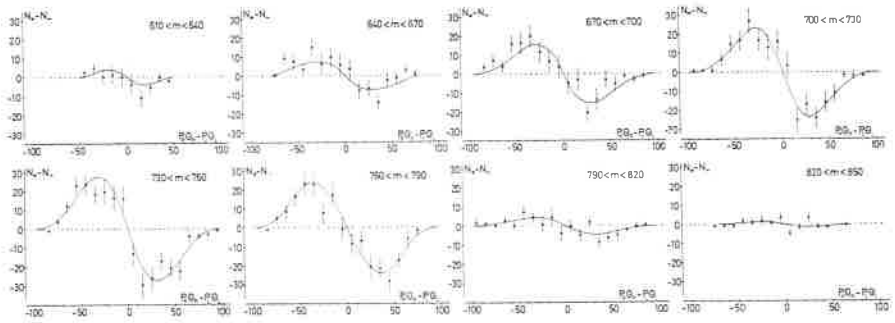

Fig. 12. – The asymmetric events for the reaction $\gamma Be \to Be\, e^+e^-$ measured by ALVENSLEBEN *et al.* The data is plotted as a function of the antisymmetric variable $p_R\theta_R - p_L\theta_L$ where the subscripts R, L denote the right or left hand solid angle (spectrometer arm). The curves are fits to the data.

In fact Alvensleben *et al.* obtained $\varphi_{\omega\varrho} = (41 \pm 22)°$ in agreement with expectation whereas Biggs *et al.* found $\varphi_{\omega\varrho} = 100°^{+38°}_{-30°}$: However, the two experiments cannot be said to disagree with each other within statistics. Given these two experiments with the errors reported there is a 1 in 4 chance of two such experiments differing by 60° or more. In a subsequent experiment intended primarily to measure the phase of A_ϱ, Biggs *et al.* ([22]) have made an independent determination of the phase of A_ω/A_ϱ. This is new data taken

under differing kinematical conditions and they obtained a value of $\varphi_{\omega\rho} = 118^{+13^\circ}_{-22^\circ}$, confirming their earlier result.

Before considering the implications of these values for $\varphi_{\omega\rho}$ it is interesting to look at the values of the phase of A_ρ and A_ω obtained in these electron pair experiments. The interference between the Bethe-Heitler term and the Compton term contributing to the process $\gamma A \to A e^+e^-$ is antisymmetric under interchange of the 4-momentum of e^+ and e^- (see ref. ([21]) for a full discussion). By measuring the count rate N_+ when e^+ is detected in a particular solid angle (e^- also detected) and also the count rate N_- when e^- is detected in the same solid angle (e^+ also detected) then the interference term is isolated by forming the combination $N_+ - N_-$. The measured interference is clearly demonstrated in the data shown in Fig. 12 and 13.

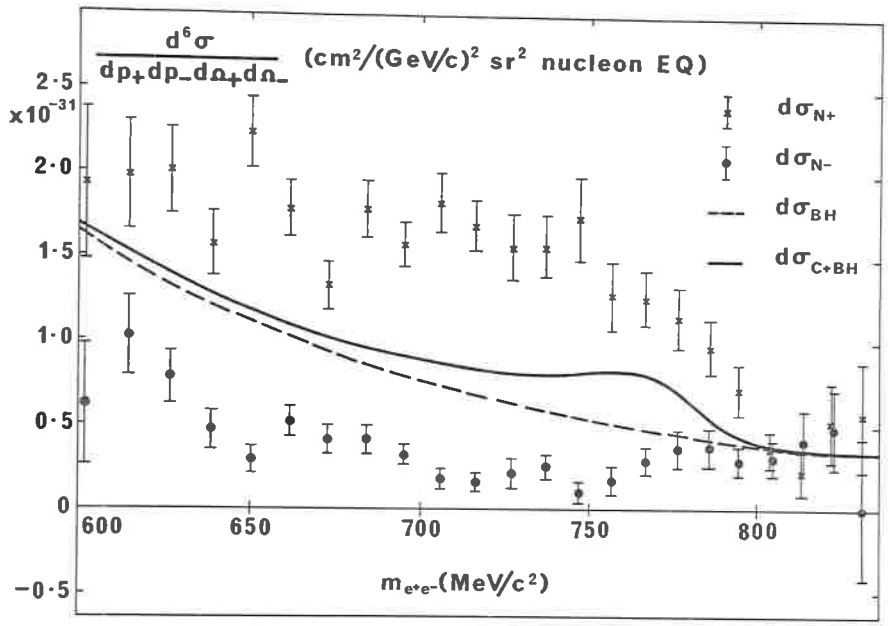

Fig. 13. – The differential cross-section for the $N_\pm$ yields plotted as a function of e^+e^- invariant mass as measured by BIGGS *et al.* The dashed line is the theoretical Bethe-Heitler (QED) cross-section and the solid line is the sum of the B-H and fitted Compton cross-sections.

The phase of A_ρ (and A_ω) relative to the Bethe-Heitler term is extracted from the interference term. In this way Alvensleben *et al.* measure the phase of A_ρ at 5.1 GeV to be $(11.8 \pm 4.4)^\circ$ leading to a phase of A_ω (corrected for mixing) of $(35 \pm 21)^\circ$. On the other hand Biggs *et al.* measure the phase

of A_ρ at 4 GeV to be $(16.5 \pm 6.2)°$ leading to a phase of A_ω of $(116 \pm 22)°$. These results for electron pair experiments are summarised in Table 3. The possibility of such a large phase for the ω production amplitude has severe implications as has already been pointed out ([23]), since it corresponds to an extremely large real part in an amplitude which is expected (from diffraction) to be predominantly imaginary.

TABLE 3.

Experiment		$\varphi_{\omega\rho}$	φ_ρ	φ_ω	φ_ω corrected for mixing
BIGGS *et al.* ([20])	γC 3.5 GeV	$100^{+38°}_{-30°}$			
ALVENSLEBEN *et al.* ([21])	γBe 5.1 GeV	$(41 \pm 20)°$	$(11.8 \pm 4.4)°$	$(53 \pm 21)°$	$(35 \pm 21)°$
BIGGS *et al.* ([22])	γC 4.0 GeV	$118^{+13°}_{-22°}$	$(16.5 \pm 6.2)°$	$135^{+14°}_{-23°}$	$117^{+14°}_{-23°}$

There is first the effect of the nucleus to consider. The size of the nucleus shifts the phase compared to what would be measured on a single nucleon. Following the formalism of ref. ([24]) where the amplitude A_ω for production on a single nucleon is given by $A_\omega = if_0(1 - i\beta)$; f_0 is real and β is the ratio of real to imaginary parts, *i.e.* $\mathrm{Arg}\, A_\omega = -\mathrm{tg}^{-1}\beta$. Then

$$A_\omega(\mathrm{Be}, C) = 2\pi f_0(1 - i\beta)\int_0^\infty b\,\mathrm{d}b \int_{-\infty}^{+\infty} \mathrm{d}z J_0\left(b\sqrt{-t_\perp}\right) \exp\left[\left(iz\sqrt{-t_\parallel}\right)\varrho(z, b)\cdot\right.$$

$$\left.\cdot \exp\left[-\tfrac{1}{2}\sigma_{\omega N}(1 - i\beta)\int_z^\infty \varrho(z', b)\,\mathrm{d}z'\right]\right.$$

Here one integrates over impact parameter b for a nucleus of density ϱ where $\sigma_{\omega N}$ gives the reabsorption of ω after production.

In Fig. 14 an attempt is made to remove nuclear effects from the phases of A_ρ, A_ω measured on carbon and beryllium. The curves are slightly different in the two cases; carbon at 4 GeV and beryllium at 5.1 GeV. These are no problems with A_ρ and the correction amounts to about 1°. In the case of A_ω it can be seen that the formalism above does not allow for a phase measured on the nucleus of more than $\sim 45°$. In the case of the result from Alvensleben *et al.* there is no difficulty provided the 18° due to mixing is removed. The measured phase then converts to $40^{+?}_{-28°}$. The result of Biggs *et al.* cannot be intepreted in the framework of this model. The dotted curve in Fig. 14 shows the freedom one has in calculating the effect of nuclear physics. The

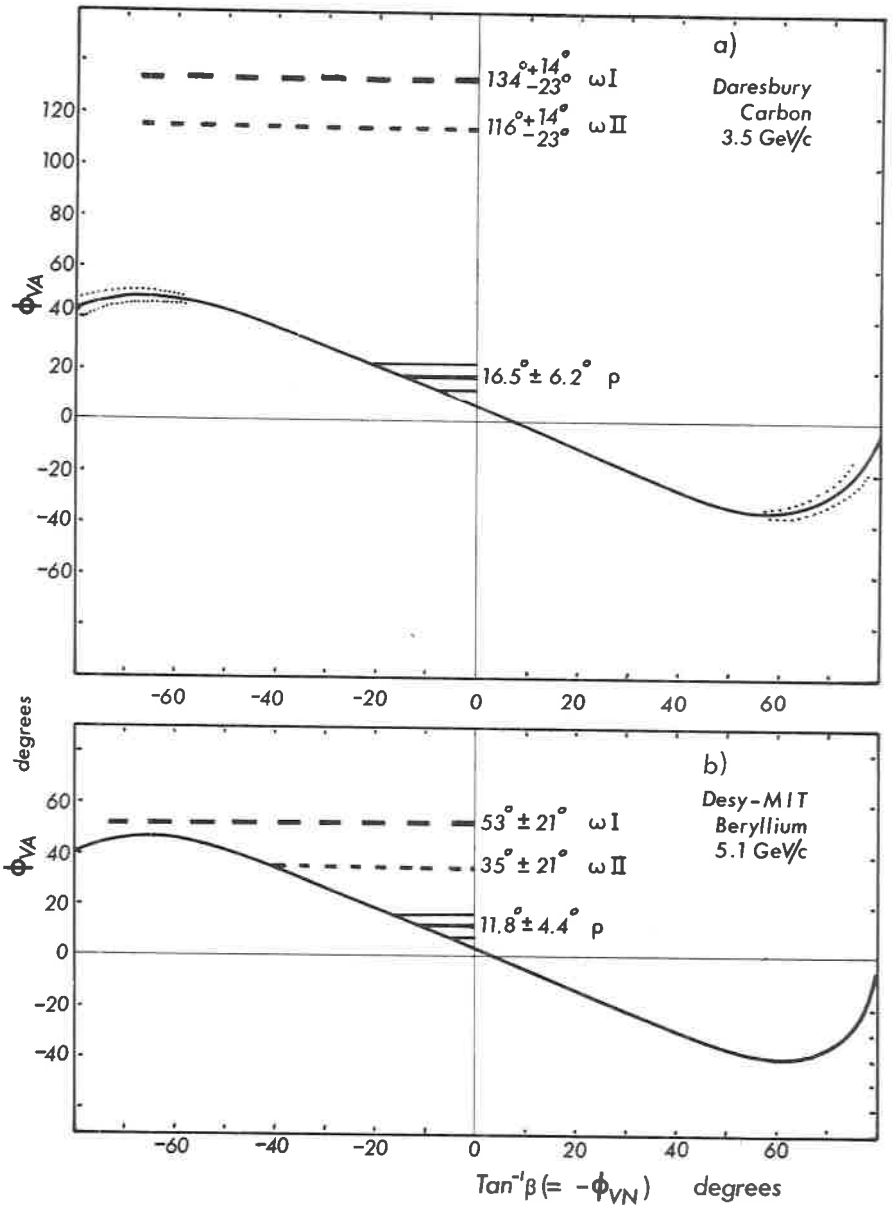

Fig. 14. – *a*) The production phase φ_{VA} on a carbon nucleus as a function of the production phase on a single nucleon φ_{VN} at 4 GeV. The measured values of BIGGS *et al.* are shown. ωI is the directly measured ω phase, ωII is the phase corrected for mixing. The dotted curve shows the variation due to various nuclear models (see text for details). *b*) The same curve for beryllium at 5.1 GeV with the results of ALVENSLEBEN *et al.*

nuclear radius has been varied within the limits of the measurement of Alvensleben *et al.* ([25]) and three nuclear shapes were tried, « Wood-Saxon », « square well » and « harmonic oscillator ». There is insufficient freedom to provide a solution.

There are various explanations.

1) Perhaps the formalism is incorrect and the nucleus has actually introduced a large phase. This is hard to accept since the ϱ behaves well.
2) The formalism is correct and *both* Daresbury experiments suffered a statistical fluctuation or systematic shift.
3) There are additional effects (2nd order mixing) to be considered which contribute to the phase of A_ω (nucleus).

If 3) fails to provide a quantitative solution then 1) and 2) can only be checked out by repeating the experiment on hydrogen (where the cross-section is considerably lower). Further to point 3) Horn ([5]) has calculated that 2nd order mass mixing

e.g.

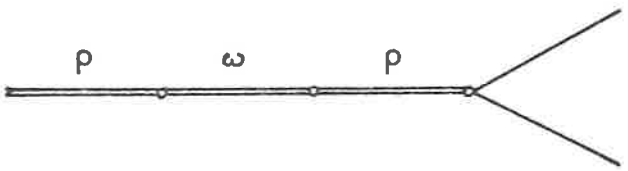

can contribute a phase $\sim 10°$ in the $\pi\pi$ case but $\sim 20°$ in the e^+e^- final state.

Also Sachs and Willemson ([4]) have pointed out that current mixing could contribute up to $\sim 9°$ to the phase in both $\pi^+\pi^-$ and e^+e^- production.

Taking these additional points into consideration we can conclude that the results of Alvensleben *et al.* for e^+e^- production are consistent with the phase of $A_\omega/A_\varrho \simeq 0°$ which can be interpreted together with all $\pi^+\pi^-$ photo-production experiments as indicating at most a small phase ($\sim 20°$) for δ. The results of Biggs *et al.* however are difficult to interpret in terms of a phase for production of ω on a single nucleon. The situation could be clarified (and perhaps altered) by a measurement of the reaction $\gamma p \to pe^+e^-$.

5. Postscript and branching ratios $\omega \to 2\pi$, $\rho \to 3\pi$.

Following a request at this conference, I have collated in Table 4, all the photoproduction and storage ring data for the $\pi\pi$ final state. This includes the data from Daresbury, SLAC, DESY and Orsay mentioned earlier and

TABLE 4.

Experiment		ξ	φ	
Daresbury [16]	γC	0.0097 ± 0.0008	$(104 \pm 5)°$	
SLAC-UCRL-TUFTS [18]	γp		$(93 \pm 22)°$	
DESY-MIT [17]	γp	0.0150 ± 0.0015	$(77 \pm 14)°$	includes systematic errors
	γC	0.0109 ± 0.0007	$(94 \pm 9)°$	
	γPb	0.0123 ± 0.0014	$(105 \pm 15)°$	
Orsay 1 [19]	e^+e^-	B.R. $= 3.3^{+2.8}_{-2.0}$ %	$(164 \pm 28)°$	
Rochester-Cornell [26]	γC	0.0118 ± 0.0012	$(93 \pm 5)°$	statistical errors only
	γAl	0.0133 ± 0.0020	$(81 \pm 6)°$	
	γPb	0.0144 ± 0.0020	$(81 \pm 7)°$	
Orsay 2 [27]	e^+e^-	B.R. $= 3.3^{+2.1}_{-1.6}$ %	$(89 \pm 15)°$	

also the new data presented at this conference from the Rochester-Cornell experiment [26] (presented by Behrends) and the Orsay experiment [27] (presented by Parrour).

The new data is of course preliminary but is in agreement with the existing results. In particular it should be noted that new results from Orsay [27] (Orsay 2 in the Table) comes from a different experiment and different group, compared to Orsay 1 [19].

In obtaining a value for the branching ratio B.R. ($\omega \to 2\pi$) using eq. (8), the various groups have used the value of ξ (and Γ_ρ where appropriate) obtained from their fits and usually a value of $\gamma_\omega^2/\gamma_\rho^2$ obtained by the same group in a different experiment. These values of $\gamma_\omega^2/\gamma_\rho^2$ have ranged from 7 to 11

and in obtaining an average value for the branching ratio it is better to average the values of ξ.

The weighted average of the values of ξ listed in Table 4 is

$$\xi = 0.0114 \pm 0.0004 .$$

The small error certainly does not reflect possible systematic effects. The question of systematic errors has been thoroughly discussed in ref. ([17]) and in any case the dominant error in calculating the branching ratio comes from $\gamma_\omega^2/\gamma_\rho^2$.

If we use $\Gamma_\rho = 125$ MeV and $\Gamma_\omega = 11.4$ MeV from the Particle Properties Tables ([29]) and $\gamma_\omega^2/\gamma_\rho^2 = (14.8 \pm 2.8)/(2.1 \pm 0.11)$ from the Orsay experiments ([30]), then

$$\Gamma_{\omega \to 2\pi} = 0.11 \pm 0.02 \text{ MeV}$$

$$\text{B. R. } (\omega \to 2\pi) = 0.1425 \frac{\gamma_\omega^2}{\gamma_\rho^2} = (1.00 \pm 0.20)\,\%$$

The formalism developed earlier is time reversal invariant, *i.e.* the off diagonal elements in the mass matrix were chosen to be equal.

This means that the partial width $\Gamma_{\rho \to 3\pi}$ can be written

$$\Gamma_{\rho \to 3\pi} = |\varepsilon|^2 \Gamma_{\omega \to 3\pi}$$

So

$$\text{B. R. } (\varrho \to 3\pi) = \xi^2 \left| \frac{A_\rho}{A_\omega} \right|^2 \frac{\Gamma_\omega}{\Gamma_\rho}$$

and this gives

$$\Gamma_{\rho \to 3\pi} = 0.01 \text{ MeV}$$

$$\text{B. R. } (\rho \to 3\pi) = 0.0084\,\% \qquad \text{which is rather small.}$$

Finally, the average value obtained for ξ leads to a value of

$$\delta = 1.79 \pm 0.18 \text{ MeV}.$$

REFERENCES

1) G. GOLDHABER, W. R. BUTLER, D. G. COYNE, B. H. HALL, J. N. MACNAUGHTON and G. H. TRILLING: *Phys. Rev. Lett.*, **23**, 1351 (1969).
2) S. L. GLASHOW: *Phys. Rev. Lett.*, **7**, 469 (1961); J. BERNSTEIN and G. FEINBERG: *Nuovo Cimento*, **25**, 1343 (1962); S. COLEMAN and H. J. SCHNITZER: *Phys. Rev.*, B **134**, 863 (1965); J. HARTE and R. G. SACHS: *Phys. Rev.*, B **135**, 459 (1965); H. R. QUINN and T. F. WALSH: *Nucl. Phys.*, **22** B, 637 (1970); S. L. GLASHOW: *Experimental Meson Spectroscopy*, ed. C. BALTAY and A. H. ROSENFELD (1970), p. 645.
3) A. S. GOLDHABER, G. C. FOX and C. QUIGG: *Phys. Lett.*, **30** B, 249 (1969).
4) R. G. SACHS and J. F. WILLEMSEN: *Phys. Rev.*, D **2**, 133 (1970).
5) D. HORN: *Phys. Rev.*, D **1**, 1421 (1970).
6) S. COLEMAN and S. L. GLASHOW: *Phys. Rev. Lett.*, **6**, 423 (1961).
7) R. GATTO: *Nuovo Cimento*, **28**, 658 (1963).
8) M. GOURDIN, L. STODOLSKY and F. M. RENARD: *Phys. Lett.*, 30 B, 347 (1969); F. M. RENARD: *Nucl. Phys.* B 15, 118 (1970); M. GOURDIN: Daresbury Study Weekend DNPL/R7 (1970), p. 95.
9) G. R. ALLCOCK: *Nucl. Phys.*, B **21**, 269 (1970).
10) G. GOLDHABER: UCRL 19850 and *Experimental Meson Spectroscopy*, ed. C. BALTAY and A. H. ROSENFELD (1970), p. 59.
11) M. ROOS: Daresbury Study Weekend DNPL/R7 (1970), p. 173.
12) W. C. JACKSON, M. BOUTING, I. J. BLOODWORTH, J. D. PRENTICE and T. S. YOON: *Bull. Am. Phys. Soc.*, **15**, 513 (1970).
13) S. HAGOPIAN, V. HAGOPIAN, E. BOGART and W. SELOVE: Florida State University preprint FSU HEP 70-8-1 (1970).
14) W. W. M. ALLISON, W. A. COOPER, T. FIELDS and D. S. RHINES: *Phys. Rev. Lett.* **24**, 618 (1970).
15) M. ABRAMOVICH, H. BLUMENFELD, F. BRUYANT, V. CHALOUPKA, S. U. CHUNG, J. DÍAZ F. MARTIN, L. MONTANET and J. RUBIO: *Nucl. Phys.*, B 20, 209 (1970).
16) P. J. BIGGS, R. W. CLIFFT, E. GABATHULER, P. KITCHING and R. E. RAND: *Phys. Rev. Lett.*, **24**, 1201 (1970).
17) H. ALVENSLEBEN, U. J. BECKER, W. BUSZA, M. CHEN, K. COHEN, R. T. EDWARDS, P. M. MANTSCH, R. MARSHALL, T. NASH, M. ROHDE, H. F. W. SADROZINSKI, G. H. SANDERS, H. SCHUBEL, S. C. C. TING and S. L. WU: DESY preprint 71.
18) K. C. MOFFEIT, H. H. BINGHAM, W. B. FRETTER, W. J. PODOLSKY, M. S. RABIN, A. H. ROSENFELD, R. WINDMOLDERS, J. BALLAM, G. B. CHADWICK, R. GEARHART, Z. G. T. GUIRAGOSSIAN, M. MENKE, J. J. MURRAY, P. SEYBOTH, A. SHAPIRA, C. K. SINCLAIR, I. O. SKILLICORN, G. WOLF and R. H. MILBURN: UCRL-19753 (1970).
19) J. E. AUGUSTIN, D. BENAKSAS, J. BUON, F. FULDA, V. GRACCO, J. HAISSINSKI. D. LALANNE, F. LAPLANCHE, J. LEFRANCOIS, P. LEHMANN, P. C. MARIN, J. PEREZ-Y-JORBA, F. RUMPF and E. SILVA: *Lettere al Nuovo Cimento*, **2**, 214 (1969).
20) P. J. BIGGS, D. W. BRABEN, R. W. CLIFFT, E. GABATHULER, P. KITCHING and R. E. RAND: *Phys. Rev. Lett.*, **24**, 1197 (1970).

21) H. ALVENSLEBEN, U. J. BECKER, M. CHEN, K. J. COHEN, R. T. EDWARDS, T. M. KNASEL, R. MARSHALL, D. J. QUINN, M. ROHDE, G. H. SANDERS, H. SCHUBEL and S. C. C. TING: *Phys. Rev. Lett.*, **25**, 1373 and 1377, (1970) and *Nucl Phys.*, B **25**, 333 and 342 (1971).
22) P. J. BIGGS, D. W. BRABEN, R. W. CLIFFT, E. GABATHULER and R. E. RAND: Daresbury preprint DNPL/P70 (1970).
23) G. GREENHUT and R. WEINSTEIN: *Phys. Lett.*, **33** B, 363 (1970); J. PUMPLIN and L. STODOLSKY: *Phys. Rev. Lett.*, **25** 970 (1970).
24) K. S. KÖLBIG and B. MARGOLIS: *Nucl. Phys.*, B **6**, 85 (1968) and R. MARSHALL: DESY Report 70/32 (1970) and Daresbury Study Weekend DNPL/R7 (1970) p. 29.
25) H. ALVENSLEBEN, U. J. BECKER, W. K. BERTRAM, M. CHEN, K. J. COHEN, T. M. KNASEL. R. MARSHALL, D. J. QUINN, M. ROHDE, G. H. SANDERS, H. SCHUBEL and S. C. C. TING: *Phys. Rev. Lett.*, **24**, 792 (1970).
26) H. J. BEHREND *et al.*: presented to this conference.
27) G. PARROUR *et al.*: presented to this conference.
28) P. DALPIAZ *et al.*: presented to this conference.
29) Particle properties tables, April 1971.
30) J. E. AUGUSTIN, D. BENAKSAS, J. C. BIZOT, J. BUON, B. DELCOURT, V. GRACCO, J. HAISSINSKI, J. JEANJEAN, D. LALANNE, F. LAPLANCHE, J. LEFRANCOIS, P. LEHMANN, P. MARIN, H. NGUYEN NGOC, J. PEREZ-Y-JORBA, F. RICHARD, F. RUMPF, E. SILVA. S. TAVENIER and D. TREILLE: *Phys. Lett.*, 28 B, 503 (1969).

ω-ρ interference in $\pi^+\pi^-$ decay mode (*)

D. BENAKSAS, G. COSME, B. JEAN-MARIE, S. JULLIAN, F. LAPLANCHE
J. LEFRANÇOIS, A. D. LIBERMAN, G. PARROUR, J. P. REPELLIN, G. SAUVAGE
Ecole Normale Supérieure, Laboratoire de l'Accélérateur Linéaire - Orsay

Abstract: A large solid angle detector has been used to observe two body events produced by electron-positron collision in the Orsay storage ring. From the $\pi^+\pi^-$ excitation curve in the ρ region we deduced the ω-ρ interference parameters.

$$A = (2.41 \pm 0.68)\%$$

corresponding to $\quad \Gamma^{1/2}_{\omega\pi\pi} = (0.63 \pm 0.18)\ \mathrm{MeV}^{1/2}$

$$\alpha = (89.1 \pm 15)^0$$

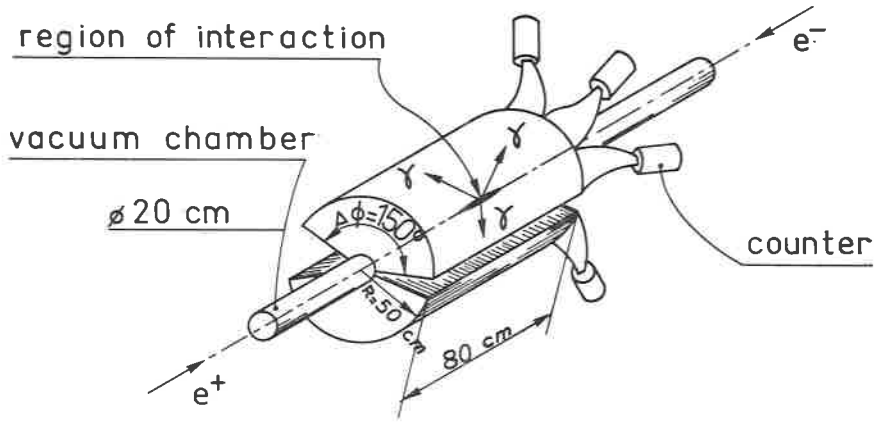

General view of the apparatus

Fig. 1

(*) Invited paper presented by G. Parrour.

This experiment has been done with the Orsay storage ring. We used a large solid angle detector ($0.6 \times 4\pi$) able to observe both charges particles and γ rays, in the decay of vector mesons produced by e^+e^- annihilations.

The apparatus is shown in Fig. 1. It has a symmetry of revolution around the vacuum chamber of the ring. The interaction region is very well defined in the radial direction ($\pm$ 1 mm) and spread over 15 cm in the longitudinal direction. The apparatus includes 2×16 optical spark chambers, the direction

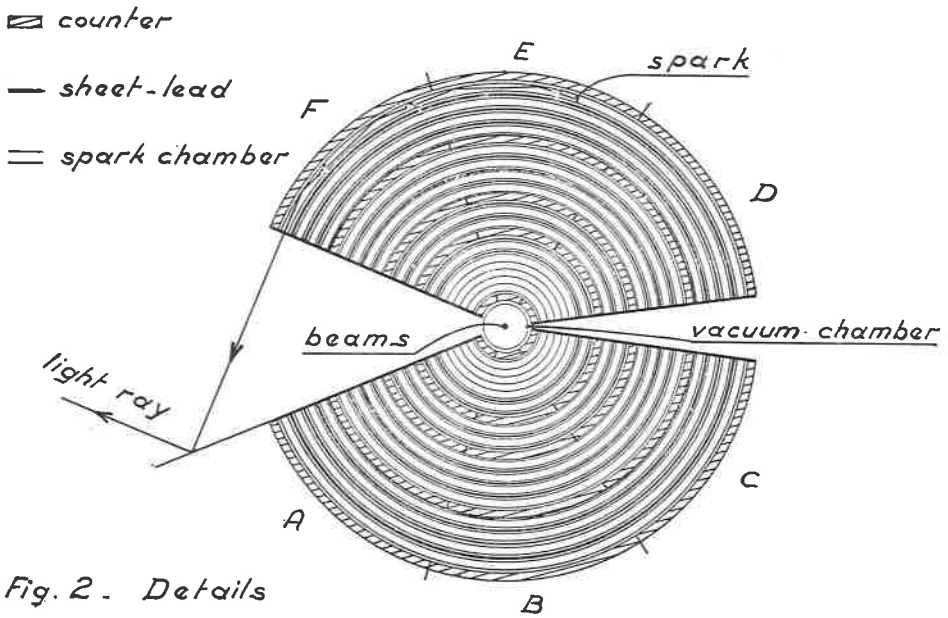

Fig. 2. Details of the arrangement of the chambers, counters, and sheets-lead.

Fig. 2. – Details of the arrangement of the chambers, counters, and sheets-lead.

of each particle is measured with the first five thin spark chambers. Electron and photon showers are observed in a sandwich made of 11 lead sheets, (0.5 radiation length each) interspaced between spark chambers, as shown in Fig. 2. Transverse and longitudinal views are photographed through an optical system by a single camera. A lead shielding above the apparatus stops all the particles coming from the beams. Counters covering this shielding are used to veto cosmic rays (anticoincidence efficiency is 99.3%). The

chambers are triggered by a logic pulse obtained with a suitable combination of the pulses given by the 2×15 scintillation counters.
For Bhabha events electron showers are very well developed. So the signature of $\pi^+\pi^-$ events is unambigous, less than 4 events of the 1800 $\pi^+\pi^-$ and 1700 e^+e^- events were not classified as obvious $\pi\pi$ or ee events at first sight.

In each photograph we also record the signals of the counters and the trigger delay with regard to the bunches. Rejection of cosmic rays has been checked in two different ways: by trigger delay and by distance from the beam. Both methods give convergent results, to better than 1%, the average corrections being 10%.

We took data at 9 energies in the ρ and ω region, 1800 $\pi^+\pi^-$ events have been taken into account. The normalization was obtained from wide angle Bhabha scattering.

The π nucleon interaction corrections are determined from the interaction actually observed in the apparatus; they are classified into 3 categories: stops, stars and scattered π with an angle greater than 12.5°, we consider the sum of these interactions to fit a nuclear cross section written as:

$$\sigma = \pi R_0^2 A^{2\alpha}$$

A: material atomic number (counters or lead);
and we find:

$$R_0 = (1.400 \pm 0.02)\ \text{fm}\,, \qquad \alpha = 0.343\ {}^{+0.008}_{-0.005}$$

In very good agreement with the expected values:

$$R_0 = 1.42, \quad \alpha = 0.333$$

Therefore, the trigger correction due to the fact that the number of counters triggered falls below the required threshold, is (1.5 ± 0.04)%, and the interaction correction coming from the stopped or scattered π in the vacuum chamber walls or in the first counter, is (8.5 ± 1.5)%.

The angular cuts are the following: in the transverse view, the $\Delta\varphi$ angle

between the two tracks has to be less than 4.5°, in the longitudinal view the $\Delta\theta$ angle has to be less than 10° for $\pi^+\pi^-$ and 15° for e^+e^- events. Moreover an event is accepted if the angle between the beam and the direction of

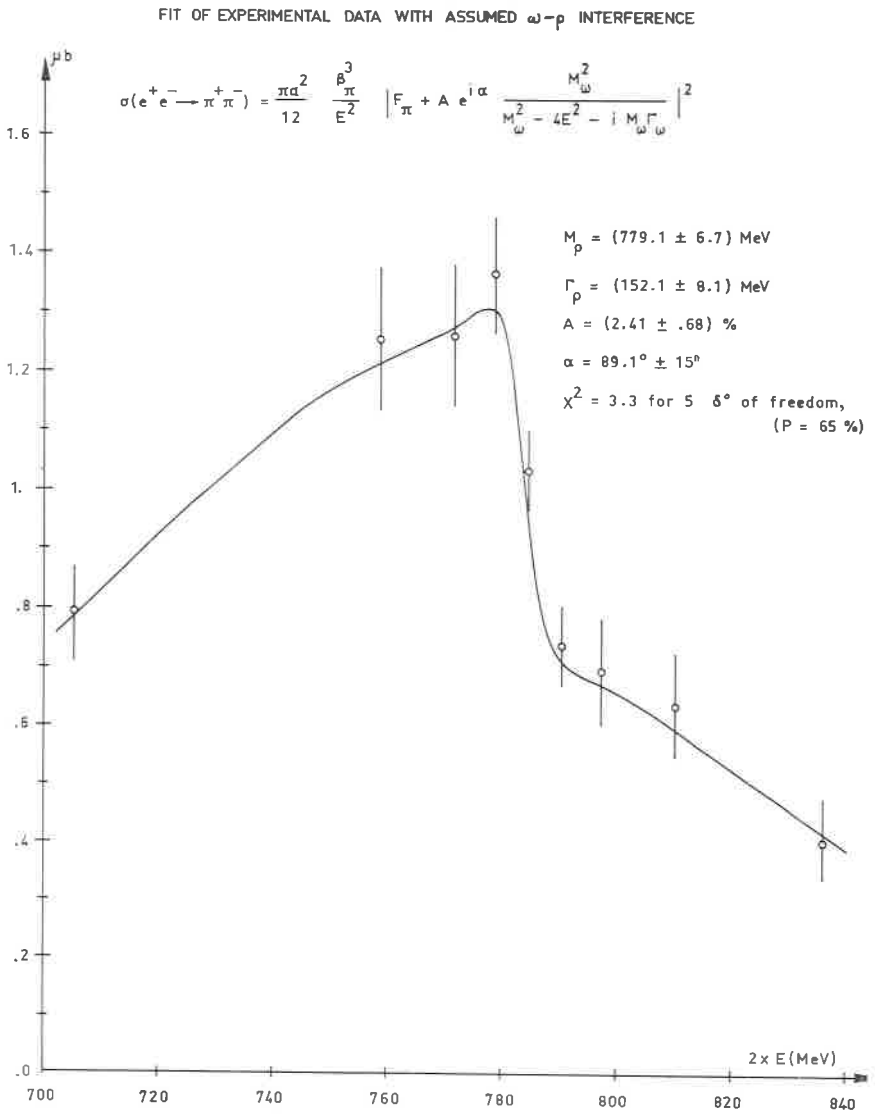

Fig. 3. – Fit of experimental data with assumed ω-ρ interference.

the tracks is greater than 52.5°. In this solid angle the tracks can cross all the spark chambers.

The radiative corrections depend on the parametrization of the cross section and on the angular cuts; their determinations are achieved by fitting the experimental data by the theoretical cross section and the probability of photon-emission convolution product.

$$\sigma_{\text{exp}} = \sigma_{\text{th}} * \varrho(k)$$

where:

$$\varrho(k)\mathrm{d}k = \beta / E^{\beta} k^{\beta-1} \mathrm{d}k$$

with:

$$\beta = 4\alpha/\pi \log(2E/\mathrm{m}_e - \tfrac{1}{2})$$

and:

$$\sigma_{\text{th}} = \frac{\pi\alpha^2\beta_\pi^3}{12E^2} \left| F_\pi + A \exp[i\alpha] \frac{M_\omega^2}{M_\omega^2 - 4E^2 - iM_\omega\Gamma_\omega} \right|^2$$

where:

$$F_\pi = \frac{M_\varrho^2(1 + \delta\Gamma_\varrho/M_\varrho)}{M_\varrho^2 - 4E^2 - iM_\varrho\Gamma_\varrho(P/P_0)^3 M_\varrho/2E}$$

with: $\delta = 0.48$, P: $\pi^\pm$ momentum, P^0: $\pi^\pm$ momentum at the $M_\varrho/2$ energy.

F_π is the simplified Gounaris-Sakurai pion form factor good enough around the ϱ peak.

The Fig. 3 shows the fit with M_ϱ, Γ_ϱ, A, α as free parameters, the best fit gives:

$$\chi^2 = 3.3 \text{ for } 5 \text{ deg. of freedom } (P = 65\%)$$

$$M_\varrho = (779.1 \pm 6.7) \text{ MeV}$$

$$\Gamma_\varrho = (152.1 \pm 8.1) \text{ MeV}$$

$$A = (2.41 \pm 0.68)\%$$

$$\alpha = 89.1° \pm 15°$$

α has also a systematic error of $\simeq 1°$ coming from uncertainty in the ω mass.

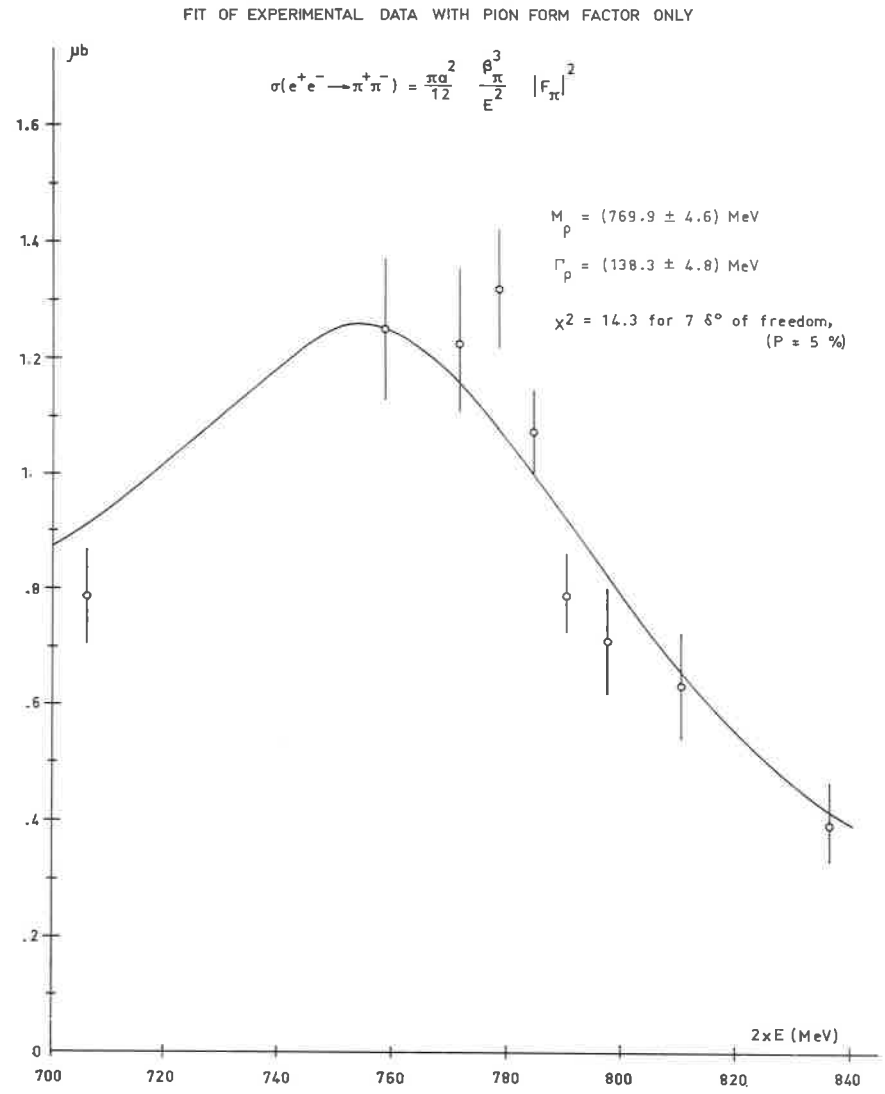

Fig. 4. – Fit of experimental data with pion form factor only.

A fit leaving the δ parameter free gives similar results:

$$\chi^2 = 2.53 \text{ for 4 degrees of freedom}$$

$$\delta = 0.34 \pm 0.6$$

$$M_\varrho = (778 \pm 7.2) \text{ MeV}$$

$$\Gamma_\varrho = (146.6 \pm 24) \text{ MeV}$$

$$A = (2.35 \pm 0.73)\%$$

$$\alpha = (89.2 \pm 15)^\circ$$

Figure 4 shows a fit with $A = 0$ (no interference), we obtain:
For δ fixed:

$$\chi^2 = 14.3 \text{ for 7 degrees of freedom } (P = 5\%)$$

$$M_\varrho = (769.9 \pm 4.6) \text{ MeV}$$

$$\Gamma_\varrho = (138.3 \pm 4.8) \text{ MeV}$$

and for δ free:

$$\chi^2 = 10.31 \text{ for 6 degrees of freedom } (P = 10\%)$$

$$\delta = -0.65 \pm 0.58$$

$$m_\varrho = 766.3 \pm 3.9$$

$$\Gamma_\varrho = (110 \pm 11.7) \text{ MeV}.$$

Our results were obtained from the whole of the data in the ρ, ω region.

Moreover, as far as the ω is concerned, preliminary results have been obtained and used, namely, M_ω and Γ_ω: The values of the ω-ρ interference parameters we observed depend only very slightly on M_ω and Γ_ω.

ω-ρ interference in the two pion decay mode in diffractive photoproduction from complex nuclei (*)

H. J. BEHREND, C. K. LEE, F. LOBKOWICZ, and E. H. THORNDIKE
University of Rochester, N. Y.

M. E. NORDBERG, Jr.
Cornell University,

A. A. WEHMANN
NAL

The interference of ρ_0 and ω in the 2π decay mode was observed in diffractive photoproduction off complex nuclei. The resulting branching ratio $\omega \to 2\pi/\omega \to 3\pi$ is $2.8 \pm \pm 0.6\%$, the difference in the decay phases $(\omega \to 2\pi) - (\rho \to 2\pi)$ is $63 \pm 16\%$.

In experiments observing the G-parity violating decay mode $\omega \to 2\pi$ one would like to extract the branching ratio $\omega \to 2\pi/\omega \to 3\pi$ and the relative phase of the $\rho \to 2\pi$ and $\omega \to 2\pi$ decays from the ρ-ω interference pattern. Therefore it is necessary to know the relative magnitude, relative phase, and degree of coherence of the production amplitudes. For strongly produced vector mesons, there is poor information on these quantities available except for the relative production cross sections. The production mechanisms for photoproduction of ρ^0 and ω mesons from complex nuclei are believed to be well understood ([1,2]) and are favorable for interference experiments, because the degree of coherence is high. However, the production cross section for

(*) Invited paper presented by H.J. Behrend.

photoproduction of ρ^0-mesons is roughly a factor of 10 higher than for ω-mesons. A possible interference pattern is therefore difficult to detect and only during the last year a small number of experiments on this subject were published ([3,4,5]).

To date there exists one other interference experiment (2π-channel) in photoproduction on nuclei (Briggs *et al.* [4]) $\gamma + C = \pi^+\pi^- + C$, at 4 GeV). Our experiment was performed at a higher energy and with three different target nuclei.

1. Experimental approach.

We have studied the process $\gamma A \to \pi^+\pi^- A$, (A = carbon, aluminum, and lead), in the $\pi^+\pi^-$ mass region of the ρ and ω. The experimental setup is shown in Fig. 1. A 9.3 GeV bremsstrahlung beam passes through a target, located

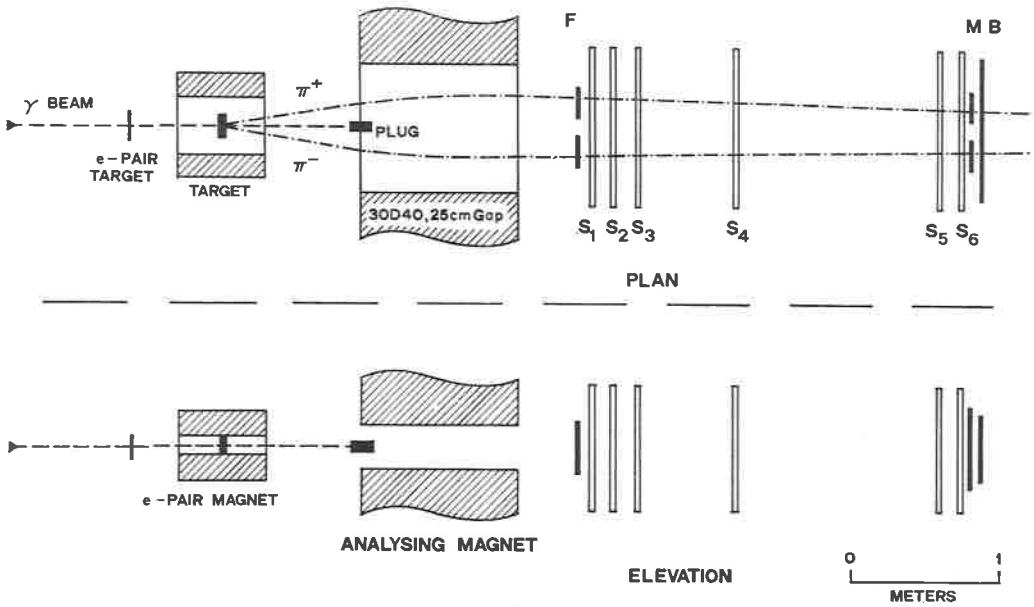

Fig. 1. – A schematic view of the apparatus. *S* are spark chambers; *F*, *M*, *B* are scintillation counters.

in the center of a small magnet (normally off), and then buries itself in a hevimet and lead plug. Pion pairs produced in the target are deflected by

the second, large magnet, and then pass through a system of trigger counters and wire spark chambers. The particle trajectory after the magnet, along with the point-like target volume, suffice to determine the particle's vector momentum, and hence the invariant mass of the $\pi\pi$ pair.

The absolute mass scale was determined by floating wire measurements with an accuracy of $\pm\frac{1}{4}\%$. The geometric detection efficiency was calculated by Monte Carlo studies. Normally a mass range of 100 MeV around the ω mass was covered in one magnet setting. To extend the mass range, a small amount of data was taken with larger trigger counters and reduced magnetic fields. The mass resolution was determined by Monte Carlo calculations, adjusted slightly on the basis of the electron transverse momentum distribution (see below); r.m.s. widths were 5.05 MeV for carbon, 4.85 MeV for aluminum, and 5.22 MeV for lead, and are believed accurate to $\pm 6\%$.

The apparatus was tested with electron-positron pairs, forward produced in a target just upstream of the small magnet. With the small magnet turned on, these particles acquire a constant transverse momentum.

Reconstruction of the distribution in transverse momentum showed a r.m.s. width of 3.11 MeV compared to 2.87 MeV predicted by the calculations. This distribution is closely related to the mass resolution, and the agreement provides a direct confirmation of the mass resolution. Several other tests were performed in a similar way with the small magnet, which could be rotated around the beam line. They proved that the apparatus is free from distortions.

The reconstructed π-pair events were subjected to cuts on dipion energy (between 7.0 and 9.15 GeV), production angle (in the first $1/e$ of the diffraction peak), and decay angle (symmetric decays, $|\cos\theta_{DK}| < 0.2$). They were then corrected for apparatus detection efficiency, and extrapolated to zero momentum transfer.

The mass spectra for Carbon, Aluminum, and Lead are shown in Fig. 2. The ρ^0-ω interference shows up very clearly as a sharp drop near 780 MeV.

2. Fitting procedure.

The following expression was used to fit the mass curves:

$$\frac{d\sigma}{dm} = Km\Gamma_\rho(m)m_\rho \left| \frac{(m_\rho/m)^2}{m^2 - m_\rho^2 + im_\rho\Gamma_\rho(m)} + \right.$$

$$\left. + \frac{\xi_A \exp[i\varphi_A]}{m^2 - m_\omega^2 + im_\omega\Gamma_\omega} \right|^2 + BG(m)\,. \qquad (1)$$

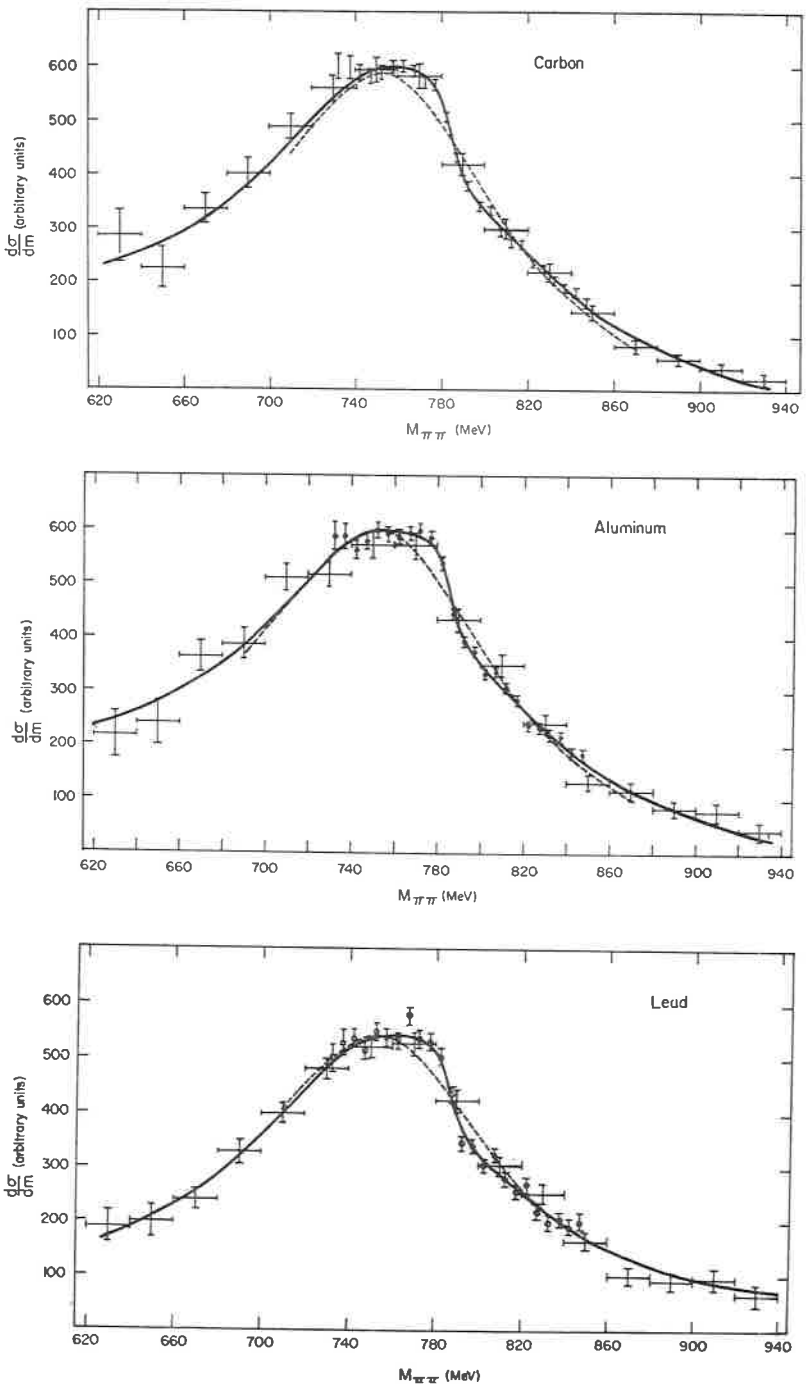

Fig. 2. – The measured mass spectra, corrected for detection efficiency.

The expression is a coherent sum of Ross-Stodolsky-modified *p*-wave Breit-Wigner for the ρ^0, and a simple Breit-Wigner for the ω. An incoherent polynomial background *BG(m)* is also included.

Aside from the background term, which is quite small, there are two parameters, ξ and φ, which give, respectively, the relative magnitudes and relative phases of the ω and ρ^0 terms. Independent of any models:

$$\xi_A^2 = \frac{\sigma_{\gamma A \to \omega A}}{\sigma_{\gamma A \to \rho_0 A}} \cdot \frac{\Gamma_{\omega \to 2\pi}}{\Gamma_{\rho^0 \to 2\pi}} \cdot \frac{m_\rho}{m_\omega} \tag{2}$$

and with the vector dominance assumption:

$$\varphi_A = \Delta\varphi\ (\gamma\text{-V coupling}) + \Delta\varphi(\text{VA} \to \text{VA scattering}) + \Delta\varphi(\text{V} \to \pi^+\pi^-)\,, \tag{3}$$

where all $\Delta\varphi's$ are phase differences between $V = \omega$ and $V = \rho^0$, for the process indicated in parantheses.

The main conclusions from the fitting procedures are the following:

1) The results are insensitive to variations in data cuts.
2) The ω mass as fitted agrees within 1 MeV with the accepted value, for subsequent studies it was held fixed.
3) Leaving the ρ-mass free or fixed to 770 MeV has little effect on the result of the experiment.
4) Letting Γ_ρ free we find $\Gamma_\rho = (160 \pm 15)$ MeV. The results are independent to the precise value of Γ_ρ (then held fixed at 145 MeV),
5) Variation of 10% in mass resolution cause 10% variation in ξ^2. Thus, accurate knowledge of the resolution is important.

Our results are given in Table I. The mass displays a small A-dependence, which has little effect on ξ or φ. Both sets of fits are statistically acceptable.

TABLE I. – *Results of two sets of fits, either fixing* m_ρ *at* 770 MeV, *or leaving it as an adjustable parameter. Errors are statistical.*

	Carbon	Aluminum	Lead
m_ρ	770 input	770 input	770 input
ξ	0.0134±0.0012	0.0135±0.0016	0.0145±0.0019
φ	94.7 ±4.5°	79.4 ±5.2°	77.8 ±6.0°
m_ρ(MeV)	767.6 ±1.4	771.1 ±1.8	771.8 ±1.7
ξ	0.0124±0.0012	0.0138±0.0018	0.0151±0.0020
φ	92.4 ±5.0°	80.3 ±5.6°	81.2 ±6.6°

3. Results.

Within statistical accuracy, ξ_A is independent of A. Using eq. (2), and the results of our previous experiments, we find $\Gamma_\omega \to \pi^+\pi^-/\Gamma_\omega \to \pi^+\pi^-\pi^0 = (2.8\pm0.6)\%$ as average for the different nuclei. Our result is consistent with, and more accurate than, all other results of branching ratios ([5,6]) except those of the Daresbury group ([4]). Part of the discrepancy is removed if their data is re-analysed using the cross section ratio 12 from our previous experiments ([1,2]), rather than their value 7, determined less directly from a leptonic decay interference experiment ([3]).

To extract the phase difference of the $V \to 2\pi$ decay amplitudes, it is necessary to know the phase difference in V-nucleus scattering and the phase difference in γ-V coupling. The latter is taken as 11° ([7]), the former we obtain from an optical model calculation ([1,2]) using ([8]) $\mathrm{tg}^{-1}\alpha_\omega - \mathrm{tg}^{-1}\alpha_\rho = -(17\pm17)°$ $\alpha_\rho = -0.24$, $\sigma_{\omega N} = (25.3\pm7.8)$ mb, $\sigma_{\rho N} = 27$ mb. These lead to a value of $(63\pm16)°$ for $\varphi(\omega \to \pi^+\pi^-) - \varphi(\rho^0 \to \pi^+\pi^-)$ ([9]). This result disagrees with the Orsay ([6]) value $(153\pm28)°$, and with a calculation by Gourdin ([7]) $(101\pm6)°$.

REFERENCES

1) H.-J. Behrend *et al.*: *Phys. Rev. Lett.*, **24**, 336 (1970); H. Alvensleben *et al.*: *Phys. Rev. Lett.*, **24**, 786 (1970).
2) H.-J. Behrend *et al.*: *Phys. Rev. Lett.*, **24**, 1246 (1970).
3) P. J. Biggs *et al.*: *Phys. Rev. Lett.*, **24**, 1197 (1970); H. Alvensleben *et al.*: *Phys. Rev. Lett.*, **25**, 1373 (1970).
4) P. J. Biggs *et al.*: *Phys. Rev. Lett.*, **24**, 1201 (1970).
5) K. C. Moffeit *et al.*: UCRL-19753 (unpublished).
6) W. W. M. Allison *et al.*: *Phys. Rev. Lett.*, **24**, 618 (1970); M. Abramovich *et al.*: Nucl. *Phys.*, B **20**, 209 (1970); J. E. Augustin *et al.*: *Lett. Nuovo Cimento*, **2**, 214 (1969); R. Bizzarri *et al.*: *Phys. Rev. Lett.*, **25**, 1385 (1970).
7) M. Gourdin *et al.*: *Phys. Lett.*, **30** B, 347 (1969); M. Gourdin: *Vector meson production and omega-rho interference* in *Proceedings of the Daresbury Study Weekend*, 12-14 June 1970, edited by A. Donnachie and E. Gabathuler (Daresbury Nuclear Physics Laboratory, Daresbury, England, 1970).
8) H.-J. Behrend *et al.*: submitted to *Phys. Rev. Lett.*
9) Here the error for the uncertainty in the ω mass in included.

ω-ρ interference in π-p interactions at 1.67 GeV/c (*)

M. Basile, D. Bollini, R. A. Bowen, P. Dalpiaz, P. L. Frabetti
T. Massam, F. Navach, F. L. Navarria, M. A. Schneegans and A. Zichichi

CERN - Geneva
Istituto Nazionale di Fisica Nucleare - Sezione di Bologna
Istituto di Fisica dell'Università - Bologna
Centre National de la Recherche Scientifique - Strasbourg

1. Introduction.

The possibility of ω-ρ mixing by electromagnetic interactions was first suggested by Glashow [1] in 1961, who pointed out that this effect could be important owing to the near degeneracy of ω and ρ masses.

Data on (ω-ρ) mixing have been obtained in colliding beams, photoproduction, and strong interaction processes [2]. The colliding beam data obtained at ACO [3] do not agree with the photoproduction results [4] and with the present theoretical expectation [5].

The purpose of this paper is to report on a study of the reaction

$$\pi^- + p \to n + \text{missing mass} \quad (1)$$
$$\qquad\qquad\quad \lfloor\!\to \pi^+\pi^-$$

performed at CERN with the Bologna-CERN neutron missing-mass spectrometer [6] coupled to a system of optical spark chambers [7] for the detection (heavy plates) and the reconstruction (thin plates) of the pions.

(*) Invited paper, presented by P. Dalpiaz.

Reaction (1) has been studied by Hagopian *et al.* ([8]) at 2.3 GeV/c; they have observed a narrow spike around the ω mass value, 4 standard deviations out of the ρ shape. For a discussion of these and other experimental results in strong production reactions, we refer to the review paper of Roos ([9]).

The data presented here were collected during the $\omega \to e^+e^-$ experiment ([10]), π-π events being accepted in the trigger as background ([7]) of the main experiment.

The missing mass to the neutron in reaction (1) was determined by the simultaneous measurements of the time-of-flight and of the emission angle of the neutron ([6]). As mentioned above thin plates optical spark chambers were used to determine the directions of the charged decay products of the missing mass in reaction (1). The incident pion momentum was 1.67 GeV/c, with $\Delta p/p = \pm 0.5\,\%$. The missing-mass resolution in the momentum transfer interval $(0.08 \div 0.42)$ $(\mathrm{GeV/c})^2$ was evaluated to be ± 8 MeV and it was checked by η and ω production in reaction (1).

2. Data analysis and results.

The pictures were scanned and measured automatically at CERN with the CRT flying-spot digitizer Luciole 66 ([11]).

The selection of the π-π events from the background was done in two steps:

i) by requiring that the acoplanarity angle between the plane of the two reconstructed tracks and the direction of the missing particle, given by the neutron detectors, be zero within experimental errors;

ii) by requiring the correlation (within experimental errors) between the angles of the two pions and the direction of the missing particle, for a two-body decay with mass given by the neutron missing mass.

Figure 1 shows the distribution of the acoplanarity angle (in absolute value) for all events without any selection. A peak at 0°, $\sim 1°$ wide, is clearly present in the spectrum superimposed on a $\sim 30\,\%$ background due to multipion production and accidental triggers. The application of the selection criteria (i) and (ii) allows the determination of the shape and the absolute level of the background. This is given by the solid line in Fig. 1.

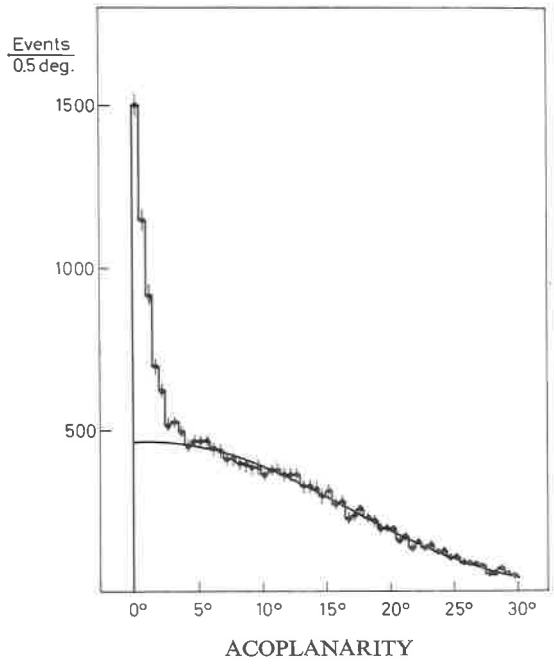

Fig. 1. – Distribution of the absolute value of the acoplanarity angle between the plane of the reconstructed tracks and the direction of the missing mass. The solid line shows the distribution of the rejected events.

Figure 2 shows the missing-mass distribution for 2874 events selected as two-body decays in the four-momentum transfer range $0.08 < t < 0.42$ $(\mathrm{GeV/c})^2$. An enhancement having a width compatible with our resolution is observed around the ω mass value, superimposed on the ρ-meson peak. The tails of the ρ peak are depressed because of the acceptance of the neutron spectrometer and of the spark chamber system. The missing-mass spectrum of Fig. 2 corrected for the acceptance of the apparatus is show in Figs. 3*a*, 3*b*. It should be noticed that while the total number of events is the same as in the experiment of Hagopian *et al.* ([8]), our statistics are double in the ω region due to our acceptance conditions.

The parametrization of the ρ-ω interference is done using two Breit-Wigner resonances for the ρ and for the ω, with a relative phase (φ):

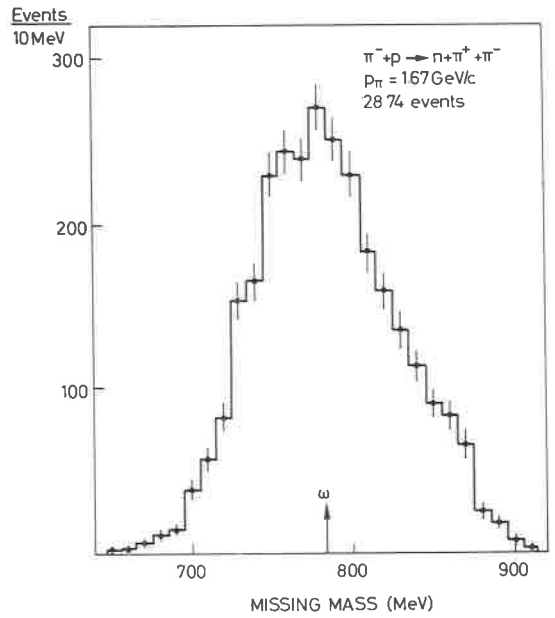

Fig. 2. – Missing-mass distribution of the selected two-body events.

$$\frac{\mathrm{d}N}{\mathrm{d}M} = A_\omega^2 |BW_\omega(m)|^2 + A_\rho^2 |BW_\rho(m)|^2 + \\ + 2\alpha A_\rho A_\omega \,\mathrm{Re}\{\exp[i\varphi] BW_\omega(m) BW_\rho^*(m)\} + BKD(m)\,, \qquad (2)$$

where

$$BW_x(m) = \frac{(2mm_x \Gamma_x(m)/\pi)^{1/2}}{(m_x^2 - m^2) - im_x \Gamma_x(m)}$$

is the Breit-Wigner formula, m is the missing mass, x stands either for ω or ρ index, A_x are the amplitudes, m_x the masses, and $\Gamma_x(m)$ (*) the widths; $0 \leqslant \alpha \leqslant 1$ is the coherence factor, and BKD is a slowly varying function to account for non-resonant dipion production.

To determine the ρ parameters and BKD(m), the spectrum of Fig. 3 has been fitted outside the ω mass region using eq. (2) with $A_\omega = 0$. The

(*) We have used $\Gamma_x(m) = \Gamma_0 (p/p_0)^3 (m_x/m)$, where p is the π momentum in the resonance centre-of-mass, and p_0 corresponds to its value for $m = m_x$ [12].

fit yields (*) $m_\rho = (770 \pm 5)$ MeV and $\Gamma_\rho = (123 \pm 8)$ MeV with about 10% BKD(m) due to non-resonant dipion production.

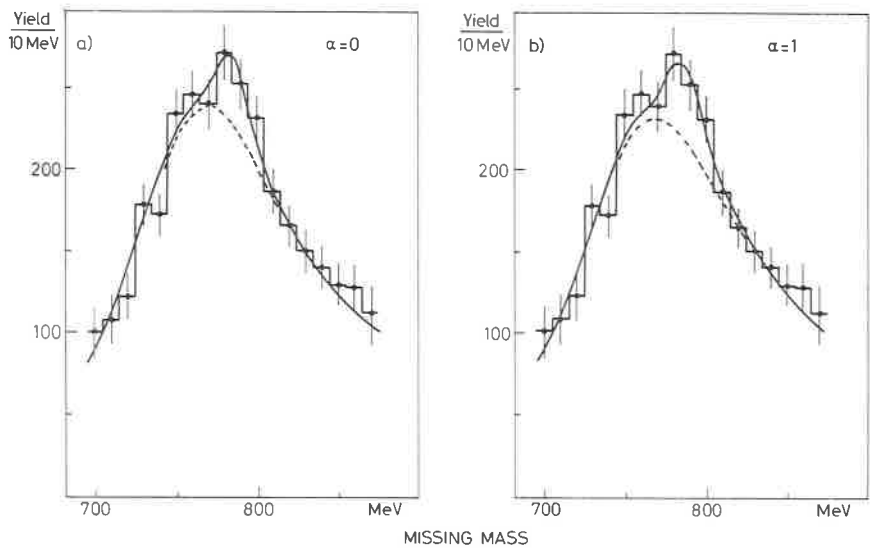

Fig. 3. – Missing-mass distribution of the selected two-body events normalized for the acceptance. The dashed line represents the contribution of BW_ρ in the fit. The solid line represents the fit with: *a*) $\alpha = 0$, *b*) $\alpha = 1$.

As it is impossible to determine both α and φ from the present data because of the limited statistics and resolution, the ω-ρ interference analysis needs some hypothesis on α. We have fitted eq. (2) to the whole spectrum with $\alpha = 0$ [no interference (Fig. 3*a*)], and with $\alpha = 1$ [complete coherence (Fig. 3*b*)].

The experimental mass resolution ($\pm$ 8 MeV) has been folded in these fits, and the ρ parameters and the BKD(m) have been kept fixed at the values quoted above. The acceptances for the processes $\rho \to \pi\pi$, $\omega \to \pi\pi$ have been calculated by Monte Carlo methods, taking into account the produc-

(*) The absolute value of the incident beam momentum was calibrated observing the production of the η meson in the reaction $\pi^- + p \to \eta + n$ at 0.8 GeV/c.

tion and decay angular distributions of incoherently produced ρ and ω mesons ([13,14]).

The amount of $\omega \to \pi^+\pi^-\pi^0$ simulating $\omega \to \pi^+\pi^-$ was evaluated and was found to be negligible. Therefore, using the known cross-sections for ρ production ([13]) in reaction (1) and for ω production ([13,14]) in the reaction $\pi^+ + n \to \pi^+\pi^-\pi^0 + p$, the following results are obtained:

	α	A_ω^2	A_ϱ^2	φ	DF	χ^2	$BR = \frac{\Gamma(\omega \to \pi^+\pi^-)}{\Gamma(\omega \to \text{total})}$
ρ	0	0	4391 ± 96	—	16	19.2	—
ρ + 3	0	128 ± 42	4173 ± 139	—	15	10.8	$(6.1 \pm 2.0)\%$
	1	12.3 ± 4.5	4072 ± 147	$-4° \pm 20°$	14	10.0	$(0.6 \pm 0.2)\%$

3. Conclusion.

The value of χ^2 obtained assuming that only the ρ -meson is present in the mass spectrum is 19.2; this value should be compared with either 10.8 or 10.0, which are the χ^2 values obtained assuming either the direct $\omega \to 2\pi$ decay, or the contructive $(\omega - \rho)$ interference being present in the mass spectrum. The probability that there is no ω, either directly or via $(\omega - \rho)$ interference going into 2π, is not greater than 1%.

If we use as an extra condition the value of BR measured in photoproduction[4] [ie. $BR = (0.80^{+0.28}_{-0.22})\%$], then our data can be interpreted as good evidence for strong constructive $(\omega - \rho)$ interferenc in the reaction:

$$\pi^- + p \to [(\rho,\omega) \to 2\pi] + n,$$

being φ consistent with zero, in good agreement with the theoretical model of A. S, Goldhaber, G. C. Fox and C. Quigg[5].

REFERENCES

1) S. GLASHOW: *Phys. Rev. Lett.*, **7**, 469 (1961).
2) For a review of the present status see:
Vector Meson Production and Omega-Rho Interference:
proceedings of the Daresbury Study Weekend, Daresbury 12-14 June 1970.
3) J. E. AUGUSTIN, D. BENAKSAS, J. BUON, F. FULDA, V. GRACCO, J. HAISSINSKY, D. LALANNE, F. LAPLANCHE, J. LEFRANÇOIS, P. LEHMANN, P. C. MARIN, J. PEREZ Y JORBA, F. RUMPF and E. SILVA: *Lett. Nuovo Cimento*, **2**, 214 (1969).
4) P. J. BIGGS, R. W. CLIFFT, E. GABATHULER, P. KITCHING and R. E. RAND: *Phys. Rev. Lett.*, **24**, 1201 (1970).
5) A. S. GOLDHABER, G. C. FOX and C. QUIGG: *Phys. Lett.*, **30** B, 249 (1969).
6) D. BOLLINI, A. BUHLER-BROGLIN, P. DALPIAZ, T. MASSAM, F. NAVACH, F. L. NAVARRIA, M. A. SCHNEEGANS, F. ZETTI and A. ZICHICHI: *Nuovo Cimento*, **61** A, 125 (1969).
7) M. BASILE, D. BOLLINI, A. BUHLER-BROGLIN, P. DALPIAZ, P. L. FRABETTI, T. MASSAM, F. NAVACH, F. L. NAVARRIA, M. A. SCHNEEGANS and A. ZICHICHI: *A large electromagnetic shower detector with high rejection power against pions*, in *Nucl. Instr. Methods*, to be published. See also: D. BOLLINI, A. BUHLER-BROGLIN, P. DALPIAZ, T. MASSAM, F. NAVACH, F. L. NAVARRIA, M. A. SCHNEEGANS and A. ZICHICHI: *Revue de Physique Appliquée*, **4**, 108 (1969).
8) S. HAGOPIAN, V. HAGOPIAN, E. BOGART and W. SELOVE: *Phys. Rev. Lett.*, **25**, 1050 (1970).
9) M. ROOS: *Proceedings of the Daresbury Study Weekend*, Daresbury, 12-14 June 1970, p. 173.
10) D. BOLLINI, A. BUHLER-BROGLIN, P. DALPIAZ, T. MASSAM, F. NAVACH, F. L. NAVARRIA, M. A. SCHNEEGANS and A. ZICHICHI: *Nuovo Cimento*, **57** A, 404 (1968), more details of the apparatus and of the electronic logic can be found in: *Nuovo Cimento*, **56** A, 1173 (1968).
11) T. F. ANDERSSON, P. M. BLACKALL, J. DAUB, A. E. HEAD, M. B. METCALF and V. J. WEIGHTS: *The measurement of spark chamber film at CERN using Luciole*, in *Proc. Int. Conf. on Programming for Flying-Spot Devices*, Munich (1967), p. 87.
12) J. D. JACKSON: *Nuovo Cimento*, **34**, 1644 (1964).
13) T. C. BACON, W. J. FICKINGER, D. G. HILL, M. W. K. HOPKINS, D. K. ROBINSON and E. O. SALANT: *Phys. Rev.*, **157**, 1263 (1967).
14) J. S. DANBURG, M. A. ABOLINS, D. I. DAHL, D. W. DAVIES, P. L. HOCH, J. KIRZ, D. H. MILLER and R. K. RADER: *Phys. Rev.*, **2** D, 2564 (1970).

SESSION I-D

Wednesday, 14 April 1971

A_1, B, and Q-region - The spin 1^+ states

Chairman: R. A. SALMERON

Secretaries: P. MAZZANTI
A. BRODY

The physics of the Q-region of $K\pi\pi$ mass (*)

M. G. BOWLER
Nuclear Physics Laboratory, University of Oxford - Oxford

1. Introduction.

I was a little perturbed to find myself listed as the only introductory speaker for this session on 1^+ states, for my invitation from the organising committee asked me to speak only on the Q region of $K\pi\pi$ mass. So apart from remarking that the A1 seems to get curiouser and curiouser, and I am glad I do not have to talk about it, I shall proceed directly to the Q.

For the benefit of those of you who are not only Meson Spectroscopists, but more specifically non-strange Meson Spectroscopists, the phenomenon known as the Q is a massive, steepsided, square topped enhancement appearing in the $K\pi\pi$ mass spectrum in a four particle final state

$$K^{\pm}p \rightarrow (K\pi\pi)^{\pm}p$$

which has for the most part been studied in $K^{\pm}$ interactions above 5 GeV/c (1). Figure 1 shows a typical $K\pi\pi$ mass spectrum—it is taken from the work of the Birmingham-Glasgow-Oxford 10 GeV/c K^+ collaboration (2). This figure shows all the salient features of the Q— the steep rise around a mass of 1.2 GeV/c^2, the rapid fall just beyond 1.4 GeV/c^2 and the flat top. In addition the Q appears to be split in this data, as in several other experiments, but the splitting is not really statistically significant, in the sense that if an evil minded theoretician produced a model that fitted the steep sides well and had a flat top, with no dip, then such a model would fit the data admirably.

(*) Introductory talk

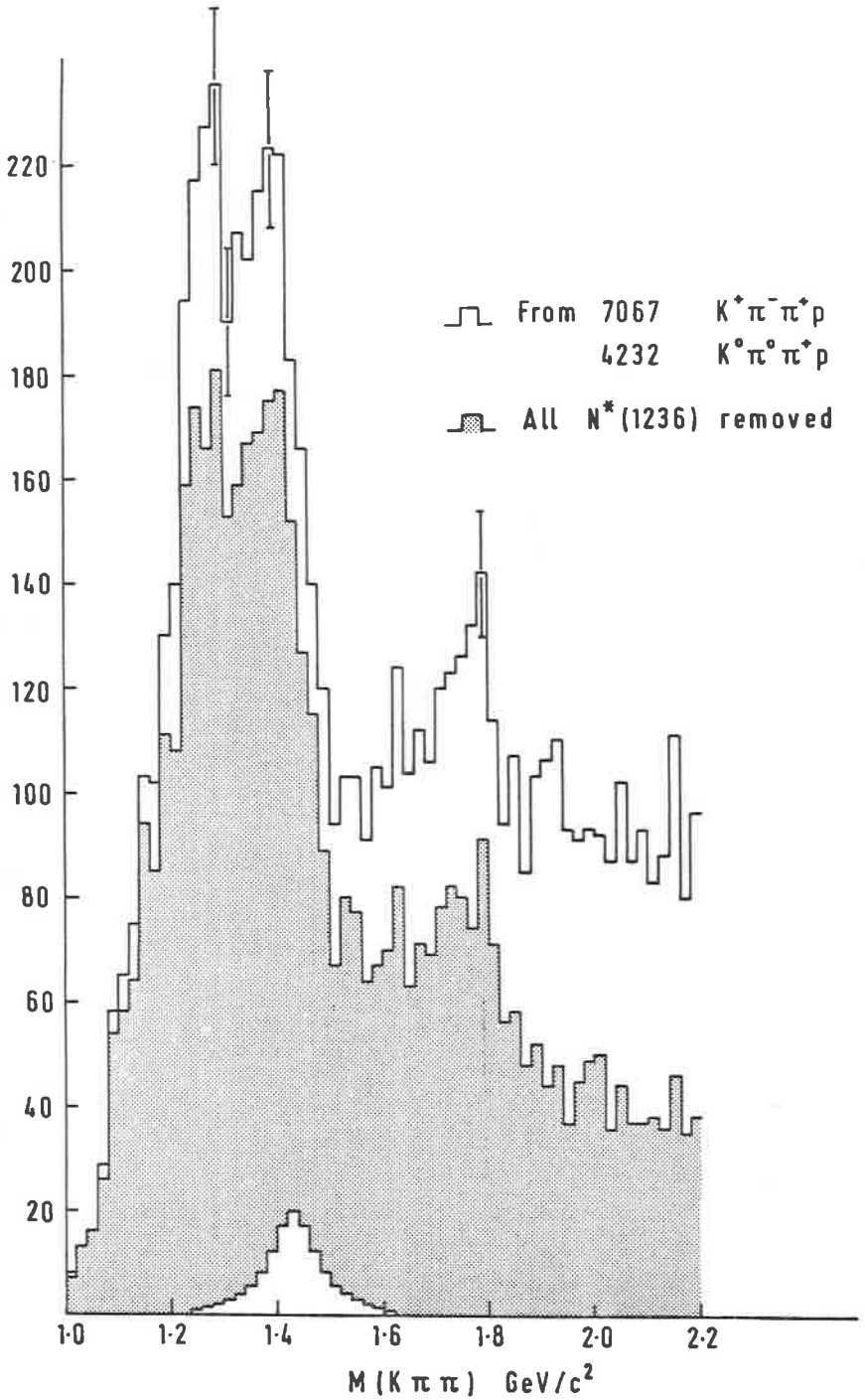
From 7067 K⁺π⁻π⁺p
4232 K°π°π⁺p
All N*(1236) removed
220
200
180
160
140
120
100
80
60
40
20
1·0
1·2
1·4
1·6
1·8
2·0
2·2
M (K π π) GeV/c²

Fig. 1.

2. What is known?

Certain facts are well established about the Q:

1) It is dominated entirely by the channels K*(890)π and Kρ. This is demonstrated in the second figure, taken again from the data I know best, 10 GeV/c K^+p (2). The figure shows the two particle mass spectra for *a*) $K^0\pi^0\pi^+$ and *b*) $K^+\pi^-\pi^+$ in the Q region (1.2÷1.4) GeV/c². The curves are the expected distributions for a spin-parity 1^+ state composed of only K*(890)π and Kρ, with no background, the relative amounts of these two channels being fitted to the data.

2) It has isospin $\frac{1}{2}$— no Q has ever been seen in reactions like $K^+p \to \to (K\pi\pi)^{++}n$.

3) Despite the reluctance of experimentalists to quote cross-section information, it is known that the production cross-section of the Q enhancement is roughly constant with laboratory momentum.

4) Production—of the whole enhancement—is very peripheral ($\sim e^{7t}$).

5) The whole region is dominantly $J^P = 1^+$ throughout. This has been got at in two ways:

i) By analysis of the angular distribution of the decay plane normal in space, which suggests, but does not actually require, 1^+.

ii) By analysis of the Dalitz plot distribution which is of course rather sensitive to the angular momentum of the decaying state. As far as I know the finest resolution with which these analyses have been made is in bins of 50 MeV/c² through the enhancement (2).

3. What are the problems?

1) *A rather trivial one— is there any* Kε *or* Kππ *background in addition to the dominant* K*(890)π *and* Kρ *channels?* It is difficult to be sure. The $K^0\pi^0\pi^+$ data is well fitted without background, while the $K^+\pi^-\pi^+$ fits shown in Fig. 2 would be improved by the inclusion of a smoothly varying background. But the $K^+\pi^-\pi^+$ channel contains $\sim 30\%$ $K^+\pi^+$ ambiguities. These come mostly from the region of the Dalitz plot where the K*(890) and ρ bands overlap, and so do not affect seriously conclusions about the Kρ channel, but may perhaps blurr the narrow K* resonance in the $K^+\pi^-$ spectrum a little.

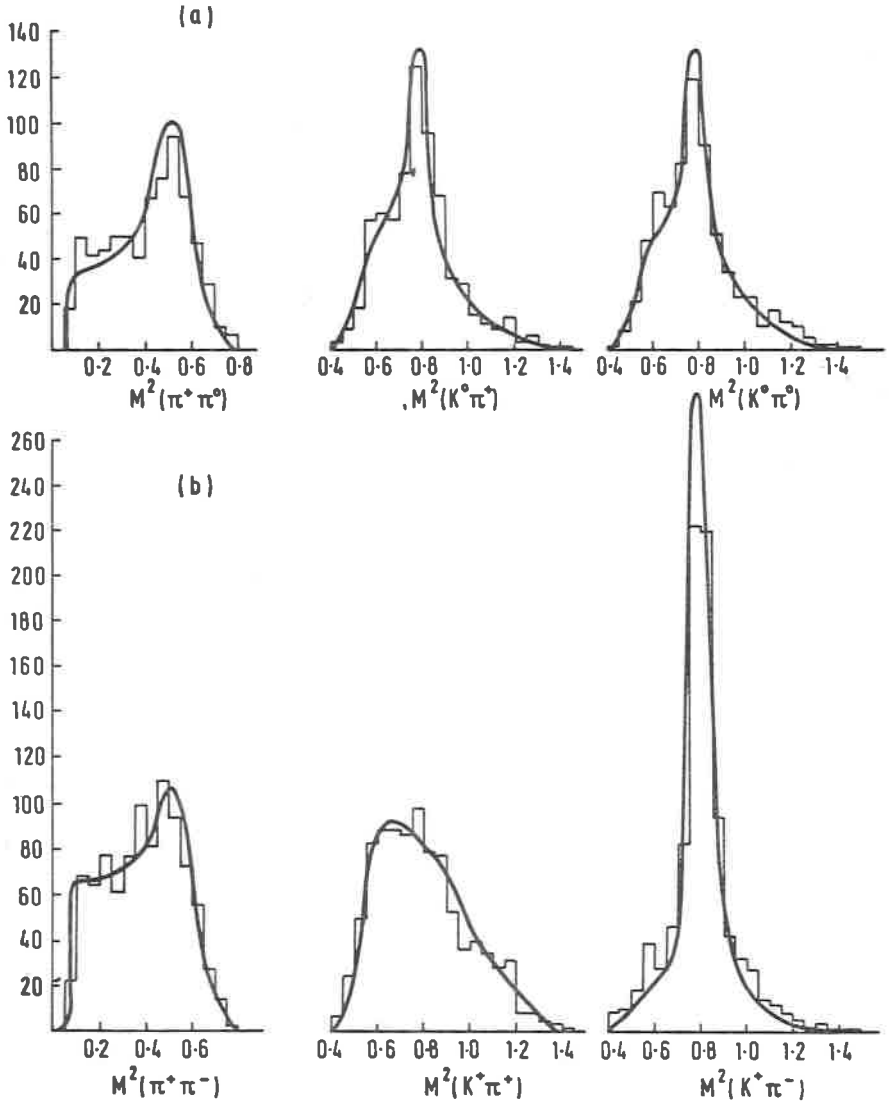

Fig. 2.

2) *Is the Q enhancement due to kinematics only, or to dynamical effects-resonances?* The problem here is that you really need to understand the strong interactions before you know how to calculate properly the effect of peripheralism à la Deck. Peripheral K*π certainly produces an enhancement

in the Q region, but it rises too soon and falls too slowly. You have to go through incredible contortions before you can get anything even qualitatively right, let alone fitting the rather extensive data.

In this connection it is worth mentioning that the people who look at coherent production of Q on nuclei (in freon and neon chambers) claim that the cross-section for interaction of the $Q^{\pm}$ in nuclear matter is about the same as that of the $K^{\pm}$, implying that the components of the Q go through a nucleus well within 10^{-13} cm of each other and so arguing for a resonance interpretation ([3]). Anything involving nuclei is inherently dirty, however, and I don't know how much confidence to place in such a conclusion, but it is a pointer. Finally, the invention of duality has taken much of the fury out of the Deck effect *vs.* resonance debate.

So let's suppose the Q is not all kinematic enhancement, which leads to the next question:

3) *One resonance or two?* The simple quark model predicts two 1^+ strange mesons in this region, so of course we want the Q to be made up of two resonances.

In Alex Firestone's review at Philadelphia ([1]) last year he showed that the Kππ spectra are fairly well fitted by two incoherent resonances, but can't be fitted by one alone. In addition, if the lower part of the Q enhancement is identified with the C meson observed in $p\bar{p}$ annihilations ([4]), the upper part must be something else. Could this something else be the well known 2^+ K*(1420)? I think that this is quite impossible. The production cross-section of the K*(1420) (known from the 3 particle final states) falls approximately as p_{lab}^{-2} above 5 GeV/c, and the K*(1420) is produced with a much flatter t distribution than the upper part of the Q. Anyway Dalitz plot analysis shows that the upper part of the Q is at least 70% 1^+.

So if we adopt a resonance interpretation for the Q, we are forced towards accepting two resonances, both 1^+, presumably superimposed on some background.

4) *What are their masses and widths?* Fitting two incoherent resonances to a compilation of high energy data, Alex Firestone obtained values

$$M_L = 1250 \pm 4 \text{ MeV/c}^2 \qquad \Gamma_L = 182 \pm 9 \text{ MeV/c}^2$$

$$M_H = 1400 \pm 6 \text{ MeV/c}^2 \qquad \Gamma_H = 220 \pm 14 \text{ MeV/c}^2 \, .$$

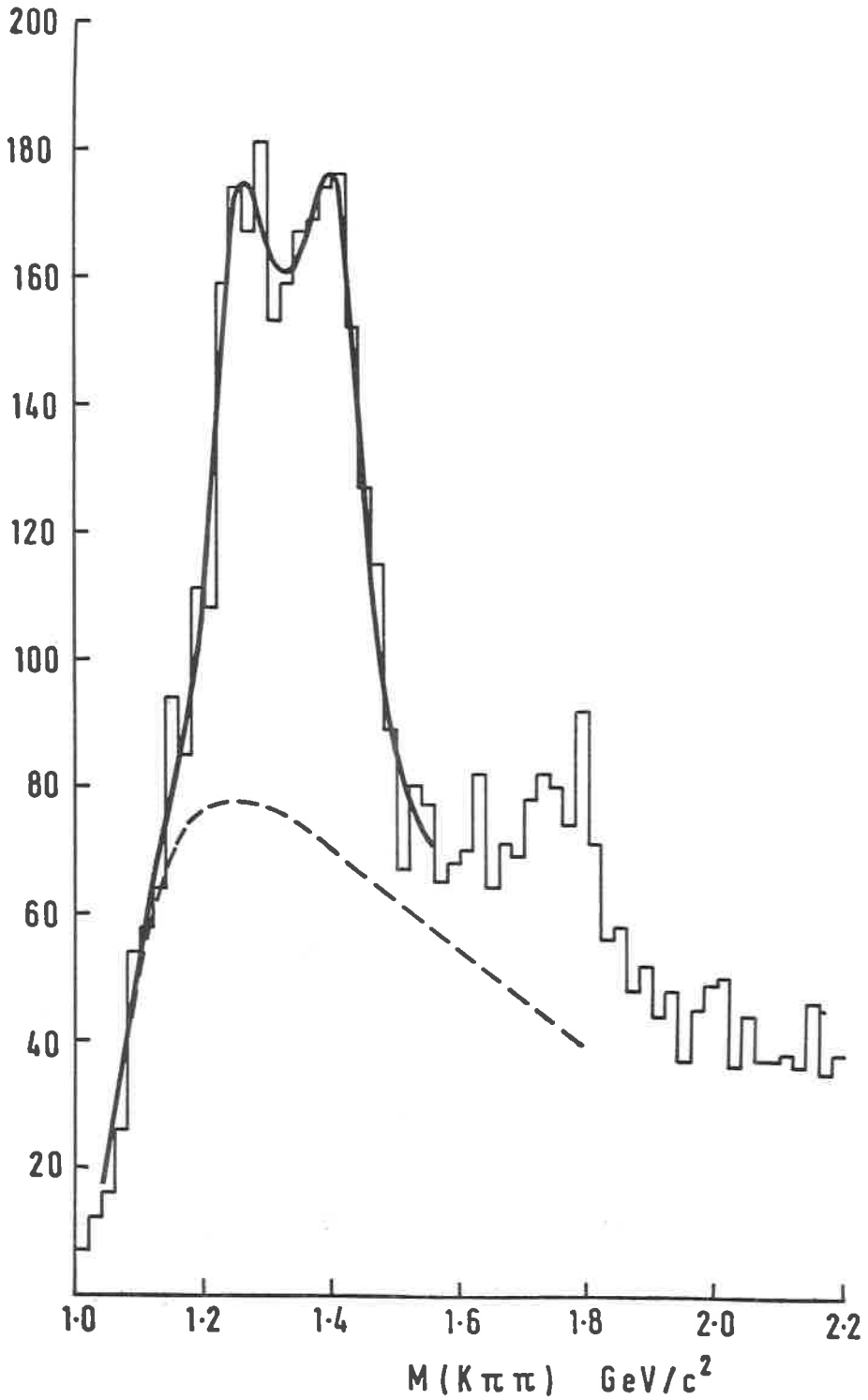

Fig. 3.

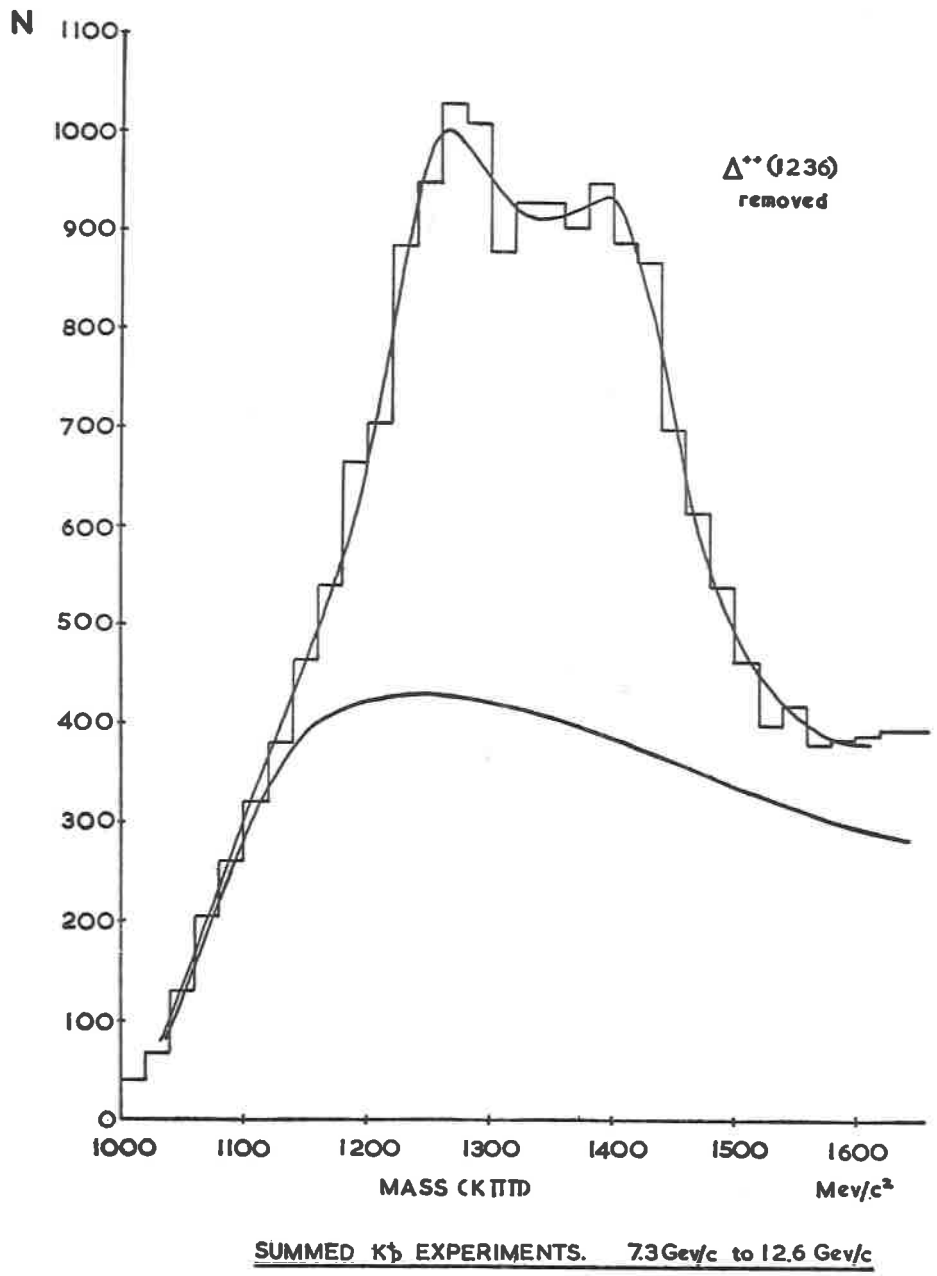
N
1100
1000
900
800
700
600
500
400
300
200
100
0
1000
1100
1200
1300
1400
1500
1600
MASS (K π π)
Mev/c²
Δ⁺⁺(1236)
removed
SUMMED K⁺p EXPERIMENTS. 7.3 Gev/c to 12.6 Gev/c

Fig. 4.

The values of these widths are too large because of background. The Birmingham-Glasgow-Oxford collaboration ([2]) found that the leading edge of the Q could not be fitted by two resonances alone and included a Deck type background in attempting to fit their $K\pi\pi$ mass spectrum at 10 GeV/c. Figure 3 shows a fit to this data with a background term and two coherent resonances. The presence of some such background is suggested by a bulge on the leading edge of the Q which does not look very impressive but becomes much more so if you try to fit it with a curve of monotonic slope.

Making a fit with such a background plus two incoherent resonances to the high energy data collected by Firestone ([1]) (there has been little new since then) I have found

$$M_L = 1263 \pm 4 \quad \Gamma_L = 118 \pm 8 \text{ MeV/c}^2$$
$$M_H = 1395 \pm 5 \quad \Gamma_H = 152 \pm 10 \text{ MeV/c}^2$$

but the fit has a confidence level $< 1\%$:

It is however curious that if I suppose the two resonances to be partially coherent then I find substantially better fits (confidence levels $\sim 70\%$) to this data and

$$M_L = 1241 \pm 4 \quad \Gamma_L = 122 \pm 7$$
$$M_H = 1423 \pm 6 \quad \Gamma_H = 141 \pm 10$$

with nearly complete coherence and a phase angle between the two Breit-Wigner amplitudes close to π. These parameters give the lower resonance in admirable agreement with the C meson and the upper degenerate with the K*(1420)—this may have some bearing on over large $K\pi\pi$ branching ratios that have been quoted for the K*(1420) in the past. This fit is shown in Fig. 4—it is worth emphasising that it is the leading and trailing edges that have most influence in determining these parameters, which are not sensitive to a split in the middle.

4. Implications of a two resonance interpretation.

The two 1^+ strange mesons which the simple quark model predicts differ in that one belongs to an octet the neutral members of which have $C = +1$, while the other belongs to an octet the neutral members of which have $C = -1$. In the limit of strict SU_3 the final $K\pi\pi$ states will differ from each

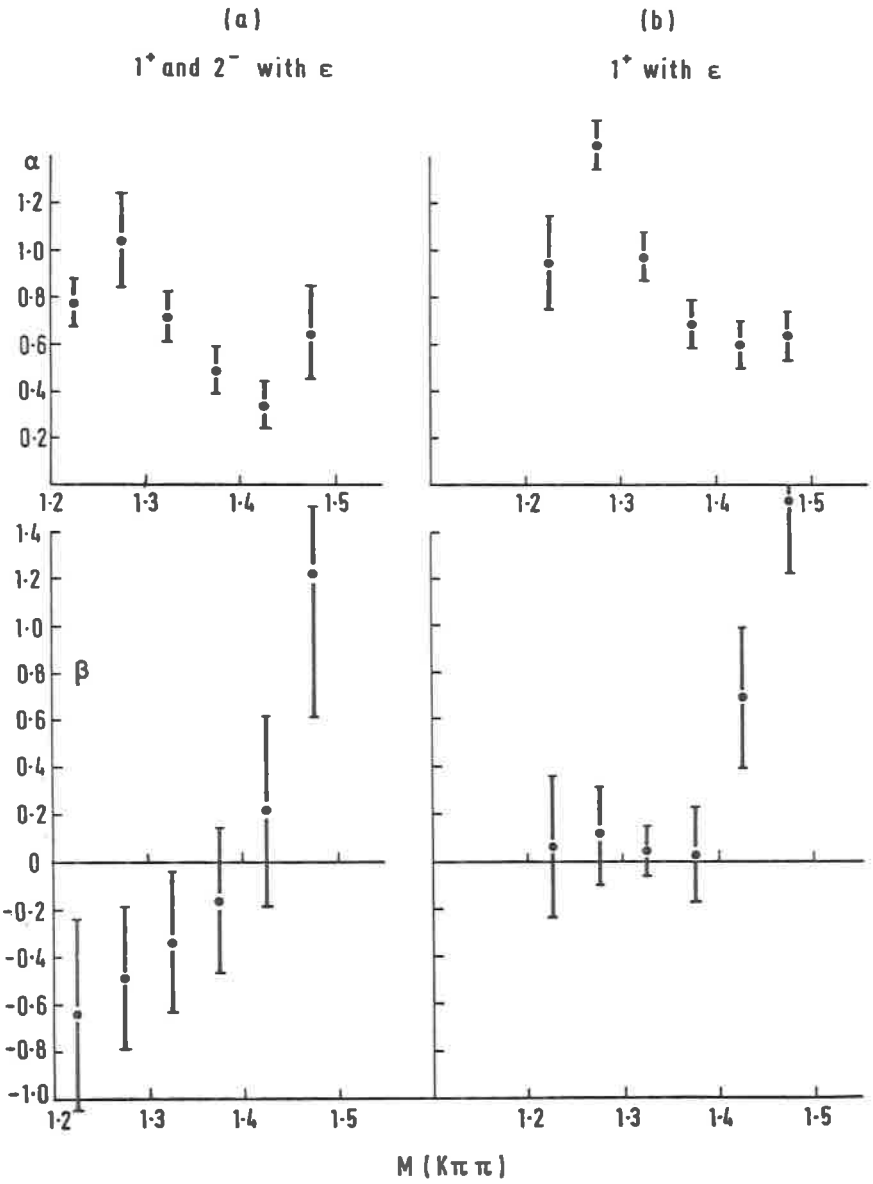

Fig. 5.

other in the following way. For the $C = +1$ octet, interference between the K*π and Kρ channels is constructive at the point where the bands cross

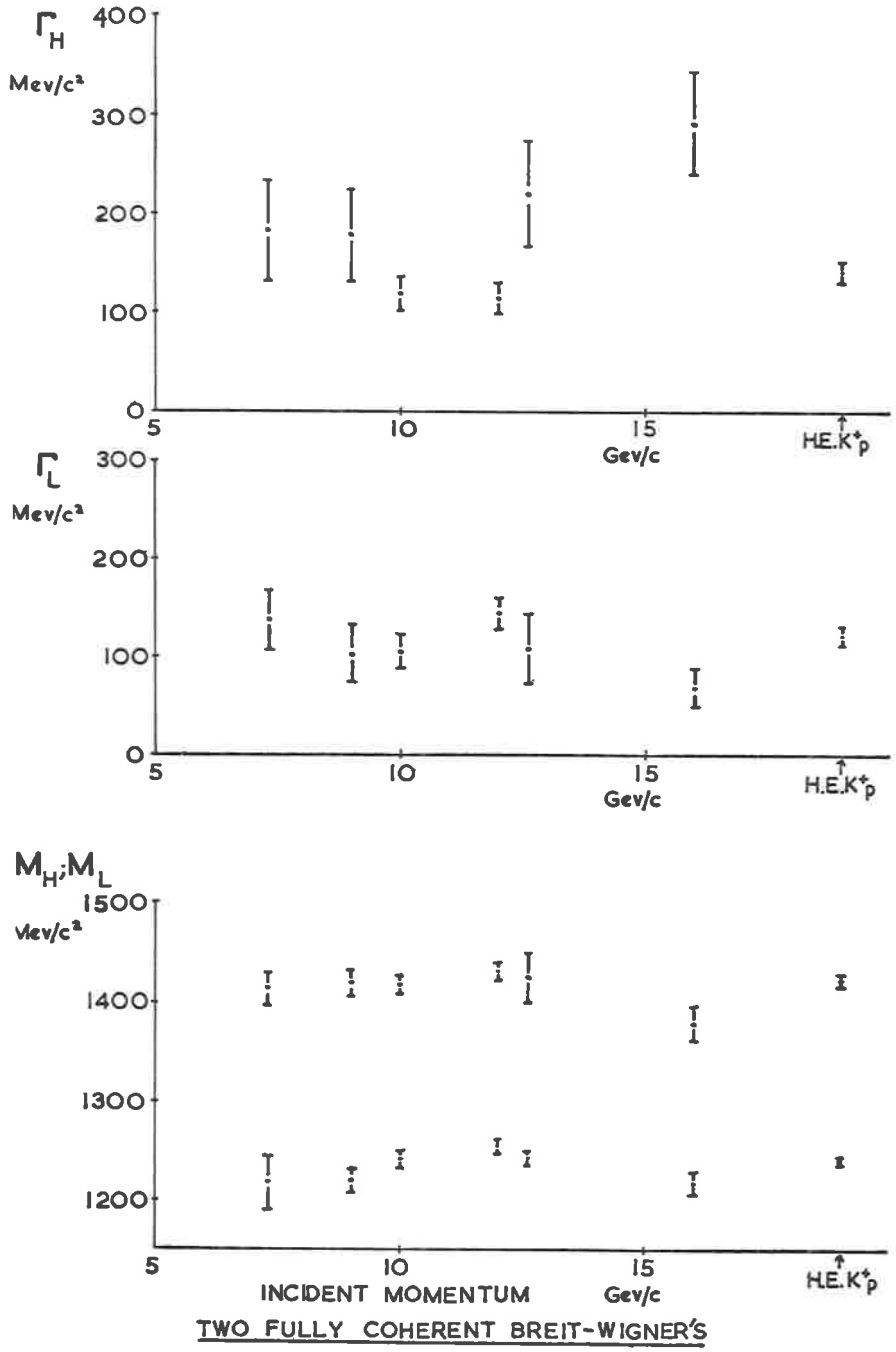
Γ_H
Mev/c²
400
300
200
100
0
5
10
15
Gev/c
H.E. K^+p
Γ_L
Mev/c²
300
200
100
0
5
10
15
Gev/c
H.E. K^+p
M_H; M_L
Mev/c²
1500
1400
1300
1200
5
10
15
INCIDENT MOMENTUM
Gev/c
H.E. K^+p
TWO FULLY COHERENT BREIT-WIGNER'S

Fig. 6.

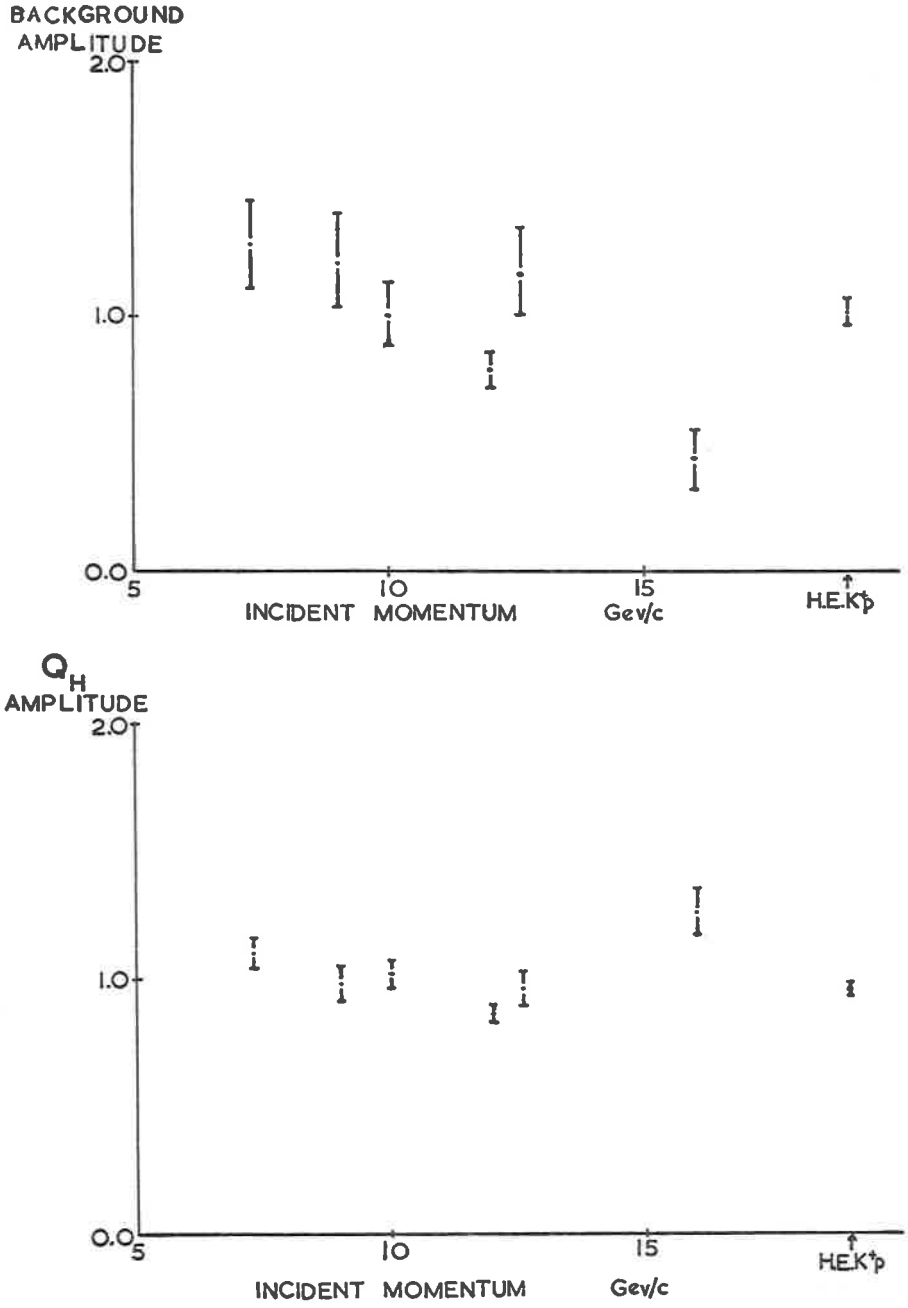
BACKGROUND
AMPLITUDE
2.0
1.0
0.0
5
10
15
INCIDENT MOMENTUM
Gev/c
H.E.K⁺p
Q_H
AMPLITUDE
2.0
1.0
0.0
5
10
15
INCIDENT MOMENTUM
Gev/c
H.E.K⁺p
MASSES AND WIDTHS FIXED

Fig. 7.

in the Dalitz plot, while for the $C=-1$ octet, interference is destructive at the point where the bands cross. If the Q consists of two 1^+ resonances, we expect the relative phase β of the Kρ and K*π channels to vary with K$\pi\pi$ mass, from $\beta\sim 0$ in the region of the strange brother of the A1 to $\beta\sim\pi$ in the region of the brother of the B. This variation of phase can be looked for in the Dalitz plot. This was done by the Birmingham-Glasgow-Oxford collaboration ([2]), and here are the results (Fig. 5).

The fairly rapid amplitude (α) and phase (β) variations are to my mind evidence independent of the K$\pi\pi$ mass spectrum of resonances in the Q region (A note for experimentalists: the $K^0\pi^0\pi^+$ channel is a better place to find the phase β than the $K^+\pi^-\pi^+$ channel. Not only does an isospin Clebsch-Gordan provide more Kρ, but also in $K^+\pi^-\pi^+$ there are the $K^+\pi^+$ ambiguities right where the bands cross and interference is maximal).

The biggest remaining problem, if you accept this interpretation of the Q as two 1^+ mesons, is the production mechanism. The production features are

i) Highly peripheral production, $\sim e^{7t}$.

ii) Roughly constant cross-section.

iii) The relative amounts of the lower and upper peaks, the positions, widths, degrees of coherence and relative phase show no evidence of variation with energy. Figure 6 shows the masses and widths.

Taking the best values of mass and width obtained by fitting two coherent resonances to the compiled high energy data, I have obtained good fits to all the individual data above 5 GeV/c, including some newer results at 16 GeV/c ([5]), allowing only the relative amounts of the two resonances and the background to vary. The results are shown in Fig. 7: there seems to be no tendency for the relative amplitude A of the upper half of the Q to the lower half to change.

Between 5 and 16 GeV/c there is no evidence that anything changes in the Q mass spectrum as a function of incident K^+ momentum. Reports of significant changes in the past have been the result of overactive imaginations working on poor statistics.

iv) The angular distribution of the normal to the K$\pi\pi$ decay plane seems independent of energy. In Fig. 8 and 9 I show the moments of the spherical harmonics Y_2^0 and Y_4^0 at 5 GeV/c ([6]) (an old experiment from CERN) and at 10 GeV/c ([2]). There seems to be no difference.

v) The Dalitz plot properties seem independent of momentum. In Fig. 5 I showed the variation of the amplitude of Kρ relative to K*π with K$\pi\pi$ mass at 10 GeV/c. In Fig. 10 I show the variation of this amplitude at 5 GeV/c ([6]). There is a striking resemblance in the behaviour of the modulus

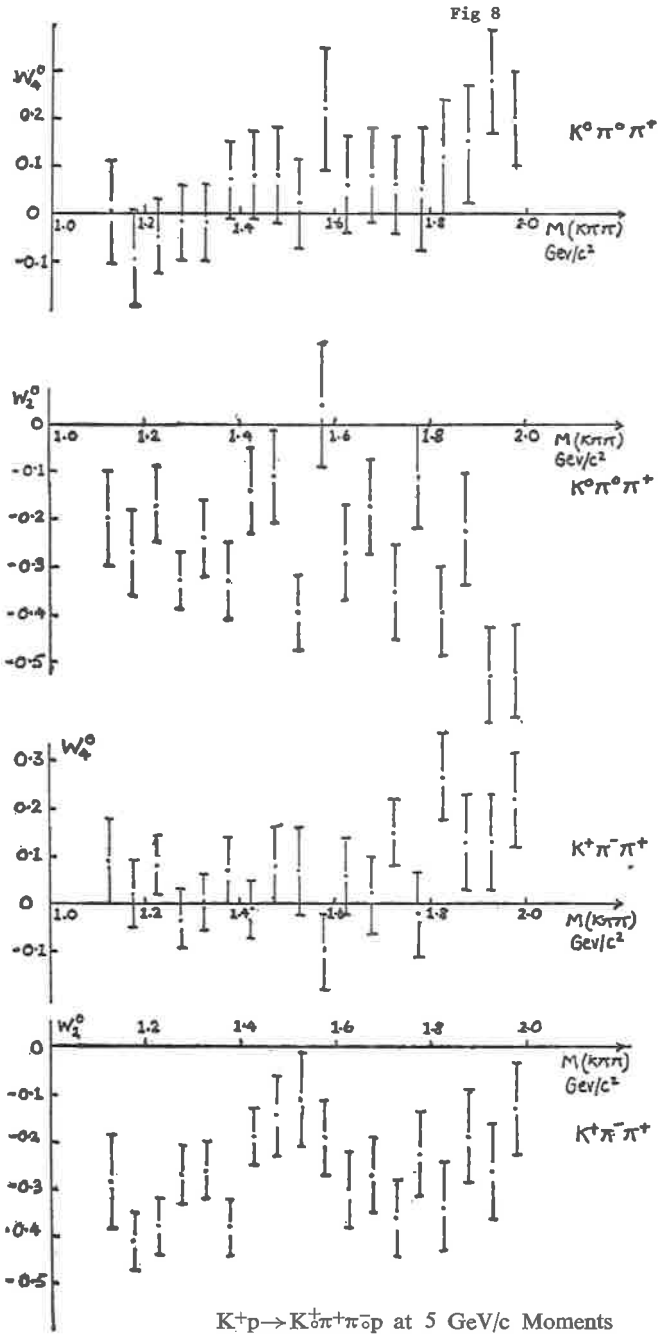
Fig 8
W_4^0
W_2^0
W_4^0
W_2^0
$K^0\pi^0\pi^+$
$K^0\pi^0\pi^+$
$K^+\pi^-\pi^+$
$K^+\pi^-\pi^+$
M(Kππ) Gev/c²
M(Kππ) Gev/c²
M(Kππ) Gev/c²
M(Kππ) Gev/c²
$K^+p \to K^+_0\pi^+\pi^-p$ at 5 GeV/c Moments

Fig. 8.

of the amplitude α; the phase β starts off in very much the same way but has a sharp drop in the fourth bin: it is of course possible that we should

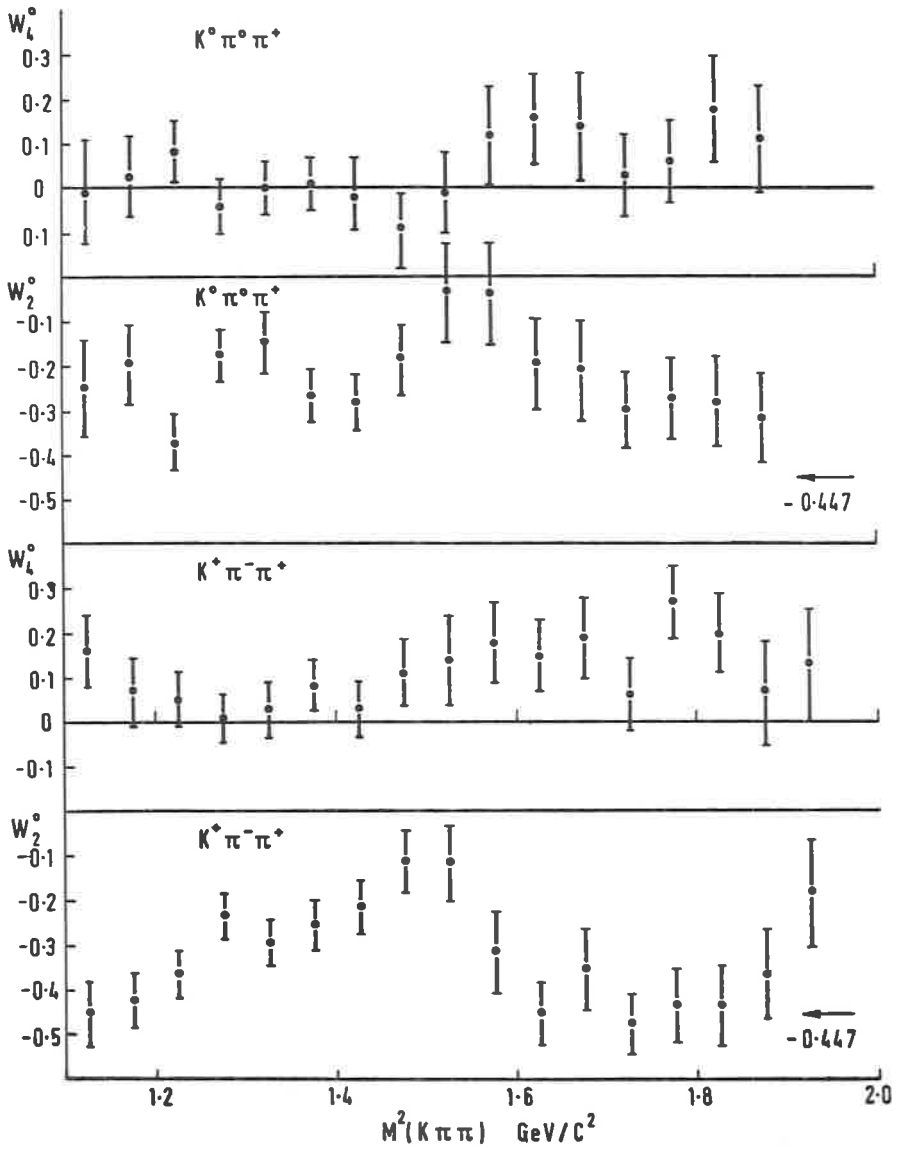

Fig. 9.

insert an extra 2π at this point: the relative phase of the two Dalitz plot amplitudes is only determined between 0 and 2π.

It seems clear that both halves of the Q have the same production mechanism (the evidence for strong coherence in the mass spectrum argues this too)

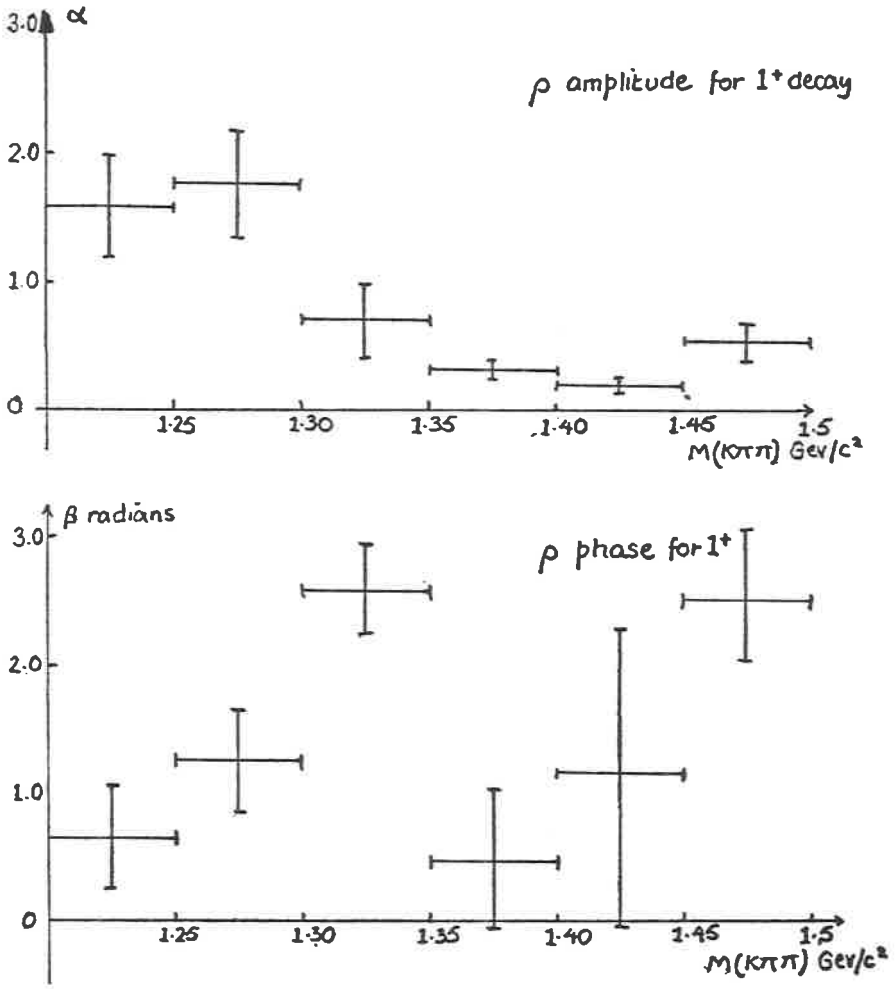

$K^+p \to K^{\pm}_{\delta}\pi^+\pi^-_{\delta}p$ at 5 GeV/c

Dalitz Plot Fit: 1^+ and 2^- with ε

Fig. 10.

and it also seems clear that the mechanism is predominantly diffraction dissociation. However, if one of these states is $C=+1$ and the other $C=-1$,

this would seem to be impossible, for one would expect diffraction dissociation to produce almost exclusively the member of the $C = +1$ octet.

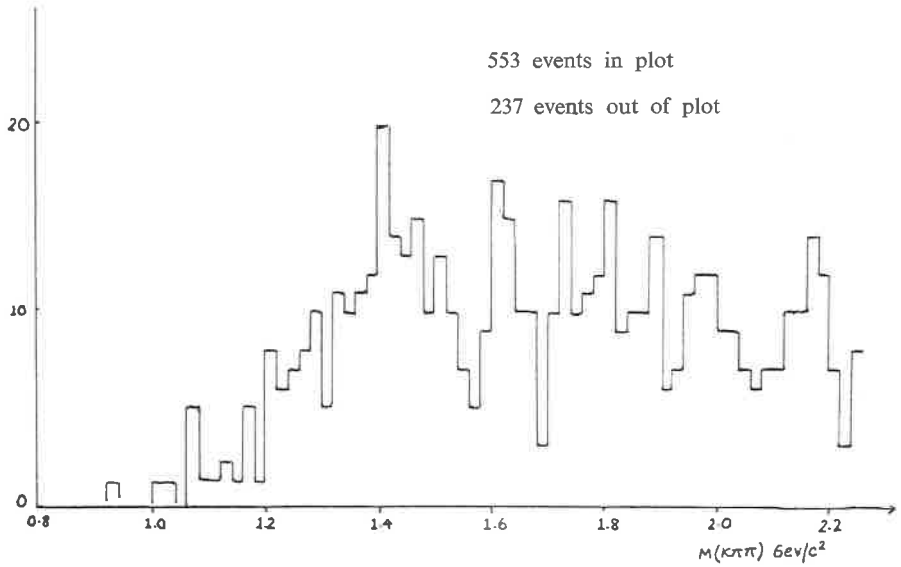

$K^0\pi^+\pi^-$ invariant mass $K^+p \to K^0\pi^+\pi^-\Delta^{++}$ at 10 GeV/c (other π^+p NOT in Δ^{++})

Fig. 11.

If indeed the picture I have built up for you is substantially correct and the Q is composed of two 1^+ strange mesons, I can see no way of avoiding the conclusion that there is substantial mixing between the strange members of the $C = +1$ and $C = -1$ octets. Such mixing, induced by SU_3 breaking forces, would mean that a predominantly $C = +1$ system could indeed be all that is produced by diffraction dissociation, but that this state would not be a nice exponentially decaying one, but would give rise to a sum of two Breit-Wigner amplitudes. This sort of situation is of course familiar from neutral K decay: if we could look with fine enough resolution at the K^0 mass spectrum in production through the strong interactions, we would see one relatively narrow peak and another broad one.

Now if you have two broad states of the same J^P, with the same decay modes and something that mixes them together, all hell is let loose. I guess

that little more information will come out of the traditional $Kp \to K\pi\pi p$ type of study—at least not without yet another order of magnitude increase

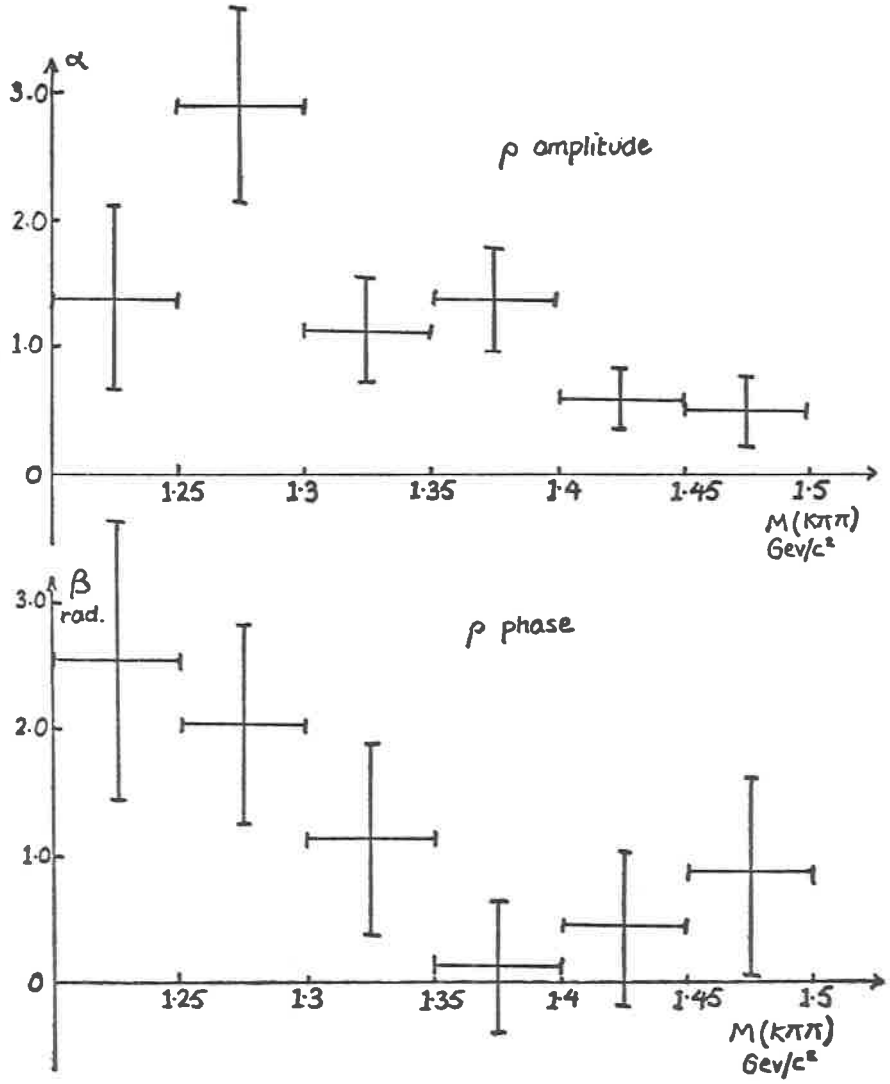

Dalitz Plot Fit: 1^+

$K^+p \to K^0\pi^+\pi^-\Delta^{++}$ (1236) at 10 GeV/c

Fig. 12.

in statistics—and I think we must try and look at nondiffractively produced Q. I should like to draw the attention of the experimentalists to the reaction

$$K^+p \to (K\pi\pi)^0 \mathcal{N}^{*++}.$$

The point is that the Q couples to $K\rho$ and the $\rho\mathcal{N}\mathcal{N}^*$ vertex is a strong one.

In Oxford John Dainton and I have had a preliminary sniff at the reaction

$$K^+p \to K^0\pi^+\pi^-\mathcal{N}^{*++}$$

in the 10 GeV/c data of the Birmingham-Glasgow-Oxford collaboration. Fig. 11 shows the $K^0\pi^+\pi^-$ mass spectrum, after selecting on the $\mathcal{N}^{*++}$, and it looks very different from the diffractively produced spectra. There is a peak at about 1.4 GeV/c², which it would be tempting to interpret as the K*(1420). However, a Dalitz plot analysis gave us the result that up to a mass of 1.5 GeV/c² this mass spectrum is dominated by 1^+— and angular information is consistent with this. Although the data is scanty, we were able to extract the $K\rho - K^*\pi$ relative amplitude. We expect of course very different results because of the (presumed) ρ exchange mechanism and they are shown in the last figure (Fig. 12).

The modulus α of the relative amplitude behaves very similarly to the diffractive case, but the phase β is extremely different, starting at π and going anticlockwise to zero rather than starting at zero and going clockwise to π.

Because of the theoretical complexities of a system of two broad mixed resonances with common decay channels, I cannot present you with a simple interpretation of the mass plots and the two sets of amplitudes I have shown you, but I suspect that they may already contain the answer to the problem of the Q.

5. Acknowledgement.

It is a pleasure to thank A. W. Lowman and J. B. Dainton for their enormous help in preparing much of the material for this talk.

REFERENCES

1) A very comprehensive review of data up to April 1970 has been given by A. Firestone, Talk presented at the 1970 Conference on Meson Spectroscopy, Philadelphia. May 1970, UCRL 19846. This paper contains exhaustive references to work up to that time.

2) K. BARNHAM *et al.*: *Nuclear Phys.*, B **25**, 49 (1970).
3) A. M. CNOPS *et al.*: PRL, **25**, 1132 (1970); M. HAGUENAUER *et al.*: *Phys. Lett.*, 34 B, 219 (1971).
4) A. A. ASTIER *et al.*: *Nucl. Phys.*, B **10**, 65 (1969).
5) Birmingham-Brussels-Saclay-CERN-Paris collaboration paper submitted to the Kiev Conference, 1970.
6) This data was taken from the world K^+ DST. Its suitability for this analysis was pointed out to me by D. C. COLLEY.

New evidence for splitting in the Q-region of $K^+\pi^+\pi^-$ Mass (*)

A. F. GARFINKEL, R. F. HOLLAND, D. D. CARMONY
H. W. CLOPP, D. CORDS, F. J. LOEFFLER, D. H. MILLER and L. K. RANGAN
Purdue University - Lafayette, Indiana
A. L. LANDER, D. E. PELLETT and P. M. YAGER
University of California - Davis, Calif.

The fact that the quark model predicts two $J^P = 1^+$ nonets of opposite C parity motivates searches for such states in the Q region (below 1400 MeV/c^2) of $K\pi\pi$ mass. Such structure was first observed by Goldhaber *et al.* [1] in 9 GeV/c K^+p experiment.

We have observed a splitting of the Q region in the reactions:

$$K^+d \to K^+\pi^+\pi^-d \qquad (714 \text{ events}) \tag{1}$$

$$K^+d \to K^+\pi^+\pi^-pn \qquad (2060 \text{ events}) \tag{2}$$

at a beam momentum of 9.04 GeV/c.

In Fig. 1*a* the $K^+\pi^-$ effective mass spectrum from reaction (1) is shown for events in the Q region. It is completely dominated by the K*(890). The unshaded histogram in Fig. 1*b* shows the $\pi^+\pi^-$ effective mass spectrum from reaction (1) for Q events. It is well described by the calculated curve which assumes pure K*(890) production. Figures 1*c* shows the $K^{*0}\pi^+$ spectrum from reaction (2). In this reaction the K* requirement was used to select the K^+ from the two positive tracks. The shaded region of Fig. 1*c* which shows substructure has the requirement that the $K^*\pi$ be produced at $|t| \leqslant$ $\leqslant 0.12$ (GeV/c)^2. Figures 1*d* shows the combined $K^+\pi^+\pi^-$ spectra of all events from reaction (1) (shaded) added to the selected sample of events

(*) Invited paper presented by D. H. MILLER.
Work supported in part by the U. S. Atomic Energy Commission.

shaded in Fig. 1*c*. The double peaks above the multi-Regge background are fitted to a mass and width of 1243 ± 8 and 70^{+26}_{-18} MeV/c² for the lower, and a mass of 1344 ± 4 and width less than 40 MeV/c² for the upper.

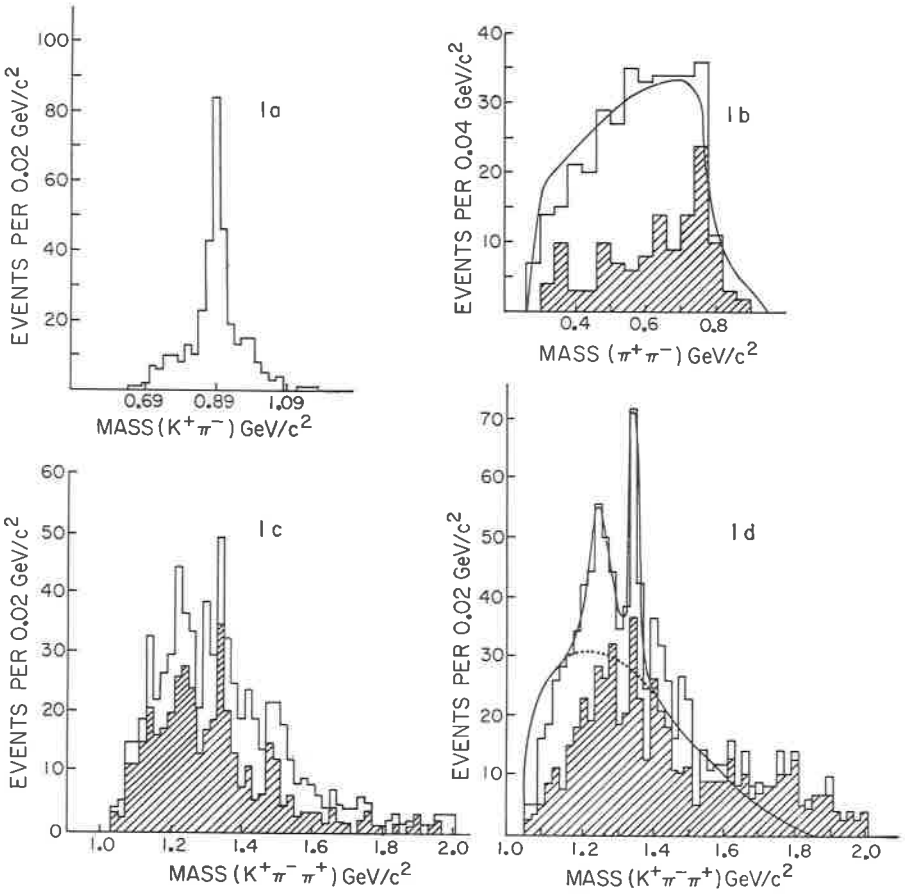

Fig. 1.

An examination of the reactions (not shown)

$$K^+d \to dK^0\pi^+ \tag{3}$$

$$K^+d \to pnK^0\pi^+ \tag{4}$$

showed no evidence for these states in the $K^0\pi^+$ spectrum. It also showed K*(1420) production to be strongly suppressed in reaction (3) relative to (4).

Angular distributions are consistent with production by pomeron exchange of spin-parity $J^P = 1^+$ states for both the K*(1243) and K*(1344).

REFERENCE

1) G. Goldhaber *et al.*: *Phys. Rev. Lett.*, **19**, 972 (1967).

An analysis of the reaction $K^+p \to Q^+p$ from 2.5 to 12.7 GeV/c (*)

H. H. BINGHAM, L. EISENSTEIN, Y. GOLDSCHMIDT-CLERMONT
V. P. HENRI and J. QUINQUARD
CERN - Geneva
F. GRARD, P. HERQUET and R. WINDMOLDERS
Laboratoire Interuniversitaire Belge des Hautes Energies - Bruxelles

We present in this talk an analysis of the reaction:

$$K^+p \to Q^+p \to K^+\pi^+\pi^-p\,, \qquad (1)$$

TABLE I. – *International* K+ *Collaboration* $K^+p \to K^+\pi^+\pi^-p$.

University	p_{inc} (GeV/c)	No. events
University of Illinois	2.5	2723
University of Illinois	2.7	4586
Brussels-CERN K+ Collaboration	3.0	1108
University of Illinois	3.2	4823
Brussel -CERN K+ Collaboration	3.5	1848
University of Chicago	4.3	1838
University of California at Berkeley	4.6	2668
Brussels-CERN K+ Collaboration	5.0	6241
Johns Hopkins University	5.5	9518
University of California at Los Angeles	7.3	11619
Brussels-CERN K+ Collaboration	8.25	4780
University of California at Berkeley	9.0	7559
Birmingham-Glasgow-Oxford Collaboration	10.0	14265
University of Rochester	12.7	3691
Total		77267

(*) Invited paper presented by R. Windmolders. Data from the International K+ Collaboration.

using a sample of ~ 77000 4-constraint events from fourteen different bubble chamber experiments with K^+ momenta from 2.5 to 12.7 GeV/c. These data were supplied by several laboratories and assembled by an international K^+ collaboration (see Table I). Result on the subsamples have already been published by the contributing laboratories and the main interest of this work is to present a systematic study at all the available energies.

1. Mass distributions and cross sections.

The $K\pi\pi$ mass distribution for the events with a $p\pi^+$ mass greater than 1.4 GeV are shown on Fig. 1 for the individual energies. At the highest K^+

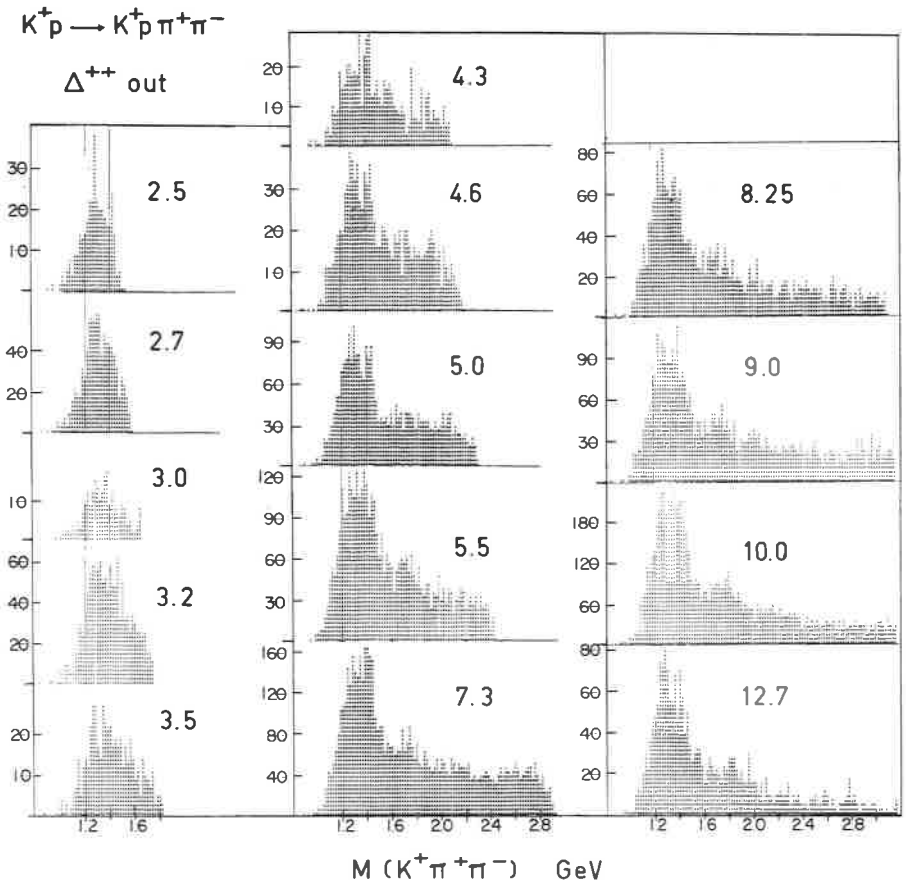

Fig. 1. – $K\pi\pi$ mass distributions for the reaction $K^+p \to K^+\pi^+\pi^-p$ at 14 energies with $M(p\pi^+) > 1.4$ GeV.

incident momenta the Q^+ signal appears very clearly above any background.

The cut on the $p\pi^+$ mass removes the $K^+\pi^-\Delta^{++}(1236)$ events which are copiously produced and also a fraction of the genuine Q^+p events. We corrected

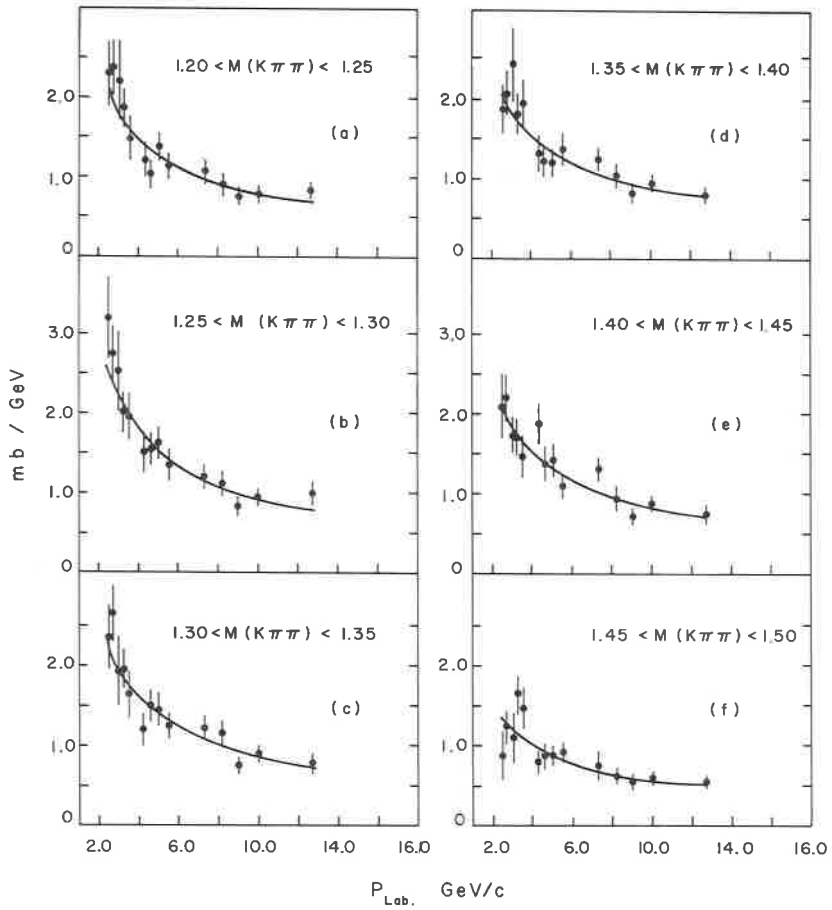

Fig. 2. – Variation of the cross-section for the reaction K+p→ Q+p with the incoming momentum.

for the loss of these events assuming that the Q decays into $K^*(892)\pi$ with angular momentum $l = 0$ and calculated the Q production cross section without removing any additional background. The results are shown on Fig. 2 for 6 intervals of the $K\pi\pi$ mass.

The energy dependence of the cross section is similar for all mass intervals and can be described by an expression of the form $\sigma_0 p_{\mathrm{Lab}}^{-n}$ with $n = 0.67 \pm \pm 0.07$. If only the 8 highest momenta are taken into account (*i.e.* $p_{\mathrm{Lab}} \geqslant \geqslant 4.6$ GeV/c) the slope is found equal to 0.58 ± 0.15.

2. Spin-parity determination.

We determined the spin-parity of the Q from the values of the moments $H(l, m, L, M)$ in the two-step decay

$$\mathrm{Q}^+ \to \mathrm{K}^{*0}\pi^+ \to \mathrm{K}^+\pi^-\pi^+ . \tag{2}$$

These moments are defined by the relation

$$H(l, m, L, M) = \langle D^L_{Mm}(\varphi_1, \theta_1, 0)\, D^l_{m0}(\varphi_2, \theta_2, 0)\rangle , \tag{3}$$

where (θ_1, φ_1) and (θ_2, φ_2) represent the Q and the K* decay angles respectively in their own rest frame.

All the moments with l, $L \geqslant 2$ were calculated for several intervals of the $\mathrm{K}\pi\pi$ mass and for 4 groups of incident momentum. Only events with $0.84 \leqslant \leqslant \mathrm{M}(\mathrm{K}^+\pi^-) \leqslant 0.94$ GeV were used. We also required that the angle between the directions of the π^+ and the recoiling proton in the Q rest frame be greater than 90°. This last condition—which will be called the « helicity cut »—removes all the $\mathrm{K}^+\pi^-\Delta^{++}(1236)$ events for incident momenta greater than 3 GeV/c and does not bias the moments used in the determination of the Q spin-parity.

It has been shown ([1,2]) that some linear combinations of the moments $H(l, m, L, M)$ must vanish for a given spin-parity independently of the production mechanism:

$$T(1) = \; H(0, 0, 0, 0) + 5H(2, 0, 0, 0) = 0 \qquad \text{for } J^p = 0^+, 1^-, 2^+, \tag{4}$$

$$T(2) = 2H(0, 0, 2, 0) - 5H(2, 0, 2, 0) - 5H(2, 2, 2, 0) = 0$$

$$\text{for } J^p = 1^-, 2^-, \tag{5}$$

$$T(3) = 2H(0, 0, 2, 0) - 5H(2, 0, 2, 0) + 5H(2, 2, 2, 0) = 0$$

$$\text{for } J^p = 1^+, 2^+: \tag{6}$$

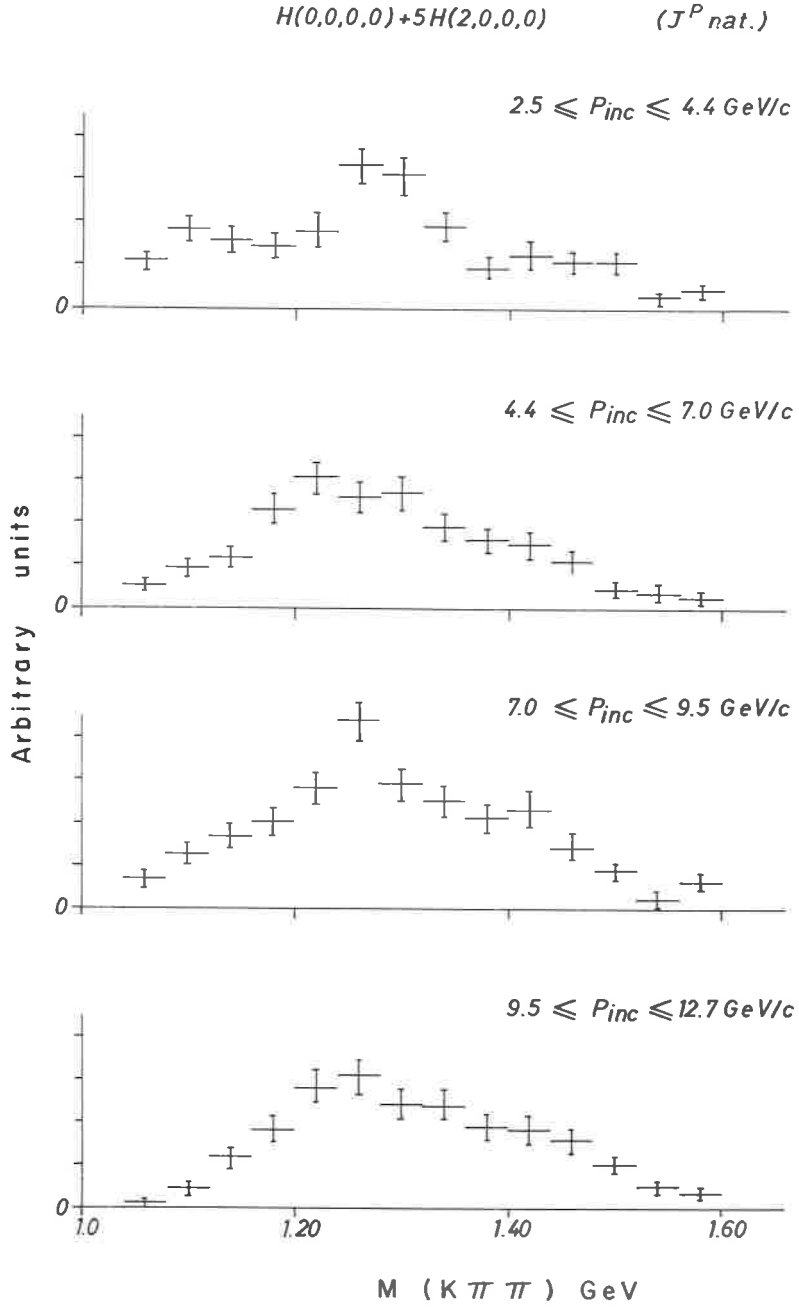
H(0,0,0,0)+5H(2,0,0,0) (J^P nat.)
2.5 ≤ P_inc ≤ 4.4 GeV/c
4.4 ≤ P_inc ≤ 7.0 GeV/c
7.0 ≤ P_inc ≤ 9.5 GeV/c
9.5 ≤ P_inc ≤ 12.7 GeV/c
0
Arbitrary units
1.0
1.20
1.40
1.60
M (K π π) GeV

Fig. 3 *a*.

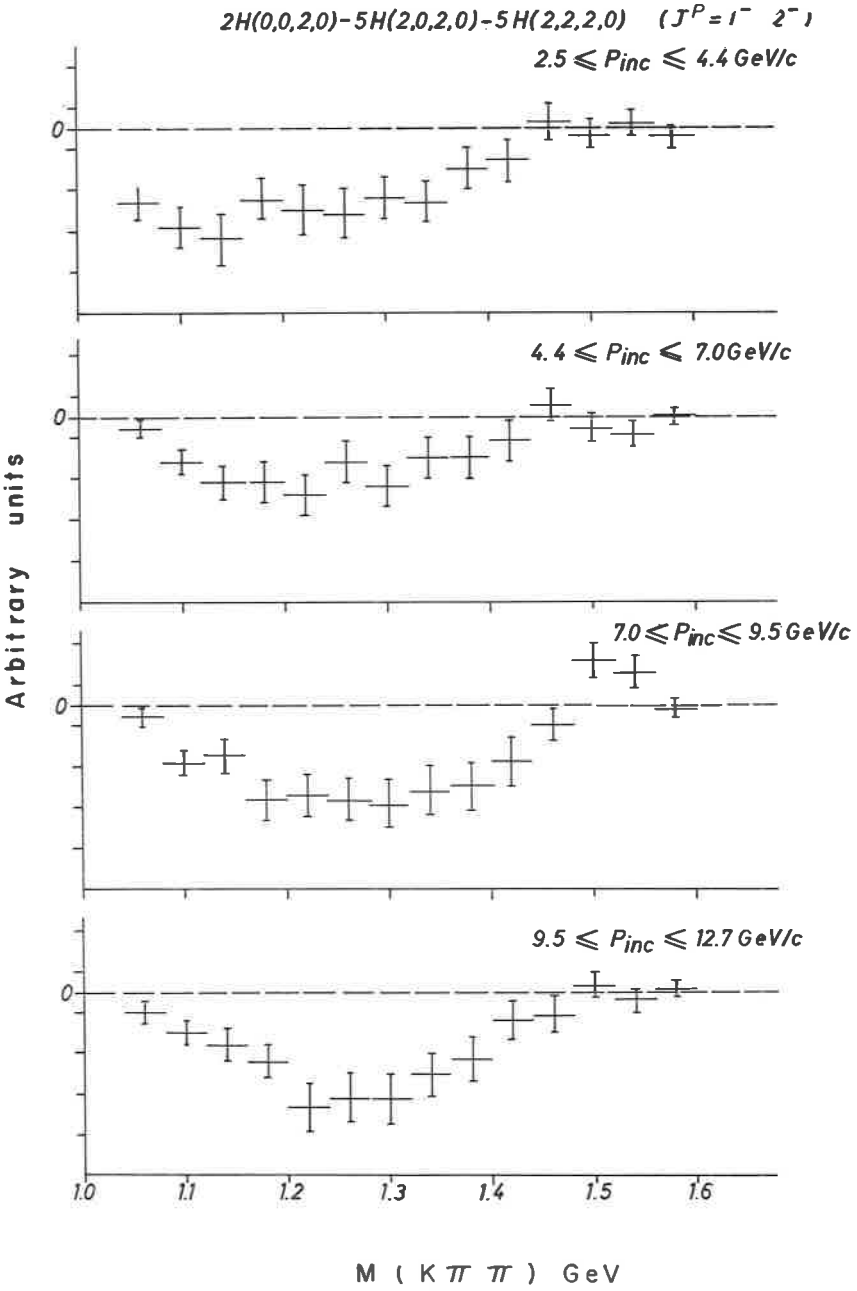
2H(0,0,2,0)-5H(2,0,2,0)-5H(2,2,2,0) ($J^P = 1^- \; 2^-$)
$2.5 \leqslant P_{inc} \leqslant 4.4$ GeV/c
$4.4 \leqslant P_{inc} \leqslant 7.0$ GeV/c
$7.0 \leqslant P_{inc} \leqslant 9.5$ GeV/c
$9.5 \leqslant P_{inc} \leqslant 12.7$ GeV/c
0
Arbitrary units
1.0
1.1
1.2
1.3
1.4
1.5
1.6
M (K π π) GeV

Fig. 3 *b*.

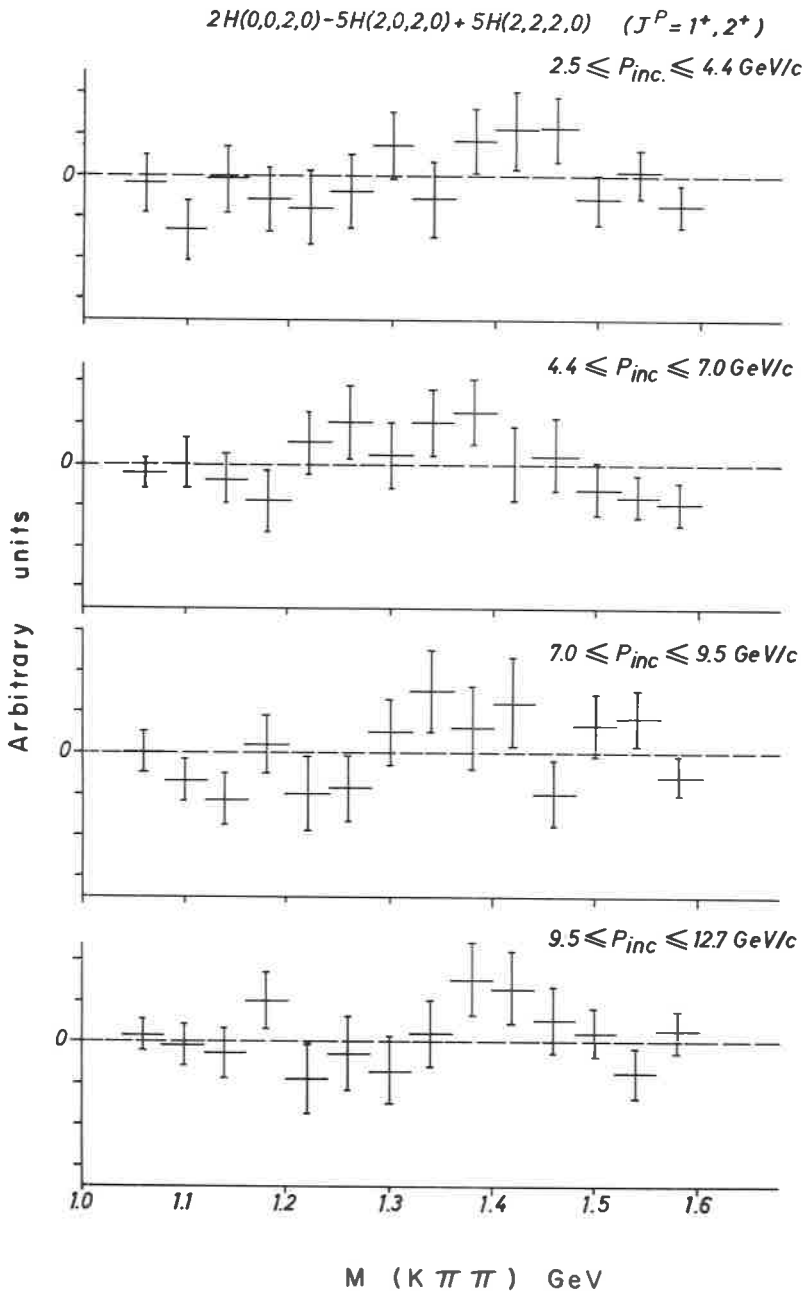

Fig. 3*c*. – Values of some linear combinations of the moments $H(l, m, L, M)$: *a*) $H(0, 0, 0, 0) + 5H(2, 0, 0, 0)$; *b*) $2H(0, 0, 2, 0) - 5H(2, 0, 2, 0) - 5H(2, 2, 2, 0)$; *c*) $2H(0, 0, 2, 0) - 5H(2, 0, 2, 0) + 5H(2, 2, 2, 0)$.

The values of $T(1)$, $T(2)$, and $T(3)$ are shown on Fig. 3 as a function of the $K\pi\pi$ mass and the incoming momentum. $T(3)$ is compatible with zero in the Q region while $T(1)$ and $T(2)$ are significantly different from zero. The Q region is thus dominated by $J^P = 1^+$ states.

3. Decay Dalitz plot.

The spin-parity of the Q can also be determined from a fit of the density of the events in the decay Dalitz plot. As an example, we show these plots on Fig. 4 for events with an incoming momentum between 7.0 and 9.5 GeV/c and for six intervals of $K\pi\pi$ mass between 1.2 and 1.5 GeV.

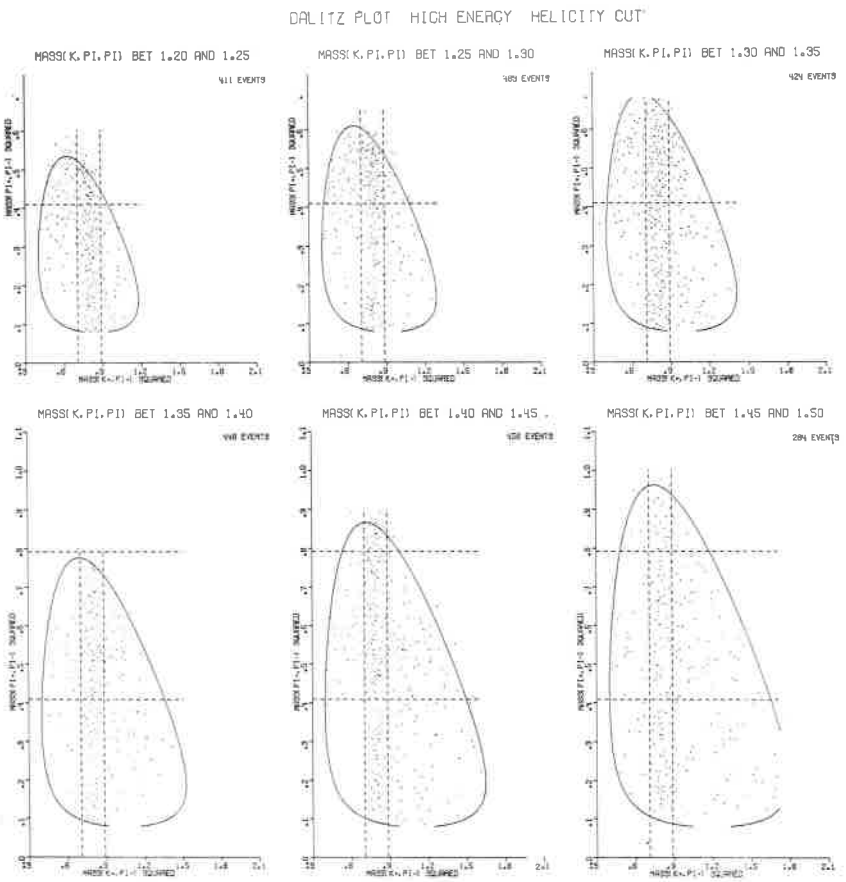

Fig. 4. – Q decay Dalitz plot for the events with an incoming momentum between 7.0 and 9.5 GeV/c.

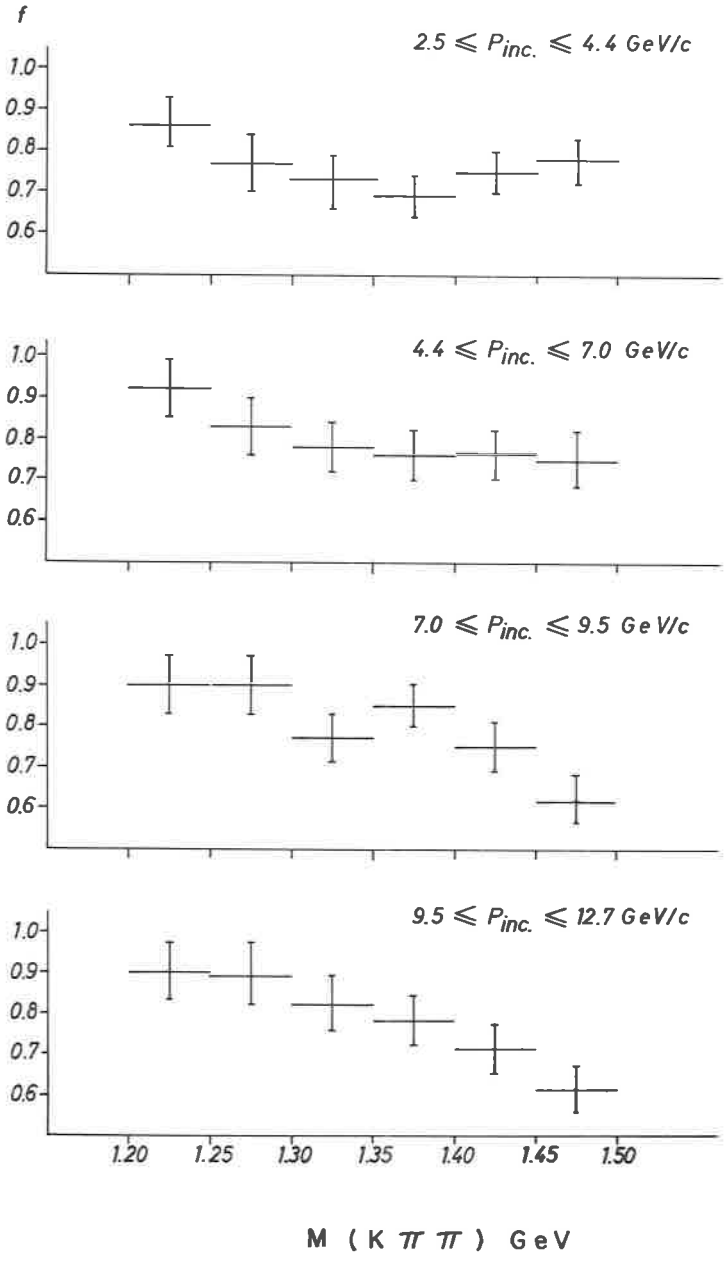
f
2.5 ≤ P inc. ≤ 4.4 GeV/c
4.4 ≤ P inc. ≤ 7.0 GeV/c
7.0 ≤ P inc. ≤ 9.5 GeV/c
9.5 ≤ P inc. ≤ 12.7 GeV/c
1.0
0.9
0.8
0.7
0.6
1.20
1.25
1.30
1.35
1.40
1.45
1.50
M (K π π) GeV

Fig. 5 *a*.

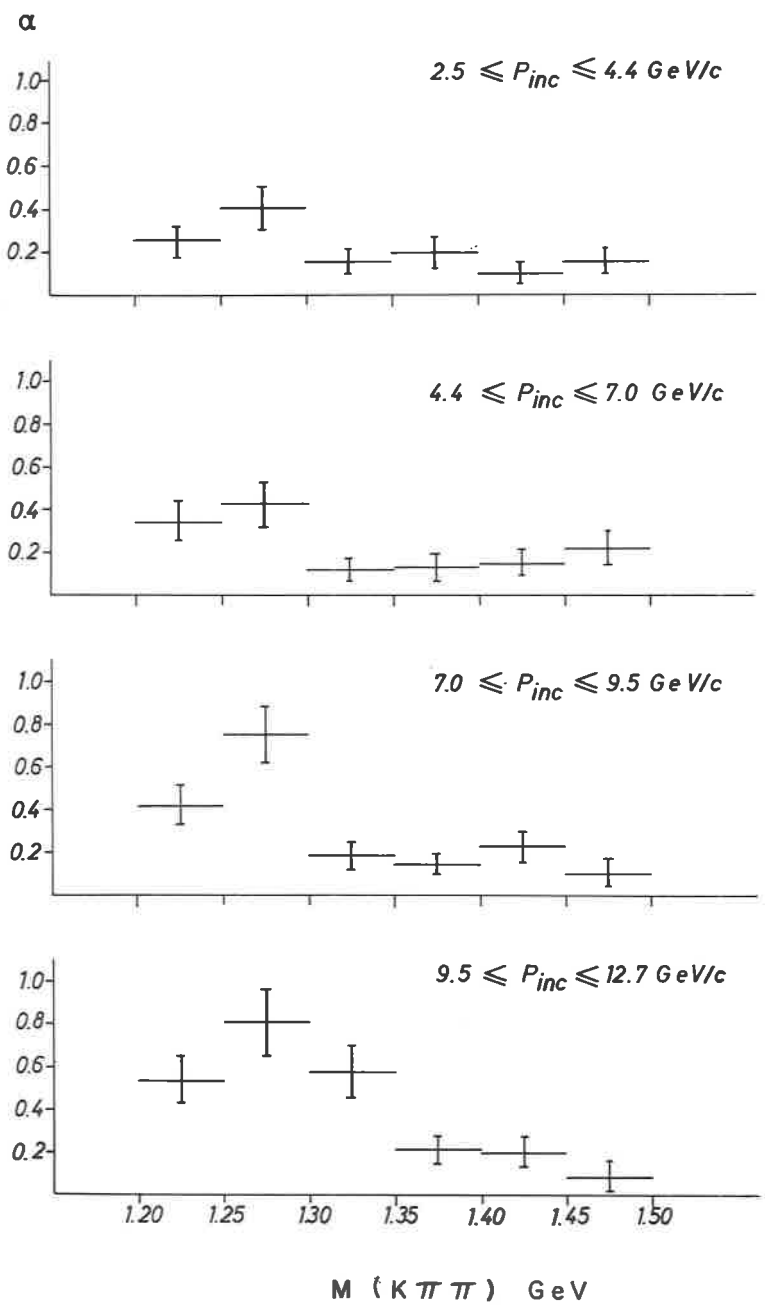
α
2.5 ≤ P_inc ≤ 4.4 GeV/c
4.4 ≤ P_inc ≤ 7.0 GeV/c
7.0 ≤ P_inc ≤ 9.5 GeV/c
9.5 ≤ P_inc ≤ 12.7 GeV/c
1.0
0.8
0.6
0.4
0.2
1.20
1.25
1.30
1.35
1.40
1.45
1.50
M (Kππ) GeV

Fig. 5*b*.

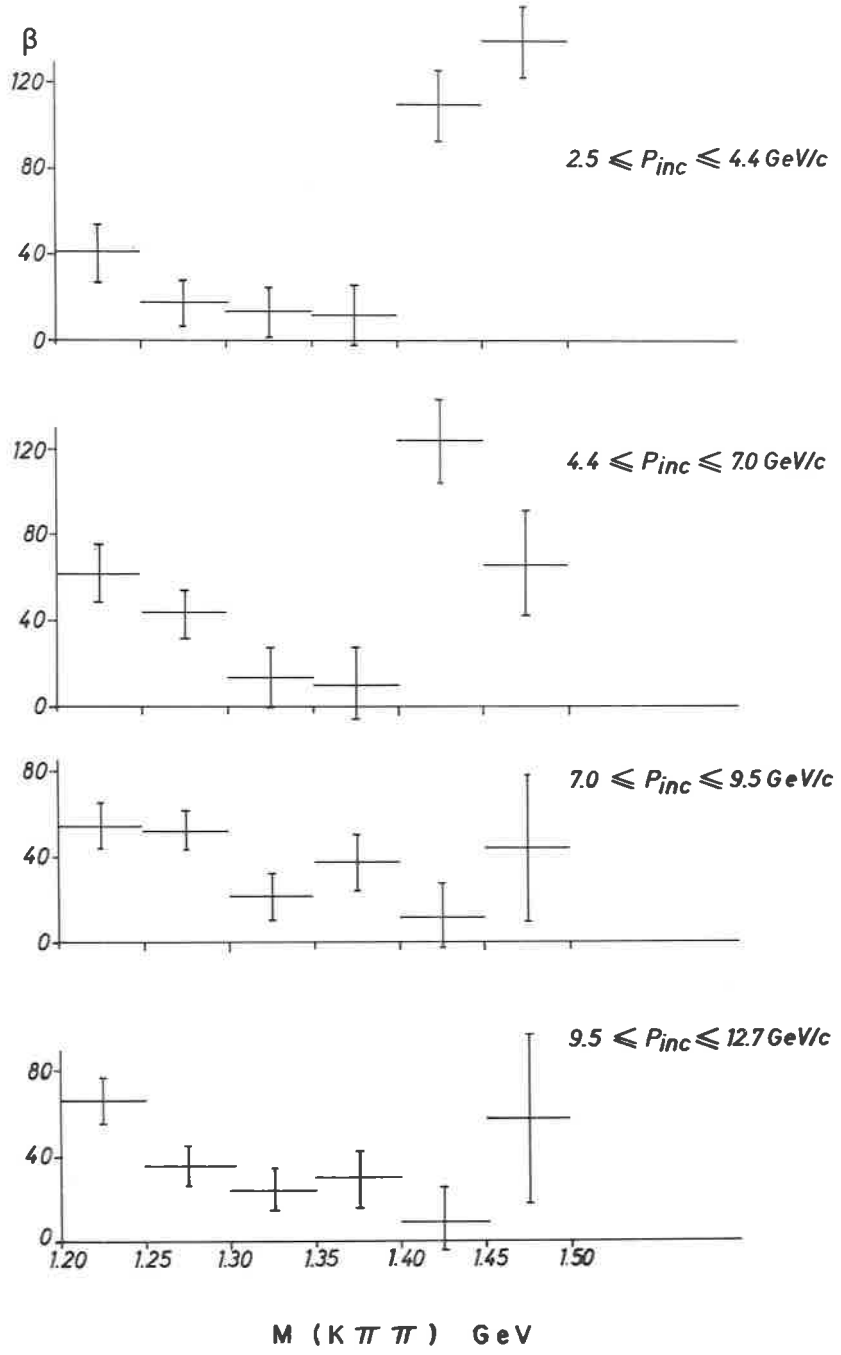

Fig. 5*c*. – Variation of the parameters describing the distribution of the events in the Dalitz plot with the $K\pi\pi$ mass: *a*) f; *b*) α; *c*) β.

The decay into K*(892)π is clearly dominant for all Kππ masses, while the Kρ decay is only visible for M(Kππ) < 1.30 GeV.

The density of the events in the Dalitz plot was parametrized as follows:

$$W\left(M^2(K^+\pi^-), M^2(\pi^+\pi^-)\right) =$$

$$= (f/N_R)|A(K^*) + \sqrt{\alpha}\exp[i\beta]\left(I(K^*)/I(\varrho)\right)^{1/2}A(\varrho)|^2 + (1-f)/N_{PS}\,. \qquad (7)$$

In this formula A(K*) and A(ρ) represent the decay amplitudes of the Q into K*(892) π and Kρ respectively and depend on the spin-parity of the Q. I(K*) and I(ρ) are the integrals of $|A(K^*)|^2$ and $|A(\rho)|^2$ over phase space and N_R, N_{PS} normalisation factors ([3]).

The last term $(1-f)$ takes into account an incoherent background which is assumed to give a uniform distribution on the Dalitz plot.

In practice a satisfactory fit could only be obtained with the assumption $J^p = 1^+$, in agreement with the results of the previous analysis. The values obtained for the 3 parameters f, α and β are shown of Fig. 5 for 4 groups of incident energies and 6 intervals of the Kππ mass between 1.2 and 1.5 GeV. It is remarkable that these parameters are very similar at all energies.

The branching ratio α shows an interesting structure: at all energies, α is maximum for $1.25 \leqslant$ M(Kππ) $\leqslant 1.30$ GeV and this maximum increases with the incident momentum. This indicates that the decay into Kρ comes mainly from events with a lower Kππ mass, a result expected from the observation of the plots on Fig. 4. The values of the phase β show that the K*π and Kρ amplitudes interfere coherently for M(Kππ) $\leqslant 1.4$ GeV. The rapid variation of the phase above 1.4 GeV may be due to the K*(1420).

4. Density matrix.

The density matrix of the Q(assumed to be a 1^+ object) has been calculated for 4 energy subsamples and several intervals of momentum transfer using the normal to the Q decay plane as analyser. We checked by a Monte-Carlo calculation that the « helicity cut » does not bias the density matrix elements and used only events with $1.20 \leqslant$ M(Kππ) $\leqslant 1.35$ GeV in order to reduce the effects due to the K*(1420).

The decay distribution of a 1^+ object decaying into 3 pseudoscalar mesons can be written in the helicity frame or in the Jackson frame as follows ([4]):

$$W(\cos\theta, \varphi) = \frac{3}{8\pi}\left(\varrho_{11}(1+\cos^2\theta) + \varrho_{00}\sin^2\theta + \sqrt{2}\,\mathrm{Re}\,\varrho_{10}\sin 2\theta\cos\varphi + \right.$$
$$\left. + \varrho_{1-1}\sin^2\theta\cos 2\varphi\right) \qquad (8)$$

where θ and φ are the polar and azimuthal angles of the normal to the Q decay plane $\boldsymbol{n} = \boldsymbol{K}^+ \times \boldsymbol{\pi}^+$. The Y axes in both frames are defined along the normal to the production plane as $\boldsymbol{Y} = \boldsymbol{K}^+_{\text{inc}} \times \boldsymbol{Q}^+$. The values of the ϱ_{ij} were computed from the following moments:

$$\varrho_{00} = 2 - 5 \langle \cos^2 \theta \rangle$$

$$\varrho_{1-1} = \tfrac{5}{2} \langle \sin^2 \theta \cos 2\varphi \rangle$$

$$\operatorname{Re} \varrho_{10} = (5/\sqrt{2}) \langle \sin \theta \cos \theta \cos \varphi \rangle \qquad (9)$$

and are shown on Table II.

Again no significant variation of the results with the incoming momentum is observed. ϱ_{00} has nearly the same value in the Jackson and in the helicity frame at least for $t < 0.25$ GeV^2 and is different from one. Re ϱ_{10} is generally different from zero in both frames.

TABLE II.

P_K^+ (GeV/c)	ϱ_{ij}	Helicity frame			
		$t < 0.08$	0.08÷0.15	0.15÷0.25	0.25÷0.40
3.0÷ 4.4	No. events		117	90	83
	ϱ_{00}		0.89 ± 0.11	0.55 ± 0.14	0.47 ± 0.16
	ϱ_{1-1}		− 0.08 ± 0.13	− 0.06 ± 0.15	− 0.14 ± 0.15
	Re ϱ_{10}		0.08 ± 0.07	0.07 ± 0.08	0.09 ± 0.09
4.4÷ 7.0	No. events	301	235	163	117
	ϱ_{00}	0.84 ± 0.07	0.82 ± 0.08	0.79 ± 0.11	0.75 ± 0.13
	ϱ_{1-1}	− 0.09 ± 0.08	− 0.08 ± 0.09	− 0.14 ± 0.11	− 0.29 ± 0.12
	Re ϱ_{10}	0.03 ± 0.05	0.20 ± 0.05	0.16 ± 0.06	0.17 ± 0.07
7.0÷ 9.5	No. events	495	322	232	115
	ϱ_{00}	0.83 ± 0.06	0.79 ± 0.07	0.67 ± 0.09	0.81 ± 0.13
	ϱ_{1-1}	0.02 ± 0.07	− 0.20 ± 0.08	− 0.09 ± 0.09	− 0.53 ± 0.12
	Re ϱ_{10}	0.04 ± 0.04	0.09 ± 0.04	0.20 ± 0.05	0.07 ± 0.07
9.5÷12.7	No. events	506	311	207	71
	ϱ_{00}	0.87 ± 0.05	0.79 ± 0.07	0.85 ± 0.09	0.52 ± 0.15
	ϱ_{1-1}	0.07 ± 0.07	− 0.03 ± 0.08	− 0.35 ± 0.10	− 0.27 ± 0.16
	Re ϱ_{10}	0.15 ± 0.04	0.15 ± 0.05	0.16 ± 0.05	0.25 ± 0.11

TABLE II (*continued*)

P_K^+ (GeV/c)	ϱ_{ij}	Jackson frame			
		$t < 0.08$	0.08÷0.15	0.15÷0.25	0.25÷0.40
3.0÷ 4.4	No. events		117	90	83
	ϱ_{00}		0.80 ± 0.12	0.53 ± 0.13	0.53 ± 0.16
	ϱ_{1-1}		−0.12 ± 0.13	−0.07 ± 0.14	−0.11 ± 0.15
	Re ϱ_{10}		−0.15 ± 0.07	−0.11 ± 0.10	−0.04 ± 0.09
4.4÷ 7.0	No. events	301	235	163	117
	ϱ_{00}	0.79 ± 0.07	0.88 ± 0.08	0.74 ± 0.09	0.78 ± 0.13
	ϱ_{1-1}	−0.11 ± 0.08	−0.05 ± 0.09	−0.17 ± 0.11	−0.28 ± 0.12
	Re ϱ_{10}	−0.11 ± 0.05	−0.12 ± 0.05	−0.19 ± 0.07	−0.17 ± 0.07
7.0÷ 9.5	No. events	495	322	232	115
	ϱ_{00}	0.77 ± 0.06	0.77 ± 0.07	0.74 ± 0.08	0.82 ± 0.13
	ϱ_{1-1}	−0.01 ± 0.07	−0.21 ± 0.08	−0.05 ± 0.09	−0.43 ± 0.12
	Re ϱ_{10}	−0.13 ± 0.04	−0.13 ± 0.05	−0.13 ± 0.06	−0.08 ± 0.07
9.5÷12.7	No. events	506	311	207	71
	ϱ_{00}	0.90 ± 0.05	0.78 ± 0.07	0.86 ± 0.08	0.80 ± 0.15
	ϱ_{1-1}	0.09 ± 0.07	−0.03 ± 0.08	−0.35 ± 0.10	−0.12 ± 0.16
	Re ϱ_{10}	−0.09 ± 0.04	−0.15 ± 0.05	−0.15 ± 0.05	−0.10 ± 0.11

If the helicity was conserved in reaction (1) either in the s-channel or in the t-channel ([5,6]), we should expect ϱ_{00} to be equal to one and all the other ϱ_{ij} to be equal to zero in the helicity or in the Jackson frame respectively. The results given in Table II show that our results disagree with these predictions, even if only the highest available energies are considered.

The Donohue-Högaasen frame ([7]), which is the frame where the density matrix is diagonal, is reached from one of the frames used previously by a rotation ψ^H or ψ^J around the normal to the production plane, where $\psi^{H,J}$ is given by the relation:

$$\operatorname{tg}(2\psi^{H,J}) = -2\sqrt{2}\,\operatorname{Re}\varrho_{10}^{H,J}/(\tfrac{3}{2}\varrho_{00}^{H,J} - \tfrac{1}{2} + \varrho_{1-1}^{H,J})\,. \tag{6}$$

The values of ψ^J are shown in fig. 6. The curves on this figure give the rotation angle χ between the Jackson frame and the helicity frame. The values of ψ^J are significantly different from zero and from χ at all energies whereas in case of s- or t-channel helicity conservation, ψ^J should be equal to either χ or 0 respectively. There is no indication from the present data, shown in

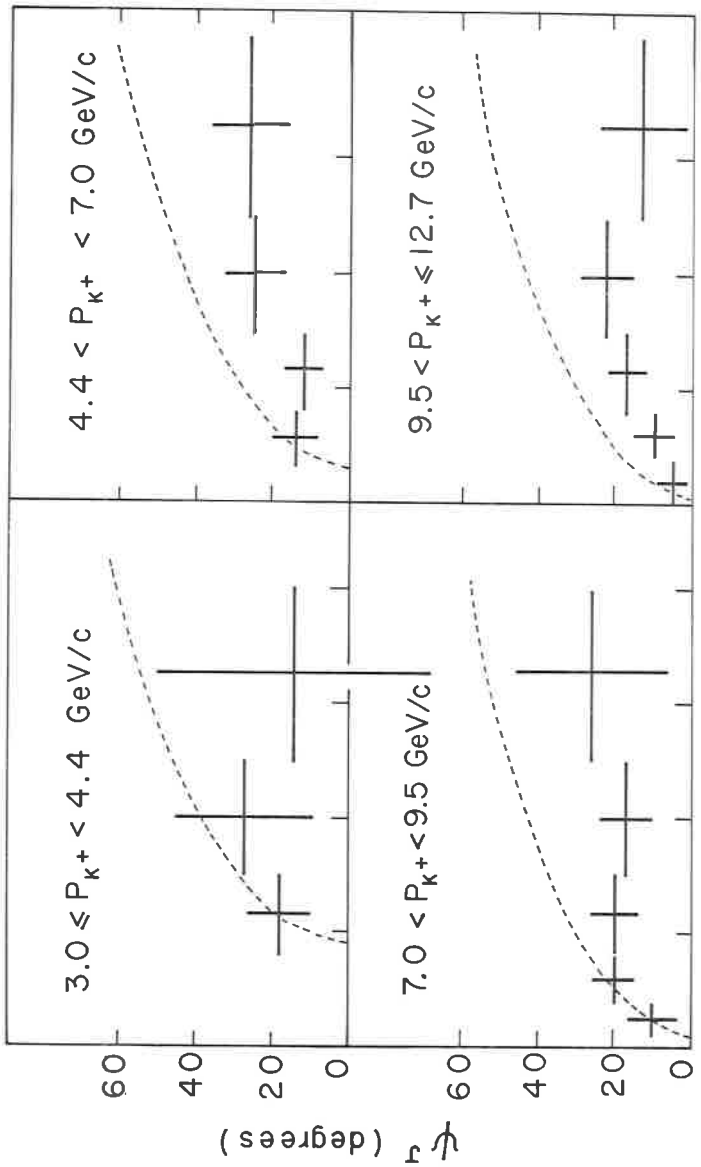

Fig. 6. – Variation of the rotation angle ψ' between the Jackson and the Donohue-Högaasen frames as function of the four-momentum transfer for $1.20 \leqslant M(K\pi\pi) \leqslant 1.35$ GeV.

Table II and Fig. 6, that they tend toward zero with increasing incident momentum.

We therefore conclude that there is no indication for *s*- or *t*-channel helicity conservation in the reaction $K^+p \to Q^+p$ at the presently available energies.

REFERENCES

1) S. M. Berman and M. Jacob: SLAC Report no. 43 (May 1965).
2) Suh Urk Chung: *Phys. Rev.*, **169**, 1342 (1968).
3) A similar analysis has been performed by the Birmingham-Glasgow-Oxford Collaboration on the 10 GeV/c data: *A study of* $K\pi\pi$ *states produced in* 10 GeV/c K+p *interactions* (Kiev Conference, 1970). In this analysis no incoherent background was used.
4) J. D. Jackson: in *High Energy Physics*, Les Houches Summer School of Theoretical Physics, Gordon and Breach Publishers (1965), p. 325.
5) F. J. Gilman *et al.*: *Phys. Lett.*, **31** B, 387 (1970).
6) J. V. Beaupré *et al.*: *Phys. Lett.*, **34** B, 160 (1971).
7) J. T. Donohue and H. Högaasen: *Phys. Lett.*, **25** B, 554 (1967).

Comparison of $A_1 - A_2$ interference between π^-p and π^+p reactions at 5 GeV/c (*)

BONN-DURHAM-NIJMEGEN-PARIS E. P. - TORINO COLLABORATION

The reactions $\pi^{\pm}p \to \pi^{\pm}\rho^0 p$ are characterized, in the low part of the $\pi\rho$ mass spectrum, by the presence of the A_2 resonance and of a wide threshold enhancement, the A_1, mainly $J^P = 1^+$, whose nature has been the subject of many discussions and different interpretations.

The aim of this paper is to compare the interference terms between A_1 and A_2 of the π^-p reactions with those of the π^+p reactions. We find that the interference terms have the same sign in π^- and π^+ initiated reactions. This is contrary to the expectations if the A_2 is produced by isovector and the A_1 by isoscalar exchange.

The experimental data used in the analysis come from the reactions $\pi^{\pm}p \to \pi^{\pm}\pi^+\pi^-p$ at 5 GeV/c (π^-p from the Illinois group [2]), π^+p from the Bonn-Durham-Nijmegen-Paris E. P. - Torino Collaboration [3]). Events with a $p\pi^+$ mass combination in the Δ^{++} mass band ((1.12÷1.32) GeV) were excluded; for the accepted events the presence of at least one $\pi^+\pi^-$ combination in the ρ^0 mass band ((0.66÷0.86) GeV) was required, and a selection of $t' = |t - t_{\min}| < 0.5$ GeV was applied. The $\pi^{\pm}\rho^0$ mass spectra are given in Fig. 1. Since, as shown in ref. [3], about 80% of the A_2 signal is concentrated in the inner half of the Dalitz plot (see Fig. 1 for the definition of inner and outer), we divide the events between inner and outer halves to have a concentrated A_2 signal in the inner half and the outer half as a control region.

To isolate the interference term between a 1^+ and a 2^+ state decaying to 3π, we analyze the moments of the distributions of the three Euler angles

---

(*) Invited paper presented by A. Werbrouck. Istituto di Fisica dell'Univ. Torino.

α, β, γ (*) which describe completely the 3π decay plane ([4]). We write in the following way the amplitude of the 1^+ and 2^+ states, produced with J component along the quantization axis (beam direction) equal to m and decaying into a 3π state with J component along the direction of the normal equal to

$$A \propto a'_m R_M D^{1*}_{mM}(\alpha, \beta, \gamma) + b'_m S_M D^{2*}_{mM}(\alpha, \beta, \gamma) , \qquad (1)$$

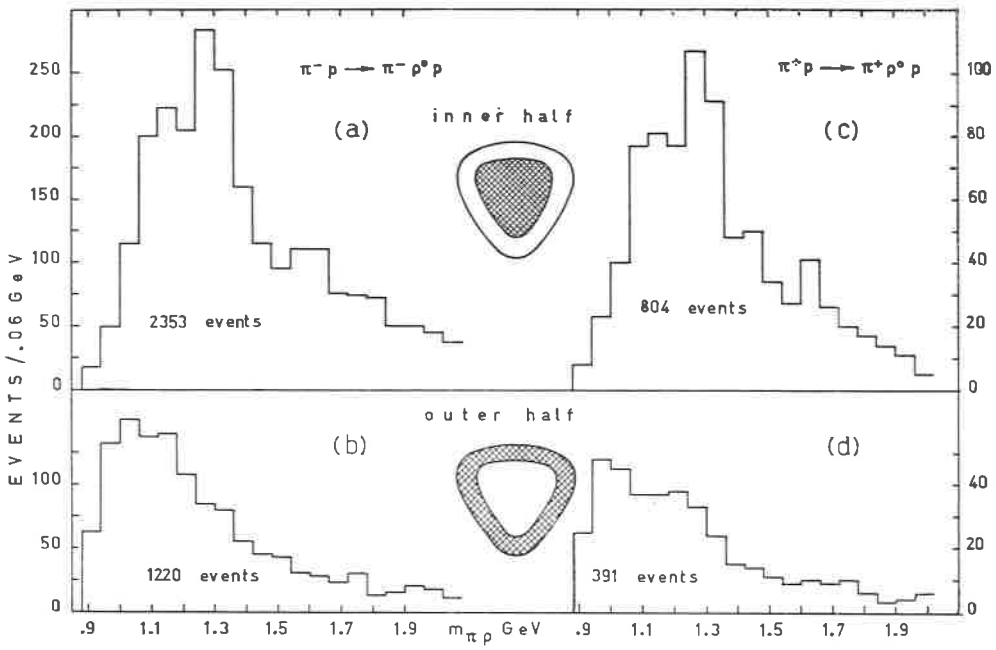

Fig. 1. – $\pi\rho$ mass spectra: *a*) and *b*) events from the reaction $\pi^-p \to \pi^-\rho^0 p$ selected in the inner and outer halves of the Dalitz plot (the inner, respectively outer, half is defined as having the radial distance divided by the maximum radial distance smaller, respectively larger, than $\sqrt{\frac{1}{2}}$, as illustrated in the insets); *c*) and *d*) same as *a*) and *b*) for the reaction $\pi^+p \to \pi^+\rho^0 p$.

M: where a'_m and b'_m are the production amplitudes, R_M and S_M are the decay amplitudes respectively of the 1^+ and 2^+ states. The parity of the states is

---

(*) The Euler angles are taken as: β and α the polar and azimuthal angles of the normal to the 3π decay plane, γ the rotation angle of the odd pion in the decay plane. The reference system, in the 3π c.m., has the z axis along the beam direction and the y axis along the normal to the production plane.

indirectly taken into account by restricting the allowed values for M (which could run from $-J$ to J) to ± 1 since only odd values of M are allowed for positive parity states, even values for negative parity. Taking the squared modulus of eq. (1) and expanding the product of D functions by use of the C.G. series we obtain the following expected angular distribution of the interference terms:

$$\frac{dN_0}{d\Omega_3} = \sum_{\substack{mm \\ MM' \\ L}} [(-1)^m(-1)^M R_M S^*_{M'} a_m b^*_{m'} C(1, 2, L; -M, M') \cdot$$

$$\cdot C(1, 2, L; -m, m') D^L_{nN}(\alpha, \beta, \gamma) + \text{c.c.}], \tag{2}$$

TABLE I. – A_1-A_2 *interference moments.*

$\langle \mathrm{Re}\, D^1_{10} \rangle$	$= \frac{8\pi^2}{3}\frac{3}{10} \mathrm{Re}\,[A_+(a_0 b^*_1 - a_0 b^*_{-1})]$
$\langle \mathrm{Im}\, D^1_{10} \rangle$	$= \frac{8\pi^2}{3}\frac{3}{10} \mathrm{Im}\,[A_+(a_0 b^*_1 + a_0 b^*_{-1})]$
$\langle \mathrm{Re}\, D^2_{10} \rangle$	$= \frac{8\pi^2}{5}\sqrt{\frac{1}{12}} \mathrm{Re}\,[-A_-(a_0 b^*_1 + a_0 b^*_{-1})]$
$\langle \mathrm{Im}\, D^2_{10} \rangle$	$= \frac{8\pi^2}{5}\sqrt{\frac{1}{12}} \mathrm{Im}\,[-A_-(a_0 b^*_1 - a_0 b^*_{-1})]$
$\langle \mathrm{Re}\,(D^2_{12} \pm D^2_{1-2}) \rangle$	$= \frac{8\pi^2}{5}\sqrt{\frac{1}{18}} \mathrm{Re}\,[\mp B_\mp(a_0 b^*_1 \pm a_0 b^*_{-1})]$
$\langle \mathrm{Im}\,(D^2_{12} \pm D^2_{1-2}) \rangle$	$= \frac{8\pi^2}{5}\sqrt{\frac{1}{18}} \mathrm{Im}\,[\mp B_\mp(a_0 b^*_1 \mp a_0 b^*_{-1})]$
$\langle \mathrm{Re}\, D^3_{10} \rangle$	$= \frac{8\pi^2}{7}\sqrt{\frac{8}{75}} \mathrm{Re}\,[-A_+(a_0 b^*_1 - a_0 b^*_{-1})]$
$\langle \mathrm{Im}\, D^3_{10} \rangle$	$= \frac{8\pi^2}{7}\sqrt{\frac{8}{75}} \mathrm{Im}\,[-A_+(a_0 b^*_1 + a_0 b^*_{-1})]$
$\langle \mathrm{Re}\,(D^3_{12} \pm D^3_{1-2}) \rangle$	$= \frac{8\pi^2}{7}\sqrt{\frac{16}{45}} \mathrm{Re}\,[\mp B_\pm(a_0 b^*_1 \mp a_0 b^*_{-1})]$
$\langle \mathrm{Im}\,(D^3_{12} \pm D^3_{1-2}) \rangle$	$= \frac{8\pi^2}{7}\sqrt{\frac{16}{45}} \mathrm{Im}\,[\mp B_\pm(a b^*_1 \pm a_0 b^*_{-1})]$
$A_\pm = R_1 S^*_1 \pm R_{-1} S^*_{-1}$,	$B_\pm = R_1 S^*_{-1} \pm R_{-1} S^*_1$

where $n = m' - m$, $N = M' - M$, $d\Omega_3 = d\alpha\, d\cos\beta\, d\gamma$ and $a_m b_m$ are the coherent parts of the a'_m b'_m amplitudes.

By the D function orthonormality properties one can calculate the expected values of the D function moments, collected in Table I, We assumed for the production amplitudes that only the $m = 0$ amplitude for the A_1 and the

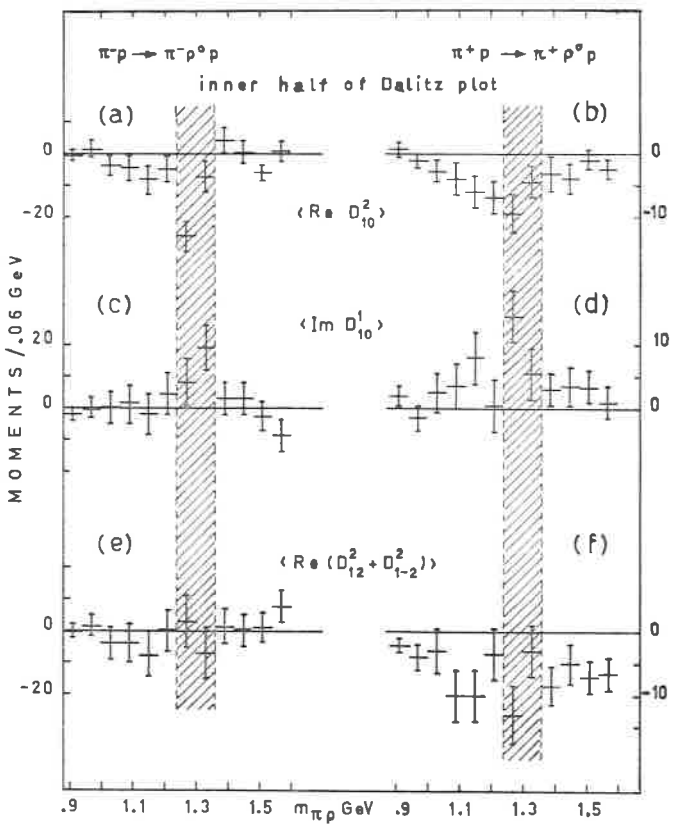

Fig. 2. – Dependence on the $\pi^{\pm}\rho^0$ mass of some D function moments proportional to the A_1-A_2 interference for $\pi^-\rho^0$ (left hand side) and $\pi^+\rho^0$ (right hand side) events in the inner half of the Dalitz plot.

$m = \pm 1$ amplitudes for the A_2 are sensibly different from zero (see ref. 2 and 3). The dependence on the production amplitudes is expressed by the factors $(a_0 b_1^* \pm a_0 b_{-1}^*)$. All the moments proportional to $a_0 b_1^* - a_0 b_{-1}^*$ are found experimentally to be compatible with zero, as expected if the A_2 is produced predominantly by natural parity exchange ([5]). We thus assume

$b_{-1} = b_1$, and write $a_0 b_1^* = |a_0||b_1| \exp[-i\delta]$, δ being the phase between the production amplitudes.

The most significant moments are shown in Fig. 2 (*) as a function of the $\pi\rho$ mass for events in the inner half of the Dalitz plot. One notices deviations at the, A_2 position which do not appear in the outer half (Fig. 3)

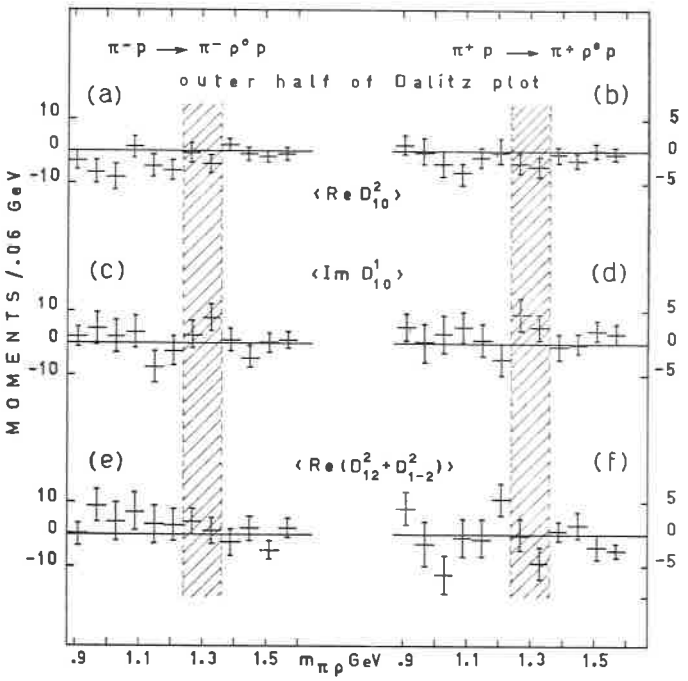

Fig. 3. – Dependence on the $\pi^{\pm}\rho^0$ mass of some D function moments proportional to the A_1-A_2 interference for $\pi^-\rho^0$ (left hand side) and $\pi^+\rho^0$ (right hand side) events in the outer half of the Dalitz plot.

and which we associate to the interference between A_1 and A_2: In fact the contributions of the direct A_1 and A_2 terms to these moments is either absent for L odd, or very small for $L = 2$, being proportional to the density matrix element ϱ_{10} which we know to be small for both states. The interference of

(*) In calculating the experimental moments we sum over the energies of the pions, except for an ordering of the equal charge pions according to their energy to avoid cancellation of the moments odd in the exchange of these pions (moments proportional to A_+ and B_+ in Table I).

the A_1 with other J^P states, which are probably present in the background, should be negligible since negative parity states cannot contribute to these moments, which have N even, and the next positive parity state, the 3^+, is still small in this region ([6]).

The interference effect appears to be similar, in Fig. 2, in π^- and π^+ data. We thus combine the π^- and π^+ moments to evaluate the phase angle δ. For this estimate we need to know the values of the $A_\pm$ and $B_\pm$ decay amplitudes, which are function of the pions energies and thus obviously depend on the decay mode of the A_1 and A_2: We calculated them assuming for the A_1 only S wave and for the A_2 only D wave decay. We obtain $\delta = -60° \pm 10°$ from the ratio $\langle \text{Im } D^1_{10} \rangle / \langle \text{Re } D^2_{10} \rangle$, averaged over $1.24 < m_{\pi\rho} < 1.36$ GeV.

The important point is that, independent of this estimate, all the moments of Fig. 2 have the same sign at the A_2 position in π^- and π^+ reactions. If the isospin exchanged in the production of the A_2 were 1, the $b_{\pm 1}$ amplitudes would have opposite sign in π^- and π^+ initiated rections, while the a_0 amplitude would have the same sign if the isospin exchanged in the production of the A_1 were zero. Under this hypothesis, all the interference moments, which are proportional to the product $a_0 b_1^*$, would have opposite sign in π^- and π^+ reactions. The fact they have on the contrary the same sign indicates that the A_1 and the A_2 are produced at least partially by the same isospin exchange.

The simplest interpretation of this interference effect is that part of the A_2 production is due to f^0 exchange and that only this part is coherent with the A_1 production amplitude. This is consistent with the fact that the f^0 exchange is more spin nonflip than spin flip, and that the A_1 production, if diffractive, should be mainly spin nonflip at the nucleon vertex. On the contrary ρ exchange is mainly spin flip at the nucleon vertex: since we sum over initial and final nucleon helicities, the interference between flip and nonflip amplitudes should average to zero. To reveal a possible interference between flip and nonflip amplitudes a polarized target should be used.

If this interpretation is correct it would also imply that the interference terms between A_2 amplitudes due to ρ^0 and f^0 exchange vanish if non polarized targets are used. This rules out the explanation of the A_2 splitting in π^-p reactions as due to the destructive interference of these two production amplitudes ([7]).

We are indebted to Dr. M. Jacob for illuminating discussions and in particular for suggesting the interpretation of the interference effect. We thank the Illinois group for giving us access to their data, and in particular Prof. G. Ascoli for helpful criticism.

REFERENCES

1) For a recent review see A. ASTIER, rapporteur's talk on *Boson Resonances at the XV International Conference on High-Energy Physics at Kiev* (1970).
2) G. ASCOLI, D. V. BROCKWAY, H. B. CRAWLEY, L. B. EISENSTEIN, R. W. HANFT, M. L. IOFFREDO and U. E. KRUSE: *Phys. Rev. Lett.*, **25**, 962 (1970).
3) G. RINAUDO *et al.* (BONN-DURHAM-NIJMEGEN-PARIS E.P.-TORINO COLLABORATION): *Analysis of the* A_1 *and* A_2 *regions in the reaction* $\pi+p\to\pi+\pi+\pi-p$ *at* 5 GeV/c, *Nuovo Cimento* **5** A, 239 (1971).
4) S. BERMAN and M. JACOB: *Phys. Rev.*, **139**, B 1201 (1965).
5) J. P. ADER, M. CAPDEVILLE, G. COHEN-TANNOUDJI and PH. SALIN: *Nuovo Cimento*, **56** A, 952 (1968).
6) D. V. BROCKWAY: *Thesis*, University of Illinois (1970); see also G. ASCOLI: talk given at this Conference.
7) D. G. SUTHERLAND: Communication at the *Second Philadelphia Meeting on Meson Spectroscopy* (May 1-2, 1970).

Observation of the B meson in the reaction $p\pi^+ \to p\omega\pi^+$ at 11.7 GeV/c (*)

DURHAM-GENOVA-HAMBURG-MILANO-SACLAY COLLABORATION

1. Introduction.

From an analysis of about 200000 pictures, obtained in an exposure of the 2.0 m HBC to a π^+ beam from the CERN PS at an incident momentum of 11.7 GeV/c, a sample of about 10500 four-prong events was fitted as belonging to the reaction

$$\pi^+ p \to p\pi^+\pi^+\pi^-\pi^0. \qquad (1)$$

In order to have a sample of events as clean as possible, severe selection criteria were applied as suggested by an analysis performed on faked events:

a) Events were accepted only when their confidence level (C.L.) was higher than 25%, to get rid of the no-fit contamination;

b) Events fitting besides reaction (1), the 4C reaction $\pi^+ p \to p\pi^+\pi^+\pi^-$ with a C.L. higher than 1% were attributed to the 4C channel;

c) For the events fitting reaction (1) with a C.L. higher than 25% more than once (for different mass assignments to the positive tracks) the hypothesys with best C.L. was accepted.

This sample has to be weighted by taking into account the different cross-sections for reaction (1) and for the reaction $\pi^+ p \to n\pi^+\pi^+\pi^+\pi^-$ and, via FAKE, the different contamination of 1C fit channel into the others. Thus a weighting factor $w = 1.19$ is given to every accepted hypothesis.

(*) Invited paper presented by S. RATTI. Istituto di Fisica dell'Univ. Milano.

d) If an event fits reaction (1) (with a C.L. higher than 25%) and simultaneously fits the reaction $\pi^+p \to n\pi^+\pi^+\pi^+\pi^-$ still with a C.L. higher than 25%, the weighting factor is reduced to $w = 0.30$.

The application of the previous selection criteria yields 6076 events which corresponds to a weighted sample of 6903 events.

Following this procedure, the cross-section for reaction (1) turns out to be:

$$\sigma = (1.48 \pm 0.15) \text{ mb} .$$

A remarkable feature of reaction (1) appears to be the production of several (3π) and (4π) resonances. Their study will be the subject of a future publication, while this paper is mainly devoted to a discussion of some characteristics of the B^+ meson observed in the $\omega\pi^+$ mass spectrum.

2. ω-meson production.

In Fig. 1 is shown the $\pi^+\pi^-\pi^0$ mass spectrum. The difficulty arising from the presence of two positive pions in the final state of reaction (1) can be overcome: in fact, if we label $\pi_f^+(\pi_s^+)$ the pion having the minimum (maximum) four-momentum transfer from the incident particle, we observe that the Δ^{++} isobar is practically produced only in the combination in which the proton is associated with the slower pion. Then in Fig. 1, we have plotted the $(\pi_s^+\pi^-\pi^0)$ mass combination for those events with $M(p\pi_s^+)$ outside the Δ^{++} region $(1.156 \leqslant M(p\pi_s^+) \leqslant 1.316 \text{ GeV/c}^2)$ and the $(\pi_f^+\pi^-\pi^0)$ mass combination for all events.

In the following, as far as the $(4\pi)^+$ mass combinations are concerned, the Δ^{++} isobar is always antiselected.

From an inspection of Fig. 1 one observes a strong ω production. A fit made by superimposing a Breit-Wigner curve upon a linear hand-drawn background gives a cross-section

$$\sigma(\pi^+p \to \pi^+p\omega) = (94 \pm 10)\,\mu\text{b}$$

where the correction for unseen neutral ω decays is taken into account. In the fit procedure, the mass of the ω meson was fixed at $M_\omega = 0.784 \text{ GeV/c}^2$. It is worth mentioning that the previously determined cross-section is unaffected by « double ω » events; actually in 10 cases only the two $(3\pi)^0$ mass combinations both lie in the ω region $(0.75 \leqslant M_\omega \leqslant 0.82 \text{ GeV/c}^2)$. The final

state $p\pi^+\omega$ includes the channel $\pi^+p \to \Delta^{++}\omega$ for which the cross-section was evaluated to be $\sigma(\pi^+p \to \Delta^{++}\omega) = (50 \pm 10)\,\mu b$.

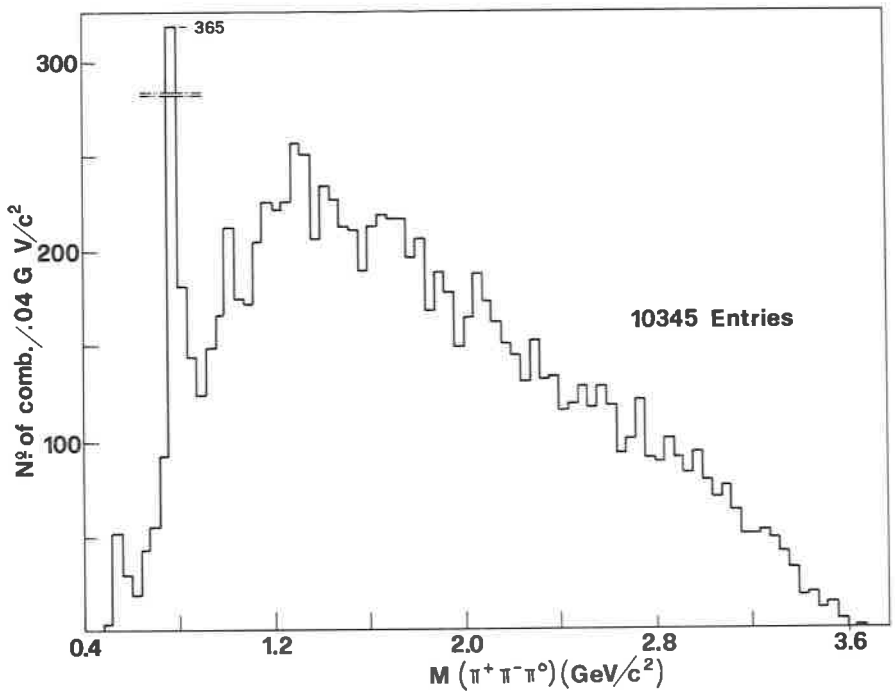

Fig. 1. – $\pi^+\pi^-\pi^0$ effective mass distribution for all events.

Furthermore Fig. 1 shows a peak in the η region and a broad enhancement in the A^0 region.

The bump at $\sim 1.0\ \mathrm{GeV/c^2}$ is discussed elsewhere [1] in connection with the h(1020) problem.

In order to have a more favourable signal to noise ratio for ω events, the procedure suggested by G. GOLDHABER *et al.* [2] was applied to our data.

This method works as follows: by taking advantage from the fact that a 1^-particle decaying into 3π must populate the central region of the Dalitz plot, one can define a suitable parameter to select a good ω sample.

By using the simplest squared 1^-decay matrix element

$$M^2 = |\boldsymbol{p}_+ \times \boldsymbol{p}_-|^2 \qquad (2)$$

($p_\pm$ indicates $\pi^\pm$ 3-momentum in the $\pi^+\pi^-\pi^0$ cm system) and normalizing it to its maximum value with

$$\lambda_\omega = \frac{M^2}{M^2_{\max}}; \quad M^2_{\max} = \frac{3}{4}\left(\frac{M^2_{3\pi}}{9} - m^2_\pi\right)^2; \qquad 0 \leqslant \lambda_\omega \leqslant 1 \tag{3}$$

one can select definite regions in the Dalitz plot by cutting on different ranges of λ_ω. If we assume the background to populate the Dalitz plot uniformly, its contribution in a selected area will be proportional to the area itself. Then, by integrating (3) we find that 50% of all ω events fall in the inner region $0.7 \leqslant \lambda_\omega \leqslant 1.0$, which contains only $\simeq 29\%$ of background events.

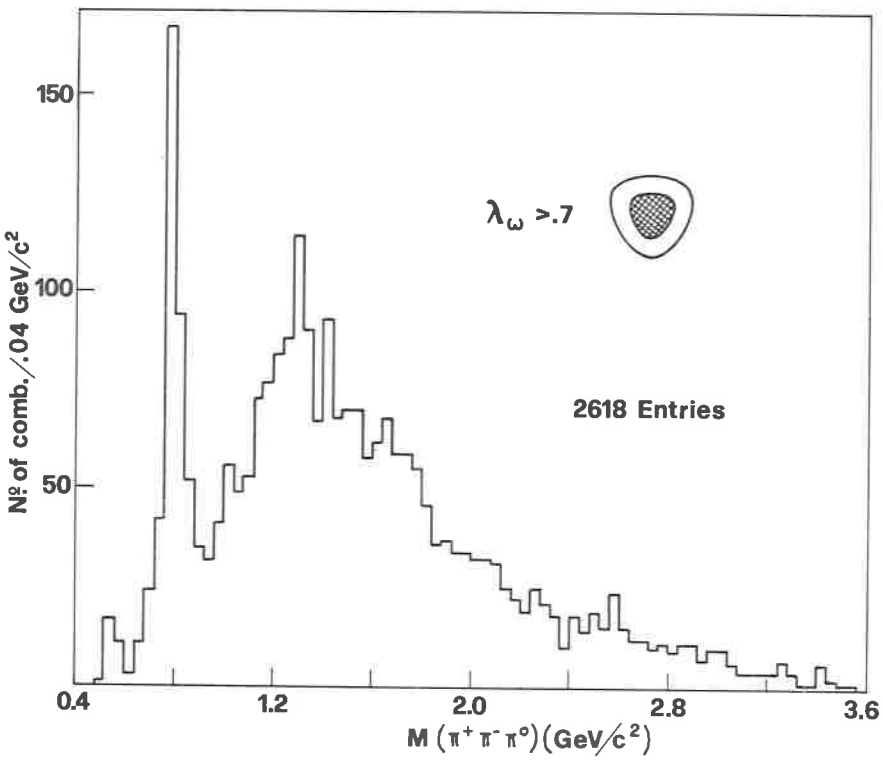

Fig. 2. – $\pi^+\pi^-\pi^0$ effective mass distribution for events having $\lambda_\omega > 0.7$.

The $(\pi^+\pi^-\pi^0)$ mass spectrum for events selected in the central region of the Dalitz plot ($\lambda_\omega > 0.7$) is reported in Fig. 2 which shows that the signal to background ratio for ω events is strongly increased with respect to that in Fig. 1.

The persistent η peak in a region where the 0^- events are unexpected is caused by the poor statistics of the η particle which is practically uniformly distributed in the whole Dalitz plot.

3. B-meson production.

In Fig. 3 the $(\omega\pi)$ mass distribution is shown. The shaded area refers to the events with $\Delta^2_{p/p} \leqslant 0.5\ (\mathrm{GeV/c})^2$. A large accumulation of events corresponding to the B^+ meson is clearly visible at about $M_{\omega\pi} \simeq 1.24\ (\mathrm{GeV/c^2})$;

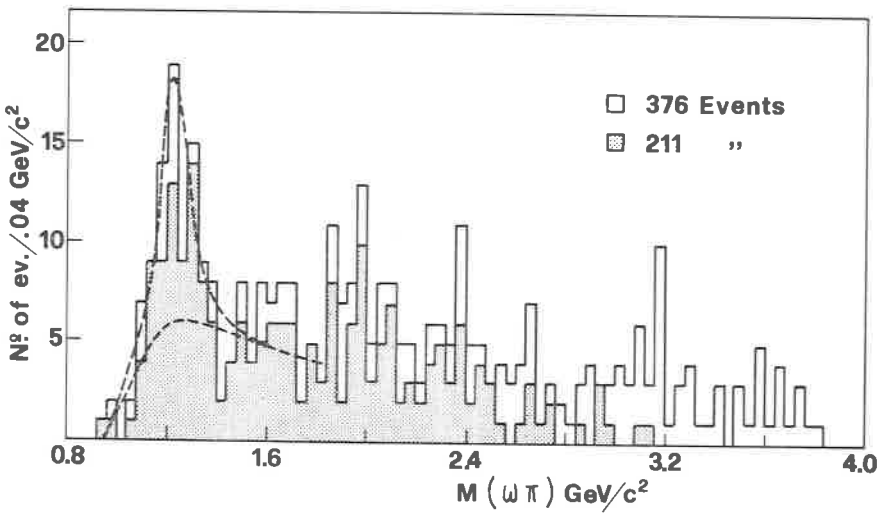

Fig. 3. – $\omega\pi$ effective mass distribution. The shaded histogram refers to the events with $\Delta^2_{p/p} \leqslant 0.5\ (\mathrm{GeV/c})^2$. The two dashed curves are explained in the text.

this peak is made more pronounced by selecting small values of the 4-momentum transfers, showing the peripheral production of such a resonance. The behaviour of the background under the B^+ peak was evaluated by plotting the $(4\pi)^+$ mass distribution for events with $M(\pi^+\pi^-\pi^0)$ lying in the two control regions $0.68 \leqslant M_{\pi^+\pi^-\pi^0} \leqslant 0.75\ (\mathrm{GeV/c^2})$ and $0.82 \leqslant M_{\pi^+\pi^-\pi^0} \leqslant 0.89\ (\mathrm{GeV/c^2})$. The lower dashed curve in Fig. 3 represents the average of the two obtained shapes, up to $M_{\omega\pi} = 1.72\ (\mathrm{GeV/c^2})$. A Breit-Wigner curve has been incoherently added to this background to obtain the characteristics of the B^+ observed resonance.

The upper dashed curve gives the result of the fitting procedure from which the free parameters come out to be:

$$M(B^+) = (1.224 \pm 0.010)\ (GeV/c^2)$$
$$\Gamma(B^+) = (0.134 \pm 0.010)\ (GeV/c^2) \qquad (4)$$

with a confidence level of $\simeq 75\%$.

The cross-section found for the two body reaction $\pi^+p \to pB^+$ is

$$\sigma(\pi^+p \to pB^+) = (15 \pm 4)\,\mu b$$

where the quoted error includes uncertainty for the assumed background and for the error in the cross-section of reaction (1).

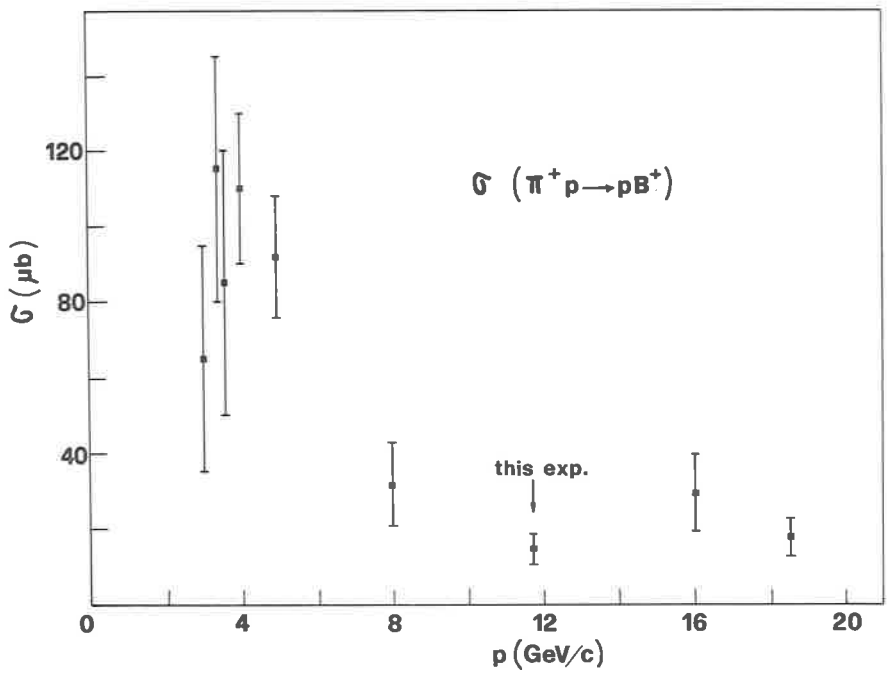

Fig. 4. – Cross-section for the reaction $\pi^+p \to pB^+$ as a function of the incoming momentum.

The above value once more contains the correction for unseen neutral ω decays. The cross-section obtained is plotted in Fig. 4 together with results

from other experiments at different energies ([3]). Our value is in agreement, within the errors, with a roughly constant B^+ production cross-section at $P_{lab} \geqslant 8$ GeV/c.

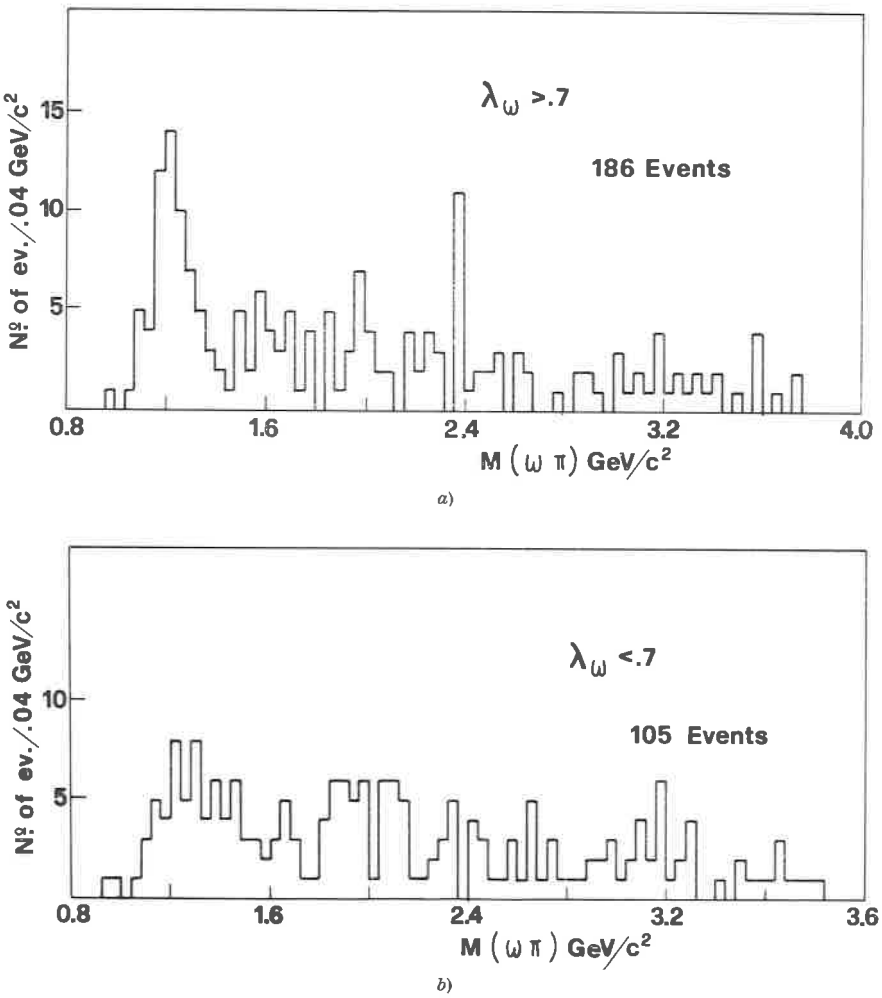

Fig. 5. – *a*) $\omega\pi$ effective mass distribution for events with $\lambda_\omega > 0.7$; *b*) $\omega\pi$ effective mass distribution for events with $\lambda_\omega < 0.7$.

To show how the $(\omega\pi^+)$ mass spectrum critically depends on the « ω » selected events, in Fig. 5*a* and 5*b* are reported the $(\omega\pi^+)$ mass distributions for events lying respectively in the inner and in the outer part of the ω Dalitz plot (we emphasize that the inner region is defined with $\lambda_\omega > 0.7$). In

Fig. 5*a* the background is drastically reduced with respect to that obtained by using all the events in the ω band (Fig. 3); on the contrary, in Fig. 5*b* there is practically no evidence of the B^+ peak since the B^+ region is completely submerged by the background shape.

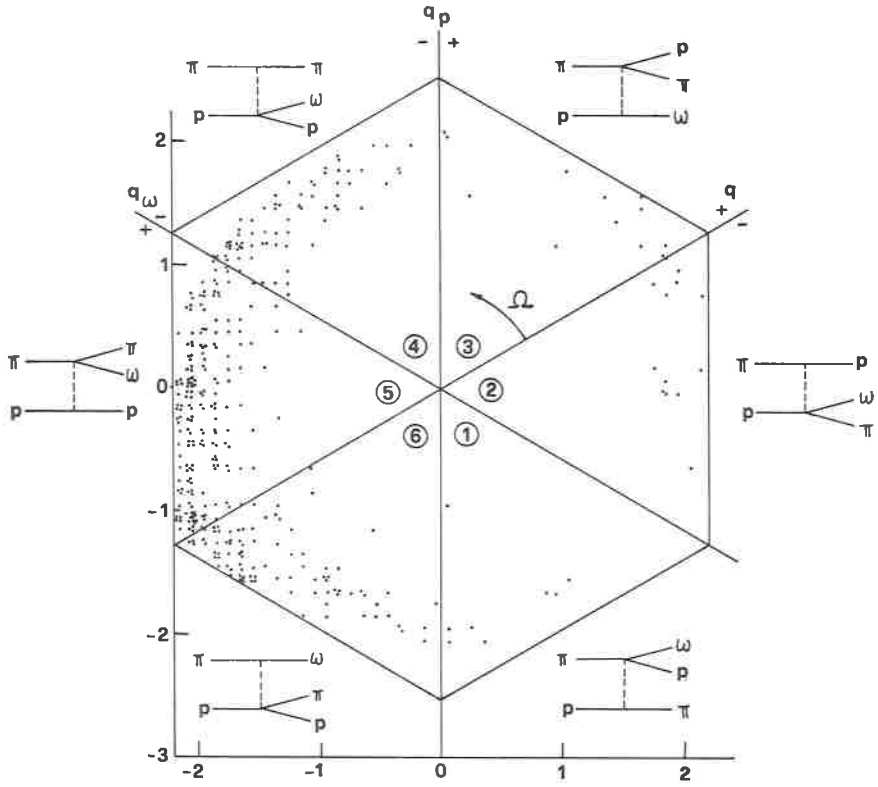

Fig. 6. – Van Hove hexagon for the reaction $\pi^+p \to \pi^+p\omega$.

Further improvement in reducing background under the B^+ signal can be obtained by using a technique suggested by L. Van Hove ([4]). In the hypothesis that all particles in a given final state have a longitudinal cm momentum (q_i) large compared to their transverse cm momentum $(p_T)_i$ and to their mass m_i, all the events should be spread along the surface

$$\sum_i |(q)_i| = W \quad (W = \text{total energy in cms}). \tag{5}$$

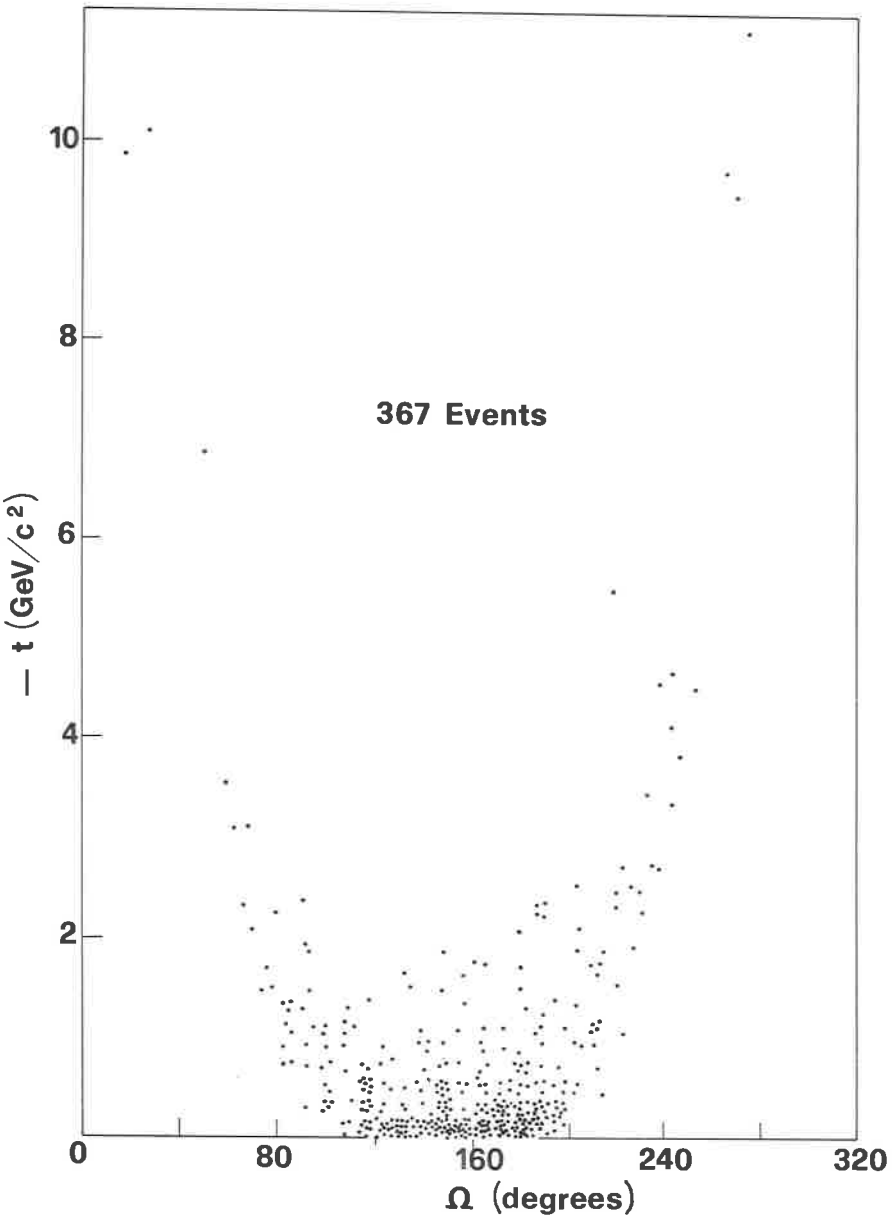

Fig. 7. – Ω angle *vs.* $t_{p/p}$ for the reaction $\pi^+p \to \pi^+p\omega$.

For a 3 particle final state, this surface reduces to the contour of a hexagon with the diagonals corresponding to:

$$(q)_1 = 0\,, \quad (q)_2 = 0\,, \quad (q)_3 = 0\,. \tag{6}$$

Such hexagon is shown in Fig. 6 for the reaction $\pi^+ p \to p\pi^+\omega$. Taking into account the set of signs of the three longitudinal momenta $(q)_p$, $(q)_{\pi^+}$, and $(q)_\omega$ it is possible to subdivide the hexagon into 6 regions; each region may be associated with a possible peripheral Feynman diagram. In Fig. 6 each region is labelled with the corresponding graph. One can observe a drastic depopulation of the regions corresponding to a baryonic exchange, *i.e.* of the regions (1), (2), (3) in the right-hand part of the hexagon.

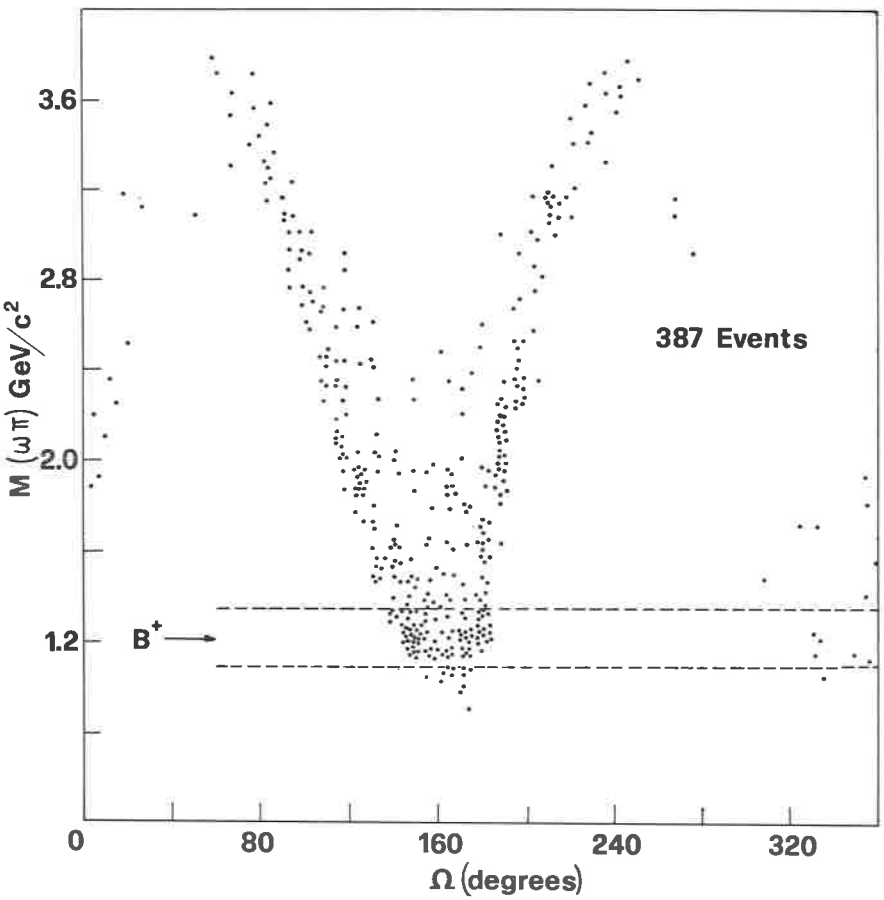

Fig. 8. – Ω angle *vs.* ωπ effective mass for the reaction $\pi^+ p \to \pi^+ p\omega$.

In Fig. 7 the Van Hove angle Ω (for the definition of Ω, see ref. ([4])) is plotted against the 4-momentum transfer, from the target to the outgoing proton. As usual, Ω starts from $q_{\pi^+} = 0$ and it increases anticlockwise. From the Figure it is evident that regions allowing a baryonic exchange are associated with large values of 4-momentum transfer. However, one has to remember that these regions contain events with a fast proton which could be a misidentified pion.

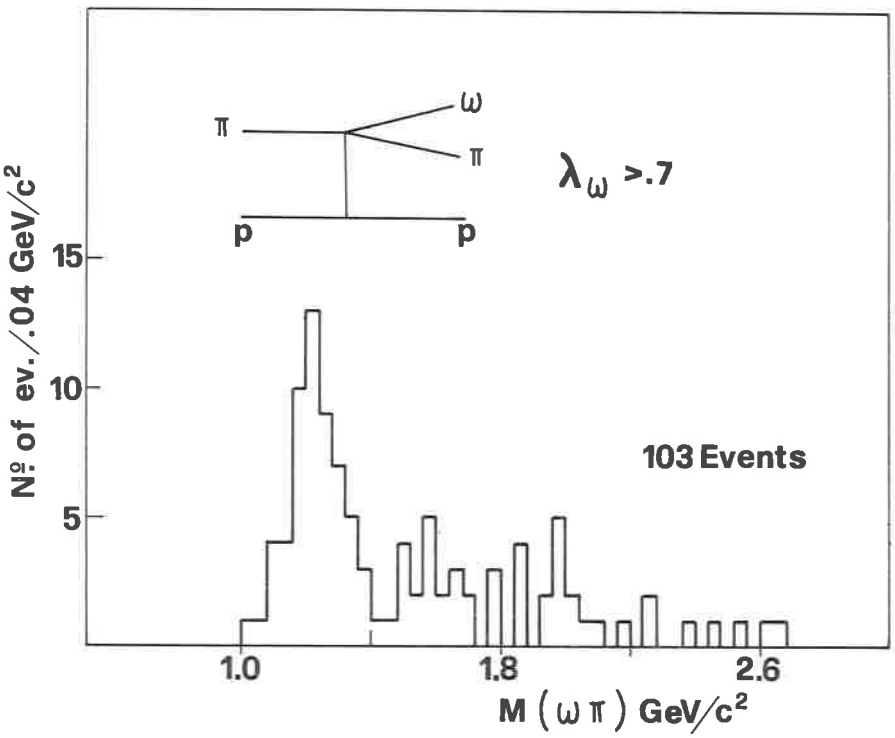

Fig. 9. – $\omega\pi$ effective mass distribution for events lying in region (5) of the Van Hove plot and with $\lambda_\omega > 0.7$.

In Fig. 8, the Ω angle is plotted against $M(\omega\pi^+)$. The main characteristic appears to be that for the majority of events in the B^+ band $(1.10 \leqslant M(\omega\pi^+) \leqslant 1.35\ (\mathrm{GeV}/c^2))$ the Ω angle lies in the range defining region (5) in the Van Hove hexagon. Such a characteristic agrees with the Feynman graph associated with this region, where the ω and π^+ particles go out from the same vertex.

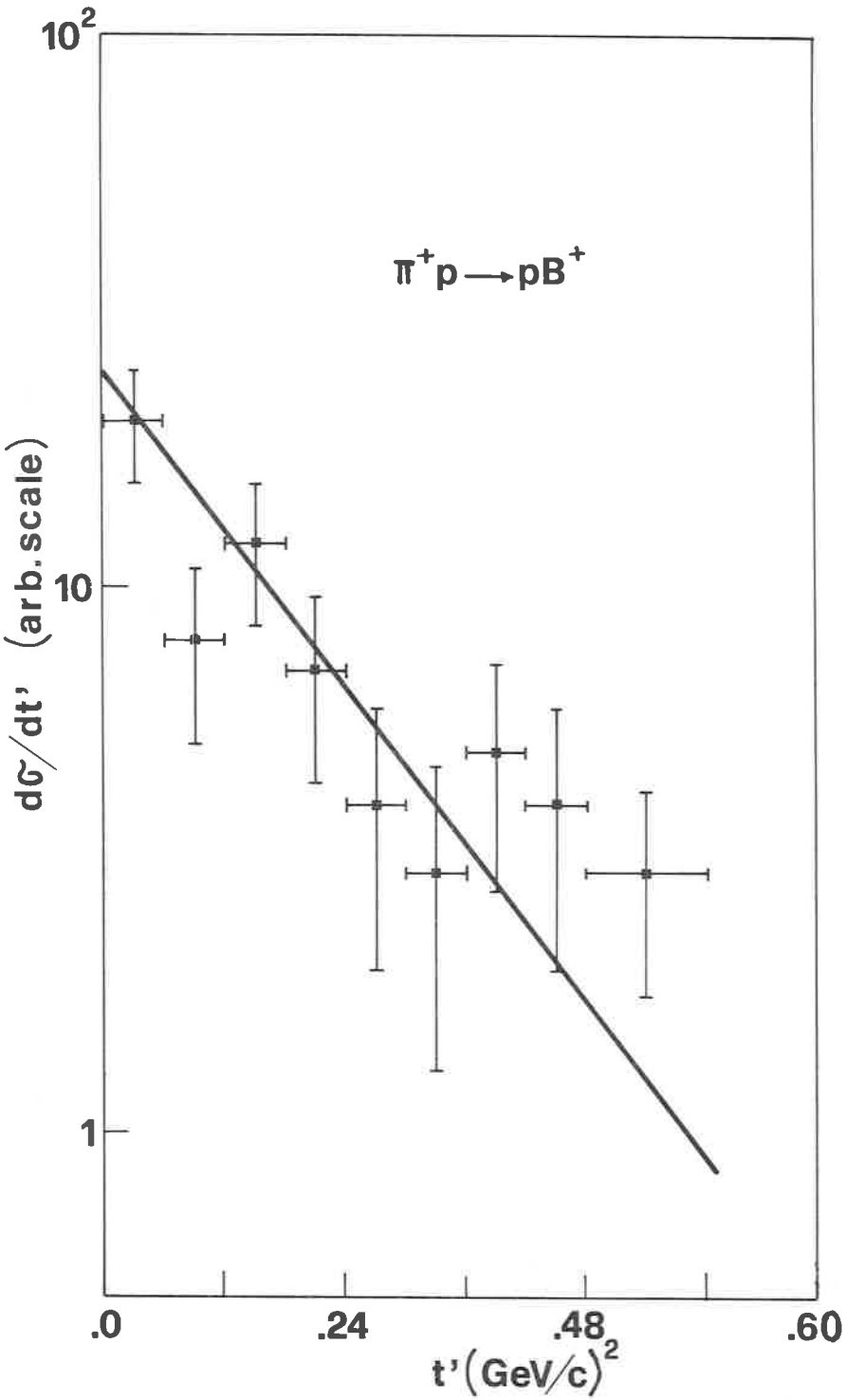

Fig. 10. – $d\sigma/dt'$ differential cross-section for the reaction $\pi^+ p \to pB^+$.

Thus, in Fig. 9 we report the $(\omega\pi^+)$ mass distribution for events in the inner part of the Dalitz plot and with $120° \leqslant \Omega \leqslant 180°$ (region 5). Under the B^+ signal there is practically no background.

Finally, in Fig. 10 $d\sigma/dt'$ for reaction $\pi^+p \to pB^+$ is plotted on an arbitrary scale. By fitting the distribution with an exponential form

$$d\sigma/dt' \simeq \exp[-At']$$

the value of the slope A comes out to be $A = (7 \pm 1)$ (GeV/c)$^{-2}$, in good agreement with the value (6.4 ± 0.8) (GeV/c)$^{-2}$ obtained at 8 GeV/c ([3f]).

REFERENCES

1) D.G.H.M.S. Collaboration: *Possible observation of the* h(1020) *meson*, (unpublished).
2) G. Goldhaber *et al.*: *Phys Rev. Lett.*, **15**, 118 (1965).
3) The data reported in Fig. 4 refer to the following experiments: *a*) 3.0 GeV/c, G. Gidal *et al.*: UCRL-17984 (1967); *b*) 3.43 GeV/c, M. Abolins *et al.*: *Phys. Rev. Let*,- **11**, 381 (1963); *c*) 3.65 GeV/c, G. Goldhaber *et al.* (see ref. ([2])); *d*) 4.0 GeV/c M. Aderholz *et al.*: *Phys. Rev.*, **138** B, 897 (1965); *e*) 5.0 GeV/c, C. L. Pols *et al.*: *Nucl. Phys.*, B **25**, 109 (1970); *f*) 8.0 GeV/c, M. Aderholz *et al.*: *Nucl. Phys.*, **B8**, 45 (1968); *g*) 11.7 GeV/c, this experiment; *h*) 16.0 GeV/c, J. Ballam *et al.*: SLAC-PUB-790 (preprint 1971); *i*) 18.5 GeV/c, M. J. Hones *et al.*: *Phys. Rev. D*, **2**, 827 (1970).
4) L. Van Hove: *Nucl. Phys.*, B **9**, 331 (1969).

The spin and parity of the D° meson (*)

M. GOLDBERG, B. MAKOWSKI, A. M. TOUCHARD
Institut de Physique Nucléaire - Paris

R. A. DONALD, D. N. EDWARDS and N. WEST
The University of Liverpool - Liverpool

The first evidence for the $D^0 \to K\bar{K}\pi$ ($M = 1285$) was found in $\bar{p}p$ annihilations at 1.2 GeV/c [1] and π^-p interactions [2]. A $\delta\pi$ decay mode has also been exhibited by several experiments [3]. D^0 is a possible candidate for the isosinglet of the $^3P_1$, $\bar{q}q$ state which corresponds to $J^{PC} = 1^{++}$, but there is up to now no unambiguous assignment of its spin parity; 0^-, 1^+, 2^- being possible [4,5], the last paper favouring 1^+.

The present study is based on the analysis of 240.000 pictures of $\bar{p}p$ annihilations at 1.1 GeV/c, taken in the 2m HBC at CERN. All events with at least one K_1^0 decay visible in the chamber have been measured. The corresponding events coming from the previous experiment at 1.2 GeV/c [1,4], have also been included. The total number is then 18931 events, more than three times the previous statistics.

The D^0 is seen in all the reactions involving an observable $(\bar{K}K\pi)^\circ$ system, generally over a high background. The most appropriate reaction to study the spin of the D^0 is the reaction $\bar{p}p \to K^0K^\mp\pi^\pm\pi^+\pi^-\pi^0$ where it is abundantly produced, mostly in association with ω^0 as shown in Fig. 1*a*. The mass and width are:

$$M = (1282 \pm 3)\ \text{MeV/c}^2, \qquad \Gamma = (56 \pm 12)\ \text{MeV/c}^2$$

$59 \pm 5\%$ of this reaction goes via the channel $D^0\omega^0$.

There is a rather low background in the $D^0\omega^0$ region, around 20%. The selection cuts for the $D^0\omega^0$ events used in the present analysis are:

$$1.26\ \text{GeV} \leqslant M_{K\bar{K}^\pm\pi^\mp} \leqslant 1.34\ \text{GeV}$$

$$0.75\ \text{GeV} \leqslant M_{\pi^+\pi^-\pi^0} \leqslant 0.81\ \text{GeV}$$

(*) Contributed paper submitted by B. Makowski

This gives a sample of 209 combinations which contains about 180 genuine $D^0\omega^0$ events.

The study of the Dalitz plot of the D^0 confirms what was stated in earlier papers: the D^0 decays via a $K\bar{K}$ scattering length and a π meson; this implies that $L_{K\bar{K}} = 0$ and then, that the D^0 has G-parity $+$ and spin and parity of the series ($J^P = 0^-, 1^+, 2^-, \ldots$). But this study was not sufficient to distinguish clearly between these hypotheses, 1^+ and 2^- being slightly favoured over 0^-.

An attempt has been made to obtain information from the associated $D^0\omega^0$ production. As shown in Fig. 1*a*, this is produced near threshold ($Q \simeq 60$ MeV). It is plausible to admit the dominance of an S wave in the final state; one has then very constraining conditions for the decay of both particles. The constraints deduced are valid for all allowed initial states.

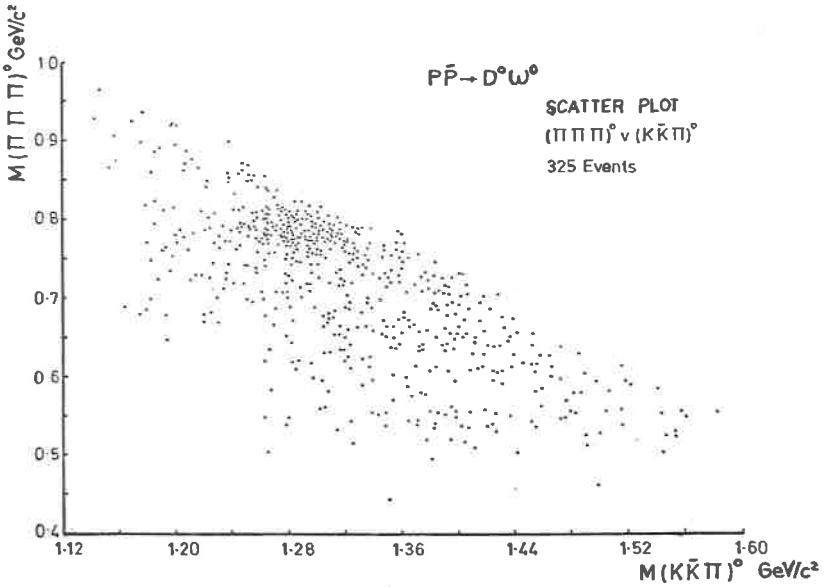

Fig. 1a

In the following we compare the experimental results to the predictions of this case. The normals to the decay planes of D^0 and ω^0 are taken as spin analyzers. The axis of quantization is the incident $\bar{p}$ direction.

It is then possible to test both spin, parity and charge conjugation assignments without any additional hypothesis on the initial state. The predictions for the spin density matrices of the D^0 and the ω^0 are given in Table I. They are deduced from the use of the joint density matrix ([8]). In the reactions $\bar{p}p \to D^0\omega^0$ the third component of the total angular momentum of the initial

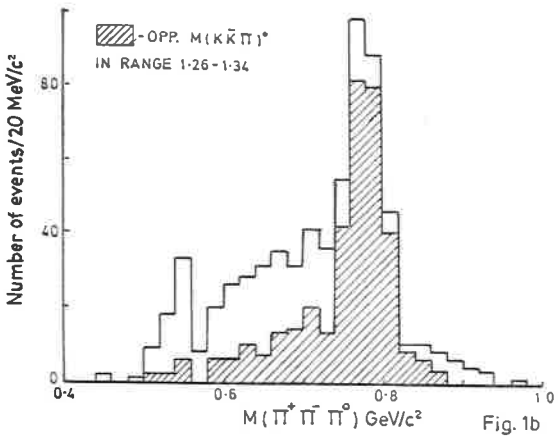

Fig. 1b

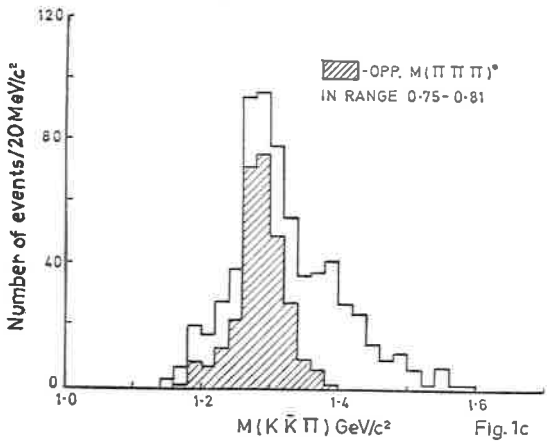

Fig. 1c

Fig. 1. – *a*) Scatter plot $M(\pi^+\pi^-\pi^0)$ *vs.* $M(K_1^0K^\pm\pi^\mp)$ 2 combinations per event. *b*) Histogram of $M(\pi^+\pi^-\pi^0)$ for $K_1^0K^\pm\pi^\mp\pi^+\pi^-\pi^0$ events. *c*) Histogram of $M(K_1^0K^\pm\pi^\mp)$ for $K_1^0K^\pm\pi^\mp\pi^+\pi^-\pi^0$ events.

state and of the spin of the final particles are denoted by λ, m, n. The transition matrix element is:

$$< D\omega|T|\lambda > = \sum_{mn} < mn|T|\lambda > M^D_m(\alpha)M^\omega_n(\beta)$$

The M being the angular dependence of the wave functions, α and β the directions characterizing the decay of the particles.

The decay distribution is:

$$W(\theta, \beta) = |\sum_\lambda \langle D\omega|T|\lambda\rangle|^2$$
$$= \sum_{\substack{m'n' \\ mn}} M_m^D(\alpha) M_n^\omega(\beta) M_{m'}^{D*}(\alpha) M_{n'}^{\omega*}(\beta) \sum_\lambda \langle mn|T|\lambda\rangle \langle m'n'|T|\lambda\rangle .^*$$

In the case of $L_{D\omega} = 0$, $\lambda = m$ and $n = m' + n'$ and the λ summation is reduced to one term.

With the $\bar{p}$ direction as the quantization axis, λ takes only the value 0 for the singlet initial state and 0, ± 1 for the triplet one.

If $J_D = 0$ the ω^0 spin orientation will be that of the initial state total angular momentum. In the other cases one has $\varrho_\omega^{00} = \varrho_{00}^D$ and $\varrho_D^{mm} = 0$ for $m \leqslant 2$ for an initial singlet state. For triplet initial state, parity conservation leads to $\varrho_{00}^{00} = 0$, then to the inequalities in Table I.

TABLE I.

$J_{D^0}^{P_D}$	Possible Initial States	
a) 0^{-+}	$^1P_1$	$\varrho_\omega^{00} = 1$
b) 0^{--} (exotic state)	$^3P_1$	$\varrho_\omega^{00} = 0$
c) 1^{++}	$^3S_1\,^3D_1\,^3D_2$	$\varrho_{00}^D < 1 - \varrho_\omega^{00}$
d) 1^{+-}	$^1S_0\,^1D_2$	$\varrho_{00}^D = \varrho_\omega^{00}$
e) 2^{-+}	$^1P_1\,^1F_3$	$\varrho_{00}^D = \varrho_\omega^{00}$ and $\varrho_{22}^D = 0$
f) 2^{--}	$^3P_1\,^3P_2\,^3F_2\,^3F_3$	$\varrho_\omega^{00} < 2\varrho_{11}^D$
g) $J > 2$		$\varrho_{mm}^D = 0$ for $m > 2$

Experimentally $\varrho_\omega^{00} = 0.58 \pm 0.05$ (see Fig. 2*b*). This excludes hypothesis *a* and *b*. Assuming $J_D^P = 1^+$ or 2^-, we have experimentally determined the diagonal elements of the density matrix of the D^0 and the joint density matrix of $D^0\omega^0$.

$J_D^P = 1^+$ gives $\varrho_{00}^D = 0.24 \pm 0.10$ which agrees with *c* but not with *d*.

For the 2^- hypothesis there are two amplitudes R_0 and R_2^+ ([7]). Taking into account the *G*-parity of the D^0 and keeping only the lower angular momenta ($l_{K\bar{K}} = 0$, $L_\pi = 2$ or $l_{K\bar{K}} = 2$, $L_\pi = 0$) the ratio R_2^+/R_0 is equal to 3. The result of the fit is the following:

$$\varrho_{00}^D = 0.18 \pm 0.12$$
$$\varrho_{11}^D = 0.15 \pm 0.09$$
$$\varrho_{22}^D = 0.26 \pm 0.07$$

Neither of the conditions d and e is satisfied. This rules out the hypothesis 2^{-+}. Concerning 2^{--}, due to the errors, definite conclusions cannot be drawn from condition *f* since $\varrho_{\omega}^{00} - 2\varrho_{11}^{D} = 0.28 \pm .0.19$

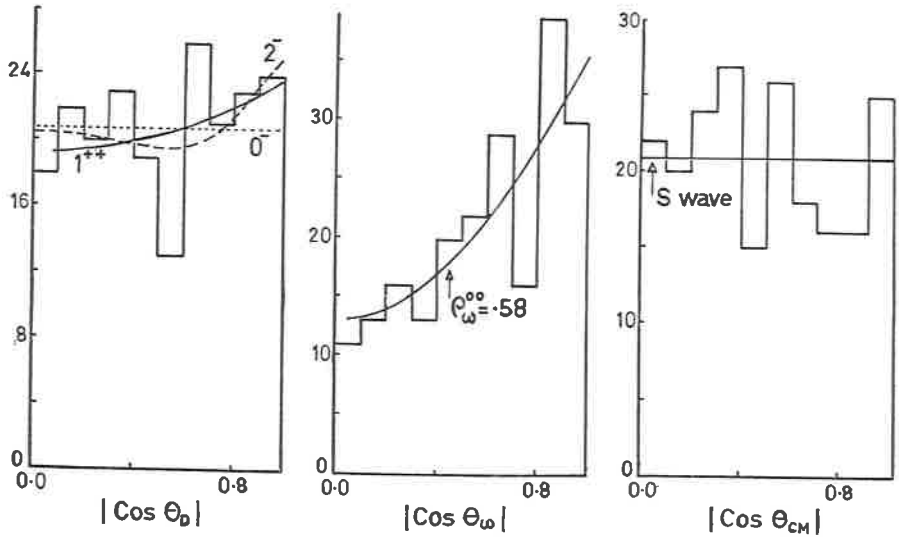

Fig. 2. – *a)* D^0 Angular distribution of the normal to the decay plane. The 2^- curve is a fit to the expression $ax^4 + bx^2 + c$. *b)* ω angular distribution of the normal to the decay plane. The curve corresponds to the fitted value $\varrho_{\omega}^{00} = 0.58$. *c)* Production angle distribution for Dω events.

We are then left with the two remaining hypotheses 1^{++} and 2^{--}. We may notice that the second one would lead to an *I*-spin equal to 1 which is in contradiction with known results ([9]). Furthermore a comparison of the log likelihood of the fits to the joint decay distribution produces much better agreement for 1^{++} than for 2^{--} (see Table II).

TABLE II.

J^{PC}	number of parameters	log likelihood
1^{++}	2	−279.24
2^{--}	3	−285.74

$J_D^{PC} = 1^{++}$ is then the only case where one gets full compatibility with experiment.

In conclusion, if $L_{D\omega} = 0$ predominates in the $\bar{p}p \to D^0\omega^0$ reaction near threshold, the only possible set of quantum numbers is $J^{PC} = 1^{++}$.

There are two necessary conditions for $L_{D\omega} = 0$: the production angle should be isotropic and the joint decay matrix element $\varrho_{00}^{00} = 0$. The experimental agreement is reasonable, see Fig. 2*c*, and the joint decay distribution gives $\varrho_{00}^{00} = 0.17 \pm 0.10$ *.

It is a pleasure to acknowledge the help of the CERN bubble chamber and P.S. crews in the acquisition of the film and our colleagues for their patient scanning, measuring and computing.

REFERENCES

1) CH. D'ANDLAU.: *Phys. Lett.*, **17**, 347 (1965).
2) D. H. MILLER *et al.*: *Phys. Rev. Lett.*, **14**, 1074 (1965).
3) C. DEFOIX *et al.*: *Phys. Lett.*, **28** B, 353 (1968); J. H. CAMPBELL *et al.*: *Phys. Rev. Lett.*, **22**, 1204 (1969); *Phys. Lett.*, **29** B, 529 (1959).
4) CH. D'ANDLAU *et al.*: *Nucl. Phys.*, B **5**, 693 (1968).
5) B. LORSTAD *et al.*: *Nucl. Phys.*, B **14**, 63 (1969).
6) H. PILKUHN and B. E. Y. SVENSSON: *Nuovo Cimento*, **38**, 518 (1965).
7) S. M. BERMAN and M. JACOB: *Phys. Rev.*, **139** B, 1023 (1965).
8) IPN-LIVERPOOL: Comunication at the *Kiev Conference*.

(*) It can be shown that in the case $L_{D\omega} = 1$, the hypothesis $J_P = 0^-$ is still excluded

SESSION II - A

Thursday, 15 April 1971

Electromagnetic interactions of mesons - Decay modes of π^0, η, ρ^0, ω, X^0 and φ - Primakoff production

Chairman: G. MORPURGO

Secretaries: E. REMIDDI
I. CORBETT

Radiative decays of mesons. (*)

M. GOURDIN
CERN - Geneva

1. General considerations.

1.1. – The subject of this introductory talk is the radiative decay of pseudoscalar mesons P and vector mesons V

$$\mathrm{P} \Rightarrow \gamma + \gamma$$

$$\mathrm{V} \Rightarrow \mathrm{P} + \gamma$$

$$\mathrm{P} \Rightarrow \mathrm{V} + \gamma$$

and a convenient theoretical framework for such a study in the broken SU_3 symmetry.

1.2. – For electromagnetic interactions the notion of U spin invariance [1,2] has been introduced on the analogy of the I spin invariance of strong interactions. One of the best success of the U spin invariance is the Coleman-Glashow relation [1] for the baryon octuplet $J^P = \frac{1}{2}^+$ which agrees very well with experiment.

In the SU_3 theory of electromagnetic interactions the assumptions made for the photon are twofold:

a) the photon is a U spin scalar;
b) the photon belongs to an adjoint representation of SU_3.

We must notice that a large number of results are independent of the assumption *b*).

(*) Introductory talk

1.3. – In the two cases of mesons considered here we have a nonet of particles ([3]), *e.g.*, a direct sum of octuplet and singlet SU_3 representations. Because of the SU_3 breaking a configuration mixing can occur between the two isoscalar members of the nonets ([4]).

A nice way to have an idea about such a mixing is to use the Gell-Mann Okubo (GM-O) mass formula ([5]) which is very successful for baryon multiplets like $J^P = \frac{1}{2}^+$ and $\frac{3}{2}^+$. Unfortunately for meson nonets the mass formula involves an a priori unknown mixing parameter and looses its predictive power for comparing the masses.

1.4. – For baryons the GM-O mass formula is linear in the particle masses. For mesons the theoretical situation is somewhat confusing. Arguments based on Lagrangian models or on propagator methods suggest to use squared masses or inverse squared masses depending on the type of SU_3 breaking we introduce ([6,7]). In our opinion this question is still open and we shall consider here both possibilities of a mass mixing formalism linear (L) or quadratic (Q) in the pseudoscalar and vector meson masses.

1.5. – More elaborated schemes of particle mixing have been proposed ([6,8,9]) using two parameters instead of one. We shall disregard these possibilities here for simplicity because the mass mixing formalism is in agreement with the Orsay data on vector meson production in electron-positron annihilation ([10,11]).

The comparison between theory and experiment involves the mixing angle θ_V for vector mesons and as an empirical fact the two values of θ_V computed with the GM-O mass formula using linear or quadratic masses are very close to each other

$$\theta_V^L = 37°, 7 \qquad \theta_V^Q = 40°, 2$$

so that a choice between these two directions is not possible in a process where only vector mesons are involved ([12]). Fortunately the situation is different for pseudoscalar mesons where the two values of the mixing angle θ_P are enough separated

$$\theta_P^L = 23°, 4 \qquad \theta_P^Q = 10°, 1$$

to imply different predictions.

1.6. – It is out of the limits of this report to discuss the general problem of SU_3 breaking for pseudoscalar and vector mesons. Let us just point out

some difficulties.

a) On what coupling constants must be applied the SU_3 or the U spin relations? ([13]);
b) Is it sufficient to take into account the large mass differences—especially for pseudoscalar mesons—only in phase space factors? ([14]);
c) Are the I spin and U spin invariances factorizable in the sense that SU_3 breaking terms depending on both I and U can be neglected as done for instance in Ref. ([1])?

These questions are obviously closely related to each other and they cannot be solved in a model independent way. Only experiments will decide if the assumptions made are reliable or not.

2. Pseudoscalar mesons.

2.1. – We study the 2γ decay mode of the pseudoscalar mesons $\mathrm{P} = \pi^0$, η^0 and X^0.

From Lorentz invariance, space reflection invariance and current conservation, the transition matrix element has the following structure

$$\langle \gamma_1, \gamma_2 | T | P \rangle = g_{\mathrm{P}} \varepsilon_{\mu\nu\varrho\sigma} p_1^{\mu} \varepsilon_1^{\nu} p_2^{\varrho} \varepsilon_2^{\sigma} \tag{1}$$

and the kinematics is indicated on Fig. 1.

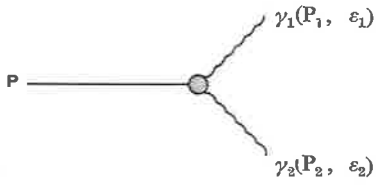

Fig. 1.

The decay width is computed from (1) to be

$$\Gamma(P \Rightarrow \gamma_1 + \gamma_2) = \frac{\pi\alpha^2}{4} m_{\mathrm{P}}^3 g_{\mathrm{P}}^2$$

where α is the fine structure constant $\alpha = 1/137$.

The best way to measure the $P \Rightarrow 2\gamma$ decay is to look at the coherent photoproduction of the P meson in the Coulomb field of a heavy nucleus, the so-called Primakoff effect ([15]) represented by the one-photon exchange diagram of Fig. 2.

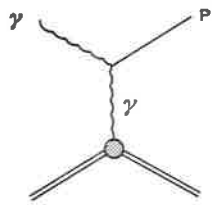

Fig. 2.

In the laboratory frame the P meson is produced at an angle θ and the angular distribution proportional to $\theta/[\delta^2 + \theta^2]^2$ has a strong narrow peak near the forward direction, because of the smallness of δ which tends to zero at high energy.

The π^0 life-time and the $\eta^0 \Rightarrow 2\gamma$ partial life-time have been measured by this method

$$\Gamma(\pi^0 \Rightarrow 2\gamma) = (11.7 \pm 1.2)\ \text{eV}\ ([16])$$

$$\Gamma(\eta^0 \Rightarrow 2\gamma) = (1.01 \pm 0.23)\ \text{keV}\ ([17]).$$

2.2. – The U spin invariance of electromagnetic interactions forbids the decay of the U spin vector P_8^1 into two photons ([18]) so that there are only two independent amplitudes describing the 2γ decay of the P mesons, one g_8 for the octuplet U spin scalar P_8^0 and one g_1 for the singlet U spin scalar P_1^0.

The mixing between the octuplet η_8 and the singlet isoscalars is written as ([7])

$$\eta^0 = \cos\theta_P \eta_8 - \sin\theta_P \eta_1$$

$$X^0 = \cos\theta_P \eta_1 + \sin\theta_P \eta_8$$

and the physical coupling constants are given in Table I.

TABLE I.

	g_8	g_1
g_{π^0}	$\sqrt{3}/2$	0
g_{η^0}	$\frac{1}{2}\cos\theta_P$	$-\sin\theta_P$
g_{X^0}	$\frac{1}{2}\sin\theta_P$	$\cos\theta_P$

2.3. – Let us now analyze the experimental data. By convention we choose g_{π^0} to be positive and in the absence of η^0-X^0 mixing the relation $g_{\eta^0}=\sqrt{3}g_{\pi^0}$ ([2]) suggests to take also $g_{\eta^0}>0$. From experiment we obtain

$$g_{\eta^0}=(0.337\pm 0.017)\ \text{GeV}^{-1}$$

$$g_{\eta^0}=(0.382\pm 0.044)\ \text{GeV}^{-1}$$

With the two values θ_p^L and θ_p^Q of the pseudoscalar mixing angle we compute the reduced matrix elements

$$g_8 = \quad (0.389\pm 0.019)\ \text{GeV}^{-1}$$

$$g_1^L = -(0.51\ \pm 0.12)\ \text{GeV}^{-1}$$

$$g_1^Q = -(1.08\ \pm 0.27)\ \text{GeV}^{-1}.$$

It is then straightforward to predict the $X^0\Rightarrow 2\gamma$ partial decay width

$$\Gamma^L(X^0\Rightarrow 2\gamma)=(5.6^{+3,5}_{-2,7})\ \text{keV}$$

$$\Gamma^Q(X^0\Rightarrow 2\gamma)=(39^{+23}_{-18})\ \text{keV}.$$

The two values differ by almost one order of magnitude and an absolute measurement of the $X^0\Rightarrow 2\gamma$ decay mode using for instance the Primakoff effect would be of the greatest interest to clarify the situation concerning the η^0-X^0 mixing. It will provide a check of the present scheme where the mass differences between the π^0, η^0 and X^0 mesons have been taken into account only through the phase space factor m_P^3 ([18]). Obviously the U spin invariance can be applied in different ways for instance on the dimensionless quantity $m_P g_P$ so that the phase space factor becomes simply m_P: such a possibility will imply a very large $X^0\Rightarrow 2\gamma$ width certainly in contradiction with experiment and the common sense.

3. Vector mesons.

3.1. – Let us now consider the radiative decay of a vector meson V

$$V \Rightarrow P + \gamma$$

or, when $m_P > m_V$ the radiative decay of a pseudoscalar meson P

$$P \Rightarrow V + \gamma$$

From Lorentz invariance, space reflection invariance and current conservation, the transition matrix element has the following structure

$$\langle \gamma, P|T|V\rangle = g_{VP\gamma}\varepsilon_{\mu\nu\varrho\sigma}p_\gamma^\mu \varepsilon_\gamma^\nu p_\nu^\varrho \varepsilon_\nu^\sigma \tag{2}$$

and the kinematics is indicated on Fig. 3

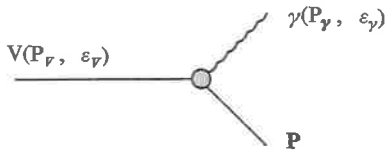

Fig. 3.

The decay widths are computed from (2) to be

$$\Gamma(V \Rightarrow P + \gamma) = \frac{\alpha}{24} g_{VP\gamma}^2 m_V^3 \left(1 - \frac{m_P^2}{m_V^2}\right)^3 \text{ when } m_V > m_P$$

$$\Gamma(P \Rightarrow V + \gamma) = \frac{\alpha}{8} g_{VP\gamma}^2 m_P^3 \left(1 - \frac{m_V^2}{m_P^2}\right)^3 \text{ when } m_P > m_V .$$

The radiative transition $\omega \Rightarrow \pi^0 + \gamma$ has been known for a long time and represents an appreciable fraction of the ω width. The world average value is [19,20]

$$\Gamma(\omega \Rightarrow \pi^0 + \gamma) = (1.12 \pm 0.20)\ \text{MeV} .$$

Two rare decay modes of the φ meson have been recently observed in an electron-positron colliding beam experiment at Orsay and the measured branching ratios are ([21])

$$B(\varphi \Rightarrow \pi^0+\gamma) = (0.19 \pm 0.08)\cdot 10^{-2}$$

$$B(\varphi \Rightarrow \eta^0+\gamma) = (1.92 \pm 0.57)\cdot 10^{-2}$$

Using, for the φ meson total width, an average value of 4 MeV ([20]) we deduce

$$\Gamma(\varphi \Rightarrow \pi^0+\gamma) = (7.6 \pm 3.2)\ \text{keV}$$

$$\Gamma(\varphi \Rightarrow \eta^0+\gamma) = (77 \pm 23)\ \text{keV}\,.$$

3.2. – From U spin invariance alone there exist five reduced matrix elements one defines as A^U_{jk} for the transition $\mathrm{V}^U_j \Rightarrow \mathrm{P}^U_k + \gamma$. The U spin index takes the values $U = 0, 1$ and two other indices j and $k = 1, 8$ indicate respectively the vector meson and pseudoscalar meson SU_3 representations. Table II gives the coupling constants $g_{\mathrm{VP}\gamma}$ for the physical transitions in terms of these five reduced matrix elements.

If, in addition, we assume that the photon belongs to an adjoint SU_3 representation we have two constraints

$$A^0_{11} = 0\,, \qquad A^0_{88} + A^1_{88} = 0$$

the second one being due to particle-antiparticle conjugation invariance.

3.3. – Let us now analyze the experimental data. We choose the phase conventions which will best agree later with the vector meson dominance model

$$g_{\omega\pi^0\gamma} > 0\,, \qquad g_{\varphi\pi^0\gamma} < 0\,, \qquad g_{\varphi\eta^0\gamma} < 0\,.$$

From experiment we compute the three coupling constants

$$g_{\omega\pi^0\gamma} = \quad (2.89 \pm 0.26)\ \text{GeV}^{-1}$$

$$g_{\varphi\pi^0\gamma} = -\,(0.16 \pm 0.02)\ \text{GeV}^{-1}$$

$$g_{\varphi\eta^0\gamma} = -\,(0.82 \pm 0.12)\ \text{GeV}^{-1}\,.$$

TABLE II

	$\frac{1}{4}(A^0_{88}-A^1_{88})$	$\frac{1}{2}A^0_{18}$	$\frac{1}{2}A^0_{81}$	$\frac{1}{2}(A^0_{88}+A^1_{88})$	A^0_{11}
$\rho \Rightarrow \pi\gamma$	1	0	0	1	0
$\rho \Rightarrow \eta\gamma$	$\sqrt{3}\cos\theta_P$	0	$-\sqrt{3}\sin\theta_P$	0	0
$X \Rightarrow \rho\gamma$	$\sqrt{3}\sin\theta_P$	0	$\sqrt{3}\cos\theta_P$	0	0
$\omega \Rightarrow \pi\gamma$	$\sqrt{3}\sin\theta_V$	$\sqrt{3}\cos\theta_V$	0	0	0
$\omega \Rightarrow \eta\gamma$	$-\sin\theta_V\cos\theta_P$	$\cos\theta_V\cos\theta_P$	$-\sin\theta_V\sin\theta_P$	$\sin\theta_V\cos\theta_P$	$-\cos\theta_V\sin\theta_P$
$X \Rightarrow \omega\gamma$	$-\sin\theta_V\sin\theta_P$	$\cos\theta_V\sin\theta_P$	$\sin\theta_V\cos\theta_P$	$\sin\theta_V\sin\theta_P$	$-\cos\theta_V\cos\theta_P$
$\varphi \Rightarrow \pi\gamma$	$\sqrt{3}\cos\theta_V$	$-\sqrt{3}\sin\theta_V$	0	0	0
$\varphi \Rightarrow \eta\gamma$	$-\cos\theta_V\cos\theta_P$	$-\sin\theta_V\cos\theta_P$	$-\cos\theta_V\sin\theta_P$	$\cos\theta_V\cos\theta_P$	$\sin\theta_V\sin\theta_P$
$\varphi \Rightarrow X\gamma$	$-\cos\theta_V\sin\theta_P$	$-\sin\theta_V\sin\theta_P$	$\cos\theta_V\cos\theta_P$	$\cos\theta_V\sin\theta_P$	$-\sin\theta_V\cos\theta_P$
$K^{*\pm} \Rightarrow K^{\pm}\gamma$	1	0	0	1	0
$K^{*0} \Rightarrow K^{0}\gamma$	-2	0	0	1	0

We assume the photon to be the U spin scalar of an octuplet. The two last columns of Table II disappear and we have only three independent parameters

$$X = A^0_{88}, \quad Y = A^0_{18}, \quad Z = A^0_{81}.$$

With the two possibilities for the mixings we compute the reduced matrix elements

$$X^L = (1.89 \pm 0.18)\ \text{GeV}^{-1} \qquad \left(\frac{Y}{X}\right)^L = 1.45 \pm 0.05 \qquad \left(\frac{Z}{X}\right)^L = -(2.13 \pm 0.50)$$

$$X^Q = (2.01 \pm 0.19)\ \text{GeV}^{-1} \qquad \left(\frac{Y}{X}\right)^Q = 1.33 \pm 0.04 \qquad \left(\frac{Z}{X}\right)^Q = -(5.88 \pm 1.22)$$

A more restrictive nonet symmetry formulated for instance in a quark model predicts (7)

$$\frac{Y}{X} = \sqrt{2} \qquad \frac{Z}{X} = -\sqrt{2}.$$

The ratios obtained with a linear mass mixing are compatible with these values.

4. Vector meson dominance.

4.1. – The P-γ-γ and P-V-γ vertices are related by the vector meson dominance as shown on Fig. 4.

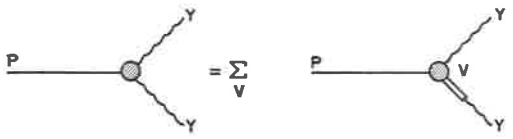

Fig. 4.

The photon is assumed to belong to an octuplet so that only the U spin scalar combination of the octuplet V_8^0 is coupled to the photon. We obtain the general relation

$$g_j = \sum_V A_{8j}^0 \frac{m_V^2}{W_V(0)} \frac{1}{f_{V^0_8}} \qquad j = 1, 8$$

where the sum $\sum_V$ extends over all possible vector mesons. The inverse vector meson propagator $[W_V(s) - s]$ has been extrapolated at $s = 0$ for a real photon where in the zero width approximation it simply reduces to m_V^2.

In the restricted vector meson dominance where only one nonet is present, using Clebsch-Gordan coefficients and taking into account phenomenologically finite width corrections ([22]) we obtain the simple proportionality

$$g_j = \frac{2}{\sqrt{3}} \frac{1}{f_{\rho\pi\pi}} A_{8J}^0 \qquad j = 1,8$$

We disregard in what follows contributions due to new vector mesons like the ρ′—if it exists— and we discuss only the restricted vector meson dominance model.

4.2. – The ratio Z/X is independent of the numerical value of the photon-vector meson coupling constant and in the two first lines of Table III we compare the VMD prediction

$$\left(\frac{Z}{X}\right)_{\text{VMD}} = \frac{g_1}{g_8}$$

with the results of the analysis made in the previous Sections. In the two last lines of the same Table, we compute the quantity X which is known from π^0 data only using the value $f_{\varrho\pi\pi} = 5.52$ which corresponds to a total ϱ meson width of 127 MeV, the ϱ meson mass being taken as $m_\varrho = 776$ MeV.

TABLE 3.

	VMD	Experiment
$(Z/X)^L$	-1.31 ± 0.30	-2.13 ± 0.50
$(Z/X)^Q$	-2.77 ± 0.70	-5.88 ± 1.22
X^L (GeV^{-1})	1.860 ± 0.093	1.896 ± 0.186
X^Q (GeV^{-1})	1.860 ± 0.093	2.018 ± 0.196

The quantitative agreement for X is good inside the errors and it can be considered as a success of the VMD model as formulated originally for meson radiative decays by Gell-Mann, Sharp and Wagner ([23]). The ratio Z/X is very sensitive to the mixing angles and a reasonable agreement can be reached with a linear mass mixing.

4.3. – In a systematic study of the vector meson dominance model we must consider the complete chain of vertices

$$\text{P-}\gamma\text{-}\gamma\,, \qquad \text{P-V-}\gamma\,, \qquad \text{P-V-V}$$

involving non-radiative transition like for instance $\omega \Rightarrow \pi^+\pi^-\pi^0$ or $\varphi \Rightarrow \varrho + \pi$. The problem in its generality has been studied by many authors ([23,24]) and more or less sophisticated models of symmetry breaking have been proposed to solve it. Let us just here emphasize three points:

a) For some relations direct contact terms have been introduced in addition to the vector meson pole contributions ([25]) with a limited success as far as the comparison between theory and experiment is concerned;

b) The corrections due to the finite width of the vector mesons are not negligible (especially for ϱ and φ) and they can be computed only in a model dependent way involving an explicit form of the vector meson propagators;

c) The three types of vertices are compared with off-mass shell vector mesons so that an extrapolation is needed for the coupling constants which are defined for on-mass shell vector mesons; such an extrapolation is generally assumed to affect only slightly the value of these coupling constants but this statement is convenient for practical purpose if certainly not exact.

4.4. – We compute the various radiative decay widths of mesons choosing as input the experimental results concerning the π^0 meson

$$\Gamma(\pi^0 \Rightarrow 2\gamma), \quad \Gamma(\omega \Rightarrow \pi^0 + \gamma), \quad \Gamma(\varphi \Rightarrow \pi^0 + \gamma)$$

and making an empirical compromise between the values of the ratio Z/X obtained in Table III:

a) linear mass mixing (LM)

$$\frac{Z}{X} = \frac{g_1}{g_8} = -1.62$$

b) quadratic mass mixing (QM)

$$\frac{Z}{X} = \frac{g_1}{g_8} = -3.94 .$$

The results are given in Table IV and compared with the available experimental data. Let us remark that the ρ meson width is also predicted by the VMD model from π^0 data only.

TABLE IV.

	LM	QM	Experiment
$\Gamma(\rho^0 \Rightarrow \pi^0\gamma)$	114 keV	126 keV	< 250 keV
$\Gamma(\omega \Rightarrow \pi^0\gamma)$	1.12 MeV	1.12 MeV	input
$\Gamma(\varphi \Rightarrow \pi^0\gamma)$	7.6 keV	7.6 keV	input
$\Gamma(\pi^0 \Rightarrow 2\gamma)$	11.7 eV	11.7 eV	input
$\Gamma(\rho^0 \Rightarrow \eta\gamma)$	108 keV	141 keV	—
$\Gamma(\omega \Rightarrow \eta\gamma)$	13.7 keV	12.7 keV	< 180 keV
$\Gamma(\varphi \Rightarrow \eta\gamma)$	93 keV	122 keV	(77 $\pm$ 23) keV
$\Gamma(\eta \Rightarrow 2\gamma)$	1.14 keV	1.68 keV	(1.01 $\pm$ 0.23) keV
$\Gamma(X \Rightarrow \rho^0\gamma)$	111 keV	1.49 MeV	see below
$\Gamma(X \Rightarrow \omega\gamma)$	12.3 keV	175 keV	—
$\Gamma(\varphi \Rightarrow X\gamma)$	1.5 keV	5.4 keV	—
$\Gamma(X \Rightarrow 2\gamma)$	9.2 keV	87 keV	see below
$\Gamma(K^{*\pm} \Rightarrow K^{\pm}\gamma)$	65 keV	72 keV	—
$\Gamma(K^{*\bar{0}} \Rightarrow K^{\bar{0}}\gamma)$	259 keV	288 keV	—
$\Gamma(\rho \Rightarrow 2\pi)$	132 MeV	150 MeV	(125 $\pm$ 15) MeV

The best way to learn something about the η^0-X^0 mixing is to have absolute measurements of the X^0 radiative decay widths for which the theoretical predictions can differ by one order of magnitude going from $\theta_P^L = 23.4°$ to $\theta_P^Q = 10.1°$.

We have only experimental indications on branching ratios and using ([19])

$$B(X^0 \Rightarrow \pi^+ + \pi^- + \gamma) = 30\,\%$$

we can predict from Table IV the X^0 meson total width and the $X^0 \Rightarrow 2\gamma$ branching ratio. This has been done in Table V inserting a finite ρ width correction of

$$\frac{\Gamma(X_0 \approx \pi^+ + \pi^- + \gamma)}{\Gamma(X_0 \approx \rho_0 + \gamma)} = 1.18$$

	LM	QM	Experiment
Γ_{X^0}	440 keV	5.8 MeV	< 4 MeV
$B(X^0 \Rightarrow 2\gamma)$	2.1 %	1.5 %	$(1.8 \pm 0.5)\,\%$ ([26])

5. Concluding remarks.

5.1. – A decisive improvement in the measurement of radiative decay of mesons is needed to hope some progress in the understanding of the broken SU_3 symmetry applied to electromagnetic interactions. The two sets of data for $P \Rightarrow 2\gamma$ and $V \Rightarrow P + \gamma$; $P \Rightarrow V + \gamma$ must be considered separately as done here in order to test first the consistency of the scheme and to learn something about the isoscalar meson mixings. This last point is very crucial. After that a relation between the vertices $P\gamma\gamma$, $PV\gamma$ and PVV can be attempted on the basis of a restricted or an extended vector meson dominance model which seems to work now in the 10 % or 15 % limit.

5.2. – All the theoretical ways of describing the radiative decays of mesons have not been discussed here even if they are a priori equally reasonable. For instance other signs for the coupling constants g_{η^0}, $g_{\omega\pi^0\gamma}$, $g_{\varphi\pi^0\gamma}$ are possible and the U spin and SU_3 relation can be applied on different quantities where mass factors have been included. The quantitative results will be different but for a scheme in agreement with experiment the qualitative feature

will be the same and the most naive approach we have presented here gives a consistent description of the available data and only new and more accurate experiments can make a selection between the various models.

5.3. – A nice way to obtain information about the radiative decay of mesons is to use the Primakoff effect. Information on the transitions

$$\rho^{\pm} \Rightarrow \pi^{\pm} + \gamma , \quad K^{*\pm} \Rightarrow K^{\pm} + \gamma , \quad X^0 \Rightarrow 2\gamma$$

can be obtained from high energy coherent production processes on a nucleus or a nucleon

$$\pi^{\pm} + A \Rightarrow \rho^{\pm} + A , \quad K^{\pm} + A \Rightarrow K^{*\pm} + A , \quad \gamma + A \Rightarrow X^0 + A .$$

Two experimental procedures can be used:

a) Detection of the produced meson near the forward direction as done for π^0 and η^0 photoproduction ([15]);

b) Detection of the recoil nucleus at very small kinetic energies in all the allowed directions ([27,28]).

A discussion of these problems cannot be done here and we just mention this very clean experimental approach.

Acknowledgements.

We thank Mr. W. Klein for his help in numerical computations and Prof. J. Prentki for reading the manuscript.

REFERENCES

1) S. Coleman and S. L. Glashow: *Phys. Rev. Lett.*, **6**, 423 (1961).
2) N. Cabibbo and R. Gatto: *Nuovo Cimento*, **21**, 872 (1962).
3) The pseudoscalar nonet is assumed to be π, K, η^0, X^0 even if the assignment $J^P = 0^-$ for the $X^0(958)$ is not unambiguously established. Other possible pseudoscalar mesons like the E(1422) are not considered here.
4) J. J. Sakurai: *Phys. Rev. Lett.*, **9**, 472 (1962); S. Okubo: *Phys. Lett.*, **5**, 165 (1963); S. L. Glashow: *Phys. Rev. Lett.*, **11**, 48 (1963).
5) M. Gell-Mann: *Phys. Rev.*, **125**, 1067 (1962); S. Okubo: *Progr. Theor. Phys.*, **27**, 949 (1962).

6) J. J. SAKURAI: *Phys. Rev.*, **132**, 434 (1963); R. F. DASHEN and D. H. SHARP: *Phys. Rev*, **133**, 1585 (1964); S COLEMAN and H. J. SCHNITZER: *Phys Rev.*, **134**, B 863 (1964); T. DAS, V. S. MATHUR and S. OKUBO: *Phys. Rev. Lett.*, **18**, 761 (1967); R. J. OAKES and J. J. SAKURAI: *Phys. Rev. Lett.*, **19**, 1266 (1967).

7) R. H. DALITZ and D. G. SUTHERLAND: *Nuovo Cimento*, **37**, 1777 (1965); **38**, 1945 (1965); F. GUERRA, F. VANOLI, G. DE FRANCESCHI and V. SILVESTRINI: *Phys. Rev.*, **166**, 1587 (1968); R. S. WILLEY: *Phys. Rev.*, **183**, 1397 (1969).

8) N. KROLL, T. D. LEE and B. ZUMINO: *Phys. Rev.*, **157**, 1376 (1967).

9) R. DUTT and S. ELIEZER: Preprint Haîfa (1970).

10) J. PEREZ-Y-JORBA: *Proceedings of the Daresbury Study Week-End*, June 1970.

11) M. GOURDIN: Lectures given at the 11-th Scottish Universities Summer School in Physics (1970).

12) Because of the small $\omega - \rho$ mass difference the comparison of $\rho \Rightarrow e^+e^-$ and $\omega \Rightarrow e^+e^-$ partial decay widths is essentially free of mass breaking ambiguities. The theoretical expression is

$$R = \frac{\Gamma(\omega \Rightarrow e^+e^-)}{\Gamma(\rho \Rightarrow e^+e^-)} \simeq \frac{1}{3}\sin^2\theta_V .$$

With the two previous mixing angles θ_V^L and θ_V^Q the predictions are

$$R_{\text{linear}} = 0.124 \quad R_{\text{quadratic}} = 0{,}139$$

both in excellent agreement with the experimental value deduced from the Orsay data ([10]):

$$R_{\text{experiment}} = 0.135 \pm 0.027 .$$

13) For instance if SU_3 symmetry holds for the quantities m_V^α / f_V where α is an integer and f_V^{-1} the dimensionless photon-vector meson coupling constant it must be also applied to the quantity $g_{VP\gamma}/m_V^\alpha$ where $g_{VP\gamma}$ is defined in eq. (2) as the vector meson pseudoscalar meson photon coupling constant.

14) As an alternative way one can break SU_3 symmetry in the coupling constants but the predictive power of the theory is highly depressed except in some specific models. See, for instance: A. ESTEVE, J. LÉON and A. TIEMBLO: *Lett. Nuovo cimento*, N **1**, 30 (1971); A. ESTEVE, J. NAVARRO and A. TIEMBLO: Preprint Madrid (1971); J. JULVE, J. LÉON and F. J. DE URRIES: Preprint Madrid (1971).

15) H. PRIMAKOFF: *Phys. Rev.*, **81**, 899 (1951); A. HALPRIN, C. M. ANDERSEN and H. PRIMAKOFF: *Phys. Rev.*, **152**, 1295 (1966).

16) G. BELLETTINI *et al.*: *Nuovo Cimento*, **66** A, 243 (1970). This result is in disagreement with the previous world average value of (7.2 ± 1.2) eV. Nevertheless we think this measurement to be more reliable.

17) C. BEMPORAD *et al.*: *Phys. Lett.*, **25** B, 380 (1967). A confirmation of this number by an independent experiment is necessary before taking it as certain.

18) See the papers of footnote ([14]), for a different type of breaking using a quark model

19) Particle Data Group (1971).

20) This value assumes the decay $\omega^0 \Rightarrow$ neutrals to be strongly dominated by the $\pi^0\gamma$ state and in particular the $\pi^0\pi^0\gamma$ mode is quoted in (19) to be less than 1% of the total A possible larger value has been reported at this conference by M. N. KREISLER for the $\pi^0\pi^0\gamma$ mode and this will imply a reduction of the $\omega \Rightarrow \pi^0\gamma$ decay width.

21) P. BENAKSAS *et al.*: Preprint Orsay LAL 1240 (1970); G. COSME: Contribution to this Conference.

22) The restricted VMD model applied to the π meson electromagnetic form factor gives the normalization constraint

$$\frac{m_\rho^2}{W_\rho(0)} \frac{f_{\rho\pi\pi}}{f_\rho} = 1$$

where the factor $m^2/W_\rho(0)$ can be interpreted as a finite width correction when the vertex functions are assumed to be constant. See ref. ([11]).

23) M. GELL-MANN, D. SHARP and W. WAGNER: *Phys. Rev. Lett.*, **8**, 261 (1962).

24) M. JACOB: Preprint CERN Th. 846 (1967); E. CREMMER: *Nucl. Phys.*, B **14**, 52 (1969); A. BARACCA and A. BRAMON: *Nuovo Cimento*, **51** A, 873 (1967); **69** A, 613 (1970); D. GREENBERG: Preprint Pittsburgh (1969).

25) W. ALLES: *Lett. Nuovo Cimento*, **3**, 163 (1970); **4**, 137 (1970); G. J. GOUNARIS: *Phys Rev. D*, **1**, 1436 (1970); **2**, 2734 (1970).

26) D. BOLLINI *et al.*: *Nuovo Cimento*, **58**, 289 (1968); M. BASILE: Contribution to this Conference.

27) L. STODOLSKY: *Phys. Rev. Letters.* **26**, 404 (1971).

28) M. GOURDIN: *Nuclear Physics* B **32** 415 (1971).

Measurement of the radiative decay modes of the φ meson, $\varphi \to \eta\gamma$, $\varphi \to \pi^0\gamma$ with the Orsay storage ring (*)

D. BENAKSAS, G. COSME, B. JEAN-MARIE, S. JULLIAN
F. LAPLANCHE, J. LEFRANÇOIS, A. D. LIBERMAN, G. PARROUR
J. P. REPELLIN, G. SAUVAGE and G. SZKLARZ
Ecole Normale Supérieure, Laboratoire de l'Accélérateur Linéaire - Orsay

Abstract: A large solid angle detector has been used to observe many body final states in the decays of the φ meson. In the decay modes $\varphi \to \to \eta\gamma$ and $\varphi \to \pi^0\gamma$ we detected 3γ. The data have been taken at the peak of the φ and the normalization is given by Bhabha scattering. The values found are

$$B_{\varphi \to \eta^0\gamma/\varphi \to \text{all}} = 0.0192 \pm 0.0057\,,$$

$$B_{\varphi \to \pi^0\gamma/\varphi \to \text{all}} = 0.0019 \pm 0.0008\,.$$

We present a measurement ([2]) of neutral branching ratios of the φ, namely $\varphi \to \eta\gamma$ and $\varphi \to \pi^0\gamma$. Results were obtained from the whole of our data at the top of the φ resonance. We have measured the events coming from e^+e^- collisions with 3γ rays in the final state. Bhabha events have been used to normalize our results from the total cross sections obtained in the previous experiments ([1]).

The apparatus is the same as the one described by G. Parrour *et al.*, in the ρ-ω interference in $\pi^+\pi^-$ decay mode paper.

1. Kinematics of $e^+e^- \to 3\gamma$ at the φ energy.

To measure the $\varphi \to \eta\gamma$ and $\pi^0\gamma$ decay modes we have analysed three γ ray events. In the reaction $e^+e^- \to 3\gamma$ the energies of the γ rays can be calculated without ambiguity if one measures the direction of emission of the γ.

(*) Invited paper presented by G. Cosme

In order to do so, we measure the conversion point of the 3 showers in the spark chambers. The origin of the event is defined as the intersection of the beams and the plane containing the three conversion points.

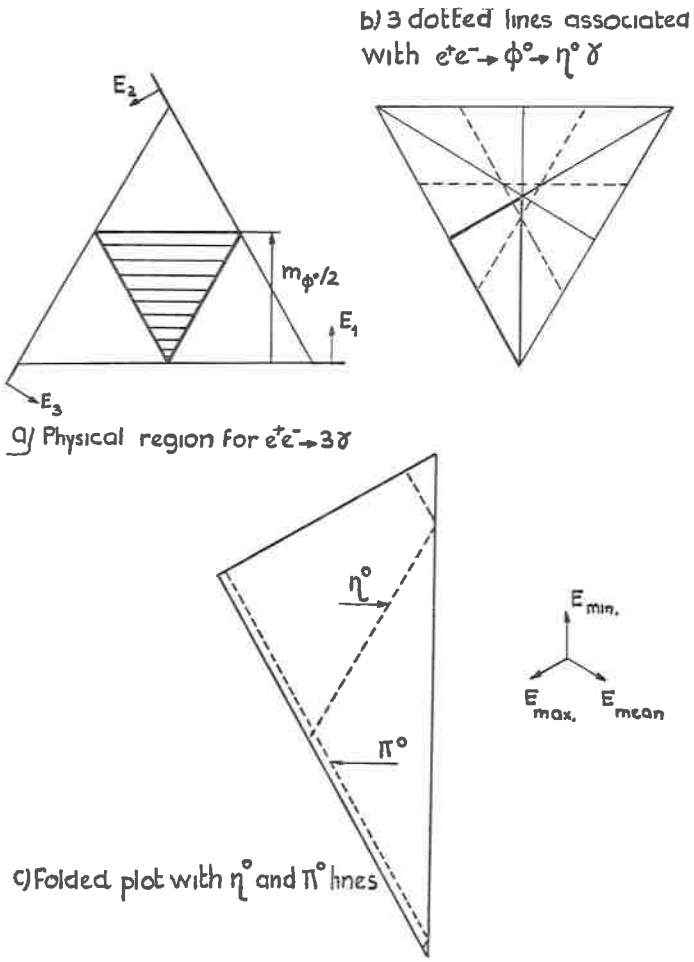

Fig. 1 *a-b-c.* – Kinematics of $e^+e^- \to 3\gamma$ at the φ energy.

In the decay $\varphi \to \eta\gamma(\pi^0\gamma) \to 3\gamma$ the γ opposite to the $\eta(\pi^0)$ has a fixed energy, $E_\gamma = 362$ MeV (501) MeV. Hence if we do a triangular Dalitz plot

(Fig. 1*a*) of the three γ ray energies E_1, E_2, E_3 an $\eta\gamma$ event lies necessarily on the 3 lines shown in Fig. 1*b*. Because of the six fold symmetry the Dalitz plot can be reduced to a sextant by ordering the γ ray energies (Fig. 1*c*).

2. Background and cuts.

Background comes from the decay mode (Fig. 3) $\varphi \to K_0^L K_0^S$, $K_0^S \to 2\pi^0 \to$ $\to 4\gamma$. To reject the $2\pi^0$ events the following three criteria have been used:

a) A photon is identified by at least two close sparks in two gaps. Spurious sparks cannot simulate photons, due to their low rate, and this has been checked using the 2γ annihilation events. All events with 4γ rays have been rejected.

b) We excluded from the Dalitz plot the region where one of the three photons had an energy lower than 100 MeV.

c) For each γ ray we calculated the ratio of the number of gaps having sparks to the total number of gaps along the photon direction counted from the conversion point. This ratio is related to the γ ray energy. A Monte Carlo program, including a shower program, was used to simulate both the $\eta\gamma$ ($\pi^0\gamma$) events and the background $2\pi^0$ events. By setting a lower limit on the sum of the ratios defined above for the three photons and the cut of the energy ($>$ 100 MeV), one could reject 76% of the generated K_0^S events giving 3 materialized γ rays in the chambers, (the mean photon energy is 125 MeV) and only 3% of generated $\eta\gamma$ (*) events (here the mean photon energy is 330 MeV).

We found experimentally that the measured events outside the region in the Dalitz plot were reduced in the same proportion, and the number of events remaining was in agreement with the number predicted from the φ production cross section and the branching ratios $\varphi \to K_0^L K_0^S$ ($K_0^S \to 2\pi^0$). This is a sensitive test of our Monte Carlo shower program. After applying these three criteria, there remain 50 events in the Dalitz plot, of which 22 events are in the η zone and 7 events in the π^0 zone (Fig. 2).

d) By using the direction of the shower of the best photon in our chambers, we have estimated the position of the collision point along the direction

---

(*) For $\pi^0\gamma$ events in the region of Dalitz plot defined below, the percentage of generated events lost by applying the same cut is $\simeq 5\%$.

of the beams. We asked the distance between this point and the calculated point (obtained with the plane defined by the three conversion points of the

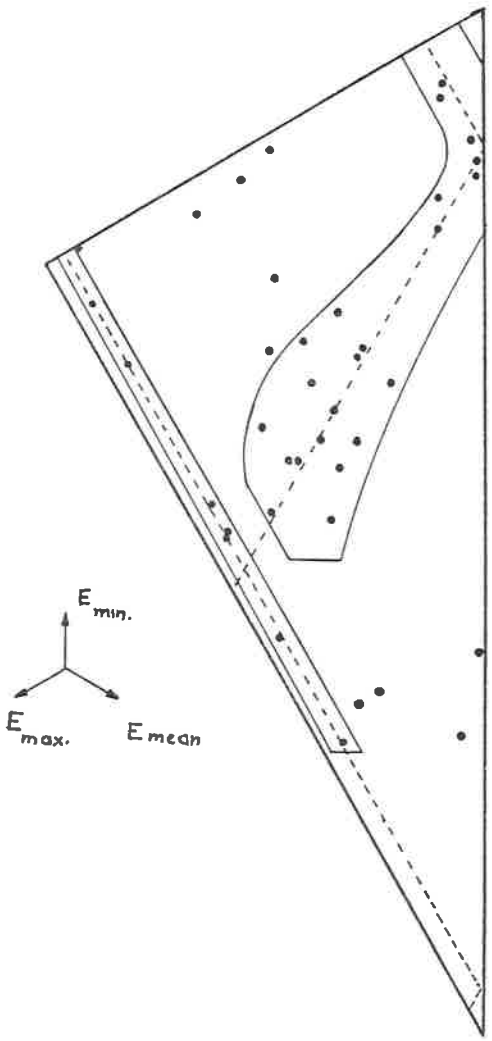

Fig. 2. – Dalitz plot with η^0 and π^0 zones of our events $e^+e^- \to \varphi^0 \to 3\gamma$.

γ rays) to be less than 6.5 cm. This cut is wide enough to avoid cutting $\eta\gamma$ and $\pi^0\gamma$ events but reduces the background by 50%.

The width of the η or π^0 zone corresponds to our resolution on the η or π^0 mass calculated from the measurement of the photon emission angles.

The widths shown on the Dalitz plot correspond to an error of $\pm 1.4°$ on the photon angles, θ and φ, due to the uncertainty of the materialisation

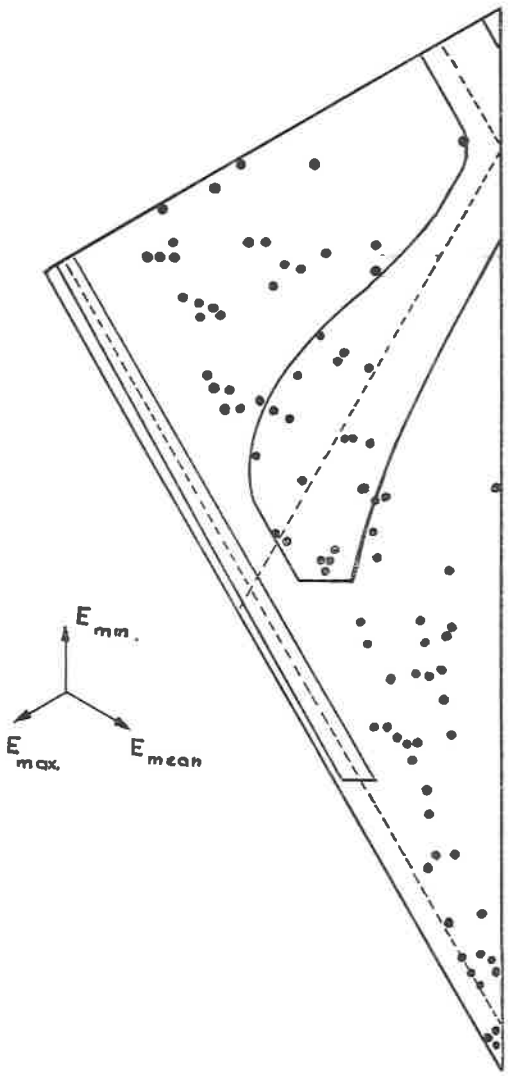

Fig. 3. – Dalitz plot of generated background events.

point. This error has been estimated by using the 2γ annihilation events at the ω energy $((2 \times 390)$ MeV$)$. The mass resolution for the η (π^0) is $\simeq 36$ MeV

($\simeq \pm$ 28 MeV). We excluded from the η zone a region corresponding to extremely asymmetrical decays ($E_{\gamma\max} > 485$ MeV) since for these cases the

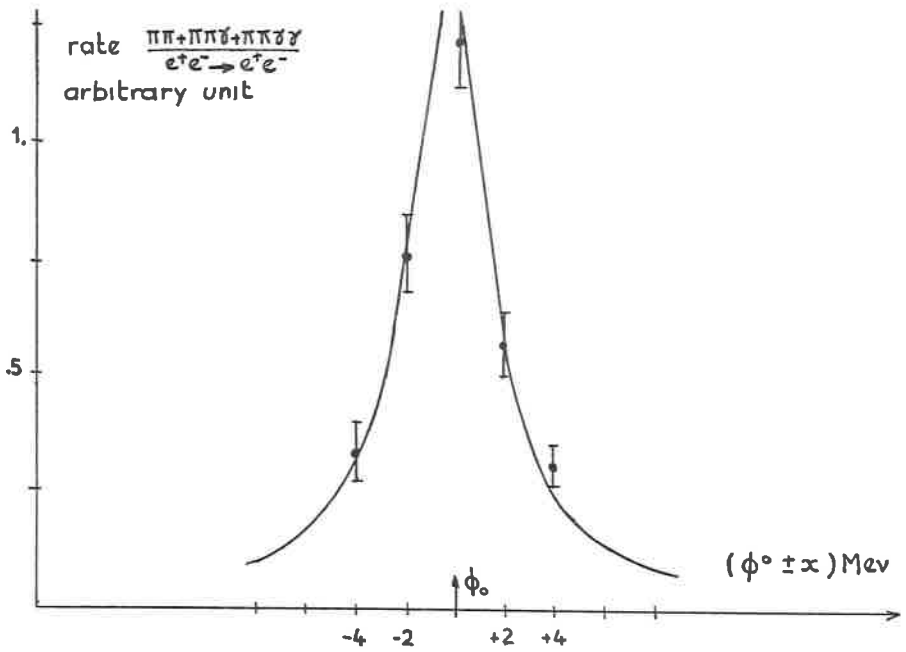

Fig. 4. – Rate $\frac{\pi\pi+\pi\pi\gamma+\pi\pi\gamma\gamma}{e^+e^- \to e^+e^-}$.

resolution on the η mass becomes too large. The decrease in efficiency due to this cut (17%) was calculated using the Monte Carlo program. The Fig. 5 shows the generated $\eta\gamma$ events.

We calculated that there were 2.7 ± 0.8 background events in the η zone, normalizing the events distribution on the Dalitz plot from the Monte Carlo program of background events (Fig. 5) by the measured background events outside the zones. In the case of the π^0 there is an expected background of 0.55 event from the $K_0^s \to 2\pi^0$ and 0.7 event from a $\eta\gamma$ decay simulating a $\pi^0\gamma$ event.

3. Normalization and experimental values $\varphi \to \eta\gamma/\varphi_{\text{total}}$ and $\varphi \to \pi^0\gamma/\varphi_{\text{total}}$.

At the present time $\varphi \to K_0^s K_0^L$ ($K_0^s \to \pi^+\pi^-$) events have not yet been analysed. So the normalization was obtained from wide angle Bhabha scat-

tering events and the previous experimental value ([2]) of the total cross section σ_T $(e^+e^- \to \varphi)$ measured at Orsay.

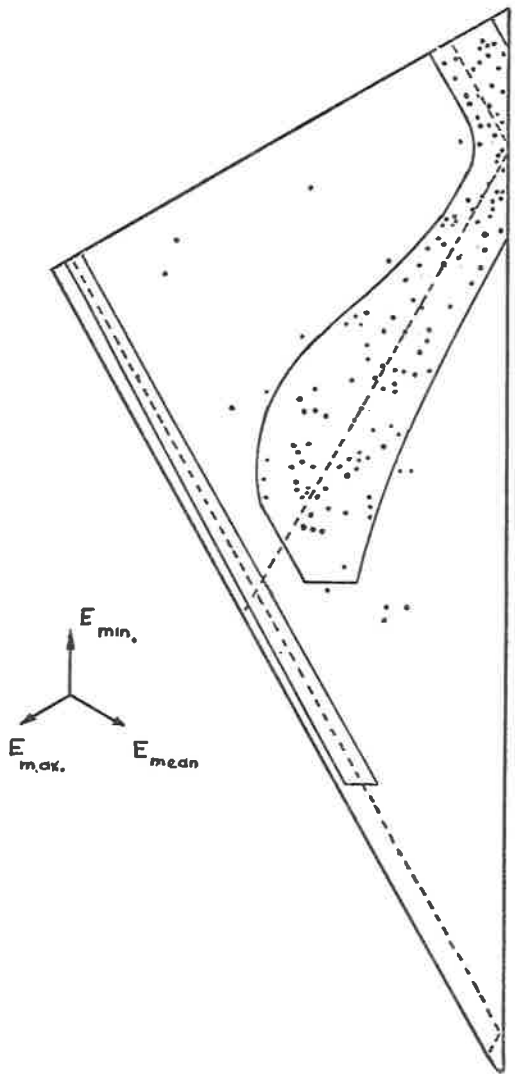

Fig. 5. – Dalitz plot of generated $\eta\gamma$ events.

The exact energy of our measurement has been determined by using $K_0^S K_0^L$ and $\pi^+\pi^-\pi^0$ events fitted by a normal Breit-Wigner formula. We have

counted the scanned $\pi^+\pi^-$, $\pi^+\pi^-\gamma$ and $\pi^+\pi^-\gamma\gamma$ events. These events, normalized by wide angle Bhabha scattering, give the rate as a function of energy as seen in Fig. 4. The analysed $\eta\gamma$ events have been taken at the point called φ and the best fit gives the center of the φ at $(\varphi - 0.3 \pm 0.14)$Mev.

The branching ratio $B = \varphi \to \eta\gamma/\varphi \to$ all is given by:

$$B_{\varphi\to\eta_0\gamma} = N(3\gamma)\cdot\frac{\sigma(e^+e^-)(1+\delta_e)}{N_{e^+e^-}}\cdot\frac{1}{\sigma_T(\varphi)\cdot(1+\delta_\varphi)}\times\frac{1}{\varepsilon}\frac{1}{B(\eta^0\to 2\gamma)},$$

where,

$\varepsilon = 0.133 \pm 0.020$	the efficiency of the apparatus for the $\varphi \to \eta\gamma$ decay mode;
$N(\eta\gamma) = 19.3 \pm 5$	the experimental number of 3γ events $\eta\gamma$ zone of the Dalitz plot;
$\sigma_T(\varphi) = 4.9 \pm 0.4\cdot 10^{-30}\,\mathrm{cm}^2$	the experimental total cross section at the determined energy of the process: $e^+e^- \to \varphi$;
$N_{e^+e^-} = 2328$	the experimental number of wide angle Bhabha events $(52°{,}5 < \theta < 90°)$;
$\sigma(e^+e^-) = 4.46\cdot 10^{-31}\,\mathrm{cm}^2$	the corresponding theoretical Bhabha cross section;
$B(\eta \to 2\gamma) = 0.382 \pm 0.02$	the branching ratio $(\eta \to 2\gamma)/(\eta \to$ all);
$1 + \delta_e = 0.97 \pm 0.02$	the radiative correction of the bhabha scattering;
$1 + \delta_\varphi = 0.75 \pm 0.02$	the radiative correction of the φ production.

From the corresponding values, we find:

$$B(\varphi \to \eta\gamma) = (1.92 \pm 0.57)\% .$$

With $\varepsilon_{\pi^0\gamma} = (0.151 \pm 0.015)$ and (5.75 ± 2.4) $\pi^0\gamma$ events we find

$$B(\varphi \to \pi^0\gamma) = (0.19 \pm 0.08)\% .$$

Previous experiments (3,4) give an upper limit

$$(\varphi \to \eta\gamma)/(\varphi \to \text{all}) < 8\% \qquad (60\%\text{ confidence level}),$$

and

$$(\varphi \to \pi^0\gamma)/(\varphi \to \text{all}) < 0.35\ \% \qquad (95\%\text{ confidence level}).$$

REFERENCES

1) J. C. Bizot, J. Buon, Y. Chatelus, J. Jeanjean, D. Lalanne, H. Nguyen Ngoc, J. Perez-y-Jorba, P. Petroff, F. Richard, F. Rumpf and D. Treille: *Phys. Lett.*, **32** B, 416 (1970).
2) D. Benaksas, G. Cosme, B. Jean-Marie, S. Jullian, F. Laplanche, J. Lefrancois, A. D. Liberman, G. Parrour, J. P. Repellin and G. Sauvage: LAL 1240 (Sept. 1970) (submitted to the *XVth Int. Conf. on High-Energy Physics*, Kiev, August 1970).
3) J. S. Lindsey and G. A. Smith: *Phys. Rev.*, **147**, 913 (1966).
4) C. Bemporad, P. L. Braccini, R. Castaldi, L. Foa, L. Lubelsmeyer and D. Schmitz: *Phys. Lett.*, **29** B, 383 (1969).

Neutral decays of the ω, η, and X^0 mesons (*)

M. N. KREISLER
Physics Department, Joseph Henry Laboratories
Princeton University - Princeton, N. J.

I would like to describe the results of a series of experiments that were performed recently at the Princeton-Pennsylvania Accelerator to study the neutral decays of the η and ω mesons.

In these experiments, the mesons were produced in the reaction

$$\pi^- p \to \left\{ \begin{array}{c} X^0 \\ \eta \\ \omega \end{array} \right\} + n \, .$$

The production of the meson was identified by measuring the momentum and angle of the neutron using large liquid scintillation counters. Single gammas from the neutral decays of the mesons were then momentum analyzed in a spark chamber-magnet spectrometer and transformed to the center of mass of the meson. After background subtraction, the momentum spectrum allows identification of the various decay modes as well as a calculation of the branching ratios.

1. Neutral decays of the $\eta(550)$ meson.

A list of the participants in that experiment ([1]) is shown in Table I.

TABLE I. – *Participants in the experiment on η neutral branching ratios.*

M. T. BUTTRAM - M. N. KREISLER - R. E. MISCHKE Joseph Henry Laboratories, Princeton University - Princeton, N. J.

(*) Invited paper

Work supported under U. S. Atomic Energy Contract N$_o$ AT (30-1) - 4159.

The known or reported neutral decay modes of the η are

$$\eta \to \pi^0\pi^0\pi^0$$
$$\to \pi^0\gamma\gamma$$
$$\to \gamma\gamma .$$

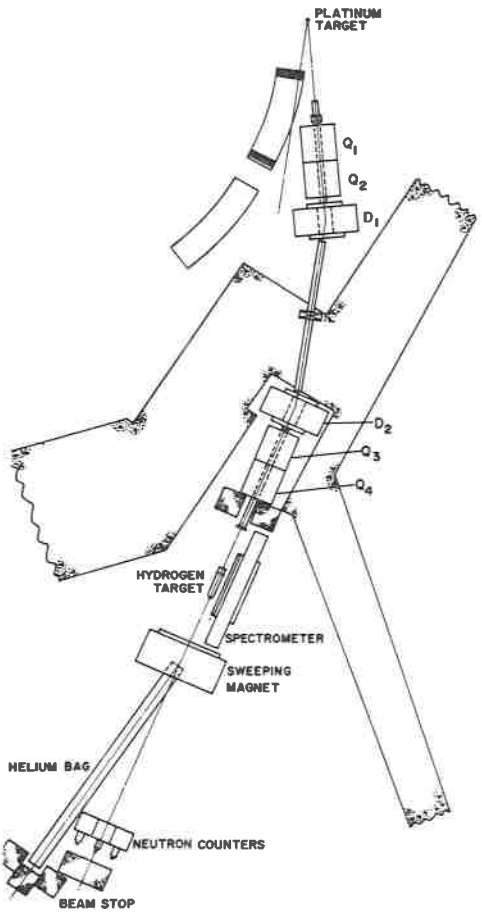

Fig. 1.

The existence of the $\pi^0\gamma\gamma$ mode seems to be uncertain despite a large number of experiments attempting to measure it with reported branching ratios varying from 0 to $> 20\%$ of all neutral decays. In addition, the branching ratios into the two major modes have suffered from large statistical fluc-

tuations. We have therefore made a precise measurement of the η branching ratios with careful attention to systematic errors.

In Fig. 1 the plan view of the experiment is shown. I call your attention to this as there may not be many future experiments using the Princeton-

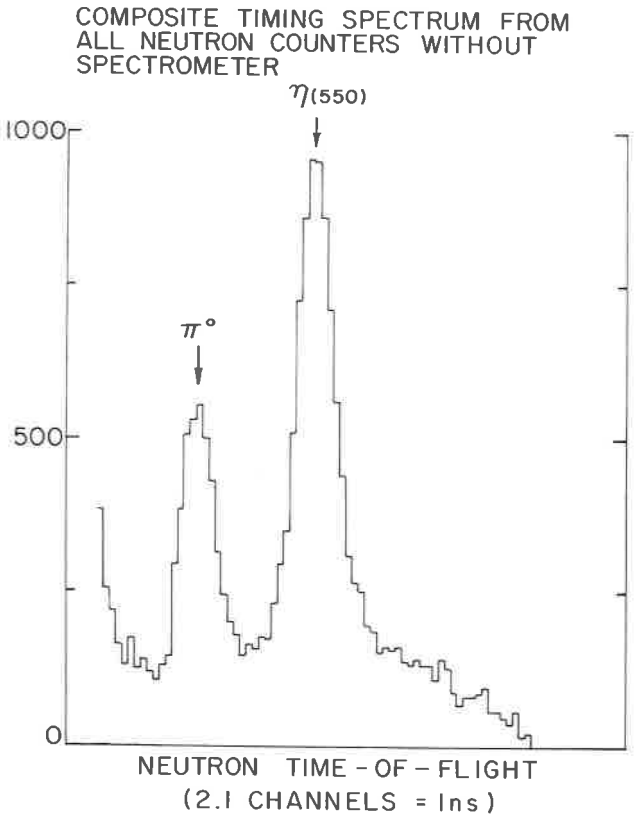

Fig. 2.

Pennsylvania Accelerator. A π^- beam, 820 MeV/c $\pm$ 1% is incident on a liquid hydrogen target 40″ long. The unscattered π^- beam is swept away from the forward direction by a large aperture sweeping magnet.

The neutron from the reaction is detected and measured in 9 large volume, 2′ cube, liquid scintillator counters in a manner that has now become standard for detecting η's. The time of flight and the angle are measured allowing knowledge of the missing mass.

One gamma from a neutral decay is momentum analyzed in a magnet-spark chamber spectrometer located at 90° with respect to the beam direction.

On the Fig. 2 we show a composite of the time of flight distribution over all 9 counters with no requirement that there be a gamma converted—only

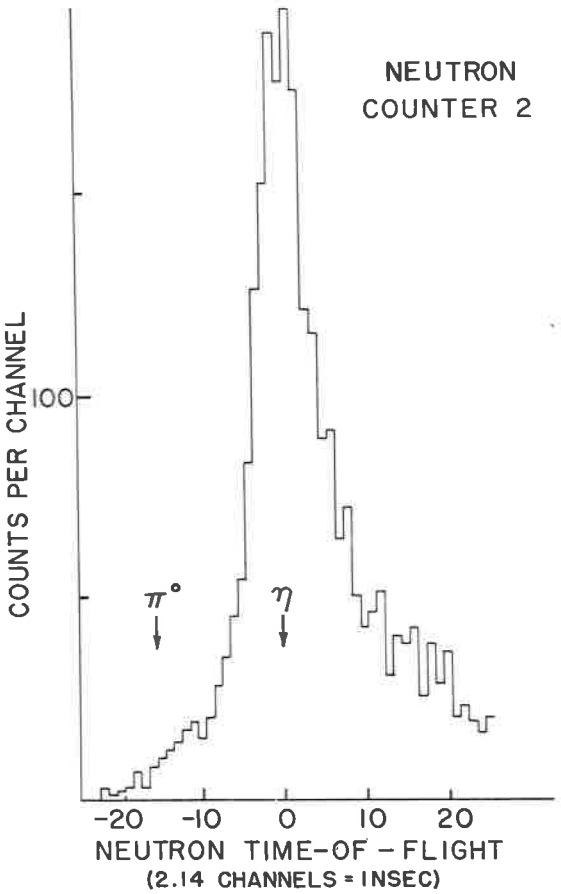

Fig. 3.

that there be a neutral final state—clear evidence for π^0 (charge exchange) and η^0 production is visible—as well as a smoothly varying background.

When the spectrometer requirement is added the background from charge exchange and low invariant masses is eliminated as shown for one of the 9 counters in Fig. 3. Unfortunately, as I arrived with the wrong size slides, I can't show the background curve (Fig. 4 added in proof showing background.)

The background was obtained in roughly the following manner, for more explicit details, see ref. [1]. The effect of the spectrometer on the mass distribution was determined experimentally by comparing the data with and without the spectrometer requirement. The η signal was assumed gaussian and the

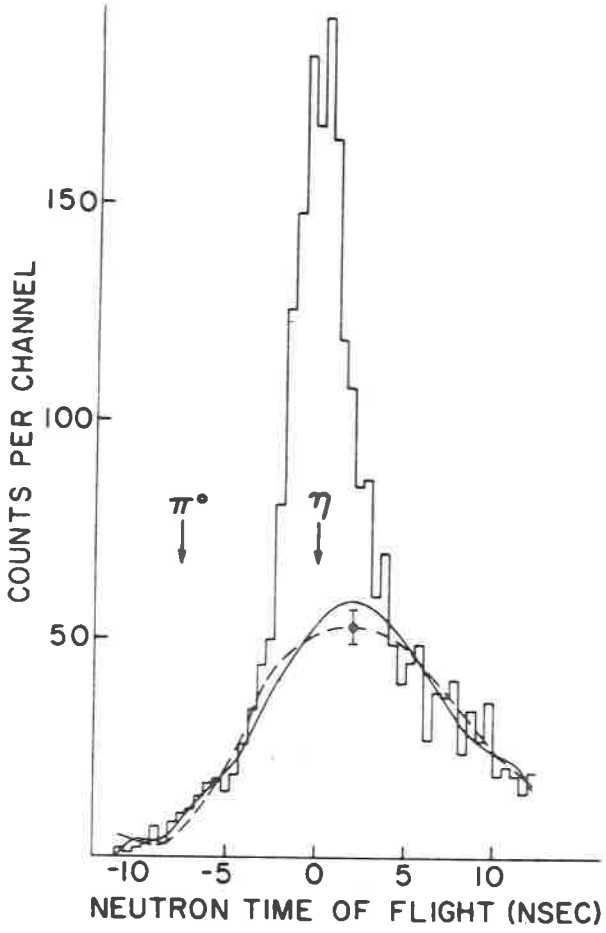

Fig. 4.

background was fit with a polynomial. The uncertainty in the background amplitude is included in the errors on the branching ratios measured by *each* counter.

The shape of the background momentum spectrum was determined by comparing the spectrum from events with invariant masses greater than the

eta with the spectrum obtained by dividing the data into small momentum intervals and measuring the amount of η signal present in each interval. Details are described in ref. (1).

On the Fig. 5 we see the shapes with which we wish to compare our subtracted spectra. Effects of measurement error, multiple Coulomb scattering

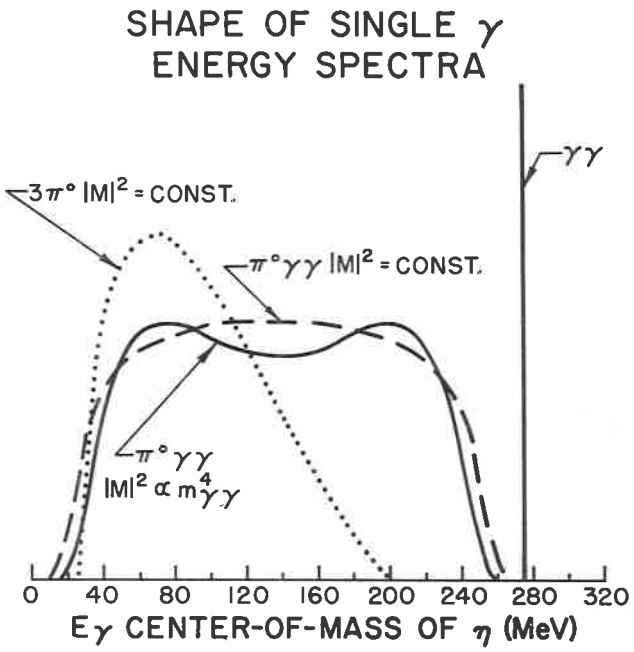

Fig. 5.

and bremstrahlung have not been included. Note that the $\gamma\gamma$ decay is essentially a δ function in the center of mass. The $3\pi^0$ spectra assumes phase space while the $\pi^0\gamma\gamma$ decay spectrum is shown with both a constant matrix element and a gauge invariant matrix element proportional to $m^4_{\gamma\gamma}$. As can be seen, our results are not sensitive to the choice of matrix element.

In Fig. 6, we show a composite of the backgrounds in all 9 counters. I remind you that the branching ratios were measured treating each counter separately.

In Fig. 7, the composite fit to the subtracted spectra is shown. Again, the same reminder applies.

Our final results, which differ slightly from our earlier results as we have redone the calculation of the effect of preconversion of gammas in the target material, are shown in Table II.

TABLE II (based on 7200 η decays).

$$\frac{\eta \to \gamma\gamma}{\eta \to \text{neutrals}} = (51.5 \pm 1.8)\%$$

$$\frac{\eta \to \pi^0\gamma\gamma}{\eta \to \text{neutrals}} = (\ 2.6 \pm 1.9)\ \%$$

$$\frac{\eta \to \pi^0\pi^0\pi^0}{\eta \to \text{neutrals}} = (45.9 \pm 2.4)\%$$

Using these results and the standard world compilation procedure, we find

$$R = \frac{\eta \to 3\pi^0}{\eta \to \pi^+\pi^-\pi^0} = 1.39 \pm 0.09\,,$$

which is less than the theoretical prediction of 1.58 ± 0.03 based on the assumption of no $\Delta I = 3$ transitions and a linear matrix element. We note that the branching ratio into $\pi^0\gamma\gamma$ is, in fact, very small.

2. Preliminary results on ω neutral decay.

The participants in that experiment ([2]) are shown in Table III. As in the η experiment, one detects the meson in the reaction $\pi^- p \to \omega n$, this time at $1445 \pm 0.5\%$ MeV/c.

TABLE III. – *Participants in the experiment on* ω *neutral branching ratios.*

J. T. DAKIN - M. G. HAUSER - M. N. KREISLER - R. E. MISCHKE - J. J. RITSKO
Joseph Henry Laboratories, Princeton University - Princeton, N. J.

The major difference between the experiments is that we placed the neutron counters at the Jacobian maximum in order to increase the rate (25′ from

the 2′ liquid hydrogen target at 34°). The neutron counters were again liquid scintillator but were 4′ long, 1′ high, and 6″ deep viewed by two phototubes,one on each end. The spectrometer was placed at $\approx 40°$ with respect to the beam.

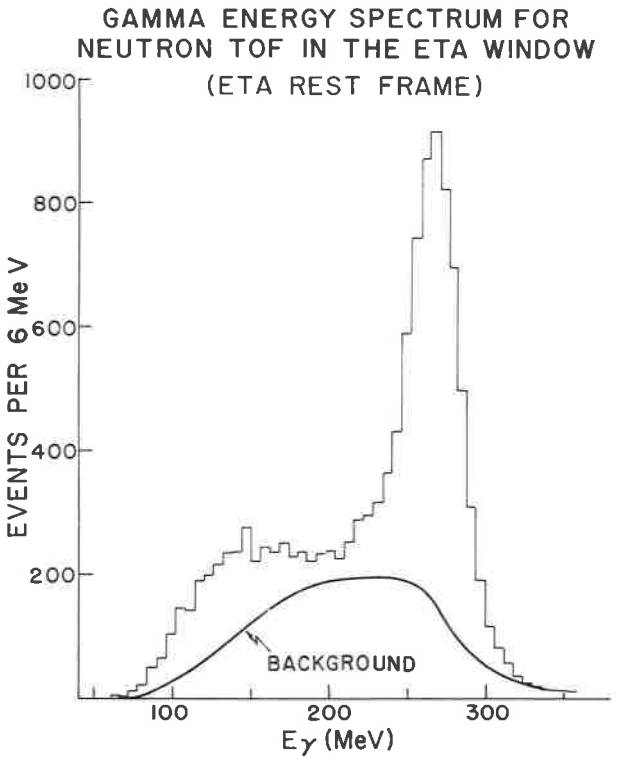

Fig. 6.

The analysis of the data is similar to that in the previous experiment. Our preliminary results ([2]) seem to be inconsistent with $\omega \to \pi^0\gamma$ as the only neutral decay. Our best fits are obtained using two decay modes $\omega \to \pi^0\gamma$ and a multi body final state, which for now we are calling $\pi^0\pi^0\gamma$.

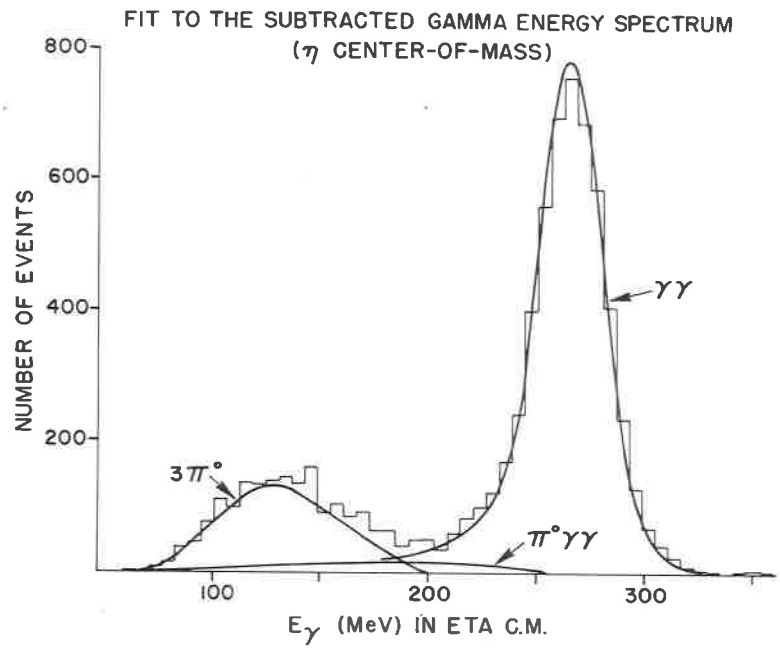

Fig. 7.

3. X⁰ neutral branching ratios.

At present, our results on the X⁰ neutral branching ratios are not complete.

I can report the preliminary results of the Minnesota group ([3]) for the X⁰ branching ratio, these are numbers which were presented at the New York APS meeting: They looked at the process

$$\pi^- p \to X^0 + n \qquad \text{at} \qquad 3.67\ \text{GeV/c}\,.$$

They claim to have seen ~ 32 events, which implies that (77 ± 14) events occurred. Since their sensitivity is 114 eV/μb they find

$$\sigma(\pi^- p \to X^0 + n) = 0.68 \pm 0.13\ \mu\text{b}\,.$$
$$\hookrightarrow \gamma\gamma$$

They then use some Michigan data on production cross section

$$\sigma_T(\pi^- p \to X^0 n) = 27 \pm 10\ \mu b\ ,$$

to calculate the branching ratio

$$X^0 \to \gamma\gamma = 2.5^{+1.5}_{-0.7}\%$$

However, most of their error is due to the uncertainty in the production cross-section.

REFERENCES

1) M. T. Buttram, M. N. Kreisler and R. E. Mischke: *Phys. Rev. Lett.*, **25**, 1358 (1970).
2) J. T. Dakin, M. G. Hauser, M. N. Kreisler, R. E. Mischke and J. J. Ritsko: *Bull. Am. Phys. Soc.*, **16**, 112 (1971); J. T. Dakin: *Thesis*, Princeton University (unpublished).
3) J. K. Randolph, E. H. Harvey, E. Marquit, E. Peterson, K. Ruddick, T. Rhodes, G. Satovich and J. Smith: *Bull. Am. Phys. Soc.*, **16**, 111 (1971).

The decay mode $X^0 \to \gamma\gamma$ and first determination of the branching ratio $X^0 \to \gamma\gamma / X^0 \to$ total (*)

M. BASILE, D. BOLLINI, P. DALPIAZ
P. L. FRABETTI, T. MASSAM, F. NAVACH, F. L. NAVARRIA
M. A. SCHNEEGANS and A. ZICHICHI

CERN - Geneva
Istituto Nazionale di Fisica Nucleare - Bologna
Istituto di Fisica dell'Università - Bologna
Centre National de Recherches Scientifiques - Strasbourg

1. Introduction.

Purpose of this paper is to present the result of an experiment designed to estabilish on the basis of higher statistics the existence of the decay mode $X^0 \to \gamma\gamma$ [1] and to measure the branching ratio $X^0 \to \gamma\gamma / X^0 \to$ total.

The reaction studied is:

$$\pi^- + p \to n + (\text{missing mass}) \quad (1)$$
$$\qquad\qquad\quad \hookrightarrow \gamma\gamma$$

at $p_\pi = 1.61$ GeV/c with $\Delta p/p = \pm 0.5\%$.

The missing mass has been calculated for each event, knowing the time-of-flight and the emission angle of the neutron measured simultaneously with the Bologna-CERN neutron missing-mass spectrometer [2]. In order to separate the $\gamma\gamma$ decay from other decay channels and from background,

---

(*) Invited paper presented by M. Basile.

we use a system of two electromagnetic shower detectors ([3]) which provide the γ-ray's directions, with a precision of $\pm 1°$, and their energies, with a precision of $\pm 15\%$.

The missing-mass resolution, due to the uncertainties in the neutron time-of-flight and position measurements, combined with the beam momentum spread and with the uncertainty on the vertex of reaction (1), is estimated to be $\pm$ 5 MeV in the X^0 mass region.

2. Experimental set-up.

The general layout of the apparatus is shown in Fig. 1. The π^- beam interacting in the 35 cm long, 5 cm diameter, liquid H_2 target is defined by the coincidence of $\overline{R}_1 \cdot U \cdot S \cdot \overline{R}_2 \cdot \overline{Q}$. The two semiconical counters V_T and V_B, in anticoincidence in the electronic trigger, surround the target almost completely, and guarantee neutral decays of the missing mass ([4]).

The two γ-ray detectors ([3]), placed symmetrically at 46° above and below the beam line, consist essentially of a shower detector of nine slices, each slice being made of a layer of lead, a two-gap optical spark chamber, and a plastic scintillator counter. In order to determine the γ-ray directions, the γ was required to convert in a 0.52 cm thick lead foil followed by a scintillation counter M in coincidence on the trigger, and by two six-gap thin-foil spark chambers, placed in front of the shower detector.

The two neutron detectors, positioned symmetrically at 20° from the beam-line, at 6 m distance from the target centre, provide the angle of emission of the neutron, its energy release, and its time-of-flight measured with respect to the U-counter. The G-counters in anticoincidence in the trigger guarantee neutral particles hitting the neutron detector.

3. Data analysis.

Some 40000 photographs of the spark chambers were taken at an average rate of 1 every 5 seconds. These photographs were scanned for events showing only one γ-ray in each γ-ray detector ($\sim 50\%$ of the total sample). No selection on the γ-ray energy using spark counting was made at this stage. The directions of the tracks in the kinematic chambers were measured on semi-automatic measuring tables, only for 31% of the $\gamma\gamma$ events (the criteria of measurability are given in ref. (3)). The reconstructed vertex of the reaction was required to be within the limits of the target.

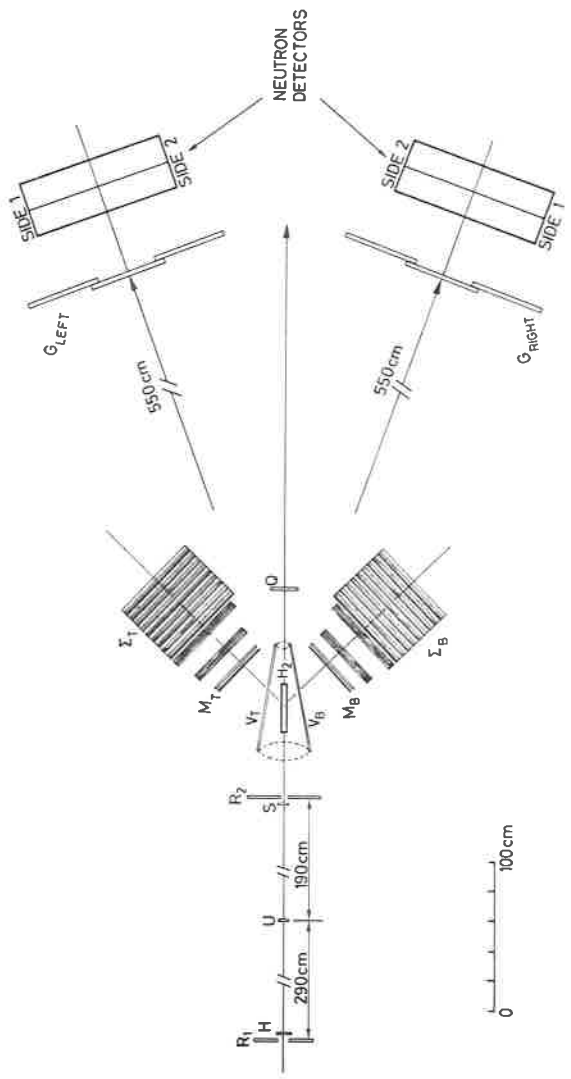

Fig. 1. – Schematic layout of the experimental set-up. The planes containing the e.m. shower detectors and the neutron detectors are at 90°.

In order to reduce the background and to improve the missing-mass resolution, only neutron time-of-flights from 32 to 50 nsec were considered, corresponding to q^2 values ranging from 0.22 to 0.50 $(\mathrm{GeV/c})^2$. Moreover, a uniform cut at 24 MeV on the energy released by the neutron was applied.

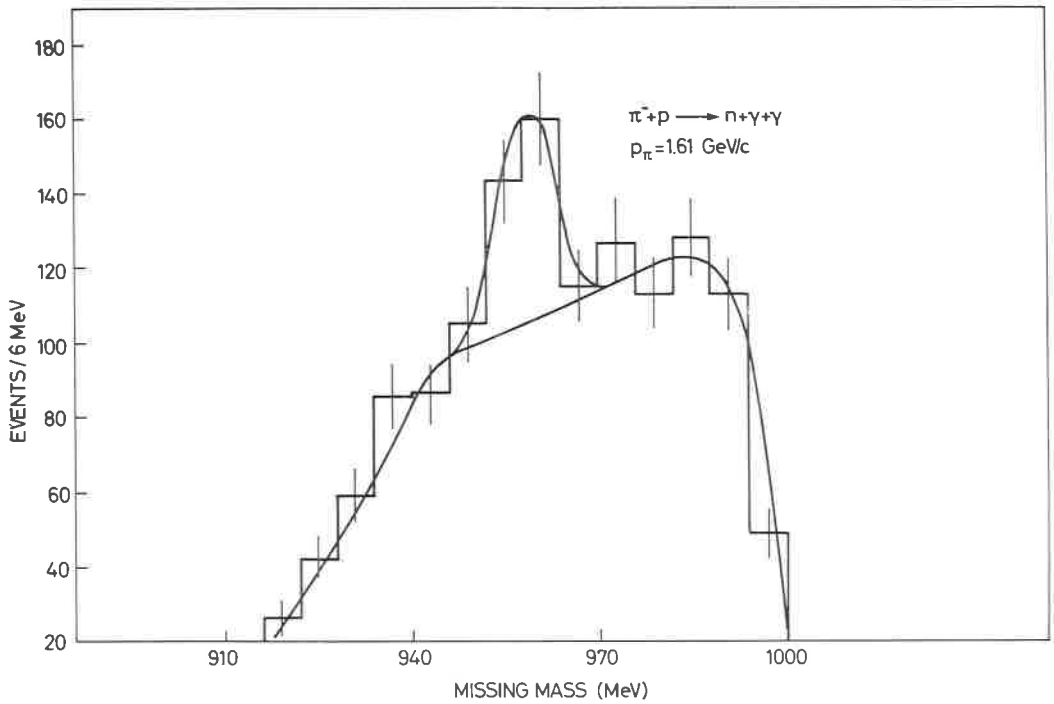

Fig. 2. – Missing-mass spectrum for selected $\pi^- + p \to n + \gamma\gamma$ events (only 2γ detected). The solid line shows the results of a fit to a Monte Carlo calculated background shape plus a Gaussian function for the X^0 peak.

The missing-mass spectrum of the ~ 1300 remaining events is shown in Fig. 2. A fit to the background by Monte Carlo leaves a ~ 10 MeV wide peak of (108 ± 20) events in the X^0 mass region. These events correspond to the neutral decay modes of the X^0 meson, *i.e.* the $\gamma\gamma$ mode and the $\eta_N \pi^0 \pi^0$ mode, of which only two γ-rays are detected. In order to separate these two decays modes, the invariant mass of the $\gamma\gamma$ system, $m_{\gamma\gamma}$, was calculated for each event using the measured opening angle between the γ-rays and the energy of each γ-ray computed from the spark-counting and from the pulse height (see ref. (3)). In fact, the Monte Carlo predicts a very good separation of the two decay channels in the $m_{\gamma\gamma}$ distribution (Fig. 3).

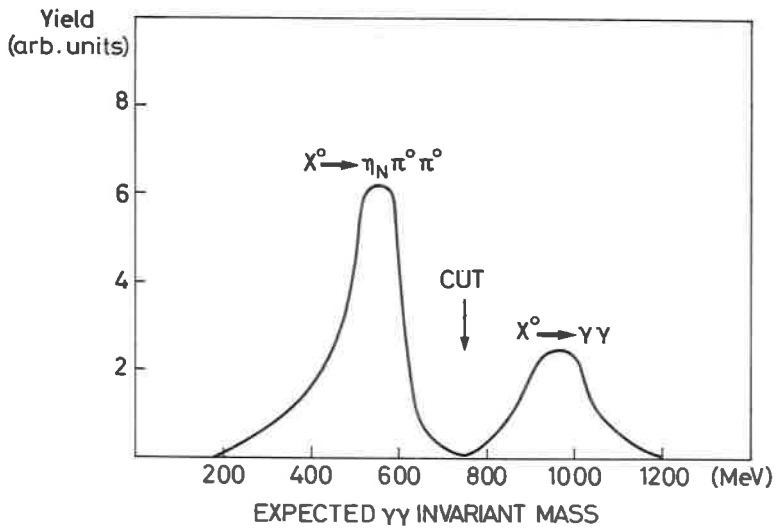

Fig. 3. – Monte Carlo predictions of the $\gamma\gamma$ invariant mass spectrum for the decays $X^0 \to \gamma\gamma$ and $X^0 \to \eta_N \pi^0 \pi^0$. The experimental resolution in determining the γ-ray energies $\Delta E_\gamma / E_\gamma = \pm 15\%$, and in the opening angle of the γ pair, $\Delta\theta_{\gamma\gamma} = \pm 1^\circ$, have been folded in the calculation. Clearly, a cut on $m_{\gamma\gamma}$ at ~ 750 MeV should make it possible to separate these two decay modes.

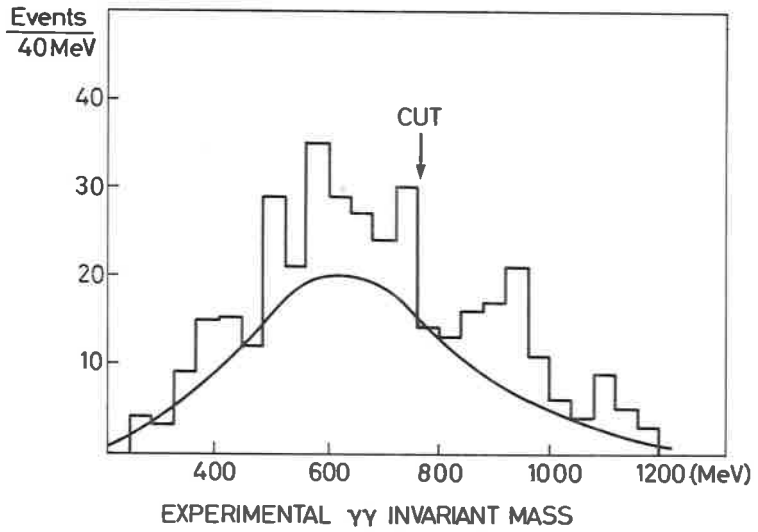

Fig. 4. – Experimental $\gamma\gamma$ invariant mass distribution for the events in the X^0 mass region ($952 <$ missing mass < 968 MeV).

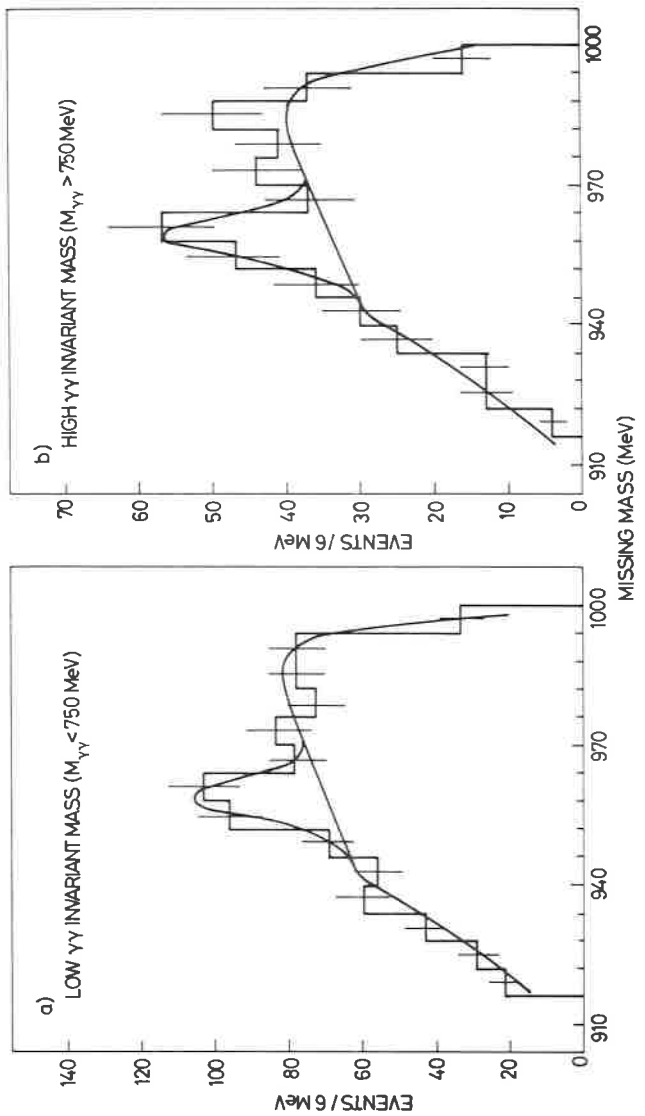

Fig. 5. – Missing-mass spectra for $\gamma\gamma$ events: *a*) with $m_{\gamma\gamma} < 750$ MeV; *b*) with $m_{\gamma\gamma} > 750$ MeV. The solid line shows the results of the fits.

The invariant mass spectrum for the events with missing mass in the range (952÷968) MeV is shown in Fig. 4. The background shape is given by the invariant mass spectrum of the events with missing mass outside the X^0 mass bins and is normalized to the observed number of background events (derived

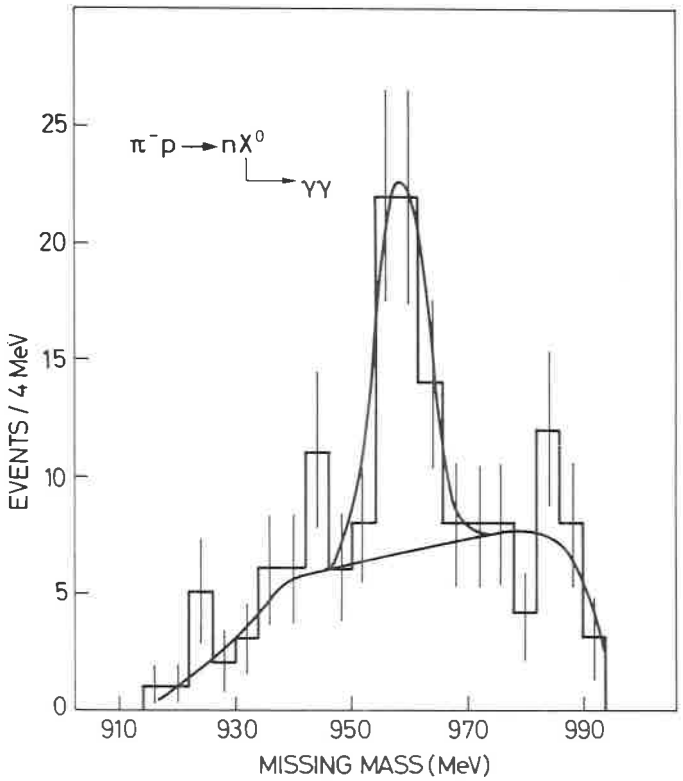

Fig. 6. – Missing-mass spectrum for $\gamma\gamma$ events with $m_{\gamma\gamma} > 750$ MeV satisfying the additional requirement of the coplanarity of the two γ-rays and the missing-mass directions. The solid line shows the result of the fit.

from the fit to the spectrum of Fig. 2). The peak, ~ 200 MeV wide, observed at ~ 900 MeV with ~ 40 events, clearly separated from the background, already shows the existence of the $\gamma\gamma$-mode. Figures *5a* and *5b* show the missing-mass spectra for the events with low invariant mass (< 750 MeV) and with high invariant mass (> 750 MeV), respectively. The backgrounds have been fitted by Monte Carlo calculated curves. Again, since the Monte Carlo (Fig. 3) shows that the cut at 750 MeV invariant mass leaves a negligible contamination from the $X^0 \to \eta_N \pi^0 \pi^0$ process, we can attribute the observed

(69 ± 17) events in Fig. 5*a* to the $X^0 \to \eta_N \pi^0 \pi^0$ decay mode and the observed (43 ± 11) events in Fig. 5*b* to the $X^0 \to \gamma\gamma$ decay mode.

In order to lower the background in the $X^0 \to \gamma\gamma$ mass spectrum, the coplanarity of the two γ-rays with the missing mass direction was constrained event by event on the basis of the geometrical reconstruction and of the neutron parameters. The mass spectrum for coplanar $\gamma\gamma$ events is shown in Fig. 6. The spectrum has been fitted to a Gaussian peak 10 MeV wide superimposed on a Monte Carlo calculated background shape. The number of events observed over a smooth and low background is 41 ± 8. The constancy of this figure, with respect to the one determined from the spectrum shown in Fig. 5*b*, proves that the separation of the $\gamma\gamma$ mode from the $\eta_N \pi^0 \pi^0$ mode is satisfactory. The $\gamma\gamma$-decay mode of the X^0 is therefore established to ~ 5 standard deviations confidence level.

The observed width of the peak in Fig. 6, (9 ± 2) MeV FWHH, when the calculated resolution is taken into account, allows the derivation of an upper limit for the natural width of the line, $\Gamma_{X^0} < 8$ MeV at 90% confidence level.

4. Results.

In order to derive the cross-section from the observed number of $X^0 \to \gamma\gamma$ events, the acceptance of the apparatus has been calculated by a Monte Carlo method. Furthermore, the conversion efficiency together with counter *M* efficiency were measured at 400 and 800 MeV with a « γ-ray beam » ([3]) and were found to be constant with energy in this region.

The measurability efficiency, *i.e.* the ratio of $\gamma\gamma$ events measured over the total number of $\gamma\gamma$ events selected, was estimated by two different methods: either using a « γ-ray beam » at 400, 800, 1100 MeV ([3]), or taking a sample of $\gamma\gamma$ events from the data. The results obtained were found to be in good agreement.

The values of these and other quantities needed for the normalization are shown in Table I.

The observed number of $X^0 \to \gamma\gamma$ events (41 ± 8) corresponds to a cross-section:

$$\sigma(\pi^- + p \to n + X^0_{\gamma\gamma}) = (1.81 \pm 0.36)\ \mu b\ .$$

TABLE I. - *Normalization for* $X^0 \to \gamma\gamma$.

γ conversion	0.370 ± 0.017
Pattern recognitions	0.31 ± 0.02
Scanning efficiency	0.92 ± 0.03
Analysis efficiency	0.98 ± 0.01
Geometrical acceptance × neutron detection efficiency	$(2.05 \pm 0.15) \cdot 10^{-3}$
N_p cm$^{-3} \times N_\pi$	$1.5 \cdot 10^{35}$
Central bar losses	0.97 ± 0.01
Neutron absorption	0.92 ± 0.01
Random vetoing	0.81 ± 0.05

Using our measured value of the total cross-section at 1.61 GeV/c ([4]), $\sigma(\pi^+ + p \to n + X^0) = (108 \pm 14)\,\mu b$, one can derive the branching ratio

$$\frac{\Gamma(X^0 \to \gamma\gamma)}{\Gamma(X^0 \to \text{total})} = (1.7 \pm 0.4)\% .$$

A consistency check can be obtained by calculating the branching ratio for the $X^0 \to \eta_N \pi^0 \pi^0$ mode.

Owing to the lower energy of the emitted γ-rays, the $\gamma\gamma$ detection efficiency turns out to be a factor of 2 lower than in the $X^0 \to \gamma\gamma$ mode. Moreover the geometrical acceptance of the γ-ray detectors is also a factor of 2 lower, with the requirement that only two γ's are detected out of the six (or ten) produced. Therefore the (69 ± 17) observed events correspond to a cross-section: $\sigma(\pi^- + p \to n + X^0_{\eta_N \pi^0 \pi^0}) = (14.4 \pm 5.0)\,\mu b$, which gives the branching ratio:

$$\frac{\Gamma(X^0 \to \eta_N \pi^0 \pi^0)}{\Gamma(X^0 \to \text{total})} = (13.4 \pm 5.0)\% .$$

Assuming that only $X^0 \to \gamma\gamma$ and $X^0 \to \eta_N \pi^0 \pi^0$ modes contribute to the $X^0 \to$ neutral decays, one can derive the branching ratio

$$\frac{\Gamma(X^0 \to \text{neutrals})}{\Gamma(X^0 \to \text{total})} = (15.1 \pm 5.0)\% ,$$

which is in good agreement with an independent measurement ([4]) performed with the neutron missing-mass spectrometer $(18.5 \pm 2.2)\%$, and with the world average ([4]) (19.0 ± 1.7).

The interest of the $X^0 \to \gamma\gamma$ branching ratio is well known and has been discussed ([1,5]). Several theoretical predictions ([6]) exist and they agree with our experimental result.

The determination of the $X^0 \to \gamma\gamma$ branching ratio is a further step towards the understanding of the η-X^0 mixing and of the old problem of the linear vs quadratic mass formula for bosons ([7]); a final answer being linked to the knowledge of the X^0 total width will be known.

REFERENCES

1) D. Bollini, A. Buhler-Broglin, P. Dalpiaz, T. Massam, F. Navach, F. L. Navarria, M. A. Schneegans and A. Zichichi: *Nuovo Cimento*, **58** A, 289 (1968).
2) D. Bollini, A. Buhler-Broglin, P. Dalpiaz, T. Massam, F. Navach, F. L. Navarria, M. A. Schneegans, F. Zetti and A. Zichichi: *Nuovo Cimento*, **61** A, 125 (1969).
3) D. Bollini, A. Buhler-Broglin, P. Dalpiaz, T. Massam, F. Navach, F. L. Navarria, M. A. Schneegans and A. Zichichi: *Revue de Physique Appliquée*, **4**, 108 (1969); M. Basile, D. Bollini, A. Buhler-Broglin, P. Dalpiaz, P. L. Frabetti, T. Massam, F. Navach, F. L. Navarria, M. A. Schneegans and A. Zichichi: *A large electromagnetic shower detector with high rejection power against pions*, to be submitted to *Nucl. Instr. and Methods*.
4) M. Basile, D. Bollini, P. Dalpiaz, P. L. Frabetti, T. Massam, F. Navach, F. L. Navarria, M. A. Schneegans and A. Zichichi: *Measurement of the* X^0 *cross-section in* π^-p *interactions at* 1.6 GeV/c *and determination of the branching ratio* $X^0 \to$ *neutrals*/$X^0 \to$ *total*, to be published in *Nuovo Cimento*.
5) D. Bollini, P. Dalpiaz, T. Massam, F. Navach, F. L. Navarria, M. A. Schneegans and A. Zichichi: *Proc. Int. Seminar on Vector Mesons on Electromagnetic Interactions*, Dubna (1969), p. 387.
6) R. H. Dalitz and D. G. Sutherland: *Nuovo Cimento*, **37**, 1777 (1965); M. Jacob: CERN Internal Report TH/846-1967 and *Proc. of High-Energy Physics Meeting*, Pisa (1967); A. Baracca and A. Bramon: *Nuovo Cimento*, **69** A, 613 (1970); F. Guerra, F. Vanoli, G. De Franceschi and V. Silvestrini: *Phys. Rev.*, **166**, 1587 (1968); P. Singer: DESY 69/35 (1969); W. Alles: *Lett. Nuovo Cimento*, **4**, 137 (1970).
7) See, for instance, the review talk of H. Harari at the *Symposium on the Present Status of* SU_3 *for Particle Couplings and Reactions*, July 1967, Argonne National Laboratory.

Evidence for the new decay mode $\varphi \to \eta\gamma$ (*)

M. BASILE, P. DALPIAZ, P.L. FRABETTI, T. MASSAM, F. NAVACH,
F.L. NAVARRIA, M.A. SCHNEEGANS and A.ZICHICHI

CERN - Geneva

Istituto di Fisica dell'Università - Bologna
Istituto Nazionale di Fisica Nucleare - Sezione di Bologna
Centre National des Recherches Scientifiques - Strasbourg

1. - Introduction

The purpose of this paper is to present evidence for the observation of the $\varphi \to \eta\gamma$ decay mode and a preliminary measurement of the branching ratio

$$R_1 = \frac{\Gamma(\varphi \to \eta\gamma)}{\Gamma(\varphi \to \text{total})} . \tag{1}$$

The experiment was performed at the CERN Proton Synchrotron (CPS) with the neutron missing-mass spectrometer of the Bologna CERN group ([1]), coupled to two electromagnetic shower detectors ([2]).

Apart from changes in the angular settings of the detectors, the set-up used is the same as the one described in a previous talk ([3]). The reaction studied is:

$$\pi^- + p \to n + MM$$

at 1.8 (GeV/c) with $\Delta p/p = \pm 1\%$. We look for neutral decays of the MM, requiring that at least two γ's from the MM decay be detected.

(*) Invited paper presented by P. L. Frabetti.

2. - Data analysis

Some 200000 pictures have been taken, of which $\sim 70\%$ are 2γ events, $\sim 30\%$ are 3γ events, and a small fraction show higher multiplicity.

The results presented here are still preliminary, as they refer to $\sim 96\%$ of the already analysed 2γ events.

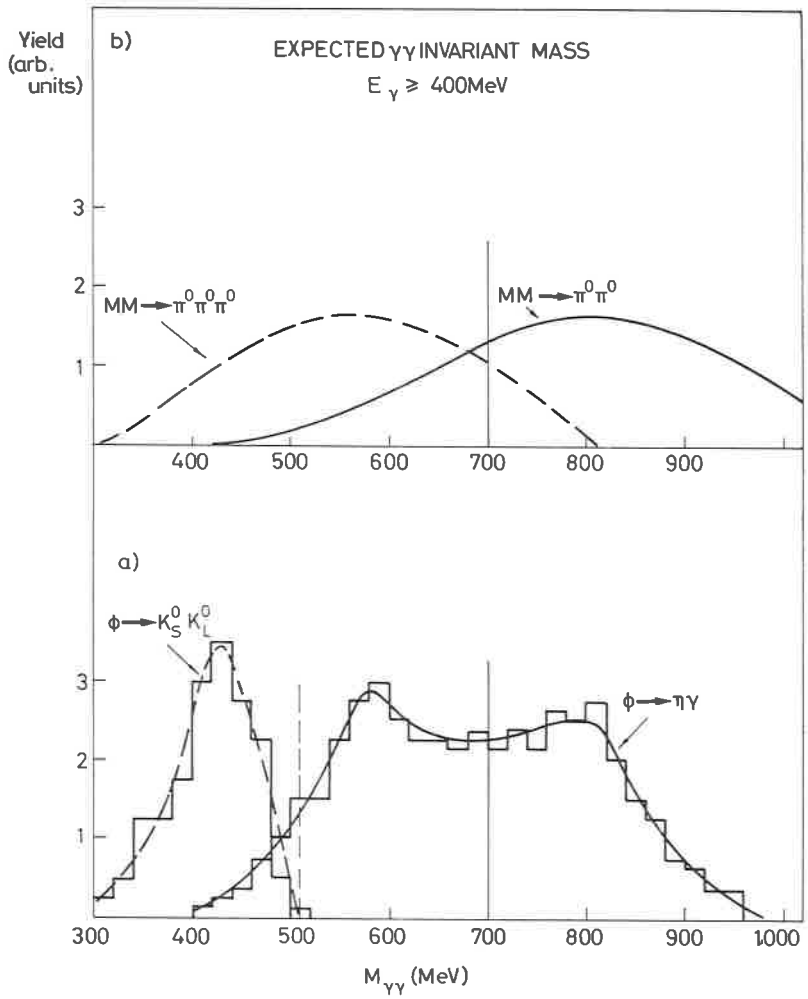

Fig. 1*a*. – Expected $\gamma\gamma$ invariant mass for the $\varphi \to \eta\gamma$ and the $\varphi \to K_S^0 K_L^0$ decay modes.
Fig. 1*b*. – Expected $\gamma\gamma$ invariant mass for $2\pi^0$ and $3\pi^0$ nonresonant production.

We measured only those events showing one converted γ-ray in each shower detector, giving well-measurable direction ([2]). The number of sparks for each γ, combined with the pulse-height information, allows the γ energy measurement with $\pm 15\%$ resolution ([2]). During the analysis, a cut at 400 MeV was applied to the energy of each γ in order to optimize the $\varphi \to \eta\gamma$ acceptance compared to background reactions. It should be noticed that such a cut on the γ energies selects, for kinematical reasons, the $\eta \to \gamma\gamma$ decay mode, with a contamination less than 1% from $\eta \to 3\pi^0$. A four-momentum transfer interval $0.2 < t < 0.5$ (Gev/c)^2 was selected during the data ana-analysis in order to reduce background and to improve the missing-mass resolution.

To detect the $\varphi \to \eta\gamma$ decay mode, we have essentially to face two problems:

i) The first is to distinguish between the $\varphi \to \eta\gamma$ decay mode and the other neutral decay mode of the φ meson, namely $\varphi \to K_S^0 K_L^0$ (with $K_S^0 \to \pi^0\pi^0$).

Figure 1*a*) shows the expected $\gamma\gamma$ invariant mass ($M_{\gamma\gamma}$) distribution, as predicted by a Monte Carlo simulation for the two different processes when a cut at 400 MeV is applied to the energy of each γ. The Monte Carlo calcu-

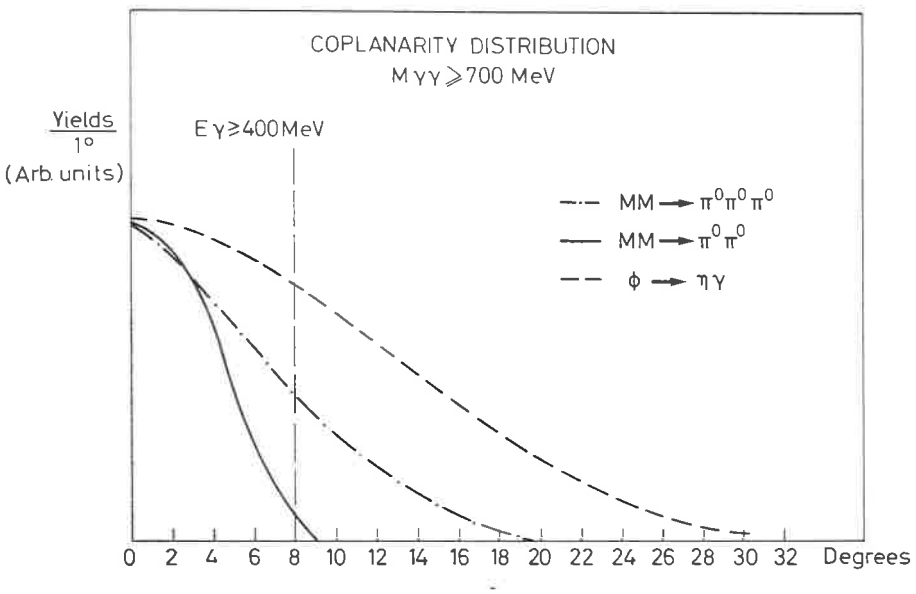

Fig. 2. – Expected acoplanarity angle distribution for $2\pi^0$, $3\pi^0$ nonresonant production and for the $\varphi \to \eta\gamma$ decay mode.

lations are done taking into account the known experimental resolution for the γ energy ($\pm 15\%$) and for the γ direction ($\pm 1°$).

From Fig. 1*a*) one can see that a cut at $M_{\gamma\gamma} = 500$ MeV enables us to distinguish between the $\varphi \to K_S^0 K_L^0$ and $\varphi \to \eta\gamma$ decay channels.

ii) The second problem is the rejection of the background coming from nonresonant multiple π^0 production, which is very important because of the small $\varphi \to \eta\gamma$ cross-section.

Figure 2 shows a comparison between expected acoplanarity angle ([3]) distribution for non-resonant $2\pi^0$ and $3\pi^0$ production and $\varphi \to \eta\gamma$.

When a cut at 8° is applied, we reject the $2\pi^0$ events with 95% efficiency, losing only 30% of $\varphi \to \eta\gamma$ events. For the $3\pi^0$ events, the cut on the acoplanarity angle is not so efficient, but a further rejection can be obtained by cutting for higher $M_{\gamma\gamma}$ values.

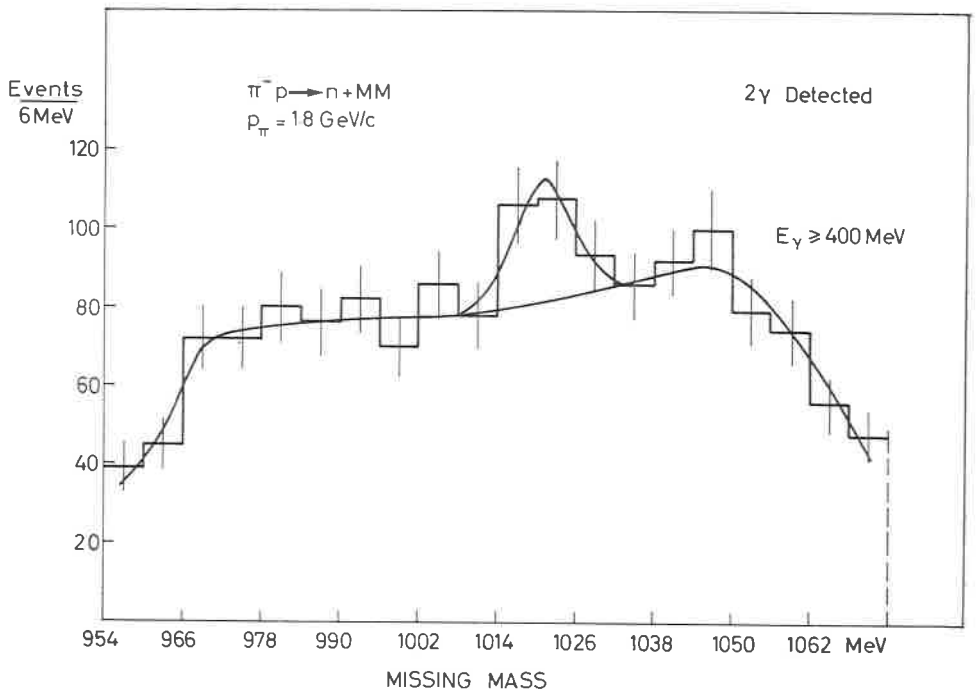

Fig. 3. – Experimental missing-mass spectrum corresponding to neutral decays of the φ meson where 2γ are detected.

Figure 1*b*) shows the expected $\gamma\gamma$ invariant mass distributions for $2\pi^0$ and $3\pi^0$ non-resonant production. It is clearly shown that a cut

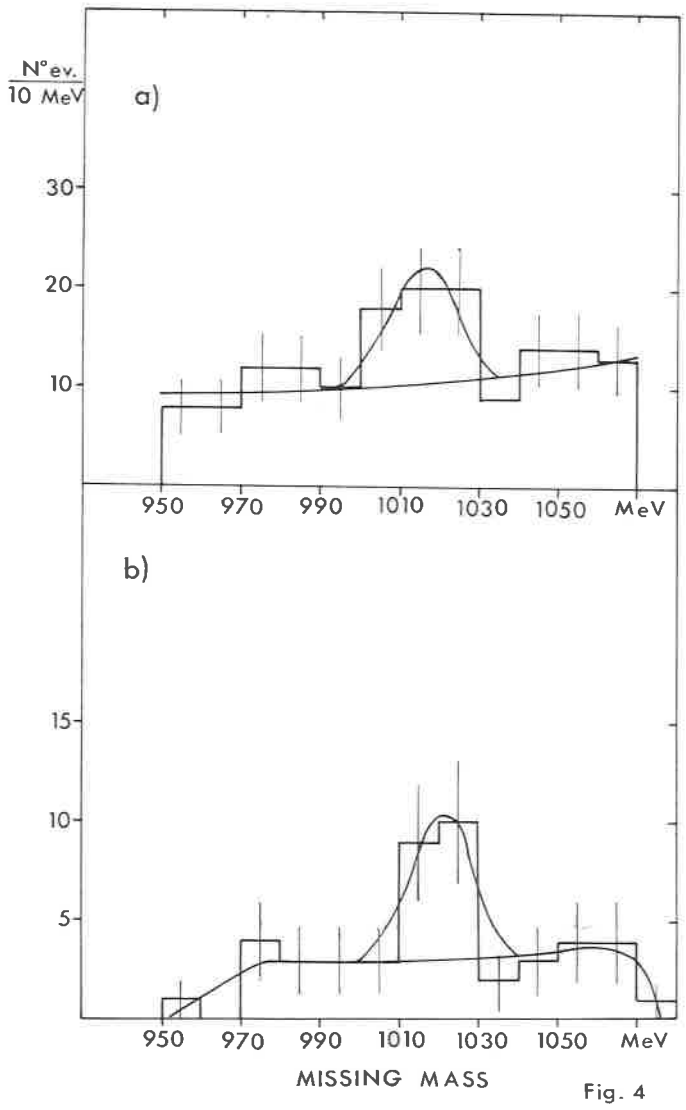

Fig. 4*a*. – Experimental missing-mass spectrum corresponding to the $\varphi \to K_S^0 K_L^0$ decay channel.

Fig. 4*b*. – Experimental missing-mass spectrum corresponding to the $\varphi \to \eta\gamma$ decay channel.

at $M_{\gamma\gamma} = 700$ MeV allows a rejection of $3\pi^0$ events with an over-all efficiency of the order of 90% for a total loss of 40% of $\varphi \to \eta\gamma$ events.

3. - Results

Figure 3) shows the missing-mass spectrum, for events with two gammas detected, with no cut applied. A clear well-resolved $\varphi \to$ neutral peak is visible, which allows some consistency check such as acceptance and beam-momentum optimization.

Figure 4*a*) shows the missing-mass spectrum for $M_{\gamma\gamma} < 500$ MeV and without coplanarity selection; therefore the observed peak (28 ± 6 events) corresponds to the $\varphi \to K_S^0 K_L^0$ decay channel.

Figure 4*b*) shows the missing-mass spectrum obtained by selecting events with $M_{\gamma\gamma} > 700$ MeV and acoplanarity angle $> 8°$, which corresponds to the $\varphi \to \eta\gamma$ channel; (13.6 ± 4.1) events are observed in the φ peak.

Using the number of observed $\varphi \to \eta\gamma$ events, the number of incident pions, the detection efficiencies, and a total production cross-section $\sigma_\varphi = (35 \pm 5)\ \mu$b at 1.8 (GeV/c) ([4]), the branching ratio (1) turns out to be

$$R_1 = (7.0 \pm 2.5)\% . \tag{2}$$

In order to check the self-consistency of our observations, we use the data of Fig. 4*a*) to derive the branching ratio

$$R_2 = \frac{\varphi \to K_S^0 K_L^0}{\varphi \to \text{total}} = (33 \pm 9)\% . \tag{3}$$

The agreement between R_2 with the known value ([4,5]) $R_2^{\text{known}} = (34.8 \pm 2.3)\%$ proves the self-consistency of our acceptances and efficiency calculations.

4. - Conclusions

The existence of the new decay mode $\varphi \to \eta\gamma$ for φ's produced in π^-p interactions is established with a confidence level better than 99% (3σ).

REFERENCES

1) D. BOLLINI, A. BUHLER-BROGLIN, P. DALPIAZ, T. MASSAM, F. NAVACH, F. L. NAVARRIA, M. A. SCHNEEGANS, F. ZETTI and A. ZICHICHI: *Nuovo Cimento*, **61** A, 125 (1969).
2) M. BASILE, J. BERBIERS, D. BOLLINI, A. BUHLER-BROGLIN, P. DALPIAZ, P. L. FRABETTI, T. MASSAM, F. NAVACH, F. L. NAVARRIA, M. A. SCHNEEGANS and A. ZICHICHI: *A large electro-magnetic shower detector with high rejection power against pions*, to be published in *Nuclear Instruments and Methods*.
3) M. BASILE, D. BOLLINI, P. DALPIAZ, P. L. FRABETTI, T. MASSAM, F. NAVACH, F. L. NAVARRIA, M. A. SCHNEEGANS and A. ZICHICHI: *Further evidence for the decay mode* $X^0 \to \gamma\gamma$ *and determination of the branching ratio* $X^0 \to \gamma\gamma/X^0 \to$ *total* (invited paper presented at this conference), submitted to *Nuovo Cimento*.
4) O. I. DAHL, L. M. HARDY, R. I. HESS, J. KIRZ and D. H. MILLER: *Phys. Rev.*, **163**, 1377 (1967); J. H. BOYD, A. R. ERWING, W. D. WALKER and E. WEST: *Phys. Rev.*, **166**, 1458 (1968); D. BOLLINI, A. BUHLER-BROGLIN, P. DALPIAZ, T. MASSAM, F. NAVACH, F. L. NAVARRIA, M. A. SCHNEEGANS and A. ZICHICHI: *Nuovo Cimento*, **60** A, 541 (1969); D. W. DAVIES, N. A. ABOLINS, O. I. DAHL, J. S. DANBURG, P. L. HOCH, J. KIRZ, D. J. MILLER and R. K. RADER: *Phys. Rev.*, D **2**, 506 (1970).
5) PARTICLE DATA GROUP: *Phys. Lett.*, **33** B, 1 (1970).
6) Upperlimits for this new decay mode of the φ meson have been reported in the literature by M. BADIER *et al.*: *Phys. Lett.*, **17**, 337 (1965), $(9\pm11)\%$ and by J. S. LINDSEY and G. A. SMITH: *Phys. Lett.*, **20**, 93 (1966), $(0\pm8)\%$; furthermore, 3γ type events in the φ mass region have been interpreted as being due to $\varphi \to \eta+\gamma$ decay made by the ACO Group $(2\pm0.75)\%$. However, these data are still unpublished.

SESSION II-B

Thursday, 15 April 1971

Intermediate mass mesons - E, F_1, R, S mesons and the L-region

Chairman: CH. PEYROU

Secretaries: F. PALMONARI
M. JOBES

Intermediate mass bosons (*)

B. R. FRENCH
CERN - Geneva

1. An introductory talk. I hope!

Items

1) E^0

2) F_1

3) $G = +1$ $(2\pi)^0_\pm$ states: $\pi^\pm\pi^0$, $\pi^+\pi^-$

4) $G = -1$ $(3\pi)^0_\pm$ states; $A_3^\pm(f^0\pi^\pm)$, $\varphi(\rho^0\pi^0)$

5) $G = +1$ $(4\pi)^+$ state

6) $G = -1$ $(5\pi)^0$ state

} R region $(1.6 \div 1.88)$ GeV

2. E^0. What is a E^0?

It is a $(KK\pi)^0$ bump seen in

$$\left.\begin{aligned} \bar{p}p &\to (K_1^0 K^\pm \pi^\mp)^0 \pi^+\pi^- \\ &\to (K_1^0 K^\pm \pi^\mp)^0 \pi^0\pi^0 \end{aligned}\right\} \text{ 0 GeV/c}$$

(*) Introductory talk

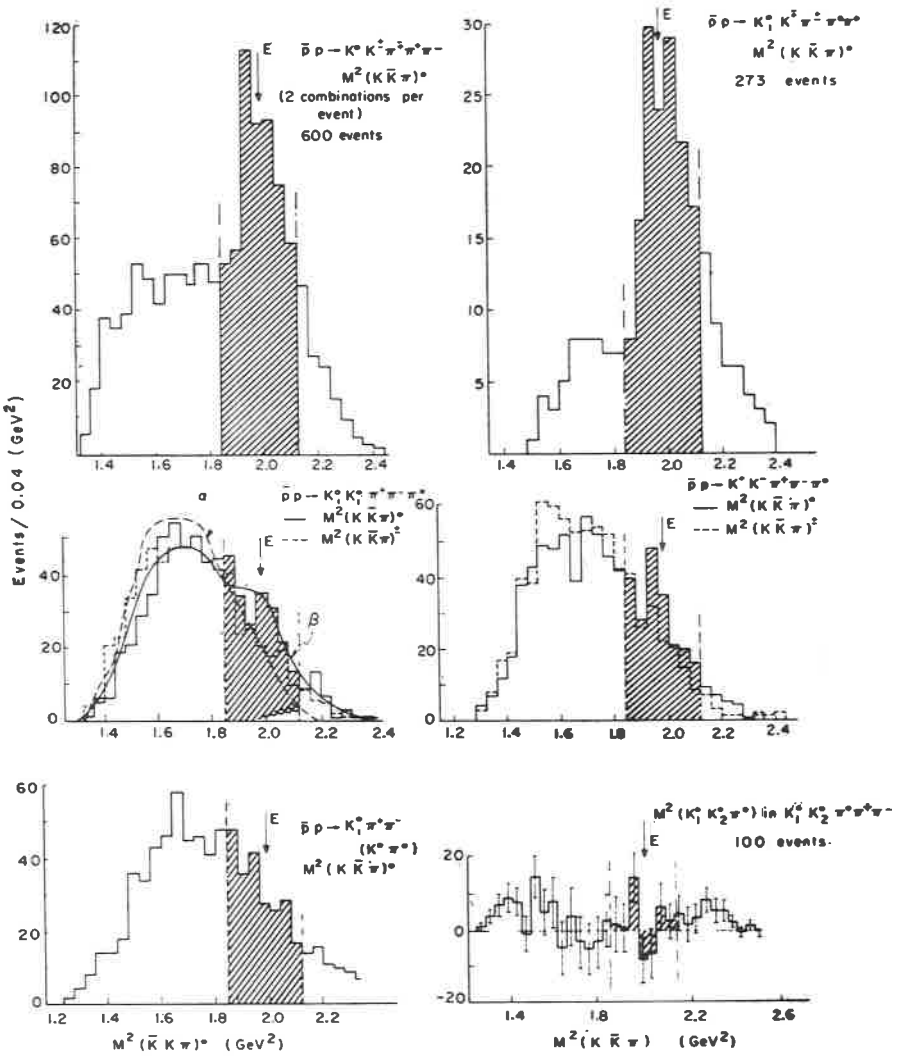

Fig. 1. - Shows the effect: $M=(1422\pm3)$ Mev, $\Gamma=(69\pm8)$ Mev, $I^G=0^+$, $J^P=0^-$ favoured by complex analysis; $I^G\ J^P$ same as η^0 and X^0; One too many for 0^- nonet.

Question 1. Why so few observations of E^0? Mainly in $\bar{p}p$ why not in $K^-p \to \Lambda^0(K^0K^+\pi^-)$?

Question 2. Can it be a radially excited state? Daughter?

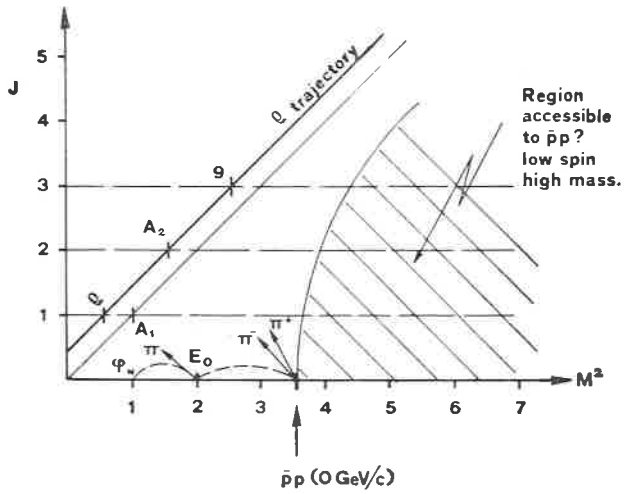

Is $\bar{p}p$ one way of putting *low* spin into *high* mass?

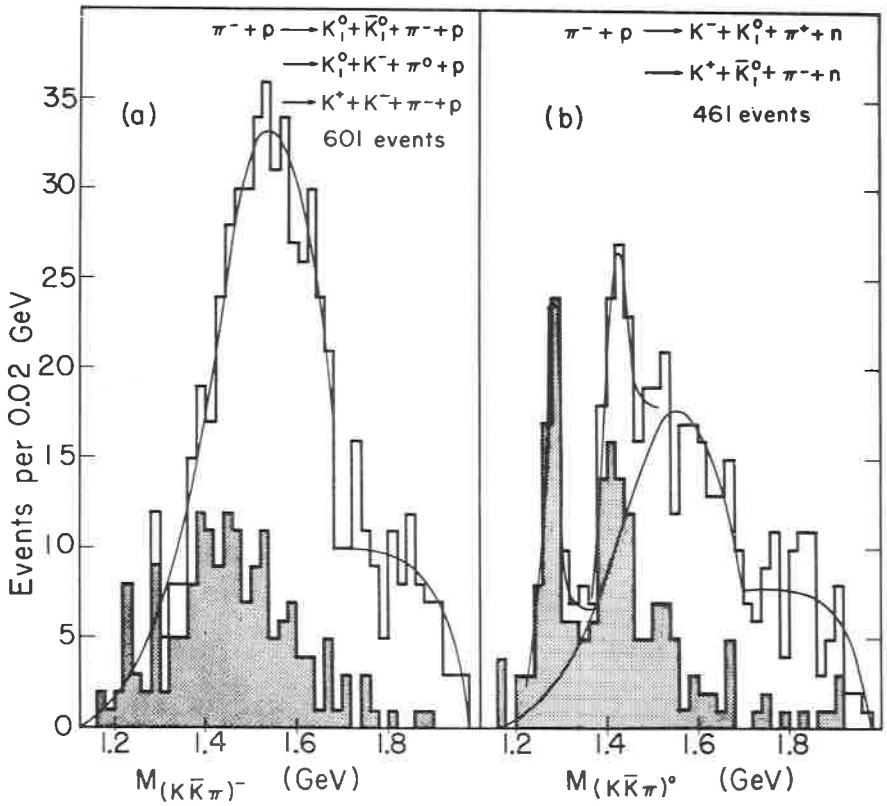

Fig. 2. - Only other observation outside $\bar{p}p$.

3. F_1. **What is** $F_1^{\pm}$?

It is a $(K_1^0 K^0 \pi^{\pm})$ bump in

$$\bar{p}p \to (K_1^0 K^0 \pi^{\pm})\pi^{\mp} \qquad \text{at 700 MeV/c}$$

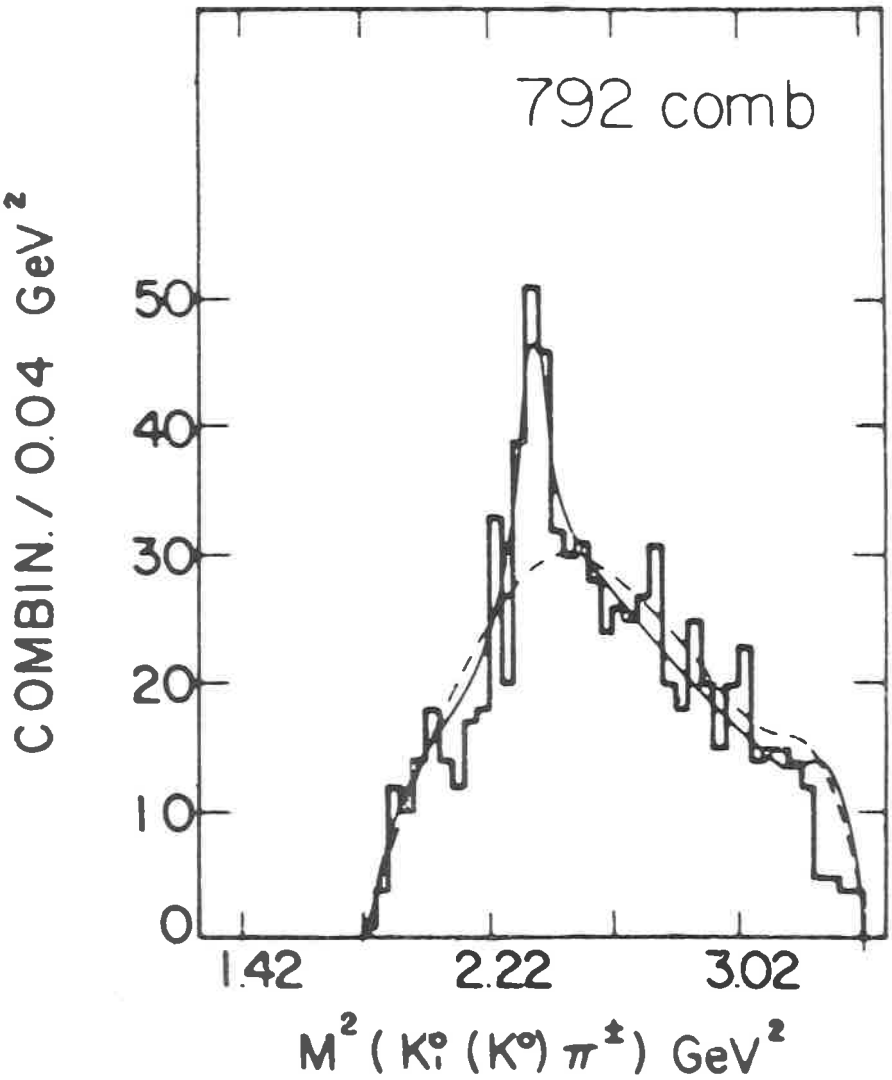

Fig. 3. - Shows the effect: $M = (1540 \pm 5)$ Mev; $\Gamma = (40 \pm 15)$ Mev; $I = 1$; $J^P =$ abnormal 1^+, 2^- favoured.

Question 1. Why only one observation?

Question 2. Can it too be radial excitation?

4. Recent work.

In $\bar{p}p$ 1,2 GeV/c, see only F_1^0!

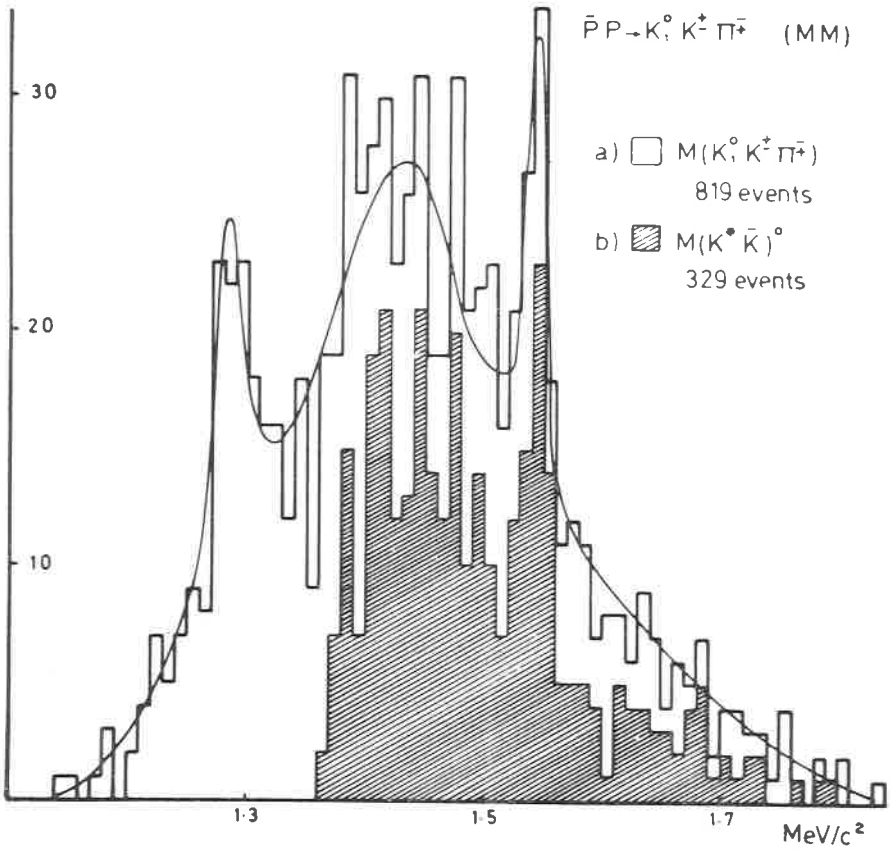

Fig. 4. - $K_1^0 K^{\pm}\pi^{\mp}$, good signal. *Reaction*: $\bar{p}p \to K_1^0 K^{\pm}\pi^{\mp}$ (MM). *Explanation:* $\bar{p}p \to F_1^0\eta^0$?.

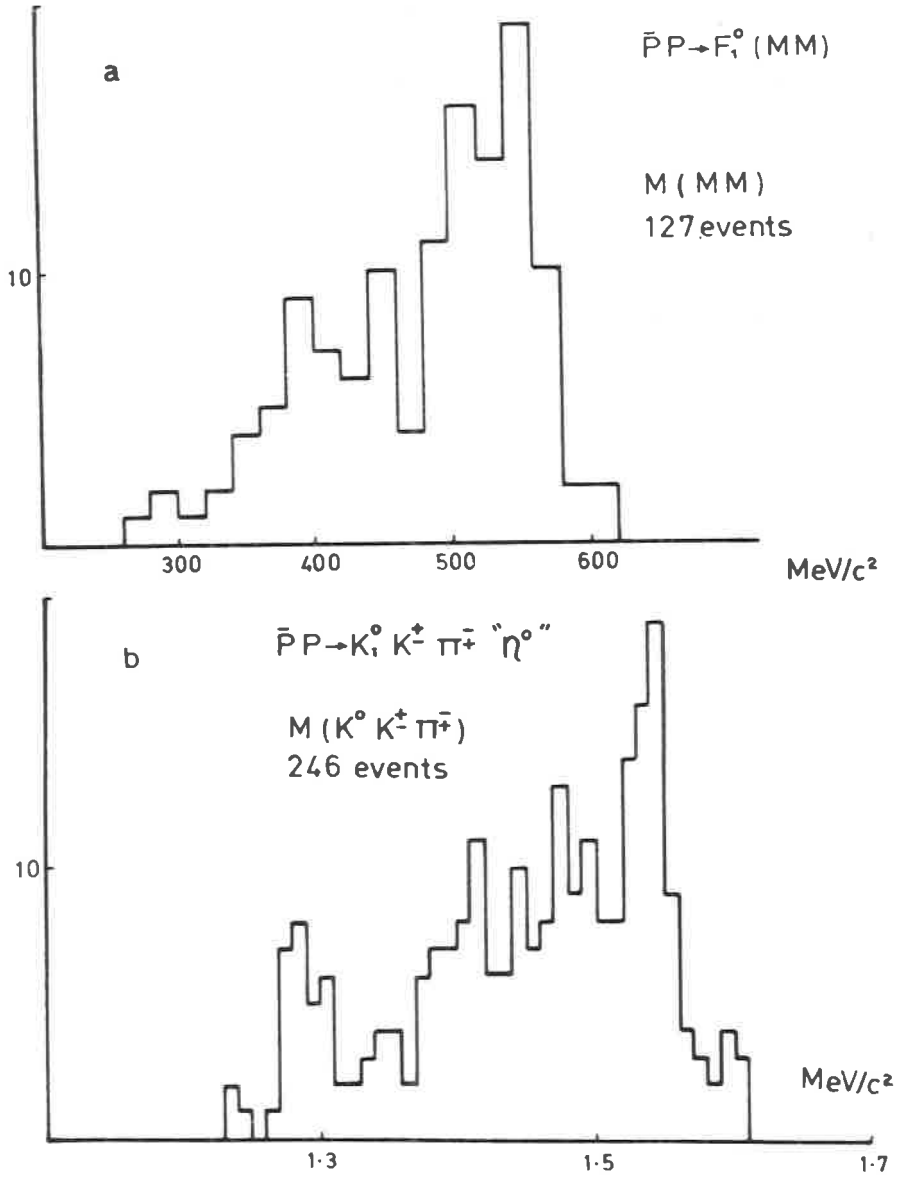

Fig. 5. - (MM) spectrum, not too good η?

5. Conclusions on E^0, F_1?

« If you will use special „nets" you will catch special fish »—sage Astier.

6. *R*-region.

$G = +1$, 2π *states first.* What have we reasonably established?

g^0 $(\pi^+\pi^-)$.

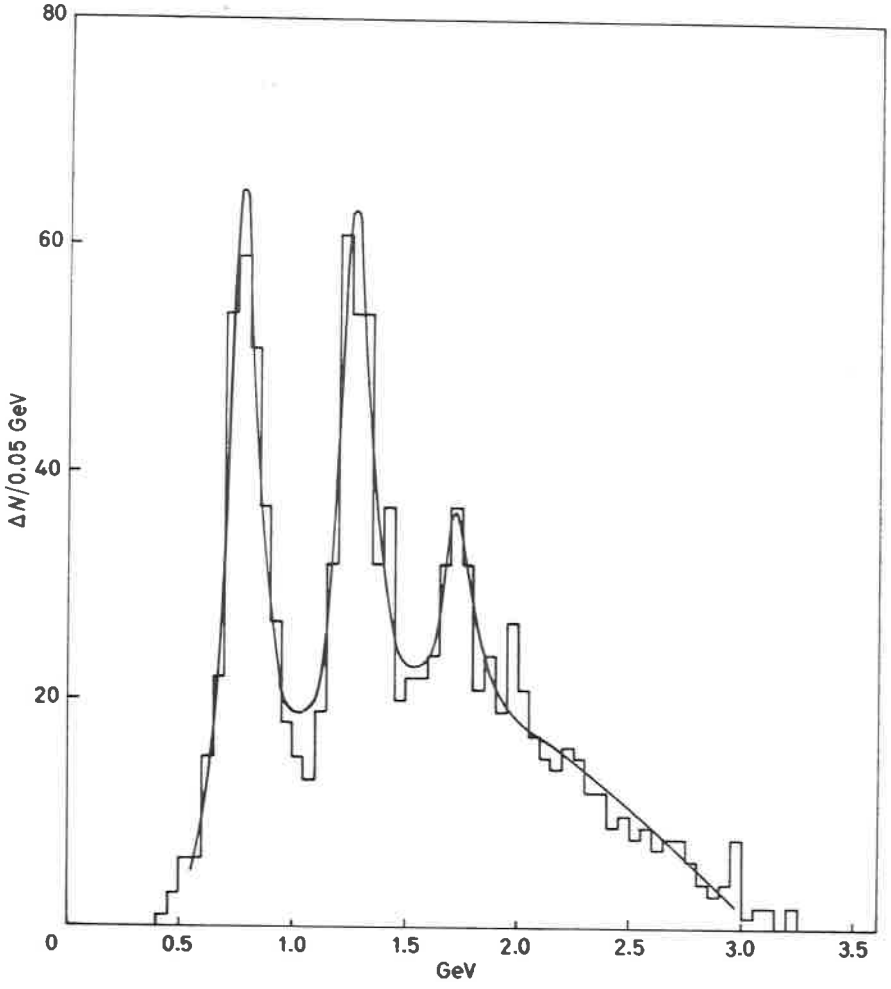

Fig. 6. - $\pi^+n \to p\pi^+\pi^-$; $t<0.04$, 9 GeV/c; $M=(1737\pm23)$ MeV; $\Gamma=(171\pm$ $\pm65)$ Mev. C. f. Vienna: 1680 ± 15, 200 ± 50.

g+ (π+π^0).

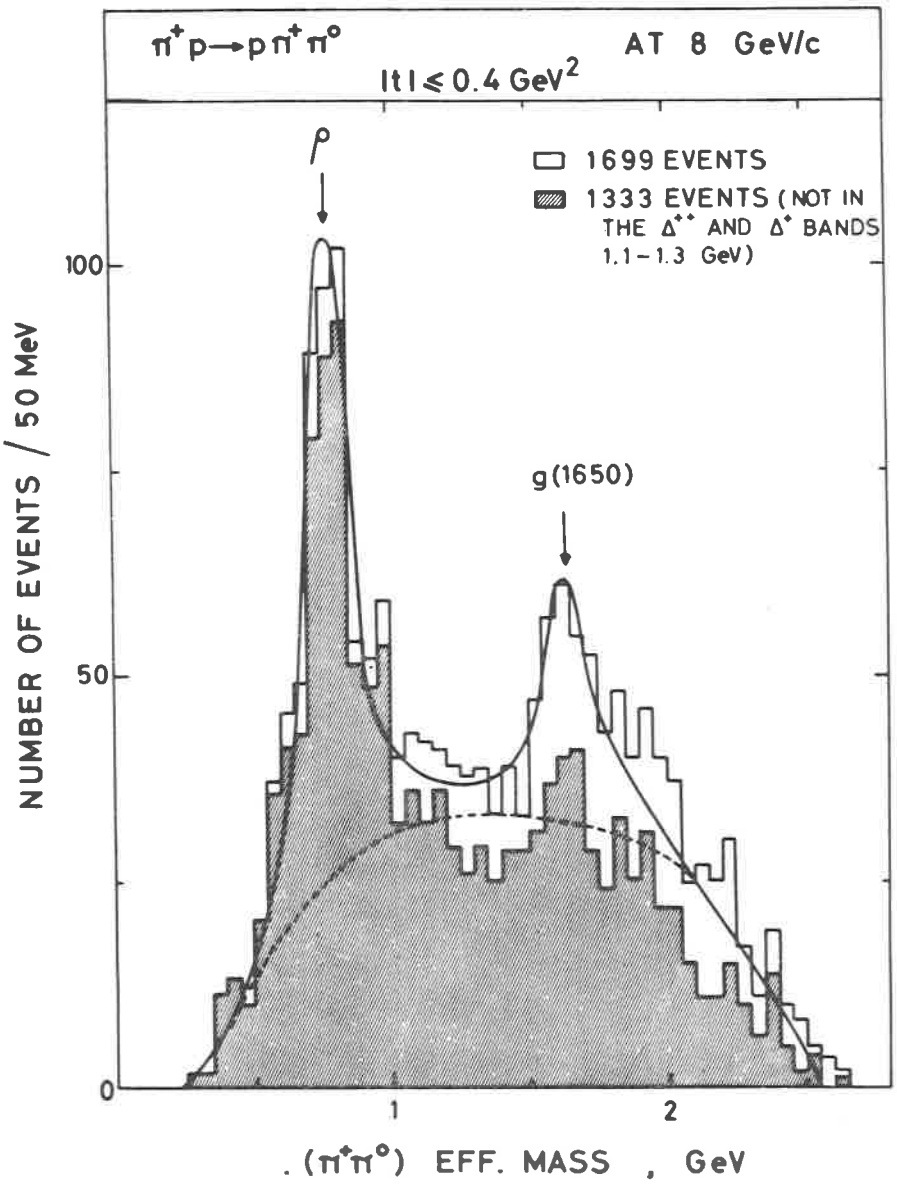

Fig. 7 - $\pi^+p \to p\pi^+\pi^0$; 8 GeV/c; $M=(1650\pm35)$ MeV; $\Gamma=(180\pm30)$ MeV
Cf. Vienna: 1640 ± 20, 120 ± 50.

Question 1. Why is $M(\pi^+\pi^-) > M(\pi^+\pi^0)$?

Question 2. Where are narrow states corresponding to MMS? (MMS = Missing Mass Spectrometer).

MMS	$R_1 = 1630 \pm 15$	$\Gamma < 21$ MeV
	$R_2 = 1700 \pm 15$	$\Gamma < 30$ MeV
	$R_3 = 1748 \pm 15$	$\Gamma < 38$ MeV

Question 3. Why no repeat of MMS expt—dangerous since A_2 split now under fire?

For questions 1 and 2—two recent results:

i) *Notre Dame*: $\pi^- p \to n\pi^+\pi^-$ 8 GeV/c.

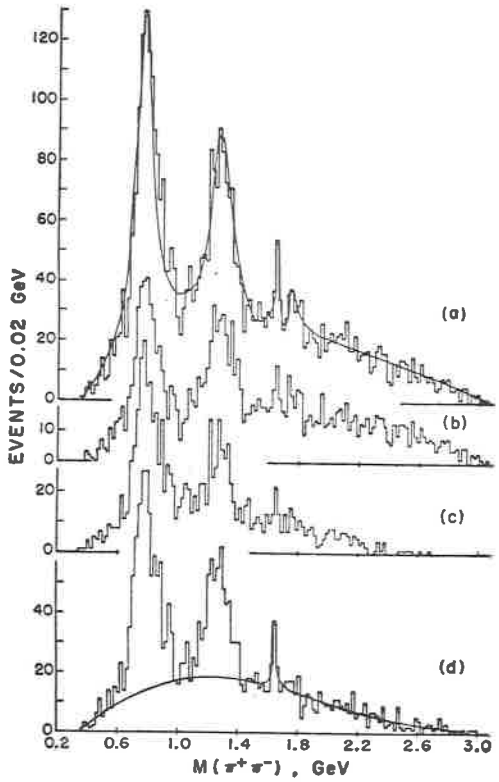

Fig. 8 - Narrow peak? $M = (1655 \pm 4)$ MeV; $\Gamma = (20 \pm 8)$ (low $t < 0.15$). + broader peak? $M = (1764 \pm 15)$ MeV, $\Gamma = (87 \pm 17)$. *a)* $\pi^- p \to n\,\pi^+\pi^-$ and $\pi^+ d \to pp\pi^+\pi^-$ *b)* $\pi^- p \to n\,\pi^+\pi^-$ *c)* $\pi^+ d \to pp\pi^+\pi^-$ *d)* as a) but $t < 0.15$.

ii) *Purdue* $\pi^+p \to p\pi^+\pi^0$ 13 GeV/c.

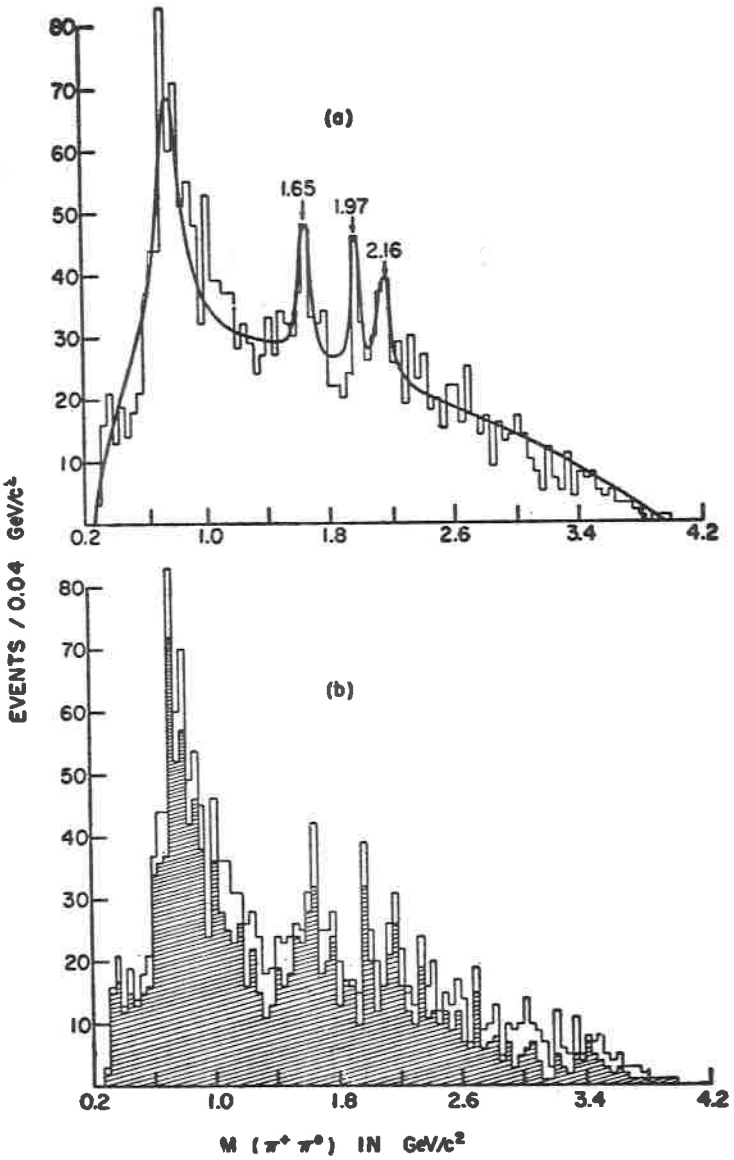

Fig. 9. - Narrow peak? $M = (1652 \pm 15)$; $\Gamma = (40 \pm 32)$ ($t < 0.3$). Notice that Fig. 9b) has Δ^{++} (1238) excluded; shaded area has $t < 0.3$ GeV².

These 2 data suggest one $I = 1$ peak at 1650 MeV + broader $I = 1$ at 1760 MeV (but more statistics needed).

Question 4. Any chance for J^P of g? May be with good statistics.

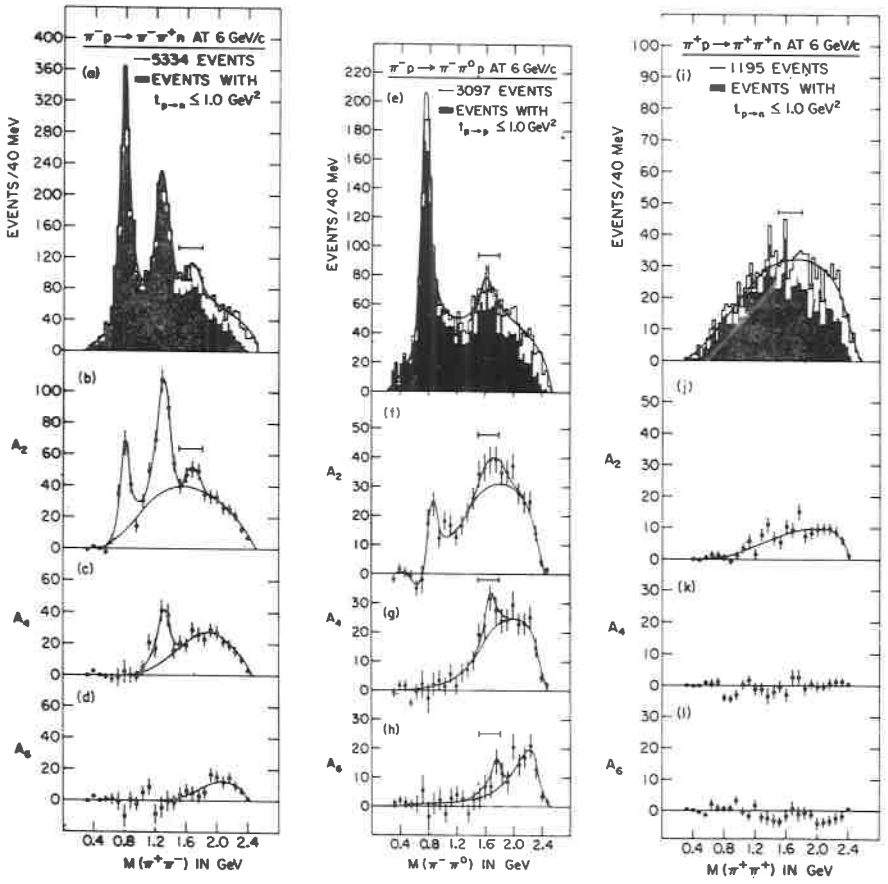

Fig. 10. - Old B. N. L. data reasonable behaviour for $\rho_0^{\pm}$, f^0; $\pi^-\pi^0$ gives bump in $A_6 \to I = 3$.

Question 5. Why no A_6 bump in $\pi^+\pi^-$?

To do. $\pi^{\pm}p \to pK^{\pm}K^0$ which shows good signal/noise at g—maybe as in $A_2 \to K^{\pm}K^0$ we will get clean J^P result.

7. Digression- narrow peaks.

Consider à la Maglic

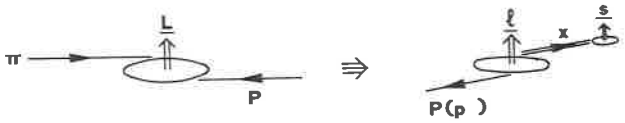

$$L \sim l + S$$

$$l \sim \frac{2p^*}{\sqrt{t}} \quad \text{is it?}$$

$$\therefore\ S \simeq L - \frac{2p^*}{\sqrt{t}}\ .$$

Thus at given L:

S small at small t;

S large at large t;

$\sigma \propto (2L+1)$; for $\exp[-8t]$, $1/7\sigma > t = 0.25$.

Question. Is this a mechanism for putting in relatively large angular momentum at given mass? *E.g.* so called Pomeron exchange gives steep t slope and gives rise to $A_1(\rho\pi)$ in S-wave and $A_3(f^0\pi)$ in S-wave. Cutting at $t > 0.2$ leaves A_2, *i.e.* $\rho\pi$ in higher angular momentum state.

8. $G = -1$, 3π states.

8.1. – $A_3(f^0\pi^-)$

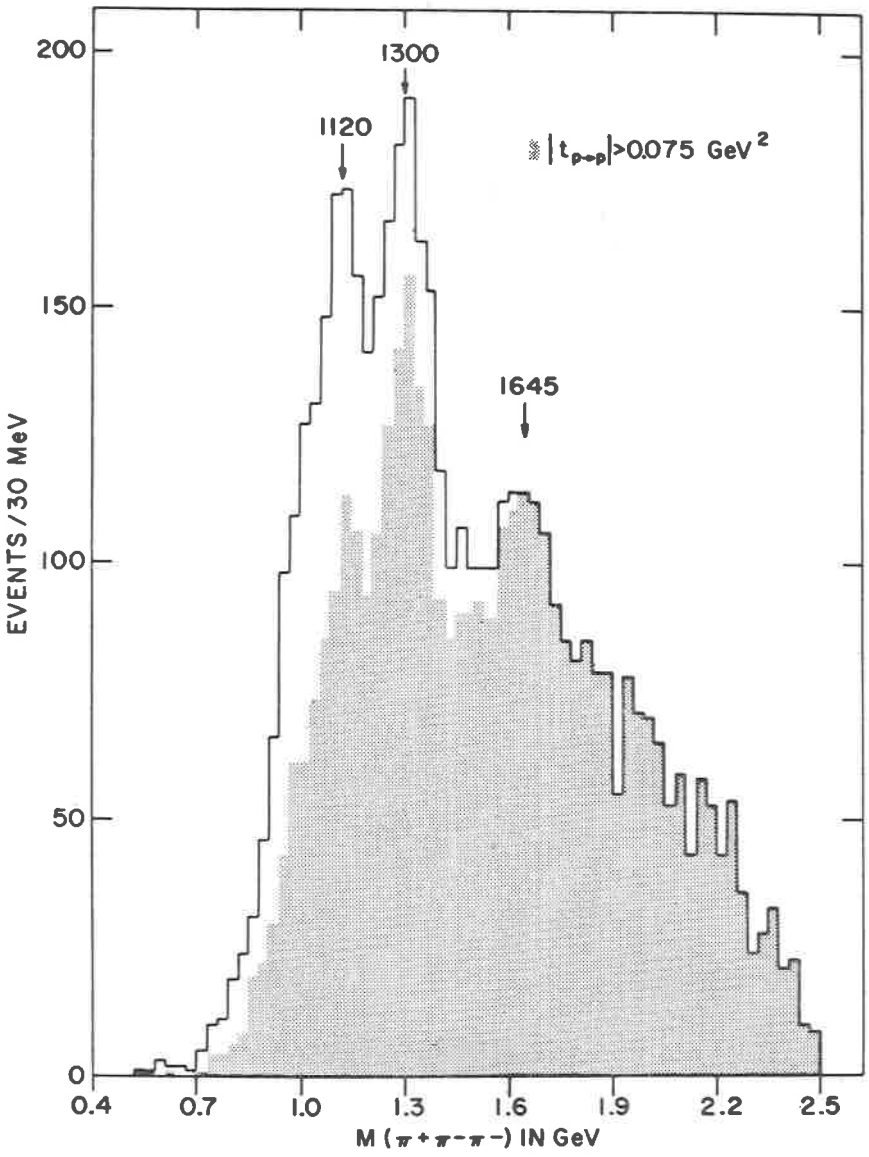

Fig. 11. - Example of A_3 BNL $\pi^- p \to p\pi^+\pi^-\pi^-$, 6 GeV/c, $t > 0.075$. No Δ^{++}. Clear peak: $M = 1645 \pm 10$ Mev; $\Gamma = 130 \pm 30$. Talk of it being a threshold effect; indeed analysis of Dalitz plot shows all $f^0\pi^-$.

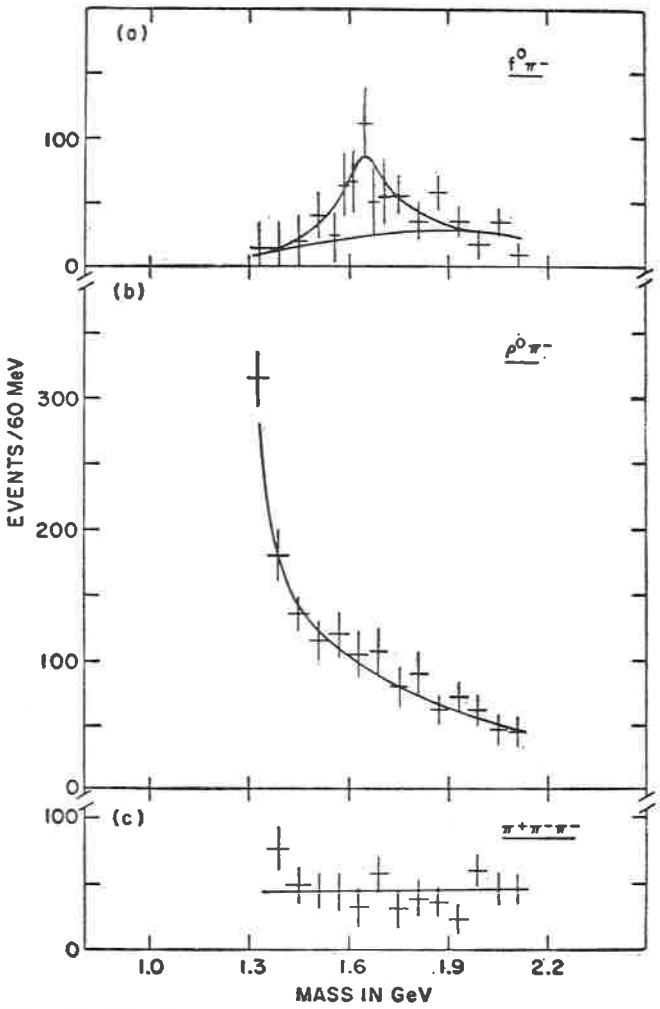

Fig. 12 - Nice B. W. shape

Question: Why no $\rho^0\pi^-$ decay? No $\pi^-\eta$, 5π,

$$\frac{d\sigma}{dt} \sim \exp[-5t]$$

$$\left.\begin{aligned} I^a &= 1^- \\ J^\rho &= 2^- \end{aligned}\right\} \text{ probable}$$

To do: Complete phase shift type analysis.

8.2. – $\varphi(1650) \to \rho^0\pi^0$.

Enhancement in $(3\pi)^0$ of $\pi^+n \to p\pi^+\pi^-\pi^0$

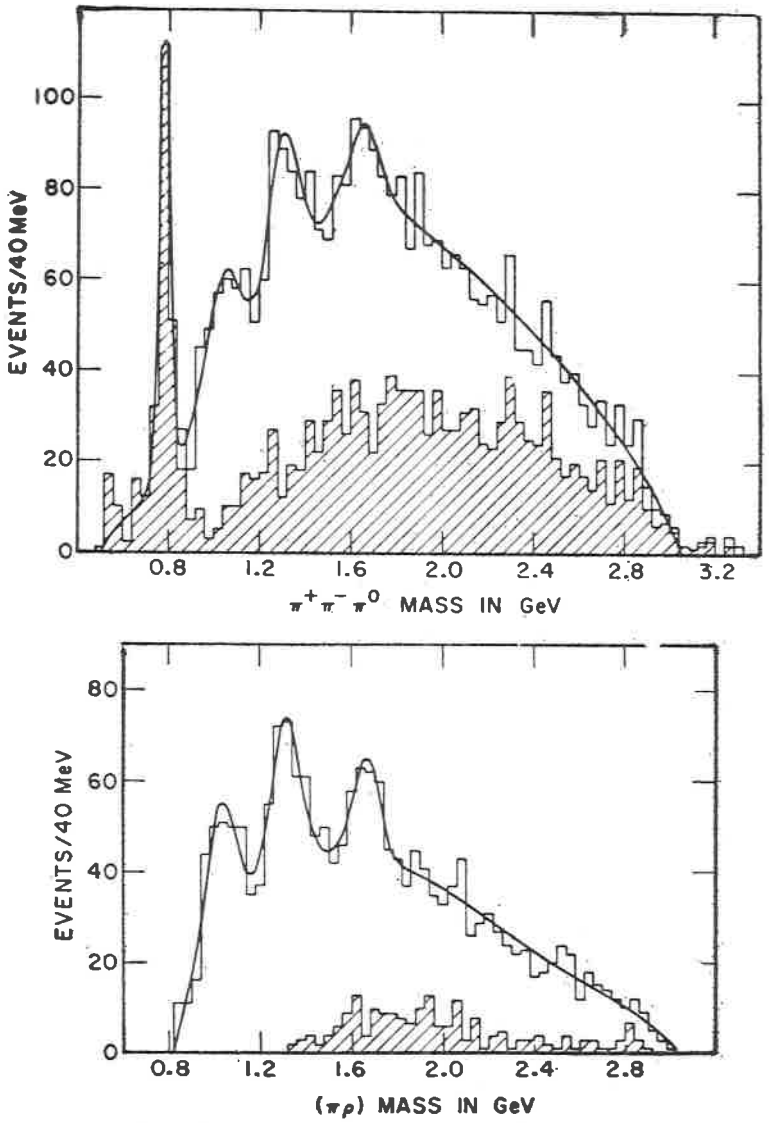

Fig. 13. - π^+d, 8 GeV/c; $M = (1670 \pm 20)$ MeV; $\Gamma = (100 \pm 40)$ MeV. No $f^0\pi^0$. Do see $\rho^0\pi^0$ ... $I^G = 0^-$, $J^P = 1^-2^\pm$ favoured. See nothing in 5π or $\omega^0\pi^+\pi^-$.

Comment. Charge exchange mechanism, *no* $f\pi$ state—special nets, special fish again?

8.3. – $\rho(4\pi)^+$.

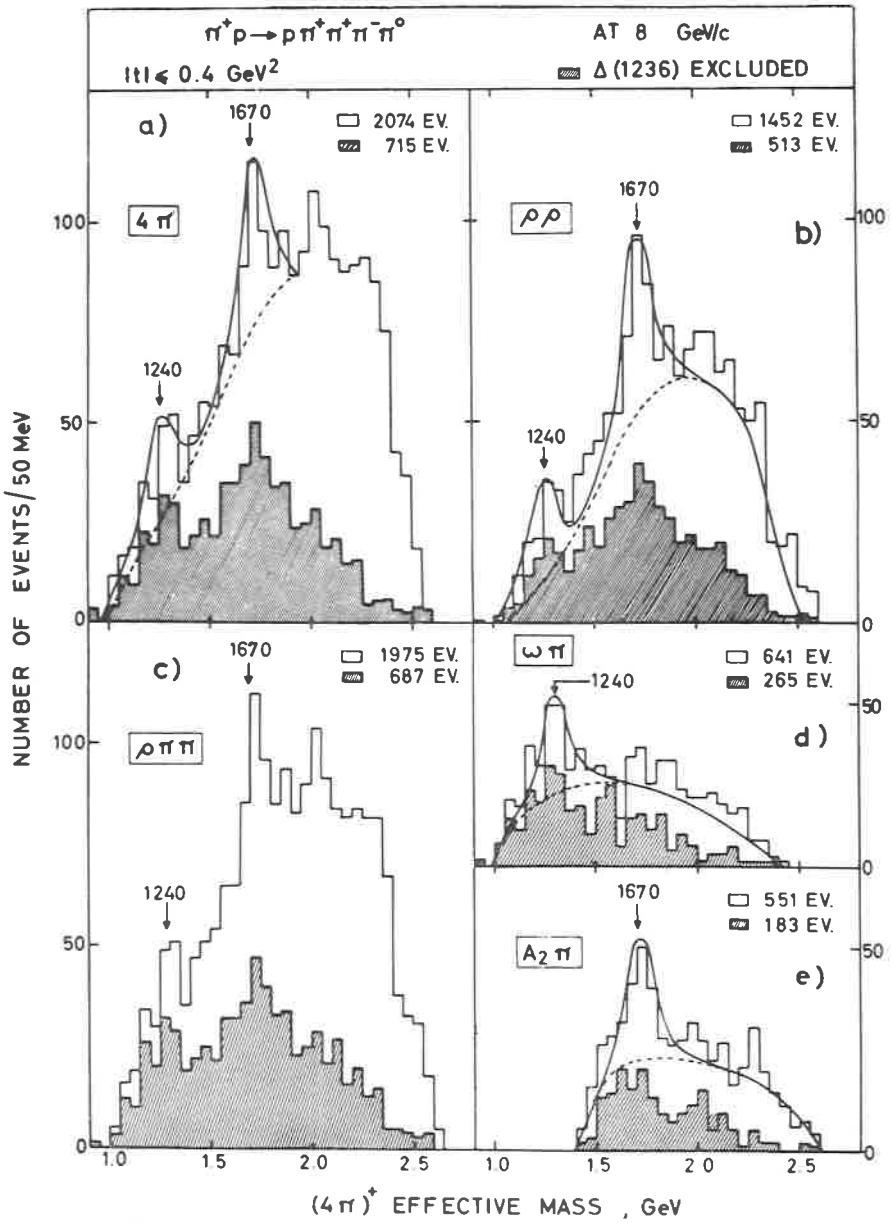

Fig. 14. - Example $\pi^+p\to p\pi^+\pi^+\pi^-\pi^0$. A.B.C. 8 Gev/c, $t<0.4$: $M=(1670\pm$ ± 30 Mev; $\Gamma=(160\pm 40)$. A. B. C. associate this with g^+-matter of taste after what we have seen.

Nice exercise. J^p multi-channel analysis - à la Abramovich *et al.* and Ascoli *et al.* require much statistic $+\geqslant$ one Zemach type man.

9. $G = -1$, 5π **state.**

$(\omega^0\pi^+\pi^-)$.

Reaction $K^-p \to \Lambda^0\pi^+\underbrace{\pi^-\pi^+\pi^-}_{\omega^0}\pi^0$ at 4.6 GeV/c.

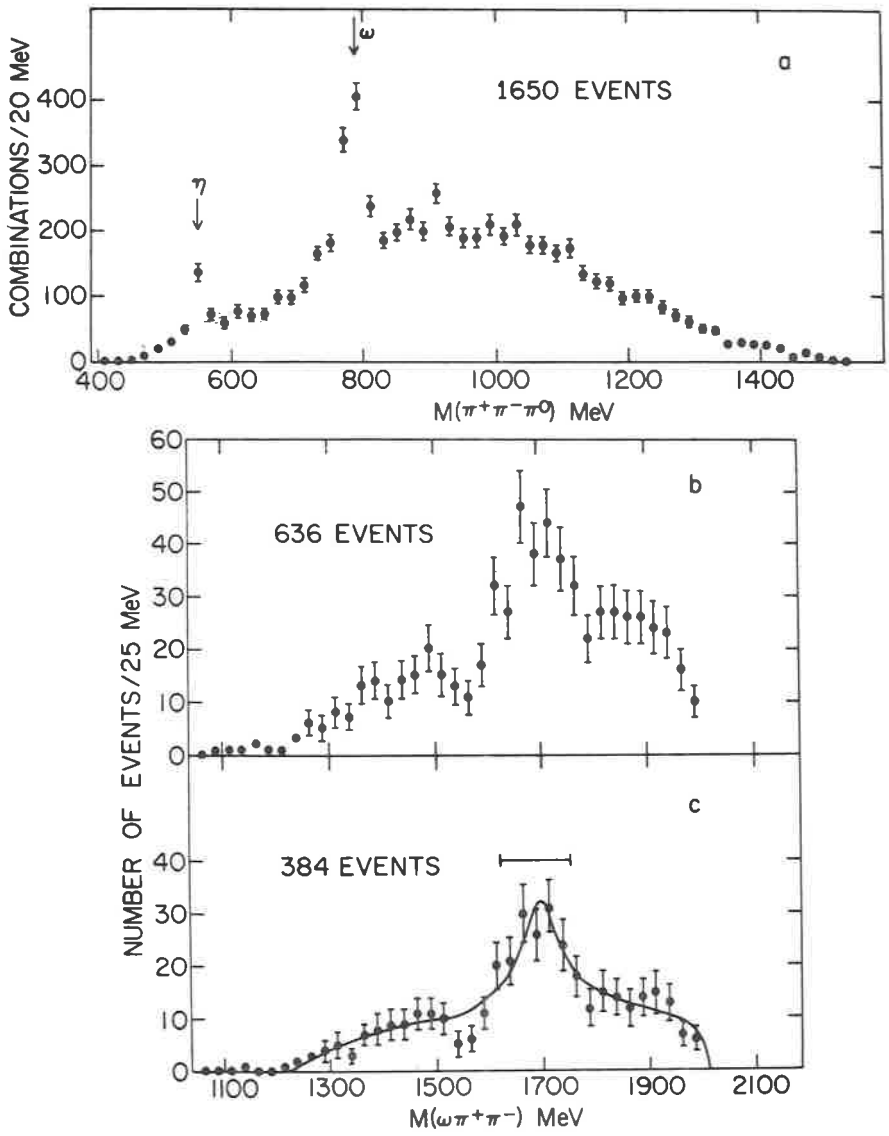

Fig. 15. – Shows the evidence: $M = (1695 \pm 20)$ MeV; $\Gamma = (90 \pm 20)$. Say they see $\omega^0\rho^0$ no $\omega^0\pi^0\pi^0$ ($I^G = 1^-$). Notice that b) is $\omega^0\pi^+\pi^-$ and c) has no y* (1385).

Question. Alternative decay mode of $f^0\pi^-$? They don't see anything in $K^-p \to \Lambda^0\pi^+\pi^-\pi^0$. However, may have K*K mode.

10. Conclusion.

None except:

a) Much more work and orders of magnitudes in statistics needed to understand what is going on.

b) Can't help being struck by the feature that each reaction produces its own characteristic scattering process,

e.g. $f^0\pi^-$, $\rho^0\pi^0$, $\omega^0\rho^0$.

c) Few states have as yet another well established decay mode,

e.g. why no $\rho^0\pi^-$ only $f^0\pi^-$?

why no $f^0\pi^0$ only $\rho^0\pi^0$?

Problems of the L-meson (*)

I. S. HUGHES
University of Glasgow - Glasgow

1. Mass and width.

All experiments at sufficiently high energy which can observe the L meson as a combination of a kaon and two or more pions find a bump at about 1760 MeV/c^2. Table I shows the masses and widths for the published data. In view of the uncertainties involved in fitting the L meson peak, the background and the Q meson tail the agreement in mass between the various experiments is satisfactory. This is also true for Γ except for the (very good statistics) Berkeley experiment which finds a very wide ($\sim$ 200 MeV) bump.

We may also however note that in the 10 GeV/c K^+ experiment ([10]) (Fig. 1) the L bump is not symmetrical showing a spike at the upper side of the bump. We also note weak evidence from this experiment that the various decay modes of the L may differ in M and Γ. These features suggest the possibility that the L may be a complex structure the components of which may have cross-sections with differing dependence on the incident momentum. Such a speculation will only be tested by experiments with much better statistics than the best of those currently available.

2. Decay modes to $K\pi\pi$. Threshold effect or resonance?

There exist apparent differences in the results of various experiments concerning the decay modes of the L. In particular the Berkeley group ([6]) present data which they interpret in terms of a threshold effect due to the K*(1420) plus a pion. We first examine the $K\pi\pi$ final state. Several variations are possible in methods of determining the proportion of different $K\pi$ and $\pi\pi$ resonances in the L bump:

We may make a series of Dalitz plots for slices of $K\pi\pi$ and then fit the plots with various degrees of sophistication. The simplest possibility

(*) Introductory talk

TABLE 1. – *Masses and widths of the* L *meson.*

Experiment	M (MeV/c^2)	Γ (MeV/c^2)
BARTSCH *et al.* 10 GeV/c K^-p(1966) ([1,9]) $K^-p \to (K^-\pi^+\pi^-)p$ (6068 events) $(K^0\pi^-\pi^0)p$ (576 events) $(K^-\pi^+\pi^-\pi^0)p$	1780 ± 15	138 ± 40
BERLINGHIERI *et al.* 12.7 GeV/c K^+p(1967) ([2]) $K^+p \to (K^+\pi^+\pi^-)p$ (395 events) $(K^0\pi^+\pi^0)p$ (359 events)	1780	80
BASSOMPIERRE *et al.* 5 GeV/c K^+p(1967) ([3]) $K^+p \to (K^+\pi^+\pi^-)p$ (6347 events) $(K^0\pi^+\pi^0)p$ (3075 events)	1760 ± 15	60 ± 20
DENEGRI *et al.* 12.6 GeV/c K^-d(1968) ([4]) $K^-d \to (K^-\pi^+\pi^-)d$ (240 events)	1600—1800	
ANDREWS *et al.* 12.6 GeV/c K^-p(1969) ([5]) $K^-p \to (K^-\pi^+\pi^-)p$ (1300 events)	1760 (my estimates)	80
BARBARO-GALTIERI *et al.* 12 GeV/c K^+p(1969) ([6]) $K^+p \to (K^+\pi^+\pi^-)p$ (14310 events) $(K^+\pi^+\pi^-\pi^0)p$ (10288 events)	1780	wide
AGUILAR-BENITEZ *et al.*, 4.6 GeV/c K^-p(1970) ([7]) $K^-p \to (K^-\pi^+\pi^-)p$ (5415 events)	1745 ± 20 ($\cos\theta^* > 0.7$, reduces Q)	100 ± 50
COLLEY *et al.* 10 GeV/c K^+p (1971) ([10]) $K^+p \to (K^+\pi^+\pi^-)p$ (14265 events) $(K^0\pi^0\pi^+)p$ (4537 events) $(K^*(1420)\pi)p$ $(K^*(890)\pi\pi)p$ $(K^*(890)\varphi)p$ $(K^*\omega)p$	1761 ± 10 1736 ± 12 1750 ± 16 1782 ± 16 1788 ± 15	91 ± 12 94 ± 17 140 ± 17 59 ± 28 56 ± 37

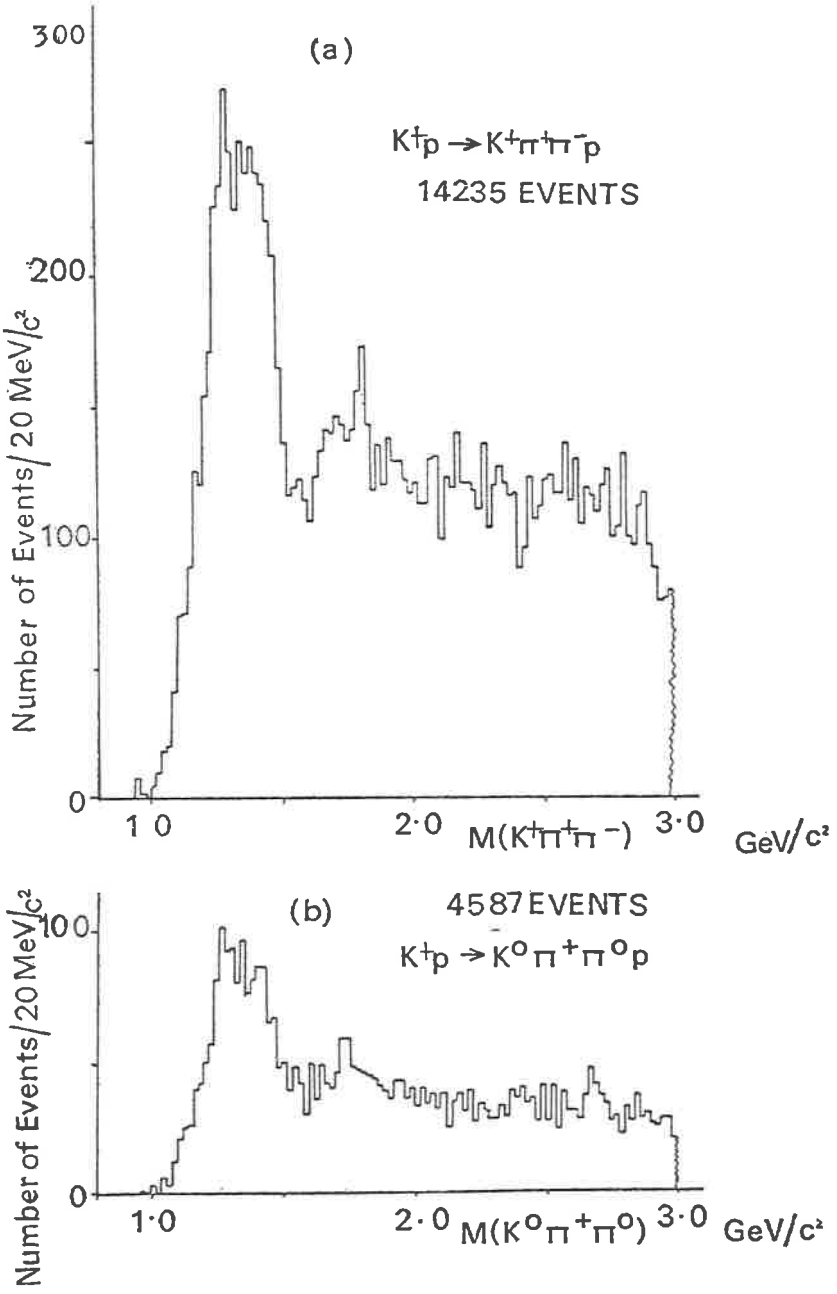
(a)
$K^+p \to K^+\pi^+\pi^-p$
14235 EVENTS
300
200
100
0
Number of Events/20 MeV/c²
1·0
2·0
3·0
M($K^+\pi^+\pi^-$)
GeV/c²
(b)
4587 EVENTS
$K^+p \to K^0\pi^+\pi^0p$
100
0
Number of Events/20 MeV/c²
1·0
2·0
3·0
M($K^0\pi^+\pi^0$)
GeV/c²

Fig. 1 *a, b.*

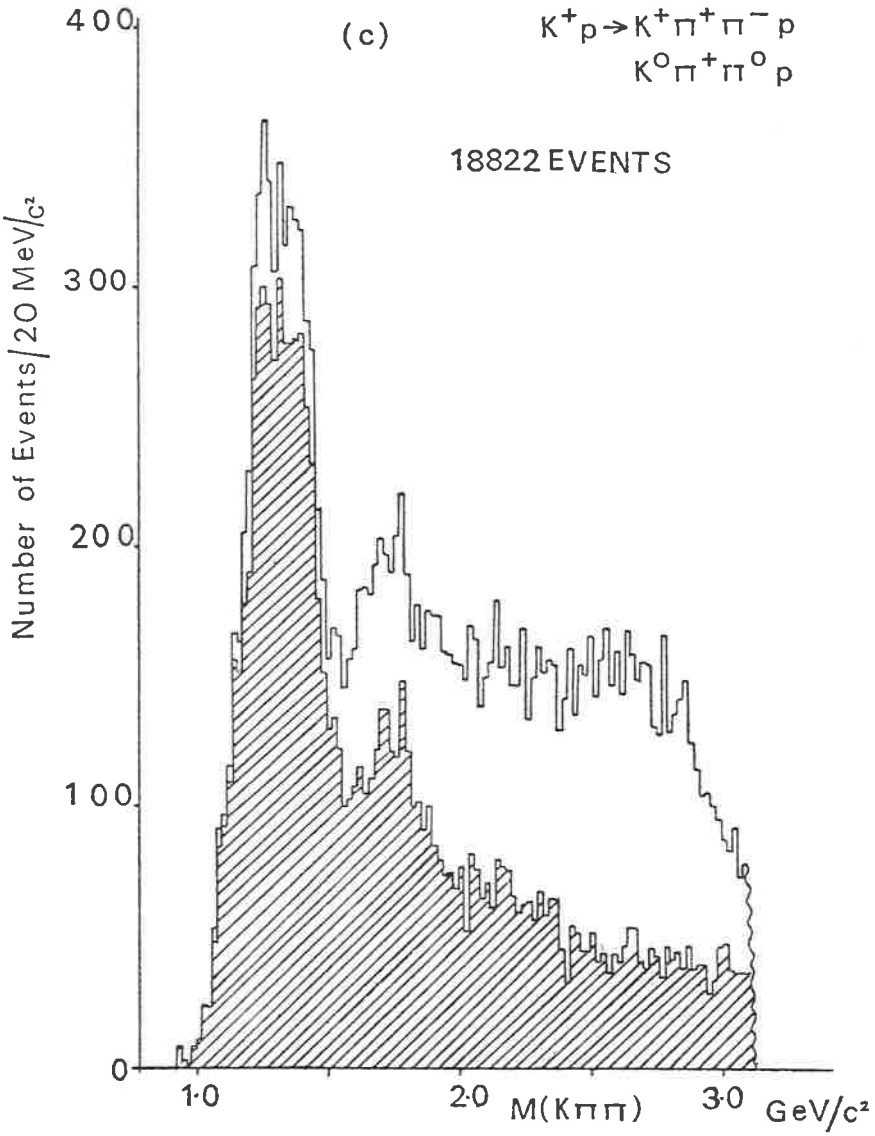

Fig. 1 *c*.

is to use uniformly populated Breit Wigner bands for say K*(890), K*(1420), Kρ, plus a uniform background. A higher degree of sophistication allows non uniform bands corresponding to different J^P and perhaps interference

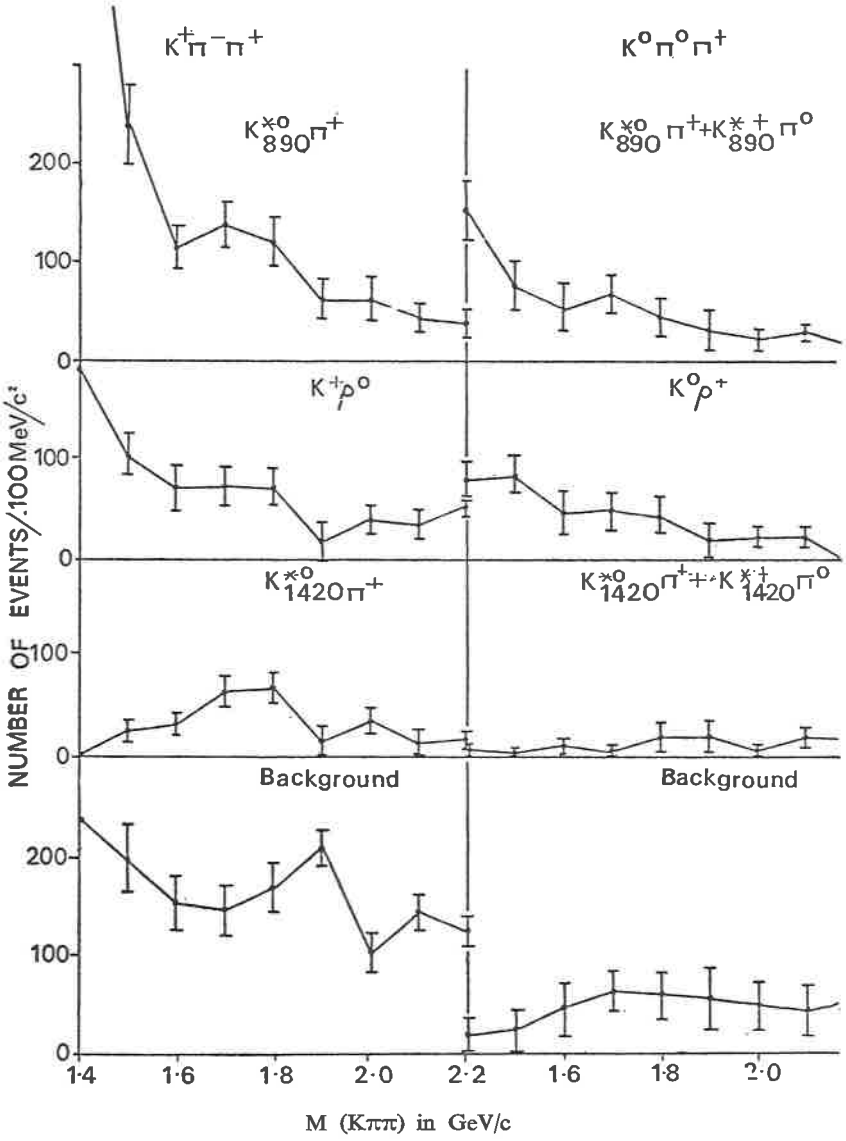

Fig. 2.

between crossing bands. An *increase* in the fraction of say K*(1420) in the L region indicates that the L *contains more* K*(1420) than the background. A smooth variation corresponds not to no K*(1420) in the L but to a propor-

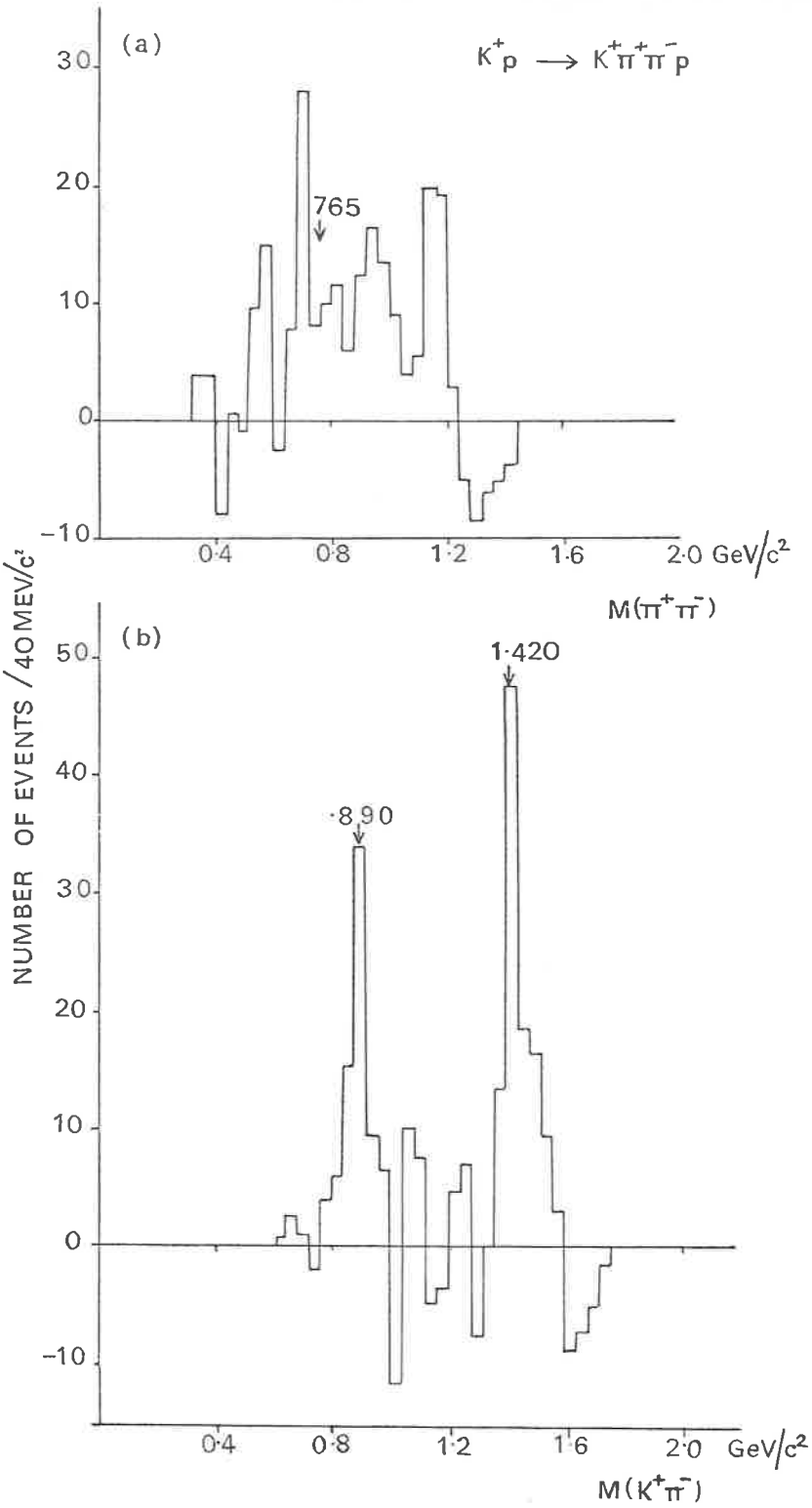
(a)
$K^+p \longrightarrow K^+\pi^+\pi^-p$
765
30
20
10
0
−10
0·4
0·8
1·2
1·6
2·0 GeV/c²
M(π⁺π⁻)
(b)
1·420
·890
50
40
30
20
10
0
−10
NUMBER OF EVENTS /40 MEV/c²
0·4
0·8
1·2
1·6
2·0 GeV/c²
M(K⁺π⁻)

Fig. 3.

tion equal to that in the background. *If the statistics are adequate* this type of analysis will provide the maximum information. Such analyses have been carried out by Bartsch *et al.* [1] (10 GeV/c K^-p), Ludlam, Sandweiss and Slaughter (12.6 GeV/c K^-) [5] and by Colley *et al.* (10 GeV/c K^+) [10]. The results for the 10 GeV/c K^+ experiment are shown in Fig. 2. In both the 10 GeV/c K^+ and K^- experiments there is clear evidence for the presence of the decay modes

$$L \to K^*(1420)\pi$$

$$K^*(890)\pi$$

and weak evidence for the modes

$$L \to K\rho$$

$$K\pi\pi$$

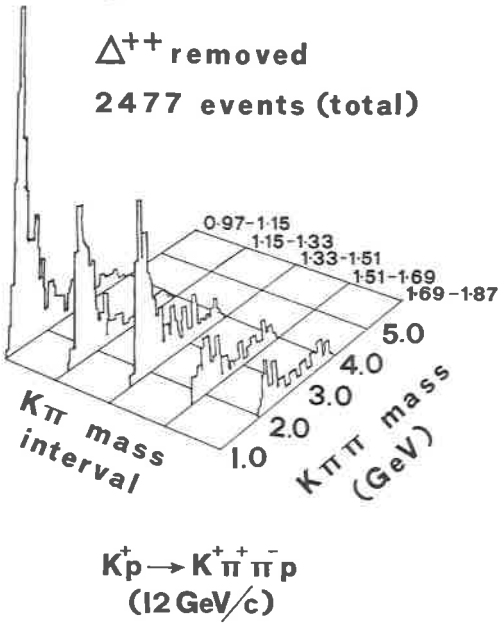

Fig. 4.

but in the (lower statistics) 12.6 GeV/c K^- experiment there is no sign of the decay $L \to K^*(890)\pi$ though the authors state that such a decay is not excluded by the data.

A less sophisticated technique, but one which may be more significant in the absence of statistics adequate to make the full Dalitz plot fit, is to make a one dimensional analysis, plotting the $K\pi$ mass spectrum for the L region minus the spectrum from bands adjacent to the L normalised to the background under the L. Such a plot is shown for the 10 GeV/c K^+ data ([10]) in Fig. 3. Again the evidence for $L \to K^*(890)\pi$ and $L \to K^*(1420)\pi$ is clear.

Another possibility is to select bands of $K\pi$ mass and then plot the spectrum of each band along with the other pion. This is the technique used in the 12 GeV/c K^+ analysis ([6]) and illustrated in Fig. 4. Figure 4 shows some threshold enhancement for each band of $M(K\pi)$ the threshold moving up as $M(K\pi)$ is increased. This has led Barbaro-Galtieri *et al.* to question the resonant nature of the enhancement. The data for 10 GeV/c K^+ show something of the same effect (Fig. 5) although here the threshold effect is only marked when the $K\pi$ actually falls into either the K*(890) or the K*(1420). On the other hand, at lower energy in a similar study of the events from the BNL K^-p experiment at 4.7 GeV/c ([7]) the threshold effect is completely absent (Fig. 6). Ludlam *et al.* ([5]) have pointed out that the constant small transverse momentum for $(K\pi\pi)$ which is characteristic of high energy processes leads to some degree of threshold enhancement at high energies though it is not adequate to account for the Q and L peaks. In the same way such a threshold enhancement is also accounted for by, for instance, the « double Regge » model. In the 12 GeV/c K^+ experiment with $K\pi$ selected to be in the K*(890) the authors state the L to be absent. However the L is so wide in this experiment that for even a moderately large branching fraction it is not clear that the L could be clearly distinguished from the background.

An alternative approach is to attempt a quantitative estimate of the number of K*(1420) events in the L to see whether the L signal could be entirely accounted for by these events. Aguilar-Benitez *et al.* ([7]) (4.6 GeV/c K^-p) obtain a branching ratio of $(20 \pm 20)\%$ for $L \to K^*(1420)\pi / K\pi\pi$. Bartsch *et* $\hookrightarrow K\pi$ *al.* (1970) ([9]) find 321 ± 60 events in the L peak but only 145 events in this region for which $M(K^-\pi^+)$ also lies in the K*(1420) $(1320 \div 1520)$ MeV/c². Equally when the K*(1420) region is antiselected the L peak remains with 166 ± 31 events. Similar results are obtained by Colley *et al.* (1971) ([10]) who find ~ 400 events in the L peak without the K*(1420) selection and

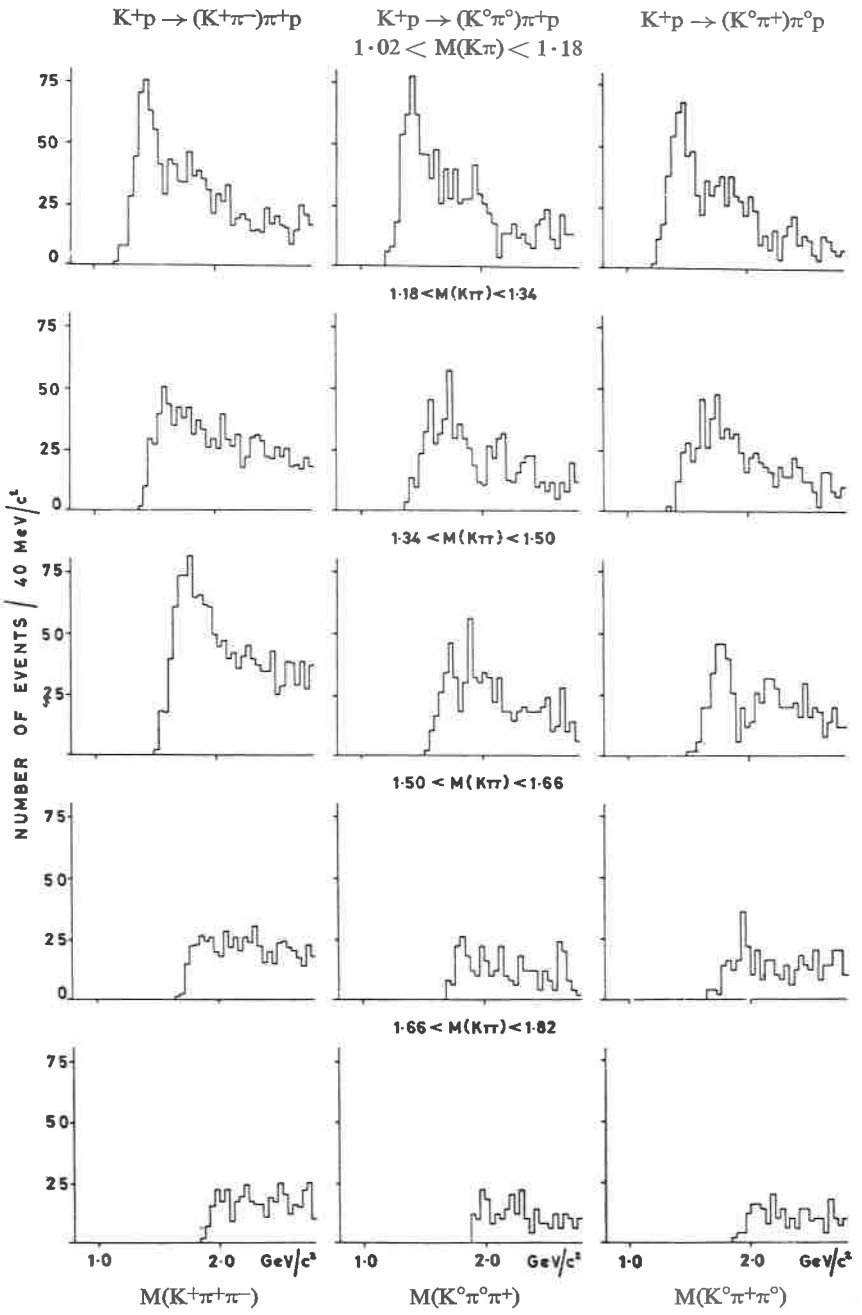
K+p → (K+π−)π+p
K+p → (K°π°)π+p
1·02 < M(Kπ) < 1·18
K+p → (K°π+)π°p
1·18<M(Kππ)<1·34
1·34 <M(Kππ)<1·50
1·50 < M(Kππ)<1·66
1·66 < M(Kππ)<1·82
NUMBER OF EVENTS / 40 MeV/c²
75
50
25
0
1·0
2·0
GeV/c²
M(K+π+π−)
M(K°π°π+)
M(K°π+π°)

Fig. 5

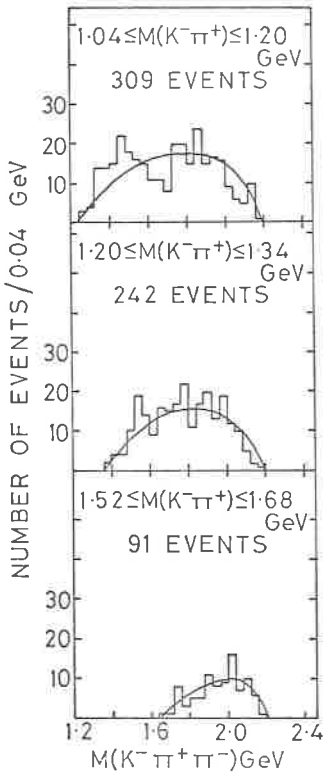

Fig. 6.

only ~ 230 with the selection. Although these numbers are in all cases approximate due to the difficulty of estimating the backgrounds, they nevertheless constitute strong evidence that the L as seen in the $(K\pi\pi)$ combination has decay modes other than $L \to K^*(1420)\pi$.

In fact, because the decay to $K\rho$ appears to be small, these « one dimensional » techniques are quite good ways to analyse the data.

We may summarise the situation for the decay $L \to K\pi\pi$ as follows:

a) There is substantial decay $L \to K^*(1420)\pi$ but this is *not* the only decay mode in $L \to K\pi\pi$.

b) Several experiments with good statistics see evidence for $L \to K^*(890)\pi$. Such a peak is far from threshold and its existence rules out the possibility that the L is « merely » a threshold phenomenon. However the 12 GeV/c K^+ data appear to be in disagreement with this conclusion.

c) $K\rho$—the evidence for the existence of this decay mode is weak.

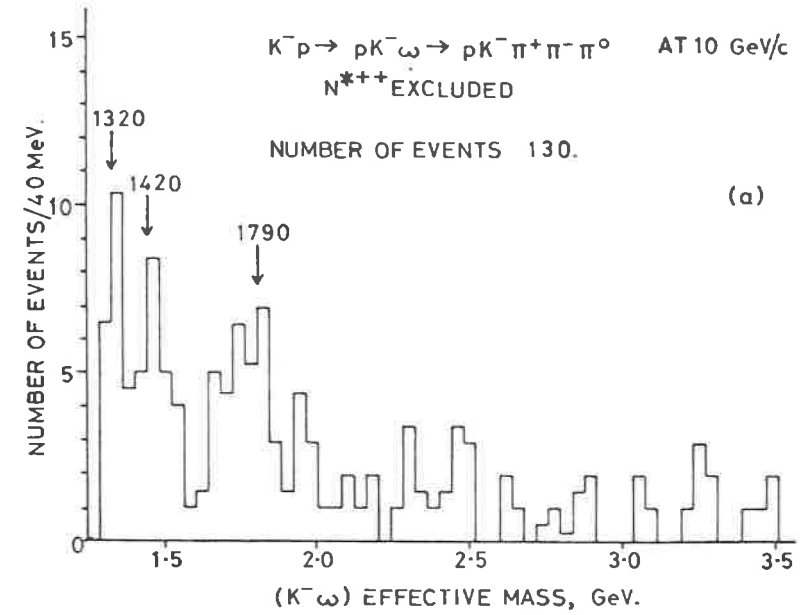
$K^-p \to pK^-\omega \to pK^-\pi^+\pi^-\pi^0$ AT 10 GeV/c
N^{*++} EXCLUDED
NUMBER OF EVENTS 130.
(a)
1320
1420
1790
NUMBER OF EVENTS/40 MeV.
15
10
5
0
1·5
2·0
2·5
3·0
3·5
$(K^-\omega)$ EFFECTIVE MASS, GeV.

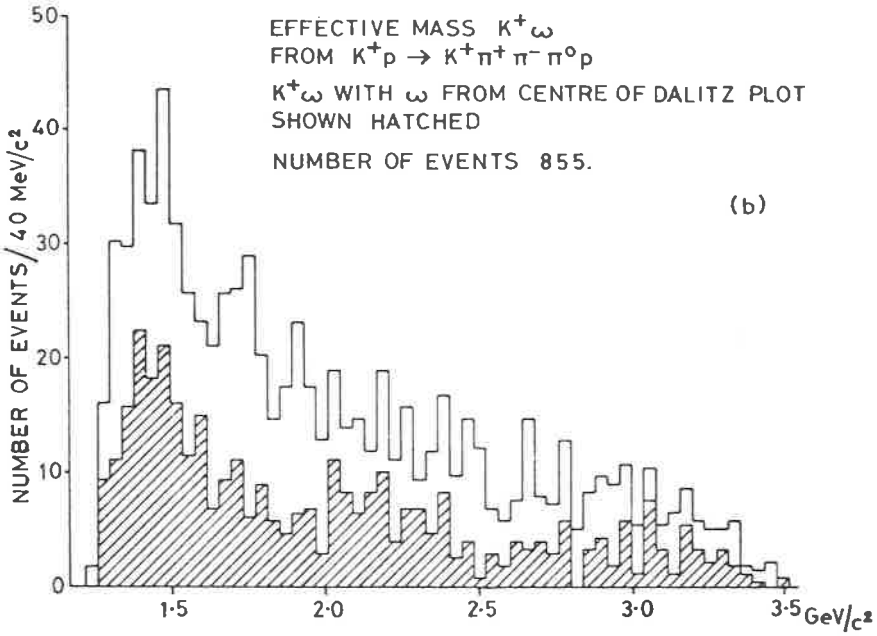
EFFECTIVE MASS $K^+\omega$
FROM $K^+p \to K^+\pi^+\pi^-\pi^0 p$
$K^+\omega$ WITH ω FROM CENTRE OF DALITZ PLOT SHOWN HATCHED
NUMBER OF EVENTS 855.
(b)
NUMBER OF EVENTS/40 MeV/c^2
50
40
30
20
10
0
1·5
2·0
2·5
3·0
3·5 GeV/c^2

Fig. 7.

3. Decay modes other than $L \to K\pi\pi$.

The 12 GeV/c K^+p ([6]), 10 GeV/c K^-p ([1]) and K^+p ([10]) experiments have studied modes of L decay other than $K\pi\pi$.

In the reaction

$$K^-p \to K^-p\omega \to K^-p\pi^+\pi^-\pi^0.$$

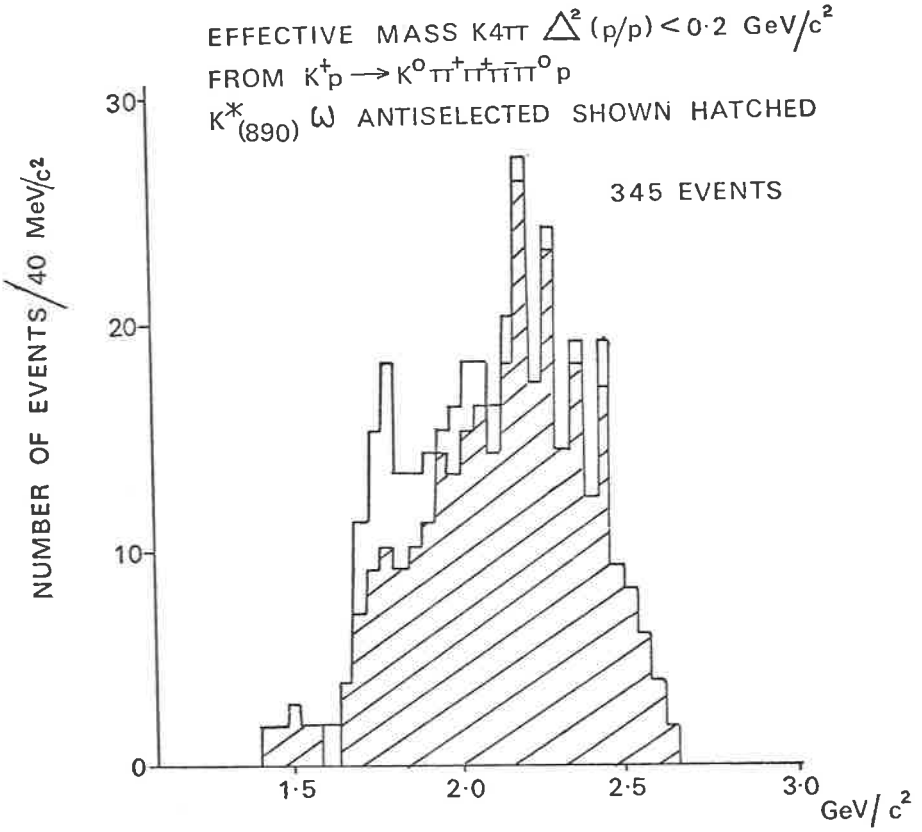

Fig. 8.

Bartsch *et al.* ([1]) claimed some evidence for the decay $L \to K\omega$. The existence of such a decay is important in that, if present, it establishes unambiguously that $I_L = \frac{1}{2}$. However the data for $L \to K\omega$ is to my mind statistically unconvincing. No evidence is found in the 12 GeV/c K^+p experiment or in the 10 GeV/c K^+p work (Fig. 7) for $L \to K\omega$. Other modes apparently

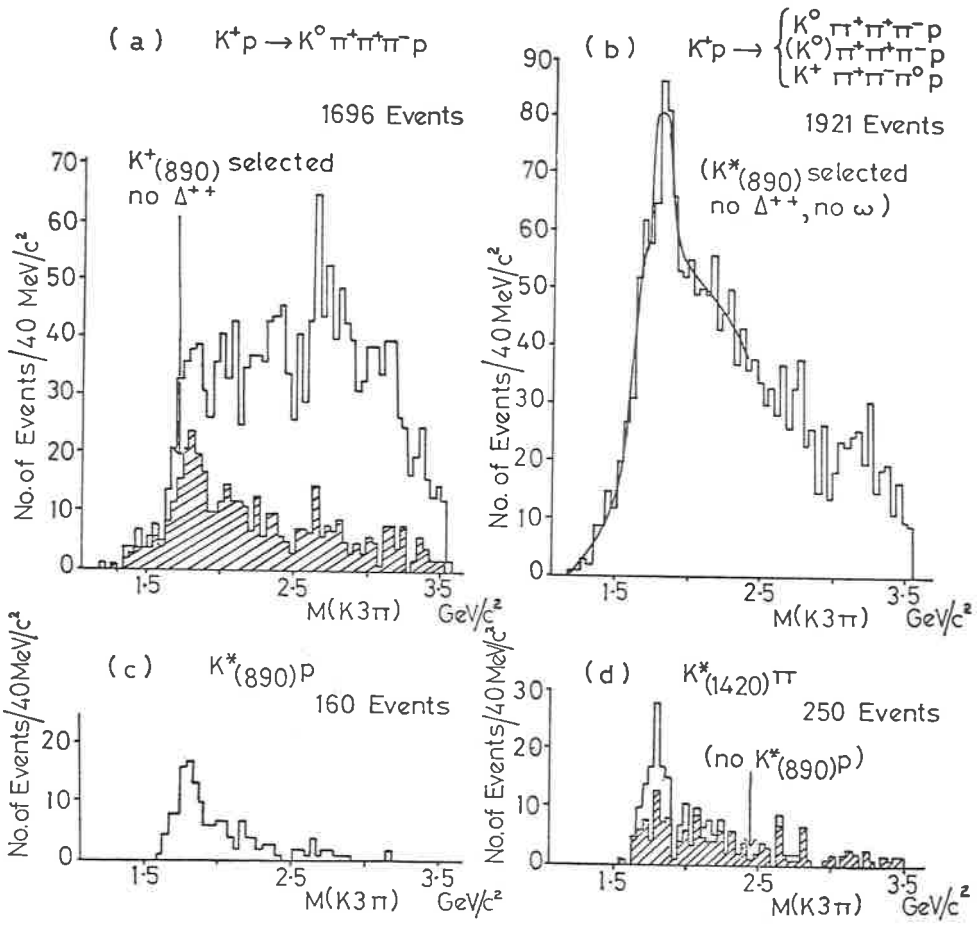

Fig. 9.

established in the 10 GeV/c K^+ experiment are

$$L \to K^*\rho \quad \text{(Fig. 8)}$$

$$K^*\omega \quad \text{(Fig. 9)}.$$

The decay $L \to K\pi$ is not seen in any experiment, nor is there any evidence for $L \to Kf$ or $K\eta$. There is no published evidence for the decay $L \to K\varphi$ but A. Pevsner informs me that the Johns Hopkins group has some weak evidence for this mode from their 12.6 GeV/c K^-d work.

4. I, J^P.

The clear L signal in the reaction $K^-d \to L^-d$ (Denegri *et al.*) [4] at 12.6 GeV/c establishes $I = \frac{1}{2}$ for the L meson. The decay ratios (*e.g.* $L^+ \to \to K^{*+}\pi^0/L^+ \to K^{*0}\pi^+$) in other experiments are consistent with this conclusion and in definite disagreement with $I = \frac{3}{2}$. The spin-parity determination is not quite so unambiguous. However the data all point to the same conclusion:

a) The absence of the decay $L \to K\pi$ suggests unnatural J^P.

b) The Dalitz plot analysis of Bartsch *et al.* [1] prefers 1^+, 2^-, 3^+ but at the available level of statistics the distinction between different J^P hypotheses is poor. The analysis of Colley *et al.* [10] tried 1^+, 2^-, 3^+ of which 1^+ gave the poorest likelihood but again the distinction is poor.

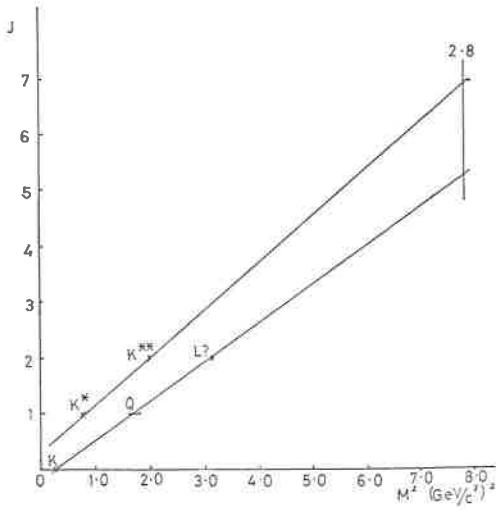

Fig. 10.

c) All experiments are consistent with formation of the L by Pomeron exchange (for instance no L is seen in $K^-p \to \overline{K}^0\pi^+\pi^-n$) requiring unnatural J^P and $m_L = 0$. The K^-d experiment of Denegri *et al.* [4] shows substantial alignment of the L as shown in the decay $L \to K^*(1420)\pi$ suggesting that the L consists of a 2^- S-wave $K^*(1420)\pi$. The other angular distributions

for the L decay are not fully explained in terms of such a model without invoking some interference from the background (or the K*(1660) ([3])), or some element of nonscalar exchange.

Thus all the evidence points towards $J^P = 2^-$ although 1^+ and 3^+ are not excluded. Such an assignment would allow the L to be placed on the K-Q trajectory (Fig. 10).

5. Summary.

The problems outstanding concerning the L are the following:

a) Conclusive establishment of the decay modes and branching fractions. (Application of some of the techniques discussed above might reveal whether the apparent discrepancy between the 12 GeV/c K^+p experiment ([6]) and other work is real and whether there is also a $K^*(890)\pi$ decay mode for the L in this experiment).

b) Establishment of J^P.

c) Data concerning production characteristics *i.e.* σ and $d\sigma/dt$ on which there is presently very little information.

For *a*) and *b*) we require very large statistics at a single high energy to enable a detailed Dalitz plot analysis. This problem may only be solved by an Omega type experiment or by a $Kd \to Ld$ study with high statistics since the background in this reaction is particularly low.

For *c*) we need detailed data at a series of energies but the problems of background subtraction are severe. Nevertheless our knowledge of the strange meson spectrum is as yet so embryonic that it seems important to establish the properties of the L, the only well established strange meson beyond the K*(1420).

REFERENCES

1) J. Bartsch, M. Deutschmann, E. Keppel, G. Kraus, R. Speth, C. Grote, J. Klugow, D. Pose, H. Schiller, H. Vogt, M. Bardanin-Otwinowska, V. T. Cocconi, P. F. Dalpiaz, E. Flaminio, J. D. Hansen, H. Hromadnik, G. Kellner, D. R. O. Morrison, S. Nowak, N. C. Barford, D. P. Dallman, S. J. Goldsack, M. E. Mermikides, N. C. Mukherjee, A. Fröhlich, G. Otter, I. Wacek and H. Wahl: *Nucl. Phys.*, B **8**, 9 (1968); *Phys. Lett.*, **22**, 357 (1966).

2) J. Berlinghieri, M. S. Farber, T. Ferbel, B. Forman, A. C. Melissinos, T. Yamanouchi and H. Yuta: *Phys. Rev. Lett.*, **18**, 1087 (1967).

3) G. Bassompierre, Y. Goldschmidt-Clermont, A. Grant, V. P. Henri, I. Hughes, B. Jongejans, R. L. Lander, D. Linglin, F. Muller, J. M. Perreau, I. Saitov, R. Sekulin, G. Wolf, W. De Baere, J. Debaisieux, P. Dufour, F. Grard, J. Heughebaert, L. Pape, P. Peeters, F. Verbeure and R. Windmolders: *Phys. Lett.*, **26** B, 49 (1967).

4) D. Denegri, A. Callahan, L. Ettlinger, D. Gillespie, G. Goodman, G. Luste, R. Mercer, E. Moses, A. Pevsner and R. Zdanis: *Phys. Rev. Lett.*, **20**, 1194 (1968).

5) J. Andrews, J. Lach, T. Ludlam, J. Sandweiss, H. D. Taft and E. L. Berger: *Phys. Rev. Lett.*, **22**, 731 (1969); T. Ludlam, J. Sandweiss and A. J. Slaughter: *Phys. Rev. D*, 2, 1234 (1970).

6) A. Barbaro-Galtieri, P. J. Davis, S. M. Flatte, J. H. Friedman, M. A. Garnjost, G. R. Lynch, M. J. Matison, M. S. Rabin, F. T. Solmitz, N. M. Uyeda, V. Waluch, R. Windmolders and J. J. Murray: *Phys. Rev. Lett.*, **22**, 1207 (1969).

7) M. Aguilar-Benitez, V. E. Barnes, D. Bassano, S. U. Chung, R. L. Eisner, E. Flaminio, J. B. Kinson, R. B. Palmer and N. P. Samios: *Phys. Rev. Lett.*, **25**, 54 (1970).

8) C. H. Chien: *Philadelphia Conference*, May 1970.

9) J. Bartsch, M. Deutschmann, G. Kraus, C. Grote, J. Klugow, W. D. Nowak, D. Pose, T. Besliu, V. T. Cocconi, P. Duinker, J. D. Hansen, G. Kellner, S. Matsumoto, D. R. O. Morrison, R. Stroynowski, J. B. Whittaker, N. C. Barford, P. J. Dornan, M. J. Losty, M. E. Mermikides, B. Buschbeck-Czapp, A. Fröhlich, M. Markytan, G. Otter and H. Wahl: *Phys. Lett.*, 33 B, 186 (1970),

10) D. C. Colley, M. Jobes, I. R. Kenyon, K. Pathak, P. M. Watkins, I. S. Hughes. J. W. P. McCormick, C. D. Procter, R. M. Turnbull and I. R. White: *Nucl. Phys.* B **26**, 71 (1971).

The R region in 13 GeV/c π^+ - nucleon interaction. (*)

D. H. MILLER, K. PALER, R. C. BADEWITZ, H. R. BARTON Jr.
T. R. PALFREY Jr., and J. TEBES
Purdue University - Lafayette, Ind.

The results to be presented in this talk come from two experiments at 13 GeV/c. These are an 8 event/μb π^+p experiment and a 10 event/μb π^+d experiment, both at 13 GeV/c, taken at SLAC in the 82 in. chamber. The new data comes from the π^+d experiment and it will be compared in part to the already published π^+p data ([1-3]). I wish to concentrate on the R region, that is the (1.6 $\rightarrow$ 1.8) GeV mass interval in the meson system. The complicated nature of this region and previous results have been discussed and reviewed by B. French ([4]) at this conference. This region contains an odd G parity resonance the « A_3 » and at least one even G parity resonance, the « g ».

We have observed the A_3 produced coherently in the reaction $\pi^+ d \rightarrow$ $\rightarrow d\pi^+\pi^+\pi^-$ at 13 GeV/c where we have used only events with a seen deuteron. Although it has been seen produced coherently before, this is the first time, to my knowledge, that it has been seen in the above reaction ([5]). This is because previous experiments at lower beam momenta have a larger t_{min} in the A_3 region causing the deuteron to break up. The data is shown in Fig. 1*a* where a clear 3π enhancement in the A_3 region is seen. The shaded histogram is obtained by selecting an f^0 in the 2π system ((1.16 $\rightarrow$ 1.32) GeV) and the dotted line is the shaded histogram subtracted from the overall data showing a smoothly varying background when the f^0 is subtracted. Figure 1*b* shows the mass of the 5π system from the reaction $\pi^+ d \rightarrow d\,5\pi$. No obvious structure is seen although it has a shape similar to the threshold enhancements seen in the 3π system. The 5π system is not produced significantly until a mass $\sim$1.5 GeV is reached and is equal to the 3π cross section above a mass $\sim$2.4 GeV. Figure 2*a* shows the $\pi^+\pi^-$ mass spectrum with two combinations/event which exhibits a clear f signal. The data are consistent with nearly

(*) Invited paper presented by D. H. Miller

100% ϱ and f production. We obtain a mass for the A_3 of $M = 1640 \pm 20$ and a $\Gamma \sim 200$ MeV with a slope $d\sigma/dt \simeq \exp[Bt]$ of $B = (30 \pm 2)$ (GeV/c)$^{-2}$. Our data on a preliminary analysis is consistent with a 100% fπ decays ([6]).

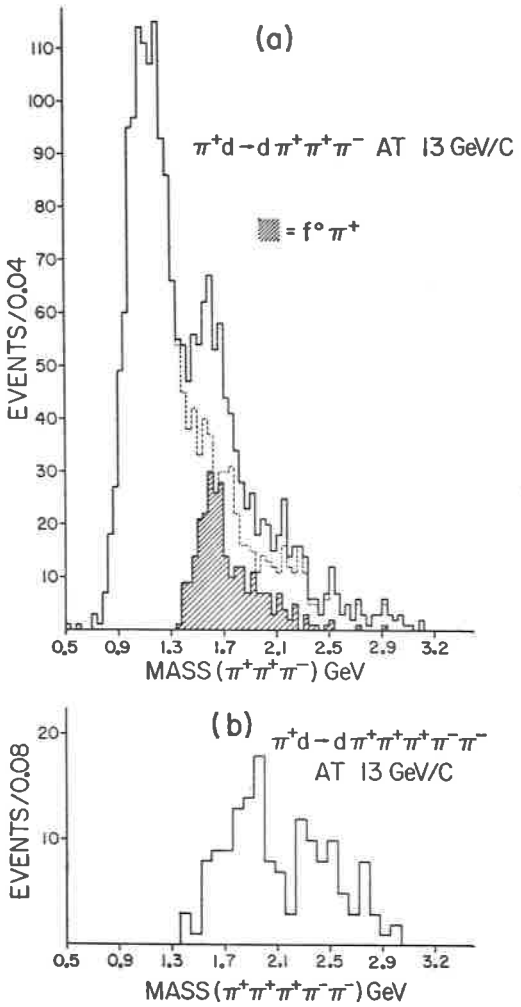

Fig. 1

Figure 2*b* shows the $\cos\theta$ of the angle between the beam and the normal to the 3π decay plane in the A_3 region ($1.48 < M3\pi < 1.72$), the solid line is a fit to pure 2^-, the dotted line to 1^+. We obtain probabilities for 1^+, 2^-, 3^+

of $< 0.01\%$, 85% and 75% respectively. The f^0 is produced with a ϱ_{00} of 0.74 ± 0.07 and is therefore strongly aligned.

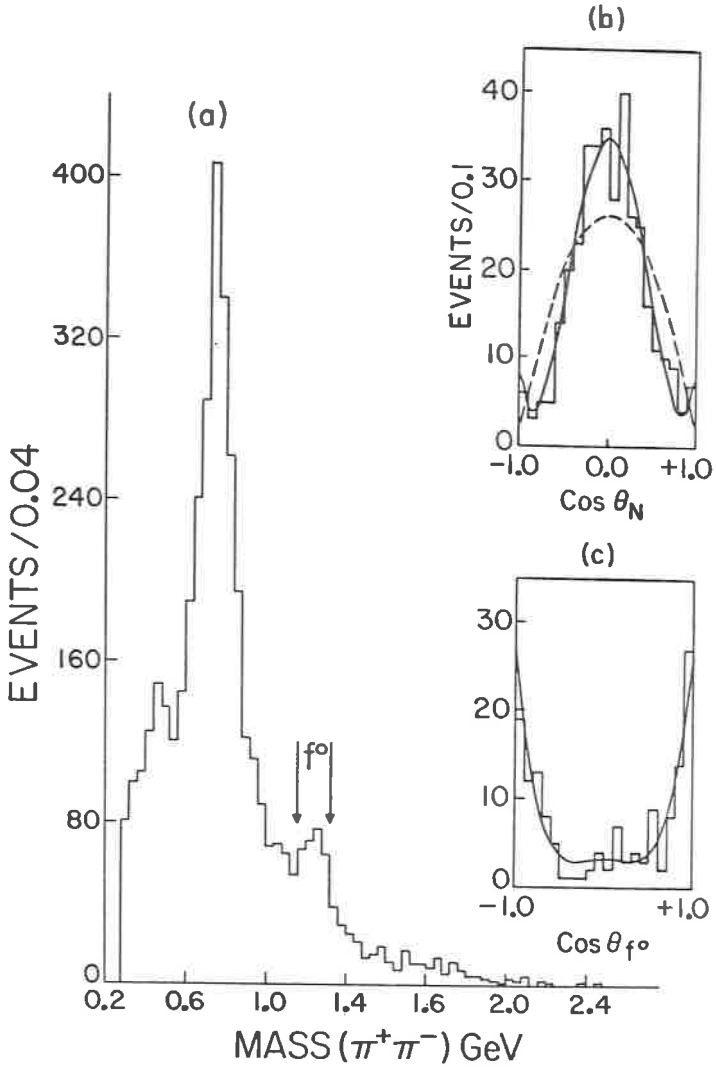

Fig. 2

I would now like to talk about the even G parity states in the R region. Figure 3*a* shows our π^+p data as shown in references 1 and 2. There is a very

strong signal in the R region of 360 ± 40 events above a smooth background and after subtraction of the $A_3 \to \pi^+\pi^0\pi^0$ (assuming the $f^0\pi$ decay is dominant);

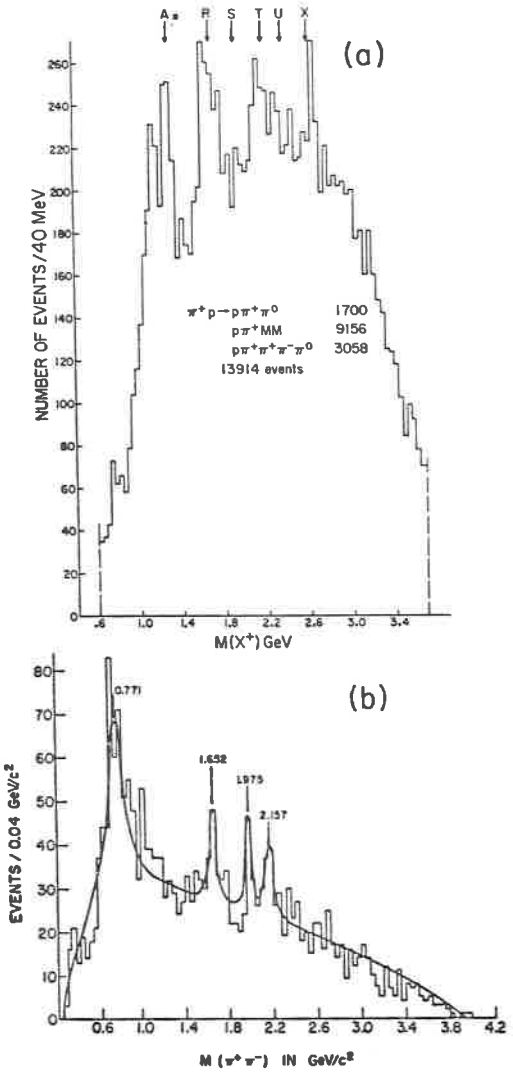

Fig. 3

there are 260 ± 50 events left due to even G parity decays into 2π and 4π. Most of this comes from the 4π state, since the 2π mass spectrum shown in

Fig. 3*b* exhibits a much narrower signal, which together with the very steep

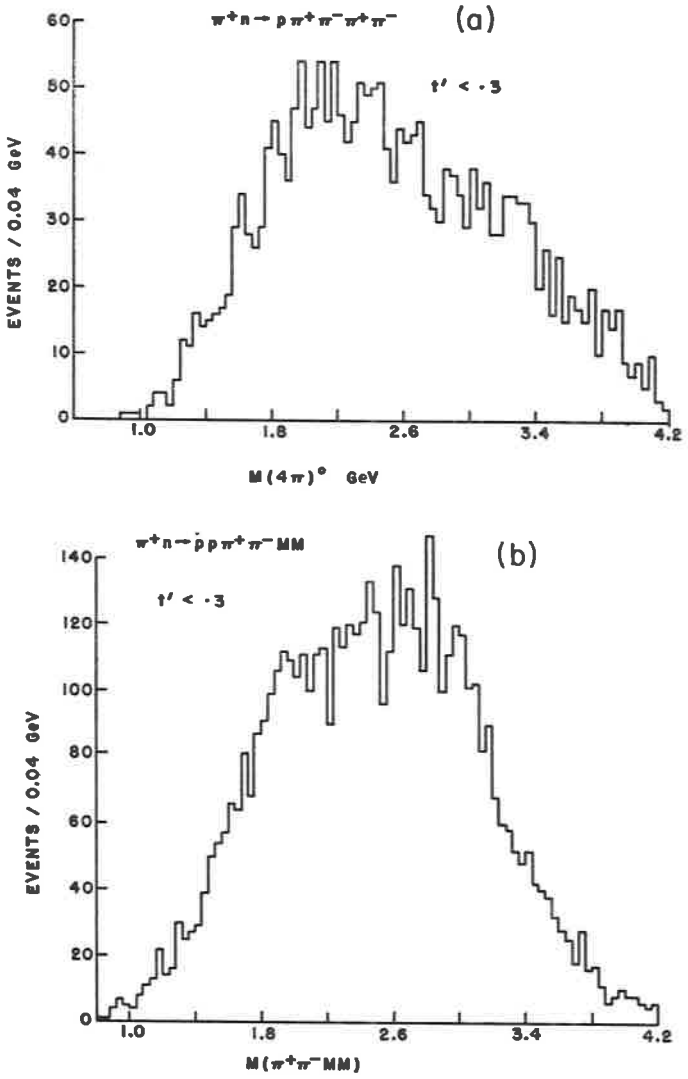

Fig. 4

sides on the enhancement in Fig. 3*a* indicates that probably more than one resonance exists in this region in agreement with the CBS results.

If the production of these states is dominated by one pion exchange (O.P.E.), then apart from some effects due to using deuterium the reaction

$$\pi^+ d \to pp X^0$$

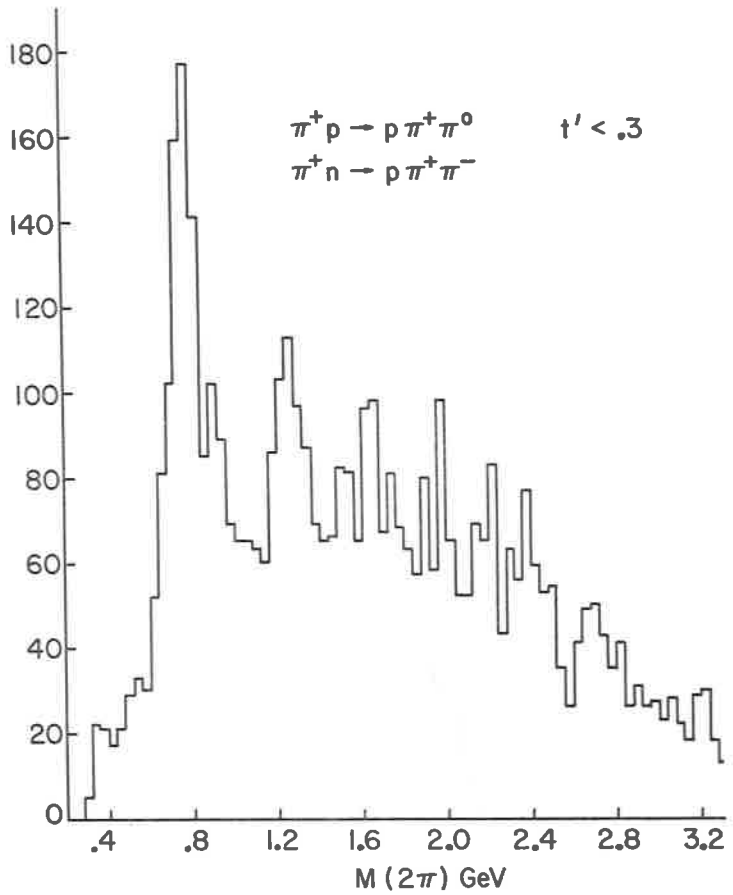

Fig. 5

where X^0 is an even G parity resonance should have twice the cross section of

$$\pi^+ p \to p X^+$$

at the same beam momenta. In fact in our $\pi^+ d$ film we have 10 events/μb compared to 8 events/μb in the $\pi^+ p$. This means we should expect by O.P.E.

a signal 2.5 times as large, *i.e.* (650 ± 126) events mainly in the $R^0 \to (4\pi)^0$ final state. I should note here that there are three possible $(4\pi)^0$ final states: $\pi^+\pi^-\pi^+\pi^-$, $\pi^+\pi^-\pi^0\pi^0$, $\pi^0\pi^0\pi^0\pi^0$. If the decay of the « R » proceeds through $\rho\rho$ or $\pi\omega^0$, as has been claimed by some authors, then no signal will be seen in the final state $\pi^+\pi^-\pi^+\pi^-$ but only in $\pi^+\pi^-\pi^0\pi^0$. Figure 4*a* shows the $\pi^+\pi^+\pi^-\pi^-$ mass spectrum and 4*b* the $\pi^+\pi^-$MM spectrum whera $MM > 2\pi^0$. No enhancement is seen in the region $1.6 \div 1.8$ in either plot. In fact, even the background is not large in this region. No enhancement is seen by taking a sub-selection demanding a ρ^0 or by selecting « ω » events in the $\pi^+\pi^-$MM final state by demanding that $M(\pi^+\pi^-) < M(\omega) - M(\pi)$. We have not analyzed the events which contain the $\pi^0\pi^0\pi^0\pi^0$ final state but it is not expected that there will be significant decays into this channel since the charge conjugation is incorrect for the observed 4π decays reported in this region.

No very significant signal is seen in $M(\pi^+\pi^-)$ from $\pi^+d \to pp\pi^+\pi^-$ in this region either, although a combined plot, Fig. 5, of $M(\pi\pi)$ from this reaction plus $\pi^+p \to p\pi^+\pi^0$ does show a narrow *g* with parameters the same as quoted in ref. (3).

The conclusions from this preliminary analysis indicate strongly that O.P.E. is not large in the *R* region and that $I = 0$ exchange, presumably ω, dominates in the π^+p data. In also appears that all of the 4π enhancement is not associated with the 2π enhancement. Both these results conflict with the assumptions of some authors ([7]) who did not, however, test them explicitly.

It is a pleasure to acknowledge the work and cooperation of the SLAC personnel and the help of members of the Purdue High Energy Physics Group.

REFERENCES

1) Published in the *Proceedings of the International Conference on Meson Spectroscopy*, Philadelphia (1970).
2) S. L. KRAMER, H. R. BARTON Jr., C. R. EZELL, J. A. GAIDOS, L. J. GUTAY, J. W. LAMSA, S. LICHTMAN, D. H. MILLER, T. MULERA, J. H. SCHARENGUIVEL and R. B. WILLMANN: *Particles and Nuclei*, **1**, 131 (1970).
3) S. L. KRAMER, H. R. BARTON Jr., L. J. GUTAY, S. LICHTMAN, D. H. MILLER and J. H. SCHARENGUIVEL: *Phys. Rev. Lett.*, **25**, 396 (1970).
4) *Review of intermediate mass meson states*, by B. R. FRENCH, given at this Conference.
5) *Review of coherent multiparticle production reactions from nuclei*, by H. H. BINGHAM: CERN preprint, D. Ph. II/Phys./70-60.
6) Our data appear to be very similar to that of CRENNEL *et al.*: *Phys. Rev. Lett.*, **24**, 781 (1970).
7) AACHEN-BERLIN-CERN COLLABORATION: *Nucl. Phys.*, B **22**, 109 (1970).

Evidence of neutral F_1 production in $\bar{p}p$ annihilations at (1.1 ÷ 1.2) GeV/c (*)

J. DUBOC, M. GOLDBERG, B. MAKOWSKI and A. M. TOUCHARD
Institut de Physique Nucleaire - Paris

R. A. DONALD, D. N. EDWARDS, J. GALLETLY and N. WEST
The University of Liverpool - Liverpool

The F_1 meson ($M = (1540 \pm 5)$ MeV/c^2, $\Gamma = (40 \pm 15)$ MeV/c^2, $G = 1$) has been observed in $\bar{p}p$ annihilations at 0.7 GeV/c by Aguilar-Benitez *et al.* [1], in the decay mode $F_1 \to K^*\bar{K}$ ($\bar{K}^*K$). In the reaction $\pi^+p \to p(K\bar{K}\pi)^+$ at 8 GeV/c, Aderholz *et al* [2] see a bump in the same spectrum centered at (1490 ± 20) MeV/c^2. Due to the errors they do not exclude that this bump could be the F_1: In this paper, we present a search for F_1 production in the $\bar{p}p$ annihilations with kaons at 1.1-1.2 GeV/c. An evidence of neutral F_1 is found in the final state:

$$\bar{p}p \to K_1^0 K^{\pm}\pi^{\mp}(MM) .$$

The present study is based on the analysis of a further 240000 pictures taken in the CERN-2 meter-Bubble-Chamber at 1.1 and 1.15 GeV/c, to which the events coming from a previous experiment [3] at 1.2 GeV/c (300000 pictures in the HBC-81 cm) have been added. All events with one or two visible K_s^0 were measured. Their numbers are 13000 and 6000 respectively. The total sample corresponds to 18 events per μb.

First, the four-body channels where the F_1 has been discovered by Aguilar-Benitez were examined:

$$\bar{p}p \to K_1^0 K^{\pm}\pi^{\mp}\pi^0 \qquad 5036 \text{ events} \qquad (1)$$

$$\bar{p}p \to K_1^0 K_1^0 \pi^+\pi^- \qquad 1252 \quad » \qquad (2)$$

$$\bar{p}p \to K_1^0(K^0)\pi^+\pi^- \qquad 3293 \quad » \qquad (3)$$

(*) Contributed paper submitted by B. Makowski

No significant peak is observed in the F_1 region in the $\bar{K}K\pi$ spectra. There is no change when a K* selection is done ($860 \leqslant M_{K\pi} \leqslant 930$ MeV/c^2). To enhance the effect, the same method as in the 0.7 GeV/c experiment, has been used, *i.e.* antiselection of $K^*\bar{K}^*$ added to the previous selection of the

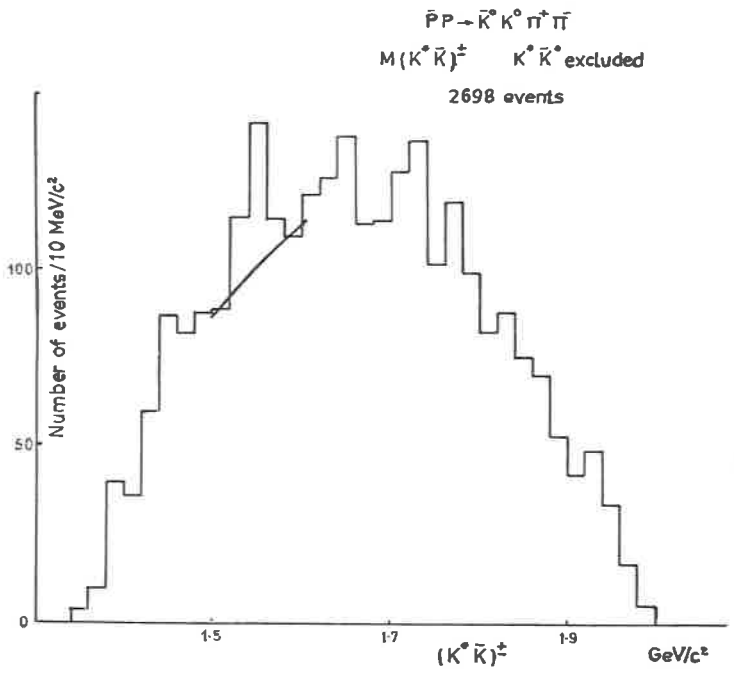

Fig. – 1. $\bar{p}p \to K^0\bar{K}^0\pi^0\pi^+\pi^-$. $(K^*\bar{K})^{\pm}$ effective mass spectrum for $K^*\bar{K}^*$ events excluded. K^*: $860 \leqslant M_{K\pi} \leqslant 930$ MeV/c^2.

K*. The result is shown in Fig. 1 for the reaction $\bar{p}p \to K^0\bar{K}^0\pi^+\pi^-$ (*i.e.* reaction (2) + reaction (3)), for which the clearest indication of the F_1 was found in ([1]). In the region of 1540 MeV/c^2 there is a small bump, the statistical significance of which is less than three standard deviations above our estimated smoothed background.

As a matter of comparison, for the reaction $\bar{p}p \to K_1^0 K_2^0 \pi^+ \pi^-$, a maximum likelihood fit gives the following results:

Channel	%
$K^{*\pm}K^0\pi^\mp$	39.2 ± 5.0
$K^{*\pm}K^{*\mp}$	27.1 ± 2.7
$\varrho^0 K_1^0 K_2^0$	1.6 ± 2.0
$\varphi\pi^+\pi^-$	7.3 ± 0.8
$F^\pm\pi^\mp$	3.0 ± 1.4

At 0.7 GeV/c [1] the last channel in the same reaction is $(14.4 \pm 2.7)\%$. This indicates a rapid decrease of the cross section with energy.

However, in reaction $\bar{p}p \to K_1^0 K^\pm \pi^\mp$ (MM) (819 events) there is a bump

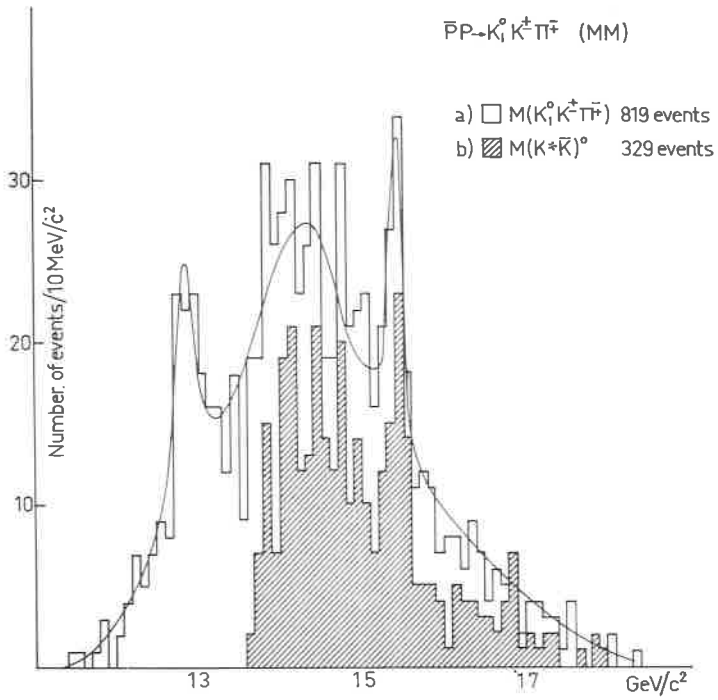

Fig. 2. – $\bar{p}p \to K_1^0 K^\pm \pi^\mp$ (MM): *a*) ($K_1^0 K^\pm \pi^\mp$) effective mass spectrum; *b*) $(K^*\bar{K})^0$ effective mass spectrum.

in the neutral $(K_1^0 K^{\pm}\pi^{\mp})$ mass spectrum enhanced in $(K^*\bar{K})^0$, as shown in Fig. 2. A Breit-Wigner formula was fitted to this distribution; the parameters obtained are:

$$M = (1543 \pm 3)\ \mathrm{MeV/c^2}\,,$$
$$\Gamma = (16 \pm 10)\ \mathrm{MeV/c^2}\ (*).$$

These are in good agreement with the values found by Aguilar-Benitez *et al.* It is then plausible to identify this peak as the neutral F_1: Comparisons of Fig. 2*a* and 2*b* shows that nearly 100% of the F_1 in this reaction decays via $K^*\bar{K}$ or $\bar{K}^*K$.

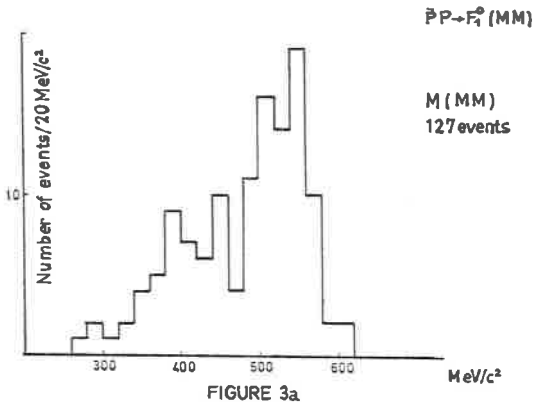

FIGURE 3a

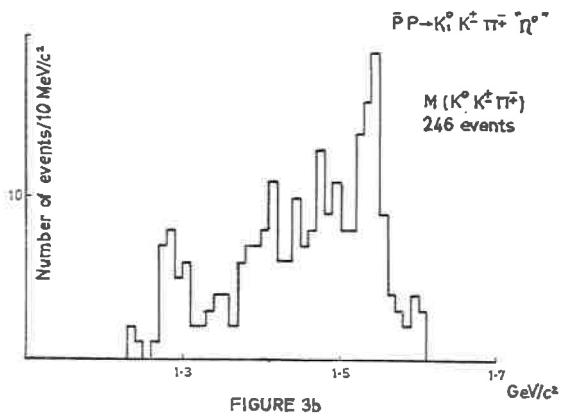

FIGURE 3b

Fig. 3. – $\bar{p}p \to K_1^0 K^{\pm}\pi^{\mp}$ (MM): *a*) (MM) missing mass spectrum opposite to F_1 $(1510 \leqslant M_{\bar{K}K\pi} \leqslant 1570)$ MeV/c²; *b*) $(K^0K^{\pm}\pi^{\mp})$ effective mass spectrum opposite to η^0 $(480 \leqslant M_{(MM)} \leqslant 580)$ MeV/c².

(*) The errors are such that the difference of the fitted widths in the two experiments is not significant.

Figure 3*a* shows the missing mass spectrum for the events having $1510\ \text{MeV/c}^2 \leqslant M(K\bar{K}\pi)^0 \leqslant 1570\ \text{MeV/c}^2$. There is an accumulation in the η^0 region. A selection on missing mass ($(480 \div 580)\ \text{MeV/c}^2$), Fig. 3*b*, enhances the F_1 signal. Hence most of the F_1 is produced via the two-body channel $\bar{p}p \to F_1\eta^0$.

Using the two-step decay of the F_1, an attempt has been made to determine its spin-parity. Events were selected according to the following conditions:

$$1510\ \text{MeV/c}^2 \leqslant M_{K\bar{K}\pi} \leqslant 1570\ \text{MeV/c}^2$$

and at least one ($K\pi$) combination between 850 and 920 MeV/c^2. This gives 76 events. 13 events give two ($K\pi$) combinations in this K* region. In this

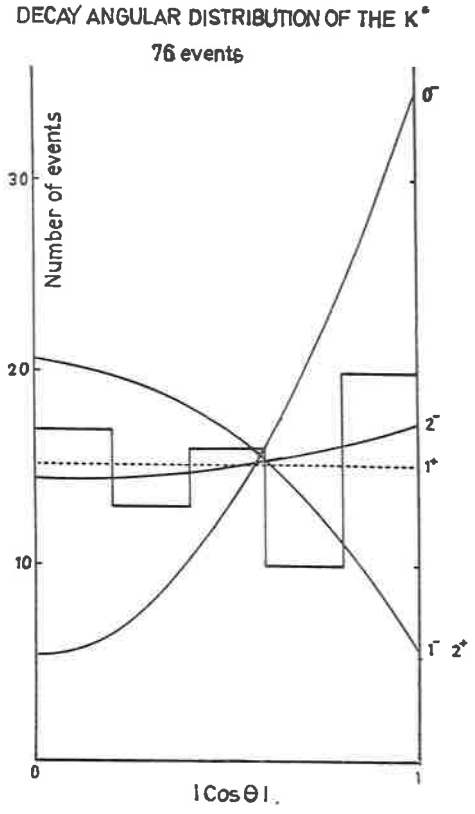

Fig. 4. – Decay angulard istribution of the K*, $1510 \leqslant M_{K\bar{K}\pi} \leqslant 1570\ \text{MeV/c}^2$, $850 \leqslant M_{K\pi} \leqslant$ $\leqslant 920\ \text{MeV/c}^2$.

case only one has been taken, that nearest to the K* mass (892 MeV/c^2).

Figure 4 shows the angular distribution of the K* decay; θ is the angle between the π in the K* center of mass system and the line of flight of the K* in the F_1 center-of-mass The predicted curves are calculated according to Table I taking into account a 35% flat background.

TABLE I (*).

$J^P_{F_1}$	0^-	1^-	1^+	2^-	2^+	
$W(\cos\theta)$	$\cos^2\theta$	$\sin^2\theta$	Constant	$3+\cos^2\theta$	$\sin^2\theta$	$\langle\chi^2\rangle = 4$
χ^2	36.1	18.7	3.9	3.4	18.7	

There is an agreement only for the 1^+ or 2^- hypotheses. Aguilar-Benitez *et al.*, in a similar way, exclude the normal series and give 1^+ and 2^- as favoured over 0^-. With the present study 0^- is now clearly excluded (see Table I).

An attempt to discriminate between these two hypotheses has been made, using the method proposed by Berman and Jacob ([4]), *i.e.* the calculation of R:

$$R = \frac{\langle 2\varrho'_{1-1}(\theta,\varphi)\sin^2\theta\rangle}{\langle[\varrho'_{11}(\theta,\varphi)+\varrho'_{1-1}(\theta,\varphi)](3\cos^2\theta-1)\rangle}$$

θ and φ being the polar and azimuthal angles of the K* with respect to the $\bar{p}$ direction in the F_1 center-of-mass, ϱ'_{ij} the density matrix elements of the K* in the helicity frame. R should be equal to $+2$ for $J^P = 1^+$ and -2 for $J^P = 2^-$ and, including 35% of background, respectively equal to $+1.3$ and -1.3.

The result is $R = -0.5 \pm 1.3$, which gives a probability of 17% for $J^P_{F_1} = 1^+$ and 54% for $J^P_{F_1} = 2^-$.

Since the F_1 is mostly produced in the two-body channel $\bar{p}p \to F_1^0\eta^0$, one has a means to obtain information about charge conjugation. The channel is produced near threshold with a low Q value ($Q < 40$ MeV), which corresponds to a wave-length greater than 1 fm. It is then reasonable to assume

(*) Because of the low Q value for the decay only the lowest value of the orbital angular momentum between the K* and the K_1^0 is considered.

that there is an *S*-wave in the final state. For the two remaining spin-parity assignments, Table II gives J^{PC} for the *S*-wave $F_1^0\eta^0$ states taking into account both possible values of the charge conjugation of the F_1.

TABLE II.

$J^{PC}_{F_1}$	1^{+-}	1^{++}	2^{--}	2^{-+}
$J^{PC}_{F_1{}^0\eta^0}$ (*S*-wave)	1^{--}	1^{-+}	2^{+-}	2^{++}
$\bar{p}p$ state	$^3S_1\,^3D_1$	does not exist	does not exist	$^3P_2\,^3F_2$

One sees that rather abundant production of the reaction $\bar{p}p \to F_1^0\eta^0$ near threshold is possible only for the two following assignments:

$$J^{PC}_{F_1} = 1^{+-} \text{ or } 2^{-+}.$$

If there exists a decay mode into pions, this would resolve the problem due to the fact that there is an opposite charge conjugation, and consequently an opposite *G*-parity in the two cases. (Since $I_{F_1} = 1$ one has $G = +1$ in the first case and $G = -1$ in the second one.)

In conclusion the reaction $\bar{p}p \to K^0\bar{K}^0\pi^+\pi^-$ at 1.1-1.2 GeV/c gives only slight evidence of $F^{\pm}\pi^{\mp}$ production. But the study of $\bar{p}p \to K_1^0K^{\pm}\pi^{\mp}$ (MM) shows a peak in the $(K_1^0K^{\pm}\pi^{\mp})$ mass spectrum, the mass, width, decay mode $(K^*\bar{K}, \bar{K}^*K)$ and decay angular distribution of which allows us to assume that it is the neutral component of the isovector F_1 found by Aguillar-Benitez *et al.*

The possible set of quantum numers is $J'^{G}_{F_1} = 1^{+-}, 2^{-+}$. A particle with the mass of the F_1 and $J^P = 2^-$, $I^G = 1^-$ would be expected as the second recurrence along the pion trajectory of slope $\alpha = 0.84$. A decay of the F_1 in an odd number of pions should be searched for.

REFERENCES

1) M. AGUILAR-BENITEZ, J. BARLOW, L. D. JACOBS, P. MALECKI, L. MONTANET, CH. d'ANDLAU, A. ASTIER, J. COHEN-GANOUNA, M. DELLA NEGRA and B. LORSTAD: *Nucl. Phys.*, B **14**, 195 (1969).

2) M. ADERHOLZ, J. BARTSCH, R. SCHULTE, R. SPETH, H. H. KAUFMANN, S. NOWAK, M. BARDADIN-OTWINOWSKA, V. T. COCCONI, J. D. HANSEN, J. LOSKIEWICZ, G. KELLNER, A. MIHUL, D. R. O. MORRISON, H. TOFTE, A. ESKREYS, K. JUSZCZAK, D. KISIELEWSKA, P. MALETI, W. ZIELINSKI, H. PIOTROWSKA and A. WROBLENSKI: *Nucl. Phys.*, B **11**, 259 (1969).

3) J. J. BARLOW, E. LILLESTOL, L. MONTANET, L. TALLONE, CH. D'ANDLAU, A. ASTIER, L. DOBRZYNSKI, S. WOJCICKI, A. M. ADAMSON, J. DUBOC, F. JAMES, M. GOLDBERG, R. A. DONALD, R. JAMES, J. LYS and T. NISAR: *Nuovo Cimento*, **50**, 701 (1967).

4) S. BERMAN and M. JACOB: Stanford Report SLAC-43 (1965).

SESSION II-C

Thursday, 15 April 1971

Non-strange mesons above $\bar{p}p$ threshold - Includes T, U, V, W, etc. mesons and studies of $\bar{p}p$ and $\bar{p}n$ interactions, cross-sections, polarization, and final states.

Chairman: I. BUTTERWORTH

Secretaries: F. L. NAVARRIA
F. HALZEN

Meson spectroscopy in the (2÷3) GeV mass region (*)

T. FIELDS
University of Birmingham - Birmingham
Argonne National Laboratory - Argonne

1. Introduction.

It is clear from the title of this session that there are many kinds of phenomena in which the heavier mesons might be observed. Furthermore, in the latest Particle Data Group (PDG) listing [1] which is being distributed at this meeting, there are some 20 candidates for nonstrange mesons in this mass range, so that the number of states as well as the diversity of experimental methods is large. In this 20 minute talk, I can only briefly review [2] some of the previous results on this complicated subject.

It should be emphasised at the outset that only one of the many possible states in this mass range is listed by the PDG as « established ». That is, only the U(2375) meets the PDG minimum criterion of having been observed with reasonably consistent properties in at least two experiments. So the first goal for experiments, that of establishing the existence of the suspected resonant states, is still very far from being reached. In this talk, I shall mention ways in which further progress toward that goal might hopefully be achieved. Until such time as the experimental situation is clarified, it seems premature to expect a pattern of states to become apparent.

An attractive possibility for mesons of mass > 2 nucleon masses is that of observing the meson in a formation reaction. Such a process, $\overline{N}N \to M$, with subsequent decay of the meson M into either $\overline{N}N$ or mesons, might be expected to lead to *s*-channel structure, *i.e.* rapid variation of cross-sections,

---

(*) Introductory talk
Work supported by the U. K. Science Research Council and the U. S. Atomic Energy Commission.

angular distributions, etc. with s. As we shall see, such s-channel effects seem to be small in many cases. Therefore, such experiments have so far been much less useful than for lower mass mesons, where formation experiments have been carried out using virtual targets (*eg.* $\pi\pi$ scattering) or with colliding e^+e^- beams.

From theoretical considerations, there is only general guidance as to what the properties of the meson states in this mass range might be. For example, it would be rather unexpected if the widths and spacing of the states were other than to correspond to a considerable overlapping of a typical state with some of its neighbours. Another example is the expectation from linear Regge trajectories that the maximum angular momenta of mesonic states in this mass range should be 5 to 10.

Given the lack of detailed theoretical expectations, the variety and difficulty of the experimental approaches, and the many unsettled questions concerning the meson mass spectrum *below* 2 GeV, it is not surprising that even the outline of a pattern has not yet emerged in this part of hadron spectroscopy. We shall, therefore, proceed by summarising typical experimental results which have been obtained in searches for mesonic states above 2 GeV, paying most attention to results whose quoted precision is reasonably definitive, while trying to determine which kinds of experiments offer the most promise of yielding definitive new results. In this survey, we must also try to allow for the natural bias against publishing results which show the *lack* of an effect at a given mass.

2. $\bar{\mathcal{N}}\mathcal{N}$ total cross-section.

To give a feeling for the difficulties which are involved in formation experiments, Fig. 1 shows the HERA compilation ([3]) of π^+p total cross-section results as well as the positions of the known Δ resonances. We see that the s-channel resonances are overlapping, and are not simply related to the bump structure. Most importantly, even with the large number of high precision π^+p experiments using electronic techniques, including studies with polarised targets, and after many sophisticated phase shift analyses, the spectrum of s-channel resonances beyond the region of large structure in σ_T is unknown.

As the results of Abrams *et al.* ([4]) show, Fig. 2, there is no large structure in $\sigma_T(\bar{\mathcal{N}}\mathcal{N})$, so one can certainly expect difficulties in identifying individual s-channel states. There is evidence for small broad peaks at 2190 MeV and 2350 MeV in $I = 1$, and at 2380 MeV in $I = 0$. These have widths of about

100 MeV, and have not been clearly correlated with effects seen in other kinds of experiments at similar masses.

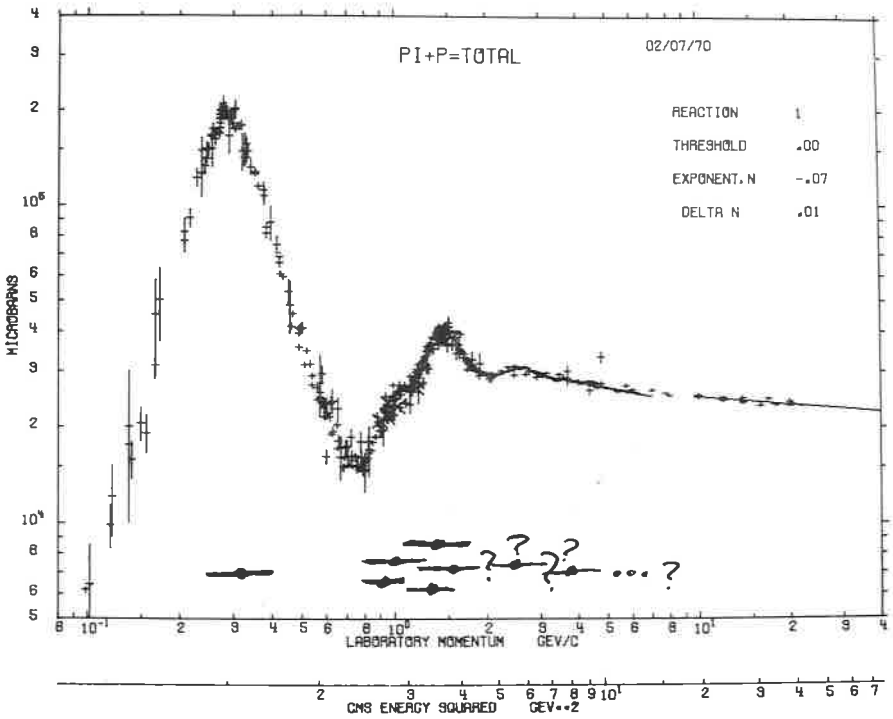

Fig. 1. – π^+p total cross-section. The positions and widths of the known Δ states are also shown.

An additional reason for expecting reduced s-channel effects in $\overline{\mathcal{N}}\mathcal{N}$ interactions is the angular momentum barrier situation compared to that for πp interactions. As shown in Fig. 3, meson resonances with $J \geqslant 5$ could be considerably decoupled from $\overline{\mathcal{N}}\mathcal{N}$ from this effect. Possibly the daughters of these states, having lower angular momentum, would not be so decoupled from $\overline{\mathcal{N}}\mathcal{N}$. On an even more speculative note, this same effect could be operative for meson daughter states even below threshold, making $\overline{\mathcal{N}}\mathcal{N}$ annihilation a likely process for observing the ε, ϱ', etc.

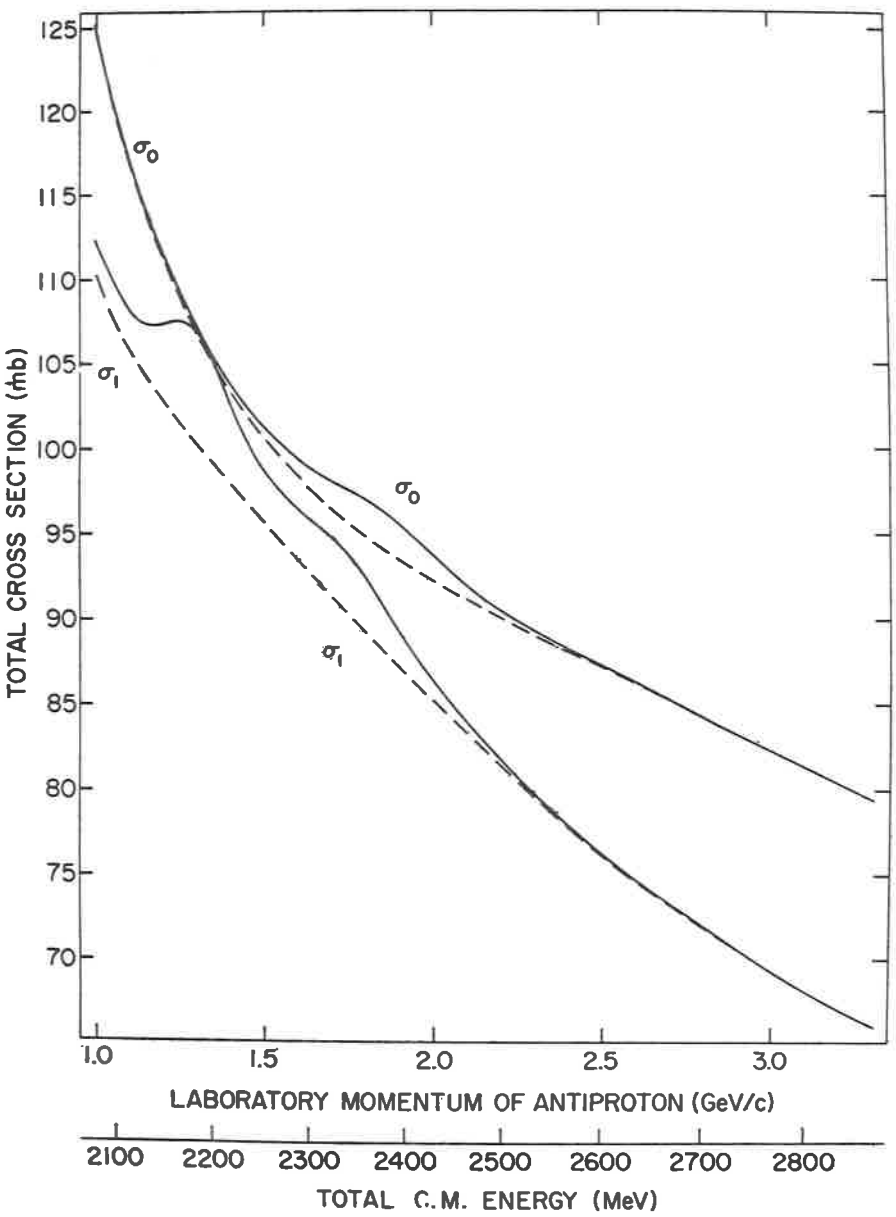

Fig. 2. – $\overline{\mathcal{N}}\mathcal{N}$ total cross-section in $I = 0$ and $I = 1$ states (ref. [4]).

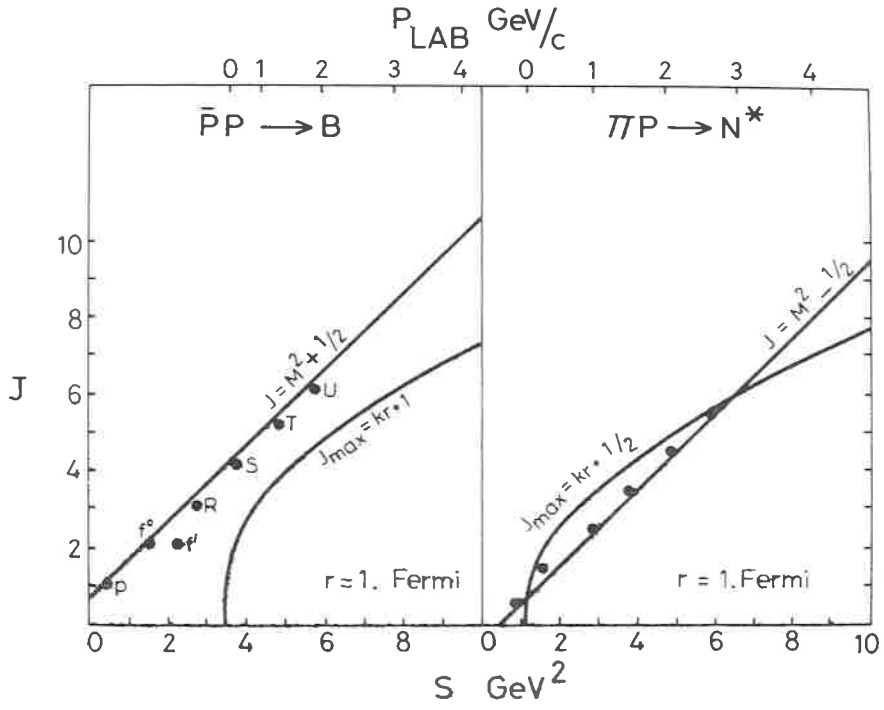

Fig. 3. – Centrifugal barriers and Regge trajectories (ref. (²)).

3. Missing mass experiments.

Figures 4 and 5 are to remind you of the MMS (⁵) and CBS (⁶) results. As shown in Fig. 4, information about the number of charged decay products can be obtained by using additional counters with a missing mass setup. Figure 5 shows a compilation of all the published CERN missing mass results. As remarked above, only the U(2375) peak is well enough confirmed to justify placing it on the wallet card. We will mention some of the other results on the U(2375) shortly. In view of the present controversies over the A_2 splitting, it is clear that further high precision missing mass experiments are needed.

A very different kind of missing mass experiment was performed by Anderson *et al.* (⁷). They looked at the reaction $\pi^- p \to pX^-$, *i.e.* backward production of mesonic states by pions. This should give information on the couplings of high mass meson states to a baryon vertex (as opposed to the coupling to mesons which is involved in the usual forward production by

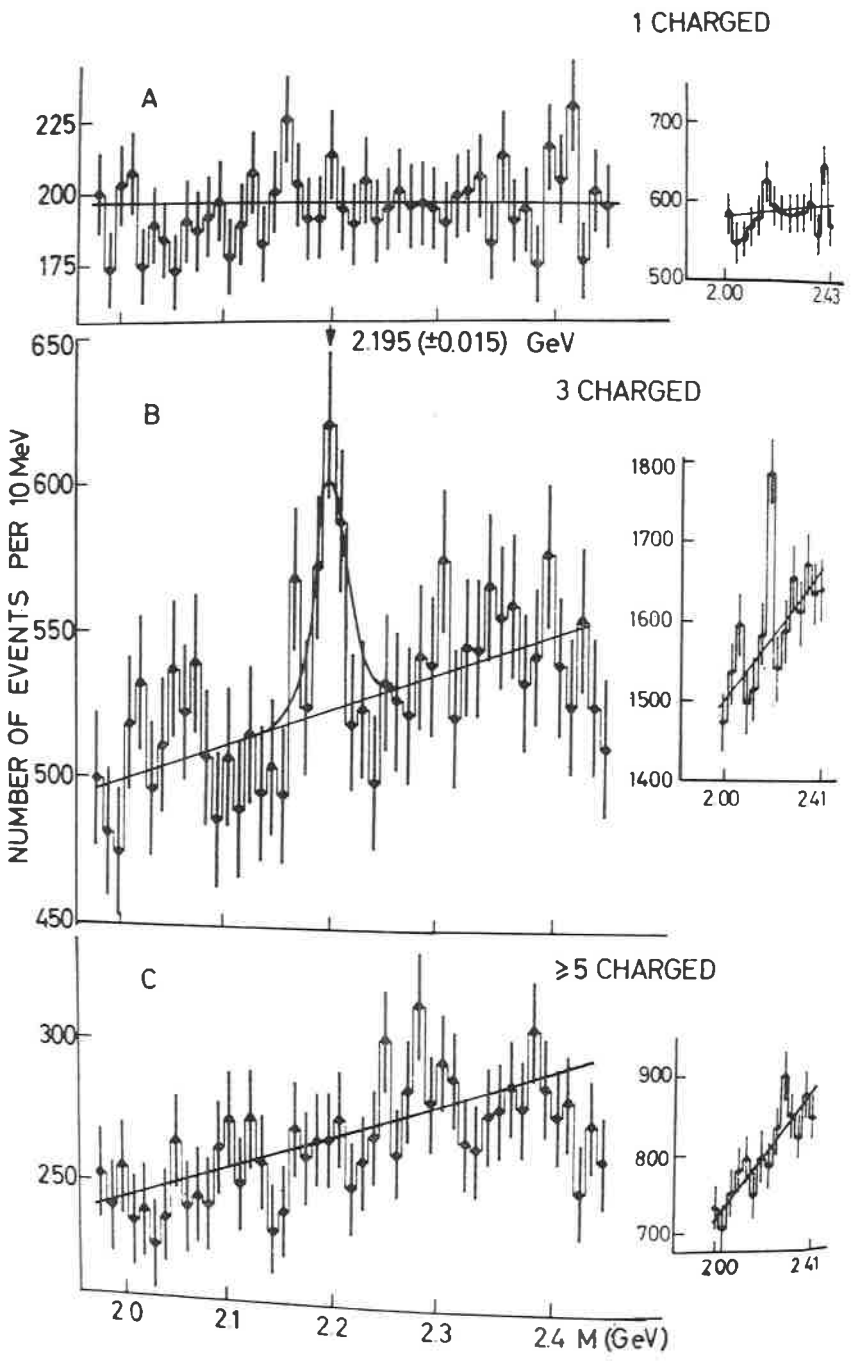

Fig. 4. – MMS result showing evidence for T(2195) decay to three charged particles (ref. [5])

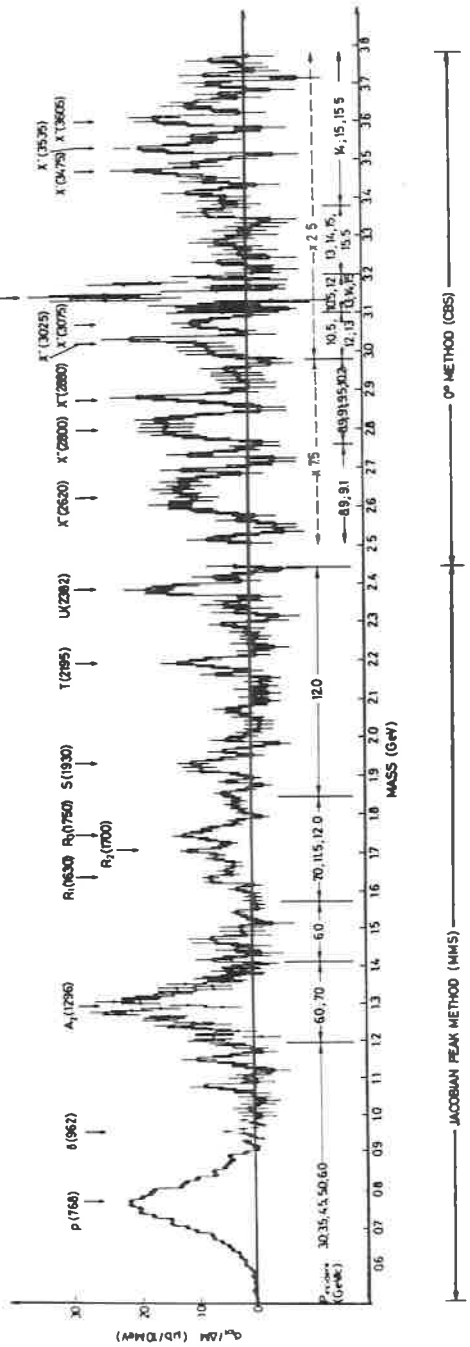

Fig. 5. – Composite spectrum from missing mass experiments.

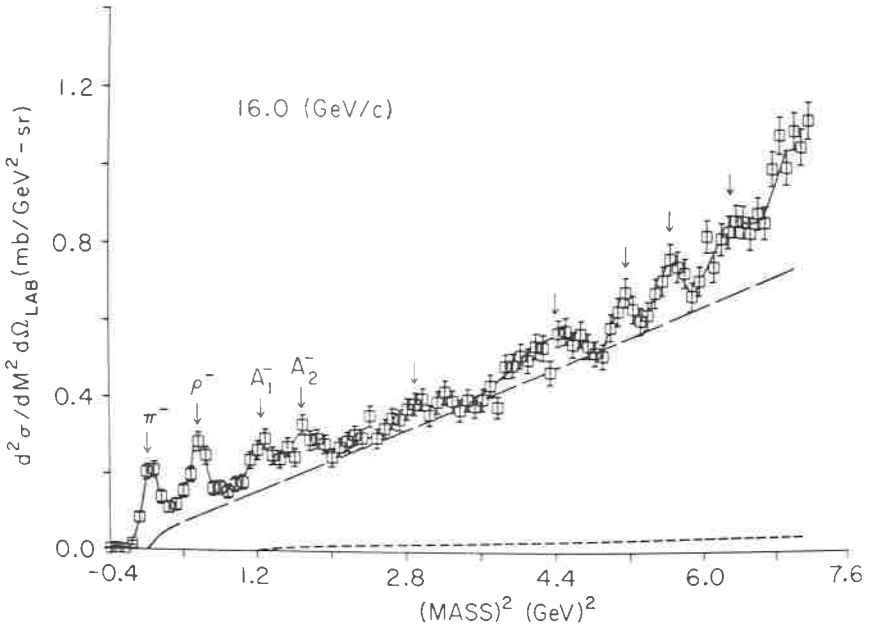

Fig. 6. – Mass spectrum from $\pi^- p \to pX^-$ at 16 GeV/c (ref (7)).

incident pions). Their results are shown in Fig. 6. One sees evidence for narrow states at 2260 MeV and 2360 MeV (the « U »?). There is also some evidence for the A_1^-. The statistical accuracy is not great enough to draw any firm conclusions, so that the graph can only be taken as tantalising.

4. Two-body annihilation.

Another important kind of data concerns the angular distribution for the processes $\bar{p}p \to \pi^+\pi^-$ and $\bar{p}p \to K^+K^-$. One might hope that the influence of *s*-channel resonances, perhaps interfering with some sort of background amplitude, would lead to a rapid *s*-dependence of the angular distribution. The results of Nicholson *et al.* (8), showing $d\sigma/d\omega$ folded about 90° cm, are given in Fig. 7. No dramatic *s*-dependence is apparent. The Legendre coefficients of the angular distributions are shown in Fig. 8. These coefficients exhibit broad maxima as function of *s*, with no evidence for *narrow* resonances. Whether the observed variations are due to broad resonances or diffraction effects cannot be resolved without better data and better models. But one should not forget that diffraction effects, which are a measure of $\overline{\mathcal{N}}\mathcal{N}$ cm momentum, will vary rapidly with *s* on account of the nearness to threshold for the $\overline{\mathcal{N}}\mathcal{N}$ system.

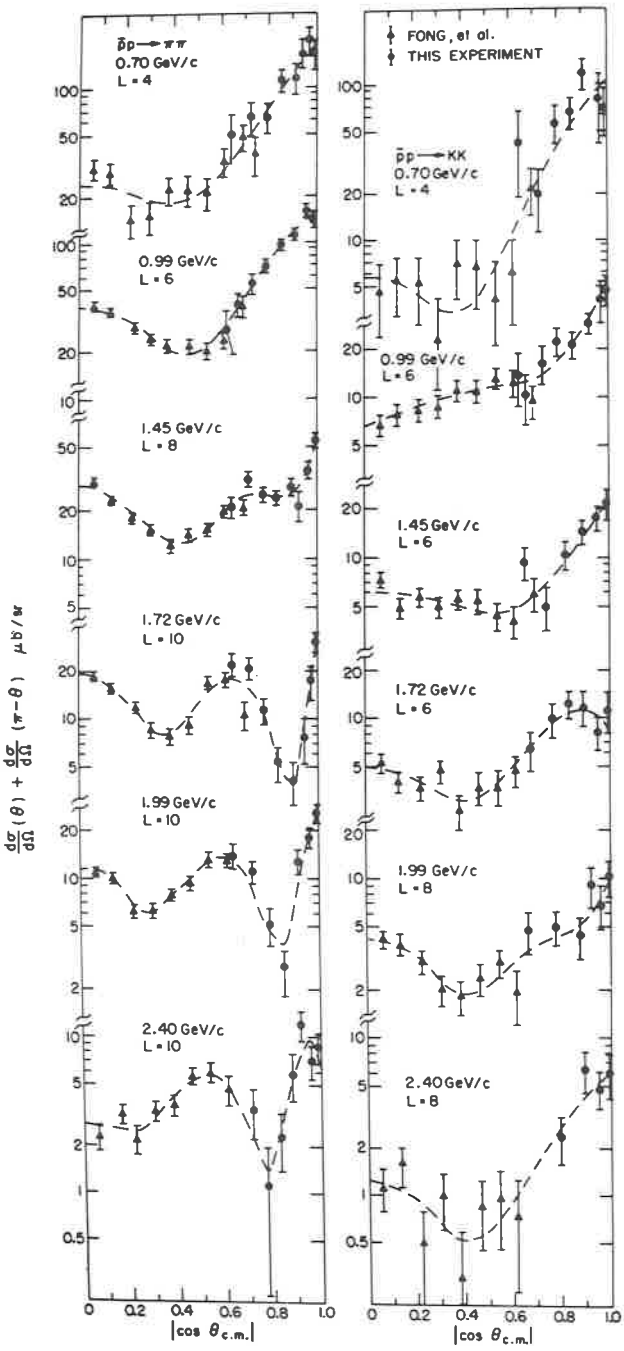

Fig 7 – Folded angular distributions for $\bar{p}p \to \pi\pi$ and $\bar{p}p \to \bar{K}K$ (ref (8)).

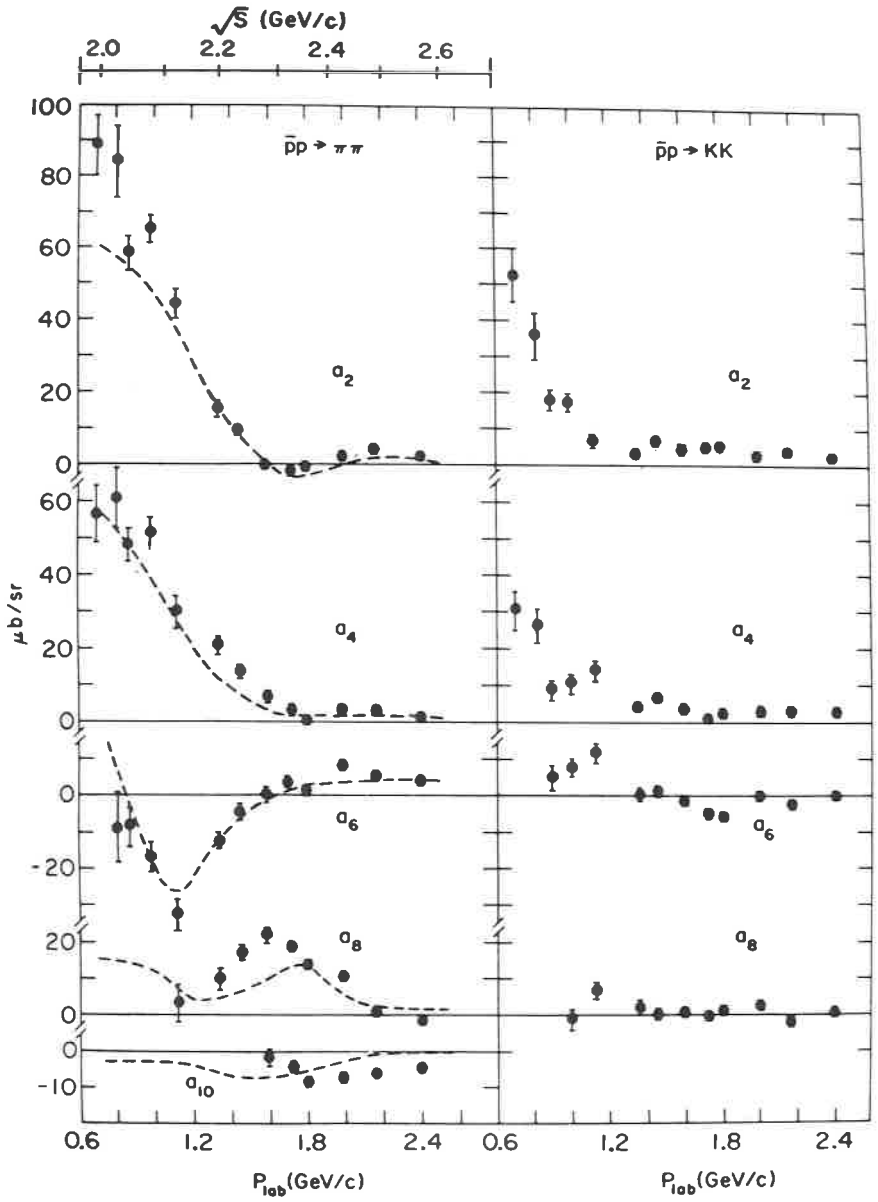

Fig 8 – Legendre coefficients for data of Fig 7

5. The U(2375).

As an aside, let me remark that the remainder of the data summarised in this talk is from bubble chamber experiments, and its statistical accuracy is

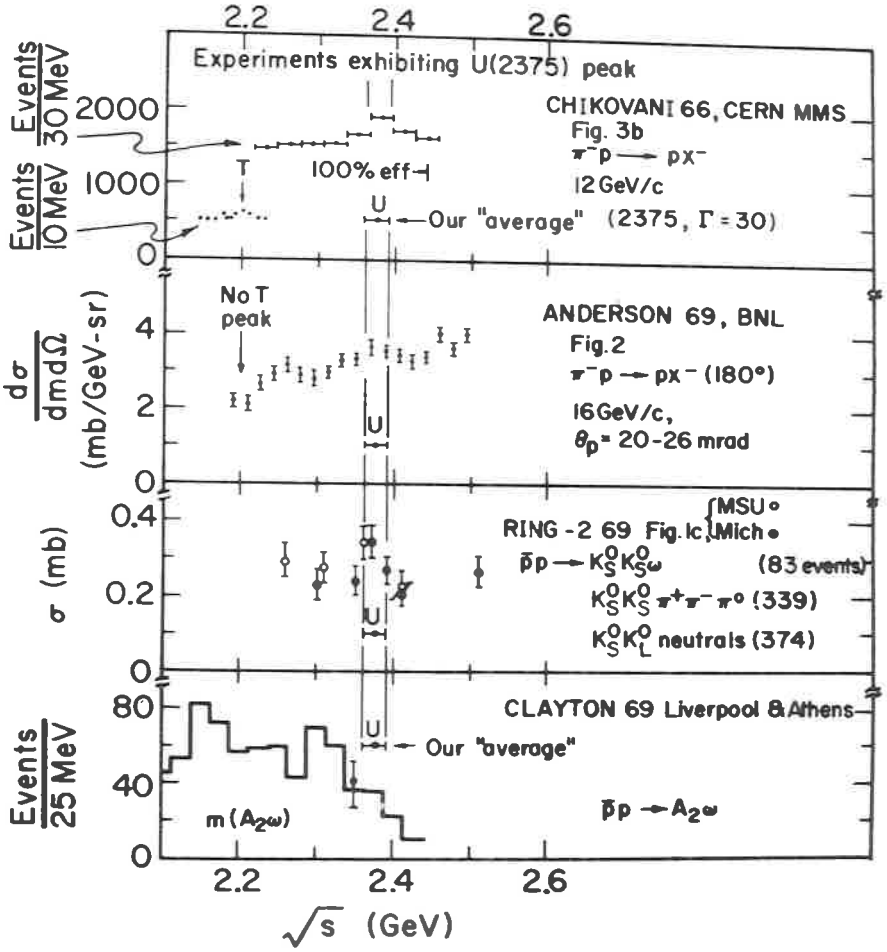

Fig 9 – PDG summary of evidence on U(2375).

generally inferior to that of the counter data discussed above. Also, bubble chamber experiments are more susceptible to the bias already mentioned, that many plots which did not show a peak are not yet in the public record.

Figure 9 is taken from the Review of Particle Properties ([9]) and summarises most of the evidence regarding the U(2375). Subsequent results ([10]) from

Michigan State, shown in Fig. 10 and 11, offer evidence for an *s*-channel

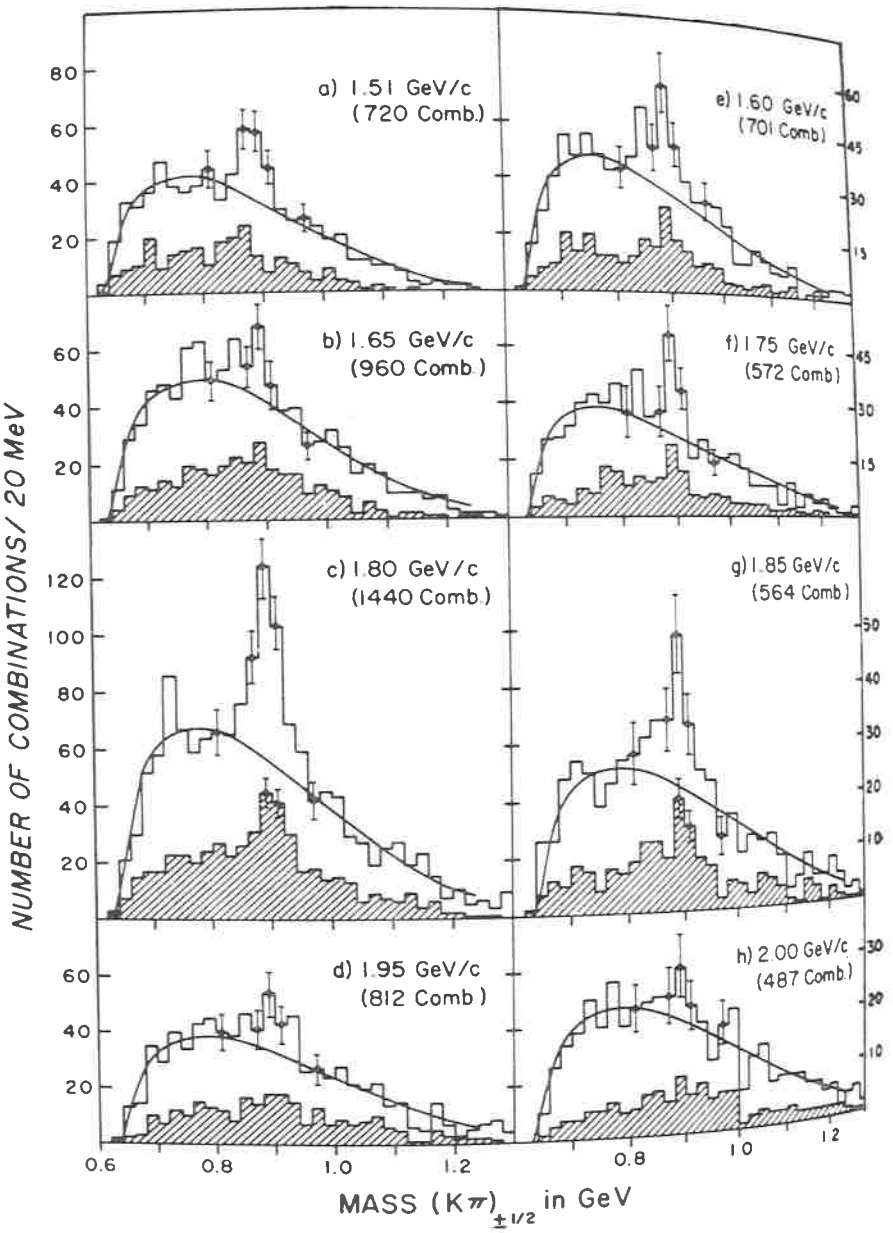

Fig 10 – Kπ mass spectra for various incident momenta anti-protons (ref [10]).

enhancement in the $I=1$ amplitude for $\bar{\mathcal{N}}\mathcal{N}\to K^*\bar{K}\pi\pi+\bar{K}^*K\pi\pi$ at about 2370 MeV, with $\Gamma\leqslant 60$ MeV. However, the previous evidence of Ring *et al.* ([11])

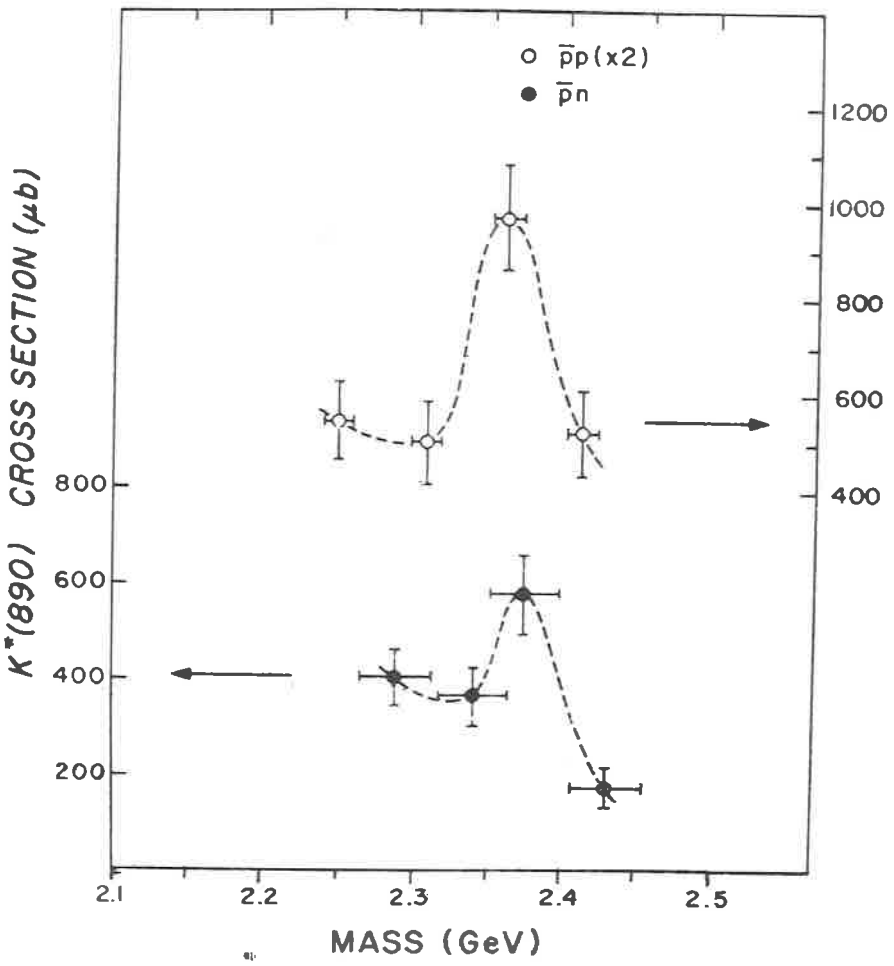

Fig. 11. - Cross-sections for the reactions $\bar{p}\mathcal{N}\to K^*\bar{K}\pi\pi$ or $\bar{K}^*K\pi\pi$ (ref. ([10])).

concerning a peak in the cross-section for $K_s^0K_s^0\pi^+\pi^-\pi^0$ is now reported ([9]) to be weaker than that shown in Fig. 9.

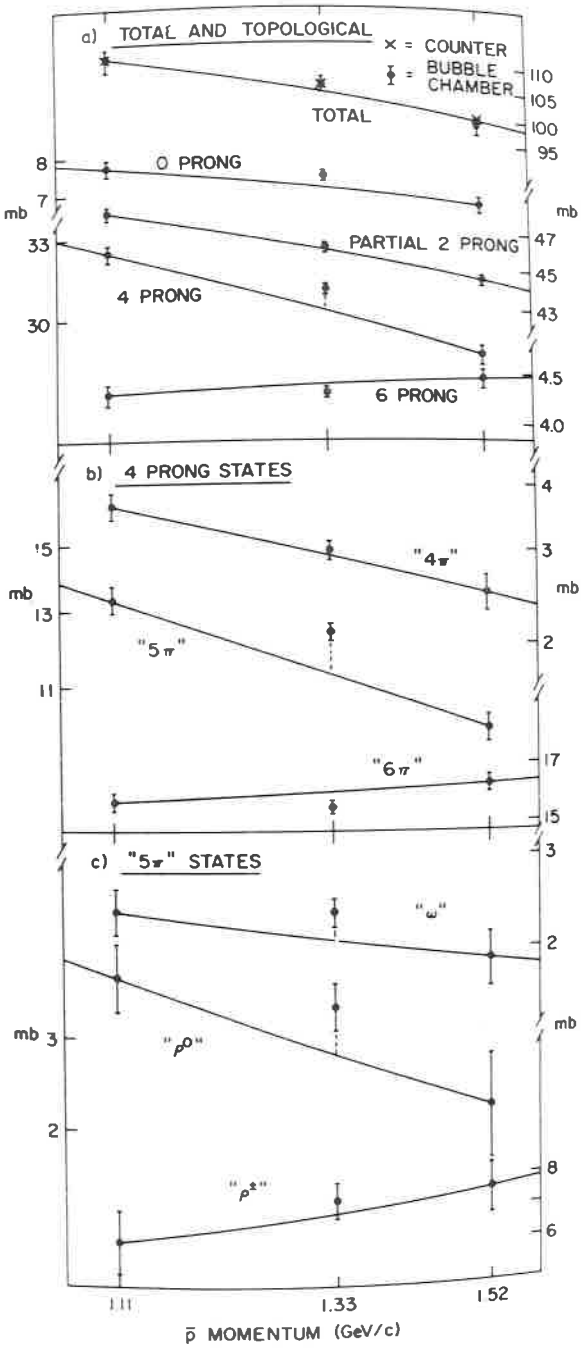

Fig. 12. – Cross-sections *vs.* $\bar{p}$ momentum (ref. [12]).

6. Other $\overline{\mathcal{N}}'\mathcal{N}'$ *s*-channel structure.

Another region in which bubble chamber data on $\bar{p}p$ annihilation *vs. s* has been obtained is near the « T(2190) ». Figure 12 shows cross-sections *vs. s* for a number of channels studied by Kalbfleisch *et al.* ([12]). Of the eleven

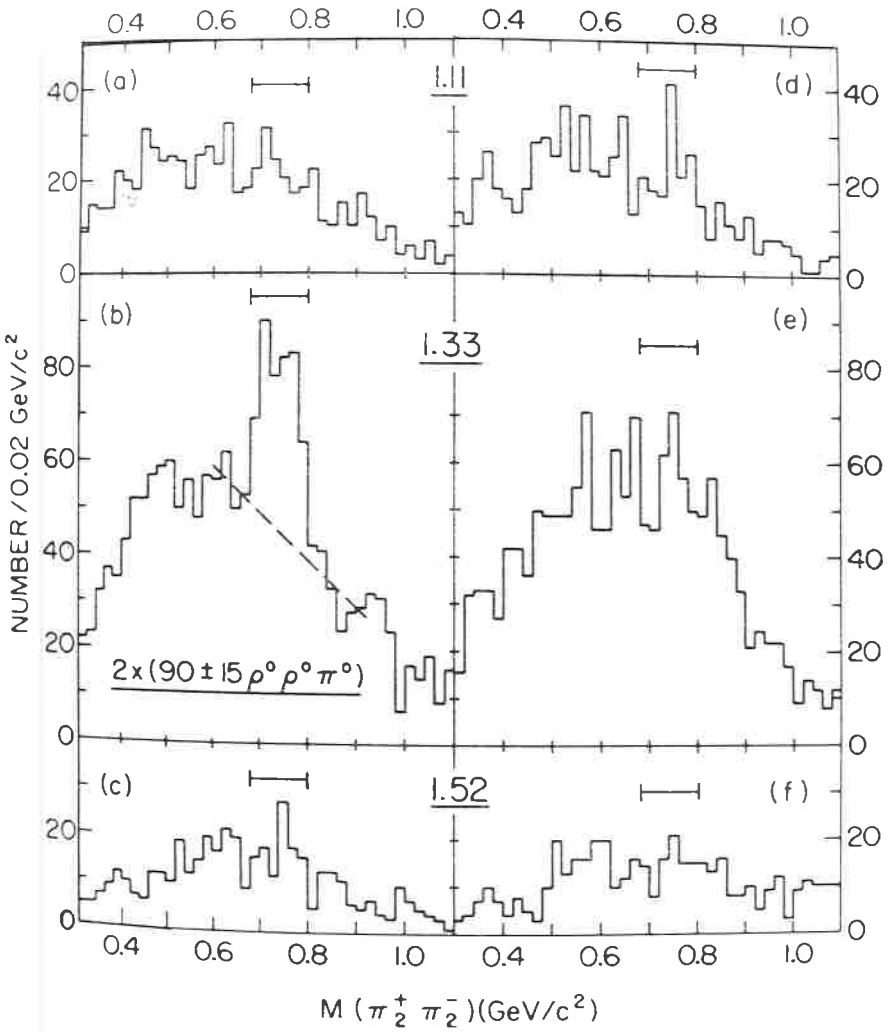

Fig. 13. – Evidence for enhancement in $\rho^0\rho^0\pi^0$ state at 1.33 GeV/c. *a*) - *c*) show $\pi^+\pi^-$ spectra from ρ^0 selected events, and *d*) - *f*) show the same for ρ^0 background selected events (ref. ([12])).

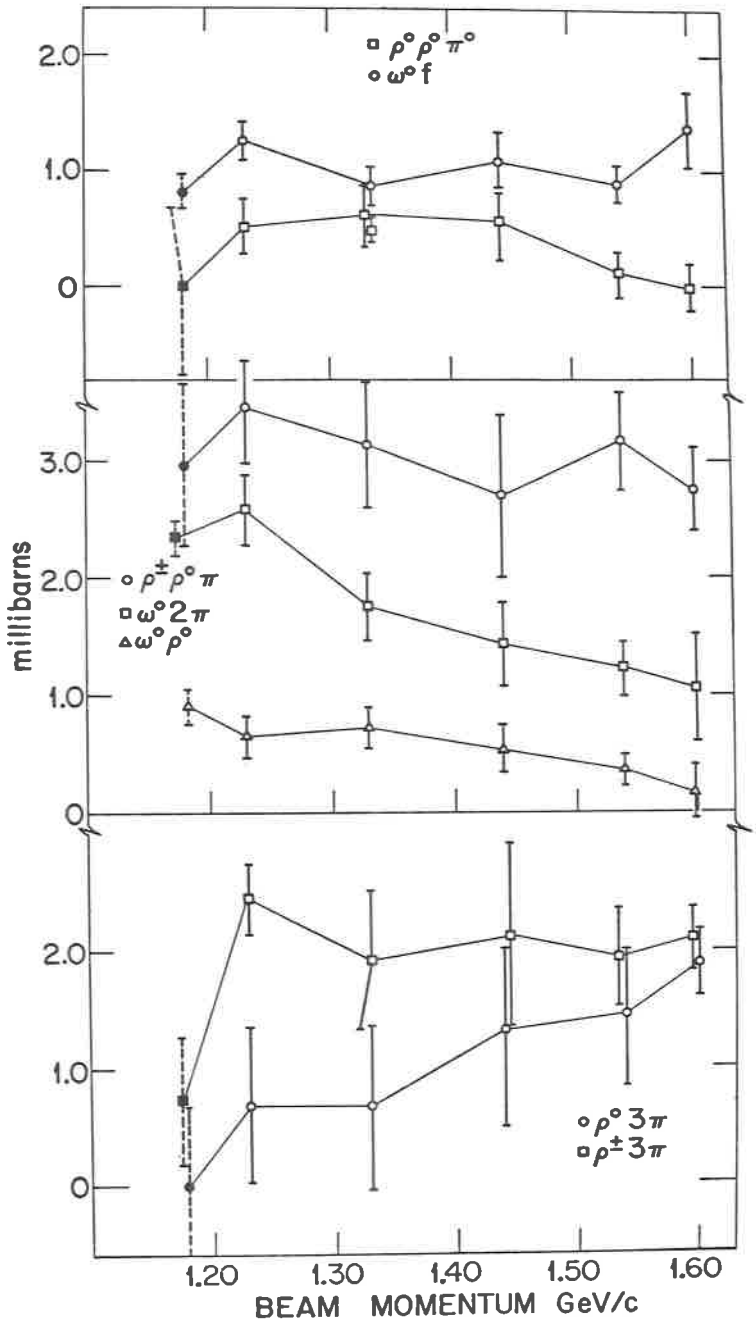

Fig. 14. – Cross-sections *vs.* $\bar{p}$ momentum (ref. [13]).

curves, the 5π cross-section shows the best evidence for a « peak ». In the $\rho^0\rho^0\pi^0$ final state, they found evidence for an enhancement, as shown in Fig. 13. A similar experiment by Cooper *et al.* ([13]) with a comparable amount of data was analysed with a Monte Carlo fit as well as in simpler ways, and did not show such a sharp energy dependence for the $\rho^0\rho^0\pi^0$ final state (Fig. 14). So further evidence is required to resolve this situation.

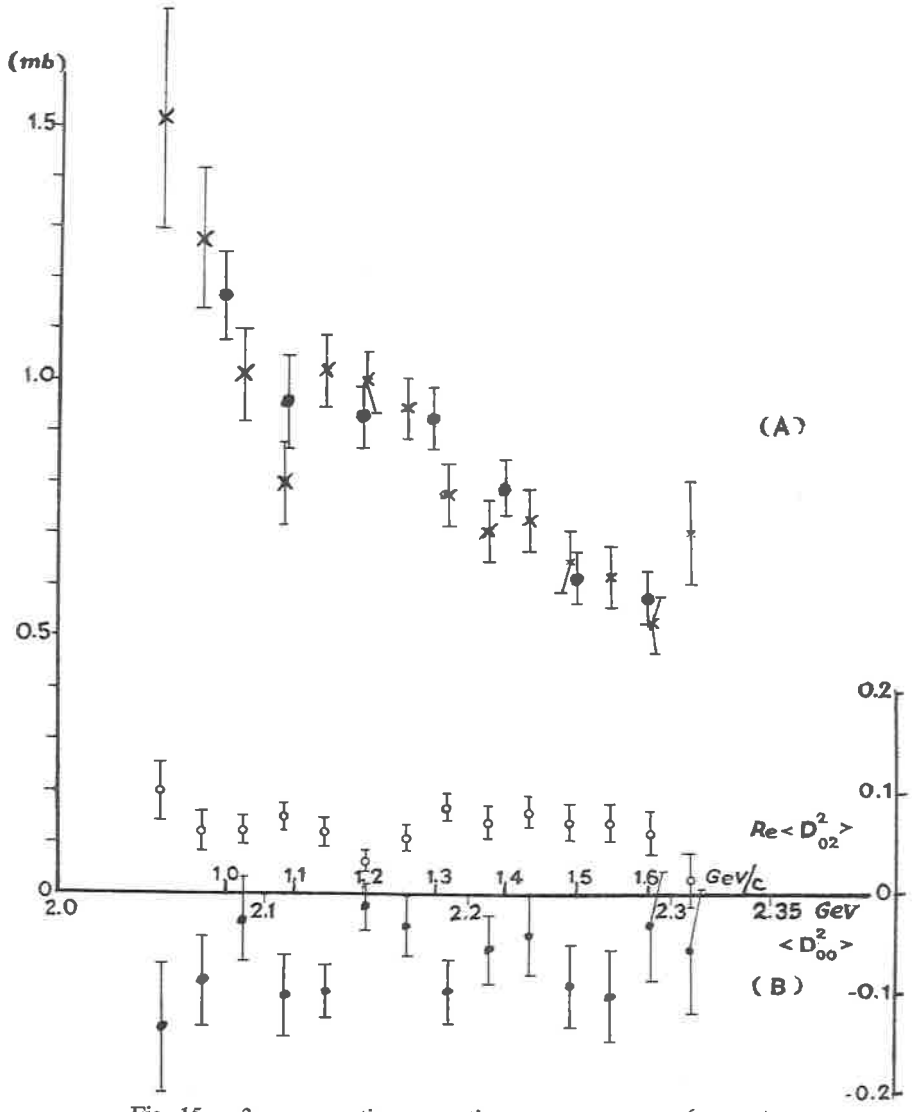

Fig. 15. – 3π cross-section *vs.* anti-proton momentum (ref. ([14])).

In a simpler kind of experiment, data have been obtained on the reaction $\bar{p}n \to 2\pi^-\pi^+$ by Bettini *et al.* [14] for $\bar{p}$ momenta from 1.0 to 1.6 GeV/c. These data exhibit striking structure in the 3π Dalitz plot, of the type previously seen in $\bar{p}n$ annihilations at rest, structure which various authors have interpreted in terms of the properties of a dual amplitude. For our present purpose, the most interesting point is whether there is evidence for a cross-section « peak » as a function of s. Figure 15 shows $\sigma(3\pi)$ as well as the moments $D^2_{00}(\varphi, \theta, \gamma)$ and $D^2_{02}(\varphi, \theta, \gamma)$ of the final state angular distribution. To quote Bettini *et al.*, « there are indications of an effect » around $(1.2 \div 1.3)$ GeV/c $(\sqrt{s} = 2166$ MeV), but the data appear to also be compatible with a smooth variation. Furthermore, the « holes » in the Dalitz plot are s-independent to a reasonable degree at least, so that the overall evidence for s variation in $\bar{p}n \to 2\pi^-\pi^+$ is still weak.

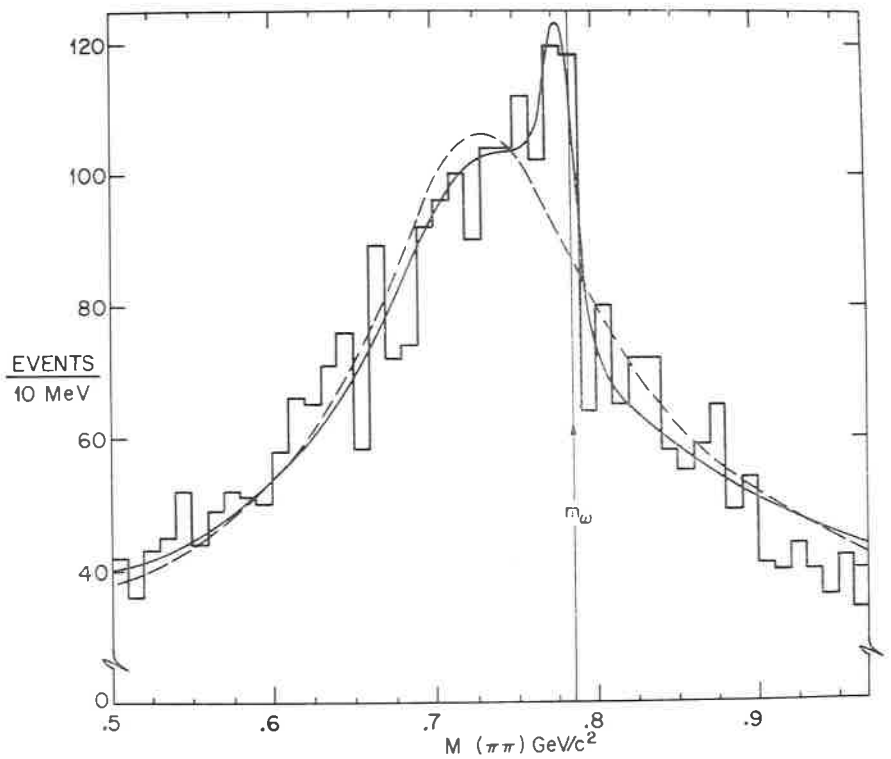

Fig. 16. – $\pi^+\pi^-$ mass spectrum, showing evidence for ρ-ω interference (ref. [15]).

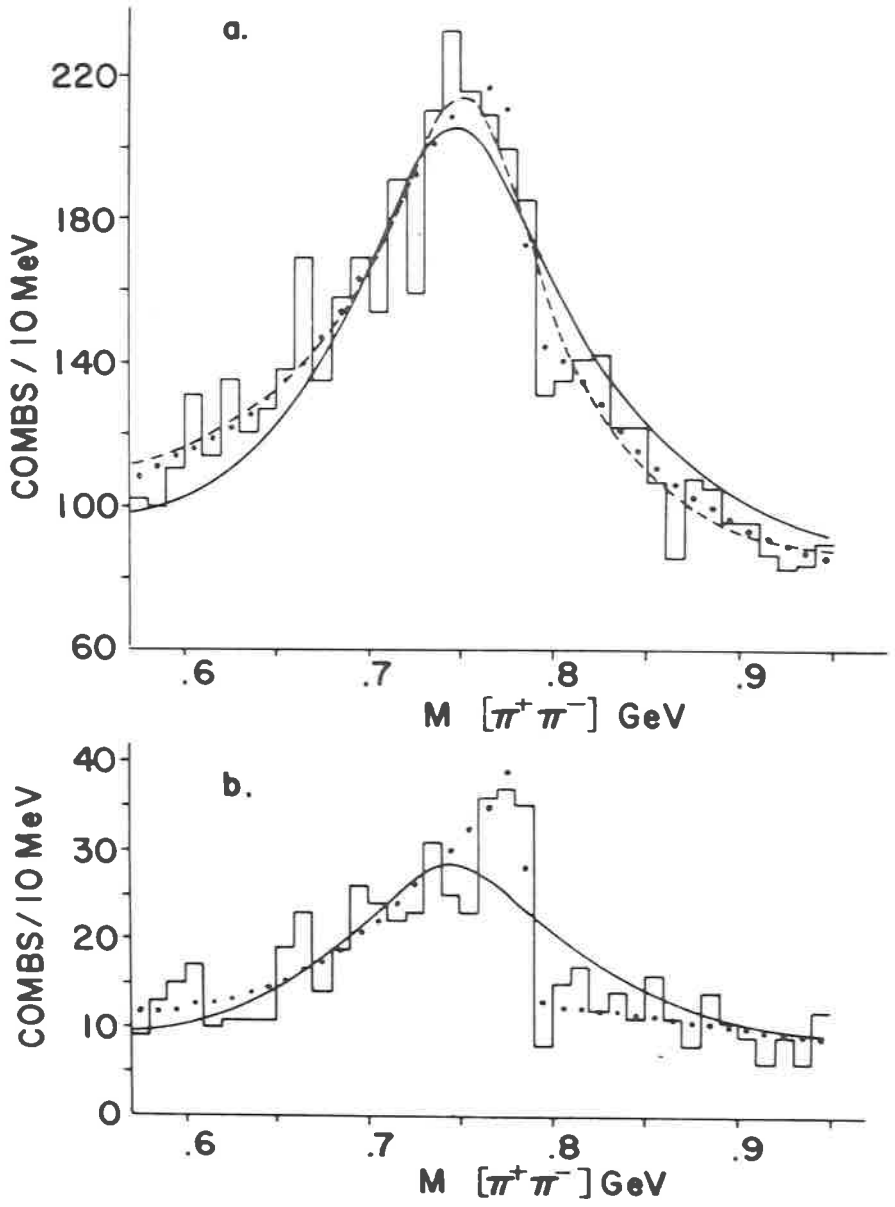

Fig. 17. – $\pi^+\pi^-$ mass spectra: *a*) shows the data with no cuts; *b*) includes only events within a t bin of -0.2 to -0.3 (ref. [16]).

7. ρ-ω interference.

Another relevant aspect of $\bar{p}p$ annihilation experiments concerns what can be learned from ρ-ω interference results. Figure 16 shows the $(\pi^+\pi^-)$ spectrum in the reaction $\bar{p}p \to 2\pi^+2\pi^-$ incident momentum of (1.2÷1.6) GeV/c, as measured by Allison *et al.* ([15]). By using the branching ratio for $\omega^0 \to \pi^+\pi^-$ determined in other experiments, these authors interpreted the observed interference pattern to mean that the $\rho^0\pi^+\pi^-$ and $\omega^0\pi^+\pi^-$ final states are highly coherent and of constant relative phase over this entire momentum range. Since these two states have opposite *G*-parity, this interpretation would then mean a complete degeneracy with respect to *G*-parity of *s*-channel resonances coupled to these final states, provided that *s*-channel resonances dominate the reaction mechanism. The results of Chapman *et al.* ([16]) on ρ-ω interference over the momentum range of (1.6÷2.0) GeV/c are shown in Fig. 17. They interpret their data as showing significantly less than 100% ρ-ω coherence, with the apparent shift and asymmetry of the ρ peak being due mainly to a ρ-background interference. Even so, their data (summed over incident energy) shows strong evidence for ρ-ω interference.

It should be emphasised that the above experiments on $\bar{p}n \to 2\pi^-\pi^+$ and on ρ-ω interference would have seemed, *a priori*, to represent sensitive ways to search for *s*-dependent effects, since the former appears to involve only a small number of *s*-channel amplitudes and since the latter measures directly a phase difference between two amplitudes. Yet these effects seem to be characterised mainly by a *lack* of *s*-dependence. Probably one can infer from this situation that a clean interpretation of individual *s*-channel resonances in the $\bar{\mathcal{N}}'\mathcal{N}'$ system will only be possible with the use of dual models.

8. Production experiments.

The last category of bubble chamber results of which I shall give examples concerns conventional « bump hunting » production experiments. Figure 18 shows the $(\pi^+\pi^0)$ mass spectrum obtained by Kramer *et al.* ([17]) from the reaction $\pi^+p \to \pi^+\pi^0p$ at 13.1 GeV/c. In addition to the peaks at lower masses, there is evidence for a peak at 2160 MeV. These peaks occur at low *t* and so are presumably associated with meson exchange processes. The positive *G*-parity is opposite to that of the possible $\rho^0\rho^0\pi^0$ enhancement at the T meson mentioned above.

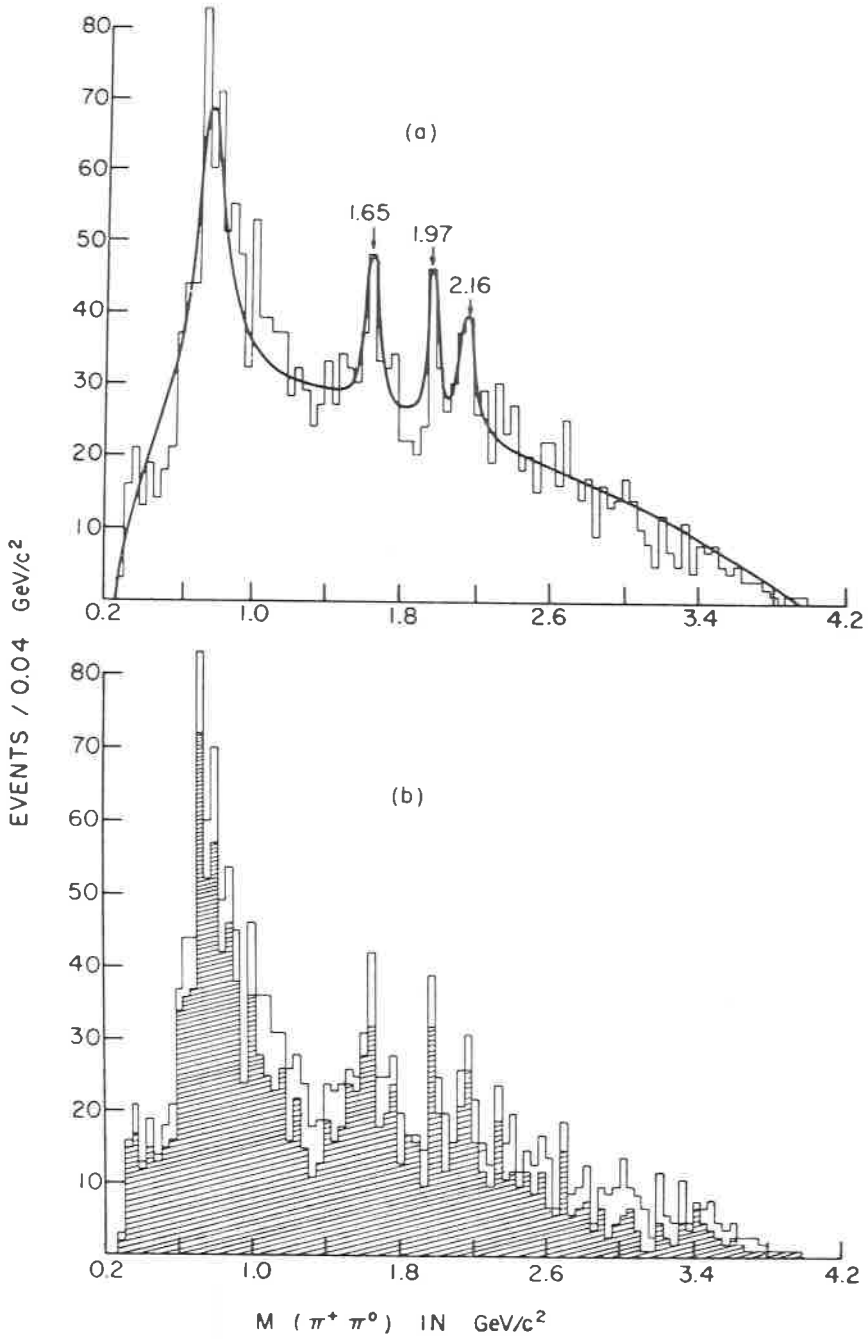

Fig. 18. – $\pi^+\pi^0$ mass spectrum. In *b*), cuts on $p\pi^+$ mass and on t have been made (ref. [17]).

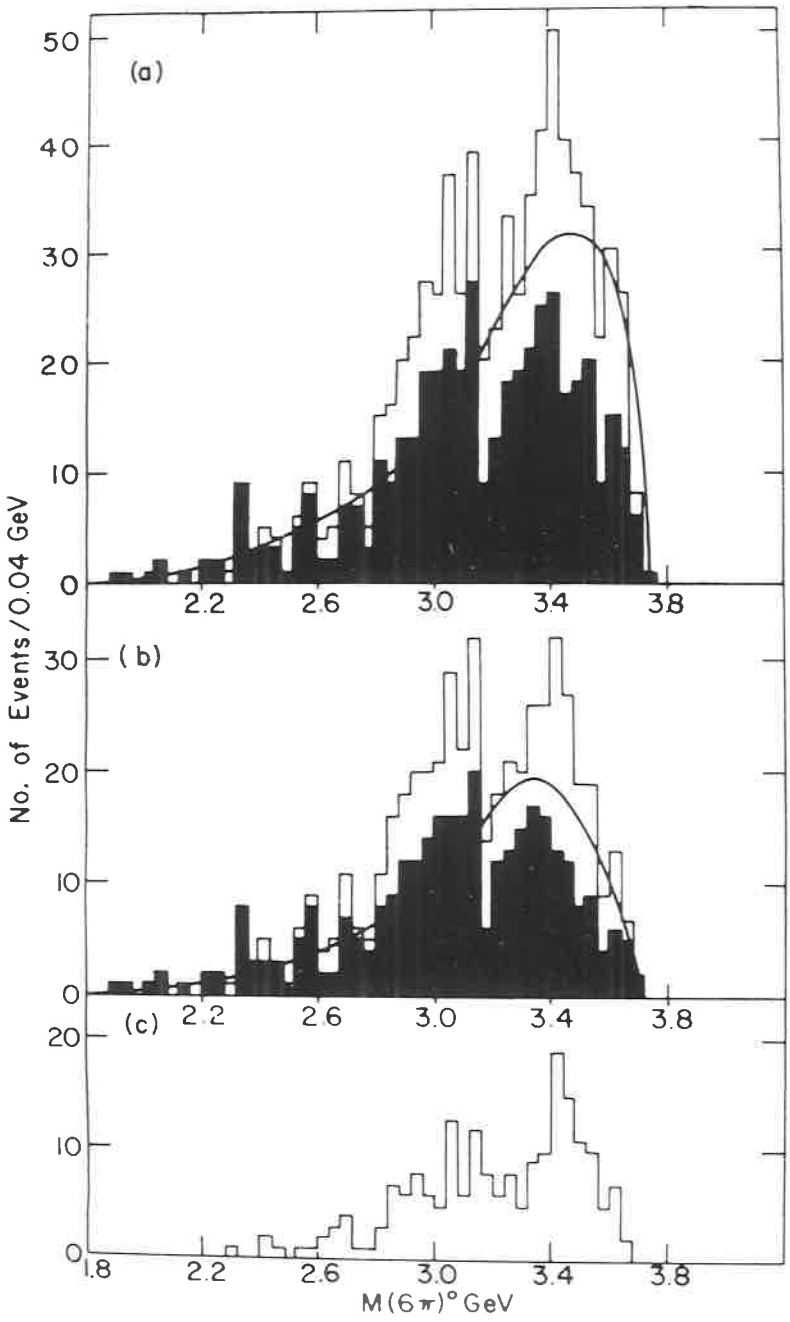

Fig. 19. – Mass spectra for 6π out of 7π in pp annihilations at 6.4 GeV/c. The shaded area shows peripheral events, and part *b*) excludes events with an ω^0 (ref. [18]).

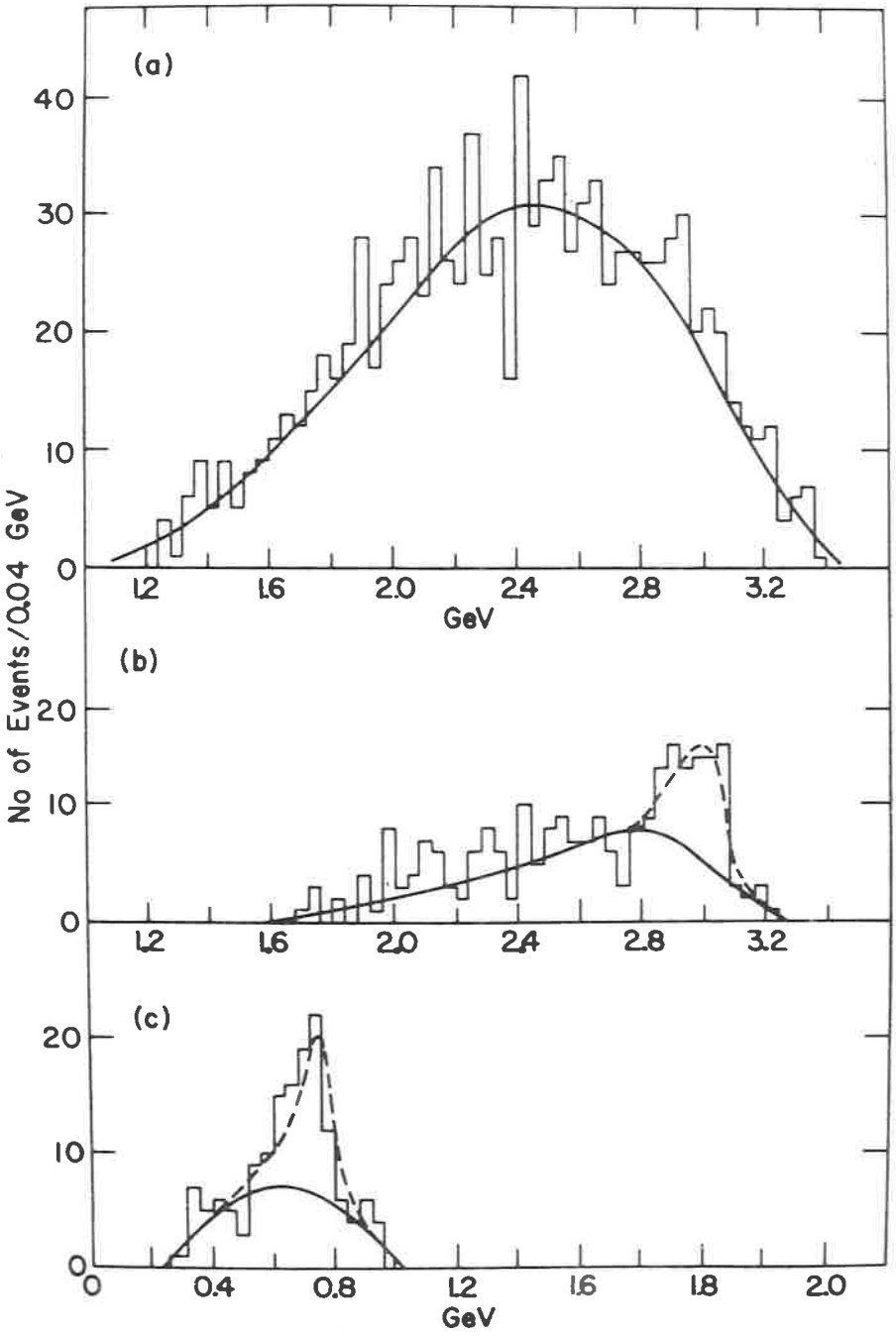

Fig. 20. – Mass spectra for 4π out of 6π are shown in *a*) and b), where the latter includes the requirement that the recoiling $\pi^+\pi^-$ system be near the ρ mass. In c) the $\pi^+\pi^-$ mass spectrum corresponding to 4π masses near 3 GeV is shown (ref. ([18])).

Using the reactions $\bar{p}p \to 6\pi$ and $\bar{p}p \to 7\pi$ at 7 GeV/c, Alexander *et al.* ([18]) have published evidence for an enhancement at 3035 MeV of width 200 MeV, decaying into 6π (Fig. 19) and 4π (Fig. 20). Note that this is a production rather than a formation experiment, but the strength of the coupling of this meson to a baryon vertex is what determines the cross-section since the exchanged particle is a baryon in $\bar{\mathcal{N}}\mathcal{N}$ annihilations.

9. Conclusion.

From this brief review of typical data on the higher mass mesons, it is clear that we are still a long way from being in a position to unravel this part of the hadron spectrum. To even establish the *existence* of the various candidates for states will require much more precise data. Production experiments, such as πp backward and $\bar{p}p$ annihilation, which involve coupling to a nucleon vertex seem particularly promising, at least for finding peaks with a reasonably low background. For nucleon-antinucleon formation experiments, the concept of duality (*i.e.* the relationships between *s*-channel and *t*-channel models, as well as the behaviour of momentum-dependent diffraction effects) must be understood more clearly before even the existing data can be reliably interpreted. Or, expressing the same idea somewhat differently, we can expect even more difficulty from overlapping resonances than has been experienced for lower mass mesons.

REFERENCES

1) Particle Properties Tables, April 1971, unpublished.
2) A review paper which is particularly useful in connection with $\bar{\mathcal{N}}\mathcal{N}$ interactions and their relationship to higher mass mesons is that of L. MONTANET in the Proceedings of the Lund Conference (1969).
3) CERN/HERA Report 70-5 (1970), unpublished.
4) R. J. ABRAMS, R. L. COOL, G. GIACOMELLI, T. F. KYCIA, B. A. LEONTIC, K. K. LI, D. N. MICHAEL: *Phys. Rev. Lett.*, **18**, 1209 (1967).
5) G. CHIKOVANI, L. DUBAL, M. N. FOCACCI, W. KIENZLE, B. LEVRAT, B. C. MAGLIC, M. MARTIN, C. NEF, P. SCHUBELIN and J. SEGUINOT: *Phys. Lett.*, **22**, 233 (1966).
6) R. BAUD, H. BENZ, B. BOSNJAKOVIC, D. R. BOTTERILL, G. DAMGAARD, M. N. FOCACCI W. KIENZLE, R. KLANNER, C. LECHANOINE, M. MARTIN, C. NEF, P. SCHUBELIN and A. WEITSCH: *Phys. Lett.*, 30 B, 129 (1969). The composite graph shown in Fig. 5 is taken from Review of Particle Properties: *Phys. Lett.*, **33** B, 72 (1970).
7) E. W. ANDERSON, E. J. BLESER, H. R. BLIEDEN, G. B. COLLINS, G. GARELICK, J. MENES, F. TURKOT, D. BIRNBAUM, R. M. EDELSTEIN, N. C. HIEN, T. J. MCMAHON, J. MUCCI and J. RUSS: *Phys. Rev. Lett.*, **22**, 1390 (1969).

8) H. NICHOLSON, B. C. BARISH, J. PINE, A. V. TOLLESTRUP, J. K. YOH, C. DELORME, F. LOBKOWICZ, A. C. MELISSINOS and Y. NAGASHIMA: *Phys. Rev. Lett.*, **23**, 603 (1969).
9) Review of Particle Properties: *Phys. Lett.*, **33** B, 71 (1970).
10) B. Y. OH, D. L. PARKER, P. S. EASTMAN, G. A. SMITH, R. J. SPRAFKA and Z. M. MA: *Phys. Rev. Lett.*, **24**, 1257 (1970).
11) RING *et al.*, Michigan and Michigan State preprint (1970).
12) G. KALBFLEISCH, R. STRAND and V. VANDERBURG: *Phys. Lett.*, **29** B, 259 (1969).
13) W. A. COOPER, W. MANNER, L. HYMAN and S. EGLI. submitted to *Phys Rev.*
14) A. BETTINI, M. CRESTI, M. MAZZUCATO, L. PERUZZO, S. SARTORI, G. ZUMERLE, M. ALSTON-GARNJOST, R. HUESMAN, R. ROSS, F. SOLMITZ, L. BERTANZA, R. CARRARA, R. CASALI, P. LARICCIA, R. PAZZI, G. BORREANI, B. QUASSIATI, G. RINAUDO, M. VIGONE, A. WERBROUCK: *Nuovo Cimento*, **1** A, 333 (1971).
15) W. W. M. ALLISON, W. A. COOPER, T. FIELDS and D. S. RHINES: *Phys. Rev. Lett.*, **24**, 618 (1970).
16) J. W. CHAPMAN, J. DAVIDSON, R. GREEN, J. LYS, B. ROE and J. C. VANDER VELDE: *Nucl. Phys.*, B **24**, 445 (1970).
17) S. L. KRAMER, H. R. BARTON, Jr., L. J. GUTAY, S. LICHTMAN, D. H. MILLER and J. H. SCHARENGUIVEL: *Phys. Rev. Lett.*, **25**, 396 (1970).
18) G. ALEXANDER, I. BAR-NIR, S. DAGAN, G. GIDAL, J. GRUNHAUS, A. LEVY, Y. OREN, and J. SCHLESINGER: *Phys. Rev. Lett.*, **25**, 63 (1970).

Study of the $\bar{p}n$ partial cross-sections between 1.0 and 1.6 GeV/c (*)

A. BETTINI, M. CRESTI, M. MAZZUCATO, L. PERUZZO
S. SARTORI and G. ZUMERLE
Istituto di Fisica dell'Università - Padova
Istituto Nazionale di Fisica Nucleare - Sezione di Padova

M. ALSTON-GARNJOST, R. HUESMAN, R. ROSS and F. F. SOLMITZ
Lawrence Berkeley Laboratory - Berkeley, Calif.

A. BIGI, R. CARRARA, R. CASALI, P. LARICCIA and R. PAZZI
Istituto di Fisica dell'Università - Pisa
Istituto Nazionale di Fisica Nucleare - Sezione di Pisa

G. BORREANI, B. QUASSIATI, G. RINAUDO, M. VIGONE and A. WERBROUCK
Istituto di Fisica dell'Università - Torino
Istituto Nazionale di Fisica Nucleare - Sezione di Torino

We shall discuss some results of a $\bar{p}n$ formation experiment in the region of the first enhancement of the total cross section [1] ($E^* \simeq 2190$ MeV) from the Berkeley-Padova-Pisa-Torino collaboration.

With the aim of carefully studying the $\bar{p}n$ partial cross sections in this energy region, we have exposed the 81 cm CERN D.B.C. to a separated beam of antiprotons at seven different momenta between 1.0 and 1.6 GeV/c; the step between two contiguous momenta (100 MeV/c) has been chosen to have, taking into account the Fermi motion, a smooth distribution of the c.m. $\bar{p}n$ energy.

The $\bar{p}n$ c.m. energy interval we can explore ranges from 2.04 to 2.32 GeV, completely enclosing the region of the bump of the total cross section. We have an average of $\frac{1}{2}$ ev/μb at each momentum setting.

One of the possible origins of the bump is a threshhold effect due to the $\bar{\Delta}N + \Delta\bar{N}$ channel.

(*) Invited paper presented by A. Bettini

The values of cross section of the reaction:

$$\bar{p}n \to \bar{p}p\pi^- , \tag{1}$$

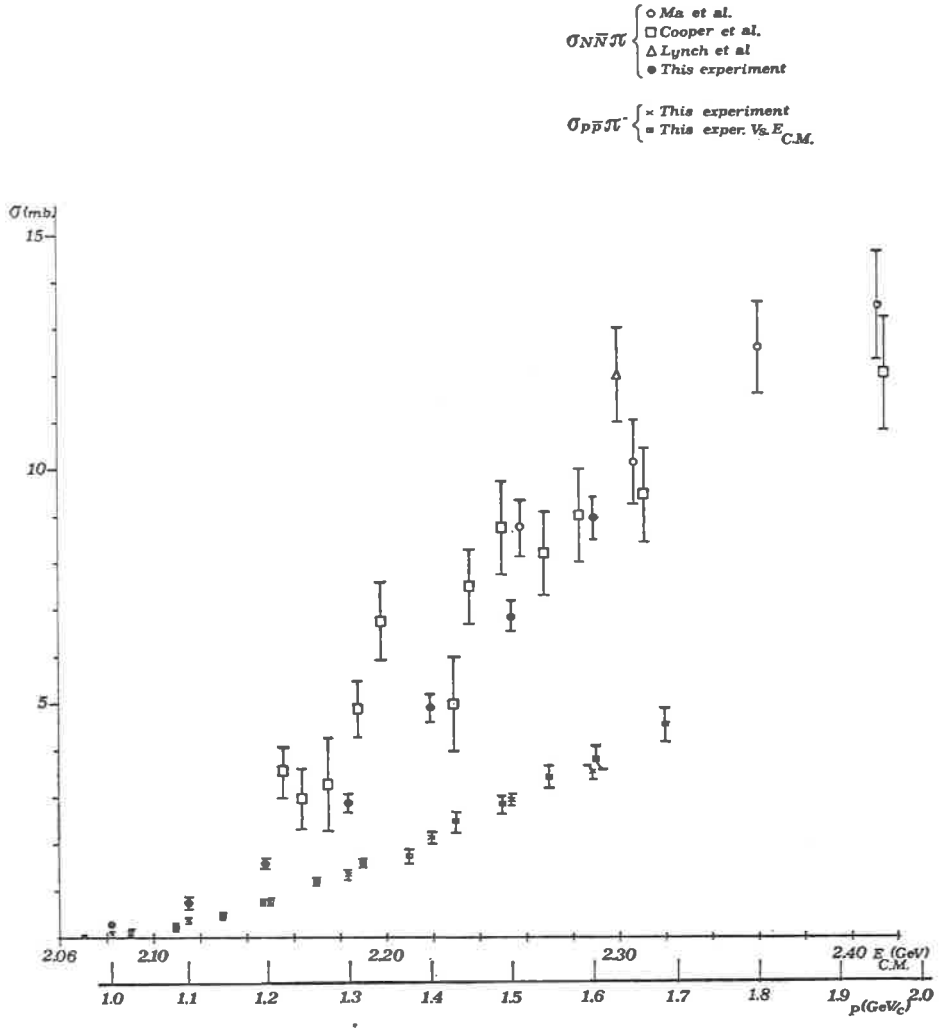

Fig. 1. – Cross-section for the reactions $\bar{p}n \to \bar{p}p\pi-$ and $\bar{p}n \to \bar{N}N\pi$ as measured by this experiment, compared with that for the reaction $\bar{p}p \to \bar{N}N\pi$ as measured by other experiments (these last have been multiplied by two to take into account the total isotopic spin).

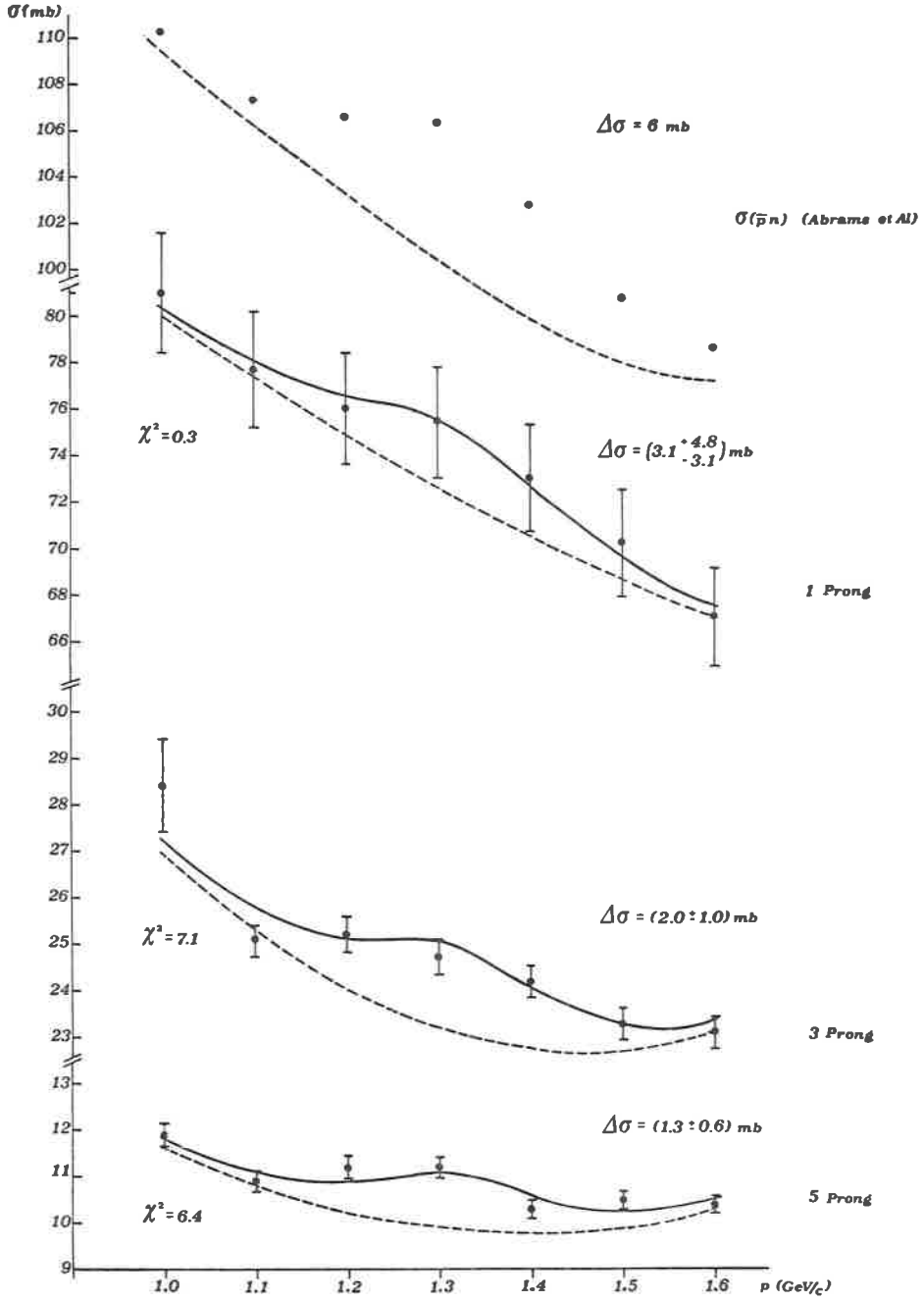

Fig. 2. – Total $\bar{p}n$ cross-section from Abrams *et al.* [1] and topological cross-sections from our experiment.

we have measured are reported in Fig. 1 as a function of incident $\bar{p}$ momentum and c.m. energy. The channel appears to be completely dominated by $\bar{\Delta}^{--}$ production; it is then reliable to apply an isobar model to evaluate the contribution of the unseen channel:

$$\bar{p}n \to \bar{p}n\pi^0 ; \tag{2}$$

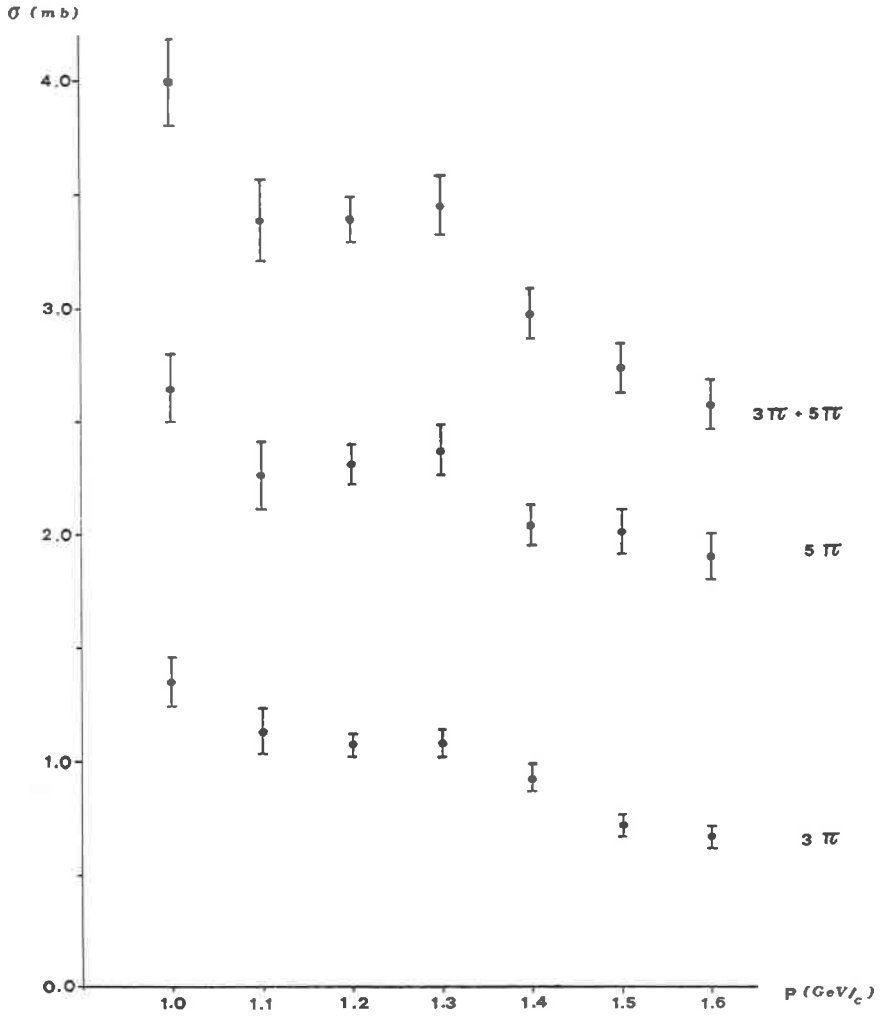

Fig. 3. – Cross-sections for the reactions $\bar{p}n \to 2\pi^-\pi^+$ and $\bar{p}n \to 3\pi^-2\pi^+$ as function of the beam momentum.

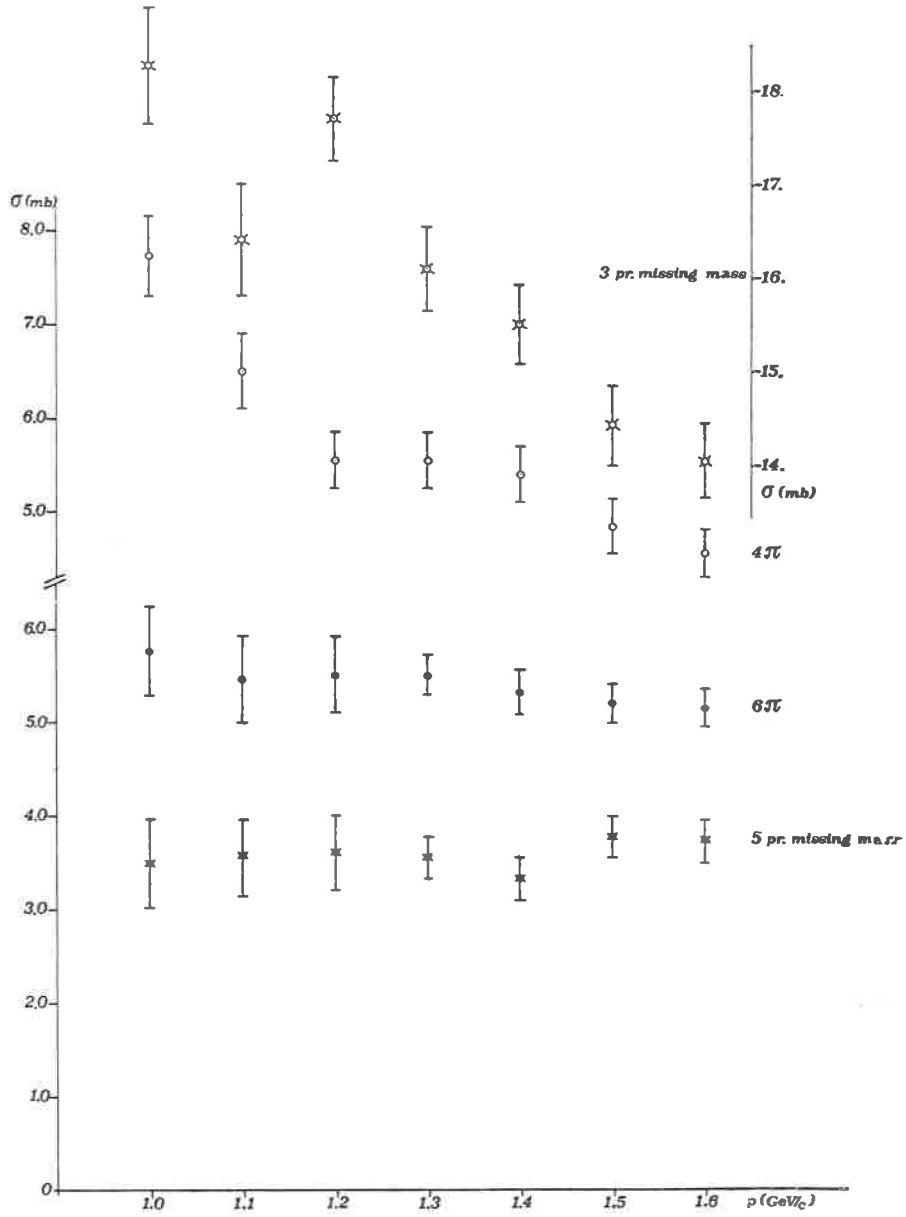

Fig. 4. – Cross-sections for the reactions $\bar{p}n \to 2\pi^-\pi^+\pi^0$, $pn \to 3\pi^-2\pi^+\pi^0$, $\bar{p}n \to 2\pi^-\pi^+$MM (see text) and $\bar{p}n \to 3\pi^-2\pi^+$MM (see text) as function of the beam momentum.

the cross section for the third one:

$$\bar{p}n \to \bar{n}n\pi^- \tag{3}$$

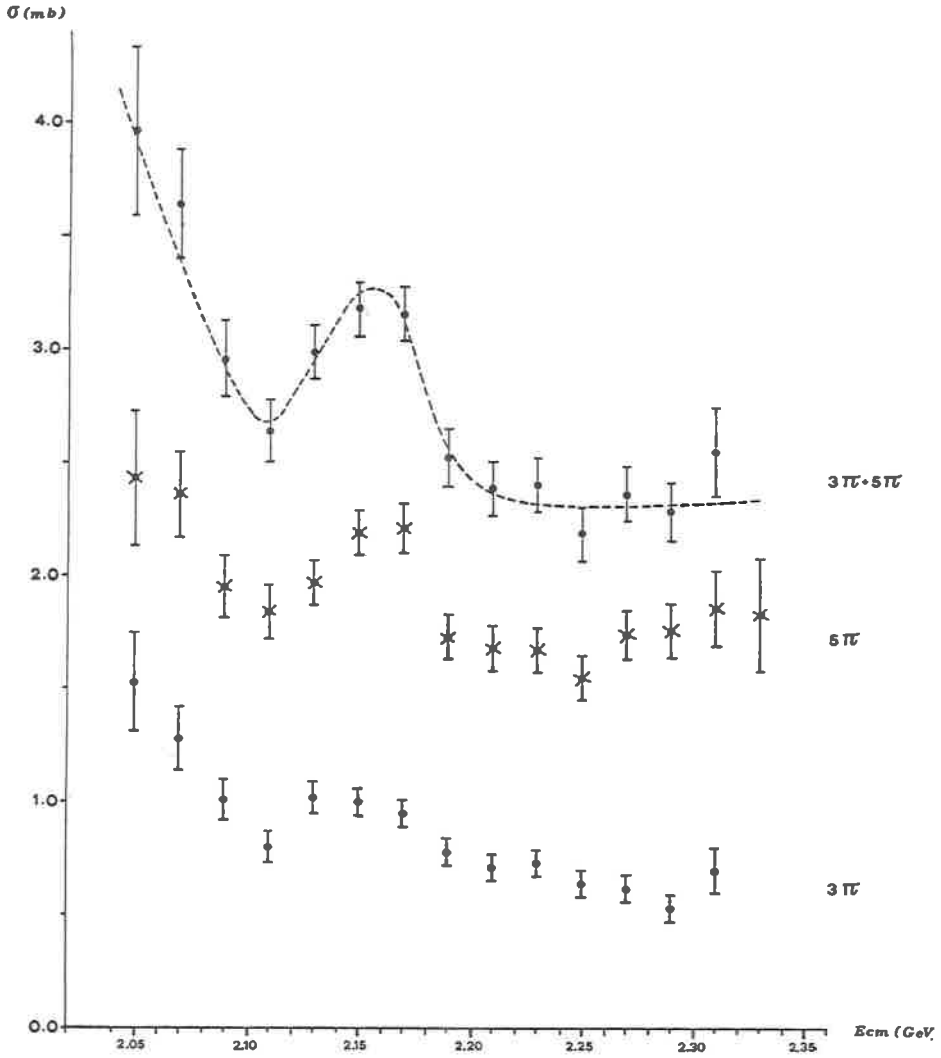

Fig. 5. – Cross-sections for the reactions $\bar{p}n \to 2\pi^-\pi^+$ and $\bar{p}n \to 3\pi^-2\pi^+$ as functions of the c.m. $\bar{p}n$ energy (Preliminary)

is equal to that of reaction (1) due to *G*-parity conservation. The values of

the cross section for the reaction $\bar{p}n \to \mathcal{N}\overline{\mathcal{N}}\pi$ evaluated in this way are reported in Fig. 1, compared to the published values of the cross section for the reaction $\bar{p}p \to \mathcal{N}\overline{\mathcal{N}}\pi$, multiplied by two to take into account isotopic spin.

As one can see, the one pion production cross section grows *at a constant rate* through all the region of the bump of the total cross section; from this observation we conclude that this channel cannot be at the origin of the 6 mb ([1]) bump. To explain the bump this cross section should have reached saturation (or at least its derivative have decreased) inside the region of the bump.

On the other hand we have positive evidence that the annihilation cross sections give contributions to the bump.

Figure 2 shows the values of the Abrams et al. ([1]) total cross section at our momentum setting (the dotted curve is the background they estimate under the resonance) and the values we measured for the cross sections of the odd-prong topologies (mainly $\bar{p}n$ interactions). The errors are point-to-point errors and do not include a 4% normalization error. The curves are fits of a Breit-Wigner function with mass and width fixed at the Abrams et al. values ($M = 2190$ MeV, $\Gamma = 85$ MeV) plus a parabolic background. Taking into account the big errors due to the ignorance of the background behaviour, we find a one-standard-deviation effect in the one-prong and two-standard-deviation effects both in 3-prong and 5-prong. No similar effect is seen in the even-prong topologies. This observation is in agreement with an assignment of $I = 1$ to the bump.

Let's consider now the physical cross section. In Fig. 3 the cross sections for the reactions:

$$\bar{p}n \to \pi^+\pi^-\pi^- \tag{4}$$

and

$$\bar{p}n \to 2\pi^+3\pi^- \tag{5}$$

are reported versus the incident $\bar{p}$ momentum. A signal is observed in both processes at the same position and with the same width; it is enhanced by summing the two cross sections. The error bars in these and in the following mentioned cross sections are point-to-point errors. A 10% systematic normalization error is not included.

The cross sections for reactions:

$$\bar{p}n \to \pi^+\pi^-\pi^-\pi^0 \tag{6}$$

and

$$\bar{p}n \to 2\pi^+3\pi^-\pi^0 \tag{7}$$

(1 *c* fits) and:

$$\bar{p}n \to \pi^+\pi^-\pi^- MM \tag{8}$$

and

$$\bar{p}n \to 2\pi^+ 3\pi^- MM \tag{9}$$

(0 *c* fits) are shown in Fig. 4. Reactions (8) and (9) are defined as those with a missing mass greater than $1\pi^0$ and include also events with missing $K^{0\prime}\bar{s}$, *i.e.* some of the charged tracks may be kaons.

These channels have not yet been studied as carefully as reactions (1)-(5); we do not yet know exactly the contamination of different categories present at each energy; this is taken into account in the big error bars given to the data points. We do not observe in these channels any big signal at 1.3 GeV/c, even though more work is needed before a definite conclusion can be reached.

At this point we note that the odd *G*-parity states seem to give the main contribution to the bump. On the other hand we note that at each momentum the datum point receives contribution from c.m. $\bar{p}n$ energies in a range of about 60 MeV due to the Fermi motion; this effect necessarily tends to wash out the variations of the cross sections. The measurement of all the momenta of the final state particles can give on the other hand a highly precise determination of the c.m. energy for each event. We could then (the deuteron wave function being known) easily compute the cross sections as a function of the c.m. $\bar{p}n$ energy. Preliminary results are shown for reaction (4) and (5) in Fig. 5.

As can be seen, both cross sections resonate. The sum of them (the curve is hand-drawn to guide the eye) shows an enhancement of $\Delta\sigma \simeq (0.7 \div 0.8)$ mb, over a guessed background. We have not yet fitted curves to find the values of the parameters of the resonance, but it appears that $M \simeq 2.160$ MeV, $\Gamma \simeq 60$ MeV.

From this observation and taking into account the contribution of the many-π^0's counterparts we can conclude that the bump in the total cross section is mainly due to $G = -1$ pionic annihilations.

The bump we observe shows up nicely, mainly for the good signal to background ratio we have due to the pure $I = 1$ initial state and to the small value of the cross sections. For comparison note that the cross section for $\bar{p}p \to 2\pi^+ 2\pi^- \pi^0$ is around 14 mb in this energy region (a factor of 7 bigger than that of reaction (5)); if a bump of the same height were to be present it would certainly be much more difficult to detect.

REFERENCE

1) R. J. Abrams *et al.*: *Phys. Rev. Lett.*, **18**, 1209 (1967).

Evidence for narrow non-strange neutral bosons of masses 2.370 and 2.610 MeV produced in $\bar{p}p$ annihilations at 5.7 GeV/c (*)

H. W. ATHERTON, L. M. CELNIKIER, M. CLAYTON, B. J. FRANEK
B. R. FRENCH, A. FRISK, B. GHIDINI
L. MANDELLI, J. MOEBES, K. MYKLEBOST, T. KHAN-NISAR
E. QUERCIGH and V. SIMAK
CERN - Geneva

Evidence for the existence of non-strange bosons of masses 2.38 GeV (U-meson region) and 2.62 GeV has been found in π^-p production experiments ([1,5]) and, in the case of the U-meson region, also in $\bar{p}p$ formation

TABLE I.

		Ref.	I	M_0 (MeV)	Γ (MeV)	Reaction	σ (μb)
X(2380) U meson	Production	([1])	$\geqslant 1$	2382 ± 24	$\leqslant 30$	$\pi^-p \to pX^-$ $(0.28 < t < 0.36)$	42 ± 14
		([3])	$\geqslant 1$	2370 ± 25	57	$\pi^-p \to pX^-$ (small u)	—
		([4])	$\geqslant 1$	2420 ± 25	$\leqslant 80$	$\pi^-p \to p\pi^0(3\pi^-2\pi^+)$	—
	Formation	([6])	1	2350 ± 10	140	$\bar{p}p \to$ all	3200
			0	2375 ± 10	190	$\bar{p}p \to$ all	2500
		([3])	1	2360 ± 25	< 60	$\bar{p}p \to K^*(890)\bar{K}\pi\pi$	420 ± 120
						$\bar{p}d \to K^*(890)\bar{K}\pi\pi p_s$	240 ± 90
X(2620)	Production	([2])	$\geqslant 1$	2620 ± 20	85 ± 30	$\pi^-p \to pX^-$	17
		([5])	$\geqslant 1$	2676 ± 27	150	$\pi^-p \to p(\pi^-\rho^-\pi^+)$	30 ± 10

(*) Invited paper presented by L. Mandelli

experiments ([6,8]) (*). This information is summarized in Table I. In this paper we present evidence for two neutrally charged resonant states of mass (2374±4) MeV and (2613±7) MeV and with narrow widths.

The evidence is obtained from a study of 12000 $\bar{p}p$ annihilations into kaons and pions at 5.7 GeV/c in the CERN 2 m HBC. Only events with at least one visible K° decay were measured. The channels used in the study were (**):

a)	$\bar{p}p \to K_1^0 K_1^0 \pi^+\pi^-\pi^0$	301 events
b)	$\to K_1^0 K_1^0 \pi^+\pi^-\pi^+\pi^-$	115 »
c)	$\to K_1^0 K_F^0 \pi^+\pi^-\pi^+\pi^-$	492 »
d)	$\to K^\pm K_1^0 \pi^\mp\pi^0\pi^+\pi^-$	1165 »
e)	$\to K_1^0 K_1^0 \pi^+\pi^-\pi^+\pi^-\pi^0$	290 »
f)	$\to K_1^0 K^\pm\pi^\mp\pi^+\pi^-$	415 »

The $K\bar{K}m\pi$ (m = 0,1 ... 4) mass spectra for the above reactions have been added up as a function of both the pion multiplicity and the charge state. Figure 1a shows one of these, the $(K\bar{K}\pi\pi)^0$ mass spectrum where two bumps at masses near 2.38 GeV and 2.62 GeV can be seen. On the other hand the $(KK\pi\pi)^\pm$ charged mass spectrum (Fig. 1*b*) shows no evidence for bumps in these regions. The curves superimposed on the histograms of Figs. 1*a* and 1*b* are fitted polynomial functions along with relativistic Breit-Wigners to describe the resonances.

The channels *a-f* have been studied individually in order to investigate all possible decay modes and/or production mechanism of these two states. Signals in the *U*-region are best seen in the $(K_1^0 K_F^0 \pi^+\pi^-)^0$ and $(K_1^0 K^\mp\pi^\mp)^0$ mass spectra of reactions *c*) and *f*) and are shown in Figs 2*a* and 2*b*. Results of fits to these spectra are given in Table II. Since the masses and widths are compatible and the production reaction is the same, *viz.* $\bar{p}p \to X^0\pi^+\pi^-$ ($X^0 \to K_1^0 K_F^0 \pi^+\pi^-$ or $K_1^0 K^\pm\pi^\mp$), we have added the two mass spectra (Fig. 2*c*) and redone the fit. Our best value for the mass is $M = (2374\pm4)$ MeV. The resulting physical width Γ^0 is always compatible with zero, and we prefer to quote in Table II its upper limit (to a 99.7% confidence level *i.e.* 3 S.D.).

(*) In the case of the reaction $\bar{p}p \to \bar{n}n$ ([7]) an effect corresponding to the signal of ref. ([6]) and ([3]) was not observed.

(**) K_F^0 stands for an unseen but fitted K^0.

The mass resolution in the *U*-region for the $K_1^0K^{\pm}\pi^{\mp}$ and $K_1^0K_F^0\pi^+\pi^-$ mass combinations are $2\sigma = 20$ MeV and $2\sigma = 30$ MeV respectively. The significance of the signal is 4.6 standard deviations.

In an attempt to obtain some information on the isotopic spin of the

TABLE II.

	Spectrum	M_0 (MeV)	Γ (MeV) 99.7% confidence	Statist. signif. (S.D.)	Signal / Backgrd.	No. of events in peaks	σ (μb)
U meson	$(K\bar{K}\pi\pi)^0$	2398 ± 10	< 33	2.7	1:5	51 ± 19	10 ± 4
X(2380)	$(K^{\pm}K^0\pi^{\mp})$	2375 ± 7	< 12	2.6	1:1	29 ± 11	6 ± 2
	$(K_1^0K_F^0\pi^+\pi^-)$	2378 ± 4	< 33	3.0	1:2.5	35 ± 12	6 ± 2
	$(K^{\pm}K_1^0\pi^{\mp})$ / $(K_1^0K_F^0\pi^+\pi^-)$	2374 ± 4	< 24	4.6	1:1.6	73 ± 16	14 ± 3
X(2620)	$(K\bar{K}\pi\pi)^0$	2620 ± 6	< 87	2.0	1:6	82 ± 39	17 ± 8
	$(K_1^0K_1^0\pi^+\pi^-)$	2616 ± 4	< 30	2.0	1:1	16 ± 8	4 ± 2
	$(K_1^0K^{\pm}\pi^{\mp}\pi^0)$	2612 ± 10	< 99	2.5	1:3.5	42 ± 17	8 ± 3
	$(K_1^0K_1^0\pi^+\pi^-)$ / $(K_1^0K^{\pm}\pi^{\mp}\pi^0)$	2613 ± 7	< 90	2.8	1:3	66^{+40}_{-24}	13^{+8}_{-5}

above state we calculated, using statistical weights ([9]) and considering all possible isotopic spin waves in the production mechanism, the number of events we would expect to see in the different observable neutral and charged $K\bar{K}\pi$ and $K\bar{K}\pi\pi$ decay modes for an $I = 0$ or $I = 1$ resonant state. The following observations may be made:

a) Since we observe a bump in the $K_1^0K_F^0\pi^+\pi^-$ spectrum and not in the $K_1^0K_1^0\pi^+\pi^-$ spectrum, the data indicate a $K_1^0K_2^0\pi^+\pi^-$ decay or a $K\bar{K}\pi^+\pi^-$ decay in which there is no restriction on the $K\bar{K}$ decay into $K_1^0K_1^0$ or $K_1^0K_2^0$.

b) In the $K^{\pm}K_1^0\pi^{\mp}\pi^0$ mass spectrum of reaction *d*) (Fig. 2*d*) we expect a minimum of (21 ± 7) events for $I = 0$ and (29 ± 9) event for $I = 1$ whereas no clear accumulation of events is seen in the U-mass region.

c) A minimum of 43 ± 15 events is predicted in the $K^{\pm}K_1^0\pi^+\pi^-$ mass spectrum of reaction *d*) (Fig. 2*g*) for $I = 1$. No bump is seen in the *U*-region ([10]).

Observation *c*) and the fact that we see no enhancement in the total charged $(KK\pi\pi)^{\pm}$ spectrum of Fig. 1*b* favour an $I = 0$ assignment for the state.

Evidence for the X(2620) structure is seen in Figs. 2*d* and 2*e* and their sum is shown in Fig. 2*f* where we have considered the bumps of Figs. 2*d* and 2*e* as representing different decay modes of the same object. The best value for the mass is (2613 ± 7) MeV. For the channels $K_1^0 K_1^0 \pi^+ \pi^-$ and $K_1^0 K^{\pm} \pi^+ \pi^0$ where the resolution is respectively $2\sigma = 22$ MeV and $2\sigma = 40$ MeV, the

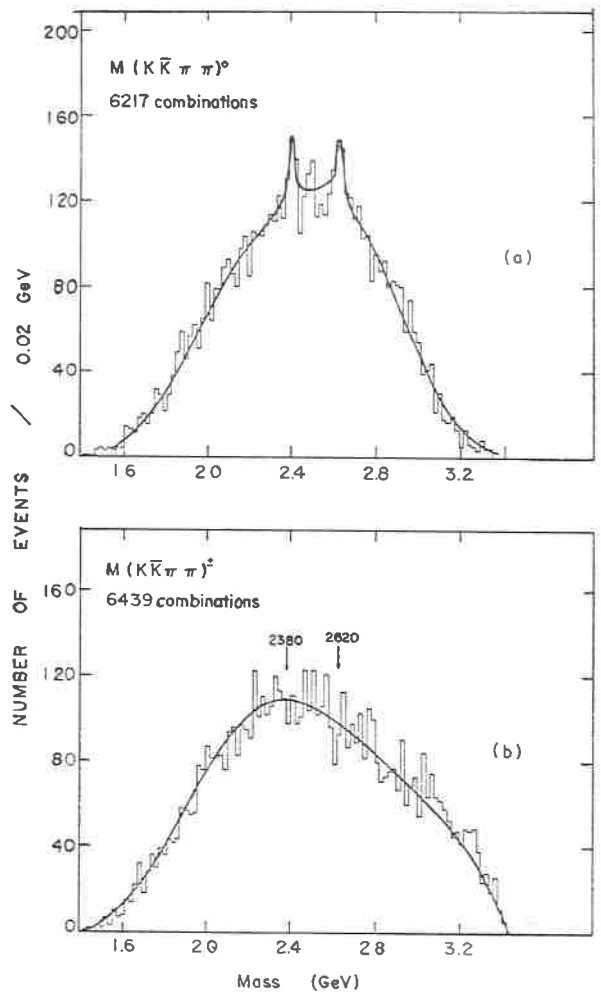

Fig. 1. – *a*) 6217 $K\bar{K}\pi\pi$ neutral combinations coming from reactions (1*a*), (1*b*), (1*c*), (1*d*) and (1*e*). The full line represents a fit of a polynomial background plus two relativistic Breit-Wigner curves. *b*) 6499 $K\bar{K}\pi\pi$ charged combinations coming from reactions (1*a*), (1*d*) and (1*e*). The full line represents a polynomial background fit.

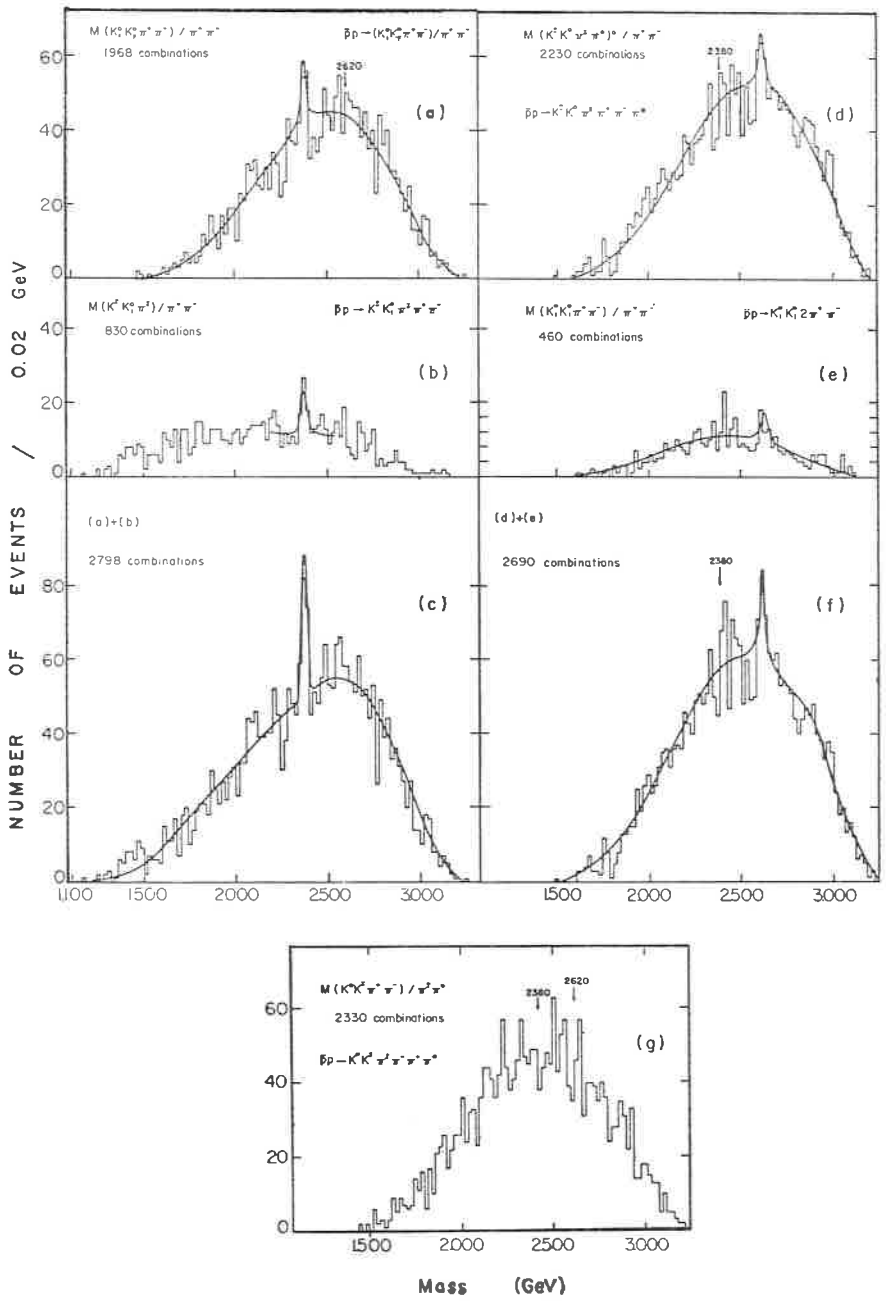

Fig. 2. – *a*) 1968 $K_1^0K_F^0\pi+\pi-$ mass combinations from reaction $\bar{p}p \to K_1^0K_F^0 2\pi+2\pi-$. *b*) 830 $K_1^0K^{\pm}\pi^{\mp}$ mass combinations from reaction $\bar{p}p \to K_1^0K^{\pm}\pi^{\mp}\pi+\pi-$. *c*) *a*) + *b*). *d*) 2230 $K_1^0K^{\pm}\pi^{\mp}\pi^0$ mass combinations from reaction $\bar{p}p \to K^{\pm}K^0\pi^{\mp}\pi+\pi-\pi^0$. *e*) 460 $K_1^0K_1^0\pi+\pi-$ mass combinations from reaction $\bar{p}p \to K_1^0K_1^0 2\pi+2\pi-$. *f*) *d*) + *e*). *g*) 2330 $K_1^0K^{\pm}\pi+\pi-$ mass combinations from reaction $\bar{p}p \to K_1^0K^{\pm}\pi^{\mp}\pi-\pi+\pi^0$. Full lines represent a fit of a polynomial background plus Breit-Wigner curves.

fit of a Breit-Wigner function with the experimental resolution folded in gives always a width compatible with zero and as before we quote in Table III the 99.7% confidence level. Since a 2σ effect is evident in the $K_1^0K_1^0\pi^+\pi^-$ mass spectrum, and no strong signal is seen in $K_1^0K_F^0\pi^+\pi^-$, we have evidence for $X(2620) \to K_1^0K_1^0\pi^+\pi^-$. Using, as before, statistical weights we predict (63 ± 25) events in the charged channel $K_1^0K^\pm\pi^+\pi^-$ which do not seem present in the spectrum of Fig. 2*g*. Furthermore in the spectrum of Fig. 1*b*, where all charged combinations are present, no signal appears favouring the assignment $I = 0$ also for this state.

For both states a search for possible decay modes $K^*\bar{K}$, $K^*\bar{K}\pi$, $K^*\bar{K}^*$, $(K\bar{K})\pi\pi$, $K\bar{K}\rho$ and $(KK\pi)\pi$ was inconclusive, as was a search for associated production via $\bar{p}p \to X^0\rho^0$. There was also no evidence for their production via the decay of some heavier boson.

We conclude that our data provide evidence for two states at the same masses and with narrow widths as the U^- meson ([1]) and the $X^-(2620)$ ([2]). However, indirect argument favours $I = 0$ in our case. Up to now, an iso-singlet state has been only found is $\bar{p}p$ formation experiment (6) at a mass of (2373 ± 10) MeV. Although the mass value agrees very well the state found in this experiment at (2374 ± 4) MeV, our narrow width is inconsistent with the width of 190 MeV.

It might be interesting to conjecture that the narrow resonances observed in production experiment correspond to states lying on the higher trajectory while the much wider structures found measuring the $\bar{p}\mathcal{N}$ total cross-sections, if really related to boson resonances, correspond to different states lying on daughter trajectories.

Furthermore an $I = 0$ assignment would indicate a degeneracy in mass of two iso-singlet and iso-triplet states which we might compare to the (ρ, ω) and (f, A_2) mass degeneracy. It should also be noted that the U(2380) bump reported here has different decay modes $(K\bar{K}\pi)$ and $(K\bar{K}2\pi)$ to that observed by Oh et al. $(K\bar{K}3\pi)$ ([8]). If the above conclusions are true the similarity in mass of such narrow objects with different *I*-spin is a striking observation at such a high value of mass.

We would like to thank Dr. A. Armenteros and Prof. Ch. Peyrou for their constant support and Dr. Jacob for discussions.

REFERENCES

1) M. N. Focacci, W. Kienzle, B. Levrat, B. C. Maglic and M. Martin: *Phys. Rev. Lett.*, **17**, 890 (1966).

2) R. BAUD, H. BENZ, B. BOSJAKOVIC, D. R. BOTTERILL, G. DAMGAARD, M. N. FOCACCI, W. KIENZLE, R. KLANNER, C. LECHANOINE, M. MARTIN, C. NEF, P. SCHÜBELIN and A. WEITSCH: *Phys. Lett.*, **30** B, 129 (1969).
3) E. W. ANDERSON, E. J. BLESER, H. R. BLIEDEN, G. B. COLLINS, D. GARELICK, J. MENES and F. TURKOT: *Phys. Rev. Lett.*, **22**, 1390 (1969).
4) A. D. JOHNSON *et al.*: submitted to *Kiev Conference* (1970).
5) C. CASO *et al.*: *Lett. Nuovo Cimento*, **3**, 707 (1970).
6) R. J. ABRAMS, R. L. COOL, G. GIACOMELLI, T. F. KYCIA, B. A. LEONTIC, K. K. LI and D. N. MICHAEL: *Phys. Rev. Lett.*, **18**, 1209 (1967) and *Phys. Rev.*, **1** D, 1917 (1970).
7) C. BRICMAN, M. FERRO-LUZZI, J. M. PERREAU, J. K. WALKER, G. BIZARD, Y. DECLAIS, J. DUCHON, J. SEGUINOT and G. VALLADAS: *Phys. Lett.*, **29** B, 451 (1969).
8) B. Y. OH, D. L. PARKER, P. S. EASTMAN, G. A. SMITH, R. J. SPRAFKA and Z. M. MA: *Phys. Rev. Lett.*, **24**, 1257 (1970).
9) J. SHAPIRO: *Suppl. Nuovo Cimento*, **18**, 41 (1960).
10) The minimum has been obtained under the hypothesis $I = 1$ for the X(2380), a $K_1^0K_2^0\pi^+\pi^-$ decay, and averaging over all $\bar{p}p$ and $\pi\pi$ isotopic spin states. If the X(2380) should more generaly decay in $K^0K^0\pi^+\pi^-$ the minimum increases by a factor two.

Upper limit to the $\bar{p}p$ coupling of the S(1929) meson (*)

R. BIZZARRI, P. GUIDONI and F. MARZANO
Istituto di Fisica dell'Università - Roma
Istituto Nazionale di Fisica Nucleare - Sezione di Roma

E. CASTELLI, P. POROPAT and M. SESSA
Istituto di Fisica dell'Università - Trieste
Istituto Nazionale di Fisica Nucleare - Sezione di Trieste

1. Introduction.

The observation with the CERN missing mass spectrometer of a very narrow resonance at a mass of 1929 MeV/c^2 [1] has stimulated the search for its possible coupling to the $\bar{p}p$ sistem. The low energy $\bar{p}p$ elastic scattering cross section is dominated by a conspicuous forward peak apparently due to diffraction, and consequently the detection of a highly inelastic resonance from the energy dependence of the elastic cross section appears very difficult. However it has been pointed out by Cline *et al.* [2] that a much better sensitivity to the possible presence of a resonant $\bar{p}p$ interaction can be achieved by looking at the energy dependence of the backward scattering cross section, away from the forward diffraction peak.

It is the purpose of this letter to show that published data on $\bar{p}p$ cross sections together with new data on $\bar{p}n$ annihilation cross section in the momentum range (350÷580) MeV/c allow to place a significant upper limit on the possible contribution of a resonant interaction to the backward $\bar{p}p$ elastic cross section, if the resonance has a mass between 1915 and 1945 MeV and a width between 10 and 40 MeV.

2. Data.

The values of the $\bar{p}p$ and $\bar{p}n$ annihilation cross sections in this energy interval are shown in Fig. 1. The $\bar{p}p$ data have already been published [3].

(*) Invited paper presented by R. Bizzarri

The $\bar{p}n$ data have been obtained in a similar way from three different exposures of the deuterium-filled 81 cm Saclay bubble chamber to a separated antiproton beam from the CERN P.S.

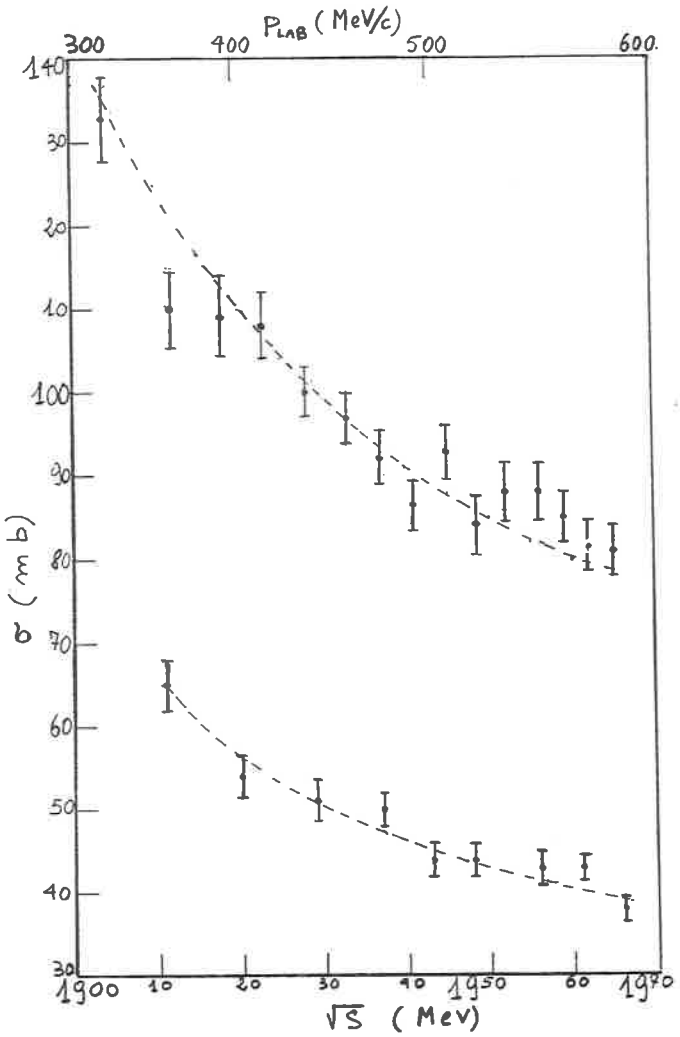

Fig. 1

The beam momenta for the three exposures were 467, 549 and 612 MeV/c at the entrance of the illuminated region of the chamber. The $\bar{p}$ interactions have been measured if they occurred in a restricted fiducial region about

48 cm long, in order to ensure at least 6 cm of illuminated track for the interacting particle. Furthermore the primary tracks were requested to enter the chamber inside a well defined beam window and within a well defined cone (0.05 sr) about the average beam direction. In this way an energy definition of the beam (r.m.s. spread of a nearly gaussian distribution) corresponding to $\pm$ 5 cm of liquid deuterium was obtained. (The absolute energy calibration of the beam is known to better than 5 MeV). For each exposure the events have then been divided into three groups 16 cm wide according to the path length of the antiproton inside the fiducial region.

From the observation of 46 km of $\bar{p}$ track, about 38 000 good interactions have been measured. A full account of the results obtained is in preparation. For the present purpose only annihilation events with an odd number of prongs have been considered. They can be interpreted as $\bar{p}n$ annihilation with the emission of a « spectator » proton too slow to give a visible track (momentum $\leqslant$80 MeV/c). This cut on the proton momentum reduces the spread on the $\bar{p}n$ total energy in the c.m.s. due to the neutron Fermi motion to a level negligible as compared to the 16 cm grouping of the data, and furthermore ensures a minimum contamination from « non spectator » events in which the proton has taken part to the reaction. 5965 such events have been found, divided into 9 energy intervals. The resulting cross section is shown in Fig. 1. From the observed number of annihilations with a visible proton track these cross sections can be estimated to represent $\sim 60\%$ of of the $\bar{p}n$ annihilation cross section. Corrections due to the shadow of the proton can be estimated to be $\leqslant 10\%$, and because of their smooth energy dependence can be neglected for our purposes.

3. Analysis.

It is apparent from Fig. 1 that the energy dependence of the annihilation cross- section is a smooth one and no evidence for bumps is seen. In fact a curve $\sigma = a\lambda\!\!\!^{-}$ gives an excellent fit to both $\bar{p}p$ and $\bar{p}n$ data (Fig. 1) ($\lambda\!\!\!^{-}$ being the wavelength of the $\bar{p}n$ relative motion). To place a quantitative limit on the possible resonance production we consider that a resonance of spin J and elasticity $x = \Gamma_{\bar{p}p}/\Gamma_{tot}$ should produce in the inelastic [4] $\bar{p}p$ cross sections an enhancement

$$\Delta\sigma(m) = \Delta\sigma(m_0)\,\frac{\Gamma_{tot}/2}{(m-m_0)^2 + \Gamma_{tot}/2} \qquad (1)$$

with

$$\begin{aligned}\Delta\sigma(m_0) &= \pi\lambda\!\!\!^{-2}(2J+1)x(1-x)\\ &\simeq \pi\lambda\!\!\!^{-2}(2J+1)x\,,\end{aligned} \tag{2}$$

m being the $\bar{\mathrm{p}}\mathrm{p}$ invariant mass.

If the I-spin of the resonance is zero no enhancement is expected in the $\bar{\mathrm{p}}\mathrm{n}$ cross section, while an $I=1$ resonance should produce a similar enhancement with intensity $\Delta\sigma'(m_0) = 2\cdot 0.6\cdot\Delta\sigma(m_0)$ (the factor 2 being due to the pure $I=1$ initial state while 0.6 accounts for the loss of energetic protons).

The data of Fig. 1 have therefore been fitted with the expression

$$\sigma(m) = c + a\lambda\!\!\!^{-} + \Delta\bar{\sigma}(m)$$

$\Delta\bar{\sigma}$ being the average of $\Delta\sigma$ over the finite size of the energy interval and c, a, $\Delta\sigma(m_0)$ being free parameters. The constant term c has been added to give to the background representation more freedom to accommodate resonances. The maximum allowed $\Delta\sigma(m_0)$ has been determined for different values of the resonance mass and width in the intervals $1915 \leqslant m_0 \leqslant 1955$ MeV/c and $10 < \Gamma < 40$ MeV. (For values of Γ outside this interval the data become rapidly insensitive to the possible presence of a resonance). In this way, for m_0 in the interval 1915÷1945 we obtain for the elasticity x the limits (at 95% confidence level)

$$\begin{aligned} x(2J+1) &< 0.15 \qquad \text{if } I=1\\ x(2J+1) &< 0.40 \qquad \text{if } I=0\,.\end{aligned}$$

A small shoulder is present in both cross sections at 1955 MeV. It has no statistical significance but its presence increases the limits we can place on $x(2J+1)$ about this value of m_0: They are $\simeq 0.5$ for $I=1$ and $\simeq 1.0$ for $I=0$.

4. Backward scattering.

If the resonance if formed by the singlet $\bar{\mathrm{p}}\mathrm{p}$ state its angular distribution is described by $|Y_j^0(\cos\theta)|^2$ and the resonant contribution to the backward cross section is

$$\frac{\mathrm{d}\sigma^R}{\mathrm{d}\Omega}(180°) = \sigma_{\mathrm{el}}\,\frac{2J+1}{4\pi} = \left(\frac{\sigma_t}{2\pi\lambda\!\!\!^{-}}\right)^2 = \left(\frac{1}{2}\,\lambda\!\!\!^{-}(2j+1)x\right)^2.$$

With the above limits on $x(2J+1)$, one obtains

$$\frac{d\sigma^R}{d\Omega}(180°) \begin{cases} < 0.06 \text{ mb/sr} & \text{if } I=1 \\ < 0.4 \text{ mb/sr} & \text{if } I=0 \end{cases} \tag{3}$$

for $1915 \leqslant m_0 \leqslant 1945$. For $m_0 = 1955$ the limits become 0.3 or 1.2 mb/sr for $I = 1$ or 0 respectively.

If the resonance is formed by the triplet $\bar{p}p$, the differential cross section will be a combination of $|Y_j^0(\cos\theta)|^2$ with $|Y_j^1(\cos\vartheta)|^2$ and $|Y_j^2(\cos\vartheta)|^2$ and the backward cross section is expected to be smaller ([5]).

The above limits should be compared with the expected diffraction background in this momentum interval. As the antiproton momentum p varies between 350 and 550 MeV/c the total c.m.s. energy varies of only 40 MeV but the momentum transfer corresponding to backward scattering varies like p. Assuming a diffraction cross section $d\sigma/dt = A \exp[-(R/2)^2 t]$ the contribution to the 160° cross section is expected to decrease from 0.6 to 0.08 mb/sr as ρ varies in the above interval. A diffractive background of the type ([6]) $d\sigma/dt = AJ_1^2(R\sqrt{|t|})/|t|$ on the contrary gives a contribution increasing with p from 0.02 to 0.5 mb/sr and going through a broad maximum of 0.6 mb/sr at ($p \simeq 620$) MeV/c. A more elaborate diffractive model ([7]) predicts instead a maximum of (≈ 0.35) mb/sr at ($p \approx 500$) MeV/c. These cross sections anyway are of comparable magnitude to the maximum expected resonant contribution.

In the presence of interference with a large non resonant amplitude the effect of a possible resonance could of course be bigger than the above limits. In this case however, due to the rapid energy variation expected for the background, the determination of the resonance properties (mass, width, spin ecc.) from this channel would be very difficult.

The above considerations apply to the 180° cross sections. In comparing with the experimental data taken over a finite angular interval, one should consider that a resonant differential cross section is expected to have a more or less sharp maximum at 180° ([8]) and therefore averaging over a finite angular interval will reduce its contribution to the cross-section. The same is not necessarily true for the diffractive background.

5. Conclusions.

The available data on the $\bar{p}p$ and $\bar{p}n$ annihilation cross-sections allow to place limits on the coupling to the $\bar{p}p$ channel of a possible boson resonance

in the mass interval (1915÷1945) MeV and 10 to 40 MeV wide. Consequently the detection of such a resonance from the study of $\bar{p}p$ elastic scattering, even in the backward direction, appears very difficult.

The main reason for the sensitivity of the inelastic cross-section to the presence of a $\bar{p}p$ resonance in this mass region rests in the large value of $\lambda\!\!\!^{-}$, the upper limit to the resonant cross-section being itself a rather high one (5 or 13 mb for $I = 1$ or 0 respectively). Therefore the detection of a possible resonance might be easier via the study of the annihilation channels.

The energy dependence of the backward $\bar{p}p$ cross-section has been studied with good statistics by the Wisconsin group ([2,9]) for $\bar{p}$ momenta between 300 and 700 MeV/c. Their most recent revised results ([9]) show the presence of a significant peak in the differential cross-section averaged in the interval $(-1.0 \leqslant \cos\vartheta \leqslant -0.9)$. This structure, approximately 40 Mev wide, occurs at a $\bar{p}$ momentum of (~ 450) MeV/c with a height of (~ 7) mb on a negligible background. In the light of the above discussion the interpretation of this peak as the effect of a unique *s*-channel resonant state appears very difficult, and it could probably be interpreted more easily as the manifestation of a secondary diffraction peak.

REFERENCES

1) G. Chikovani *et al.*: *Phys. Lett.*, **22**, 233 (1966); M. N. Focacci *et al.*: *Phys. Rev. Lett.*, **17**, 890 (1966).
2) D. Cline, J. English, D. D. Reeder, R. Terrel and J. Twitty: *Phys. Rev. Lett.*, **21**, 1268 (1968).
3) U. Amaldi Jr. *et al.*: *Nuovo Cimento*, **46**, 171 (1966).
4) Since no appreciable bumps are present in the energy dependence of $\bar{p}p$ elastic cross-section (ref. ([3])), the elasticity x of a possible resonance is expected to be small. For this reason we have made the search in the inelastic cross-section, instead that in the total one, and we shall neglect x compared to 1 in formula (2). Another reason to study only the inelastic cross-section is that in $\bar{p}d$ interaction a clear separation between scattering on neutron and on proton is impossible due to the small average momentum transfer.
5) The scattering amplitude is the average of four amplitudes characterized by a spin index i ($i = S, M_s$) and for each of them the optical theorem $\mathrm{Im}\, T_{ii} = \sigma_i$ holds. A resonant amplitude is purely imaginary and gives a symmetric angular distribution (neglecting interference with nonresonant background). For the single $\bar{p}p$ state only one T_{ii} is different from zero and eq. (3) follows. For the triplet state three amplitudes can contribute and the backward cross-section has the upper bound given by eq. (3) and a lower bound 3 times smaller.
6) B. Conforto *et al.*: *Nuovo Cimento*, **54 A**, 441 (1968).

7) J. K. YOH *et al.*: *Phys. Rev. Lett.*, **23**, 506 (1969).
8) J. LYS: University of Michigan Bubble Chamber Group, Research note no. 91/68 (unpublished).
9) D. CLINE, J. ENGLISH and D. D. REEDER: *Evidence for a narrow, high spin boson state with mass* 1925 MeV, paper presented at the *Kiev Conference*, April 1970, and circulated preprint.

Search for heavy neutral mesons in $\bar{p}p$ annihilations (*)

K. COHEN, B. MAGLIC, J. NOREM
F. SANNES, M. SILVERMAN and K. VOSBURGH
The State University of New Jersey - Rutgers, N. J.

G. CVIJANOVICH and M. S. MATIN
Upsala College of New Jersey - Upsala, N. J.

We are attempting to measure the energy dependence of the $\bar{p}p$ annihilations to look at direct channel formation of heavy meson ($2.1 < M < < 2.8$ GeV). Evidence ([1,3]) in favour of this process has been seen in

1) total cross sections;
2) backward elastic scattering;
3) angular distributions and forward backward asymmetries in $\bar{p}p \to \pi\pi$;
4) specific final states such as $KK\omega$, $\rho\rho\pi$, etc. seen in bubble chamber experiments.

We are now attempting a new experiment which combines some of the selectivity of a bubble chamber with the statistics of a total cross section type experiment. Good mass resolution should also be possible, ($\Delta M = \pm 5$ MeV).

Assuming the ratio of decays of heavy mesons into $\bar{p}p$ states is a small fraction of the total because of the large numbers of annihilation channels open, one would expect that the resonant signal should be largest in the third of the total cross section which is due to annihilation. Elastic scattering and inelastic scattering comprise the remaining two thirds of the total cross section.

In the reaction

$$a + b \to a' + b' + c + d + \ldots$$

(*) Invited paper presented by J. Norem.

the particles a' and b', when observed in the centre of mass, tend to continue in the direction they were giving before the interactions. Created particles tend to be produced with comparatively little momentum in the centre-of-mass.

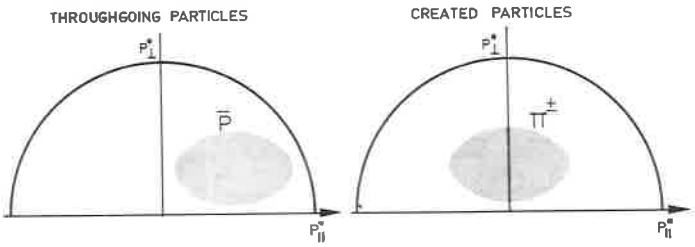

Fig. 1A

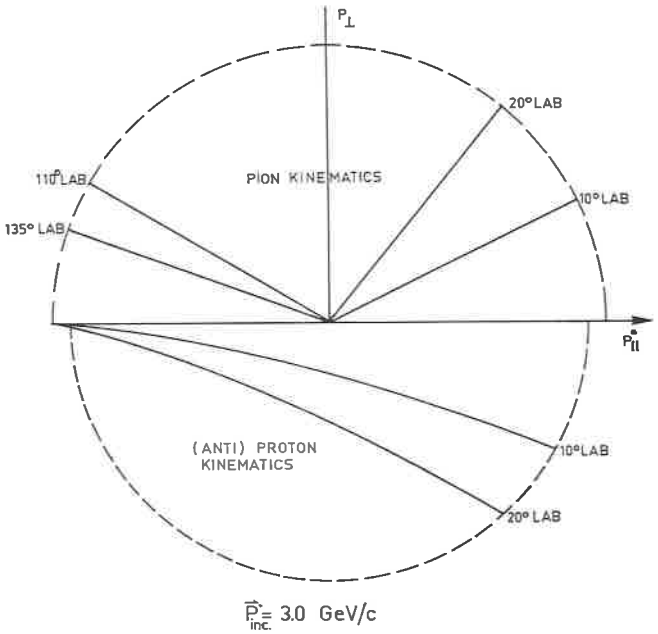

Fig. 1B

This behaviour is shown in Fig. 1*a*. The thermodynamic model ([4]) gives a particularly clear picture of this behaviour. Annihilation states are similar to reactions where only created particles exist, and the products are roughly isotropic in the centre-of-mass.

If one considers the kinematics of the $\bar{p}p$ situation shown in Fig. 1*b* it can be seen that the majority of antinucleons surviving an interaction are fairly well collimated forward in the Lab. whereas meson products are much

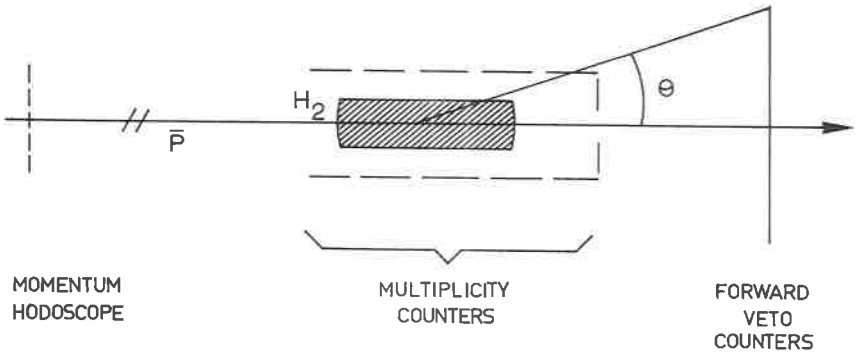

Fig. 2a

more istropic. Using this fact we can isolate annihilations simply by looking at $\bar{p}p$ interactions where particles do not go forward.

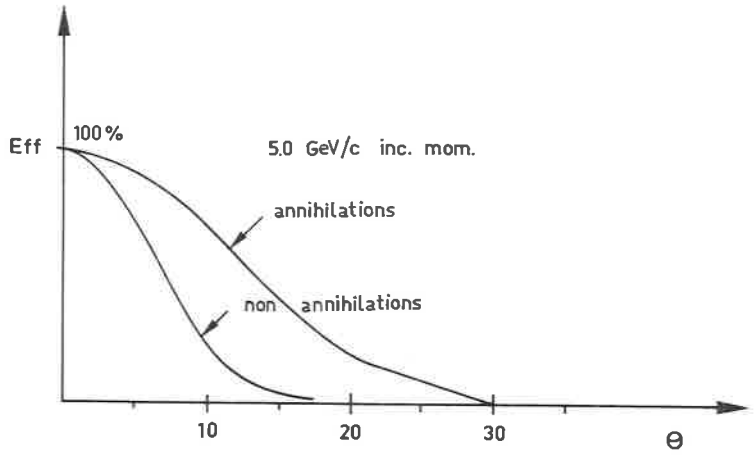

Fig. 2b

Our apparatus is shown in Fig. 2*a*. A hydrogen target is followed by large anti-counters and surrounded by counters to measure multiplicity.

The efficiency of the apparatus for detecting annihilation and nonannihilation final states is shown in Fig. 2*b*. This efficiency is dependent on charged multiplicity and incident energy. In all cases, however, the efficiency for non-annihilation events drops off much faster than for annihilations of the same multiplicity.

We will also attempt to look at charged multiplicity because annihilation final states have higher multiplicities than non-annihilations, particularly at low energies. By this means we hope to isolate the cause of the « bumps » in the total cross sections ([5]) at 1.3 and 1.7 GeV/c either as a resonance:

$$\bar{p}p \to M \to \text{pions} \qquad (0, 2, 4, 6, \ldots, \text{prongs})$$

or as a single pion threshold effect ([6]):

$$\left.\begin{aligned} \bar{p}p &\to \bar{p}p\pi^0 \\ &\quad \bar{n}p\pi^- \\ &\quad \bar{p}n\pi^+ \end{aligned}\right\} (0, 1, 2 \text{ prong}) .$$

Unfortunately, because of problems in scheduling and target stability it is not possible to present data at this time.

REFERENCES

1) L. Montanet: *Proceedings of the Lund Conference on Elementary Particles*, Lund, Sweden (June 1969) (Berlinska Boktryckerict, Lund, Sweden, 1969).
2) G. R. Kalbfleisch: in *Experimental Meson Spectroscopy*, edited by Baltay and Rosenfeld (Columbia Univ. Press, New York, 1970).
3) G. A. Smith: *Experimental Meson Spectroscopy*, edited by Baltay and Rosenfeld (Columbia Univ. Press, New York, 1970).
4) R. Hagedorn: *Nucl. Phys.*, B **24**, 93 (1970).
5) R. J. Abrams, R. L. Cool, G. Giacomelli, T. F. Kycia, B. A. Leontic, K. K. Li and N. Michael: *Phys. Rev. Lett.*, **18**, 1209 (1967).
6) W. A. Cooper, L. G. Hyman, W. Manner, B. Musgrove and L. Voyvodic: *Phys. Rev. Lett.*, **20**, 1059 (1968).

Antinucleon - Nucleon two body reactions at 1,2 GeV/c(*)

NEUCHATEL-LAUSANNE COLLABORATION

We have analysed two pronged events and zero pronged events with associated odd pronged stars produced by antiprotons of 1.2 GeV/c in hydrogen bubble chambers. In order to select the two body events, we have applied a test of coplanarity to the two pronged stars in the scanning procedure.

1. Elastic scattering.

About 20000 pictures taken at 1,20 GeV/c incident momentum were scanned in order to find elastic scattering collisions in a limited fiducial volume. In order to eliminate the large number of diffraction events, stars containing protons which stopped in the chamber were eliminated. The selected events were measured with IEP ENETRA and processed with standard programms THRESH and GRIND.

Figure 1 represents the angular distribution obtained for the reaction $\bar{p}p \to \bar{p}p$ for $\cos\theta^* \leqslant 0{,}5$. One sees the characteristic dip-bump structure of antiproton-proton elastic scattering. The distributions measured at 1.18 GeV/c by R. Cooper ([2]) and at 1.23 GeV/c by a Liverpool-Rutherford Laboratory Collaboration ([3]) are in very good agreement with ours and the summed distributions depict with precision the positions of the two minima at:

$$\cos\theta^* = \quad 0.35 \quad \text{or} \quad t = -0.36 \ (\text{GeV/c})^2$$

$$\cos\theta^* = -0.65 \quad \text{or} \quad t = -0.90 \ (\text{GeV/c})^2 .$$

(*) Contributed paper submitted by E. Jeannet. Institute de Physique de l'Université Neuchâtel.

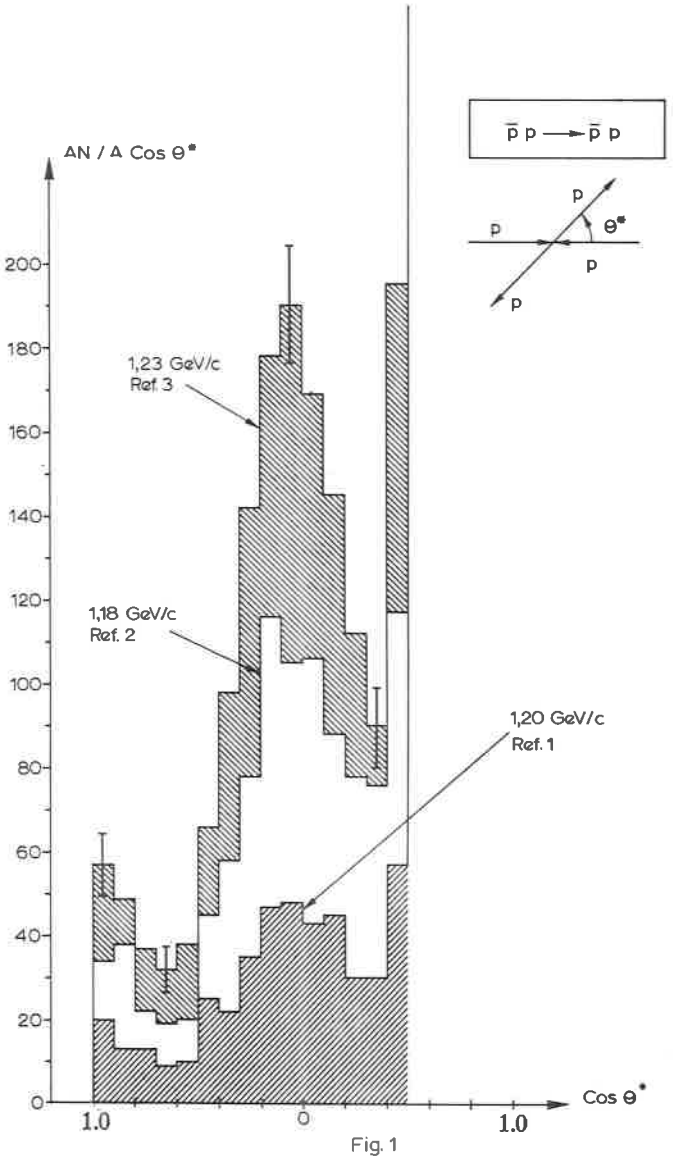

Fig. 1

Figure 2 represents the values of the momentum transfer squared (t_{min}) corresponding to minima of $d\sigma/d\Omega$ as a function of the center of mass momentum (log scale) found by different authors ([4]).

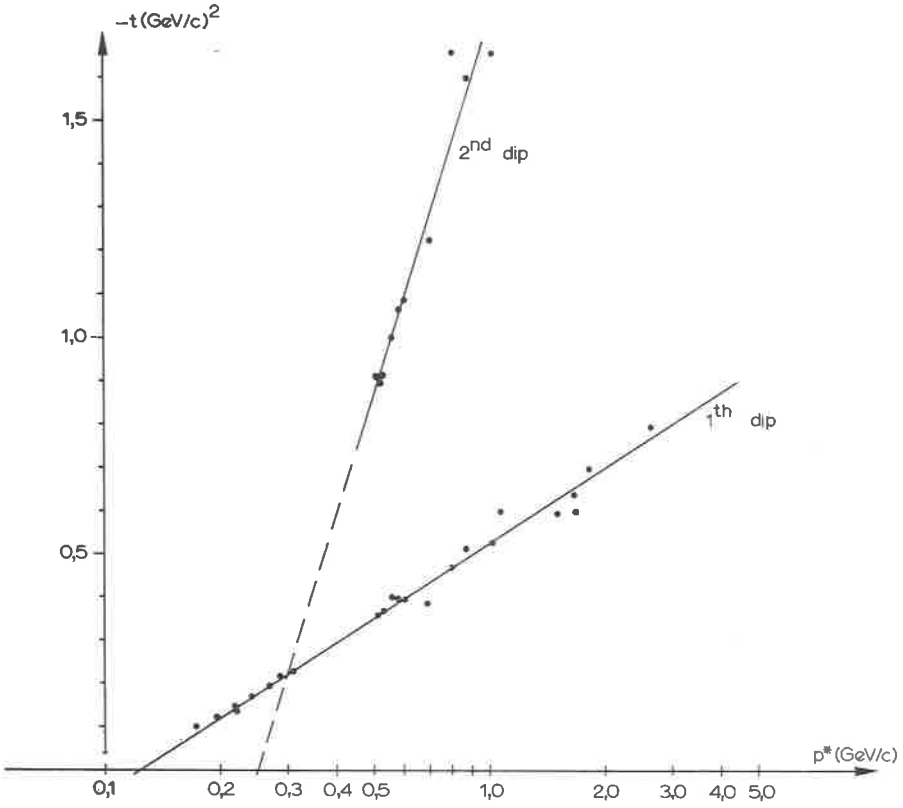

Fig. 2

This figure shows a clear connection between $t_{\min}$ and p^*. The empirical relation:

$$-t = a \ln (p^*/p_0)$$

with $a = 0{,}25\ (\mathrm{GeV/c})^2$, $p_0 = 0{,}12$ GeV/c for the first minimum and $a = 1.49\ (\mathrm{GeV/c})^2$, $p_0 = 0.25$ GeV/c for the second one, adequately describes the positions of these minima. The parameter p_0 can be interpreted as the linear momentum threshold which allows the angular momenta $l = 1$ and $l = 2$ for an impact parameter of $R \simeq 1.5$ fm.

In an extension of this experiment, 30000 pictures taken for incident momenta of 1.12, 1.23, 1.30 and 1.36 GeV/c were specially scanned for

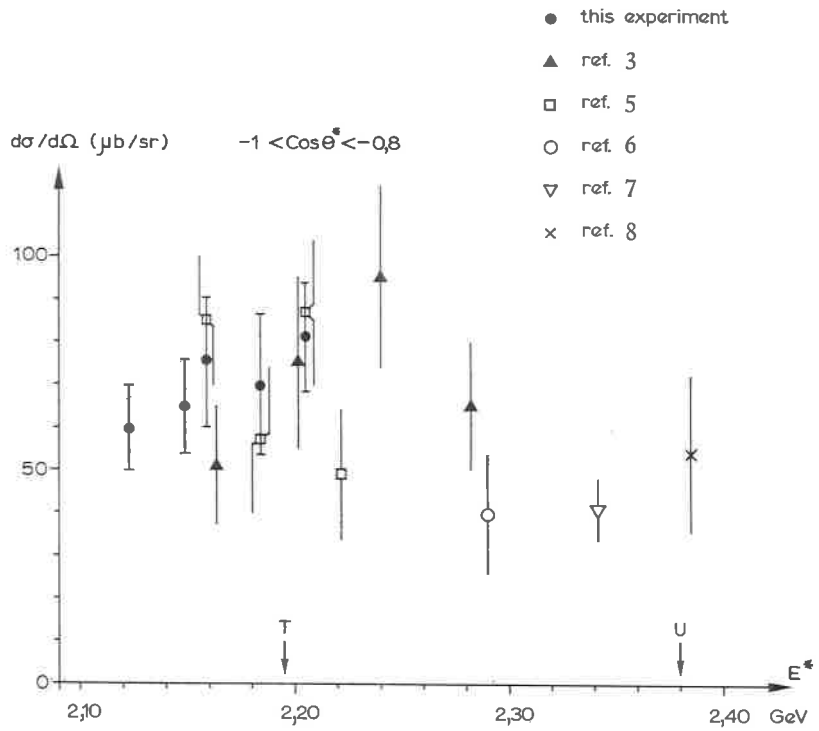
this experiment
ref. 3
ref. 5
ref. 6
ref. 7
ref. 8
dσ/dΩ (μb/sr)
−1 <Cosθ*<−0,8
100
50
0
T
U
E*
2,10
2,20
2,30
2,40 GeV

Fig.3

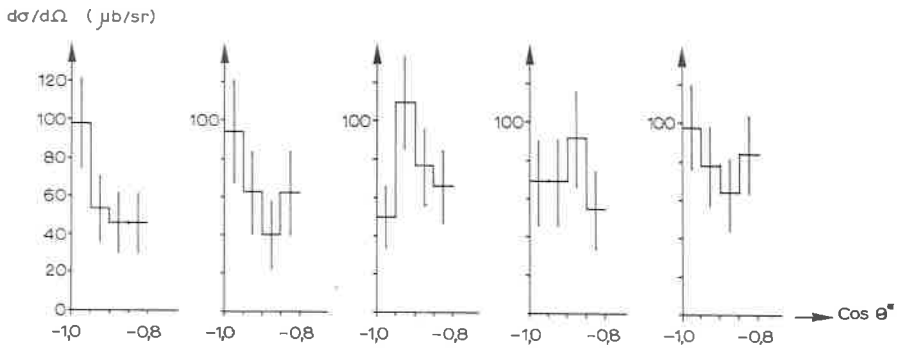
dσ/dΩ (μb/sr)
120
100
80
60
40
20
0
−1,0
−0,8
Cos θ*
p = 1,12 GeV/c
E* = 2,12 GeV
1,20 GeV/c
2,15 GeV
1,23 GeV/c
2,16 GeV
1,30 GeV/c
2,18 GeV
1,36 GeV/c
2,20 GeV

Fig 4

backward scattering. Figure 3 represents our results for the elastic differential cross section ($\cos\theta^* \leqslant -0.8$) compared with the results of other experiments. No fine structure corresponding to the effect of the meson T(2195) in the direct channel can be seen.

Figure 4 represents the differential cross section obtained by combining our results with those of references ([2,3]); the normalization is calculated on the basis of our scanning.

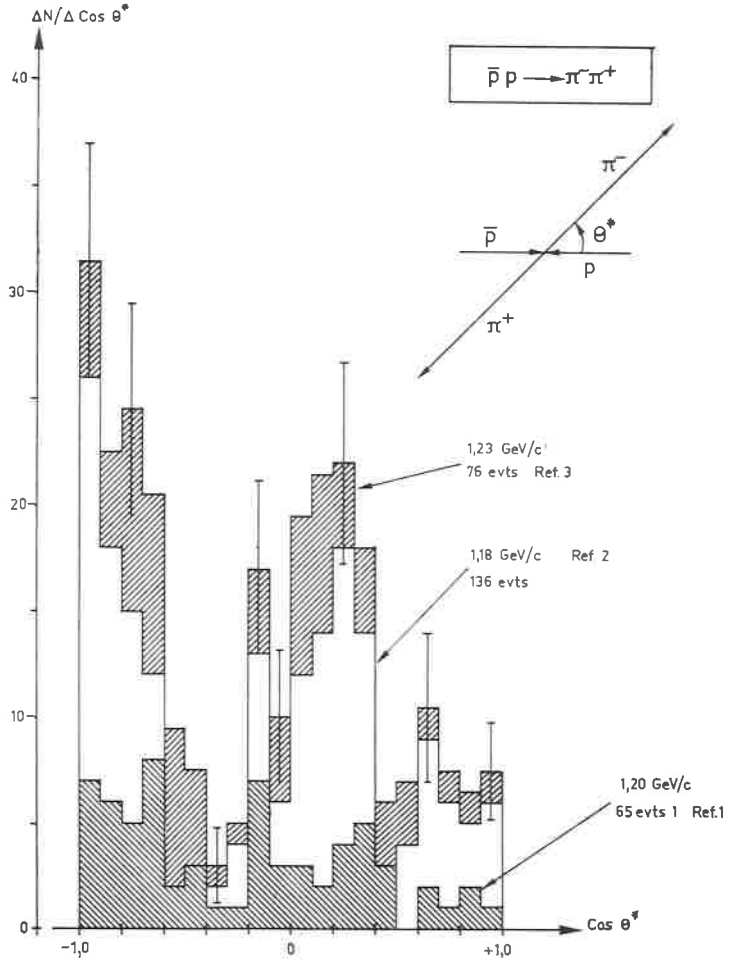

Fig. 5

2. $\bar{p}p$ annihilations into $\pi^-\pi^+$ and K^-K^+.

These types of events were also observed in our scanning for elastic scattering at 1.20 GeV/c. We have found the following cross sections:

$$\sigma(\bar{p}p \to \pi^-\pi^+) = (157 \pm 20)\ \mu b$$

$$\sigma(\bar{p}p \to K^-K^+) = (\ 40 \pm 10)\ \mu b\ .$$

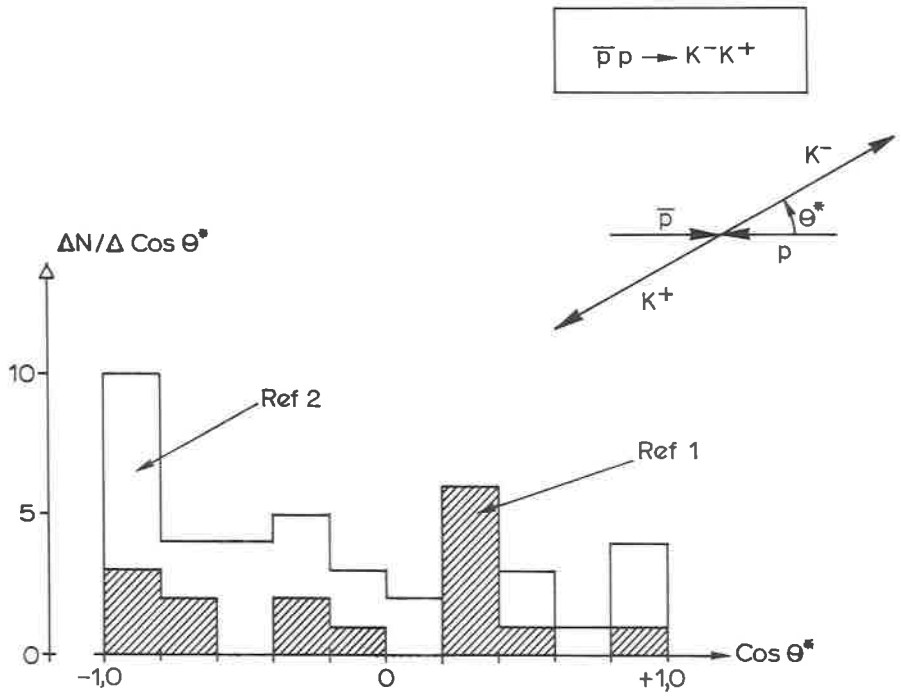

Fig.6

The π^- angular distribution is strongly anisotropic, with the π^- preferentially emitted at $\theta^* \simeq 80°$ and $\theta^* \simeq 180°$. Figure 5 represents the combined results of references [1,3]. Figure 6 shows the combined distribution for the $\bar{p}p \to K^-K^+$ angular distribution [1,2].

3. Charge exchange: $\bar{p}p \to \bar{n}n$.

A total of 113000 pictures taken at 1.12, 1.18 and 1.20 GeV/c incident momenta were scanned for zero pronged events with associated stars (47000 pictures taken in HBC 81 were examined for 3, 5 and 7 pronged stars, the rest, taken in HBC 200, were examined only for 5 and 7 pronged stars). The 1178 events found were analysed kinematically for the process: $\bar{p}p \to \bar{n}n$ followed by $\bar{n}p \to$ pions, with the following results:

4 C	FIT:	150 events,
1 C	FIT:	565 events,
NO	FIT:	463 events,

(No fit events are multineutrals, kaonic annihilations or incorrect associations).

The number of stars incorrectly associated with zero pronged events was evaluated to be 6% of the total number of observed stars.

Figure 7 shows the angular distribution of the antineutrons. Each event was given a weight equal to the inverse of its detection probability $P = 1 - \exp[-L/\lambda]$ where L is the potential path of the antineutron in a definite fiducial volume and $\lambda = 1/N\sigma$ is the mean free path of antineutrons in for the observed star events. A correction for the 6% of incorrect associations has been incorporated.

The charge exchange distribution is strongly peaked in the forward direction and displays some structure at large angles.

The measured charge exchange cross section was found to be

$$\sigma_{ex} = (6.8 \pm 0.4)\ \text{mb}$$

when corrected for inelastic charge exchange and zero pronged annihilation events. The differential cross section for $\cos\theta \leqslant -0{,}8$ was found to be

$$d\sigma/d\Omega = (340 \pm 70)\ \mu\text{b/sr}$$

This cross section is 5.2 ± 1.5 times larger than the differential elastic cross section at the same angles (see Fig. 3). This result is in contradiction with

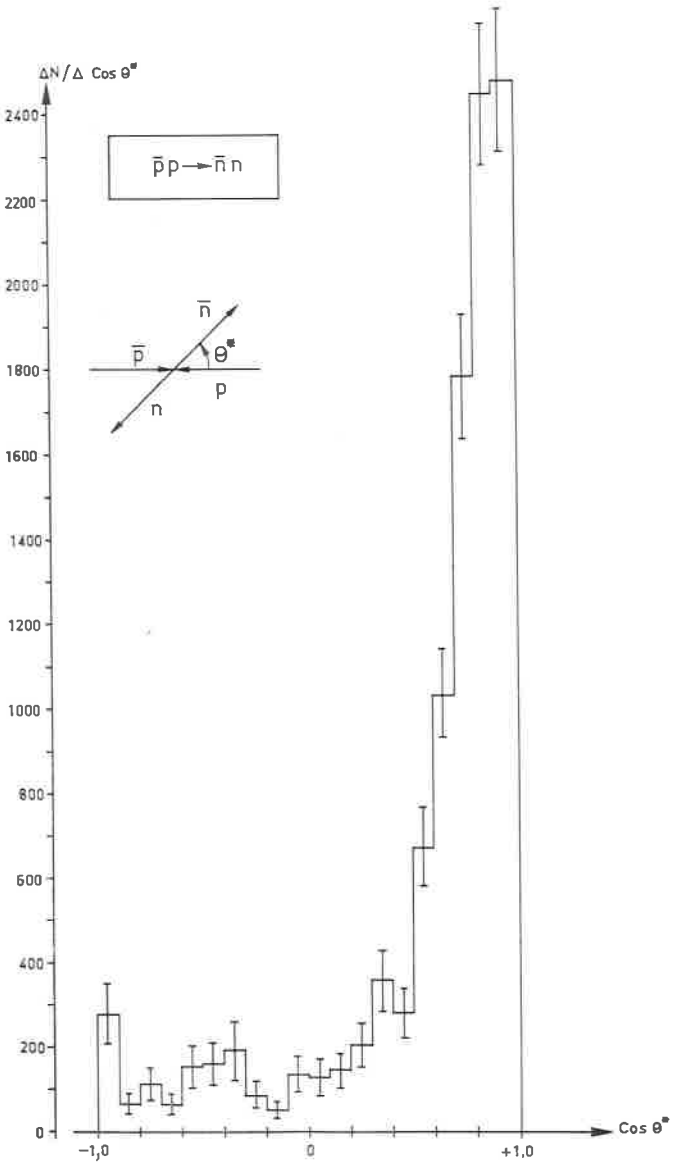

Fig. 7

the hypothesis of a process dominated by a bosonic resonance in the direct channel which predict equal differential cross section for $\bar{p}p \to \bar{p}p$ and $\bar{p}p \to \bar{n}n$ at $\theta^* = 180°$.

REFERENCES

1) M. BOGDANSKI: *Thesis*, Université de Neuchâtel (1971).
2) R. COOPER: *Thesis*, University of Liverpool (1969).
3) R. A. DONALD *et al.*: Preprint (communication to the *Kiev Conference*, 1970).
4) D. D. CLINE *et al.*: *Phys. Rev. Lett.*, **21**, 1268 (1968); CH. D'ANDLAU *et al.*: Preprint Collège de France (1970); ref. (1) and (3); C. DAUM *et al.*: *Nucl. Phys.*, B **6**, 617 (1968); T. FERBEL *et al.*: *Phys. Rev.*, **137** B, 1250 (1965); K. BOCKMANN *et al.*: *Nuovo Cimento*, **42** A, 954 (1966); T. KITEGAKI *et al.*: *Phys. Rev. Lett.*, **21**, 175 (1968); T. FERBEL *et al.*: *Phys. Rev.*, **173**, 1307 (1968); D. BIRNBAUM *et al.*: *Phys. Rev. Lett.*, **23**, 663 (1969).
5) W. A. COOPER *et al.*: *Nucl. Phys.*, B **16**, 155 (1970).
6) J. LYS *et al.*: *Phys. Rev. Lett.*, **21**, 116 (1968).
7) Z. M. MA *et. al.*: *Communication to the XIV th International Conference on High Energy Physics*, Vienna (1968).
8) G. R. LYNCH *et al.*: *Phys. Rev.*, **131**, 1276 (1960).

Search for a direct channel effect in the reaction $\bar{p}p \to \rho^0 \rho^0 \pi^0$ in the c.m. energy-range (2.10 ÷ 2.22) GeV (*)

H. BRIAND, J. DUBOC, B. DURUSOY and F. LEVY
Institut de Physique Nucléaire - Paris
R. A. DONALD, D. N. EDWARDS and J. K. GIBBINS
The University of Liverpool - Liverpool

115000 4 prong antiproton-proton annihilations have been measured and analyzed in a formation experiment where the incident antiproton momentum lies in the range 1.1÷1.47 GeV/c. Several observations have been done in this energy range (2.10÷2.22 GeV) which covers widely the T meson region ([1-7]).

55000 5π events have been identified and studied in order to search confirmation for a possible direct channel effect at the T position ([6]), in the reaction:

$$\bar{p}p \to \rho^0\rho^0\pi^0 .$$

For technical reasons, the results presented here correspond only to half of the statistics.

In order to avoid biases due to energy loss in the 2 m hydrogen bubble chamber the number of events at each point has been connected, not to the nominal energy value, but to the total energy in the $\bar{p}p$ c.m. system, calculated for each event after measurement and fit. In this way, the energy range is divided into energy bands and we give in Table I, the number of 4 prong and 5π events in each band.

(*) Contributed paper submitted by F. Lévy.

TABLE I.

c.m. Energy	2.10÷2.12	2.12÷2.14	2.14÷2.16	2.16÷2.18	2.18÷2.20	2.20÷2.22
No. of 4 prong events	7941	15381	3323	13944	18210	8952
No. of 5π events	3099	5981	1223	4803	6387	2947

In this Table:

— all 5π events with probability $< 10\%$ have been rejected;

— 5π events with (MM²) beyond 4 standard deviations from the central $M^2_{\pi^0}$ value have been removed.

As presented in Fig. 1, the distribution $m(\pi^+\pi^-)$ associated with a ρ^0 (defined as $0.680 \leqslant m_{\varrho^0} \leqslant 0.800$ GeV/c_2) exhibits in the whole energy range a bump at the position of the ρ^0 which is particularly obvious at 1.33 GeV/c. However, the intensity of the peak is very sensitive to contamination of events with more than one π^0 and it has been necessary to practise missing mass and probability cuts, much more severe than those mentioned above.

An empirical extrapolation law has been obtained using a 3×2 matrix cuts at Γ, $\Gamma/2$ missing mass squared and 10, 20, 30% probability. A maximum likelihood fit at energy E has been done for these 6 possibilities and the results (presented in Table II) have been properly corrected for the cuts. The correction coefficient is obvious for probability cuts; it is written between brackets for cuts in the Gauss curve.

TABLE II.

	$\Gamma/2$ (1/0.45)		Γ (1/0.76)	
0.30	155	344	227	299
	221	469	324	426
0.20	162	360	265	348
	202	449	331	435
0.10	162	360	279	367
	180	400	310	486

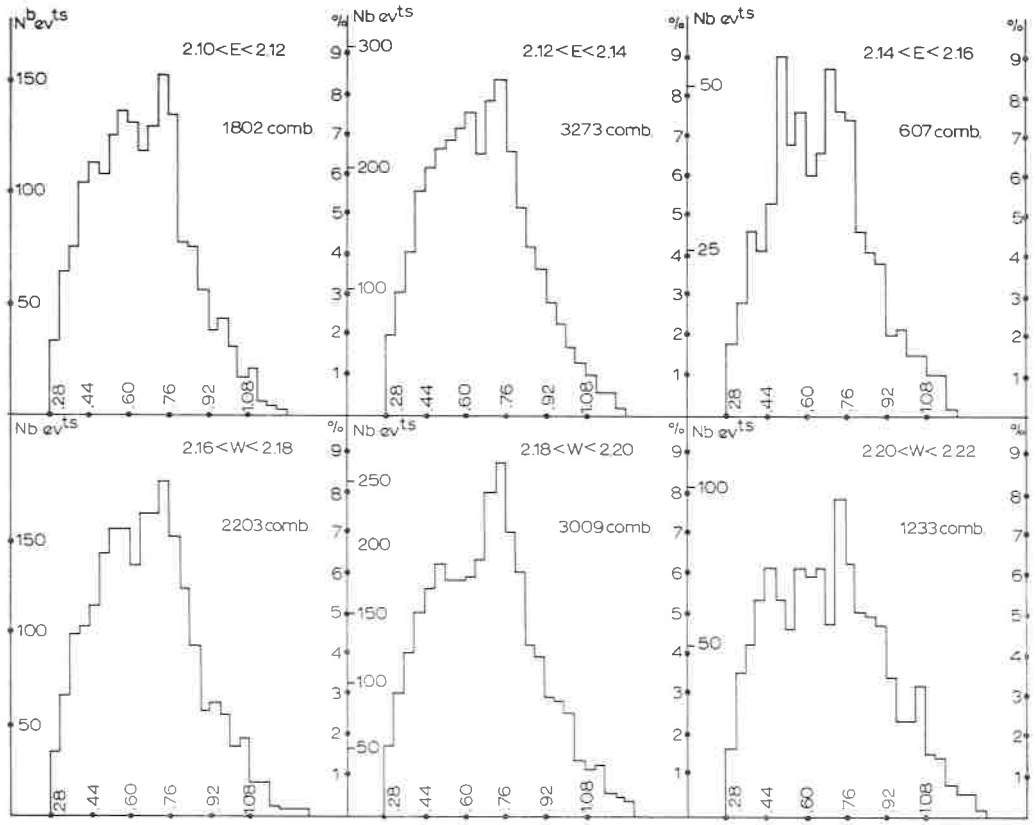

Fig. 1. – Distribution of $M(\pi^+\pi^-)$ associated with a ρ^0 at six regions of center-of-mass energy spanning the T meson.

The idea is the following: if we start from different experimental values (corresponding to different cuts), we should get the same final figure after appropriate physical corrections. In fact, we get 6 different figures but their dispersion around the central value:

$$\bar{n} = 444 \pm 30$$

is much smaller than the uncertainly resulting from the fit: $n = 435 \pm 140$. This result gives us confidence in our method.

Cuts at 20% probability and one (MM^2) standard deviation have been accepted and used in our fitting procedure.

A maximum likelihood fit has been performed at the 6 energy values

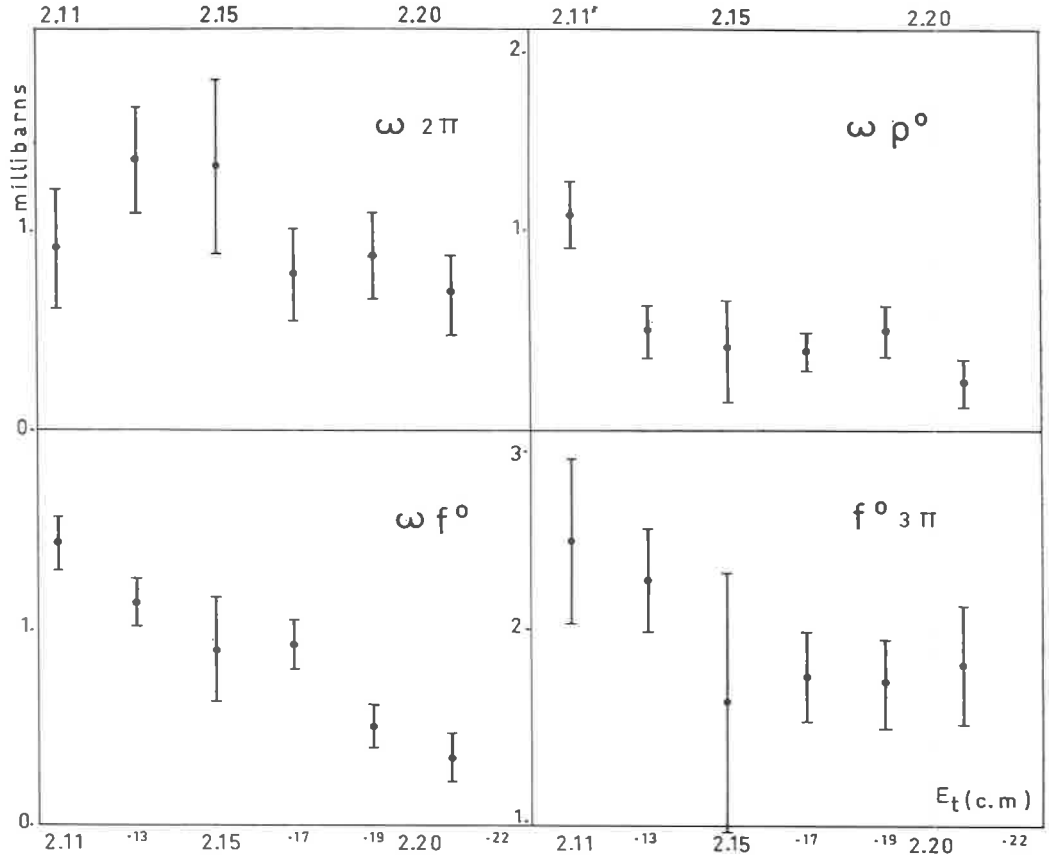

Fig. 2. – Results of a maximum likelihood fit for reactions: $\bar{p}p \to \omega 2\pi$, $\omega\rho^0$, ωf^0, $f^0 3\pi$,

TABLE III.

$\Gamma_\rho = 120$ MeV/c²	2.10 ÷2.12	2.12÷2.14	2.14÷2.16	2.16 ÷2.18	2.18 ÷2.20	2.20 ÷2.22
$\rho^0 3\pi$	1.51 ±1.05	1.62±0.68	0	1.261±0.68	0.483±0.56	1.73 ±0.8
$\rho^\pm 3\pi$	0.159±0.80	1.52±0.52	0	2.04 ±0.57	1.546±0.44	1.289±0.60
$f^0 3\pi$	2.44 ±0.42	2.24±0.26	1.62±0.65	1.76 ±0.22	1.74 ±0.22	1.82 ±0.30
$\omega 2\pi$	0.913±0.30	1.36±0.27	1.32±0.44	0.78 ±0.23	0.88 ±0.22	0.68 ±0.20
$\rho^0\rho^0\pi^0$	0.67 ±0.40	0.83±0.27	0.22±0.33	0.61 ±0.25	0.79 ±0.23	0.07 ±0.21
$\rho^0\rho^\pm\pi^\mp$	4.96 ±0.73	3.50±0.52	5.09±0.60	2.53 ±0.44	3.44 ±0.44	2.56 ±0.50
$\omega\rho^0$	1.07 ±0.15	0.50±0.12	0.39±0.26	0.40 ±0.10	0.50 ±0.13	0.24 ±0.12
ωf^0	1.43 ±0.14	1.13±0.12	0.89±0.26	0.91 ±0.12	0.51 ±0.11	0.35 ±0.12
φ	1.26 ±0.98	0.45±0.75	2.58±0.72	0.92 ±0.69	1.26 ±0.57	1.26 ±0.77

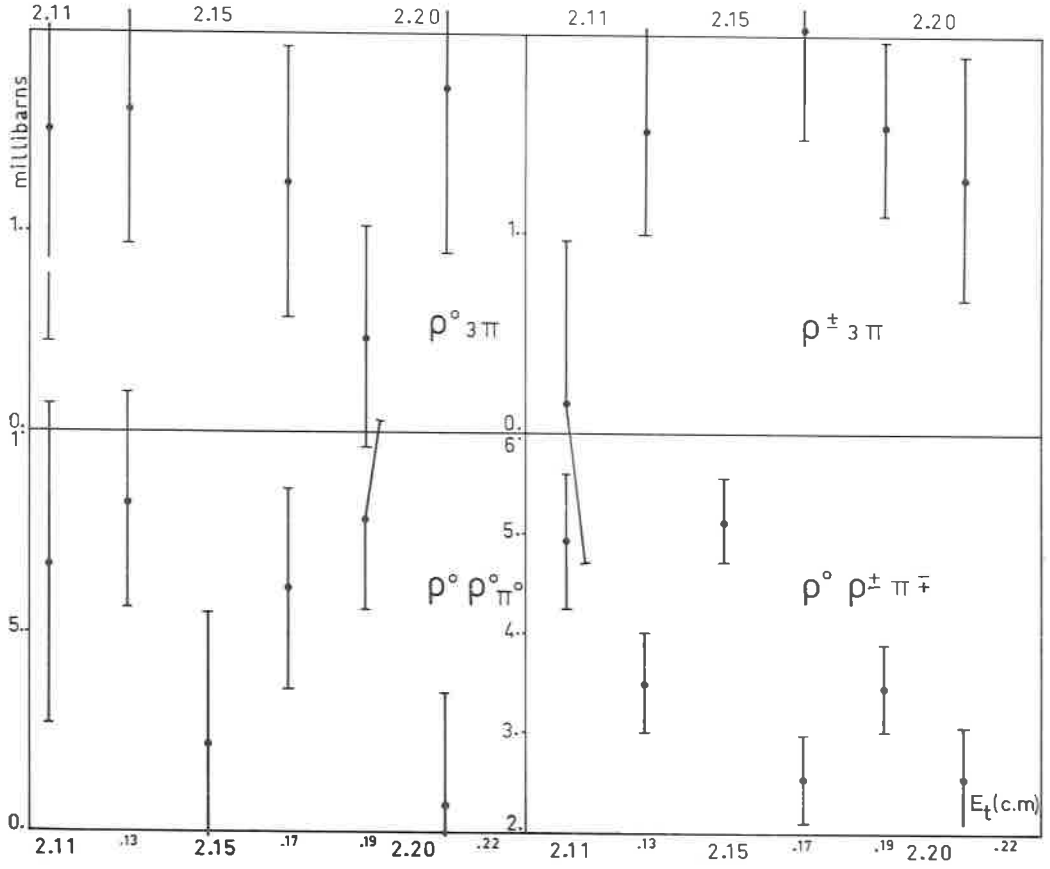

Fig. 3. – Results of a maximum likelihood fit for reactions: $\bar{p}p \to \rho^0 3\pi$, $\rho^{\pm} 3\pi$, $\rho^0\rho^0\pi^0$, $\rho^0\rho^{\pm}\pi^{\mp}$.

in the energy range mentioned above, using besides phase space the matrix elements $\rho^0 3\pi$, $\rho^{\pm} 3\pi$, $f^0 3\pi$, $\omega 2\pi$, $\rho^0\rho^0\pi^0$, $\rho^0\rho^{\pm}\pi^{\mp}$, ωf^0, $\omega\rho^0$.

The resulting number of events in each channel is corrected for the cuts and expressed in terms of cross sections in Table III, Fig. 2 and 3 in the whole energy range.

The normalization to known cross sections (namely cross-section for 4 prong events which has been measured and properly corrected for contamination) is done in the following way:

Let σ_T be the total 4 prong cross section at energy E corresponding to N events on the D.S.T. at the same energy. Let n be the number of 5π events

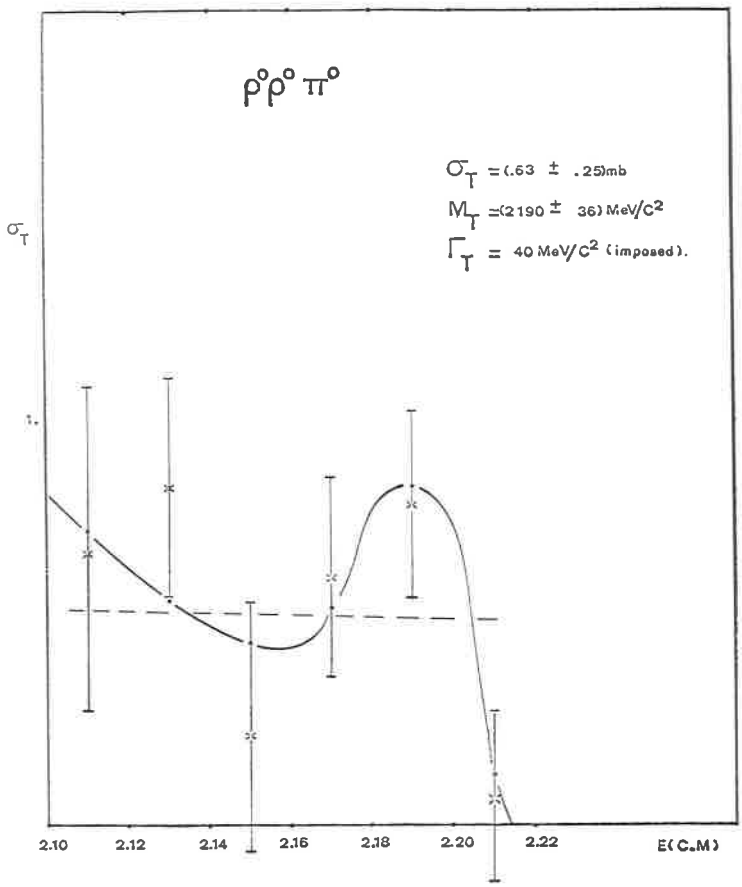

Fig. 4. – χ^2 fit for the results of the channel $\bar{p}p \to \rho^0\rho^0\pi^0$.

(fitted + corrected) which is related to the channel $\bar{p}p \to \rho^0\rho^0\pi^0$ at energy E, then

$$\sigma_{\bar{p}p\to\rho^0\rho^0\pi^0} = \frac{\sigma_T n}{N}.$$

Figure 4 illustrates the numerical values for $\rho^0\rho^0\pi^0$ and shows the results of χ^2 fits which can give descriptions of the bump observed around 2.19 MeV/c². A straight line and a Breit-Wigner super imposed on a parabolic background give equally good fits.

If the experimental results are interpreted in terms of a Breit-Wigner function the position of the bump is:

$$M = (2190 \pm 36)\ \mathrm{MeV/c^2},$$

as well as the cross section

$$\sigma = (0.63 \pm 0.25)\ \mathrm{mb}\,,$$

and the background constants have been fitted, taking the width Γ as an imposed value (40 MeV/c²).

One concludes that the channel $\rho^0\rho^0\pi^0$ exists over the whole of the energy range (2.10÷2.22) GeV/c².

However, it seems prudent to us not be too affirmative before getting more information in the momentum range around 1.5 GeV/c. Many pictures at this point, are being measured. It should permit a better knowledge of the phenomenon.

REFERENCES

1) R. J. Abrams *et al.*: *Phys. Rev. Lett.*, **18**, 1209 (1967).
2) G. Chikovani *et al.*: *Phys. Lett.*, **22**, 233 (1966).
3) W. A. Cooper *et al.*: *Phys. Rev. Lett.*, **20**, 1059 (1968).
4) M. Baubillier *et al.*: Communication at the *Lund Conference* (1969).
5) G. R. Kalbfleisch *et al.*: *Phys. Lett.*, **29** B, 259 (1969).
6) H. Briand *et al.*: Communication at the *Kiev Conference* (1970).
7) G. R. Kalbfleisch: *Proceedings of the Conference on Meson Spectroscopy* (1970).

SESSION II-D

Thursday, 15 April 1971

Meson splitting: A_2, f^0, K^*, etc.

Chairman: W. JENTSCHKE

Secretaries: P. L. BRUNINI
W. BLUM

Meson splitting (*)

T. MASSAM
Istituto Nazionale di Fisica Nucleare - Sezione di Bologna

1. Introduction.

I have to summarize what was known to me about splitting before this conference, so in spite of the high statistics results to be presented, I will stick to the rules and know nothing about them, leaving to the authors the pleasure of perhaps up-ending all I will say.

Previous experimental reviews tended to use, as reference for comparing and classifying experiments, the relative probabilities of the fits to different shapes, which emphasized the controversy of « dipole » or « not dipole » ([1,2]). In this introduction, I will concentrate mainly on the classification of the experiments themselves because, when looking at some of the results, my interpretation did not agree with that suggested by the goodness of fit numbers obtained. This classification is to try and show up any systematic effects which might give a clue to the answers of some of the questions on the splitting and, perhaps form a new basis for future discussion.

The two main question to be answered are:

i) What is the A_2 splitting—is it really there—is it a property of the A_2 or is it just some sort of background effect?

ii) If it is really there, what is the mechanism which produces it?

Other questions, which would help us answer these are:

— Under what conditions is the A_2 seen to be split? To have clear understanding of this is of major importance.

— How is the A_2 produced? Could there be any mechanism in the production process which could give a structure? How could we test it by experiment.

— Are other members of the 2^+ nonet split—is it just one individual or is it the whole family which is odd?

(*) Introductory talk

2. Classification of the experiments.

The classification which I have made is according to the ability of the experiments to show up structure, as shown in Fig. 1. The abscissa is the standard

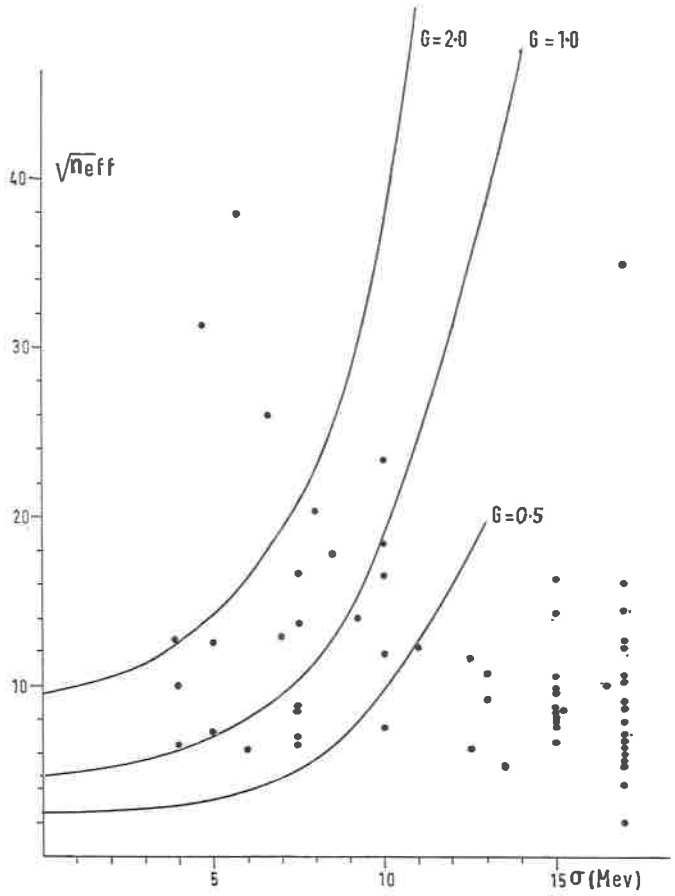

Fig. 1. – Showing the mass resolution and effective number of events of the A_2 experiments σ is the standard deviation. $n_{\text{eff}} = (1+b)n/\{(0.22+b/3)\ (0.78+2b/3)\}$ where n is the number of A_2 events in a 45 MeV central region of the A_2 and b is the ratio of background to A_2 events in the same region. The lines show the numbers of events needed to obtain a G standard deviation effect for a dipole, using the rough analysis described in the Appendix. Detailed analysis of the mass spectrum gives 2 to 4 times higher significance. The curves form a guide for ordering the significance of the experiments.

TABLE 1. – A_2 *experiments.*

$\|i\rangle$	$\|f\rangle$	A_2 Decay	Reference	P (GeV/c)	t' (GeV/c)^2	$N(A_2)$	B/A_2	n_{eff}	σ (MeV)	N
π^-p	A_2^-p	$\pi^+\pi^-\pi^-$	(3) MMS G4*a*	6.0	0.24÷0.42	118	4.9	5.9	13±3	
			(3) G4*b*	7.0	0.22÷0.28	113	3.3	7.0	13±3	
			(3) G7	7.0	0.20÷0.26	255	2.6	10.2	8.5	9
			(3) G6*bc*	7.0	0.15÷0.20	210	5.9	7.2	12.5	
			(3) G6*f*	7.0	0.26÷0.31	51	6.3	3.4	13.5	
			(4) CBS G15	2.65	0	369	4.9	10.3	7.5	8
			(4) CBS G3*a*	7.0	0.19÷0.29	226	1.0	16.1	10.0	12
			(4) CBS G3*b*	7.0	0.19÷0.29	156	1.2	12.5	10.0	15
			(5) CERN	3.9	< 0.84	84	2.5	6.9	17.5G	
			(6) Illinois	5.0÷7.5	0.02÷0.62	250	0.1	32	38G	
			(7)	4.5	All.	50	1.3	7.1	37G	
			(8) WT	7.0	> 0.15	122	1.2	11.0	15G	
			(8) WT	25.0	> 0.10	20	1.0	4.8	30G	
			(9) LRL	3.2 + 4.2	All.	127	1.8	9.8	15G	
			(10) LRL	1.5 to 5.2	< 0.65	22	0.5	6.4	15G	
			(11) BNL	6.0	0.08÷0.62	32	1.0	6.4	7.5G	19
			(12) Notre Dame	8.0	0.5	53	0.6	9.4	20G	
			(13) Notre Dame	8.0	0.5	25	1.1	4.8	18	
			(14) TAW	3.0	All.	32	1.25	5.5	25G	
			(15) SLAC	16.0	All.	16	2.5	3.0	30G	
π^-p	A_2^-p	$(K\bar{K})^-$	(4) CBS (*h*)	7.0	0.19÷0.29	70	0.3	13.5	10	17
			(16) Brookhaven	20.3	< 0.7	200	0.1	28.6	4.7	2
			(17) CERN-Münich	17.2	< 0.7	320	0.2	32.0	5.7	1
			(10) LRL	1.5 to 5.2	< 0.65	22	0.6	6.0	15G	
			(18) LRL	3 + 4	All.	34	0.5	8.0	15G	
π^-p	A_2^-p	$(\eta\pi)^-$	(4) CBS G9	11.0	0.19÷0.29	25	1	5.3	10	24
			(6) Illinois	5.0	0.13÷1.5	12	0.3	5.6	15G	
			(19) Notre Dame	8.0	< 1.6	20	1.0	4.8	7.5	22
π^-p	A_2^0n	$\pi^+\pi^-\pi^0$	(20) CERN-Bologna	3.2	0.3÷0.6	800	7.4	13.9	8.0	5
π^-p	A_2^0n	$K_1^0K_1^0$	(18) LRL	3 + 4	All.	20	0.6	5.8	15G	
			(11) BNL	6.0	0.08÷0.62	21	1.0	5.2	7.5G	21
π^+p	A_2^+p	$\pi^+\pi^-\pi^+$	(4) CBS G14*b*	2.65	0	68	2.8	5.9	7.5	18
			(21) BBFO	5.1	< 1.25	27	2.0	4.3	30G	
			(22) LRL	7.0	> 0.18	306	1.4	10.5	6.7	3
			(23) BDNPT	5.0	< 0.5	50	1.9	5.9	15G	
			(24) LRL	3.7	0.1÷2.0	88	1.5	8.7	7.0	10
			(25) LRL	3.7	All.	4.5	2.7	1.0	30G	
			(26) ABBHLM	3.7	All.	35	0.9	6.6	30G	
			(23) BDNPT	5.0	< 0.5	28	1.5	4.8	5.0	14
π^+p	A_2^+p	$K^+\bar{K}^0$	(22) LRL	7.0	All.	41	0.3	10.4	3.8	4

TABLE 1. – *Continued*

$\|i\rangle$	$\|f\rangle$	A_2 Decay	Reference	P (GeV/c)	t' (GeV/c)^2	$N(A_2)$	B/A_2	n_{eff}	σ (MeV	N
π^+p	A_2^+p	$\eta\pi^+$	([22]) LRL	7.0	All.	49	0.3	11.3	9.2	16
π^+n	A_2^0p	$\pi^+\pi^-\pi^0$	([8]) WT	7.0	All.	61	0.9	8.6	30G	
			([27]) BBFO	5.1	0.4	70	0.4	12.8	30G	
			([28]) Michigan	3.65	< 0.8	20	0.25	7.6	30G	
			([29]) BOTP	8.0	All.	18	1.0	4.6	30G	
			([30]) Purdue	2.7	All.	50	1.4	6.8	15	
π^+d	A_2^+NN	$K^+\bar{K}^0$	([31]) BPBF	5.1	< 1.2	10	0.3	5.1	6	20
π^+p	$A_2^0\Delta^{++}$	$\pi^+\pi^-\pi^0$	([32]) LRL	3.7	$0 \div 1.0$	60	1.0	8.2	10	23
			([33]) Notre Dame	18.5	All.	15	1.0	4.4	30G	
K^-n	$A_2^-\Lambda^0$	$\pi^+\pi^-\pi^0$	([34]) BNL	3.9	All.	37	1.3	6.0	15	25
K^+p	$A_2^0K^0p$	$\pi^+\pi^-\pi^0$	([35]) LRL	9.0	< 0.32	30	2.3	4.3	30G	
$\bar{p}p$	$A_2^\pm\pi^\pm$	$\pi^+\pi^-\pi^\pm$	([36]) LP	$1.1 \div 1.4$		74	2.0	7.2	30G	
			([37]) Liverpool	1.2		109	1.7	9.1	7.5G	11
			([38]) CC	0		180	3.9	8.2	11G	
$\bar{p}p$	$A_2^\pm\pi$'s	$K^\pm\bar{K}^0$	([39]) CERN	3.6		71	2.3	6.5	4.0	7
			([40]) CCL	$0 \div 1.2$		104	2.0	8.4	5.0	6
			([41]) CCIL	0		110	1.5	9.5	24G	
$\bar{p}p$	$A_2^0\pi$'s	$K_1^0K_1^0$	([39]) CERN	3.6		20	1.3	4.5	4.0	13
$\bar{p}p$	$A_2^\pm\pi^\mp$	$\eta\pi^\pm$	([42]) CC	0		19	1.1	4.5	12.5	

Abbreviations:

BBFO = Bari-Bologna-Florence-Orsay
LRL = Lawrence Radiation Laboratory
WT = Wisconsin-Toronto
CC = CERN-College De France
LP = Liverpool, Institut de Physique Nucléaire-Paris
BPBF = Bari, Paris, Bologna, Florence
BOTP = Brookhaven, Oak Ridge, Tennessee, Pennsylvania
TAW = Toronto, Argonne, Wisconsin
BDNPT = Bonn, Durham, Nijmegen, Paris, Torino
ABBBHLM = Aachen, Berlin, Birmingham, Bonn, Hamburg, London (IC), München
CCL = CERN, College de France, Liverpool
CCIL = CERN, College de France, Institut de Physique Nucléaire (Paris), Liverpool
BNL = Brookhaven National Laboratory
G = My estimate of the resolution.

TABLE II. – A_2 *graphs used in the comparisons.*

Reaction \ Decay	$\rho\pi$	$K\bar{K}$	$\eta\pi$
$\pi^-p \to A_2^-p$	(3) MMS (G7) (4) CBS (G15) (4) CBS (G3*b*) (11) BNL	(4) CBS (*h*) (16) BNL (17) CERNMünich	(4) CBS G9 (19) Notre Dame
$\pi^-p \to A_2^0n$	(20) CERN-Bologna	(11) BNL	
$\pi^+p \to A_2^+p$	(4) CBS (G14*b*) (22) LRL (24) LRL (23) BDNPT	(22) LRL (31) BPBF	(22) LRL
$\pi^+p \to A_2^0\Delta^{++}$	(32) LRL		
$\bar{p}p \to A^{\pm}\pi^{\mp}$	(37) Liverpool	(39) CERN (40) CCL	
$\bar{p}p \to A_2^0\pi$'s		(39) CERN	
$K^-n \to A_2^-\Lambda^0$	(34) BNL		

(Abbreviations and references are as in Table I).

deviation of the mass resolution and the ordinate is the square root of the effective number of events, that is, the number of A_2 events in a central, 45 MeV wide, section of the peak, corrected for the reduction in the statistical significance caused by the background. [Appendix I defines this more precisely and Table I gives a list of the experiments included on the graph (Ref. 3 to 41)]. The lines are contours of equal significance, G, and have been calculated for a dipole shape of resonance. For a broader type of structure, the lines would have a slower increase in numbers of events needed as a function of the resolution, but by inspection, the ordering of the experiments will not change significantly. I have included all experiments above the lower contour (plus two or three just below it). This corresponds to where most authors are no longer prepared to say anything about structure—it is the order of the experiments rather than the position of the cut which is relevant. Each experiment has been assigned a statistical merit number by inspection of the diagram. Thus, on the graphs, results will be numbered between 1 (for high statistical

significance) and 25. Experiments 1 to 4 have $G > 2$, and experiments 5 to 14 have G between 1 and 2. Table II shows the selected experiments, which have been grouped according to the production process and the decay process. Vertically, there are π^-p, π^+p, $\bar{p}p$ and K^-n interactions, whilst in the final state, $\rho\pi$, $K\bar{K}$ and $\eta\pi$ decay modes have been studied. Each process has its own merits and problems, among which, I will point out a few:

3. General features of the experiments.

i) Most data is available in experiments with three pions in the final state, but they have the highest background, with a background to peak ratio usually greater than 1, especially if $(\pi\pi)$ combinations inside the ρ band have not been selected.

ii) The $K\bar{K}$ experiments have lower total statistics, but are more reliable in general because of the much lower background level: background/peak ~ 0.3.

iii) The $\eta\pi$ experiments also have low statistics and low background, but generally the mass resolution is less since there is always an un-reconstructed neutral particle in the decay products.

iv) Care must be taken in interpreting the $K_1^0K_1^0$ spectra since there may be interference with the f^0 which also has a $K\bar{K}$ decay mode.

v) In the production of charged A_2 mesons in π^-p and π^+p interactions, both isoscalar and isovector exchange amplitudes are allowed, but in the exchange reactions $\pi^-p \to nA_2^0$ and $\pi^+p \to \Delta^{++}A_2^0$, no isoscalar exchange is allowed, so if there are mass dependent production effects, these could show up differently in these four interactions.

vi) $K^-n \to A_2^-\Lambda^\circ$ has strangeness-changing exchange, so again could be different.

vii) $\bar{p}p$ annihilation has no restriction about exchange mechanism, so high statistics, high resolution experiments would be particularly interesting.

4. Background problems.

Before comparing the results in the various classes, I will show some results which are particularly relevant to the background problems in the $\rho\pi$ final state, quoting in particular two of the groups who have made partial wave analyses of the $\rho\pi$ system in π^-p interactions. Figure 2 shows the results of Abramovich *et al.* (5). Fig. 2 (a) shows the raw mass spectrum, with indications

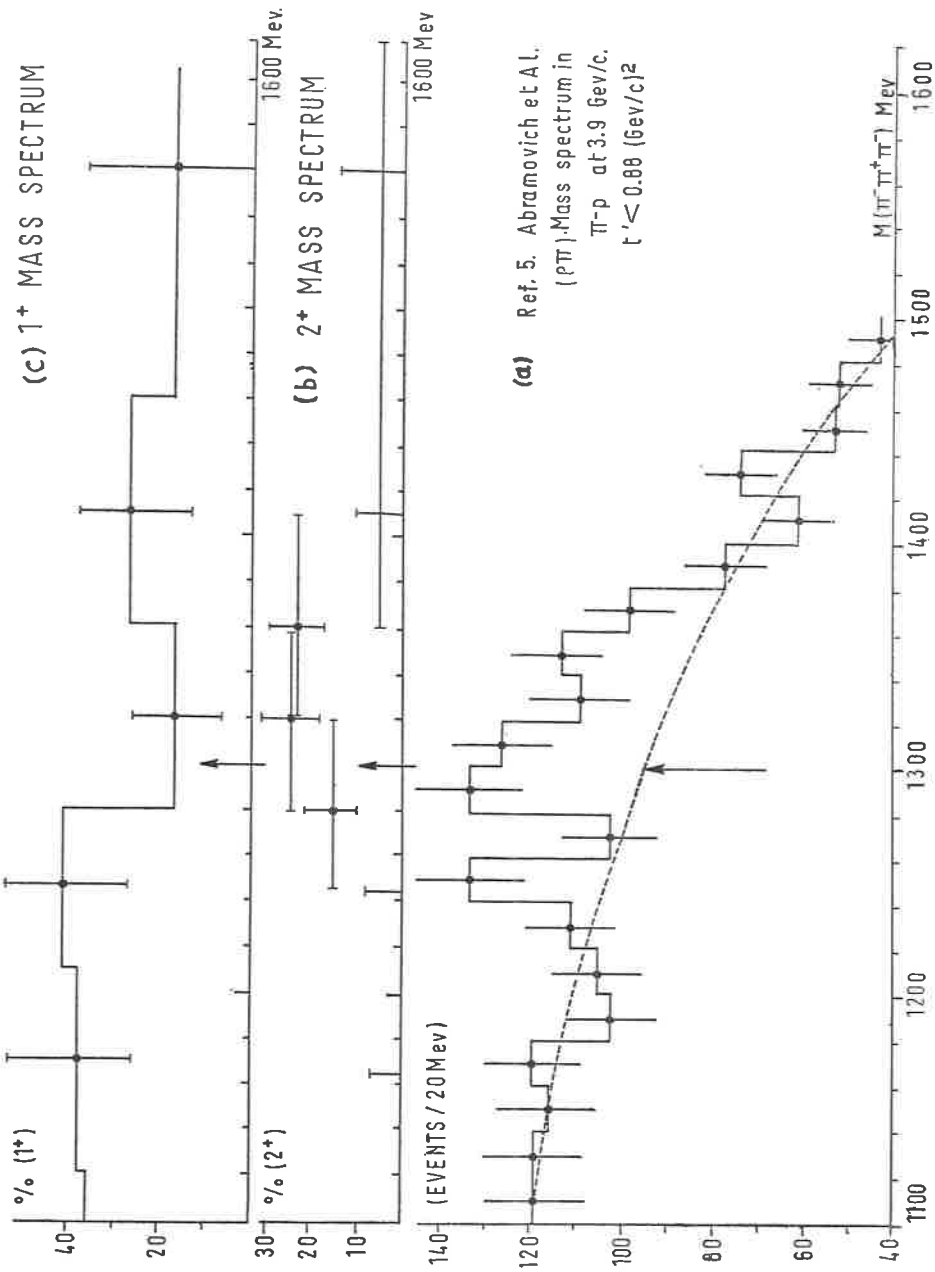

Fig. 2. – $(A_2^- \to \pi^-\pi^+\pi^-)$ mass spectrum in $\pi^-p \to A_2^-p$. *a*) Total mass spectrum. *b*) The $J^P = 2^+$ contribution. *c*) The $J^P = 1^+$ contribution. This illustrates the shift in apparent mass caused by the 1^+ background shape.

of what might be a dip. When they project out just the 2^+ partial wave contribution to the mass spectrum, Fig. 2*b*, the peak is displaced 40 MeV higher. The binning needed for the analysis is too wide to examine structure. The 1^+ state, shown in Fig. 2*c* shows a step which could displace the peak.

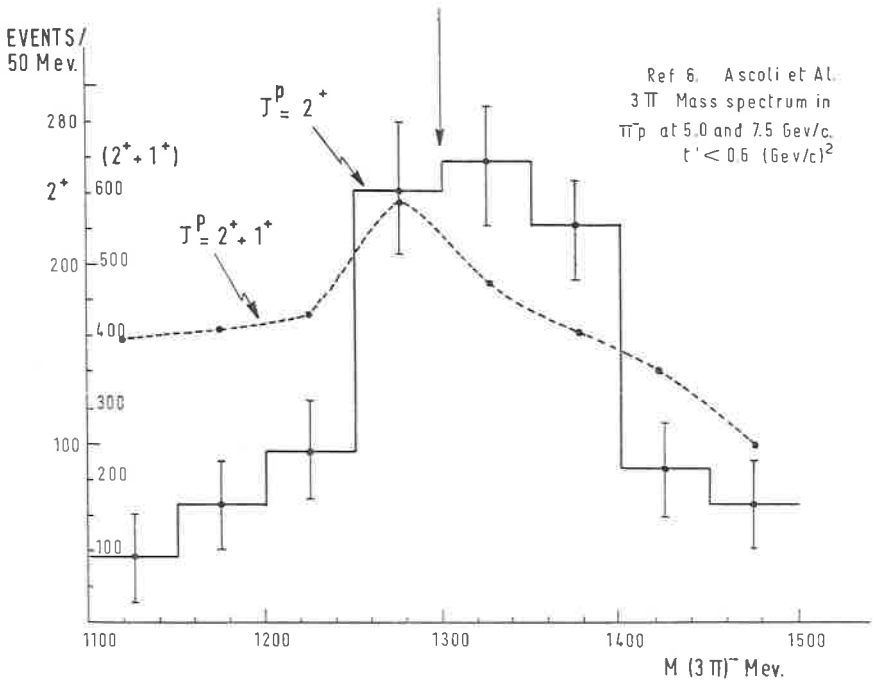

Fig. 3. – $(A_2^- \to \pi^-\pi^+\pi^-)$ mass spectrum in $\pi^-p \to A_2^-p$. This illustrates the shift in apparent mass which occurs when the $J^P = 1^+$ background is added to the $J^P = 2^+$ resonant state.

This behaviour shows up clearly in the results of Ascoli *et al.* ([43]). In Fig. 3 is shown the 2^+ contribution alone, and also the sum of the 2^+ and 1^+ contributions. Note again the shift in the peak position, which has been caused just by adding the 1^+ contribution, shown alone in Fig. 4. The pronouced step at 1300 MeV emphasises the importance that this type of analysis be carried out with even higher statistics and smaller bin width. (Suppose the step really overshoots, then this would be an excellent way to manufacture a splitting).

There could also be complications in antiproton annihilation experiments. Clayton *et al.* ([44]), in another Zemach type partial wave analysis of three

pion states in $\bar{p}p \to 5\pi$ have observed another peak at the A_2 position, but with $J^P = 1^-$. Again the need for partial wave analysis is demonstrated.

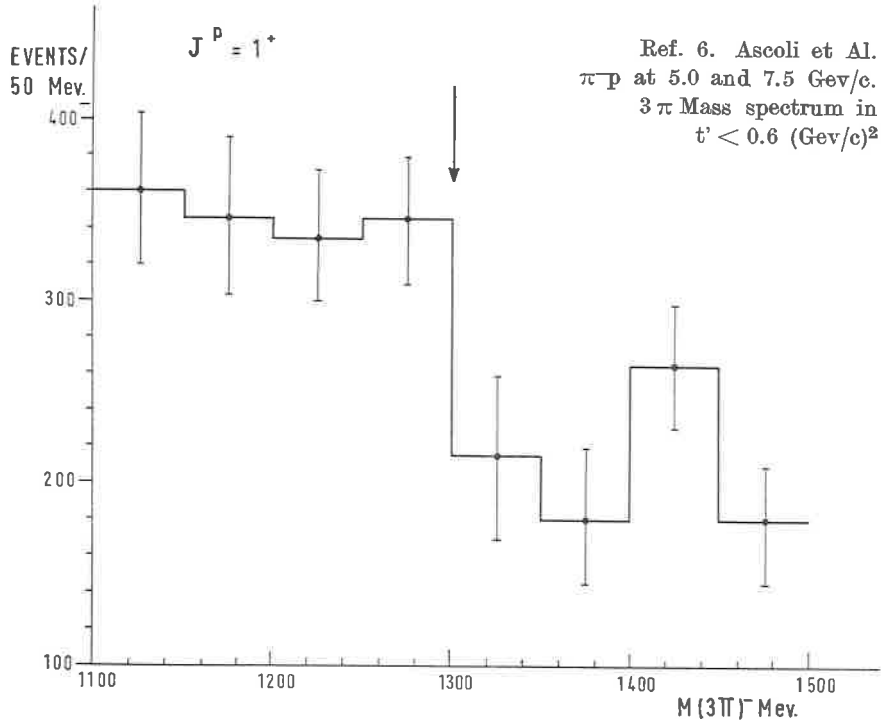

Fig. 4. – Showing the change in shape of the 1^+ background which occurs under the A_2 peak.

5. Comparisons of results on A_2 spectra.

To obtain direct comparisons of experiments I have redrawn the relevant mass spectra using a unique mass scale. They are too numerous to be shown in detail so I have superimposed the results of each class, after having drawn freehand curves to touch all the error bars. Normally one would draw smoother curves, but I have done this to counteract the tendency to take into account a 1.5 standard deviation point only when it is at the centre of the A_2 peak. So, if the wriggles outside the peak are equal to the splitting, do not trust it!

The results are given for each production mechanism, following Table II.

On each graph, the experiments are indicated in the key, which also shows the bin width and the statistical uncertainty at the peak of the curve. N is the statistical significance number.

6. Reaction $\pi^- p \to A_2^- p$.

1) $A_2^- \to \rho\pi$, Fig. 5. All these experiments are at low t' between 0.2 and 0.4 (GeV/c)^2 and at momenta between 2 and 7 GeV/c. They all show

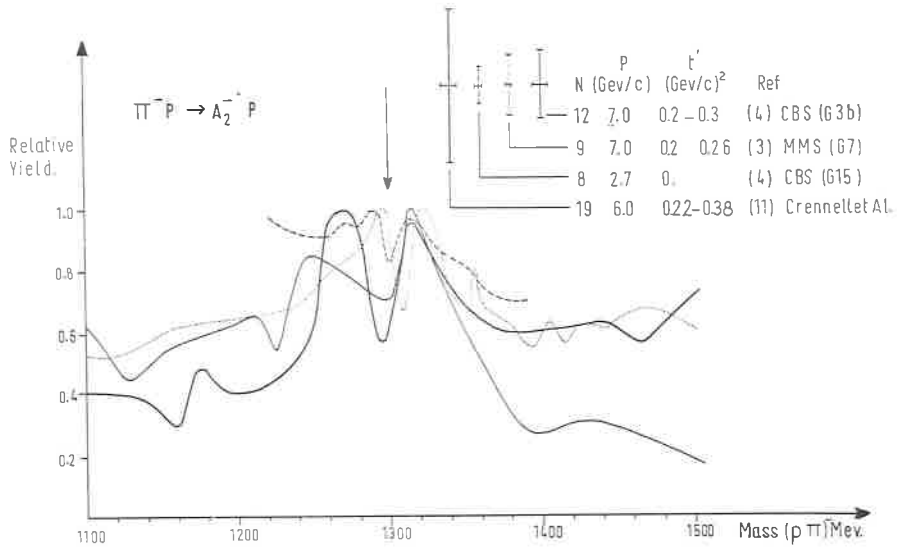

Fig. 5. – Summary of the mass spectra in $\pi^- p \to p A_2^-$; $A_2^- \to (\pi^+\pi^-\pi^-)$. The experiments are of intermediate significance. No clear dependence on momentum or on $t'(=t-t_{\text{minimum}})$ is seen.

a two-peaked structure, which is very regular at the A_2^H, but varies from experiment to experiment at A_2^L. However, in the actual data a two peak fit does give an adequate description.

2) $A_2^- \to K\overline{K}$, Fig. 6. At low p and low t', there are two peaks, but at higher p and t', the mass spectrum looks like A_2^H with a shoulder instead of a peak in the A_2^L position. Note also that the results of Grayer *et al.* could be a narrow A_2 on a wide resonance. This sequence of graphs strongly suggests the broad-narrow type of Breit-Wigner interference mechanism.

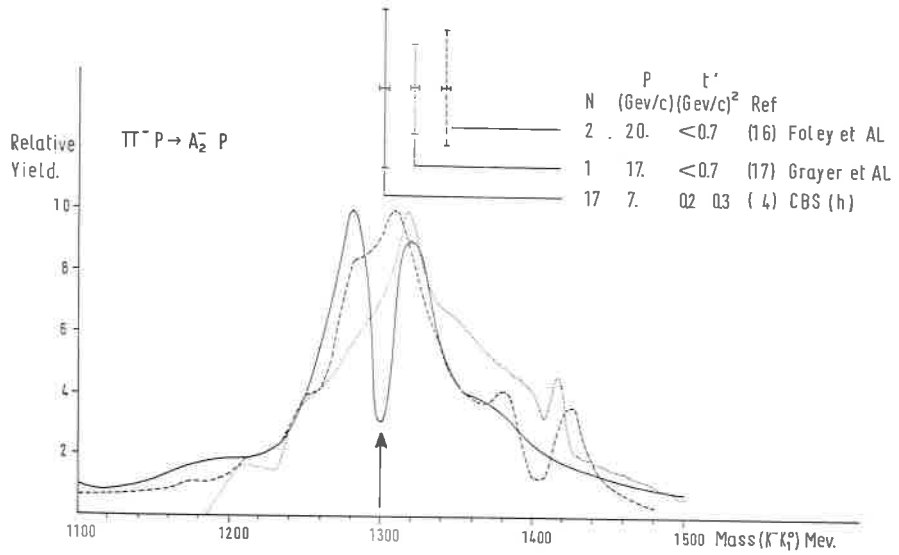

Fig. 6. – Summary of the mass spectra in $\pi^- p \to p A_2^-$; $A_2^- \to K^- K_1^0$: At higher P, A_2^L disappears or forms a shoulder.

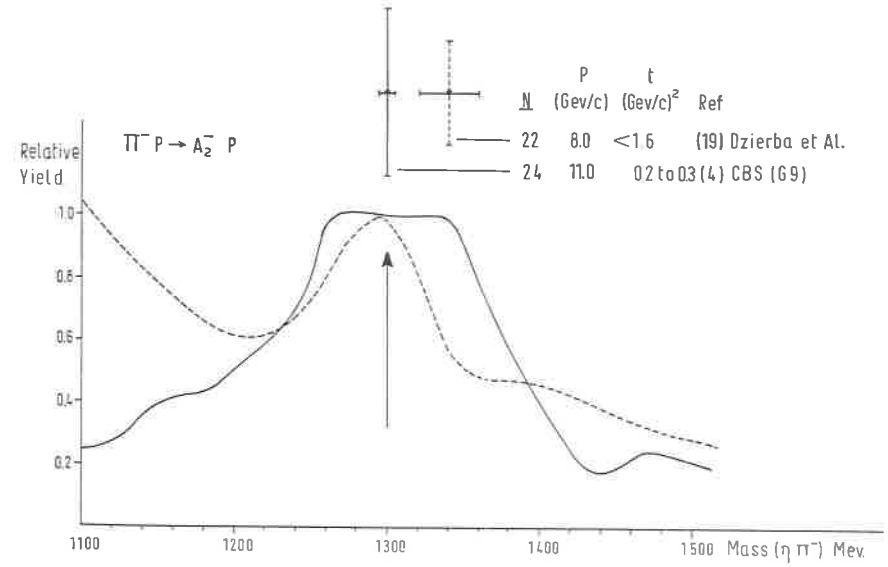

Fig. 7. – Summary of the mass spectra in $\pi^- p \to p A_2^-$; $A_2^- \to \eta \pi^-$. Both experiments are in the lowest significance band, and no conclusion can be reached.

3) $A_2^- \to \eta\pi^-$, Fig. 7. At present, these results are not really good enough to say anything about shape (*N* high). The CERN Boson Spectrometer result can be drawn as a flat-topped curve compatible with a simple peak or a peak with structure. Dzierba *et al.* have similar resolution and statistics, but the binning in the published data is too broad to give further indications.

7. Reaction $\pi^- p \to n A_2^0$.

4) $A_2^0 \to \pi^+\pi^- +$(*neutrals*), Fig. 8. There is only one experiment in this mode, and it shows a two peak structure.

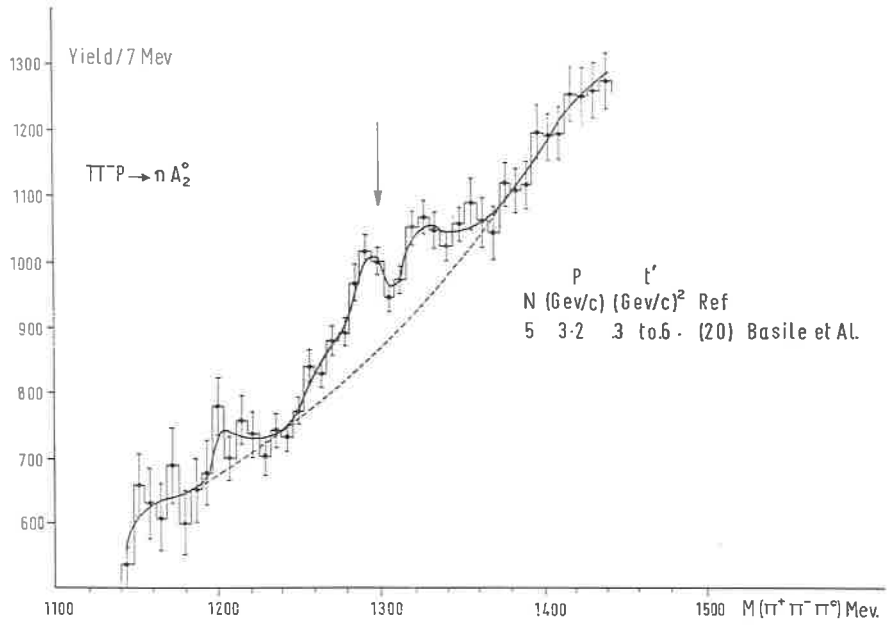

Fig. 8. – Mass spectrum in $\pi^- p \to A_2^0$; $A_2^0 \to (\pi^+\pi^- +$ neutrals). This intermediate significance experiment shows a minimum at the centre of the A_2 peak.

5) $A_2^0 \to K_1^0 K^0$, Fig. 9. Again there is only one experiment, which shows just a narrow resonance at the A_2 position. This could be either an A_2 structure or an effect of interference with f^0.

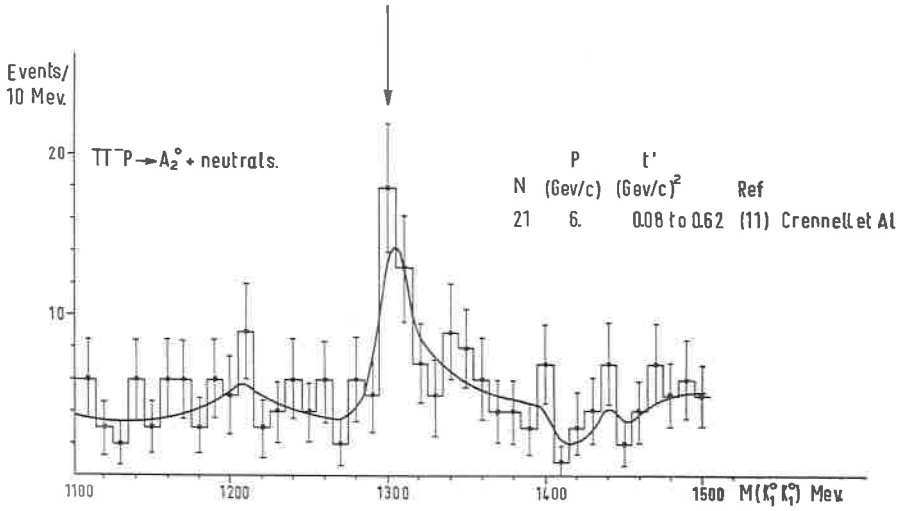

Fig. 9. – Mass spectrum in $\pi^- p \to$ neutrals + A_2^0; $A_2^0 \to K_1^0 K_1^0$: There is just one narrow peak near the A_2^E position. f^0 interference?

8. Reaction $\pi^+ p \to p A_2^+$.

6) $A_2^+ \to \rho\pi$, Fig. 10. t' range from 0.1 (GeV/c)^2 to 2.0 (GeV/c)^2 in these experiments, for momenta from 2.7 GeV/c to 7 GeV/c. There are

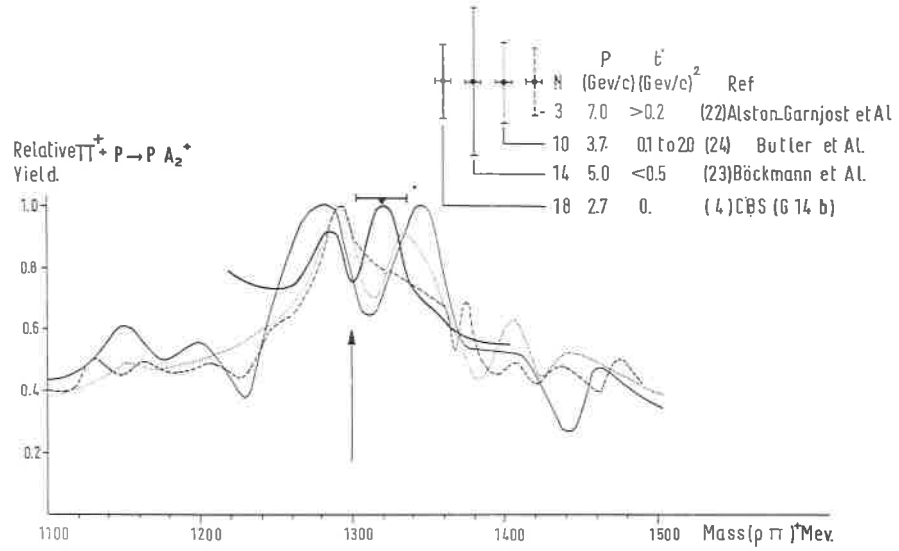

Fig. 10. – Summary of the mass spectra in $\pi^+ p \to p A_2^+$; $A_2^+ \to (\pi^+\pi^-\pi^+)$. Notice that as P increases, the A_2^E seems to be supressed to form a shoulder.

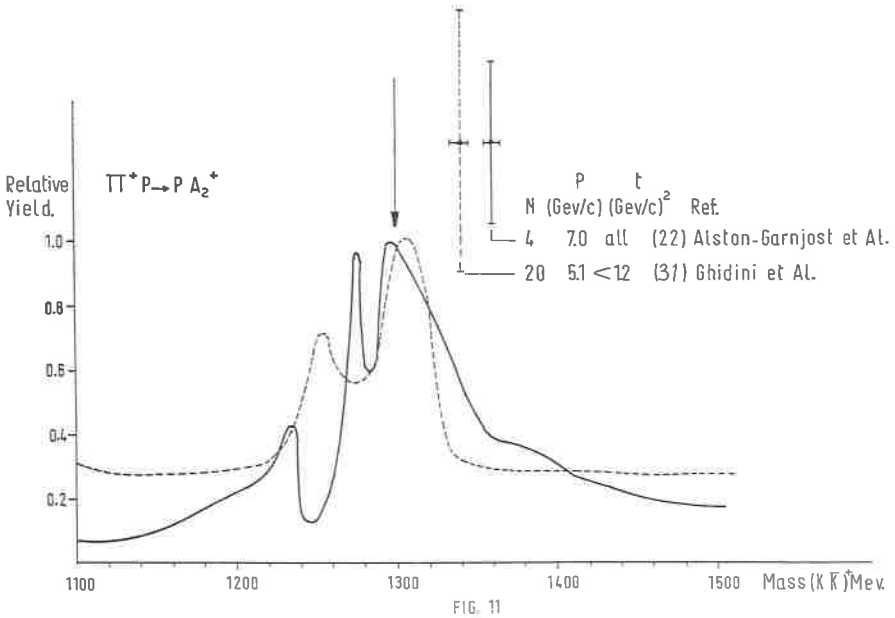

Fig. 11. – Summary of the mass spectra in $\pi^+ p \to p A_2^+$; $A_2^+ \to (K^+ K_1^0)$. Though the solid curve has a high-significance number, the dip which had to be drawn is only a 2.5 standard deviation effect. The structure in the broken curve is only a 1.3 standard deviation effect.

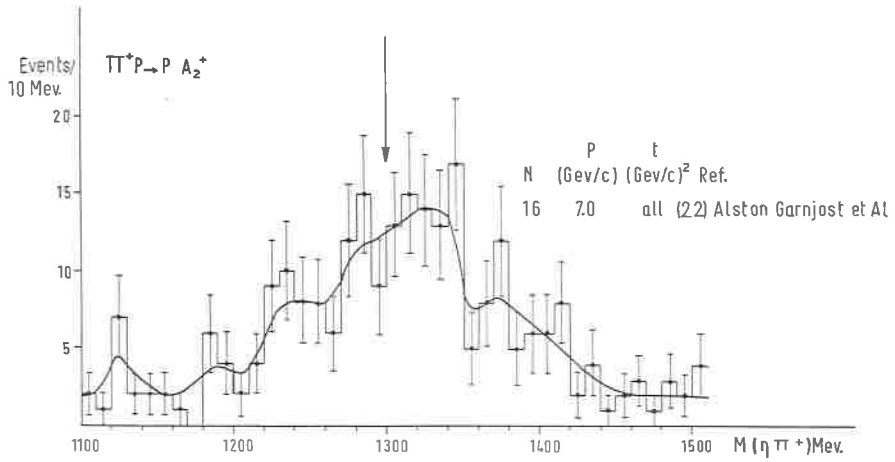

Fig. 12. – Mass spectrum in $\pi^+ p \to p A_2^+$; $A_2^+ \to \eta \pi^+$.

differences in shape which can be associated with incident pion momentum rather than with t'; at 2.7 GeV/c, the A_2^H is the stronger, at 3.7 (GeV/c) it is not as strong and then at 7 GeV/c it just forms a shoulder on the mass spectrum. The data at 5 GeV only partly follow this pattern in that the two peaks are equal at this intermediate energy. Also A_2^H and A_2^L are more widely separated. The 27 Gev/c curve has a large mass uncertainty as shown on the graph.

7) $A_2^+ \to KK$, Fig. 11. Both experiments show a narrow peak with a low mass satellite in just one or two bins, the main peak being centred near 1300 MeV rather than at A_2^H. The significance of the structure is low: a 2.5 standard deviation hole in the solid curve and only about 1.3 standard deviations in the broken curve. A similar shape will be noticed in one of the f^0 results.

8) $A_2^+ \to \eta\pi^+$, Fig. 12. A broad resonance, wriggly, but with no clear structure to be seen near 1300 MeV.

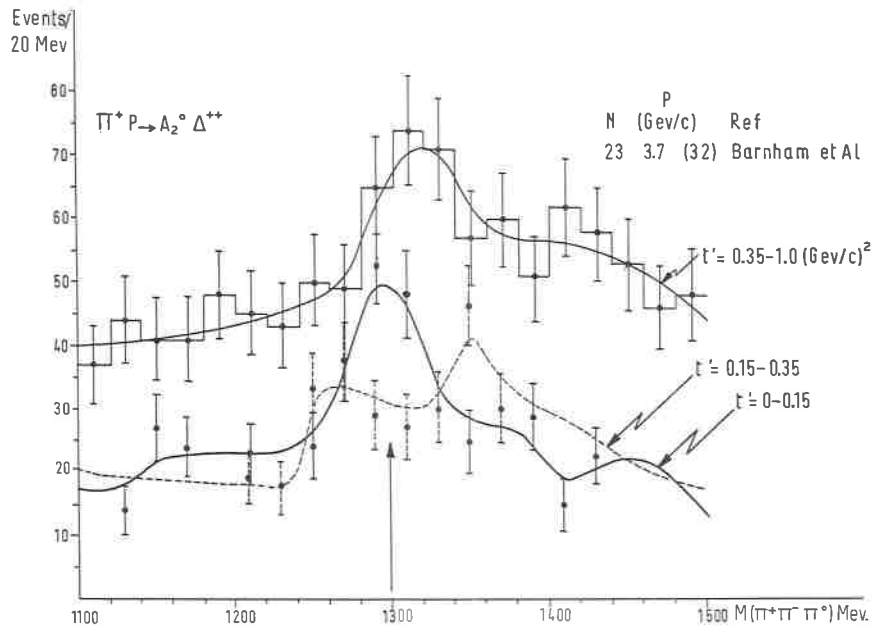

Fig. 13. – Mass spectra in $\pi^+p \to \Delta^{++}A_2^0$; $A_2^0 \to \pi^+\pi^-\pi^0$. Notice the shift in mass of the A_2 from low t' to high t', and notice also the «background shape» when the A_2 is absent at the intermediate t' value.

9) *Reaction* $\pi^+p \to \Delta^{++}A_2^0$; $A_2^0 \to \rho\pi$, Fig. 13. In this reaction, the A_2^0 changes shape with four momentum transfer. When $d\sigma/dt$ is plotted as a

function of t, there is a dip at $t = 0.6$ which corresponds to the nonsense zero, $\alpha_\rho = 0$, of the ρ trajectory. The authors then plot the mass spectra for low t' ($t' = 0$ to $0.15\,(\mathrm{GeV/c})^2$), for intermediate t' corresponding to the dip ($t' = 0.15$ to $0.35\,(\mathrm{GeV/c})^2$) and high t' ($t' = 0.35$ to $1.0\,(\mathrm{GeV/c})^2$). There are two effects to be noticed. At low t, the A_2 central mass is at (1297 ± 4) MeV, whereas at high t the mass is at (1317 ± 6) MeV a 2.8 standard deviation shift. At the intermediate value of t, the shape is quite different. Supposing that it is some residual A_2, then it looks like an A_2 structure but with the two possible peaks widely separated by 90 MeV. If it is not A_2, then it is the shape of the background, which makes one suspect the validity of the smooth first or second order polynomial background subtractions which have to be made in the high background situations found also in some of the other interactions. It is interesting to compare this shape with that found in the 7 GeV data in Fig. 5 (CBS Oct 69(G3*b*)).

9. Reaction $\bar{p}p \to A_2\pi$.

10) $A_2^\pm \to \rho\pi$. Fig. 14. There is evidence for a dip, the wriggle at 1300 MeV being in two channels whereas other wriggles are only single channel fluctuations.

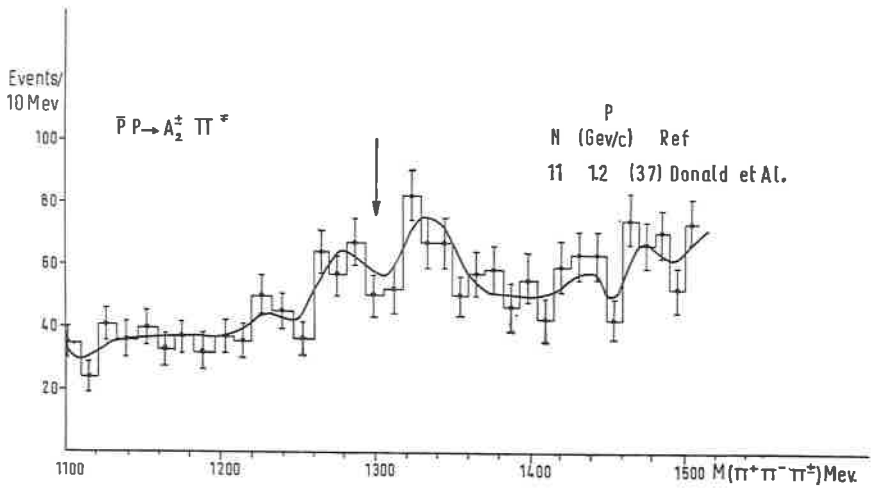

Fig. 14. – Mass spectrum in $\bar{p}p \to A_2^\pm\pi^\pm$; $A_2^\pm \to (\pi^+\pi^-\pi^\pm)$. An intermediate significance experiment showing a dip.

11) $A_2^{\pm} \to \overline{K}K$, Fig. 15. There are wriggles in both curves near 1300 MeV, but it is difficult to draw any conclusion or see any regularity on the basis of just these experiments.

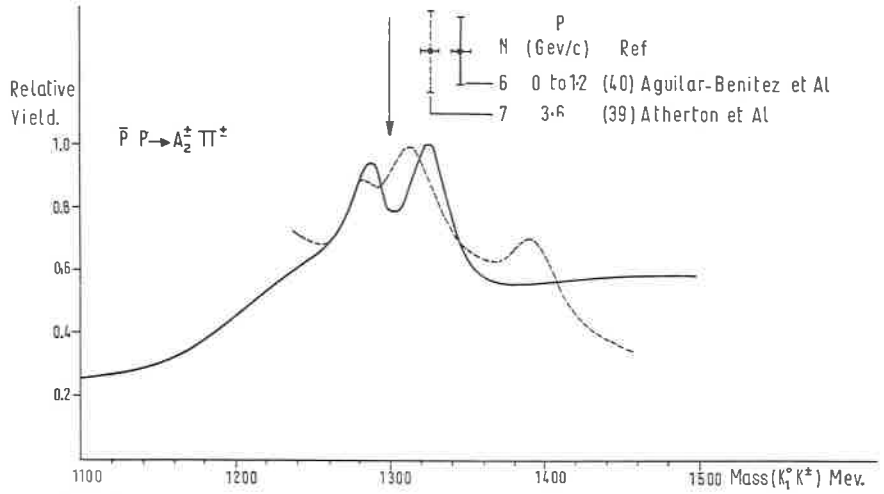

Fig. 15. – Summary of the mass spectra in $\bar{p}p \to A_2^{\pm}\pi^{\mp}$; $A_2^{\pm} \to (K^{\pm}K_1^0)$. Intermediate significance experiments, but difficult to draw conclusions.

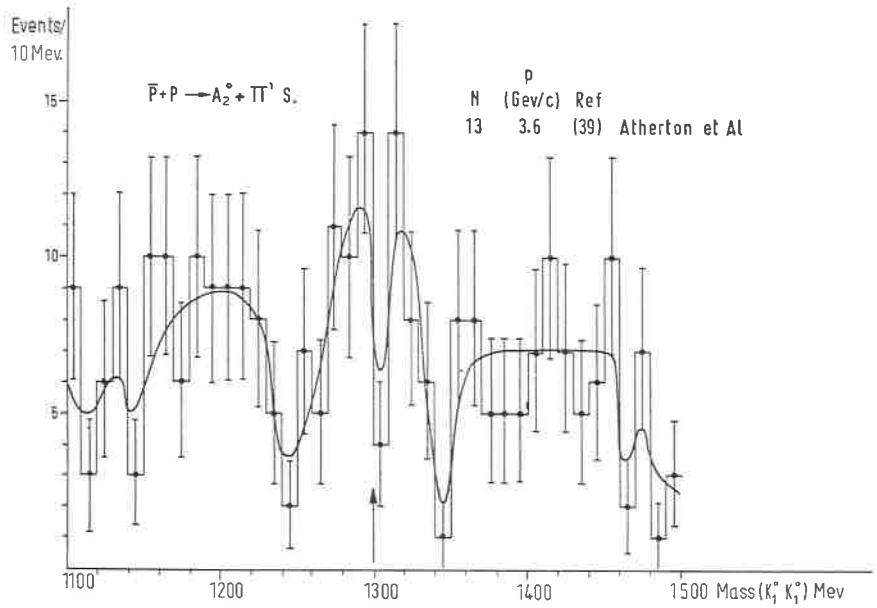

Fig. 16. – Mass spectrum in $\bar{p}p \to A_2^0$ + pions. $A_2^0 \to K_1^0K_1^0$: Near the boundary between low and intermediate significance bands. Structure statistical fluctuations or f^0 interference?

12) $A_2^0 \to K_1^0 K_1^0$, Fig. 16. The single bin hole at 1300 is 2.7 standard deviations, but it is consistent with the wriggles on the side of the A_2 peak. If the central hole is to be considered a structure, so should the holes at 1245 and 1345 MeV. Remember, here again there could be interference from the f^0.

10. Reaction $K^- n \to A_2^- \Lambda^0$.

13) $A_2^- \to \rho\pi$, Fig. 17. This result has somewhat lower effective statistics than the rest of the data. I have included it because it is the only experiment of its kind, and because the result has been quoted as giving a lower mass

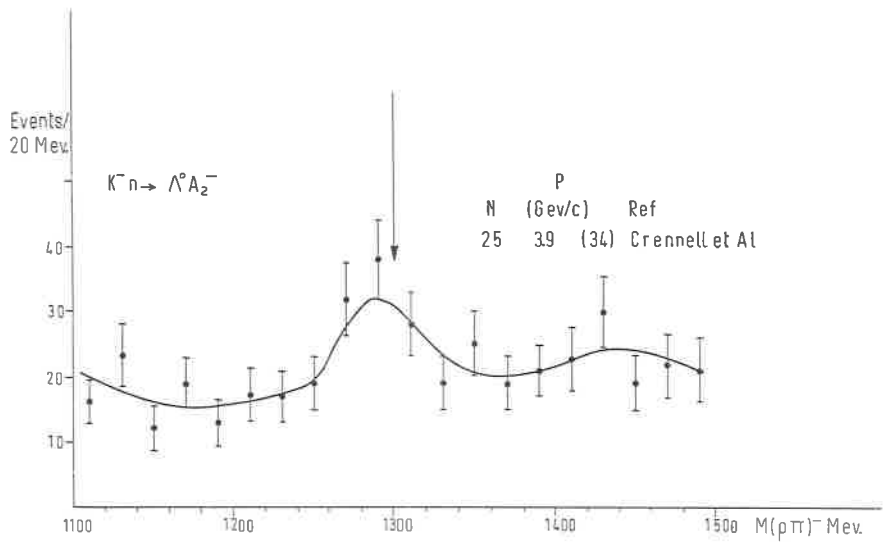

Fig. 17. – Mass spectrum in $K^- n \to \Lambda^0 A_2^-$; $A_2^- \to (\rho\pi)^-$.

value and narrower width than usual $M = (1289 \pm 10)$ MeV, $\Gamma = 40$ MeV. However, the inclusion of background effects similar to those shown above could change both these results.

11. Conclusions on A_2 mass spectra.

In the $(\rho\pi)^{\pm,0}$ and $(K\bar{K})^{\pm}$ final states, there is structure but it does not have any clear systematic behaviour. There is no evidence for a dependence

on t, but in two cases there is a hint of a dependence on incident beam momentum in πp interactions—the A_2^H shows up more strongly in $(K\overline{K})^-$ at higher energies, whereas in $(\rho\pi)^+$ it is depressed at higher energies. The $(K\overline{K})^-$ data in particular suggest the interference of a broad and a narrow resonance. There is also a narrow structure for $(K_1^0K_1^0)$ decay modes, but this could be the result of f^0 interference.

12. Production mechanism of the A_2.

There are some inconsistencies, but a pattern is showing. ρ^0 and/or f^0 exchange might be expected to predominate in $\pi^{\pm}p \to A_2^{\pm}p$ and $\pi^-p \to A_2^0n$ Different groups draw different conclusions about the exchange mechanism from their results on decay angular correlations. Carroll *et al.* [8] find that up to 25 GeV, the ρ helicity state population in the $(\rho\pi)$ decay mode is con-

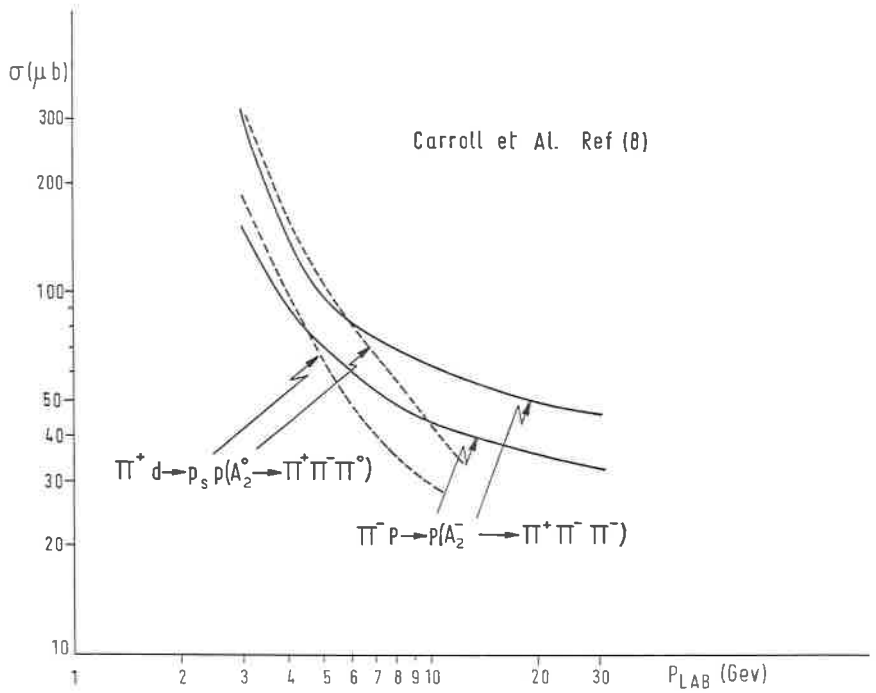

Fig. 18. – Showing the dependence of A_2 production cross-section on beam momentum in $\pi\mathcal{N}$ interactions. Broken curve is with charge exchange. Solid curve without charge exchange. The two curves change shape above 6 to 7 GeV/c.

sistent with just ρ exchange. However, as pointed out at this conference, A_1 and A_2 interfere and so there must be a considerable isoscalar part of the amplitude for this to happen. The production cross-sections also support the existence of an isoscalar contribution.

Figure 18 shows the error bands of the observed cross-sections drawn using the results shown in ref. ([8]) for $\pi^- p \to p A_2^-$ and $\pi^+ n \to p A_2^0$. For pure ρ exchange, when the *I*-spin coefficients and the fraction of the final states which are observed are taken into account, the A_2^0 curve should be four times higher than the A_2^- curve. However, they are nearly equal at low energy, which indicates an f^0 amplitude roughly 1.7 times the ρ exchange amplitude. Above 6 to 7 GeV, the two error bands part, indicating that f^0 exchange starts to predominate. Note that this energy corresponds to the energy at which one starts to see shoulders rather than peaks in the mass distribution. If this is not coincidence, then it supports the idea that the mass spectrum might depend on the production mechanism. However, the observation of two peaks in $\pi^- p \to n A_2^0$, where f^0 exchange cannot take place, contradicts this ([20]).

13. Are other members of the 2^+ nonet split?

The K*(1420). There have been several experiments which showed the K*(1420) mass spectrum ([45–50]), but just one precision measurement designed

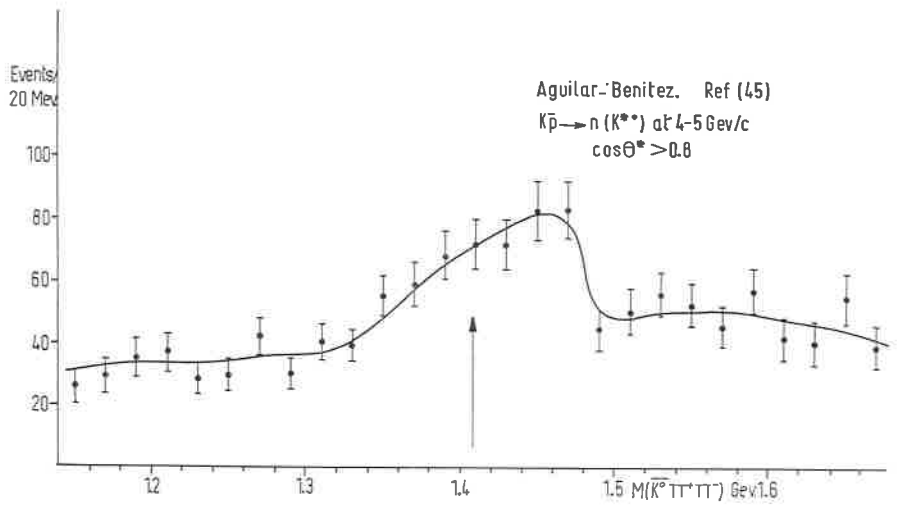

Fig. 19. – Mass spectrum of $K^*(1420) \to (\bar{K}^0\pi^+\pi^-)$ produced in $K^- p \to n K^{*0}$. This is one of the two experiments which give indications of an asymetric shape.

to look for structure ([49]). None of the experiments show any convincing structure, though two of them ([45,47]) show a sharp edge on the high mass

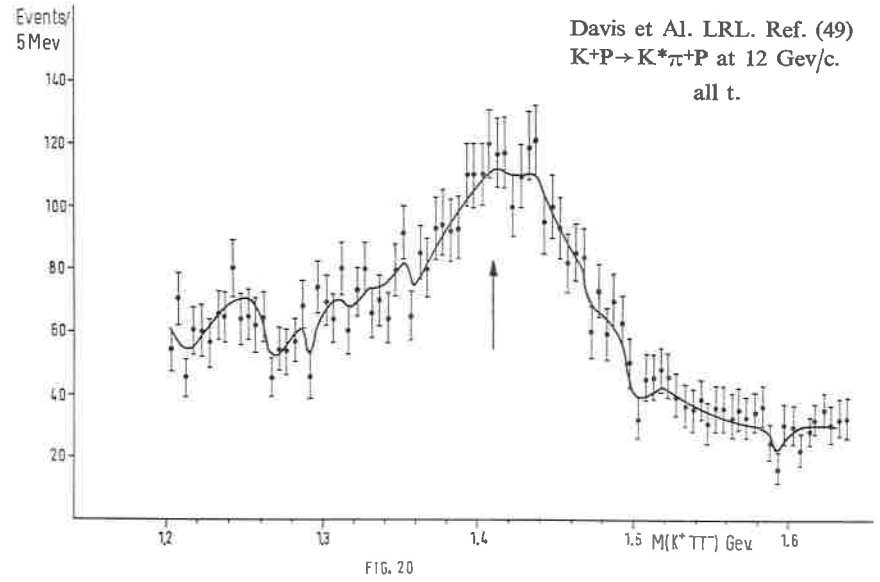

Fig. 20. – Mass spectrum of $K^*(1420) \to (K^+\pi^-)$ produced in $K^+p \to K^{*0}\pi^+p$. This high statistics high resolution spectrum shows no clear structure.

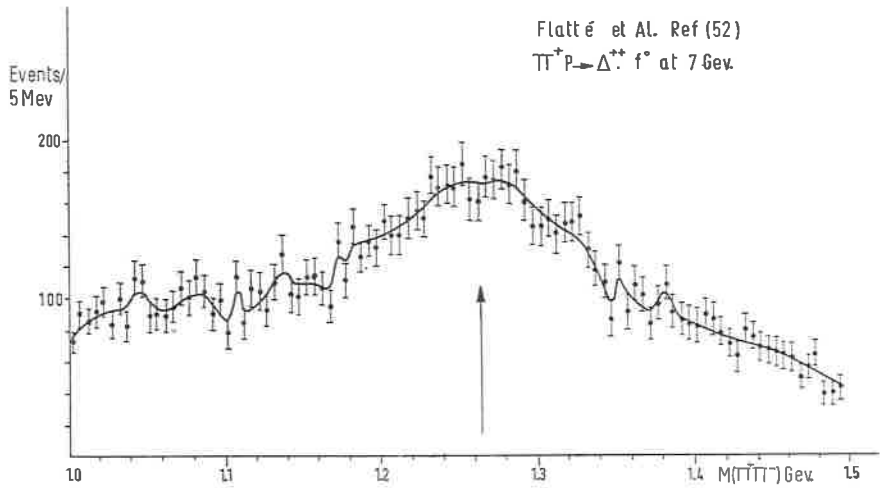

Fig. 21. – Mass spectrum of $f^0 \to (\pi^+\pi^-)$ produced in $\pi^+p \to \Delta^{++}f^0$. No structure is seen in this experiment which was designed to be able to see fine structure.

side of the resonance. Figure 19 shows one example of this sharp edge ([45]) and Fig. 20 shows the results of the LRL ([49]) experiment.

The $f^0(1260)$. As the number of experiments on f^0 increases ([51–58,21,30,31,36,19]), controversy increases. (Also statistical fluctuations have this behaviour.) Of these experiments, two groups have presented evidence for a structure ([55,58]), and one high statistics experiment ([52]) has found none. Figure 21 shows the high statistics measurement of Flattè *et al.* These is no evidence of any structure, in the peak, which is greater than wriggles in the rest of the curve.

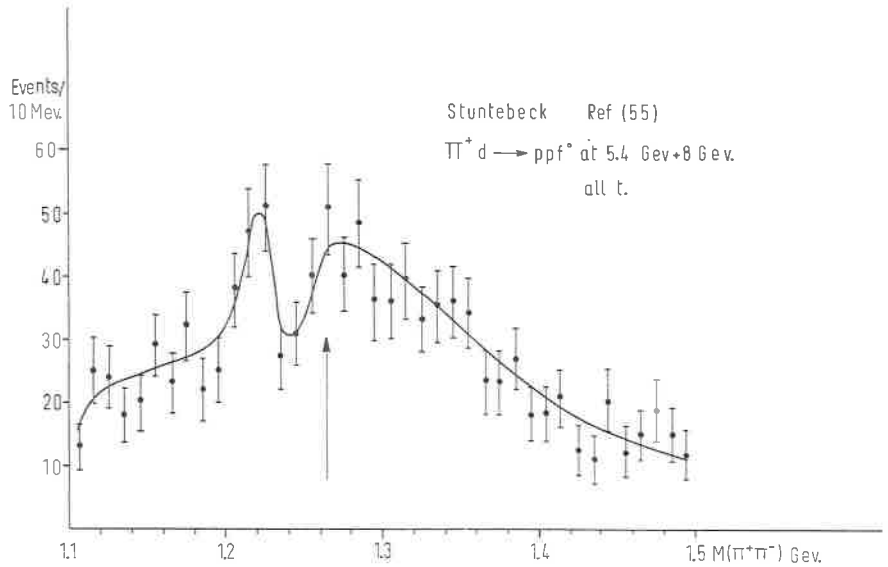

Fig. 22. – Mass spectrum of $f^0 \to (\pi^+\pi^-)$ produced in $\pi^+ d \to ppf^0$.

Only one experiment, Stuntebeck *et al.*, Fig. 22 ([55]), has shown a direct structure in the mass spectrum obtained in $\pi^- p \to f^0 n$ and also in $\pi^+ d \to pp f^0$. However, the χ^2 values give only a factor of four higher probability that the true distribution is a double pole rather than a single Breit Wigner, and both have acceptable χ^2. (Probability for a single Breit Wigner = 15%).

The second experiment shows an unusual effect which may or may not be an f^0 splitting type of effect. Ehrlich *et al.* ([58]) looked at the reaction $pp \to pp f^0$, and plotted the mass spectrum after selecting the momentum transfer to the proton. When only one proton was peripheral, they saw the f^0 at a mass of 1246 MeV and with a $J \geqslant 2$ decay distribution. However, when both protons were peripheral, they observed a displaced peak with a mass 1190 MeV

and $J = 0$ decay characteristics. This shift is comparable with the distance between the peaks in Stuntebeck *et al.*, though the mass values are quite different.

14. Conclusion.

In conclusion, the present indications are against a splitting which is a property of the whole nonet, unless it is a structure with a full width of less than 10 MeV in the K*(1420) and the f^0. There is some indication of a systematic dependence of the shape of the A_2 mass spectrum on incident pion energy in $\pi^{\pm}p$ interactions, but there is still no single experiment which has produced a result which could not be statistically compatible with one or other of the original two extreme cases of single Breit Wigner and Dipole. In some experiments, on both the A_2 and f^0, there is also the added complication that the background is not a smooth function of the mass.

Appendix. Classification of experiments.

For example consider the two-peaked shape superimposed on a background. Consider three equal mass intervals near the peak.

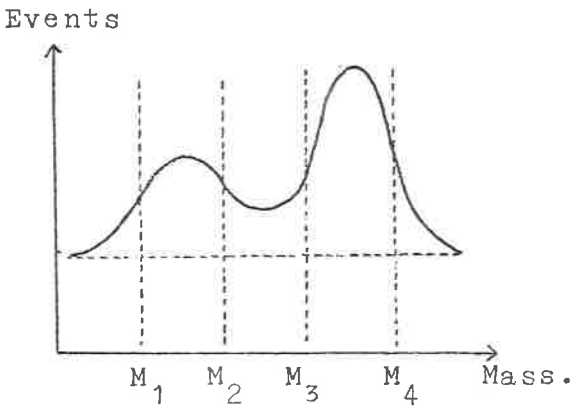

Let n = the number of A_2 in the $M_1 - M_4$ interval;
bn = the total background in this region;

f = the fraction of the A_2 in the $M_2 - M_3$ interval (f is a function of the resolution);
f_B = this fraction if the curve were a Breit Wigner. This varies much more slowly with resolution.

The apparent value of f is then

$$f' = (fn + bn/3)/(n + bn) = (f + b/3)/(1 + b) .$$

The statistical uncertainty in f, using binomial statistics, is

$$\{(f + b/3)\cdot(1 - f + 2b/3)/(1 + b)\}^{\frac{1}{2}}/\{n^{\frac{1}{2}}(1 + b)\} .$$

If the curve were a simple Breit Wigner, a value f'_B should be found, so the significance of any deviation is given by

$$G = \frac{f' - f'_B}{\text{Error}} = \frac{f - f_B}{\text{Error } (1 + b)} = (f - f_B)\sqrt{\frac{n(1 + b)}{(f + b/3)(1 - f + 2b/3)}} .$$

The term $f - f_B$ depends only on the resolution, σ.

The square root term depends on n, b and, through f, also on the resolution. However, in practical cases, f varies between 0.15 and 0.3, so setting $f = 0.32$ only introduces a $\pm 10\%$ error. Then the contribution to G may be written as the product

$$G = (f - f_B)\sqrt{n_{\text{eff}}}$$

where the quantity n_{eff}, which is proportional to the effective numbers of events, depends only on the number of events and on the background level:

$$n_{\text{eff}} = \frac{n(1 + b)}{(0.22 + b/3)(0.78 + 2b/3)} .$$

To draw contours of constant G in the (n_{eff}, σ) plane it is then necessary to introduce a specific shape, so as to calculate f.

REFERENCES

1) B. French, Rapporteur talk: *14th International Conference on High Energy Physics* Vienna (1968).
2) A. Astier, Rapporteur talk: *15th International Conference on High Energy Physics* Kiev (1970).

3) MMS; May 1965 (G4*a*); Oct. 1965 (G4*b*); Jan. 1967 (G6*b*, G6*c*, G6*f* and G7). These graphs are taken from ref. (*j*) below. The dates identify the measurement, and the numbers preceeded by G are the figure numbers in ref. (*j*).
4) CBS: March 1968 (G14*b*); April-May 1968 (G15), ref. (*j*); June-Oct. 1969 (G3*b*), ref. (*g*); June-Oct. 1969, ref. (*h*); Jan-Feb. 1970 (G9), ref. (*k*). The results of the CERN, MMS and SBS group have been published in the following: (*a*) B. LEVRAT *et al.*: *Phys. Lett.*, **22**, 714 (1966); (*b*) M. N. FOCACCI *et al.*: *Phys. Rev. Lett.*, **17**, 890 (1966); (*c*) G. CHIKOVANI *et al.*: *Phys. Lett.*, **25** B, 44 (1967); (*d*) G. CHIKOVANI *et al.*: *Philadelphia Conference on Meson Spectroscopy*, April 1968; (*e*) H. BENZ *et al. Phys. Lett.*, **28** B, 233 (1968); (*f*) G. CHIKOVANI *et al.*: *Phys. Lett.*, **28** B, 526 (1968); (*g*) R. BAUD *et al.*: *Phys. Lett.*, **31** B, 401 (1970); (*h*) R. BAUD *et al.*: *Phys. Lett.*, **31** B, 397 (1970); (*i*) C. NEF: CERN NP 70-20 and Thesis, University of Geneva. (*j*) W. KIENZLE, Review talk: *Philadelphia Conference on Meson Spectroscopy*. April 1968; (*k*) R. BAUD *et al.*, Invited paper: *Philadelphia Conference on Meson Spectroscopy*, May 1970.
5) M. ABRAMOVICH *et al.*: CERN/DPH II/Phys. 70-20 and *Nucl. Phys. B*, submitted 29-7-1970.
6) G. ASCOLI *et al.*: *Phys. Rev. Lett.*, **20**, 1321 (1968)
7) G. V. BEKETOV *et al.*: ITEF 816.
8) J. T. CARROLL *et al.*: *Phys. Rev. Lett.*, **25**, 1393 (1970).
9) S. U. CHUNG *et al.*: UCRL 16881, *Rev.* (1967).
10) S U. CHUNG *et al.*: *Phys. Rev. Lett.*, **12**, 621 (1964).
11) D. J. CRENNELL *et al.*: *Phys. Rev. Lett.*, **20**, 1318 (1968).
12) N. M. CASON *et al.*: *Phys. Rev. Lett.*, **18**, 880 (1967).
13) J. W. LAMSA *et al.*: *Phys. Rev.*, **166**, 1398 (1968).
14) A. W. KEY *et al.*: *Phys. Rev.*, **166**, 1430 (1968).
15) J. BALLAM *et al.*: *Phys. Rev. Lett.*, **21**, 934 (1968).
16) K. J. FOLEY *et al.*: *Phys Rev. Lett.*, **26**, 413 (1971).
17) G. GRAYER *et al.*: *Phys. Lett.*, **34** B 333 (1971).
18) O. I. DAHL *et al.*: *Phys. Rev.*, **163**, 1377 (1967).
19) A. R. DZIERBA *et al.*: Preprint University of Notre Dame.
20) M. BASILE *et al.*: *Lett. Nuovo Cimento*, **4**, 838 (1970).
21) N. ARMENISE *et al.*: *Lett. Nuovo Cimento*, **2**, 501 (1969).
22) M. ALSTON-GARNJOST *et al.*: UCRL 20129.
23) K. BÖCKMANN *et al.*: *Nucl. Phys.*, B **16**, 221 (1970).
24) W. R. BUTLER *et al.*: Paper submitted to *15th International Conference on High Energy Physics*, Kiev (1970).
25) G. GOLDHABER *et al.*: *Phys. Rev. Lett.*, **12**, 336 (1964).
26) M. ADERHOLZ *et al.*: *Phys. Lett.*, **10**, 226 (1964).
27) N. ARMENISE *et al.*: *Phys. Lett.*, **25** B, 54 (1967).
28) G. BENSON *et al.*: *Phys. Lett.*, **16**, 1177 (1966).
29) I. R. KENYON *et al.*: *Phys. Rev. Lett.*, **23**, 146 (1969).
30) R. J. MILLER *et al.*: *Phys. Rev.*, **178**, 2061 (1969).
31) B. GHIDINI *et al.*: Paper submitted to *15th International Conference on High Energy Physics*, Kiev (1970).
32) K. W. J. BARNHAM *et al.*: UCRL 20050.
33) N. N. BISWAS *et al.*: *Phys. Rev.* D2 2529 (1970).

34) D. J. CRENNELL *et al.*: *Phys. Rev. Lett.*, **22**, 1327 (1969).
35) G. ALEXANDER *et al.*: *Phys. Rev.*, **183**, 1168 (1969).
36) H. BRIAND *et al.*: Paper submitted to *15th International Conference on High Energy Physics*, Kiev (1970).
37) R. A. DONALD *et al.*: *Nucl. Phys.*, B **12** 325 (1969).
38) J. DIAZ *et al.*: *Nucl. Phys.*, B **16**, 239 (1969).
39) H. ATHERTON *et al.*: CERN/DPH II/Phys. 70-26.
40) AGUILAR-BENITEZ *et al.*: *Phys. Lett.*, **28** B 62 (1969).
41) G. CONFORTO: *Nucl. Phys.*, B **3**, 469 (1967).
42) P. ESPIGAT *et al.*: CERN/DPH II/Phys. 71-7.
43) G. ASCOLI *et al.*: COO-1195-193 (1970).
44) J. CLAYTON *et al.* (Liverpool-Athens): Private communication.
45) M. AGUILAR-BENITEZ *et al.*: *Phys. Rev. Lett.*, **25**, 1362 (1971).
46) G. ALEXANDER *et al.*: *Phys. Rev.*, **183**, 1168 (1969).
47) G. BASSOMPIERRE *et al.*: *Nucl. Phys.*, B **13**, 189 (1969).
48) G. CHARRIERE *et al.*: CERN/D Phys. II/Phys. 70-30.
49) P. J. DAVIS *et al.*: *Phys. Rev. Lett.*, **23**, 1071 (1969).
50) A. FIRESTONE *et al.*: UCRL 19813.
51) S. M. BEAUPRE *et al.*: CERN/DPH II/Phys. 70-42.
52) S. M. FLATTÈ *et al.*: UCRL 20273.
53) B. GAIDOS *et al.*: COO 1428-248.
54) B. LÖRSTAD *et al.*: *Nucl. Phys.*, B **14**, 63 (1969).
55) P. H. STUNTEBECK *et al.*: *Phys. Lett.*, **32** B 391 (1970).
56) N. N. BISWAS *et al.*: *Phys. Rev. D* **2**, 2529 (1970).
57) W. BEUSCH *et al.*: Paper submitted to the *15th International Conference on High Energy Physics*, Kiev (1970).
58) R. EHRLICH *et al.*: Preprint Rutgers, The State University New Brunswick, New Jersey.

Measurements of the A_2^- and A_2^+ mass spectra (*)

D. Bowen, D. Earles, W. Faissler, D. Garelick
M. Gettner, M. Glaubman, B. Gottschalk, G. Lutz, J. Moromisato
E. I. Shibata, Y. W. Tang and E. von Goeler
Northeastern University at Boston - Boston, Mass.

H. R. Blieden, G. Finocchiaro, J. Kirz and R. Thun
State University of New York at Stony Brook - Stony Brook, N. Y.

I am reporting on an experiment carried out at BNL by a collaboration between Northeastern University at Boston and the State University of New York at Stony Brook.

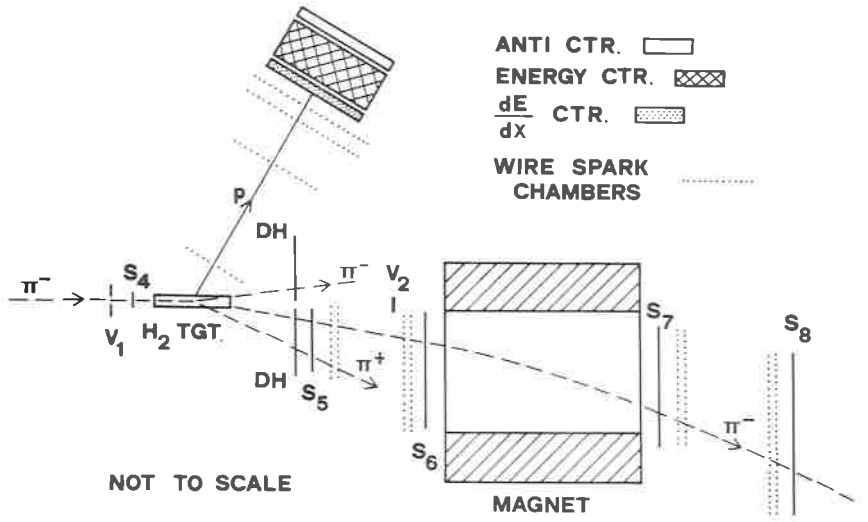

Fig. 1. – Detector arrangement. The symbols $S_1, S_2, \ldots, S_8$ label aperture-defining scintillation counters; V_1 and V_2 label veto counters; and DH label the decay hodoscope. The beam enters the detector region from the left after traversing a Čerenkov counter, for π identification, and three beam hodoscopes which determined the momentum, angles, and lateral position of the incident particle at the hydrogen target.

(*) Invited paper presented by G. Lutz.

The main objective of the experiment has been to study the reaction

$$\pi^- p \to p(MM)^-$$
$$\qquad\quad \lfloor\to \pi^-(MM)^0 .$$

Figure 1 shows the double arm spectrometer built for this experiment. The proton telescope consists of 4 spark chambers which measure the direction of the proton followed by 5 identical proton detectors which subdivide the vertical aperture. Each proton detector consists of a thin scintillation counter which measures the energy loss dE/dx, a thick block of scintillator which measures the energy E of the proton ([11]) and an anticounter vetoing particles which do not stop in the proton counter. Also recorded is the time of flight of the proton (TOF). The proton is identified by consistency between E and dE/dx and between E and TOF. The forward magnetic spectrometer measures the direction and momentum of the pion. Although this spectrometer was not used for measuring A_2 decay, it proved to be very useful to monitor the stability of the beam and to measure the mass resolution of the experiment. There are also some hodoscope counters (DH) to measure the charged decay multiplicity of the resonance.

In our first measurements in June 1970 we tried to reproduce the A_2 splitting ([1]) in order to check the quality of our apparatus. When we did not see any indication of a split, we made some changes on the target in order to increase the mass resolution. A high statistics run on the A_2 has been done in the period October-November 1970 with negative pions at 5 and 7 GeV/c and positive pions at 5 GeV/c.

I will now explain how we measure the resolution and stability of the experiment. The missing mass is given by

$$M^2 = (p_b + m - p)^2 = m_\pi^3 -$$
$$- 2T(E_b + m) + 2P_b P \cos\theta$$
$$P = \sqrt{T(T + 2m)}$$
$$t = -2mT .$$

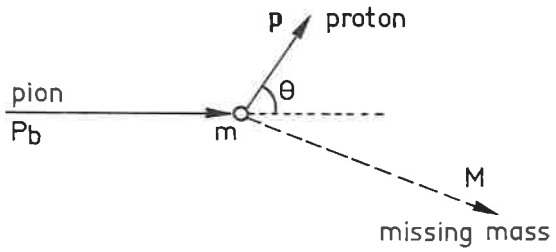

Three measured quantities enter in the missing mass, the beam momentum P_b, the proton kinetic energy T, and the proton scattering angle θ. The kinematics for a beam of 7 GeV/c is shown in Fig. 2. Note that we measure the A_2 in a region close to the Jacobian peak and therefore are insensitive to the energy resolution of the proton counter.

The mass resolution has been measured by two methods, one giving an upper limit for the resolution, the other giving the precise value of the mass

resolution. The upper limit for the mass resolution has been obtained by observing the (missing mass)^2 spectrum of a narrow « resonance »—the pion. Frequent measurements of the pion have been done at 5 GeV and 7 GeV by changing the angle of the proton telescope by about 20°. In addition at 7 GeV the pion data have been taken simultanously with the A_2 data since at this beam energy a larger mass range is covered by the proton telescope. All

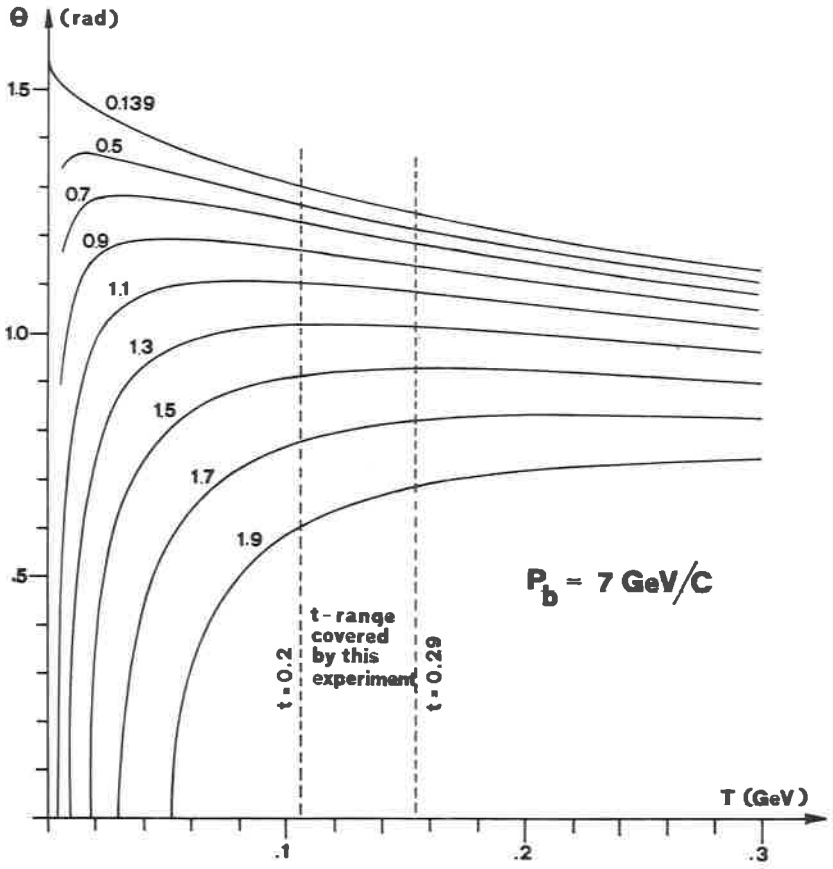

Fig. 2. – Kinematics for the reaction $\pi^{\pm}p \to p(MM)^{\pm}$ at 7 GeV/c beam momentum. Plotted is the proton scattering angle θ *vs.* the proton kinetic energy T for fixed missing mass.

calibration data taken at the same beam momentum have been summed up, so the measured resolution includes drifts in the beam momentum and the proton energy calibration. These drifts have also been monitored separately and are inconsequential effects in this experiment.

Knowing that the mass resolution at the pion is sensitive to both angle and energy resolution of the proton, while at the A_2 only the angle is important—as seen from the error derivatives in Table I—one gets an upper limit for the mass resolution by assuming that the width of the missing mass square

TABLE I. – *Error derivatives for a beam of* 7 GeV/c. The derivatives are given for the pion mass and the A_2 mass at the center and at both ends of the t range covered by this experiment. All quantities are given in GeV and radians.

MM	T	t	$\partial M^2/\partial P_b$	$\partial M^2/\partial\theta$	$\partial M^2/\partial T$
0.1396	0.107	0.200	0.0287	— 6.21	— 7.51
	0.131	0.245	0.0351	— 6.86	— 7.42
	0.155	0.290	0.0416	— 7.33	— 7.45
1.3	0.107	0.200	0.267	— 5.49	0.75
	0.134	0.245	0.275	— 6.18	— 0.74
	0.155	0.290	0.280	— 6.67	— 1.52

peak of the pion is due to the angular resolution only. The angular resolution then predicts the mass resolution at the A_2 mass. Added to this resolution is the contribution from the beam which has been measured separately by observing elastic scattered pions with the fast spectrometer. A small fraction of these data have been taken at the same time as the A_2 data were being recorded, and thus include any drifts in beam momentum.

TABLE II. – *Experimental resolutions* (FWHM) *and their contributions to the* A_2 *mass resolution*. Proton resolutions are for $0.20 \leqslant |t| \leqslant 0.29$ (GeV)^2.

Beam momentum (GeV)	5	7
Proton production angular resolution (mr)	8.6 ± 0.4	8.6 ± 0.4
Contribution to A_2 mass resolution (MeV)	13 ± 0.7	20 ± 1.0
Proton energy resolution (MeV)	5.0 ± 1.0	5.0 ± 1.0
Contribution to A_2 mass resolution (MeV)	3.0 ± 0.5	1.0 ± 0.5
Beam momentum resolution (MeV)	54 ± 2.0	61 ± 2.0
Contribution to A_2 mass resolution (MeV)	8.0 ± 0.4	6.4 ± 1.0
Total A_2 *mass resolution* (MeV) ($M = 1.30$ GeV)	16 ± 1.0	21 ± 1.0

The *upper limit* for the mass resolution obtained by this method is 19 MeV for the 5 GeV data and 25 MeV for the 7 GeV data. With the statistical accurancy of our experiment a mass resolution of this magnitude is clearly sufficient to detect two peaks 40 MeV apart.

The precise value of the mass resolution has been extracted from the elastic scattering events, where both the proton and the scattered pion have been detected. From these data it is possible to extract separately both the

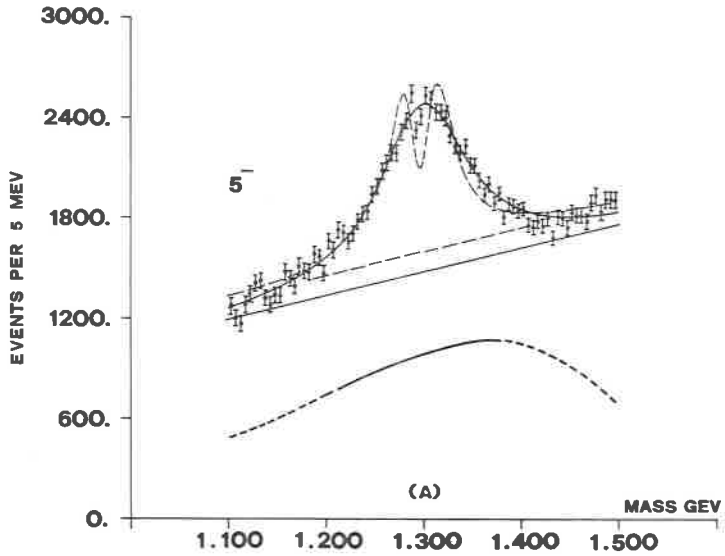

Figs. 3*a*-3*c*. – Mass spectra at 5–, 5+, and 7– GeV. The solid lines through the data are the Breit-Wigner fits, and the solid straight lines beneath the data are the associated fitted linear backgrounds. The dashed lines in the region of the data are the dipole fits (Γ dipole = 28 MeV, fixed) and their associated backgrounds. The calculated detection efficiencies *vs.* mass are shown (arbitrary units) as dashed lines ($1.10 \leqslant M \leqslant 1.22$ GeV and $1.38 \leqslant M \leqslant 150$ GeV) and as solid lines ($1.22 \leqslant M \leqslant 1.38$ GeV, « resonance » region). The detection efficiencies have been normalized so that at $M = 1.300$ MeV the ordinates on the graphs indicate the actual number of events detected in the experiment per 5 MeV bin.

proton angular resolution and the proton energy resolution. The experimental resolution of each of the measured quantities and its contribution to the A_2 mass resolution is listed in the Table II. The mass resolution is heavily dominated by the proton scattering angle resolution which in turn is dominated by multiple scattering of the proton and can be calculated quite well from the amount of material in the proton path. The calculated value of the angular resolution agrees with the measured value given in the table.

A number of tests have been done to check the stability of the experimental conditions and the consistency of data taken at different times and in each proton counter. No difficulties have been found and only a small fraction of the data has been omitted due to technical failures. The elastic scattering

cross section and their t-dependence agrees well (within $\pm 10\%$) with published values ([6]). This checks the event selection criteria and the detection efficiency correction.

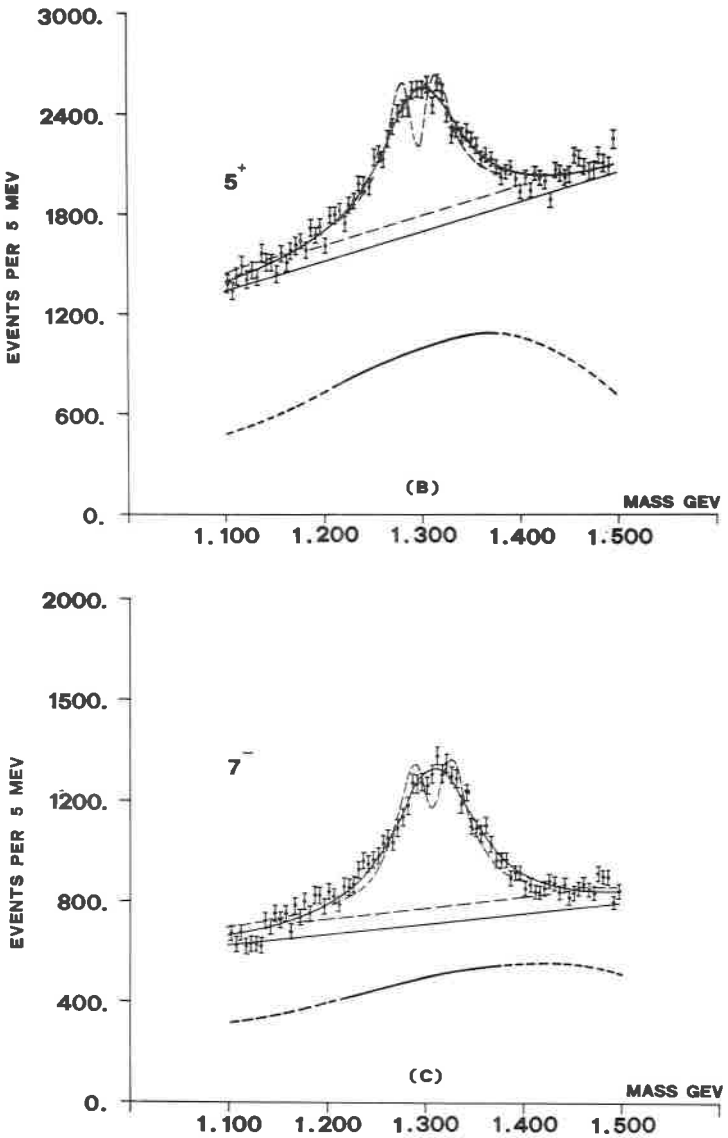

The A_2 spectra divided by the detection efficiency are shown in Fig. 3. There are 28 000 A_2^- events above background at 5 GeV, 24 000 A_2^+ events at 5 GeV

and 17000 A_2^- events at 7 GeV. The statistical precision is better than 3% per 5 MeV bin.

The results of fits to the data are summarized in Table III. All of the A_2 data are

TABLE III. – *Results of the fits.* The data are fitted over the interval $1.1 \leqslant M \leqslant 1.5$ GeV with a Breit-Wigner, B, (or a dipole, D), distribution plus a linear, L, or linear plus quadratic, Q, background. The number of degrees of freedom for the entire interval $1.1 \leqslant M \leqslant 1.5$ GeV is 75 for the L fits and 74 for the Q fits. χ_T^2 and χ_R^2 are the total χ^2 for the regions $1.1 \leqslant M \leqslant 1.5$ GeV and $1.22 \leqslant M \leqslant 1.38$ GeV, respectively. The quantity $\Sigma \equiv (\chi_d^2 - \chi_B^2)/\sqrt{60}$ is the difference in χ^2 for the D and B fits for $1.22 \leqslant M \leqslant 1.38$ GeV divided by the approximate expected fluctuation in χ^2 for this mass interval. P_R is the probability of the fit calculated from the χ^2 in the region $1.22 \leqslant M \leqslant 1.38$ GeV. M_0, Γ, and R are the resonance mass, width, and signal to background ratio (at $M = M_0$) given by the fits. The uncertainties listed with M_0, and Γ include the effects of possible systematic errors associated with determining these quantities.

Resonance and background distribution used	Beam momenta (GeV)	R	M_0 (MeV)	Γ (MeV)	χ_T^2	χ_R^2	P_R	Σ
B + L	5–	0.79	1299 ± 6	105 ± 5	114	31	41%	—
D + L	5–	—	1299 ± 6	26 ± 1	368	238	10^{-34}	27
D + L (*)	5–	—	1298 ± 6	28 (*)	374	252	10^{-37}	29
B + L	5+	0.52	1300 ± 6	99 ± 5	94	27	62%	—
D + L	5+	—	1300 ± 6	25 ± 1	271	179	10^{-26}	20
D + L (*)	5+	—	1300 ± 6	28 (*)	283	200	10^{-27}	22
B + L	7–	0.89	1309 ± 4	103 ± 5	100	29	51%	—
D + L	7–	—	1308 ± 4	27 ± 1	231	135	10^{-15}	14
D + L (*)	7–	—	1308 ± 4	28 (*)	231	138	10^{-16}	14
B + Q	5–	0.82	1300 ± 6	118 ± 9	109	30	46%	—
D + Q	5–	—	1298 ± 6	23 ± 1	243	114	10^{-11}	11
D + Q (*)	5–	—	1298 ± 6	28 (*)	281	166	10^{-21}	18
B + Q	5+	0.61	1300 ± 6	113 ± 9	89	27	62%	—
D + Q	5+	—	1301 ± 6	22 ± 1	195	94	10^{-8}	9
D + Q (*)	5+	—	1299 ± 6	28 (*)	234	146	10^{-17}	15
B + Q	7–	0.81	1309 ± 4	96 ± 9	99	29	51%	—
D + Q	7–	—	1309 ± 4	23 ± 1	138	58	0.16%	4
D + Q (*)	7–	—	1308 ± 4	28 (*)	159	87	10^{-7}	7

(*) For these fits the dipole width was fixed at $\Gamma = 28$ MeV.

clearly compatible with a Breit Wigner resonance and rule out a dipole regardless of the form of background assumed (7).

REFERENCES

1) The A_2^- splitting has been observed in experiments of the CERN Missing Mass Spectrometer Group ([2-5]).
2) B. LEVRAT *et al.*: *Phys. Lett.*, **22**, 714 (1966).
3) G. CHIKOVANI *et al.*: *Phys. Lett.*, **25** B, 44 (1967).
4) H. BENZ *et al.*: *Phys. Lett.*, **28** B, 233 (1967).
5) R. BAUD *et aq.*: *Phys. Lett.*, **31** B, 397 (1970).
6) C. T. COFFIN *et al.*: *Phys. Rev.*, **159**, 1169 (1967).
7) The energy and t range covered by this experiment agrees with that of the original CERN Missing Mass Experiment ([2-3]). Several other experiments ([8-10]) in which no dipole-like shape was found observed the A_2 under conditions differing from those of the CMMS experiments and thus do not necessarily contradict the CMMS findings.
8) M. ALSTON-GARNJOST *et al.*: *Phys. Lett.*, **33** B, 607 (1970).
9) G. GRAYER *et al.*: *Phys. Lett.*, **34** B, 333 (1971).
10) K. J. FOLEY *et al.*: *Phys. Rev. Lett.*, **26**, 413 (1971).
11) B. GOTTSCHALK: *Rev. Sci, Inst.*, **40**, 22 (1969).
B. GOTTSCHALK *et al.*: *Nucl. Inst. and Meth.* 97, 291 (1971).

Study of the A_2^- from the reaction $\pi^- p \to K_S^0 K^- p$ at 4.5 GeV/c (*)

KWAN-WU LAI

Physics Department, Brookhaven National Laboratory - Upton, N. Y.

I would like to present a recent study of A_2^- from the reaction $\pi^- p \to K_S^0 K^- p$ at 4.5 GeV/c in the 80 in. hydrogen bubble chamber by D. J. Crennell, H. A. Gordon, J. M. Scarr, and myself.

1. Experimental details.

The most controversial question in meson spectroscopy is the possible fine structure in the A_2 mass spectrum particularly in the $K\bar{K}$ decay mode. To investigate this question, we report in this paper the results of a study of $A_2^- \to K_S^0 K^-$ from a sample of 542 events from the reaction

$$\pi^- p \to K_S^0 K^- p \qquad (1)$$

where the K_S^0 decays by the charged mode.

The data come from 500000 pictures obtained in the Stanford Linear Accelerator Center (SLAC) 82 in. hydrogen bubble chamber exposed to a separated 4.5 GeV/c π^- beam ([1]). These events were measured on the Brookhaven National Laboratory Flying Spot Digitizer and processed through the standard BNL analysis programs ([2]). Because of the importance of the experimental resolution in searching for structure in the A_2 mass spectrum, all the experimental details have been scrutinized. We used ~ 5000 four-constraint four-prong events as well as ~ 40000 K_S^0's and Λ's to study systematic errors in the reconstruction and fitting of the events as a function

(*) Invited paper

Work performed under the auspices of the U. S. Atomic Energy Commission.

of their location in the chamber. The statistical distributions (pulls) of these events as well as the K_S^0 and Λ mass distributions suggested some small adjustments in the geometrical and magnetic field constants ([3]). The known spatial dependence of the beam momentum was calibrated with a sample of four-prong four-constraint events by fitting for the beam momentum. We concluded that the beam momentum was known to $\pm 0.3\%$ at any point in the chamber. Two methods were employed to check the realiability of the mass resolution calculated by the fitting program. First, the events of reaction (1) were fitted as if the reaction were $\pi^- p \to p K^- \pi^+ \pi^-$. The $\pi^+\pi^-$ effective mass distribution is well fitted by a Gaussian of mass (498.9 ± 0.2) MeV and full width at half maximum of (8 ± 1) MeV. The resolution calculated from measurement errors propagated through the kinematic fitting process is also found to be 8 MeV. Secondly, the events were fitted to reaction (1) but with the proton mass unconstrained. A fit to the distribution of masses recoiling from the $K_S^0 K^-$ yields a proton mass of (939 ± 1) MeV with a full width at half maximum of (8 ± 0.5) MeV in good agreement with the propagated resolution of 9 MeV. Therefore, we can infer that the resolution full width at half maximum of the $K_S^0 K^-$ mass in the A_2^- region cannot be very different from the calculated value of (8 ± 1) MeV.

2. Mass and width.

The Dalitz plot for the $K_S^0 K^- p$ final state is shown with the mass-squared projections in Fig. 1*a*. The marked A_2^- and $\Lambda(1520)$ bands do not cross. Hence, removing the $\Lambda(1520)$ will not affect the analysis of the A_2^- but will reduce the background on the high mass side. Figure 1*b* shows the $K_S^0 K^-$ mass spectrum near the A_2^- (plotted in 10 MeV bins because the resolution is 8 MeV full width at half maximum). There is no significant dip near the A_2^- mass (1.3 GeV) in the $K_S^0 K^-$ mass spectrum such as that reported in the 7 GeV/c $\pi^- p$ CERN experiment for $A_2^- \to K_S^0 K^-$ ([4]). A single Breit-Wigner resonance form plus a linear background was fitted to this mass spectrum by the maximum likelihood method ([5]); the result is shown by the solid curve in Fig. 1*b* where the resonance has mass (1313 ± 7) MeV and width 125^{+19}_{-16} MeV ([6]). A similar fit with a two parameter « dipole » plus a linear background yields two acceptable solutions with masses (1296 ± 2) and 1314^{+4}_{-3} MeV, respectively ([7]). The latter fit is shown dashed in the figure. In an attempt to measure the acceptability of these fits we have calculated a χ^2 in the mass region from 1100 to 1500 MeV and obtain probabilities of 80%

for the single Breit-Wigner resonance, 13% and 19% for the dipole fits ([8]). However, the χ^2 calculation depends greatly on the choice of bin size, so we also quote the ratio of the likelihoods which is 240:1 with the Breit-Wigner fit favored over either dipole fit.

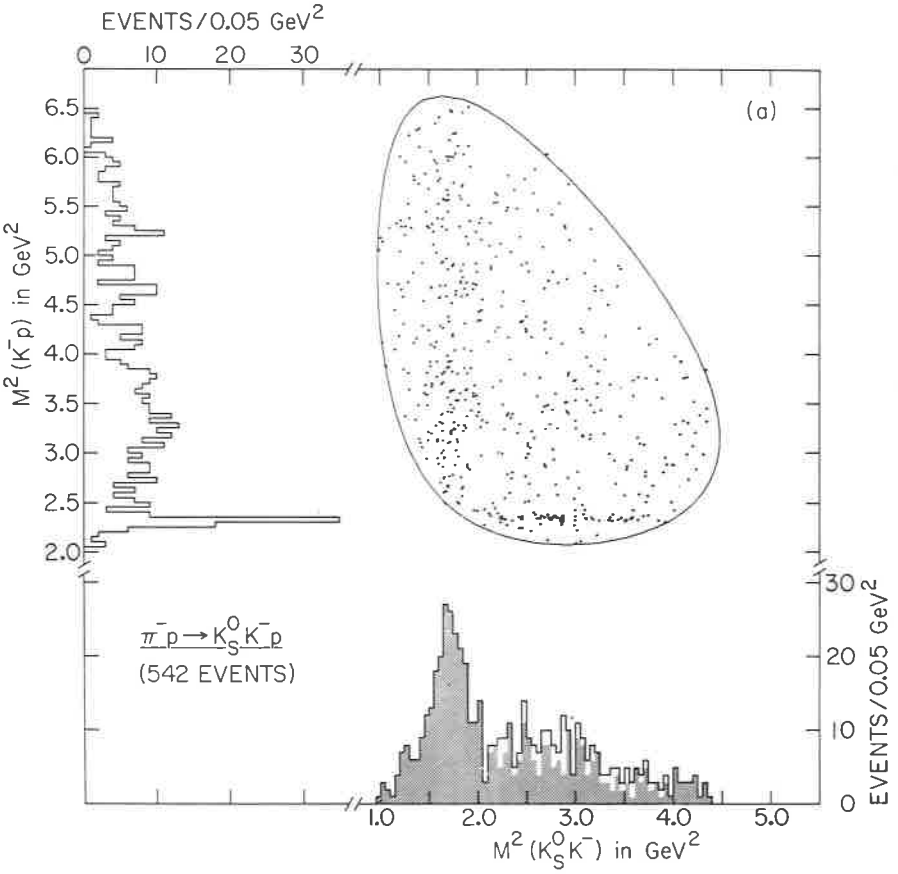

Fig. 1. – *a*) Dalitz plot and mass squared projections. Shaded area is the events with $Y_0^*(1520)$ removed.

To check further on systematic errors of the mass and width of these fits, we fit the narrow $\Lambda(1520) \to K^- p$ from the same final state and obtain a mass of $(1519 \cdot 6 \pm 1.4)$ MeV and a width of 11^{+3}_{-2} MeV. They are in excellent agreement with the established values. This gives additional confidence in our understanding of the systematics in this experiment. Therefore we conclude

that, with the present statistics, we favor the single Breit-Wigner resonance interpretation even though we cannot rule out the « dipole » assumption on the χ^2-probability basis alone. However, we do not see the split in the $A_2^- \to K_S^0 K^-$ reported by the 7 GeV/c π^-p CERN experiment (with 0.2

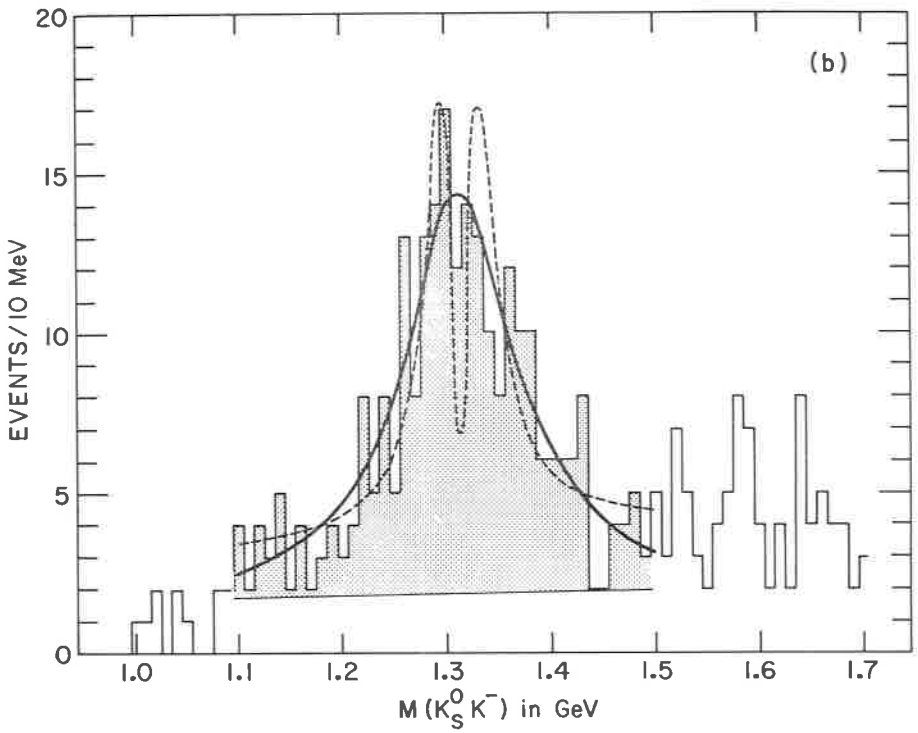

Fig. 1. – *b*) $K_S^0 K^-$ mass with solid curve indicating fit of data to a simple Breit-Wigner fit, solid line the background for that fit; the dotted line indicates the best dipole fit. Excess events in the (1.5÷1.7) GeV mass region are attributed to the g(1630)–meson (see text for details).

$< |t| < 0.29$ GeV^2) although we have a resolution less than half as broad. In fact, our data show remarkable similarity to the Berkeley 7 GeV/c π^+p data for $A_2^+ \to K_S^0 K^+$ (9).

3. Production and decay correlations.

The production angular distribution of A_2^- can best be studied in the $K_S^0 K^-$ decay mode because of the small background ($< 20\%$) in the mass

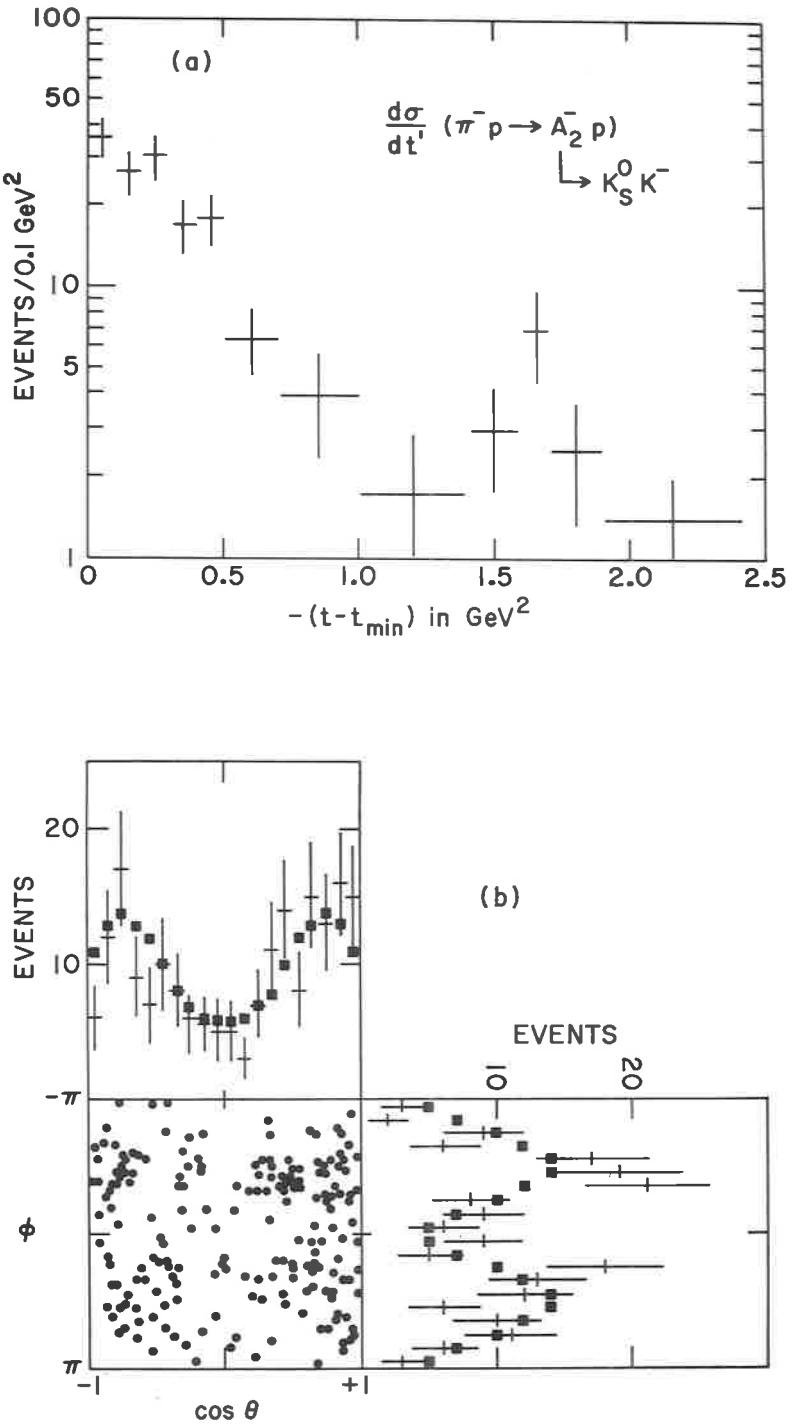

Fig. 2. – *a*) Differential cross-section for events in the A_2 region (1.2÷1.4 GeV). *b*) Decay and angular distributions for events in the A_2 region. Solid squares indicate best fit to the data.

region $(1.2 \div 1.4\ \text{GeV})$. Figure 2*a* displays this distribution as a function

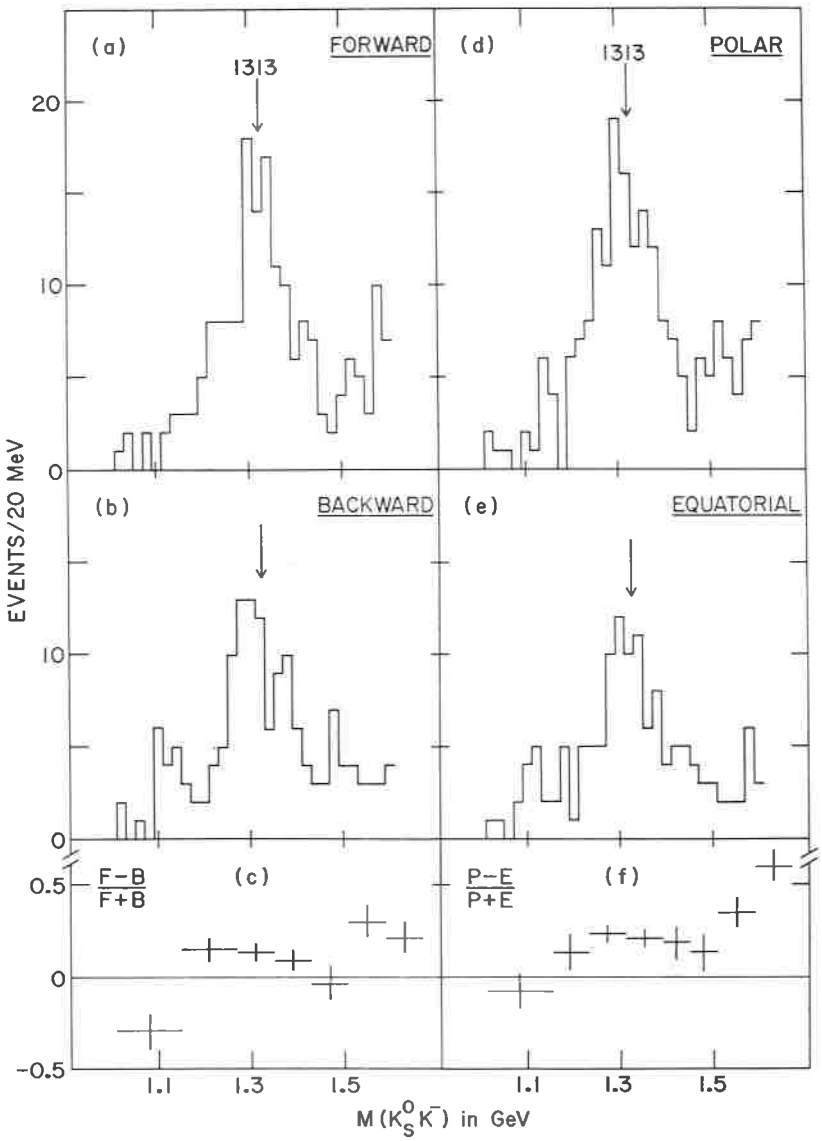

Fig. 3. – *a-b-d-e*) $K_S^0K^-$ mass distributions for various selections on the decay angle $\cos\theta$ with respect to K_S^0 in the Gottfried-Jackson frame (see text for details). Arrows at 1.313 GeV indicate central value of best fit to the total $K_S^0K^-$ mass spectrum for A_2^-: *c*) and *f*) are forward-backward and polar-equatorial asymmetry as a function of $K_S^0K^-$ mass.

of $t' = t - t_{\min}$ which can be fitted by the functional form $\sim \exp[bt']$ up to $|t'| \simeq 1$ GeV^2 with a value of $b = (3 \pm 0.5)$ GeV^{-2}. There is a significant break in the distribution at $|t'| \sim 1.0$ GeV^2. Because of the limited t range studied so far by the counter experiments, the structure of the $A_2^- \to K_S^0 K^-$ production at large t region has not been revealed. We will return to this point after our examination of the decay correlations of the $A_2^- \to K_S^0 K^-$ as shown in Fig. 2*b*. Because of the 4π-solid angle detection in this experiment, escape corrections for the events in the A_2^- mass region are negligible ($< 3\%$). There are four clusters of events in the scatter-plot of $\cos\theta$ vs φ with respect to K_S^0 in the Gottfried-Jackson frame for the A_2^- events. A maximum likelihood fit to the decay angles gives spin-density matrix elements of $\varrho_{0,0} = 0.14 \pm 0.05$, $\varrho_{1,1} = 0.34 \pm 0.03$ and $\varrho_{1,-1} = 0.24 \pm 0.04$ with all the other elements consistent with zero ([10]). A study of the events adjacent to the A_2^- shows that a background subtraction does not change these values of $\varrho_{m,n}$. At this energy the values of $\varrho_{1,1}$ and $\varrho_{1,-1}$ do not reach the maximum allowed value ($\varrho_{1,1} = \varrho_{1,-1} = 0.5$) for a pure ϱ exchange. In addition, the value of ϱ_{00} seems to be non-zero. We have also studied the spin-density matrix elements as a function of t' and find only ϱ_{00} is different for $|t'| < 0.3$ GeV^2 ($\varrho_{00} = 0.28 \pm 0.07$) compared to $|t'| > 0.3$ GeV^2($\varrho_{00} = 0.12 \pm 0.06$). These facts, plus the break observed at ~ 1.0 GeV^2 in A_2^- production, may suggest that trajectories other than the ϱ contribute to A_2^- production.

4. Experimental comments.

Since this experiment has the largest sample of bubble chamber events in the $K_S^0 K^-$ decay of the A_2^- from $\pi\mathcal{N}$ interactions, some experimental comments are necessary when one compares the 4π-solid angle $K_S^0 K^-$ results (bubble chamber) with those of limited solid angle (counter). It is known that interference between states of different J^P may affect the $K_S^0 K^-$ mass spectrum if one does not detect all of the solid angle of $K_S^0 K^-$ decay. To illustrate this point, Fig. 3 shows the $K_S^0 K^-$ spectra in the A_2^- region subjected to the following cuts in the $K_S^0 K^-$ rest frame: $\cos\theta > 0$, $\cos\theta < 0$, $|\cos\theta| > 0.5$, and $|\cos\theta| < 0.5$ corresponding to forward, backward and polar, equatorial regions as shown in Figs. 3*a-b-d* and *e* respectively. These show that a possible mass shift of ~ 10 MeV as well as a width difference of as much as ~ 20 MeV or both can be achieved by these cuts ([11]). Furthermore, the forward-backward asymmetry $((F - B)/(F + B))$ observed in Fig. 3*c* indicates interference between the A^- and the other amplitude(s) does indeed exist, whereas the

asymmetry in $((P-E)/(P+E))$, as shown in Fig. 3*f*, is expected because of the nature of the A_2^- decay. Therefore, it is clear that different decay region of $A_2^- \to K_S^0 K^-$ from this experiment may exhibit different mass distributions of the A_2^-. This observation will make direct comparisons of $K_S^0 K^-$ mass spectra between the « all » solid angle (such as bubble chamber) experiments and the « limited » solid angle (such as counter) experiments very difficult. This comment does not apply, of course, to missing mass experiments where no requirements were made of the decay products.

5. Concluding remarks.

The $A_2^- \to K_S^0 K^-$ observed in our experiment at 4.5 GeV/c for all t values does not show the «split» as seen in the 7 GeV/c π^- CERN experiment for $A_2^- \to K_S^0 K^-$ for $|t| = 0.2$ to 0.29 GeV^2. In fact their « dipole » fit (60%) to the $A_2^- \to K_S^0 K^-$ cannot rule out the assumption of a single Breit-Wigner fit (5%) ([4]). Our mass resolution, $\Gamma = 8$ MeV, is more than a factor of two better than that experiment ($\Gamma = 20$ MeV). On the other hand, our result agrees well with that of the 7 GeV/c π^+ Berkeley result. Therefore, it is reasonable to conclude that, within the limited statistics, the $A_2^- \to K_S^0 K^-$ and $A_2^+ \to K_S^0 K^+$ exhibit no obvious difference. In view of the recent 17 GeV/cπ^-p CERN ([12]) and 20.2 GeV/c-π^-p BNL ([13]) experiments of $A_2^- \to K_S^0 K^-$ (no split), we further suggest that the structure (or non-structure) $A_2^- \to K_S^0 K^-$ has no energy dependence between 4.5 and ~ 20 GeV/c.

The narrow structure in the $K_S^0 K_S^0$ mass spectrum from the 6 GeV/c π^-p experiment ([14]) is not observed in this experiment.

REFERENCES

1) For a description of the beam see S. FLATTÉ, Lawrence Radiation Laboratory Berkeley Group A Physics Note no. 646 (1968), unpublished.
2) The one event ambiguous with another hypothesis was removed from the sample.
3) The magnetic field was changed by 0.3% and the index of refraction of the hydrogen was changed by 1.2%. These changes result in a root-mean-square change of 2.1 MeV in the K^0K^- mass in the A_2^- region, negligible compared to the resolution (8 MeV).
4) R. BAUD *et al.*: *Phys. Lett.*, **31** B, 397 (1970); P. SCHUBELIN: private communication.
5) A simple Breit-Wigner form $[\Gamma^2/((M-M_0)^2+\Gamma^2/4)]$ was used.
6) The width and, to a lesser extent, the mass are slightly dependent on the mass limits (1.1÷1.5 GeV) and the background. The quoted errors reflect this uncertainty.

7) The experimental resolution has been folded into the « dipole » expression

$$\left[\Gamma^2(M-M_0)^2 \Big/ \left((M-M_0)^2+\frac{\Gamma^2}{4}\right)^2\right].$$

8) Bins were combined so that no contribution to the χ^2 had less than 10 events. The $P(\chi^2)$ did not change whether the entire mass region $(1.1 \div 1.5$ GeV) was used in this way or only the events within one full width were used.

9) M. ALSTON-GARNJOST *et al.*: *Phys. Lett.*, **33 B**, 607 (1970).

10) We fit the events assuming $J^P = 2^+$; for example see J. D. JACKSON: *Nuovo Cimento*, **34**, 1644 (1964).

11) Using the same type of fit as for the overall mass spectrum, we obtain for the forward events $M = 1320 \pm 9$, $\Gamma = 152 \pm 25$; backward $M = 1297 \pm 12$, $\Gamma = 77^{+26}_{-19}$; polar $M = 1313 \pm 9$; $\Gamma = 145 \pm 25$; equatorial $M = 1313 \pm 12$, $\Gamma = 90^{+30}_{-22}$.

12) G. GRAYER *et al.*: CERN-Munich Preprint (1970).

13) K. J. FOLEY *et al.*: *Phys. Rev. Lett.*, **26**, 413 (1971).

14) D. J CRENNELL *et al.*: *Phys. Rev. Lett.*, **20**, 1318 (1968).

Mass spectra of A_2^- and f^0 (*)

G. GRAYER, B. HYAMS, C. JONES and P. SCHLEIN
CERN - Geneva

W. BLUM, H. DIETL, W. KOCH, H. LIPPMANN, E. LORENTZ
G. LÜTJENS, W. MÄNNER, J. MEISSBURGER, U. STIERLIN and P. WEILHAMMER
Max Planck Institut für Physik und Astrophysik - Münich

We have measured the reaction

$$\pi^- p \to p K^- K^0 \quad \big\lfloor \to \pi^+\pi^-$$

with 17.2 GeV incident π^-, using a magnet spectrometer with magnetostrictive wire spark chambers.

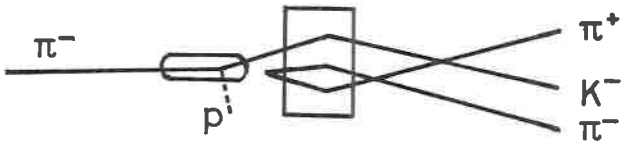

Fig. 1

Figure 1 shows the appearance of an event schematically. The incident beam momentum and the outgoing K^-, $\pi^+\pi^-$ momenta are measured. The proton is identified as a sharp peak in the missing mass associated with the observed particles.

The invariant mass resolution at the A_2 mass has been calculated analytically and by Monte Carlo programs. Both calculations lead to the result that the resolution is determined almost entirely by multiple scattering. If this is so we must expect that our observed K^0 width will be independent of the K^0 energy. Figure 2 shows the measured K^0 width (standard deviation) observed, and this confirms the result of the resolution calculation. This enables us to calculate our resolution for the A_2 as $\Delta M(A_2) = (5.7 \pm 0.6)$ MeV.

(*) Invited paper presented by B. Hyams

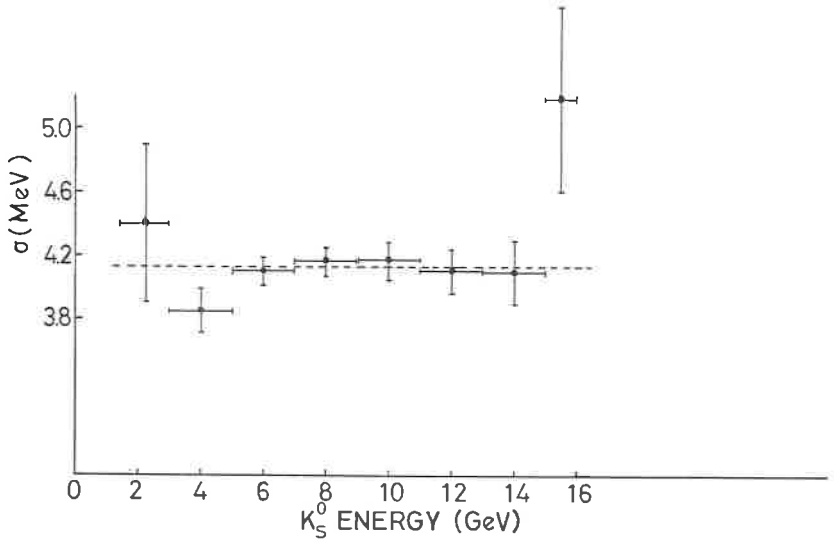

Fig. 2

Figure 3 shows the invariant mass spectrum of the K^-K^0 system. Fitting a spin 2 Breit Wigner resonance to the data leads to a χ^2 with probability 32%.

We have measured the reaction

$$\pi^- p \to n\pi^+\pi^-$$

at 17.2 GeV, observing the outgoing $\pi^+\pi^-$ and identifying the neutron by a peak in the missing mass spectrum. I mention our results in the f^0 region, where the mass resolution is ± 6.5 MeV. Figures 4 and 5 show the $\pi^+\pi^-$ invariant mass spectra of 15,108 events in the f^0 region. They fit well to a single broad spin 2 Breit-Wigner resonance.

Finally I will describe preliminary results obtained from an experiment now in progress, measuring

$$\pi^- p \to pK^-K^0$$

at 9.8 GeV. We expect to have around 900 events in the A_2 region with a mass resolution of $\Delta M = \pm 6.0$ MeV. Figure 6 shows preliminary data on 422 events, which show no sign of a split.

We conclude that the A_2^- and f^0 are broad spin 2 resonances, with no sign of dipoles, splits or structures required by the data.

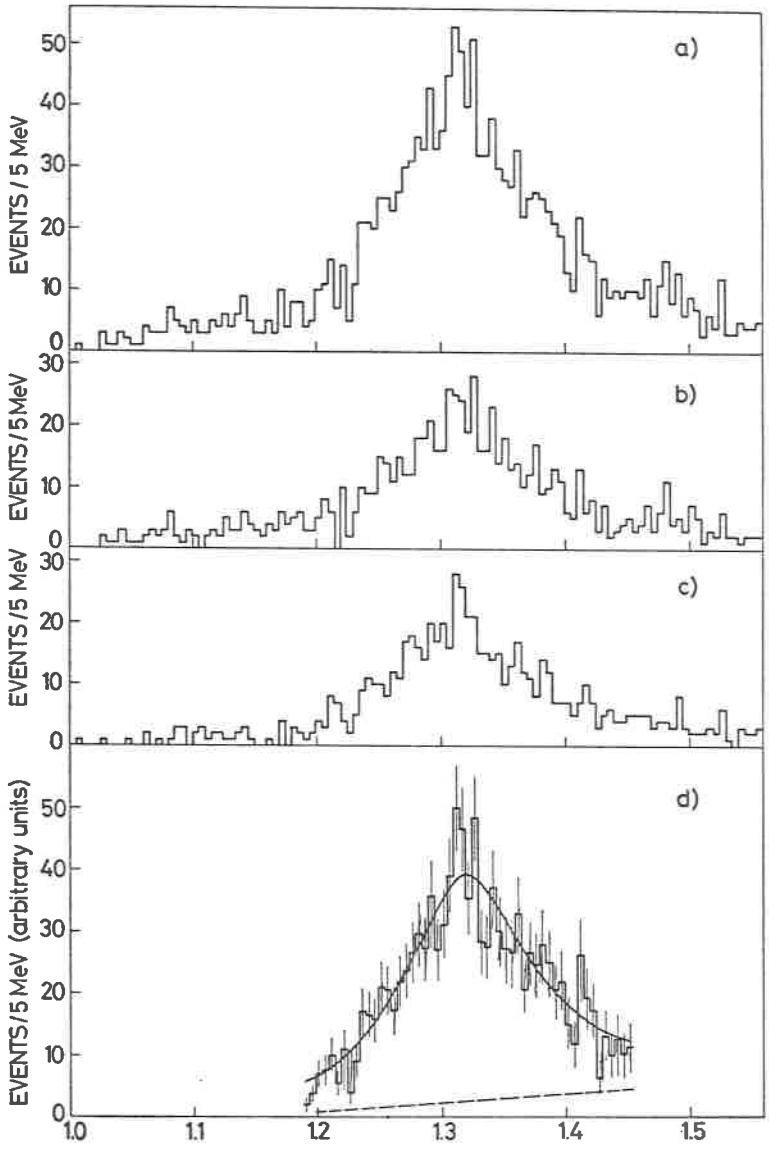

Fig.3 $K^-K^0_S$ invariant mass:

a) all $|t|$, unweighted;

b) $|t| < 0.2$, unweighted;

c) $0.2 < |t| < 0.7$ $(GeV/c)^2$, unweighted;

d) weighted $0.0 < |t| < 0.7$ $(GeV/c)^2$.

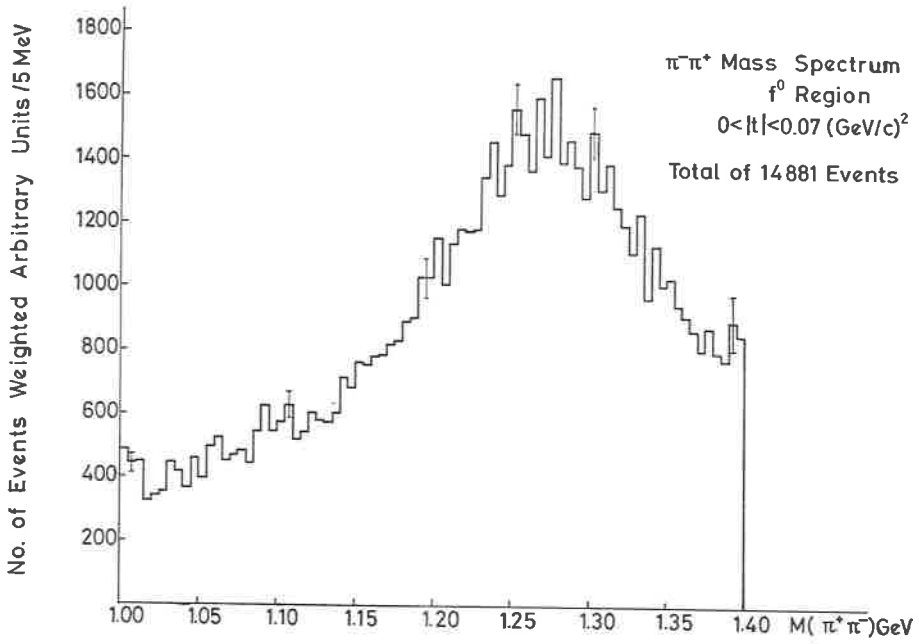
No. of Events Weighted Arbitrary Units/5 MeV
1800
1600
1400
1200
1000
800
600
400
200
1.00
1.05
1.10
1.15
1.20
1.25
1.30
1.35
1.40
M(π⁺π⁻)GeV
π⁻π⁺ Mass Spectrum
f⁰ Region
0<|t|<0.07 (GeV/c)²
Total of 14881 Events

Fig. 4

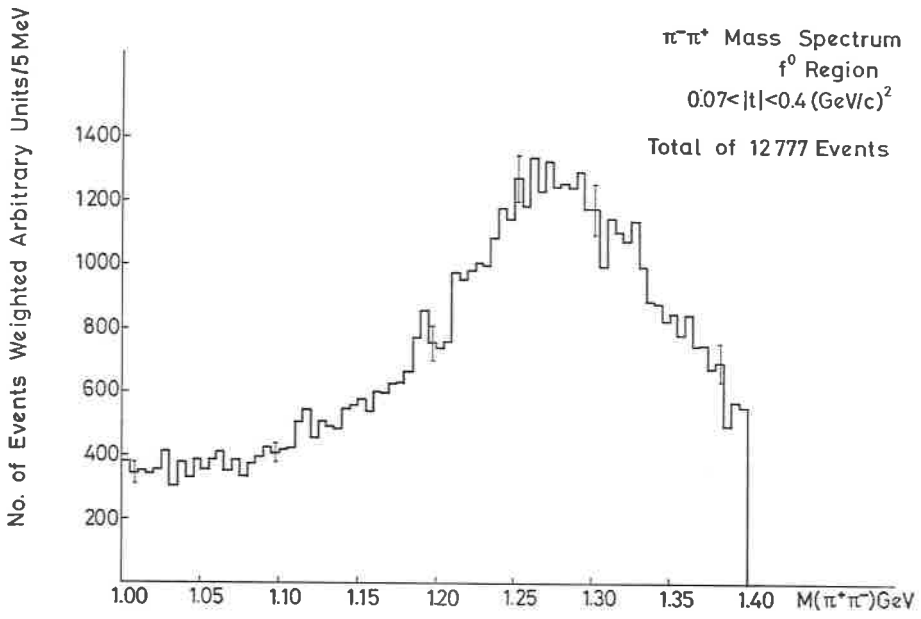
No. of Events Weighted Arbitrary Units/5 MeV
1400
1200
1000
800
600
400
200
1.00
1.05
1.10
1.15
1.20
1.25
1.30
1.35
1.40
M(π⁺π⁻)GeV
π⁻π⁺ Mass Spectrum
f⁰ Region
0.07<|t|<0.4 (GeV/c)²
Total of 12777 Events

Fig. 5

The 17.2 GeV data which lead to this conclusion cannot be in contradiction to data at 7 GeV since other states may be present at 7 GeV. However, our preliminary 9.8 GeV/c data suggest a contradiction with the missing mass experimental observation of a split which could hardly vanish at 9.8 GeV/c. Until the analysis of our data is complete this remains a suggestion, not a confirmed contradiction.

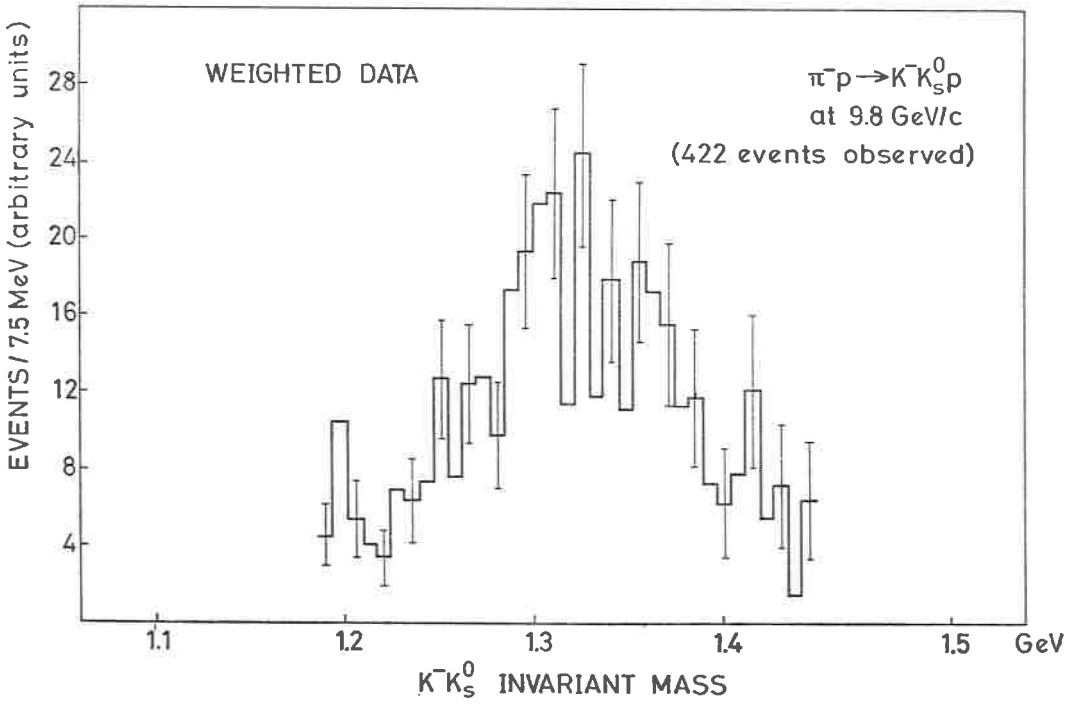

Fig. 6

Mass structure in the D^0 region (*)

J. DUBOC, M. GOLDBERG, B. MAKOWSKI and A. M. TOUCHARD
Institut de Physique Nucléaire - Paris

R. A. DONALD, D. N. EDWARDS, J. GALLETLY and N. WEST
The University of Liverpool - Liverpool

This experiment is based on the analysis of the events coming from $2.4 \cdot 10^5$ $\bar{p}p$ annihilations at 1.1 and 1.15 GeV/c to which have been added the events used in a previous experiment, which represents $\frac{1}{3}$ of the whole statistics ([1,2]).

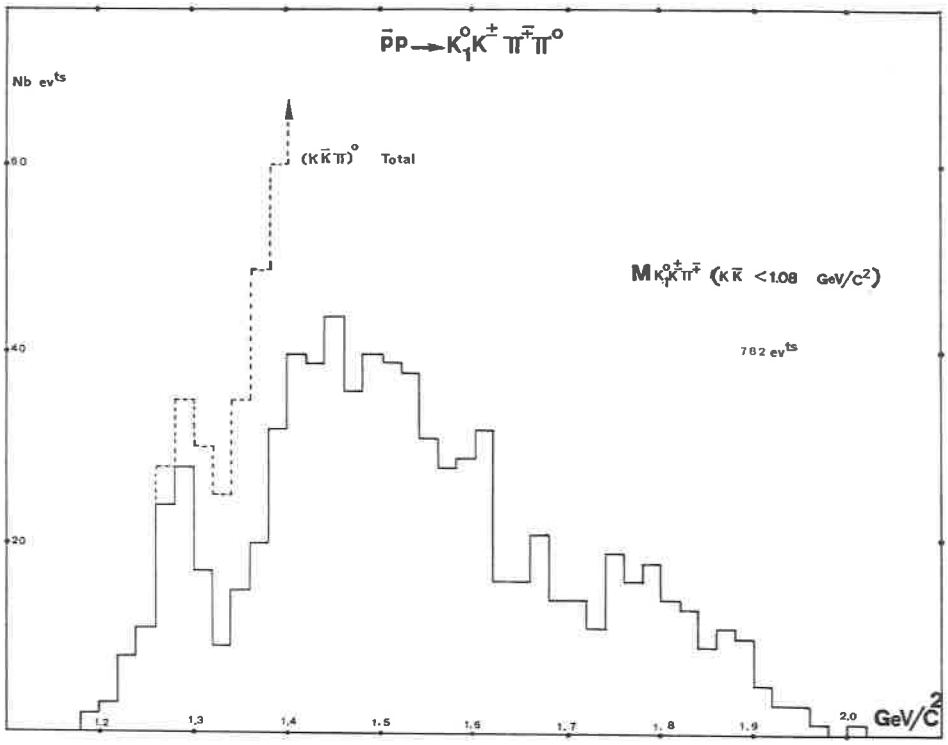

Fig. 1. – $\bar{p}p \rightarrow K_1^0 K^{\pm}\pi^{\mp}\pi^0$, ($K_1^0 K^{\pm}\pi^{\mp}$) effective mass spectrum with $K\bar{K} < 1.08$ GeV/c^2. The dotted histogram corresponds to the whole ($K_1^0 K^{\pm}\pi^{\mp}$) spectrum.

(*) Invited paper presented by B. Makowski

The following reactions have been studied:

(1)	$\bar{p}p \to K_1^0 K^{\pm}\pi^{\mp}\pi^0$	5036 events
(2)	$\bar{p}p \to K_1^0 K^{\pm}\pi^{\mp}\pi^+\pi^-$	1117 »
(3)	$\bar{p}p \to K_1^0 K_1^0 \pi^+\pi^-\pi^0$	867 »
(4)	$\bar{p}p \to K_1^0 K^{\pm}\pi^{\mp}\pi^+\pi^-\pi^0$	338 »
(5)	$\bar{p}p \to K_1^0 K^{\pm}\pi^{\mp}$(MM)	819 »

The D^0 meson is observed in all these reactions (see Figs. 1-5).

$$\bar{p}p \to K_1^0 K^{\pm}\pi^{\mp}\pi^+\pi^-$$

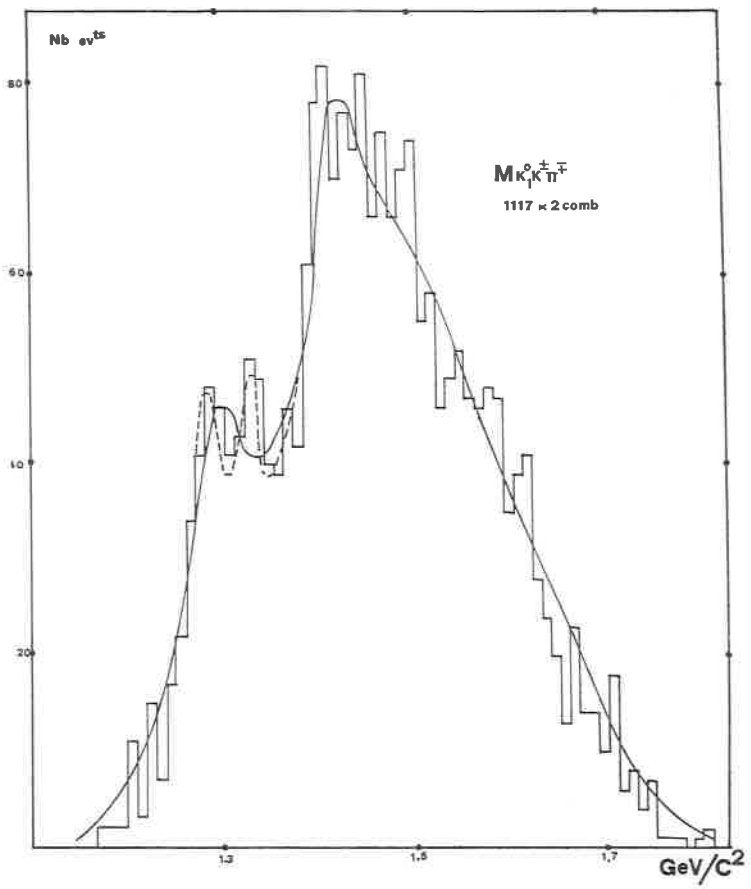

Fig. 2. – $\bar{p}p \to K_1^0 K^{\pm}\pi^{\mp}\pi^+\pi^-$, ($K_1^0 K^{\pm}\pi^{\mp}$) effective mass spectrum. The curves correspond to the fit listed in Table I.

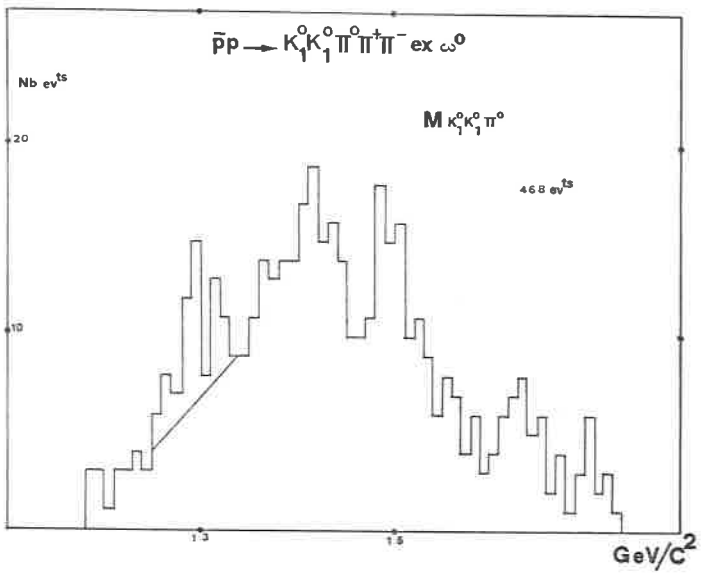

Fig. 3. – $\bar{p}p \rightarrow K_1^0 K_1^0 \pi^+ \pi^- \pi^0$, ($K_1^0 K_1^0 \pi^0$) effective mass spectrum, ω^0 events excluded.

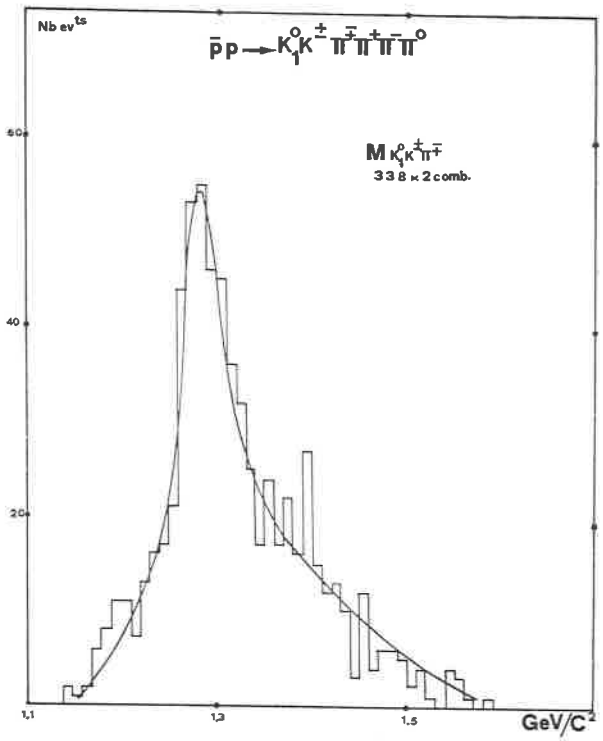

Fig. 4. – $\bar{p}p \rightarrow K_1^0 K^{\pm} \pi^{\mp} \pi^+ \pi^- \pi^0$, ($K_1^0 K^{\pm} \pi^{\mp}$) effective mass spectrum.

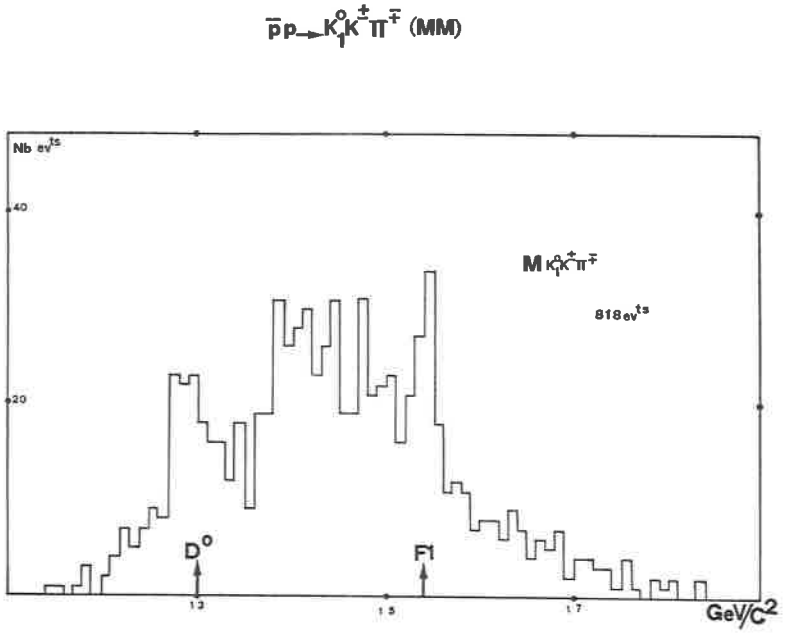

Fig. 5. – $\bar{p}p \to K_1^0 K^{\pm}\pi^{\mp}$(MM), ($K_1^0 K^{\pm}\pi^{\mp}$) effective mass spectrum.

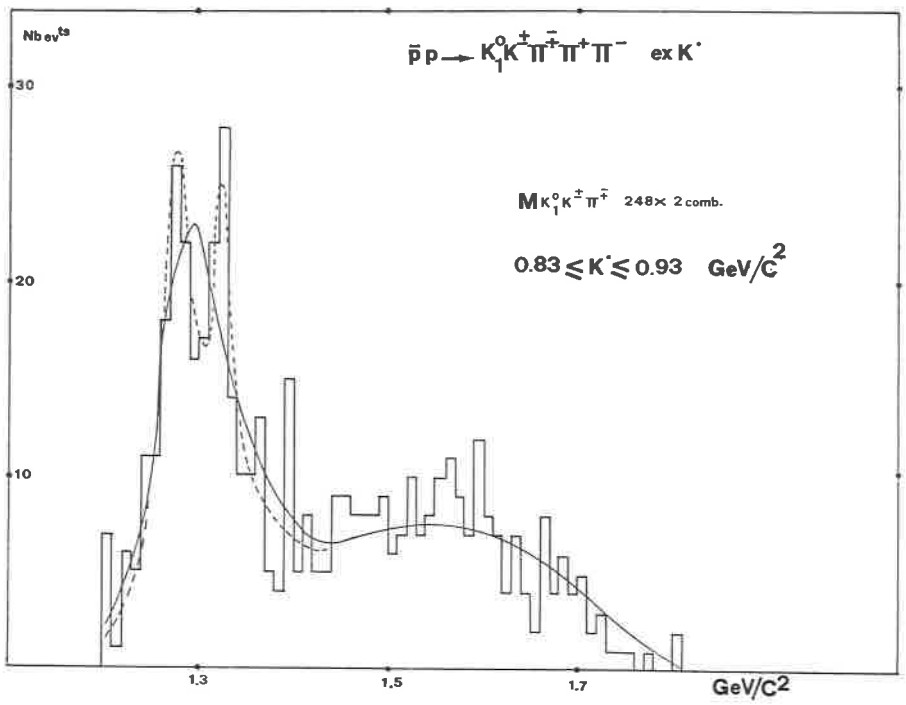

Fig. 6. – ($K_1^0 K^{\pm}\pi^{\mp}$) effective mass spectrum in $\bar{p}p \to K_1^0 K^{\pm}\pi^{\mp}\pi^{+}\pi^{-}$ with K* events excluded ($0.83 \leq M(K\pi) \leq 0.93$ GeV/c^2). The dotted curve corresponds to the two Breit-Wigner hypothesis (see text).

At first sight there seems to be a discrepancy between the $(K\bar{K}\pi)^0$ spectra of the five-body reactions and the others in the D^0 region. Two peaks appear in the spectra of reactions (2) and (3), while there is a clear Breit-Wigner form in the others. The statistical significance of these two peaks has been tested on the $(K\bar{K}\pi)^0$ spectra with the hypotheses of one or two incoherent Breit-Wigner's, by maximum likelihood method, and cleared by χ^2 values obtained from M.L. results. The fit taking into account two coherent Breit Wigner's gives the same result with a phase angle $\varphi = 200°$

As there is considerable background under the D^0, due to K* production, Fig. 6 shows the $(K\bar{K}\pi)^0$ distribution for all events of reaction (2) with no $(K\pi)_{I_z=\pm 1/2}$ combinations in the K* region.

TABLE I.

Histogram	Hypothesis	% mass width	χ^2 and probability	
			evaluated on complete histogram	evaluated over the mass-range (1.26÷1.34) GeV/c²
$K^0K^{\pm}\pi^{\mp}$ total	1 BW	(20±10)%	57/57	5.8/8
		(1288±5) MeVc/²		
		(62±27) MeV/c²	47%	67%
	2 BW	D_L (15±7)%		
		(1282±5) MeV/c²		
		(42±18) MeV/c²	50.3/51	1.2/8
		D_H (5±5)%		
		(1326±8) MeV/c²	50%	100%
		(20±20) MeV/c²		
$K_1^0K^{\pm}\pi^{\mp}$ ex K*	1 BW	(80±8)%	56.7/58	13/8
		(1276±5) MeV/c²		
		(77±16) MeV/c²	55%	8%
	2 BW	D_L (50±6)%		
		(1274±3) MeV/c²	48.6/57	1.9/8
		35 MeV/c²		
		D_H (18±4)%		
		(1323±4) MeV/c²	82%	98%
		20 MeV/c²		

The results are summarized in Table I. Whilst the confidence levels of these two hypotheses are of the same order on the overall spectra, they are

quite different in the D^0 region. However the 8% probability for the one Breit-Wigner case is not low enough to exclude it.

The maximum likelihood fit to the overall $K_1^0 K^{\pm}\pi^{\mp}\pi^-$ channel gives a difference of the log likelihood equal to 6 in favour of the two Breit-Wigner hypothesis.

Since the expected change in Log L due to the $(n_1 - n_2)$ extra parameters is given by the rule that 2Δ Log L follows a χ^2 law with $(n_1 - n_2)$ degrees of freedom, this corresponds to a ratio of probability of 200 in favor of the two Breit-Wigner hypothesis.

This effect cannot be ignored, but is not sufficient to conclude that there are two peaks in the D^0 region, and more data seems required, because there are only 163 events in D^0 peaks, after cuts.

REFERENCES

1) C. D'ANDLAU *et al.*: *Phys. Lett.*, **17**, 347 (1965); J. BARLOW *et al.*: *Nuovo Cimento*, **50**, 701 (1967); C. D'ANDLAU *et al.*: *Nucl. Phys.*, B **5**, 693 (1968).

2) Communications to the Kiev International Conference of High-Energy Physics (1970).

Evidence for structure in the f° mass region (*)

S. M. SCARROTT, J. V. MAJOR, and D. KEMP
University of Durham - Durham

R. CONTRI, D. TEODORO and G. TOMASINI
University of Genoa - Genoa

E. CALLIGARICH, S. RATTI and G. VEGNI
University of Milan - Milan

G. DE ROSNY, J. HUC, B. TERRAULT and R. SOSNOWSKI
Ecole Polytechnique - Paris

K. H. NYGYEN, M. BARRIER and J. QUINQUARD
EP - L.P.N.H.E.

DURHAM-GENOA-MILAN-PARIS (EP, LPNHE)

Evidence for possible structure in the f^0 mass region is presented for the reaction

$$\pi^+ d \to p_s p \pi^+ \pi^- \qquad (1)$$

(p_s proton spectator) at an incident pion momentum of 11.7 GeV/c.

The data comes from a bubble chamber experiment using the CERN 2 m DBC and the results are presented for 1704 events that give 4-C fits to reaction (1).

In Fig. 1 the dipion invariant mass spectrum in 40 MeV bins is shown for 3-prongs, 4-prong and 3 and 4-prong events. (A 3-prong event corresponds to a non-visible spectator whereas in 4-prong events the spectator is seen). In this figure peaks corresponding to the ρ^0 and f^0 mesons are apparent. However, in all plots there is an indication of structure in the f^0 region.

This structure is more obvious in Fig. 2 when the bin width is reduced to

---

(*) Invited paper presented by S. M. Scarrott.

20 MeV bins. The f^0 region has a dip centred on 1260 MeV and the two subsidiary maxima at 1220 and 1310 MeV respectively each with a width of ~ 50 MeV. The dip corresponds to a 4 standard deviation effect. However,

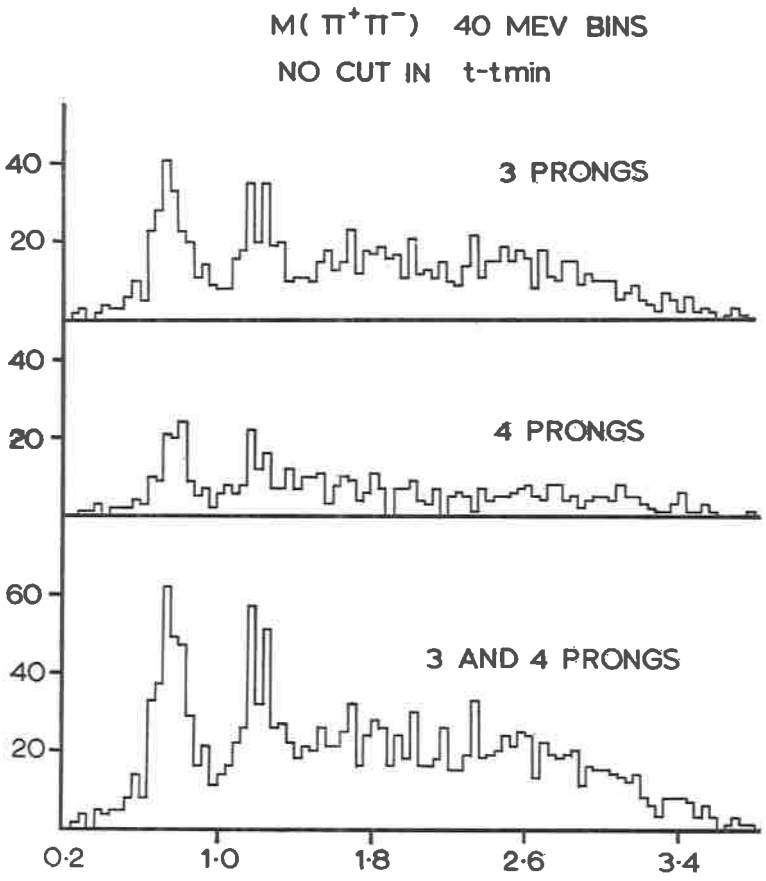

Fig. 1. – The dipion mass spectrum, M($\pi^+\pi^-$), for 3 and 4-prong events. There is no restriction on t'. The plotting resolution is 40 MeV.

a 6 s.d. effect can be observed if both a t'-cut of 0.15 and a missing mass selection of $0.010 < MM^2 < 0.003$ are made.

Further, a possible structure in the region above the ρ^0 at a mass of about 850 MeV is also evident. This is also observed in π^+p interactions at 11.7 GeV/c ([1]) and also in π^+d interactions ([2]). The structure is shown in greater detail in Fig. 3 where the mass plot is given in 10 MeV intervals.

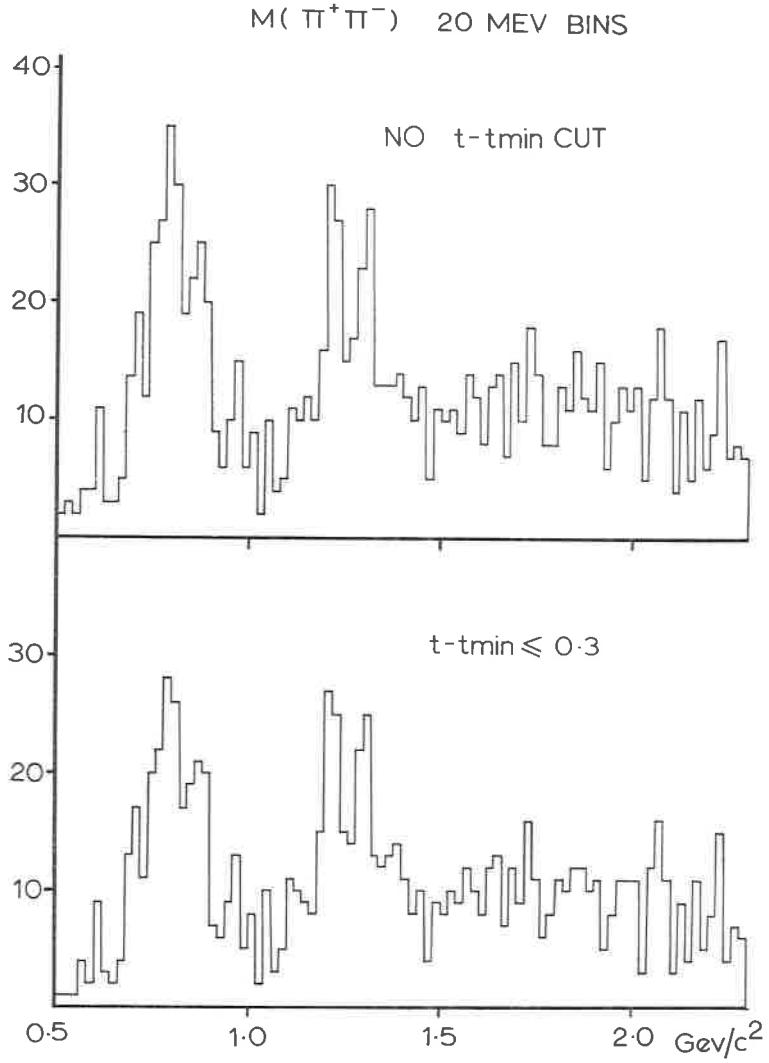

Fig. 2. – The dipion mass spectrum for 3 and 4-prong events with 20 MeV plotting resolution with: *a*) no restriction on t' and *b*) with $t' \leqslant 0.3$ (GeV/c^2)^2.

The Jackson angular distribution for the whole f⁰ mass peak (1.160÷÷1.360 MeV) is given in Fig. 4*a* and it is consistent with that which has previously been presented for the f⁰ meson. In Figs 4*b* and 4*c* the same distributions are given for each part of the f⁰ region (1.260÷1.360 MeV).

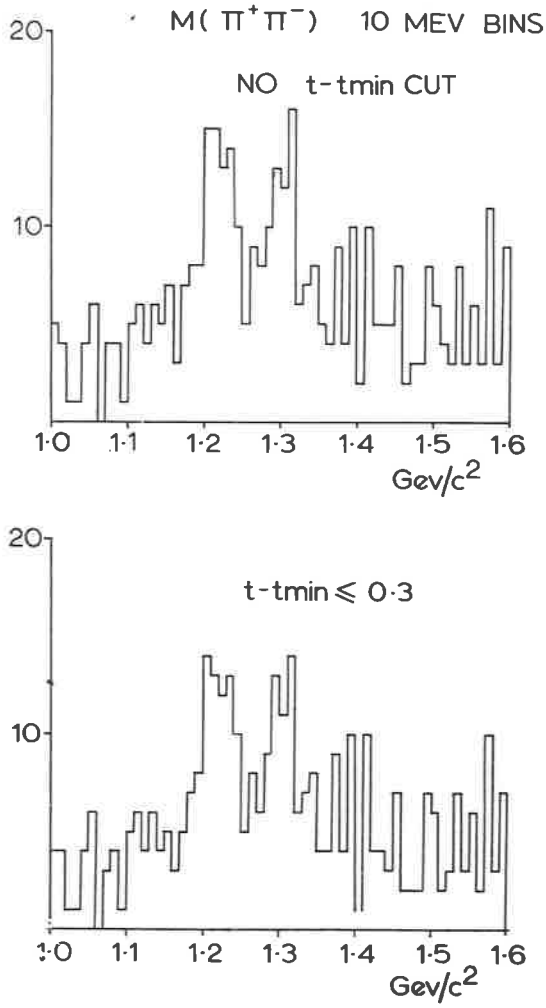

Fig. 3. – The dipion mass spectrum for 3 and 4-prong events with 10 MeV plotting resolution with: *a*) no restriction on t' and *b*) with $t' \leqslant 0.3$ (GeV/c^2)^2.

Both are consistent with the same spin parity assignment.

The f^0 mass distribution has been preliminarily fitted with:

a) a single Breit-Wigner curve;

b) two incoherent Breit-Wigner curves;

TABLE I. – *Results of fitting in the* f^0 *mass region.*

	Fitted (MeV) parameters	χ^2/degrees of freedom	Confidence level
1) Single Breit-Wigner resonance with constant incoherent background	$M = 1252$ $\Gamma = 150$	22.2/13	$\sim 5\%$
2) Two incoherent Breit-Wigner resonances and constant incoherent background	$M_L = 1216$ $\Gamma_L = 59$ $M_H = 1304$ $\Gamma_H = 36$	5.7/12	90%
3) Two coherent Breit-Wigner resonances and constant incoherent background	$M_L = 1213$ $\Gamma_L = 27$ $M_H = 1311$ $\Gamma_H = 14$ $\delta = 137°$	6.4/11	80%
4) Dipole model	$M = 1259$ $\Gamma = 57$	11/414	$\sim 70\%$

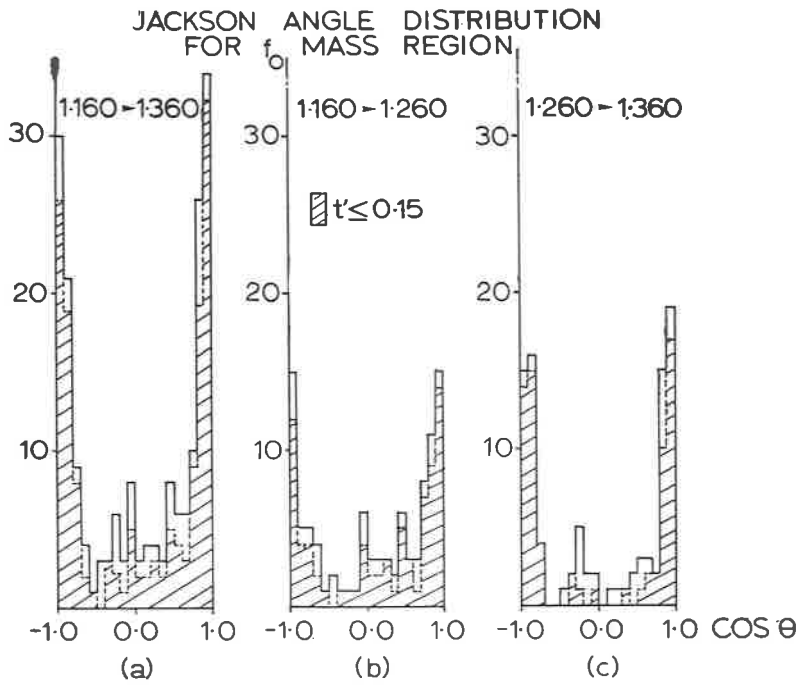

Fig. 4. – Jackson angular distributions in the f^0-region: *a*) for the low mass peak; *b*) for the high mass peak; *c*) for the whole f^0 region.

c) two coherent Breit Wigner curves;

d) a symmetric dipole.

In all cases a constant incoherent background was assumed.

The results of the fitting are summarised in Table I. The single Breit-Wigner fit is only acceptable at a confidence of 5% whereas much better fits are produced using double Breit-Wigner expressions.

It is concluded that although a single peak without structure is not excluded it is much more probable that the f^0 mass peak is split into two parts centred approximately at 1220 and 1310 MeV respectively each with a full width ~ 50 MeV. The decaying resonances producing the peaks both appear to have the same spin parity.

REFERENCES

1) Private communication by S. RATTI (π^+p Collaboration at 11.7 GeV/c, Durham-Genoa-Hamburg-Milan-Saclay).

2) *a*) π^+d at 13 GeV/c. See invited paper Session II-B by D. H. MILLER. *b*) π^+d at 6 GeV/c. Private communication by A. ENGLER.

A possible complication in the A_2 meson situation (*)

J. CLAYTON, P. MASON, H. MUIRHEAD and K. WHITELEY
University of Liverpool - Liverpool

R. RIGOPOULOS (*), P. TSILIMIGRAS and A. VAYAKI-SERIFIMIDOU
Nuclear Research Centre - Democritos Athens

We have observed an enhancement in the $\pi^+\pi^-\pi^0$ meson mass spectrum in the A_2 region in the process $\bar{p}p \to 2\pi^+2\pi^-\pi^0$ at 2.5 GeV/c. In Fig. 1 we display this mass spectrum together with a maximum likelihood fit (a

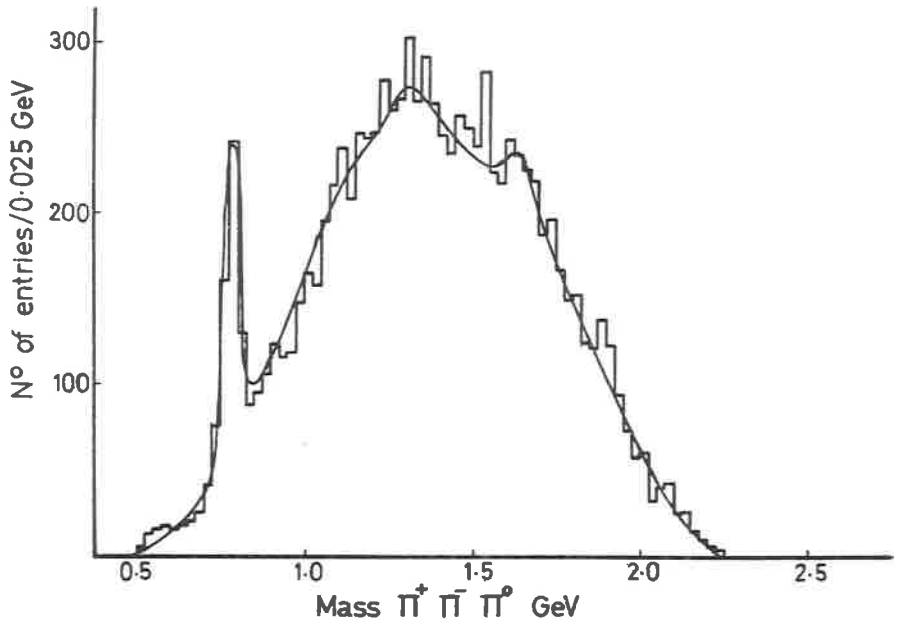

Fig. 1. – Mass spectrum of $\pi^+\pi^-\pi^0$ mesons from $p\bar{p} \to 2\pi^+2\pi^-\pi^0$ at 2.5 GeV/c. Four combinations per event.

(*) Contributed paper submitted by P. Mason

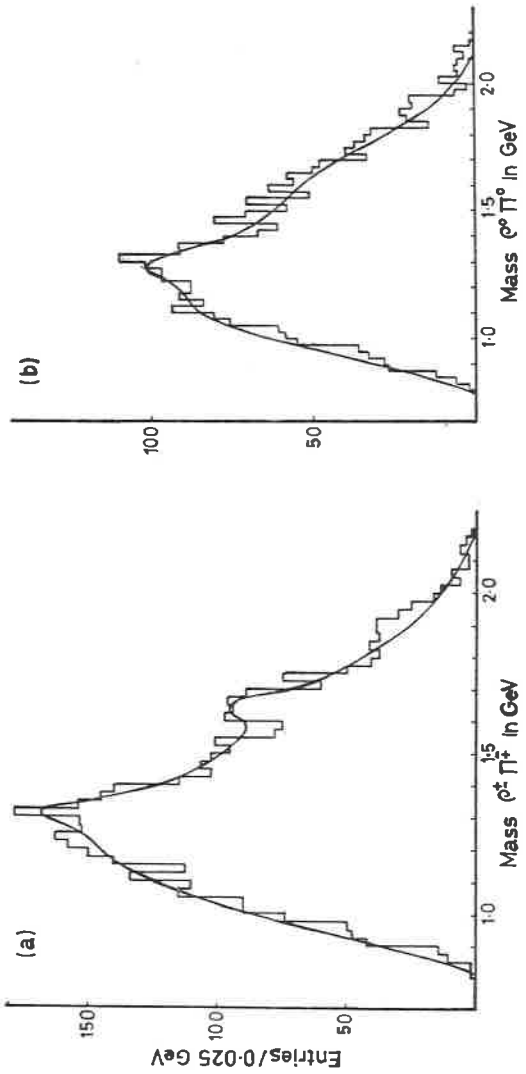

Fig. 2. – Mass spectrum of $\rho\pi$ mesons. A ρ meson is defined as any $\pi\pi$ combination with mass in the interval 0.675 to 0.850 GeV.

mass and width of 1.318 and 0.90 GeV were imposed as imput data to this fit). The fit yielded 0.088 ± 0.020 particles per event in the A_2 enhancement.

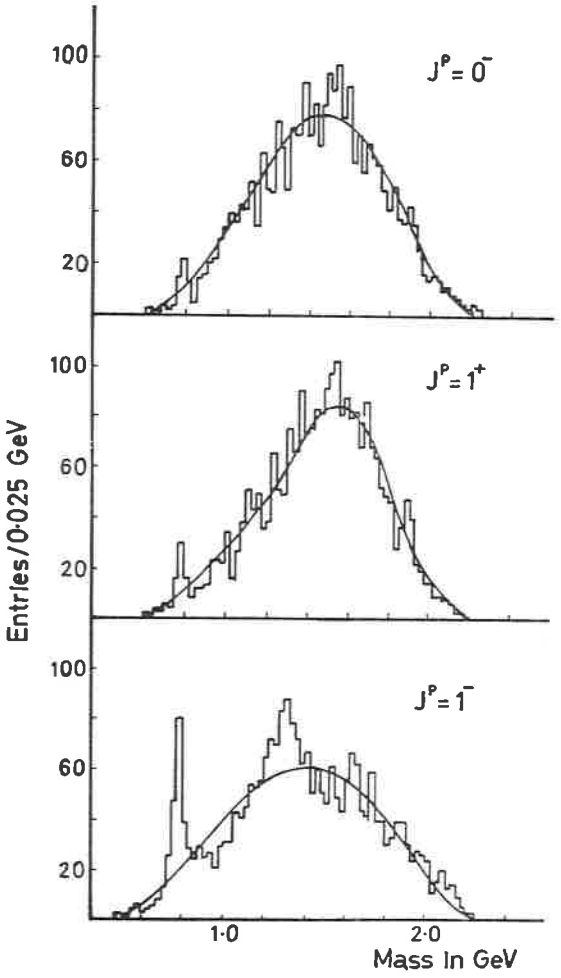

Fig. 3. – Mass spectra for $\pi^+\pi^-\pi^0$ for isospin zero systems selected by maximum $d\Gamma/\Gamma$. One combination per event.

This peak corresponds to a system with overall charge zero. No similar enhancements were found in the $\pi^{\mp}\pi^{\mp}\pi^{\pm}$ mass spectrum. The absence of a charged equivalent to the enhancement at 1.32 GeV is surprising for an isospin

assignment $I = 1$, since the Clebsch-Gordan coefficients favour the charged systems.

The dominant decay mode of this enhancement is $A^0 \to \rho^{\pm}\pi^{\mp}$. In Fig. 2 we display mass spectra for $\pi^+\pi^-\pi^0$ associated with $\rho^{\pm}$ and ρ^0 cuts on the data (a ρ meson was defined as pion pair within the mass interval 0.675 to 0.850 GeV). Enhancements are present both in the $\rho^{\pm}\pi^{\mp}$ and $\rho^0\pi^0$ channels. An isospin one meson cannot decay to $\rho^0\pi^0$, however. Figure 2 does not offer proof that the system we observe has isospin zero, since kinematic reflections from the ρ^+ and ρ^- channels automatically lead to enhancements in the ρ^0 region for $\pi^+\pi^-$ when the parent 3π system has mass $\sim 1{,}3$ GeV.

The resonances appearing in Fig. 1 suffer from poor signal to noise ratios due to the fact in order to plot the $\pi^+\pi^-\pi^0$ mass spectrum from $\bar{p}p \to 2\pi^+2\pi^-\pi^0$ we must take four combinations per event. We have attempted to improve the signal to noise ratio and at the same time assign possible quantum numbers to the enhancement by adapting a technique which was first discussed by Goldhaber ([1]). A decay amplitude was assumed for a specific spin-parity, using the technique developed by Zemach ([2]); the probability $d\Gamma/\Gamma$, where $d\Gamma$ is an element on the Dalitz plot, was then calculated for each of the four possible configurations for each event. The configuration which yielded the biggest probability was accepted as the most likely and plotted on the mass spectrum. In this way we narrowed our four choices down to one. Calculations were carried out for isospin 0 and 1 states, and $J^P = 0^-$, $1^{\pm}$, $2^{\pm}$, $3^{\pm}$.

In Fig. 3 we display the mass spectra for the systems $I = 0$, $J^P = 0^-$, 1^+ and 1^-. The peak expected for the ω meson in the 1^- plot can be seen, together with an enhancement in the A_2 region.

We have analysed the mass spectrum in this figure, together with the other spin-parity values, and the data is displayed below.

Resonance	$J^P = 0^-$	1^+	1^-	2^+	2^-	3^+	3^-	
ω	0.005±	0.015±	0.068±	0.028±	0.004±	0.020±	0.059±	$I = 0$
	±0.005	±0.005	±0.010	±0.005	±0.005	±0.010	±0.010	
	0.031±	0.045±	0.034±	0.045±	0.036±	0.020±	0.058±	$I = 1$
	±0.005	±0.010	±0.005	±0.010	±0.010	±0.005	±0.010	
A	0.011±	0.000±	0.120±	0.006±	0.005±	0.000±	0.129±	$I = 0$
	±0.020	±0.020	±0.020	±0.020	±0.020	±0.020	±0.020	
	0.010±	0.017±	0.029±	0.058±	0.019±	0.000±	0.108±	$I = 1$
	±0.020	±0.020	±0.020	±0.020	±0.020	±0.020	±0.020	

The similarity of the Dalitz plots for many spin-parities—especially the 1^-, 2^+, 3^- where all the plots vanish at the boundary—do not allow us to pick a specific value for the spin-parity with our available statistics. Nevertheless it is encouraging that our most likely assignement for the ω meson is $I = 0$, $J^P = 1^-$. An inspection of the table shows that most likely quantum numbers for the A are $I = 0$, $J^P = 1^-$, 3^- or $I = 1$, $J^P = 3^-$. The expected value of $I = 1$, $J^P = 2^+$ yields a peak smaller by a factor of two.

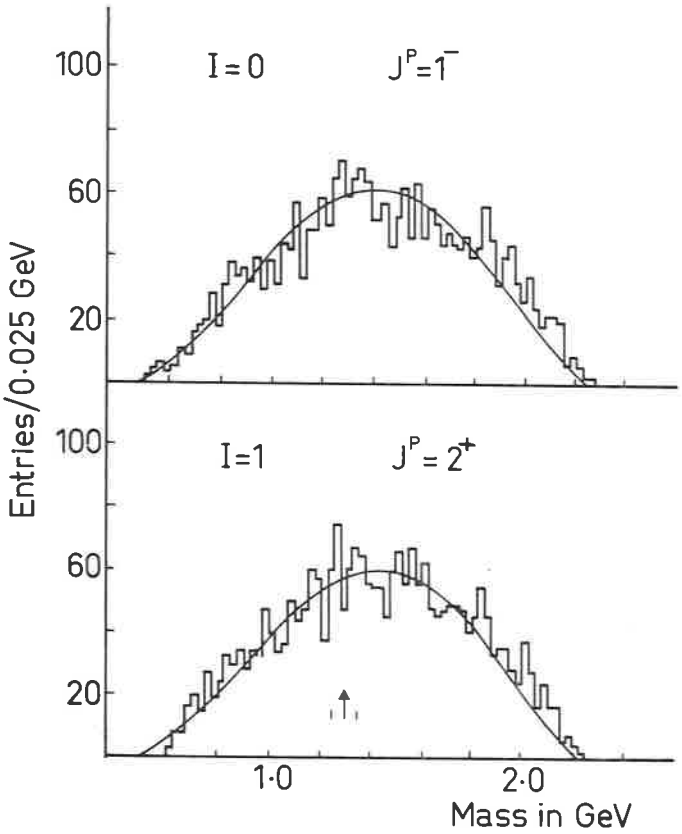

Fig. 4. – Mass spectra for $\pi^+\pi^+\pi^\mp$ selected by $d\Gamma/\Gamma$. One combination per event. The solid lines in Figs. 3 and 4 represent events generated by the CERN program FOWL and selected in the same way as the experimental data. These distributions have been normalised to the total number of events found experimentally. The arrow and vertical lines in Fig. 4 indicate respectively the expected position of the A peak and width, as they appear in Figs. 1, 2 and 3.

Finally in Fig. 4, we display data for $I = 0$, $J^P = 1^-$ and $I = 1$, $J^P = 2^+$ treated in the same manner for $\pi^\pm\pi^\pm\pi^\mp$ mesons. No obvious peaks can be seen.

At present the consensus of opinion ([3]) appears to be that an $I = 0$, $J^P = 0^+$ meson exists with a mass close to that of the ρ meson. It is tempting to speculate as to whether we have observed an $I = 0$, $J^P = 1^-$ system associated with the A_2 meson. Data from antiproton experiments at momenta near 2.5 GeV/c could be used to confirm or disprove this point. It would also be of interest to examine the 1.3 GeV mass region using the colliding electron-positron beam technique.

Further data on the channel $p\bar{p} \to 2\pi^+2\pi^-\pi^0$ and on the resonant technique will appear in forthcoming articles from this collaboration.

REFERENCES

1) G. Goldhaber: CERN Report 67-24, vol. 3.
2) C. Zemach: *Phys. Rev.*, **133 B**, 1201 (1964).
3) A. Astier: Rapporteur's report to *Kiev Conference* (1970).

SESSION III - A

Friday, 16 April 1971

Hadron production by colliding e^+e^- beams

Chairman: E. LOHRMANN

Secretaries: S. GRAFFI
A. KEMP

Production of multibody events by e^+ and e^- colliding beams (*)

FRASCATI-ROMA-MARYLAND-PADOVA COLLABORATION (**)

Preliminary results obtained with the Frascati storage ring « Adone » by the so-called « mu-pi » group, were reported at the Kiev International Conference, on September 1970 (1). The composition of the « mu-pi » group, with the injection of a few new young members, is given in Table I. In the

TABLE I. – *Composition of the « μ-π Group of Adone »* (*Frascati-Roma-Maryland-Padova Collaboration*).

G. BARBIELLINI	M. NIGRO
B. BORGIA	L. PAOLUZI
F. CERADINI	R. SANTONICO
M. CONVERSI	P. SPILLANTINI
F. GRIANTI	L. TRASATTI
M.GRILLI	V. VALENTE
E. IAROCCI	R. VISENTIN
A. MULACHIÉ	G. T. ZORN

last months the group has been mostly engaged in the elaboration of the data concerning the tests of quantum-electrodynamics and in projecting a new version of the apparatus, more suitable for recording the multibody events. The analysis of these events—carried out in particular by M. Grilli, M. Nigro, V. Valente and some of the younger members—has been therefore completed only for part of them.

As we shall see the new data presented here are consistent with those presented at Kiev. If the particles observed in the multibody events are mostly

(*) Invited paper presented by M. Conversi.

(**) See Table I for the composition of the group.

charged pions, then these events are produced with a cross section of the order of that of the annihilation into muon pairs. Let me recall that such a process occurs with a total cross section of 20 nb at the energy $E = 1$ GeV/beam.

The « main apparatus » is shown in Fig. 1. The adjective « main » is used here to distinguish it from another apparatus, also mounted over the

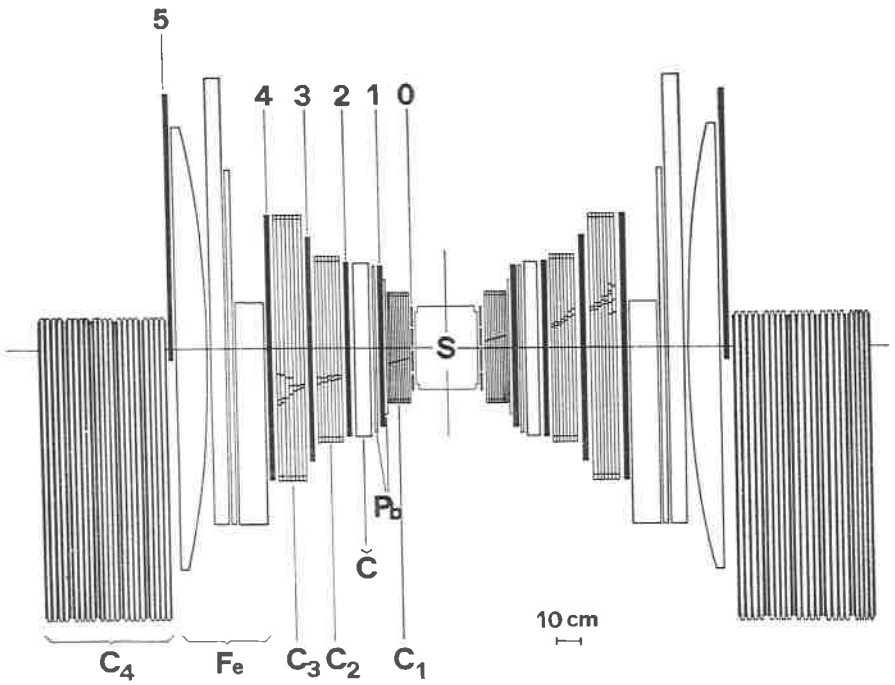

Fig. 1. – The « main apparatus », used to record Bhabha scattering at wide angle ($53° < \theta < 127°$), annihilation into muon pairs and production of hadronic states by positron and electron colliding beams.

same straight section of Adone and runned in parallel to the former, which measures the machine luminosity. The measurement of this quantity is especially important for the tests of quantum electrodynamics made through inspection of wide angle Bhabha scattering (WAS) and annihilation into muon pairs. Even if these two processes will not be discussed here, it should be recalled that they can be detected and identified with high efficiency by the apparatus shown in Fig. 1. The muons of course do not undergo appreciable radiation losses and have therefore a definite range, which is usually

measured by their stopping in the end chambers, C_4: High energy electrons and positrons, on the other hand, have a high probability ($\sim 95\%$ at $E = 1$ GeV) to develop a visible electromagnetic shower in either of the two telescopes which are placed on opposite sides of the vacuum chamber of Adone. These telescopes contain, in fact, about 6 radiation lengths of sensitive material (scintillation counters, numbered from 0 to 5, and thick plate spark chambers, placed between the « directional » thin foil chambers, C_1, and the end chambers C_4). The chambers C_1 are used to reconstruct the origin of the events. In order to be considered as « good candidates », the events have to show in C_1 tracks coming from a point of the region where the e^+ and e^- bunches collide. This region is the source, S, of all « good events ». While its transverse dimension are of the order of 1 mm, the source length is several tens of cm at beam energies of the order of 1 GeV. In our experiment this length is

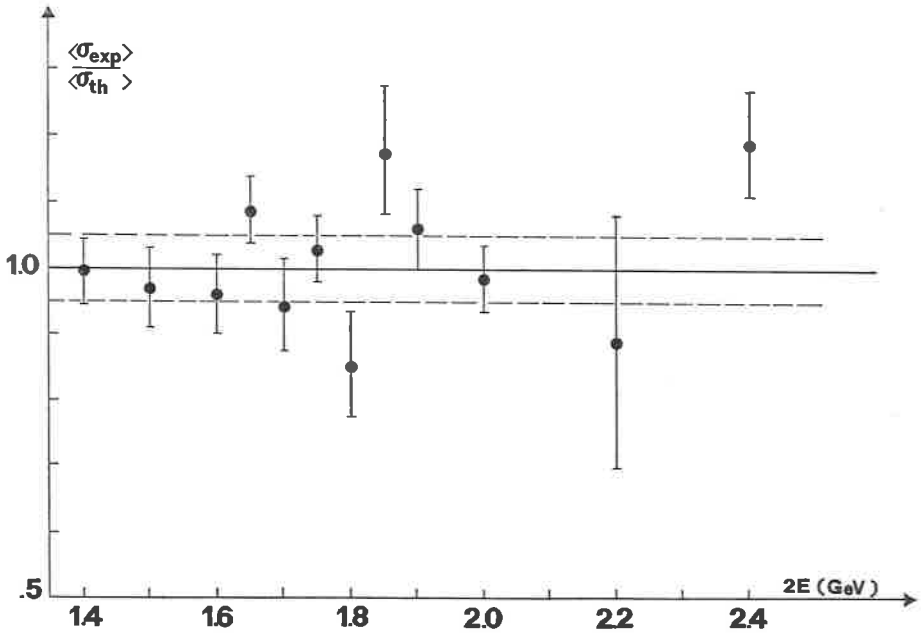

Fig. 2. – Results on electron-positron elastic scattering. The quantity $\langle \sigma_{th} \rangle$ is the Bhabha cross-section integrated over the detecting apparatus. The corresponding experimental quantity, $\langle \sigma_{exp} \rangle$, is obtained using the results of two types of measurements: those carried out with the apparatus of Fig. 1 and those carried out simultaneously with a « monitoring system » which detects small angle Bhabha scattering ($3° < \theta < 6°$). The latter process is unaffected by a possible breakdown of quantum electrodynamics at large momentum transfers. The two dashed lines are limits for estimated systematic uncertainties. The experimental points are reported with their statistical errors alone.

derived from the observed distribution of the points origin of well identified WAS events. I wish just to mention that the results obtained with the main apparatus on the WAS events, reported in Fig. 2, confirm the validity of quantum electrodynamics down to distances of 0.03 fm, for the high space-like momentum transfers involved ([2]).

Any event with more than two visible tracks in the chambers C_1 will be of course considered as a multibody event. But also events with two visible tracks can be due to multibody events, if the tracks are not collinear and especially if they are not coplanar with respect to the beam direction. Some of the particles emitted in a multibody event may, in fact, remain unobserved, either because they are neutral, or because they are emitted outside the solid angle of the detecting apparatus. Background tests carried out with only one beam circulating in Adone show the existence of an appreciable background among the two–track events. No appreciable background is observed instead in the multibody events with $t \geqslant 3$ visible tracks. We shall consider separately, in what follows, the multibody events with at least three visible tracks in the chambers C_1, and those with only two visible tracks ($2t$).

A multibody event is detected by our apparatus if its charged particles reach counter 2 of one telescope and counter 4 of the other one. These criteria of minimum penetration could not be released without bringing the trigger rate of the events, recorded on film, at an intolerable value. These criteria impose, on the other hand, rather severe limitations for the minimum energy of the secondary particles. If we assume for instance that these particles are all pions, then the minimum kinetic energy is 180 MeV for the pion at counter 4. 85 MeV for the pion going through counter 2 and about 20 MeV for any other pion observed in addition to the former two.

In order to determine the response of our telescopes to electrons of various energies and, thereby, to estimate, in particular, the probability that a given single track in the telescopes is due to an electron, we have performed calibration measurements with electrons from the Frascati 1 GeV electronsynchrotron. The energies E_e of the electrons were between 100 and 500 MeV. It should be pointed out that for $E_e \geqslant 700$ MeV the response of the telescopes is already contained in the main runs carried out at Adone, so that there is not need for calibration measurements with electron beams.

The calibration measurements have been taken with the apparatus sketched in Fig. 3. There are three small scintillation counters, A, B, C, used to define the electron beam. The remaining part of the equipment reproduces one of the two telescopes mounted over Adone, up to the spark chamber C_3 of Fig. 1. The « directional chamber » is the « thin foil chamber » C_1 of Fig. 1 and the counters D, E correspond to counters 2, 3, respectively.

With this equipment we have first measured, at various energies of the electron beam, the probabilities that an electron gives a signal in counters *D* and *E*, *i.e.* in counters 2 and 3 of Adone's « main apparatus ». These

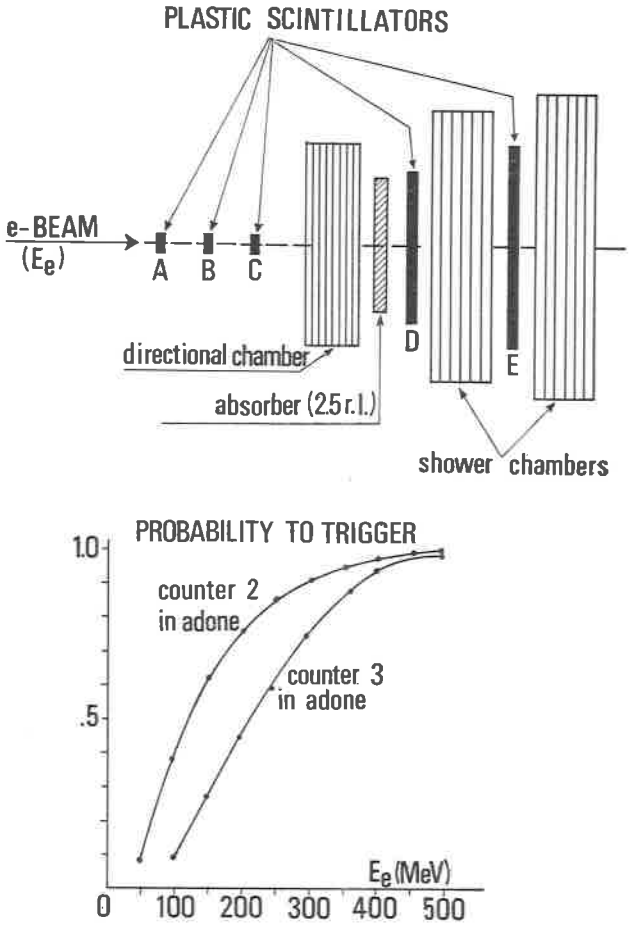

Fig. 3. – Apparatus used for calibration measurements at the Frascati electron-synchrotron. The results of these measurements are reported in Table II and partly in this Figure, as curves giving the probability for an electron of energy E_e to trigger counter 2 or counter 3 in the « main apparatus » of Fig. 1.

probabilities are reported in Fig. 3 and in Table II as a function of the beam energy. In the last column of the table the probability that the electron gives a signal in counter 4 of our main apparatus is also given. This probability has been estimated on the basis of the other two measured probabilities. The

conclusion of these measurements and calculations is that electrons of energy below (200÷250) MeV have but a small probability to produce a signal in counter 4. Multibody events of electromagnetic nature would not be recorded, therefore, if involving only electrons not in excess of some 200 MeV.

TABLE II. – *Results of the calibration measurements.*

Calibration apparatus					ADONE apparatus		
E_e (MeV)	No. of events	Percent frequency of event appearance as			Percent probability to trigger counter		
		e.m. (*) shower	single (**) track	« intermediate »	2 (measured)	3 (measured)	4 (estimated)
100	42	~50	0	50	35	10	1
150	63	~70	0	30	60	27	3
200	219	80	1	19	75	44	7
250	89	~90	0	10	85	59	15
300	178	94	1	5	90	75	28
400	191	96	1	3	95	94	70
500	283	98	1	1	99	98	95
750	(1065)	> 99	0	< 1	~100	~100	~100

(*) At least 4 sparks not aligned, within 20°, in each « shower chamber ».
(**) At least 3 sparks aligned in each « shower chamber ».

Conclusions:

a) Negligible probability of single track appearance, at all E_e's.
b) High probability for shower identification at $E_e > 250$ MeV.

A total of about 1000 pictures have been taken, at various energies E_e, to observe the behaviour of the electrons in the « shower chambers ». For the identification of an electromagnetic shower we require the presence, in each of the two chambers of Fig. 3, of at least 4 sparks not aligned and in at least two different gaps, within a cone of 20° aperture around the direction of the primary electron. As one can see from the table, well identified *showers are produced with a* rather *large probability* at all energies, and in particular *for* $E_e > 250$ MeV. On the other hand, at all energies there is a negligible probability that an electron appears as a single track, *i.e.*—in our definition—as

a sequence of three or more aligned sparks in each chamber. Therefore *single tracks appearing in the multibody events cannot be due to electrons* of any energy. There are, however, farly frequent « intermediate cases », particularly at the lower energies, in which the event is not well identified as a shower or as a single track.

I shall now discuss separately the two main categories of multibody events: those showing only two tracks ($2t$) and those showing more than two tracks ($3t$, $4t$, ...) in the directional chambers C_1. Of course for all events we require: *a*) that they come from a point of a fiducial region around the « source » S; *b*) that they occur within a short time interval around the instant of crossing of the bunches at the straight section of Adone where our apparatus is mounted.

The results reported hereafter refer to the analysis of events collected in runs (taken at beam energies ranging from 0.7 to 1.05 GeV/beam) during which a number $N_{\text{WAS}} = 1590$ of well identified WAS events were recorded. These runs represent $\sim\frac{1}{4}$ of the total runs carried out at Adone. As the analysis proceeds, the results may undergo of course some changes. Also for this reason the following results are still to be considered as preliminary.

Two-track events have been considered as possible candidates for multibody events whenever the two tracks observed in chambers C_1 were either not collinear within 10°, or not coplanar with respect to the beams' direction within 5°. The bahaviour of the particles in the thick plate « shower chambers » C_2, C_3 was then examined. If the particles produce showers in either telescope, thay are identified as electrons and the corresponding event is classified as a WAS event in which the collinearity and/or the coplanarity has been lost due to radiative corrections. If, on the other hand, the particles exhibit single track behaviour in the telescopes, then we know, from the calibration measurements discussed before, that they cannot be electrons. In these cases the corresponding event is retained as a multibody event. Simultaneously to the $N_{\text{WAS}} = 1.590$ WAS events, 34 two-track events were recorded, with the two observed particles exhibiting « single track » behaviour in the « shower chambers » of both telescopes. The two photon annihilation process ([3]) $e^+e^- \to e^+e^- \mu^+\mu^-$ may well be responsible for some of these 34 events, since muons of the energies involved would behave just as most of the observed particles (all those not showing nuclear scattering). By integrating the differential cross-section given by Greco ([3]) over our apparatus, we have found that 7 of the 34 events are expected to arise from this four-body process. These events should be essentially coplanar with respect to the beams' direction, because the two secondary electrons are emitted nearly in the same direction of the

primary ones. It is interesting to note that 8 of the 34 events are indeed coplanar to within 5°. Of the $34 - 7 = 27$ remaining events, 6 ± 4 are expected to be spurious events, on the basis of background measurements performed with only a single beam, or with two separated beams circulating in Adone. Then we conclude that there are $N_{2t} = 21 \pm 9$ genuine hadronic multibody events among the two-track events, corresponding to the $N_{\mathrm{WAS}} = 1590$ WAS events. The large error includes also some uncertainties in the normalization of the background events to the other events.

In order to obtain a value for the cross section of the process responsible for these observed events, one needs of course to make some assumption on the process itself. If we assume that the observed events arise mostly from the process

$$e^+e^- \to \pi^+\pi^-\pi^+\pi^-\pi^0 \tag{1}$$

then we can evaluate, by a Montecarlo calculation, the probability that our apparatus detects such a process as a 2-, 3,- 4-track event. This calculation has been performed taking into account the effective distribution of the e^+, e^- interaction points. Assuming isotropic distribution of the emitted particles, energy distribution according to phase space, and pion absorption in matter as from data available in the current literature, the detection efficiency of our apparatus for two-track events is found to be $\sigma_5^{(2t)} = 0.025$. Then for the total cross section of the multibody process, we obtain

$$\sigma^{(2t)}_{(4\pi+\pi^0)} = (20 \pm 9)\ \mathrm{nb} \tag{2}$$

Of course there are other processes which may contribute to the two-track events, *e.g.* $e^+e^- \to \pi^+\pi^-\pi^0$. Assuming for the cross section of this three-body process a value of 10 nb, which is the upper limit indicated by the « gamma gamma group » at Adone, we find that 4 of the 21 observed events should come from this channel. This yields $\sigma^{(2t)}_{(4\pi+\pi^0)} \simeq 16$ nb.

More-than-two-track events need no background subtraction because, as mentioned already, no event of this type has been observed in many hours of background runs.

In the sample considered here, corresponding to $N_{\mathrm{WAS}} = 1.590$ well identified WAS events, there are 49 three-track and 5 four-track events.

We can safely retain as hadronic events 6 of the 49 three-track events, because in these 6 cases all tracks exhibit in the shower chambers (S.C.) the « single track behaviour » which excludes their electronic nature. There are,

however, other 19 events which may also be at least in part of hadronic nature. In fact in these 19 cases two of the three particles show single track behaviour, while the third particle goes either outside the shower chambers (13 cases) or has the « intermediate » behaviour (6 cases) observed in the calibration test. We have instead excluded the remaining 24 events ($49 - 6 - 19 = 24$) because they have tracks either with doubtful behaviour (12 cases) or with associated *e.m.* showers (12 cases). These « mixed » events are not yet understood.

The situation can be summarized as follows. We have:

49 observed three-track events of which

12 with doubtful track behaviour in S.C. and

12 with associated showers. This leaves

25 good hadronic candidates of which

6 with full single-track behaviour in S.C.

13 with two « single-tracks » and one track outside S.C. and

6 with two « single-track » and one « intermediate » behaviour.

The two extreme cases corresponding to retaining only 6 or keeping 25 of the 49 three-track recorded events, lead to the cross-sections listed in Table III, computed on the basis of the Montecarlo calculation mentioned above. These results refer to an average energy $\overline{E} \approx 0.9$ GeV/beam.

TABLE III. – *Estimated cross-sections for 3-track events.*

Number of hadronic 3-track events	Cross-section in nanobarn for e^+e^- annihilating into 4 charged pions +	
	$0\,\pi^0$	$1\,\pi^0$
6	5	7
25	12	17

In spite of the large uncertainty exhibited by these numbers, it seems reasonable to conclude that events of hadronic nature are produced with a cross-section of the order of 10 nb.

From the analysis of the 25 three-track events of presumed hadronic nature, we have observed a $(17 \pm 3.5)\%$ percentage number of nuclear interactions (scattering with $\theta > 25°$) in agreement with the 14% value expected on the

basis of known measurements of pion absorption in matter. This yields further support to the view that these events are indeed of a hadronic nature. The measurement of the pulse-heights in counters 2 and 3 of the main apparatus

TABLE IV. – *Energy distribution of observed multi-body hadronic events.*

Total beam energy (MeV)	Hadronic events (3 tracks)	Associated e^+e^- pairs	Hadrons e^+e^- pairs
$2\bar{E} = 1600$ $(1500 < 2E < 1700)$	20	1180	$(1.7 \pm 0.7)\%$
$2\bar{E} = 1850$ $(1750 < 2E < 1900)$	19	1170	$(1.6 \pm 0.7)\%$
$2\bar{E} = 2050$ $(2000 < 2E < 2100)$	21	1130	$(1.9 \pm 0.7)\%$

show, moreover, that the observed tracks are mostly consistent with minimum ionizing particles.

The energy dependence of the cross section of the hadronic events, given in Table IV indicates a $1/s$ law ($s = 4E^2$, total c.m. available energy). The data include now also those reported at the Kiev Conference.

REFERENCES

1) G. BARBIELLINI *et al.*: Frascati Report LNF-70/38 (1970), unpublished.
2) G. BARBIELLINI *et al.*: Frascati Report LNF-71/13 (submitted to *Phys. Lett.*).
3) M. GRECO: Frascati Report LNF-71/1 (1971) (to be published on *Nuovo Cimento*). See this paper also for previous references on these two photon annihilation processes.

Multiple production from e^+e^- annihilation, and a first observation of $\gamma + \gamma$ interaction ($e^+e^- \to e^+e^-$ + others) (*)

C. BACCI, R. BALDINI-CELIO, G. CAPON, C. MENCUCCINI
G. P. MURTAS, G. PENSO, A. REALE, G. SALVINI, M. SPINETTI and B. STELLA

University of Rome

1. Introduction.

We have studied the reaction

$$e^+e^- \to \text{multiple particle production} \tag{1}$$

using the Frascati electron-positron storage ring at center of mass energies $2E$ between (2×700) and (2×1200) MeV. Most of our results ($\approx 75\%$) have been taken in the interval $(1900 < 2E < 2100)$ MeV.

More specifically, the processes we report here are hose exhibiting at least three particles (a photon is also considered a particle in this case) in the final state, one at least of them being charged.

As we shall see, it is a good hypothesis to assume that our events (1) are mostly hadronic in nature. We develop now this hypothesis.

The most probable hadronic processes (1), when considering the limits $(1400 < 2E < 2400)$ MeV, include the following:

$$e^+e^- \to \pi^+ + \pi^- + \pi^0(\eta, \gamma)\,, \tag{2}$$

$$e^+e^- \to \pi^+ + \pi^- + \text{two or more neutral particles}\,, \tag{3}$$

$$e^+e^- \to \pi^+ + \pi^- + \pi^+ + \pi^-, \tag{4}$$

$$e^+e^- \to \text{multiple hadronic events}\,, \tag{5}$$
with 4 charged particles plus at least one neutral,

(*) Invited paper presented by G. Salvini.

$e^+e^- \to n$ charged pions, m neutral particles, (6)

with $n \geqslant 6$; $m \geqslant 0$.

In the reactions above a pair of pions may be substituted by a pair of K's.

We shall interpret our events with reactions (2)-(6), on the following basis:

— We have observed nuclear interactions of the charged particles in the plates of the spark chambers, which ensure their hadronic nature; this is only a statistical observation, which may confine the muons to be less than 25%.

— We have multiple hadronic events (for instance at least two charged pions and one shower) at energies ($2E < 2000$) MeV. This makes improbable at these energies any origin different from the annihilation diagram:

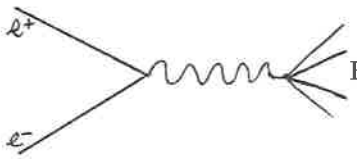

(7)

For instance, the events from the $\gamma\gamma$ interaction ([1]) have a cross section definitely lower than our results.

We assume therefore in the following that our multiple events go through the one photon annihilation diagram (7). With this in mind, the questions to consider in connection to our experimental results are the following:

1) Whether the present situation can be explained by the existence of the ϱ, ω, Φ mesons only, or we should enlarge the vector boson family.

2) How large is the amplitude of the $J^P = 1^-$ final state in diagram (7).

3) The behaviour with energy of the cross sections for processes (1): do they follow an $1/E^2 \equiv 1/S$ law?

2. The experimental apparatus.

Our apparatus is similar to the one described in a previous paper ([2]), and it is shown in Fig. 1. It mainly consists in four blocks of scintillation counters and spark chambers and scintillation counters above and below the target area. It may detect charged particles with efficiency close to one, and γ rays

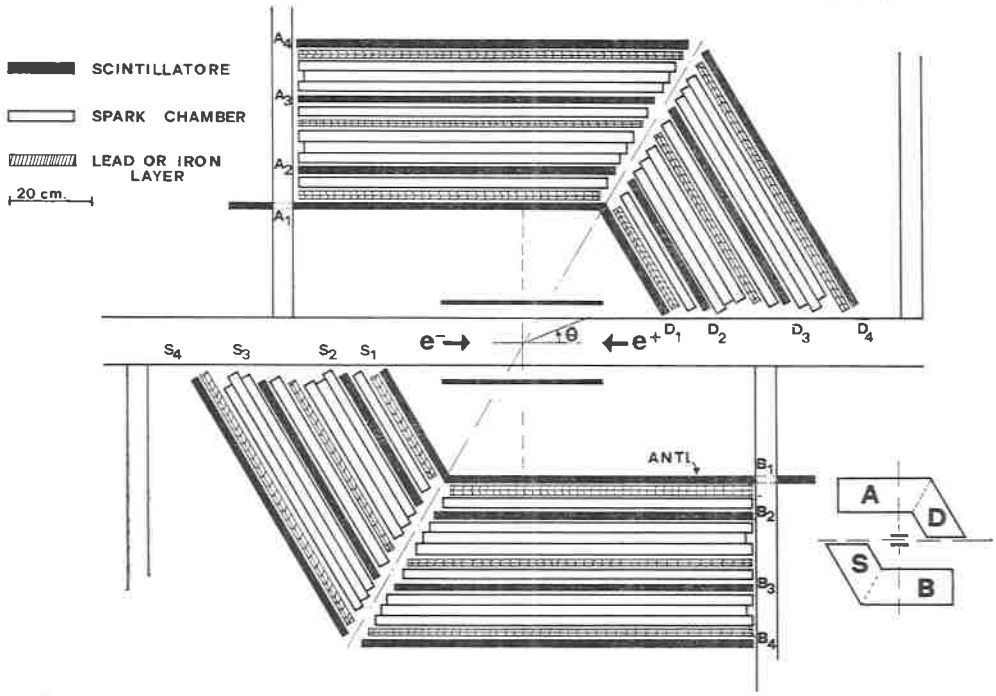

FIG.1

with an energy dependent efficiency, which is typically $\approx 80\%$ for an energy E: $\geqslant$250 MeV.

The apparatus could not be triggered by two charged particles only, so that our information has been collected through the following triggers:

a) at least three « particles » (charged particles or photons) in three at least of the four blocks;

b) at least one neutral (charged) in blocks I, II above and one charged (neutral) in the blocks below the e^+e^- beams;

c) only neutrals, at least one in the blocks above, and one below.

3. Results.

With this apparatus we have obtained in the last six months two hundred events, of which 84 coming from trigger *a*) have been analyzed. The total luminosity of Adone, for the 84 events we report, has been $L_t = 200 \cdot 10^{32}$ cm^{-2}.

The cross section for the processes (1) is, as usual, given by

$$\sigma = \frac{N}{L_t \varepsilon}$$

N being the total number of the events for each specified process; L_t the total luminosity of Adone in that same period. The luminosity has been measured by using as a monitor the $e^+e^- \to e^+e^-$ scattering at small momentum transfer ([3]).

Efficiency ε represents the probability of detecting the considered hadronic events in our apparatus. This is a most difficult point, which deserves a few words of explanation. In fact the value of ε depends on the particular angular and energy distribution of the considered events, and it is not possible to measure with certainty those distributions with the apparatuses which are presently in operation at Frascati. They are far from covering the 4π solid angle and have rather sensible cuts in energy (our apparatus covers $\approx 0.2 \cdot 4\pi$ solid angle and requires at least 100 MeV for a pion to be detected).

The efficiencies ε we have used to evaluate the cross sections σ we are reporting have been evaluated therefore under the hypothesis of pure phase space momentum distribution. The evaluation has been made by the Monte-Carlo method taking into account the details of our experimental apparatus. the length of the interaction region, the probability for detection of the γ rays and the nuclear interactions of the charged particles. In the evaluation of ε we have assumed the tracks to be pions and the showers to be due to photons.

The events have been distributed according to the number of showers and tracks observed, and range from events with two (one) tracks and one (two) showers up to events with four tracks and three showers.

We divide our events in two main categories: one is that of the hadronic events with only two charged pions $\pi^\pm$ produced, together with γ rays, that is processes (2) and (3); the other is that of the hadronic events coming from reactions with at least four charged particles in the final state, that is processes (4) to (6).

Due to energy cuts the detection efficiency of events with a total of more than 6 charged particles turns out to be rather small at our total energies.

The results are summarized in Table I.

TABLE I. – *Experimental results at average energy* $2E = 2\times1000$ MeV, *for the multiple hadronic production.*

Type of process	Lower limit of σ (cm^2)	Upper limit of σ (cm^2)
I) $e^+e^- \to$ 2 charged pions + neutrals (processes (2) and (3))	$0.6\cdot10^{-32}$	$1.5\cdot10^{-32}$
II) $e^+e^- \to$ at least four charged + any number of neutrals	$0.3\cdot10^{-32}$	$0.8\cdot10^{-32}$
III) $e^+e^- \to$ any multiple process with at least 3 particles, two being charged	$0.9\cdot10^{-32}$	$2.3\cdot10^{-32}$

Row III is the addition of rows I and II.

We have tried to separate in row I the processes $\pi^+\pi^-\pi^0$ and $\pi^+\pi^-\gamma$ from the others, by selecting the events in which the charged pions and the photon where close to coplanar. From this analysis we can only get an upper limit to the cross section to processes $e^+e^- \to \pi^+\pi^-\pi^0$ and $\pi^+\pi^-\gamma$; this is

$$\sigma(e^+e^- \to \pi^-\pi^+\pi^0(\gamma)) \leqslant 10^{-32}\ \mathrm{cm}^2 .$$

The lower limits given in Table I have been obtained by comparison of the cross sections estimated for different groups of events (each group having a given number of tracks and showers). We have also made use of the fact that efficiency ε does not increase indefinititely with the number of particles, but it reaches a maximum, due to the limited number of the particles which can be created and the decrease of their average energy when the multiplicity increases.

The results given in Table I refer mostly to the energy interval $(1900 < 2E < 2100)$ MeV. Preliminary analysis at other energies is in progress. The preliminary indication is that the total cross section for processes (1), does not decrease with energy with a simple $1/E^2$ law, but rather tends to remain high with increasing energy.

4. Conclusions on the multiple processes.

When going back to our initial questions, the interpretation of our results

gives the following indications:

A) There are multiple hadronic events, with three or more hadrons in the final state. The cross sections for these processes (see Table I) remain in the region covered by the « point like » cross section for bosons (spin 0) pair production (which is $\approx 0.6 \cdot 10^{-32}$ cm^2 at $2E = 2000$ MeV), and the cross section for μ pair production (which is $\approx 2.4 \cdot 10^{-32}$ cm^2 at this same energy).

B) The absolute values and energy dependence of our cross sections for multiple production do not indicate until now the existence of new vector bosons beyond ρ, ω, φ. One can try to express this fact, with a conservative limit, which is valid only at energies $2E$ around 2000 MeV: if we assume for a possible new 1^- boson a width Γ_ν of the order of 150 MeV, and we also assume that it decays mostly in three or more hadrons, its coupling to the *e.m.* field should be lower than the corrisponding coupling of the ϱ by at least a factor ten, that is: $4\pi/\gamma_\nu^2 \simeq 0.2$, being $4\pi/\gamma_\varrho^2 \simeq 2$.

C) The multiple events we are presenting may find some explanations in recent models, which were mostly considered after the discovery in Frascati of an appreciable hadronic production.

One possibility is the « extension » to our energies of the tails of the ρ, ω, φ particles, with new multihadronic decays. This has been studied recently by some authors ([4]), and will be discussed in this Conference by Renard.

Recently, Bramon and Greco ([5]) have analyzed the bump observed at DESY and SLAC in the photoproduction process $\gamma p \to \pi^+\pi^- p$ at forward angles, under the hypothesis that it is due to a new vector boson, the ρ', which has the quantum numbers of the ρ, and may decay in multihadronic modes. The corresponding cross sections are not incompatible with our values listed in Table I.

In addition to these interpretations, we recall the jet model of Cabibbo *et al.* ([6]), which is probably mostly effective at asymptotic energies, but still may provide multiple hadronic production with $\sigma \approx 10$ nanobarns at our energies.

5. Events with the electron and the positron surviving the collision (a first evidence of γ-γ interactions).

Besides the events described above, we have detected processes with at least two prongs (charged or neutrals, tracks or showers) in the apparatus

and a surviving electron or positron emitted at very small angle ($\approx 0°$) with respect to the e^+e^- beam line. Events of this kind could come, for instance, from second order electromagnetic processes in the e^+e^- collisions, of the type

$$e^+e^- \to e^+e^- + \text{others}\,,$$

which have been calculated by many authors [1], and are usually expressed in the graph:

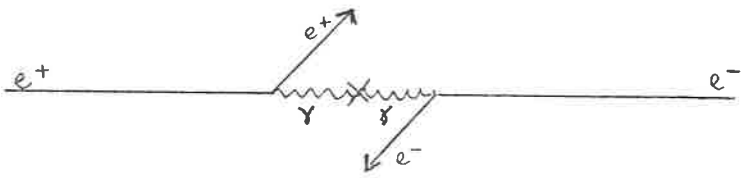

In order to detect these events in a first explorative stage we have installed two counters at the upstream and downstream edges of the bending magnets of Adone respectively [7] (see Fig. 2). By doing this we essentially use the

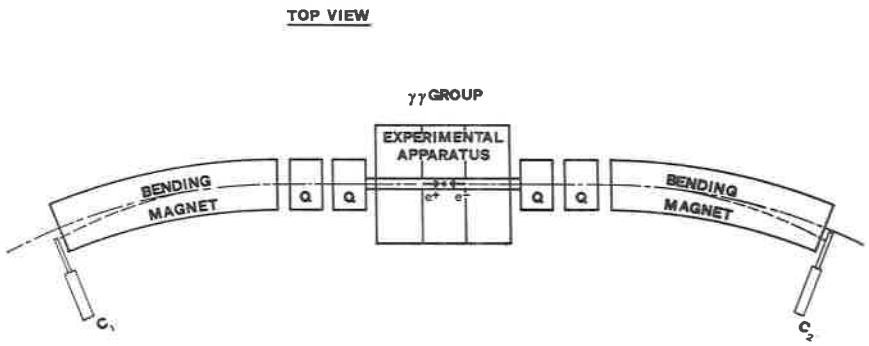

Fig. 2

Adone bending magnets as momentum analyzers for the $e^\pm$ emitted in the forward direction. So far, due to the position of the counters (installed right at the exit of the magnets), only a small fraction of $e^+(e^-)$ are detected ($\approx(80 \div 90)\%$ of the single beam energy is required to get a coincidence).

Experimental data with the small counters have been collected for a total integrated luminosity of about $(750 \times 10^{32})\,\text{cm}^{-2}$ at an aveage energy of 1000 MeV for each beam. These data are now under analysis. After a rough

selection, a total of about 50 events have been chosen for a further analysis and a large part of these events appears as 2 electrons ($\approx 70\%$). This is what one could expect, on basis of the theoretical calculation of the γ-γ interactions ([1]).

Events with 2 charged non showering particles are also present.

At present time we are installing long counters all along the doughnut inside the bending magnets so to be able to detect also lower energy electrons and positrons and to know their energy through a standard tagging technique.

REFERENCES

1) N. A. ROMERO, A. JACCARINI, P. KESSLER and J. PARISI: *Lett. Nuovo Cimento*, **4**, 933 (1970).; S. J. BRODSKY, T. KINOSHITA and H. TERAZAWA: *Phys. Rev. Lett.*, **25**, 972 (1970).
2) C. BACCI *et al.*: in publication, internal note L.N.F. 71/16.
3) G. BARBIELLINI *et al.*: *Atti Accademia dei Lincei*, **44**, 233 (1968).
4) G. KRAMER, J. L. URETSKY and T. F. WALSH: *Phys. Rev.*, D **3**, 719 (1971).
5) A. BRAMON and M. GRECO: Internal Note LNF 71/8.
6) N. CABIBBO, G. PARISI and M. TESTA: *Lett. Nuovo Cimento*, **4**, 35 (1970). See also S. D. DRELL, D. J. LEVY and T. M. YAN: *Phys. Rev.*, D **1**, 1617 (1970).
7) F. AMMAN: *Lett. Nuovo Cimento*, **1**, 729 (1969).

Proof of hadron production in e^+e^- interactions. (*)

V. ALLES-BORELLI, M. BERNARDINI, D. BOLLINI, P. L. BRUNINI, E. FIORENTINO, T. MASSAM, L. MONARI, F. PALMONARI and A. ZICHICHI

CERN - Geneva
Istituto Nazionale di Fisica Nucleare - Bologna
Istituto di Fisica dell'Università - Bologna
Laboratori Nazionali di Frascati - Frascati (Roma)

1. Introduction.

The purpose of this paper is to show that in e^+e^- interactions at centre-of-mass energies above the ρ, ω, φ region, hadronic final states are abundantly produced.

Since the first observations [1] with the Frascati colliding beams, of processes with large cross sections, many theoretical models have been presented in the literature [2] to predict large hadronic cross sections in e^+e^- interactions. The crucial point was, however, to establish the hadronic nature of the observed processes.

2. The experimental set-up.

The experimental set-up (**) consists of four similar telescopes, two on each side of the colliding beam axis. They were designed to cover

(*) Invited paper presented by A. Zichichi.

(**) The experimental set-up will be reported elsewhere [3-5], here we will mention only a few relevant points.

the maximum possible solid angle consistent with having sufficient telescope thickness for good particle identification. The use of the various elements in each telescope is as follows:

i) kinematic chambers—to allow precise vertex reconstruction of an event;

ii) thin and thick plastic scintillation counters—to allow a fast trigger with good pulse-height analysis and time-of-flight measurement;

iii) heavy-plate spark chambers—to allow a discrimination between electrons (which generate electromagnetic showers), muons (which do pratically nothing) and pions (which suffer nuclear scattering or interactions).

3. Data taking and analysis.

The ADONE energies and the corresponding luminosities available for the data reported here are given in Table I. The electronic trigger was such

TABLE I.

E (MeV)	L_I (10^{32} cm^{-2})
700	74
750	175
950	630
970	235
1050	1075
1200	449

as to accept all reactions with at least two charged particles in the final state. All events showing at least three sparks in the heavy-plate spark chambers have been reconstructed in space using the tracks in the thin-plate spark chambers. Furthermore the pulse-heights in the thick scintillation counters and also the time-of-flight of each of the two particles in the final state were recorded and analysed off-line. The time-of-flight information is particularly useful for excluding cosmic-ray events as discussed in ref. 5. The pulse-height information has so far not been exploited because the heavy-plate spark chamber pictures already give the required discrimination between electrons, muons, and hadrons. The monitor was a small-angle telescope which was sensitive to the elastic scattering $e^+e^- \to e^\pm e^\mp$, at very small momentum tran-

sfers, varying from $-0.8\cdot10^{-3}$ GeV^2 to $-4.6\cdot10^{-3}$ GeV^2, the average over the monitoring telescope being $-2\cdot10^{-3}$ GeV^2 (*).

3.1. *Selection of* $h^\pm h^\mp$ *final states.* – The reactions searched for were

$$e^+e^- \to h^\pm h^\mp \tag{1}$$

$$e^+e^- \to h^\pm h^\mp + \text{anything}, \tag{2}$$

where $h^\pm$ stands for hadron.

The crucial point here was to show that final states supposedly of hadronic nature were not the result of background simulation from the much more abundant reactions

$$e^+e^- \to e^\pm e^\mp \tag{3}$$

$$e^+e^- \to e^\pm e^\mp + \text{anything} \tag{4}$$

$$e^+e^- \to \mu^\pm \mu^\mp \tag{5}$$

$$e^+e^- \to \mu^\pm \mu^\mp + \text{anything} \tag{6}$$

In order to do this, it was necessary to exploit all information contained in the heavy-plate spark chamber pictures. This may be done by means of six parameters whose purpose is to obtain an objective pattern recognition in terms of quantities directly measurable in a picture. On the basis of these parameters an event is defined by a point in a six-dimensional space, and may be assigned to one of three main subdivisions of the space:

i) *The hypervolume where* $e^\pm e^\mp$ *events fall*: Special calibration data have been taken with a fifth telescope, analogous to the other four of the actual experiment, using electron beams from 350 MeV/c to 1000 MeV/c at the CERN Proton Synchrotron (PS). This large energy range has been chosen in order to take account of $e^\pm e^\mp$ final states with large radiative emission. On the basis of these calibration data, it has been possible to identify in the six-dimensional space a hypervolume where at 760 MeV/c $(100\pm3)\,\%$ and at 1000 MeV/c $(99.0\pm0.7)\,\%$ of the electrons fall.

(*) Our metric is – for space-like and + for time-like quantities.

ii) *The hypervolume where* $\mu^{\pm}\mu^{\mp}$ *events fall*: Here again special calibration data, using muons from 760 MeV/c to 1000 MeV/c at CERN PS, allowed the identification of the hypervolume containing $(100.0 \pm 0.1)\%$ of the muon events.

iii) *The hypervolume where* $h^{\pm}h^{\mp}$ *events fall*: This hypervolume is obtained from (i) and (ii) by requiring that the penetration in this volume of an electron is $< 10^{-2}$ and of a muon is $< 10^{-2}$. Some of the hadronic patterns are bound to fall in this « non-leptonic » hypervolume. Limiting ourselves to the case: $h^{\pm} \equiv \pi^{\pm}$ and again using known particle beams at the PS (pions from 760 MeV/c to 1000 MeV/c), we have determined that $(71 \pm 3)\%$ of the pions give patterns in the non leptonic hypervolume.

Thus the six-parameter method allows the detection of a pion pair with $(50 \pm 4)\%$ efficiency, the rejection of a $(e^{\pm}e^{\mp})$ pair with $< 10^{-4}$ rejection power and the rejection of a $(\mu^{\pm}\mu^{\mp})$ pair with 2×10^{-3} rejection power.

iv) *Simulation of* $h^{\pm}h^{\mp}$ *from* $(e^{\pm}e^{\mp})$ *and* $(\mu^{\pm}\mu^{\mp})$ *final states*: On the basis of the calibration data mentioned above the background level from leptonic pairs is estimated to be:

$$h^{\pm}h^{\mp} \text{ simulated by } (e^{\pm}e^{\mp}) \text{ pairs} = N(e^{\pm}e^{\mp}) \times P_{e\bar{e}}^{\pi\pi} \leqslant 1 \text{ event}$$

$$h^{\pm}h^{\mp} \text{ simulated by } (\mu^{\pm}\mu^{\mp}) \text{ pairs} = N(\mu^{\pm}\mu^{\mp}) \times P_{\mu\bar{\mu}}^{\pi\pi} \leqslant 1 \text{ event}$$

where $N(e^{\pm}e^{\mp})$ and $N(\mu^{\pm}\mu^{\mp})$ are the total numbers of $(e^{\pm}e^{\mp})$ and $(\mu^{\pm}\mu^{\mp})$ pairs measured in the same data runs as the hadronic events reported here, and $P_{e\bar{e}}^{\pi\pi}$, $P_{\mu\bar{\mu}}^{\pi\pi}$ are the probabilities that a $(e^{\pm}e^{\mp})$ or a $(\mu^{\pm}\mu^{\mp})$ pair simulates a $(\pi^{\pm}\pi^{\mp})$ pair. Thus the observed $h^{\pm}h^{\mp}$ events cannot be due to background from leptonic pairs produced in $e^{+}e^{-}$ interactions.

An independent cross-check is obtained using « internal » calibration data. We take all events having an electron (or a muon or a pion pattern) in one telescope and we measure the six parameters in the picture from the telescope on the opposite side. The results of the « internal » calibrations are in excellent agreement with the « external » calibration data. On the basis of these « internal » calibrations the rejection power for $(e^{\pm}e^{\mp})$ pairs, in the energy interval proper to this experiment, is found to be better than 1.5×10^{-6}; this value is better than the other one from the « external » calibrations because of the higher number of « electrons » available. The rejection power for muons turns out to be the same as that from « external » calibrations. These results confirm that the $h^{\pm}h^{\mp}$ events observed cannot be generated by $(e^{\pm}e^{\mp})$ or $(\mu^{\pm}\mu^{\mp})$ pairs produced in $(e^{+}e^{-})$ interactions.

In fact these rejection powers against leptons are sufficiently large that, for the data presented here, a more relaxed criterium, based on the observatron of a pion pattern on either side, can be used. With this criterium the electron and muon contaminations are estimated to be $\sim 5\,\%$ of the hadronic events, while the hadronic pattern recognition efficiency is $(77\pm7)\,\%$.

3.2. *Other background sources.* – The other background sources investigated are cosmic rays and beam-gas interactions.

Cosmic rays: In order to check the correct performance of our apparatus, we continuously take cosmic-ray film. In a sample of film corresponding to $\sim$half the sensitive data-taking time, no event of the $h^\pm h^\mp$ class has been found; thus the events observed cannot be accounted for by cosmic-ray background.

Beam-gas interactions: Special runs at various ADONE energies have been taken with only one circulating beam. Here the monitor is the total current loss. In a sample of beam-gas interaction data corresponding to $\sim 40\,\%$of the data taking luminosity, no event of the type $h^\pm h^\mp$ has been found: the observed events cannot be taken as being due to beam-gas interaction background.

4. Results.

The R distribution of all $(h^\pm h^\mp)$ events with $|\varphi| \leqslant 5°$, is shown in Fig. 1. R is the supplement of the angle subtended by the directions of the two particles; φ is the angle between the two planes, each of which contains one particle and the beam direction. The peak at small angles ($R \leqslant 7.5°$) is the proof that collinear $h^\pm h^\mp$ events are produced in e^+e^- interactions. Events with $R > 7.5°$ cannot be explained in terms of first-order radiative corrections (dotted line). These corrections have been calculated following the work of Bonneau and Martin ([6]), where the peaking approximation ([7]) is removed. These events can be understood from Fig. 2, which shows the acoplanarity distribution of the events with $R > 7.5°$. The dotted histogram is the result of Monte Carlo calculations normalized to the total number of events with $|\varphi| > 5°$. This distribution clearly shows that the non collinear-but coplanar hadronic events are the tail of reaction (2).

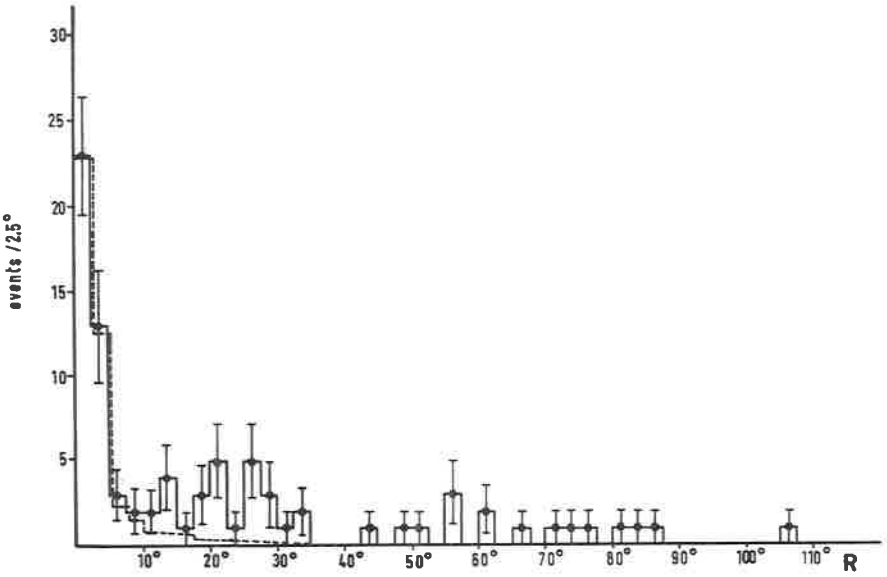

Fig. 1. – R distribution of all $h^{\pm}h^{\mp}$ events with $|\varphi| \leqslant 5°$. The dotted histogram shows the effect of the radiative corrections.

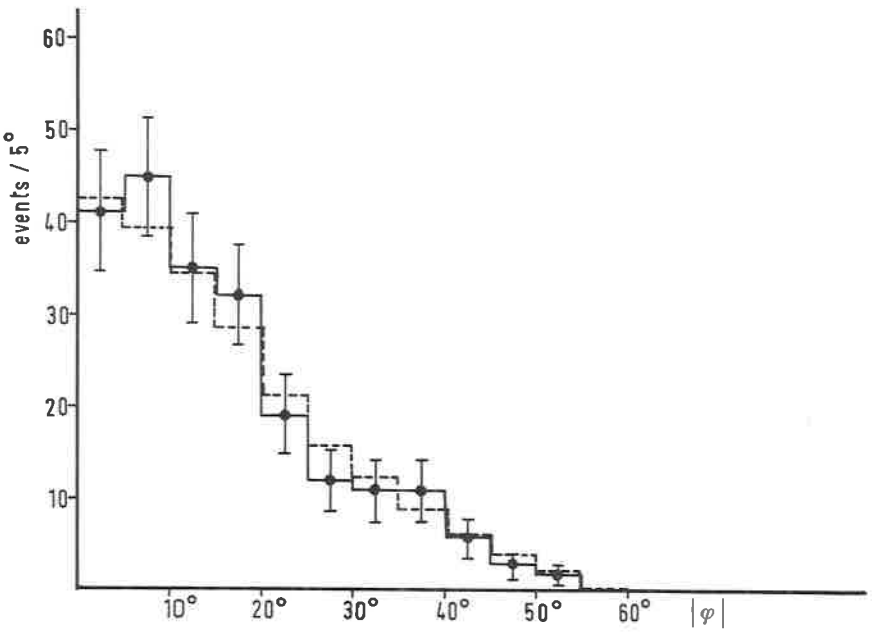

Fig. 2. – $|\varphi|$ distribution of all $h^{\pm}h^{\mp}$ events with $R > 7.5°$. The dotted histogram shows Monte Carlo expectations, normalized to the total number of events with $|\varphi| > 5°$.

From the geometrical analysis, the events can be divided into three classes:

i) Events with $R \leqslant 7.5°$ and $|\varphi| \leqslant 5°$—collinear and coplanar.

ii) Events with $R > 7.5°$ and $|\varphi| \leqslant 5°$—non-collinear but coplanar.

iii) Events with $R > 7.5°$ and $|\varphi| > 5°$—non-collinear non coplanar.

4.1. *s-dependence of reaction* (1): $e^+e^- \to h^\pm h^\mp$. – The events belonging to class i) are the best candidates for the simple two-body hadronic annihilation reaction: $e^+e^- \to h^\pm h^\mp$. The s-dependence of these events is shown in Fig. 3 where the ordinate is the ratio

$$\alpha_1 = \frac{e^+e^- \to h^\pm h^\mp (\text{with } R \leqslant 7.5° \text{ and } |\varphi| \leqslant 5°)}{e^+e^- \to e^\pm e^\mp (\text{with any } R)}$$

The value of this ratio expected for e^+e^- annihilation into a pair of point-like pions is shown by the dotted line.

4.2. *s-dependence of reaction* (2): $e^+e^- \to h^\pm h^\mp +$ *anything*. – The events belonging to the classes (ii) and (iii) are all due to the multibody annihilation reaction $e^+e^- \to h^\pm h^\mp +$ anything. The s-dependence of the observed ratio

$$\alpha_2 = \frac{e^+e^- \to h^\pm h^\mp (\text{with } R > 7.5° \text{ and } |\varphi| > 5°)}{e^+e^- \to e^\pm e^\mp (\text{with any } R)}$$

is reported in Fig. 4. The background subtraction from beam-gas interaction has been applied. In order to derive from this ratio the values of the cross-section, it is necessary to make assumptions about relative contributions of the various channels of e^+e^- hadronic annihilation to our observed two-body final states. For the time being we prefer to present our data without making any model-dependent hypothesis.

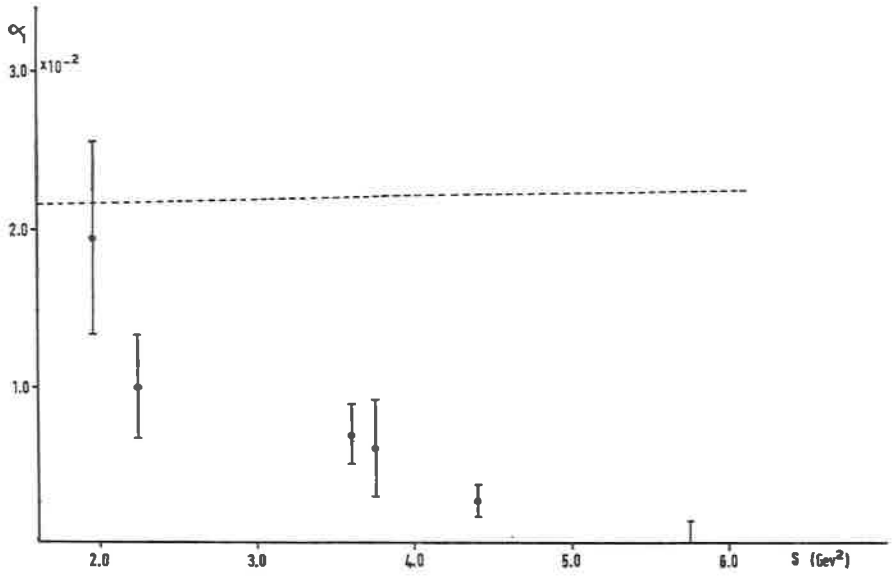

Fig. 3. – s-dependence of the ratio $\alpha_1 = \dfrac{e^+e^- \to h^\pm h^\mp \text{ (with } R \leqslant 7.5^\circ \text{ and } |\varphi| \leqslant 5^\circ)}{e^+e^- \to e^\pm e^\mp \text{ (all R)}}$.

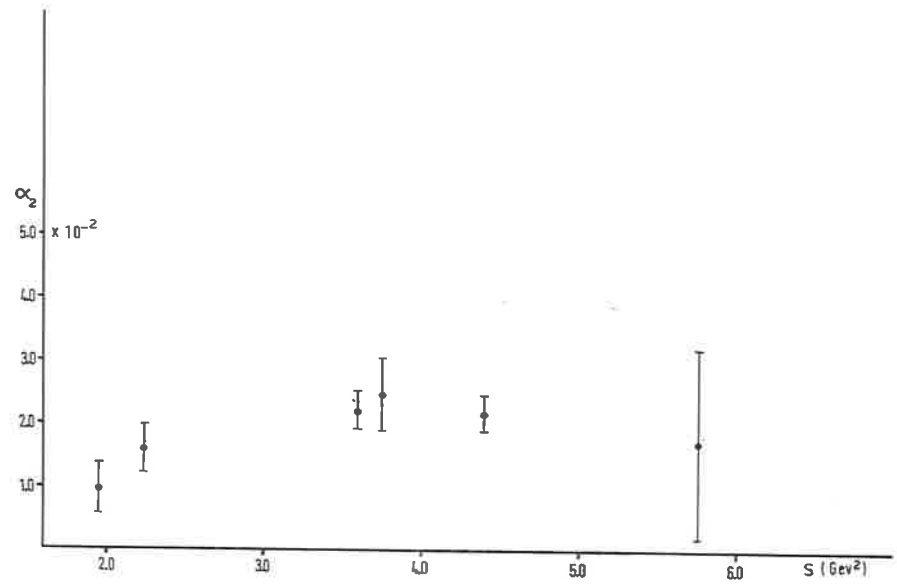

Fig. 4. – s-dependence of the ratio $\alpha_2 = \dfrac{e^+e^- \to h^\pm h^\mp \text{ (with } R > 7.5^\circ \text{ and } |\varphi| > 5^\circ)}{e^+e^- \to e^\pm e^\mp \text{ (all R)}}$.

REFERENCES

1) Papers submitted to the *XV International Conference on High-Energy Physics*, Kiev, August 1970, by all the Groups working with ADONE.
2) For a review see N. CABIBBO: Invited paper to this Conference.
3) V. ALLES-BORELLI *et al.*: *Proceedings of the VIII Course of the International School of Subnuclear Physics*, Erice, July 1970, published by Academic Press in *Elementary Processes at High-Energy*, A. Zichichi ed., p. 790.
4) V. ALLES-BORELLI *et al.*: *Direct Check of* QED *in* e^+e^- *Interactions at High* q^2 *Values*, to be submitted to *Il Nuovo Cimento*.
5) V. ALLES-BORELLI *et al.*: *Check of Quantum Electrodynamics and of Electron-Muon Equivalence*, to be submitted to *Il Nuovo Cimento*.
6) G. BONNEAU and F. MARTIN: *Thesis*, Laboratoire de Physique Théorique et Hautes Energies, Orsay.
7) S. TAVERNIER, *Thèse de Doctorat de 3-me cycle*, Orsay, RI 68/7 (May 1968).

Hadron production in e^+e^- collisions from the tail of the ρ, ω and φ mesons (*)

J. LAYSSAC and F. M. RENARD

Departement de Physique Mathématique, Faculté des Sciences - Montpellier

We present a model for the multihadron production in e^+e^- collisions which is simply based on the conventional Vector Dominance Model. It is well known [1] that the vector dominance model works rather wèll for time-like photons in the range of energy including the ϱ, ω and φ mesons. One may therefore assume that this model still works for a larger energy range, for example up to 2.0 or 3.0 GeV; the hadronic interaction of the photon would still be governed by the ρ, ω and φ mesons only. This is the basis of our model in which the whole production of hadrons comes from the tails of the ϱ, ω and φ propagators; the final states are only those which are strongly coupled to these mesons. It is also supposed that the dominant contributions come from the enhancements due to the final two-body or quasi-two-body states formed with mesons and resonances. One had already noticed [2] this possibility in the case of $e^+e^- \to 4\pi$ with the strong effect of the $\varrho \to \pi\omega$ mode.

This model is now applied to the production of pions (4π, 5π, 6π) and of η+pions, $K\overline{K}$+pions in the range of energy $E_{tot}^{cm} < 3$ GeV which is presently accessible with Adone. The corresponding processes are those corresponding to the diagram 1 and 2 and for which the thresholds are below 3 GeV. The coupling constants are taken either from experimental widths or from VDM, SU_3 or quark models. The explicit forms of the couplings, widths and cross-sections may be found in our previous papers [3].

Each particular quasi-two-body mode $e^+e^- \to R + R'$ give a cross-section which presents the characteristic bump due to the threshold effect at the opening of the corresponding channel. It is the addition of the various

---

(*) Invited paper presented by F. M. Renard.

modes which compensates the decreasing effects of the photon and vector meson propagators in the energy ranges where many resonances are strongly coupled to the ϱ, ω and φ mesons.

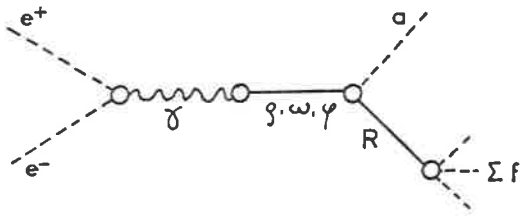

Diag. 1

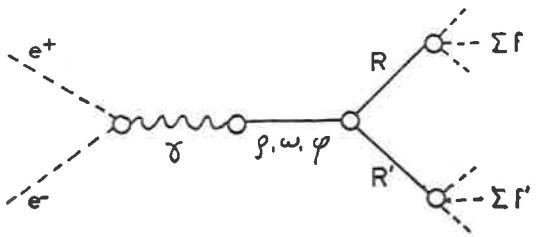

Diag.2

In fact for $e^+e^- \to 4\pi$ the important modes are $\pi\omega$, πA_1 and ϱf, the corresponding cross-section is shown in Fig. 1. The reaction $e^+e^- \to 5\pi$ is dominated by the states πB, ϱA_1, ϱA_2 and shown in Fig. 2. The 6π production is essentially given by the modes ωA_1, ωA_2 and ϱB (Fig. 3). The η+pions production occurs dominantly through the states $\eta\varrho$, ηB and $\delta\omega$ (see Fig. 4). The $K\overline{K}$+pions cross-sections have been calculated from the various modes $K^*\overline{K}^*$ related by SU_3 to the non-strange modes. Figure 5 shows the total cross-sections respectively for the sums of the pionic, η+pions and $K\overline{K}$+pions production. One has also drawn the total hadronic production and the total cross-section for four charged particles which result from the above modes. The total hadronic cross-section is rather constant around $(3 \cdot 10^{-32})$ cm^2

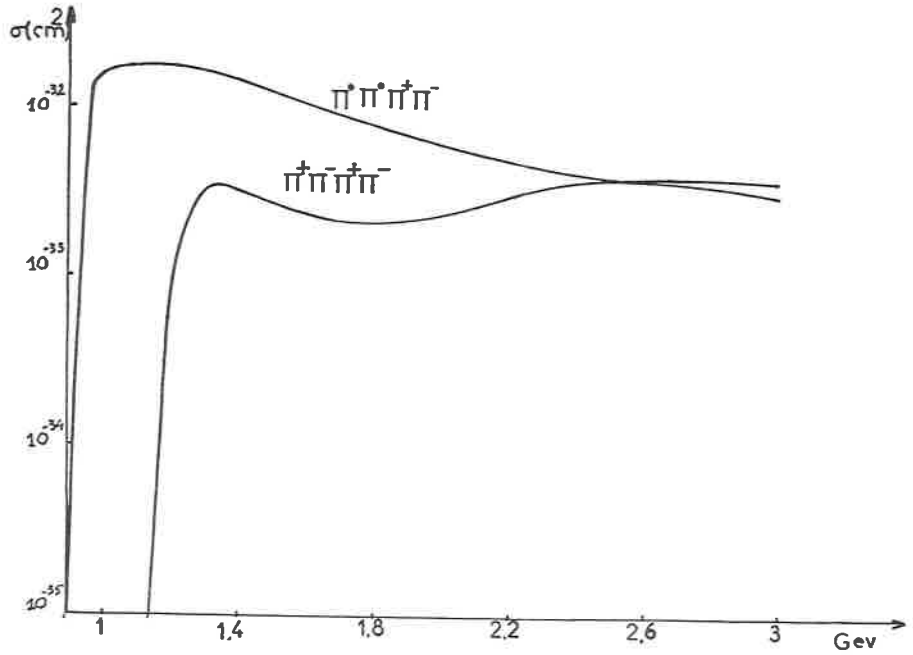
σ(cm²)
10⁻³²
10⁻³³
10⁻³⁴
10⁻³⁵
π°π°π⁺π⁻
π⁺π⁻π⁺π⁻
1
1.4
1.8
2.2
2.6
3
Gev

Fig 1

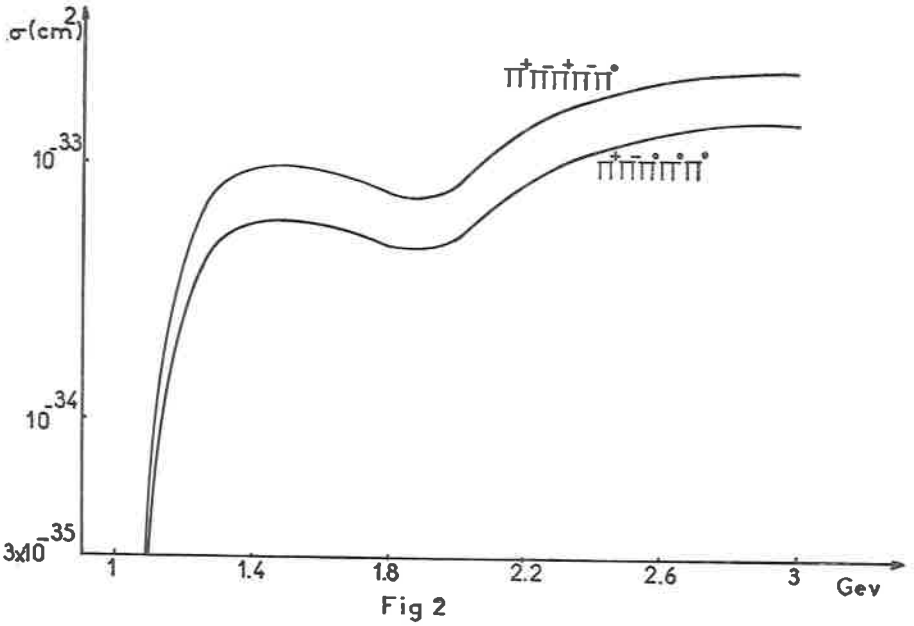
σ(cm²)
10⁻³³
10⁻³⁴
3x10⁻³⁵
π⁺π⁻π⁺π⁻π°
π⁺π⁻π°π°π°
1
1.4
1.8
2.2
2.6
3
Gev

Fig 2

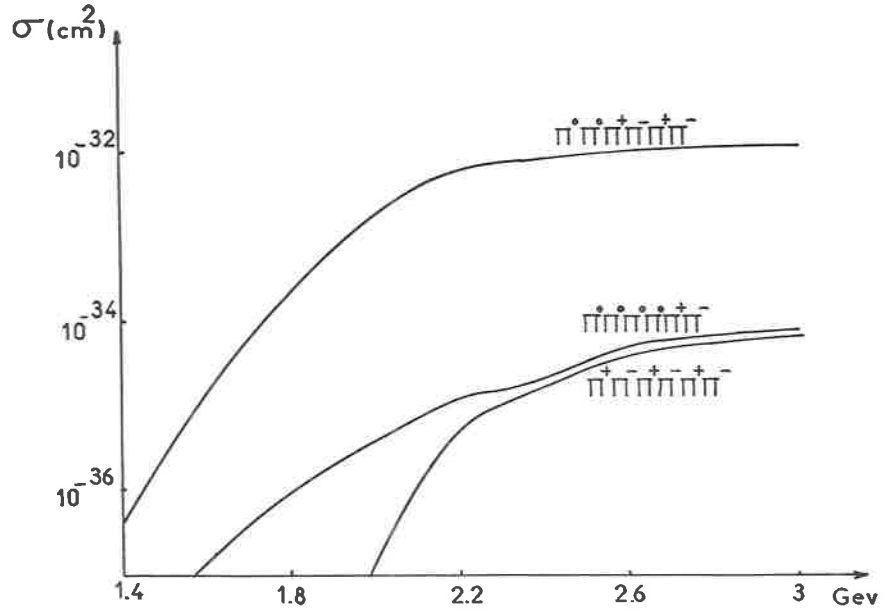
σ(cm²)
10⁻³²
10⁻³⁴
10⁻³⁶
1.4
1.8
2.2
2.6
3
Gev

Fig 3

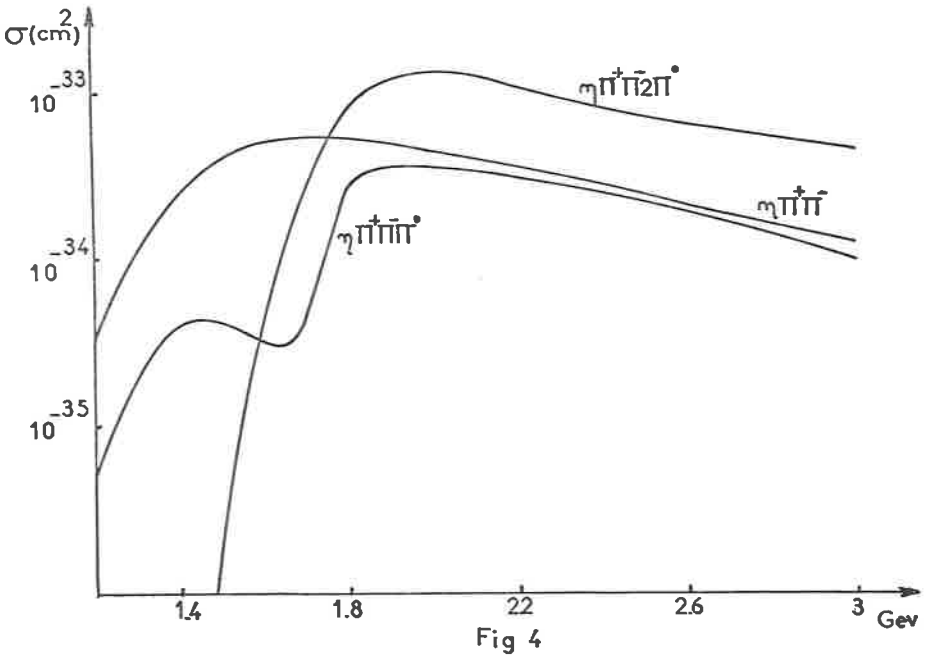
σ(cm²)
10⁻³³
10⁻³⁴
10⁻³⁵
1.4
1.8
22
2.6
3
Gev

Fig 4

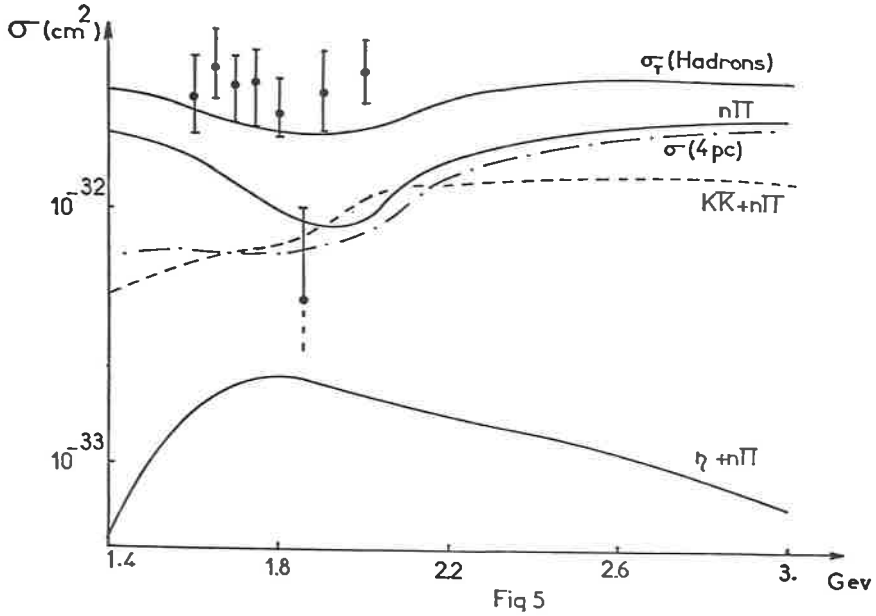

Fig 5

between 1.4 and 3 GeV, with two small maxima essentially due to the dominant effects of the $\pi\omega$ mode around 1.4 GeV and of ρA_1, ρA_2, ρf and ωf around 2.8 GeV.

The four charged particles production appears to be slightly smaller than the one observed at Adone in the 1970 preliminary mesurements ([4]), but the energy dependence is similar.

In addition to these total cross-sections, one should compare with experiments the kinematical distributions of the final particles. The validity of our model would be tested if the characteristic quasi-two-body mass spectra were observed. In this case a precise fit of the experimental results will give the coupling constants of the various resonances. This may be used also to test various symmetry models (SU_3, quark models) in particular the internal symmetry properties of the electromagnetic current ($|\Delta I| \geqslant 1$, $|\Delta U| = 0$ and octet behaviour).

The energy dependence of the cross-sections will also give us informations on the s-dependence of the coupling constants and width, in particular for the vector meson propagators. This is an important problem which arises if one wants to apply our model for higher energies. Also the increasing number of opened channels and higher resonances limits the applicability of this model above 3 GeV. In this energy range, the asymptotic descriptions

using the concepts of partons and scale invariance may be more reliable. However if it works, the merit of this model will be to give a simple connection between the range of application of the VDM in the vicinity of the ϱ, ω and φ mesons and the asymptotic one.

REFERENCES

1) J. J. SAKURAI: *Balaton Symposium on Hadron Spectroscopy* (1970).
2) F. F. M. RENARD: *Nuovo Cimento*, **64**, 979 (1969); G. KRAMER, J. L. URETSKY and F. WALSH: DESY Report 70/44.
3) J. LAYSSAC and F. M. RENARD: *Lett. Nuovo Cimento*, **1**, 197 (1971) and *Nuovo Cimento* **6** A, 134 (1971).
4) B. BARTOLI *et al.*: contribution to the Kiev Conference (1970).

An experimental possibility to detect higher order electromagnetic processes at Adone (*)

G. BARBIELLINI
Laboratori Nazionali del C.N.E.N. - Frascati (Roma)

S. ORITO
University of Tokyo - Tokyo

To detect the almost real $\gamma\gamma$ collisions, we propose to install a tagging system utilizing the bending magnets of ADONE. A main purpose is the experimental check against the contaminations on the 1γ (annihilation) processes coming from the higher order electromagnetic reactions such as $e^+e^- \to e^+e^-e^+e^-$, $e^+e^-\mu^+\mu^-$ or $e^+e^-e^+e^-e^+e^-$. The system also allows us to investigate the hadronic 2γ processes such as $e^+e^- \to e^+e^-\pi^+\pi^-$ or the production of $c = +1$ resonances like $e^+e^- \to e^+e^-\eta'$. Furthermore it is possible by this scheme to get a clean identification of the radiative vector meson productions.

1. Purposes.

1.1. *Contamination on annihilation processes.* – Figure 1 shows possible diagrams of the higher order electromagnetic processes in the $e^\pm$ collision. Recent calculations ([1-4]) show relatively large cross-sections of these 2γ and 3γ processes already at GeV region. This implies a possibility to investigate the almost real $\gamma\gamma$ collisions by using the existing or coming $e^\pm$ colliding beam machines.

At the same time, it also indicates some danger of contaminations coming from these 2γ (or 3γ) processes on the 1γ (annihilation) processes. For ex-

(*) Invited paper presented by G. Barbiellini.

ample, the 2γ process $e^+e^- \to e^+e^-\mu^+\mu^-$ is expected to have a total cross-section of 70 nb at beam energy of 1.5 GeV. This contributes to an effective

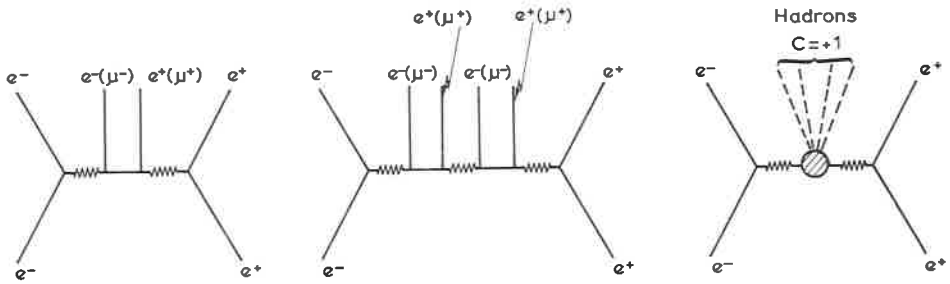

a) $2\gamma \to$ leptons b) 3γ, leptons c) $2\gamma \to$ hadrons

FIG.1 Higher order electromagnetic processes in e^+e^- collision

cross-section of 2 nb ([5]) for the muon pairs with each kinetic energy larger than 150 MeV to be detected by a wide angle detector covering $\theta = (90 \pm 40)°$, $\Delta\Phi/2\pi = 0.8$ ([5]). About 10% of them (effective cross-section of 0.2 nb) will give the collinear track within $\pm 5°$. In the same way, we expect a cross-section of 0.3 nb ([5]) for the collinear $e^\pm$ with each kinetic energy larger than 150 MeV coming from the 2γ process $e^+e^- \to e^+e^-e^+e^-$.

These values are appreciably large if compared to the corresponding effective cross-section of 0.4 nb expected for the annihilation process $e^+e^- \to \to \pi^+\pi^-$ ([6]). It should be noticed that there exist some difficulties, in most of the detectors being used at ADONE, to distinguish these low energy muons or electrons from the pions. For the complete rejection of such contaminations, a clean experimental identification of the 2γ (3γ) processes would be valuable.

1.2. *Hadronic* 2γ *processes.* – The investigation of the hadron production by $\gamma\gamma$ collision is extremely interesting in itself, since essentially no experimental information is available at this moment. For the reaction $e^+e^- \to e^+e^-\pi^+\pi^-$, a total cross-section of 4 nb is expected at beam energy of 1.5 GeV (assuming the point like pion). This corresponds to an effective

cross-section of 0.1 nb for the pion pairs with each kinetic energy more than 150 MeV to be detected by the wide angle detector covering ([5]) $\theta = (90 \pm 40)°$, $\Delta\Phi/2\pi = 0.8$. This will give about 20 events for 100 days assuming an average luminosity of $10^{32}\ \mathrm{cm^{-2}\,hr^{-1}}$. It would be also worthwhile to notice that some calculations ([7]) give even twice as large cross-section as for the point-like pion due to the hadronic corrections.

Other hadronic processes which can be investigated are the production of $c = +1$ resonances through $\gamma\gamma$ collision. For example, the cross-section for the reaction $e^+e^- \to e^+e^-\eta'(960)$ is expected to be ([4]) $1.2 \cdot 10^{-35}\ \mathrm{cm^2\ (KeV)^{-1}}\ \Gamma 2\gamma$ at beam energy of 1.5 GeV where $\Gamma 2\gamma$ is the 2γ decay width of the resonance. Putting the branching ratio $\Gamma 2\gamma/\Gamma = 0.1$ ([8]) and the upper limit 4 MeV for the total width Γ, we can get a cross-section of 5 nb, which results into an event rate similar to the $e^+e^- \to e^+e^-\pi^+\pi^-$. Therefore, we have a good chance, at least, to reduce the upper limit for Γ by a factor 10.

1.3. *Radiative production of the vector mesons.* – Recent calculation by C. Bernardini ([9]) demonstrates a cross-section of $(1 \sim 10)$ nb for the reactions $e^+e^- \to \varrho\gamma$, $\omega\gamma$, $\varphi\gamma$. It would be interesting to detect this kind of events.

2. Experimental method.

A characteristic kinematical feature of the 2γ (or 3γ) processes is the extremely small angle (typically an order of mrad) between the surviving $e^\pm$ and the beams. In order to tag the almost real γ's by these forward-going $e^\pm$, we propose to use the bending magnet of ADONE as the momentum analyzer.

Figure 2 shows the experimental arrangement, which consists of two scintillation counters (F1, F2) inside the magnet, two lead glass counters set at zero degree ($\gamma 1$, $\gamma 2$) and a wide angle detector (W).

The $e^\pm$ which has lost the energy by the irradiation of almost real photon travels essentially in the beam direction, passing through the quadrupole magnets, swept out by the bending magnet of ADONE, and is detected by the scintillation counter inside the magnet. The scintillator will be 2.7 m long, 7 cm high, 3 cm thick, viewed by two photomultipliers from both sides. The time difference measurement between the tubes gives us a position accuracy of ± 5 cm, which corresponds to a momentum accuracy of $\pm 2\%$. The small but nonzero angular spread of $e^\pm$ causes a slight difference of orbit even for the same momentum. Considering all these, a

typical momentum accuracy is estimated to be of $\pm 3\%$. The momentum range covered is between $0.2E$ and $0.85E$, where E is the beam energy. The range can be extended up to $0.9E$ by adding a small counter at the exit of the magnet.

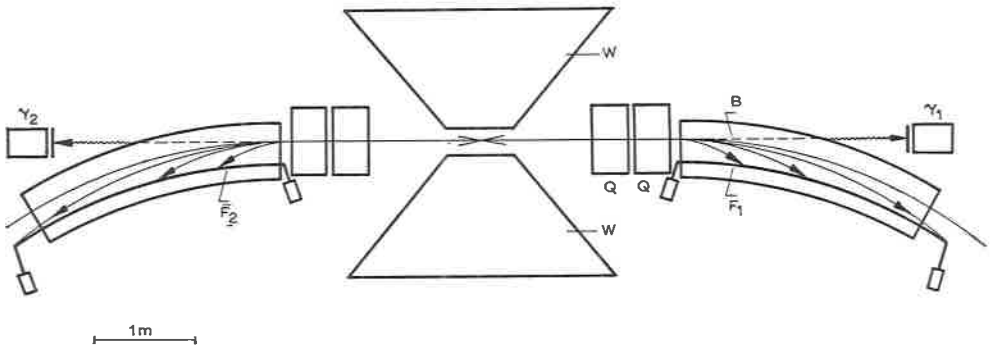

FIG. 2 Experimental arrangement

For the wide angle detector, any apparatus existing or being prepared at ADONE can be used, although a lower threshold energy for the trigger and a larger solid angle is preferable.

Block diagram of the logic is shown in Fig. 3. We take the coincidence $F1\overline{\gamma 1}\ F2\overline{\gamma 2}W$ for the 2γ (3γ) processes. The coincidence requirement for the forward going $e^{\pm}$ will be necessary for the clean identification of the events. The background will mainly come from the beam $e^{\pm}$ which loses energy by the real bremstrahlung with the residual gas. This contribution for the accidental rate is expected to be about 1% for the normal operating condition of ADONE ([10]). The anticoincidence requirement for the lead glass counter $\gamma 1$ or $\gamma 2$ will finally avoid any ambiguity coming from this kind of backgrounds.

For the $2\gamma \to 2$ body processes such as $e^+e^- \to e^+e^-\pi^+\pi^-$, approximate coplanarity can be used for the identification.

The invariant mass M and the velocity β of the 2γ system are well determined from the measured momentum of the forward going $e^{\pm}$. Typical accuracies are $\Delta M = \pm 40$ MeV and $\Delta\beta = \pm 0.07$. This also serves as a kinematical constraint for the angle and energies of the two final state particles. The resonance production by 2γ process would be clearly recognized by the peak in the invariant mass.

For the radiative production of the vector mesons, we require the logic signal $\gamma 1 W \overline{F1}$ or $\gamma 2 W \overline{F2}$. The anticoincidence requirement for F_1 and F_2 will be essential since otherwise the accidental rate would be as high as

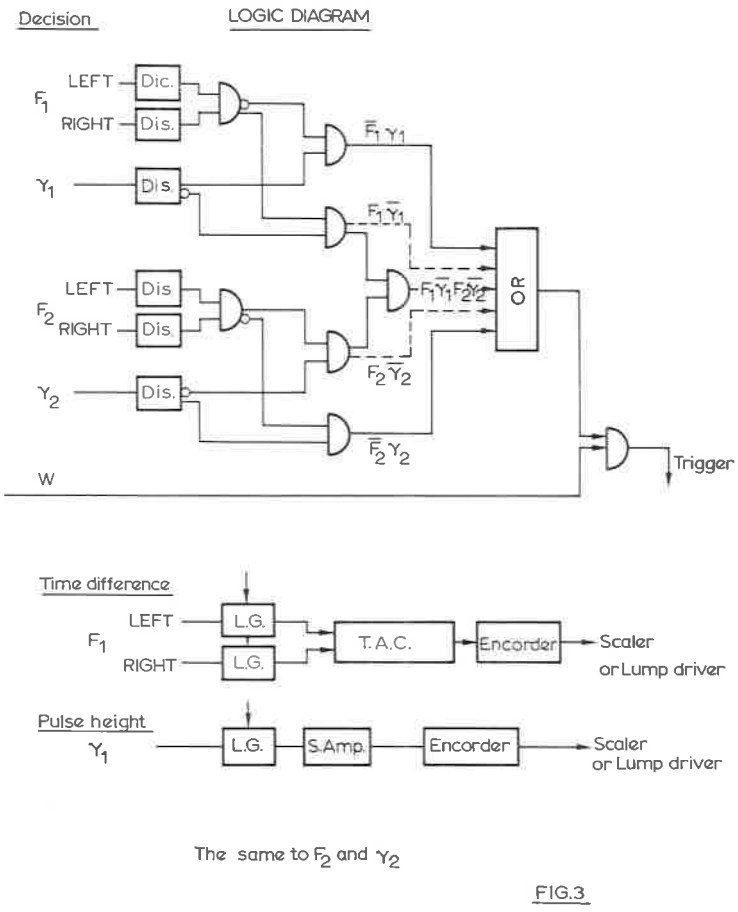

FIG.3

10% ([10]) which mainly comes from the beam-gas bremstrahlung. The energy of the γ-ray can be measured with an accuracy of $\pm 10\%$, which will be sufficient to identify this kind of event through the kinematical constraints.

3. Installation.

Figure 4 shows the position of the scintillator inside the magnet. For the installation, the vacuum pipe has to be taken out. This can be done during the shut-down of ADONE scheduled from mid-March of this year

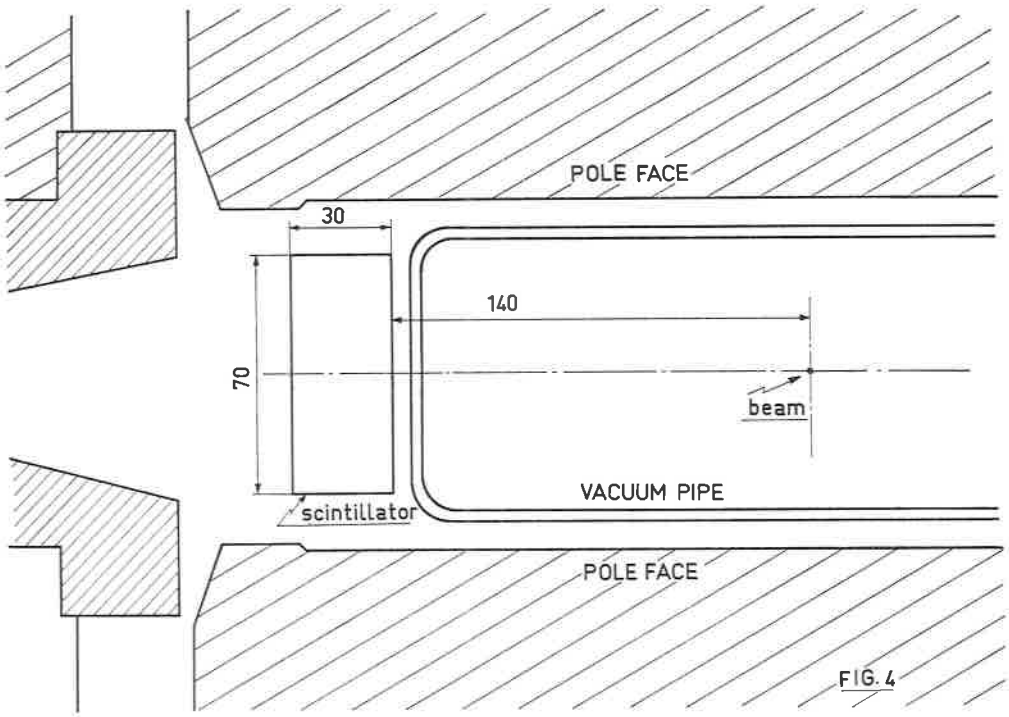

for about one month. No significant difficulty is foreseen. The scintillator can be ready mid-March, and the test with the electron beam will be finished before the end of March.

Sincere thanks are to Dr. M. Greco for stimulating discussions. We are deeply indebted to the experimental and the machine groups of ADONE for useful discussions. Finally, we wish to thank Prof. M. Conversi for his encouragements.

REFERENCES

1) N. A. Romero, A. Jaccarini, P. Kessler and J. Parisi: Paris preprint (1970).
2) V. M. Budnev and I. F. Ginzburg: Novosibirsk report TF 55 (1955).
3) S. J. Brodsky, T. Kinoshita and H. Terazawa: *Phys. Rev. Lett.*, **25**, **14**, 992 (1970).
4) M. Greco: LNF 71/1.
5) Inefficiency of 0.5 due to the source spread is taken into account.
6) Assumed one half of the point-like cross-section.
7) J. T. Manassah and S. Matsuda: Princeton preprint (1971).
8) M. Roos *et al.*: *Phys. Lett.*, **33** B, 1 (1971).
9) C. Bernardini: Frascati preprint (1971).
10) We assume the beam intensity 50 mA (10^{11} particles circulating), lifetime of 3 h. The loss rate is $\sim 10^{11}/10^4$ s$\sim 10^7$ s. This corresponds to 1 particle lost per bunch per turn. Since our tagging system is looking about 10% of the whole circumference of ADONE, we expect 0.1 background for each bunch for each tagging system, that means 10% accidentals for each wide angle event. Requiring the coincidence for the two forward going $e^{\pm}$, the accidental rate is expected to be $0.1 \cdot 0.1 = 0.01$.

Hadron production through photon-photon collisions in electron-positron storage rings (*)

P. KESSLER
Collège de France

This talk concerns the continuation of the theoretical work our group has performed for more than two years on photon-photon collisions in electron-positron storage rings ([1]). This group is composed of N. Arteaga-Romero, A. Jaccarini, J. Parisi and myself.

From the start, we suggested that the following type of experiments should be performed. Reactions of the type $e^-e^+ \to e^-e^+A^-A^+$ (where $A = e, \mu, \pi, K, ...$) should be studied in fourfold coincidence experiments where the outgoing electron and positron would be detected at very small angles with respect to their incident directions, whereas the particles $A^\pm$ produced would be measured at large angles with respect to the beam axis (see Fig. 1*b*). We were then able to show that, under such conditions, practically only one Feynman diagram, *i.e.* diagram (*a*) of Fig. 1, contributes to the cross-section measured. Since there the two space-like photons exchanged are « almost real » (q^2, q'^2 very small), one then really measures the process $\gamma+\gamma \to A^-+A^+$.

We were also able to show that fairly high counting rates can in principle be achieved—in the cases: $A = e, \mu, \pi$—with electron-positron storage rings of the next generation (beam energy ~ 2 GeV, luminosity $\sim 10^{32}$ cm^{-2} s^{-1}). However, till now, we had not yet considered entirely realistic conditions, *i.e.* all cut-off parameters which should appear in an experiment.

Here we are considering five parameters on which the cross-section measured for any of these processes should depend:

i) the beam energy E_0;

ii) a maximal angle θ_{max} for both the scattered electron and positron; we thus take: $\theta, \theta' \leqslant \theta_{max}$ (see Fig. 1*b*);

(*) Invited paper

iii) a minimal angle $\psi_{\min}$ for both produced particles $A^{\pm}$, such that: $\psi_{\min} \leqslant \psi$, $\psi' \leqslant \pi - \psi_{\min}$ (see Fig. 1*b*); it is indeed well known to colliding-

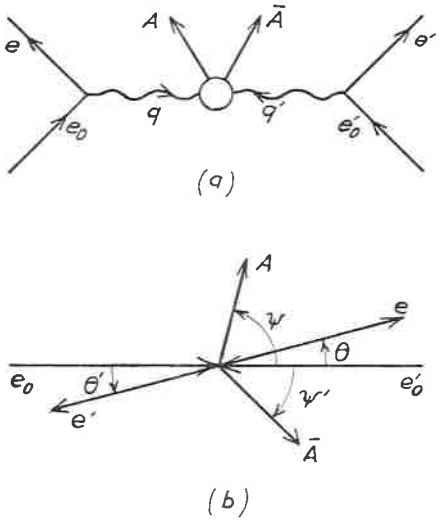

Fig. 1. – *a*) Main Feynman diagram for $e^-e^+ \to e^-e^+A\bar{A}$. *b*) Kinematic scheme for $e^-e^+ \to$ $\to e^-e^+A\bar{A}$ (for simplicity, azimuthal angles were left out).

beam specialists that the detection device for the particles produced cannot be set up too near to the beam axis);

iv) a minimal relative energy loss $\chi_{\min}$ for both the scattered electron and positron; we must have: $\chi, \chi' \geqslant \chi_{\min}$, where we define:

$$\chi = (E_0 - E)/E_0 , \qquad \chi' = (E_0 - E')/E_0 ,$$

calling E and E' the respective energies of the scattered electron and positron. The parameter $\chi_{\min}$ is to be introduced because, in order to separate itself from the beam and thus to be detectable, the (practically forward) scattered electron or positron must have lost some part of its energy;

v) a maximal relative energy loss $\chi_{\max}$ for both the electron and the positron, such that: $\chi, \chi' \leqslant \chi_{\max}$: Indeed, the $e^{\pm}$ particles scattered must have kept some appreciable part of their energy in order to be detected.

There may be additional cut-off parameters in an experiment, such as limitations on the azimuthal angles measured. But we considered them as unimportant.

Among the five parameters defined

$$E_0 \quad \theta_{\max} \quad \psi_{\min} \quad \chi_{\min} \quad \chi_{\max},$$

we shall show that only the first, the third and the fourth play a crucial role.

Figure 2 shows the behaviour of the integrated cross-section as a func-

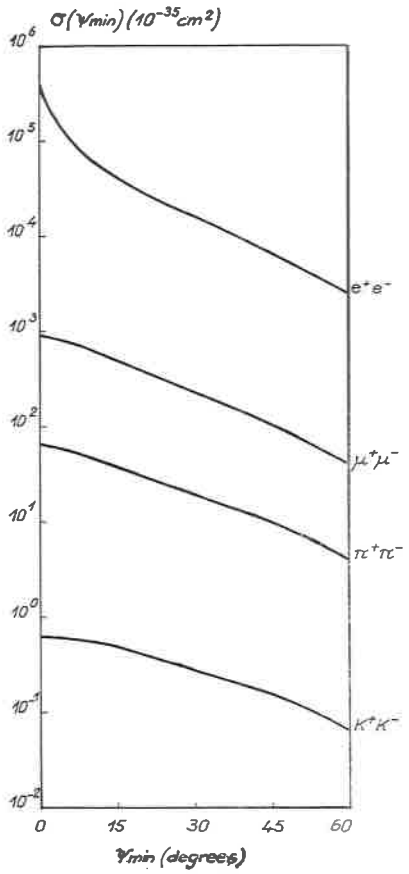

Fig. 2. – $\sigma(\psi_{\min})$ for electron pair production (with invariant mass $M>50$ MeV), muon, pion and kaon pair production. $E_0 = 2$ GeV, $\theta_{\max} = 4$ mr, $\chi_{\min} = 0$, $\chi_{\max} = 100\%$.

tion of $\psi_{\min}$, for A = e, μ, π, K (*), under following conditions: $E_0 = 2$ GeV, $\theta_{\max} = 4$ mr, no cut-off on χ and χ'.

Figure 3 shows the variation of the integrated cross-section with $\chi_{\min}$, under following conditions: $E_0 = 2$ GeV, $\theta_{\max} = 4$ mr, no cut-off on ψ and ψ', $\chi_{\max} = 100\%$.

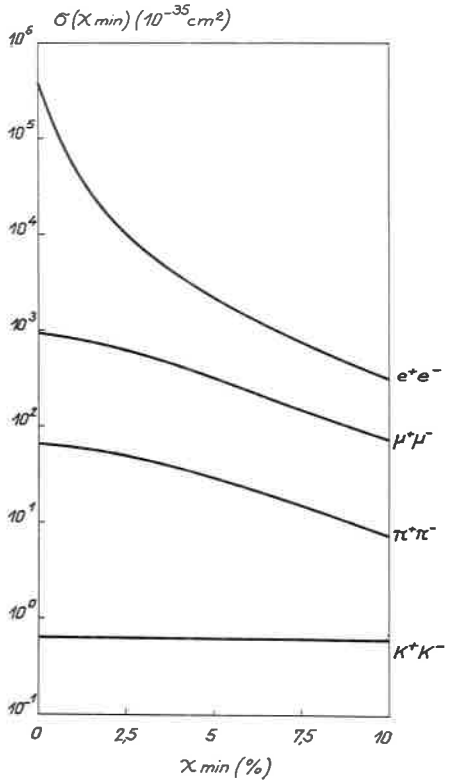

Fig. 3. – $\sigma(\chi_{\min})$ for electron pair production ($M > 50$ MeV.), muon, pion and kaon pair production. $E_0 = 2$ GeV, $\theta_{\max} = 4$ mr, $\psi_{\min} = 0$, $\chi_{\max} = 100\%$.

One can see from Figs. 2 and 3 how critical both parameters $\psi_{\min}$ and $\chi_{\min}$ are, especially for produced particles of low mass. That such a mass effect appears for both of them is easily explainable: particles with lower

(*) In all our calculations for the case A = e, a minimal invariant mass of 50 MeV was introduced for the pair e^-e^+ produced.

Lepton pair production—although less interesting in itself than hadron pair production—was included in all our calculations, because it may serve for calibration experiments.

mass are more forward-backward peaked, and thus more affected by the cut-off $\psi_{\min}$, on the other hand, they have a lower threshold for pair production and are thus more affected by $\chi_{\min}$ (because of the relation: $M_{\min} = 2\chi_{\min}E_0$, M being the invariant mass of the pair produced).

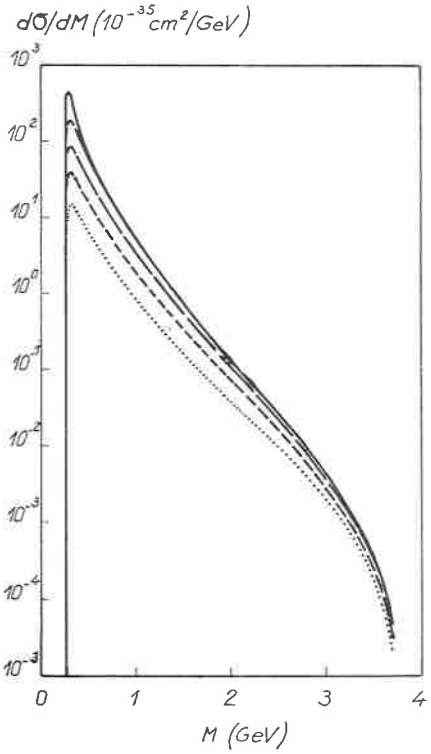

Fig. 4. – Effect of $\psi_{\min}$ on the invariant mass distribution $d\sigma/dM$ in pion pair production; $E_0 = 2$ GeV, $\theta_{\max} = 4$ mr, $\chi_{\min} = 0$, $\chi_{\max} = 100\%$. ——— $\psi_{\min} = 0$; ——– $\psi_{\min} = 15°$. — — — $\psi_{\min} = 30°$; – – – $\psi_{\min} = 45°$; · · · $\psi_{\min} = 60°$.

It is quite interesting to see how the cut-offs $\psi_{\min}$ and $\chi_{\min}$ operate on the invariant mass spectrum of the pair produced. This is shown in Figs. 4 and 5 for the case $A = \pi$. One notices that $\psi_{\min}$ is effective at any value of M, though somewhat more at the lower values; as for $\chi_{\min}$, it is mainly effective in the threshold region.

Figure 6 shows the behaviour of the integrated cross-section as a function of $\theta_{\max}$ (for $E_0 = 2$ GeV, $\psi_{\min} = 45°$, $\chi_{\min} = 5\%$, $\chi_{\max} = 70\%$). It can

be seen that, after a few milliradians, each curve tends rapidly towards a plateau.

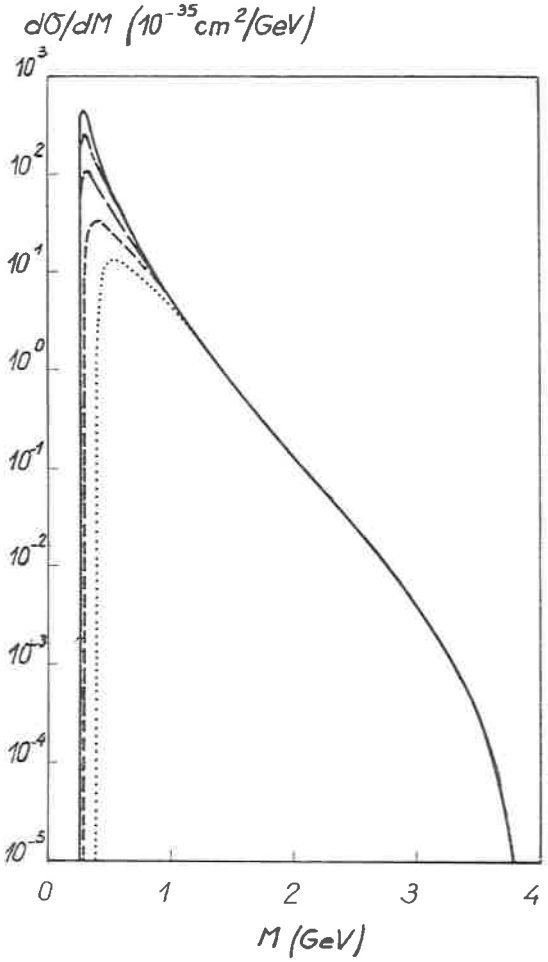

Fig. 5. – Effect of χ_{min} on the invariant mass distribution $d\sigma/dM$ in pion pair production. $E_0 = 2$ GeV, $\theta_{max} = 4$ mr, $\psi_{min} = 0$, $\chi_{max} = 100\%$. ——— $\chi_{min} = 0$; —— – $\chi_{min} = 2.5\%$; — — — $\chi_{min} = 5\%$; – – – $\chi_{min} = 7.5\%$; · · · $\chi_{min} = 10\%$.

Figure 7 shows the variation of the integrated cross-section with χ_{max} (for $E_0 = 2$ GeV, $\theta_{max} = 4$ mr, $\psi_{min} = 45°$, $\chi_{min} = 5\%$). One notices that for the lighter particles (A = e, μ, π) the curves shown tend to be flat already above $\chi_{max} \approx 20\%$.

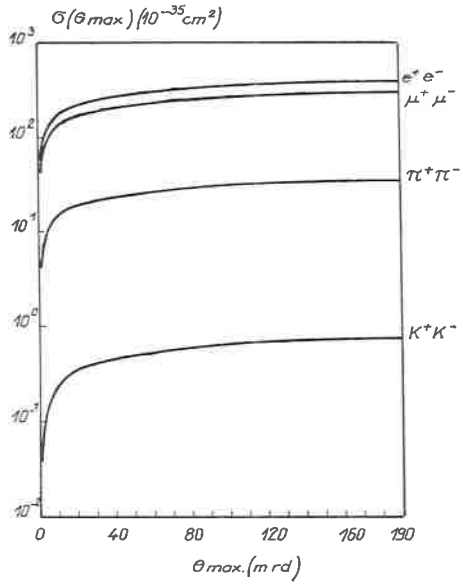

Fig. 6. – $\sigma(\theta_{max})$ for electron, muon, pion and kaon pair production. $E_0 = 2$ GeV, $\psi_{min} = 45°$, $\chi_{min} = 5\%$, $\chi_{max} = 70\%$.

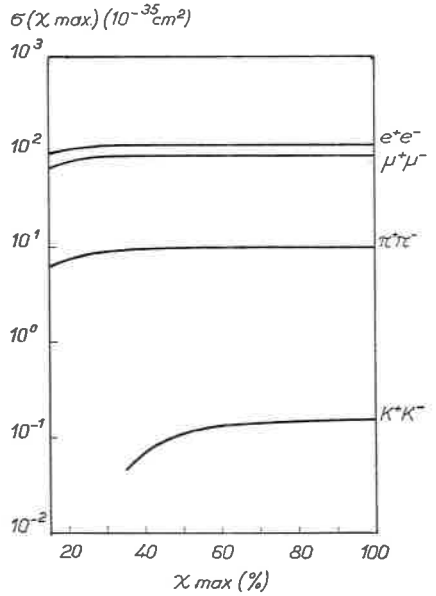

Fig. 7. – $\sigma(\chi_{max})$ for electron, muon, pion and kaon pair production. $E_0 = 2$ GeV, $\theta_{max} = 4$ mr, $\psi_{min} = 45°$, $\chi_{min} = 5\%$.

Obviously, the uncritical character of θ_{max} and χ_{max} is related to the fact that the primary electrons (positrons) tend to be scattered practically forward and with small energy loss.

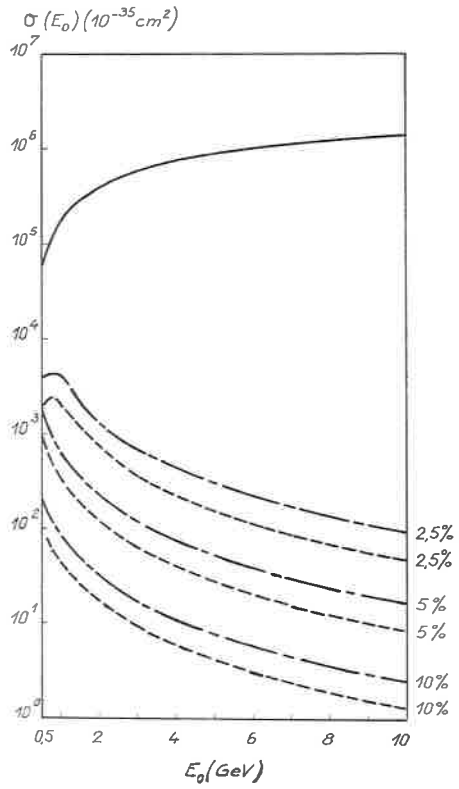

Fig. 8. – $\sigma(E_0)$ for electron pair production ($M > 50$ MeV). ——— $\theta_{max} = 4$ mr, no other cut-off. All other curves: $\theta_{max} = 4$ mr, $\chi_{max} = 70\%$, χ_{min} as indicated; ——— $\psi_{min} = 30°$; – – – $\psi_{min} = 45°$.

Let us now consider the energy behaviour of the integrated cross-sections with more or less realistic cut-offs. This behaviour is shown in Figs. 8, 9, 10, 11 for A = e, μ, π and K respectively. Here the values of θ_{max} and χ_{max} were fixed (at 4 mr and 70% respectively) and various values were taken for ψ_{min} (30°, 45°) and χ_{min} (2.5%, 5%, 10%). For reference, we also show the curve obtained with $\theta_{max} = 4$ mr and no other cut-off.

One notices that—except to some extent for the case A = K—the energy behaviour is quite strikingly modified by introducing the realistic cut-offs.

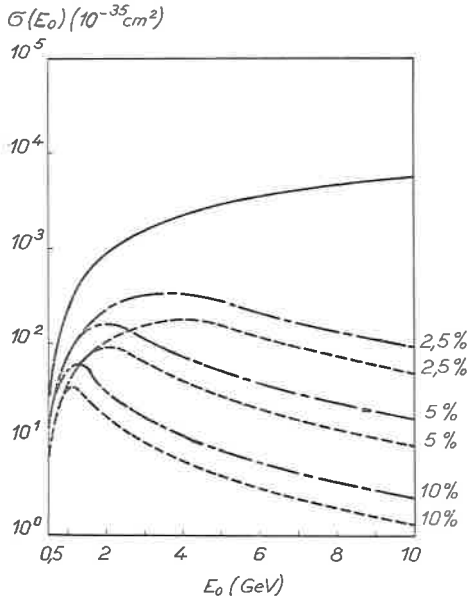

Fig. 9. – $\sigma(E_0)$ for muon pair production. All curves are characterized as in Fig. 8.

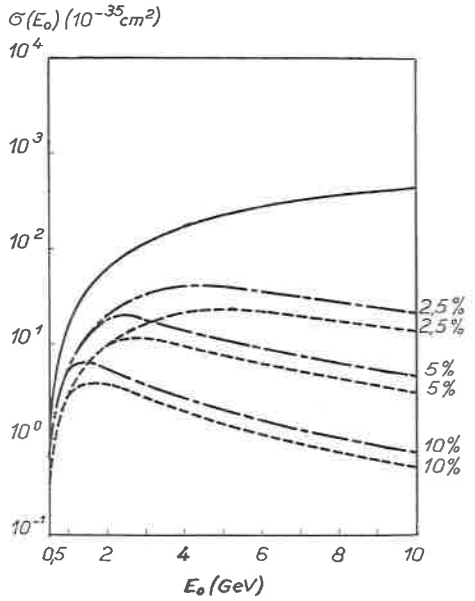

Fig. 10. – $\sigma(E_0)$ for pion pair production. All curves are characterized as in Fig. 8.

It can be easily understood—from the relation: $M_{min} = 2\chi_{min}E_0$—that it is essentially χ_{min} which becomes more and more effective at higher and higher beam energies. In the case of electron pair production, the energy behaviour is completely reversed with respect to the « unrealistic » curve shown for reference, and the combined effect of χ_{min} and ψ_{min} becomes really heart-breaking at high-energy. For muon and pion pair production, there appears

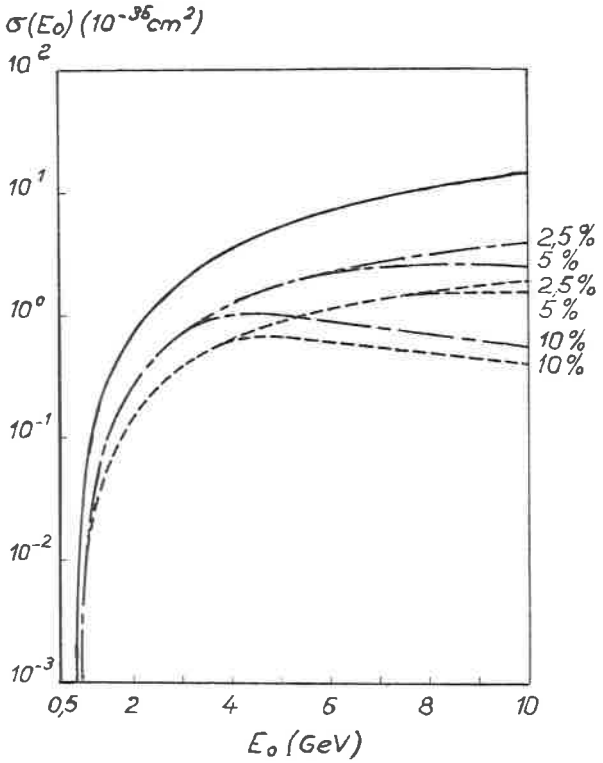

Fig. 11. – $\sigma(E_0)$ for kaon pair production. All curves are characterized as in Fig. 8.

to be an optimum in E_0; it is a fortunate circumstance that this optimum is essentially located in the region $E_0 \sim (2 \div 3)$ GeV, where the beam energy of storage rings of the next generation should lie.

In Table I, we show the cross-sections to be expected for $E_0 = 1$, 2 and 3 GeV, under following conditions: $\theta_{max} = 4$ mr, $\psi_{min} = 45°$, $\chi_{min} = 5\%$, $\chi_{max} = 70\%$ (*).

(*) These conditions were retained as the most realistic after discussion with Prof. Haissinski (Orsay). We also received some advice on that subject from Prof. Waloschek (DESY).

TABLE I. – $\sigma(E^0)$ *in* 10^{-35} cm^2.

	A = e	A = μ	A = π	A = K
$E_0 = 1$ GeV	343	38	3	0.01
$E_0 = 2$ GeV	119	91	10	0.15
$E_0 = 3$ GeV	63	63	11	0.4

It appears from these « realistic » figures that photon-photon collision experiments, producing electron, muon and pion pairs, should become possible with storage rings of the next generation. (We must of course assume that the Born approximation which we applied throughout does not lead to a gross overestimation for pion pair production; we think that most theorists will agree on this assumption, since mainly pion pairs with small invariant masses are to be produced).

We now consider another type of reactions which are also to be analysed as photon-photon collisions, namely

$$e^- + e^+ \to e^- + e^+ + X \quad (X \to 2\gamma),$$

where X is a pseudoscalar particle, *i.e.* π^0, η or η'. The two decay photons now play the role of A and $\overline{A}$ in Fig. 1. Figures 12, 13 and 14 show the

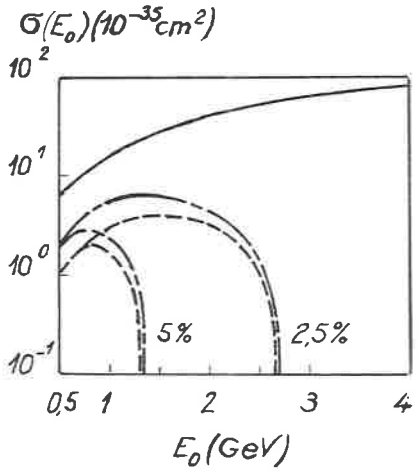

Fig. 12. – $\sigma(E_0)$ for the process $e^- + e^+ \to e^- + e^+ + \pi^0$. ——— $\theta_{max} = 4$ mr, no other cut-off. All other curves: same process, followed by decay into 2γ: $\theta_{max} = 4$ mr, $\chi_{max} = 70\%$, χ_{min} as indicated; ——— $\psi_{min} = 30°$; – – – $\psi_{min} = 45°$.

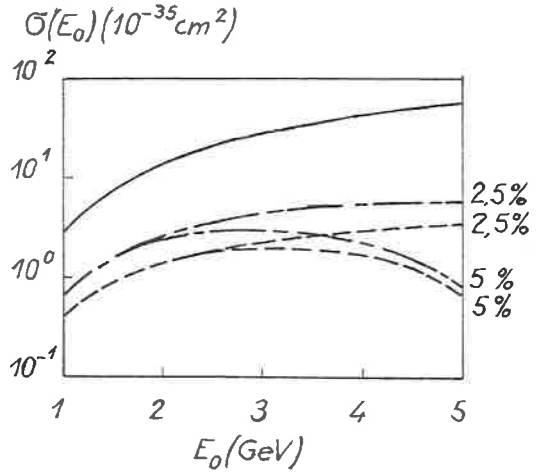

Fig. 13. – $\sigma(E_0)$ for the process $e^- + e^+ \to e^- + e^+ + \eta$. All curves are characterized as in Fig. 12.

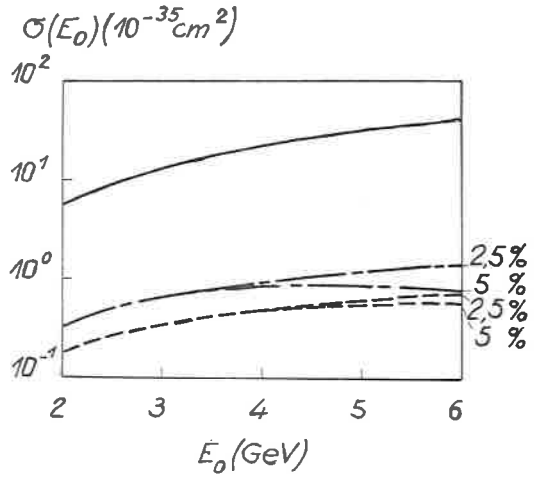

Fig. 14. – $\sigma(E_0)$ for the process $e^- + e^+ \to e^- + e^+ + \eta'$. All curves are characterized as in Fig. 12.

energy behaviour of the cross-section for production of π^0, η and η' respectively. Here again, more or less « realistic» curves ($\theta_{max} = 4$ mr; $\chi_{max} = 70\%$; $\chi_{min} = 2.5\%$ or 5%; $\psi_{mln} = 30°$ or $45°$) are compared with the « unrealistic » one (cross-section for $e^- + e^+ \to e^- + e^+ + X$, with $\theta_{max} = 4$ mr, no other cut-off). It is to be noticed, in particular, that, due to the low mass of π^0,

the cut-off χ_{min} acts in such a way that the type of experiment defined here can only be performed, as far as π^0 production is concerned, at relatively low beam energy.

Table II shows the cross-sections to be expected at: $E_0 = 1$, 2 and 3 GeV, and: $\theta_{max} = 4$ mr, $\psi_{min} = 45°$, $\chi_{min} = 5\%$, $\chi_{max} = 70\%$.

TABLE II. – $\sigma(E^0)$ *in* 10^{-35}- cm^2.

	$X = \pi^0$	$X = \eta$	$X = \eta'$
$E_0 = 1$ GeV	1.68	0.39	0.07
$E_0 = 2$ GeV	—	1.36	0.18
$E_0 = 3$ GeV	—	1.98	0.34

To obtain these figures, we used the following values for the decay rates; $\Gamma(X \to 2\gamma)$: 11 eV for π^0, 1 keV for η, 5 keV for η'; for the branching ratios $\Gamma(X \to 2\gamma)/\Gamma(X \to \text{total})$: 100% for π^0, 40% for η, 10% for η'.

The above Table shows that π^0 and η production can also probably be studied, through the type of fourfold coincidence experiments defined here, with e^-e^+ storage rings of the next generation. For η', the counting rates predicted seem a bit too low; however, it is possible that we underestimated the strength of the coupling of the $\eta'\gamma\gamma$ vertex (some theorists set it one or two orders of magnitude higher).

The last point I want to mention concerns the possible contamination of annihilation measurements by our processes (a point which recently received much attention in connection with the experiments at ADONE). We want to stress that, theoretically, this risk of contamination exists indeed, not only for the so-called noncoplanar events (interpreted as multi-hadron production), but also for the so-called colinear events (interpreted as two-hadron production). It is usually assumed that the 2-photon events studied by us are mostly coplanar but not colinear. However, we recently calculated the distribution of these events with respect to the « noncolinearity angle » (under the conditions of the experiments performed at ADONE), and we found that about 15% of them are actually colinear within 5°. How far these events might possibly have contaminated the annihilation measurements at ADONE (in the sense that low-energy leptons might have been mistaken for high-energy pions) is of course mainly an experimental question.

REFERENCES

1) N. Arteaga-Romero, A. Jaccarini and P. Kessler: *Compt. Rend.*, **269** B, 153, 1129 (1969); *Photon-photon collisions with electron-positron colliding beams*, Internal Report PAM 70-02 (April 1970). J. Parisi: *Etude du processus* $e^-e^+ \to e^-e^+(0^-)$, Thèse de troisième Cycle, Univ. of Paris (Febr. 1970). A. Jaccarini: *Etude des processus* $e^-e^+ \to e^-e^+\pi^-\pi^+$ *et* $e^-e^+K^-K^+$, Thèse de troisième Cycle, Univ. of Paris (July 1970). A. Jaccarini, N. Arteaga-Romero, J. Parisi and P. Kessler: *Lett. Nuovo Cimento*, **4**, 933 (1970). N. Arteaga-Romero, A. Jaccarini, P. Kessler and J. Parisi: *Phys. Rev.* D **3** 1569 (1971), J. Parisi, N. Arteaga-Romero, A. Jaccarini and P. Kessler: *Lett. Nuovo Cimento*, **1**, 935 (1971).

The work of some other authors on the same subject should also be mentioned:

F. Low: *Phys. Rev.*, **120**, 582 (1960).

F. Calogero and C. Zemach: *Phys. Rev.*, **120**, 1860 (1960).

J. C. Le Guillou: *Compt. Rend.*, **261**, 326 (1965).

P. C. De Celles and J. E. Goehl jr.: *Phys. Rev.*, **184**, 1617 (1969).

V. E. Balakin, V. M. Budnev and I. F. Ginsburg: *JETP Lett.*, **11**, 388 (1970).

V. G. Serbo: *JETP Lett.*, **12**, 39 (1970).

S. J. Brodsky, T. Kinoshita and H. Terazawa: *Phys. Rev. Lett.*, **25**, 972 (1970).

M. Greco: *Multiple electromagnetic processes in high-energy* e^-e^+ *collisions*, Internal Report LNF 71/1 (Jan. 1971).

SESSION III - B

Friday, 16 April 1971

Electromagnetic production of vector mesons using hadronic targets

Chairman: G. SALVINI

Secretaries: P. L. FRABETTI
P. GENSINI

Electromagnetic production of vector mesons on nucleons

D. SCHMITZ
Physikalisches Institut der Universität, - Bonn

In this talk I report on the present status of photoproduction of vector mesons on nucleons. I restrict myself mainly to the high energy region above *s*-channel resonances.

As on overall property of photon induced processes one observes a large similarity between photoproduction of hadrons and hadronic reactions in three respects:

i) The energy dependence of photoreactions is the same as for hadronic reactions showing resonance structure at low energies and simple *s*-dependence at high energies.

ii) Photoproduction of pseudoscalar mesons exhibits a striking similarity with inelastic hadronic reactions, both in *s* and *t*-dependence.

iii) Photoproduction of vector mesons is mainly diffractive, being closely related to the elastic hadron scattering.

In Fig. 1 and 2 examples for i) and ii) are given. Figure 1 shows a comparison of the photon absorption cross-section onprotons and the total π^0p cross-section. The photon data are taken from experiments of two completely different types, namely:

1) From e^-p [1] and μ^+p [2] inelastic scattering with an extrapolation to $q^2 = 0$;
2) From absorption measurements of real photons [3,4,5].

Not included are bubble chamber results, which in general agree with the data given. Considering the completely different methods applied the agreement between the data is remarkable.

(*) Introductory talk

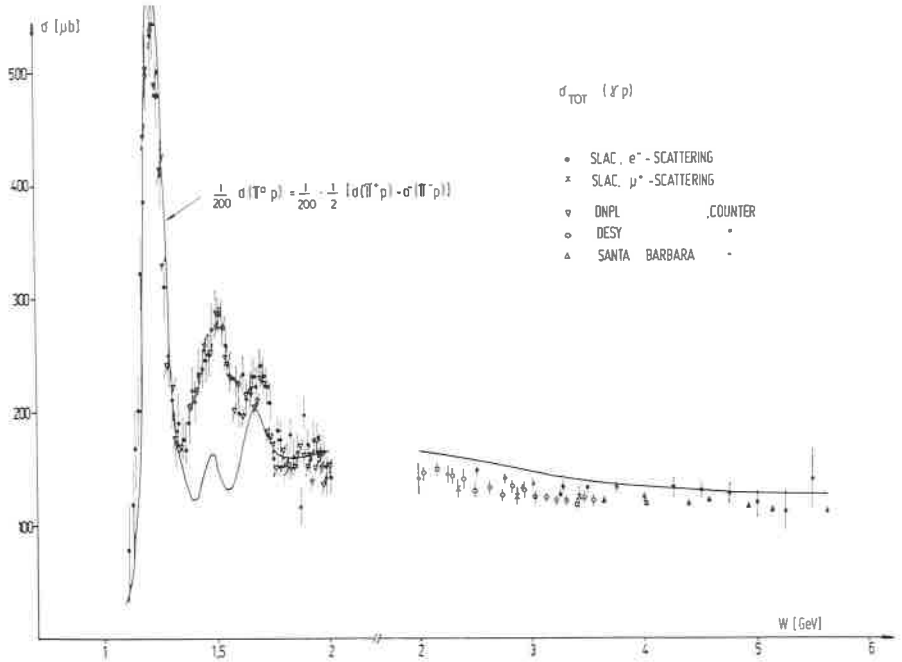

Fig. 1. – Total photon absorption cross-section as a function of c.m. energy. Data are taken from ref. ([1,2,3,4,5]). Solid line: total π^0p cross-section.

The total π^0p cross-section ([6]) scaled by a factor 1/200 is shown by the solid line. Both cross-sections show a pronounced resonance structure below $W = 2$ GeV and a smooth nearly s-independent energy behaviour in the high energy region. In particular the s-dependence at high energies is the same for both processes. This suggests a parametrization for the total photon absorption cross-section in terms of a simple Reggepole-model:

$$\sigma_{\gamma N}(k) = \sum_i c_i k^{\alpha_i(0)-1} \tag{1}$$

where k is the photon energy

$$k = \frac{s - M^2}{2M} = \frac{W^2 - M^2}{2M} . \tag{2}$$

The $\alpha_i(0)$ at $t = 0$ are the intercepts of the contributing trajectories. The leading trajectories with charge conjugation $\eta_c = +1$ and isospin 0 or 1 are the Pomeron $(\alpha_p(0) = 1)$ and the f and A_2 mesons $(\alpha_f(0) \sim \alpha_{A_2}(0) \sim 0.5)$.

A fit ([7]) to the total γ-proton and γ-neutron absorption cross-sections using the simple form

$$\sigma_{\gamma N} = \sigma_{0,N} + a_N k^{-\frac{1}{2}} \tag{3}$$

give the results:

$$\sigma_{\gamma p} = (98.1 \pm 2.6) + (65.2 \pm 6.6) k^{-\frac{1}{2}}\ \mu b \tag{4}$$

$$\sigma_{\gamma n} = (95.6 \pm 5.7) + (48.3 \pm 15.4) k^{-\frac{1}{2}}\ \mu b \tag{5}$$

$$\Delta = \sigma_{\gamma p} - \sigma_{\gamma n} =$$

$$= (2.5 \pm 6.3) + (16.9 \pm 16.8) k^{-\frac{1}{2}}\ \mu b . \tag{6}$$

In the high energy limit the cross-section is finite and in the order of 100 μb. The difference between neutron and proton data may indicate a non negligible $I = 1$ exchange with the A_2 as candidate. Indications for such a contribution are also found at incoherent ρ-production on deuterium ([8]).

Figure 2 shows for π^0 and η production a comparison between photon reactions $\gamma p \to \pi^0 p$ and $\gamma p \to \eta p$ ([9,10,11,12]) and charge exchange $\pi^- p$ scattering $\pi^- p \to \pi^0 n$ and $\pi^- p \to \eta n$ ([13,14]). The similarity between the corresponding reactions is striking. The π^0 production shows a characteristic dip at $t \sim -0.5\ \mathrm{GeV}^2$ which is definitely not seen in η production. The smooth fall off at higher t values with a slope of approximately $\exp[3t]$ is common to all pseudoscalar photo-production processes. In the various processes only in the small t-region bumps or spikes are seen, which can easily be related to contribution of π, ω or ρ t-channel exchange. In particular in π^0 production the maximum at $t = -0.1\ \mathrm{GeV}^2$ and the dip at $t = -0.5\ \mathrm{GeV}^2$ can be explained by reggeized ρ or ω-exchange. The dip can be reproduced either by a zero of the Reggepole-amplitude at the wrong signature point or by a destructive interference of the pole contribution without wrong signature zeros and a smooth cut contribution. The sharp increase of the cross-section in the very forward direction for the $\gamma p \to \pi^0 p$ and $\gamma p \to \eta p$ processes is due to the Primakoff effect.

I turn now to the photoproduction of vector mesons. The diffractive character of these processes is explained very naturally in the vector dominance model (VDM). In the VDM the hadronic part of the electromagnetic

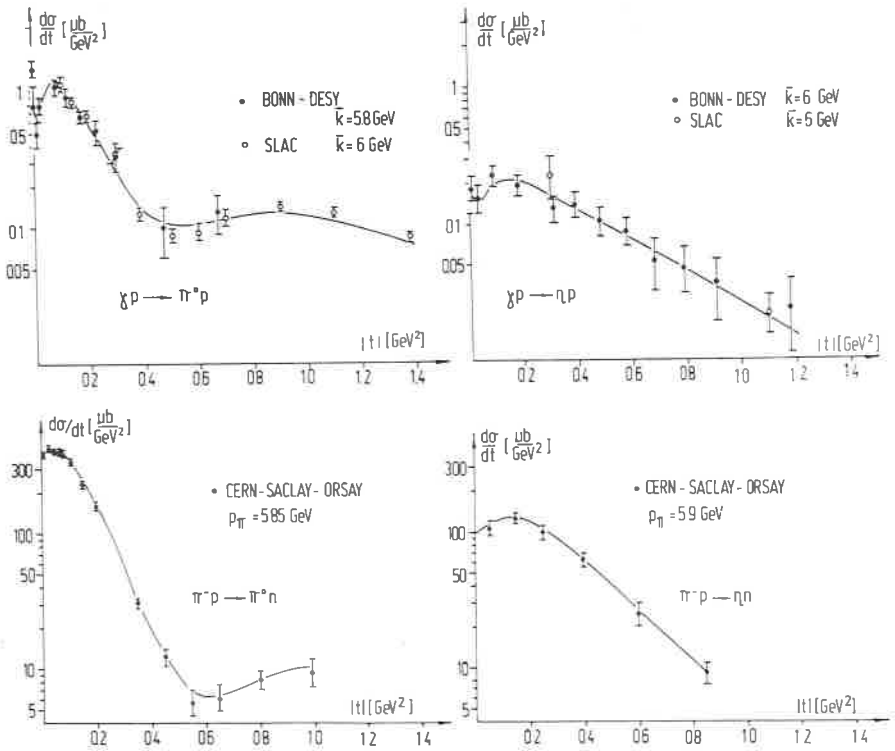

Fig. 2. – Comparison of the photoproduction cross-sections $\gamma p \to \pi^0 p$ [9,11] and $\gamma p \to \eta p$ [9,11,12] with the charge exchange reactions $\pi^- p \to \pi^0 n$ [13] and $\pi^- p \to \eta n$ [14].

current is connected with the fields of vector mesons, which have the same quantum numbers as the photon ($J^p = 1^-$, $\eta_c = +1$, $I = 0, 1$) by:

$$j_\mu^{(x)} = -\left[\frac{m_\varrho^2}{2\gamma_\varrho}\varrho_\mu^{(x)} + \frac{m_\omega^2}{2\gamma_\omega}\omega_\mu^{(x)} + \frac{m_\varphi^2}{2\gamma_\varphi}\varphi_\mu^{(x)}\right].$$

$$= -\sum_v \frac{m_v^2}{2\gamma_v} v_\mu^{(x)}.$$

The γ_v are the photon-vector meson coupling constants.

Assuming that the amplitudes change very little by extrapolating from $m = 0$ to the real vector meson mass and neglecting interference terms one obtains from this the well known relation:

$$\sigma(\gamma p \to x) = \frac{\alpha}{4}\sum_v \frac{1}{\gamma_v^2/4\pi}\sigma(vp \to x) \qquad (8)$$

which relates photoproduction to the same vector meson induced process.

In particular, vector meson-photoproduction is linked to the scattering of vector mesons

$$\frac{d\sigma}{dt}(\gamma p \to vp) = \frac{\alpha}{4}\sum_{v'}\frac{1}{\gamma_{v'}^2/4\pi}\frac{d\sigma}{dt}(v'p \to vp) \tag{9}$$

$$\sim \frac{\alpha}{4}\frac{1}{\gamma_v^2/4\pi}\frac{d\sigma}{dt}(vp \to vp).$$

In the quark model the vector meson scattering cross-sections are given by the $\pi\mathcal{N}$ and $K\mathcal{N}$ elastic scattering:

$$\frac{d\sigma}{dt}(\rho p) = \frac{d\sigma}{dt}(\omega p) = \frac{d\sigma}{dt}(\pi_0 p) = \frac{1}{2}\left[\frac{d\sigma}{dt}(\pi^+ p) + \frac{d\sigma}{dt}(\pi^- p)\right] \tag{10}$$

$$\frac{d\sigma}{dt}(\varphi p) = \frac{d\sigma}{dt}(K^+ p) + \frac{d\sigma}{dt}(K^- p) - \frac{d\sigma}{dt}(\pi^+ p). \tag{11}$$

Figures 3 and 4 show the differential cross-section for ρ and φ production derived from the SLAC missing mass experiment ([9]). The $\gamma p \to \rho p$ cross-section is almost constant with energy and falls off exponentially with t the slope being approximately exp [7t]. The solid lines give the s and t dependence of the combined VDM and quark model predictions in complete agreement with the data. From the energy independent normalization constant fitted to the experimental points the authors derive a ρ-photon coupling constant of

$$\frac{\gamma_\rho^2}{4\pi} = 0.61 \tag{12}$$

in reasonable agreement with the storage ring value of

$$\frac{\gamma_\rho^2}{4\pi} = 0.52 \pm 0.02\,. \text{ ([15])} \tag{13}$$

The differential cross-section of the φ photoproduction is seen in Fig. 4. At the energy of 6 GeV data from DESY bubble chamber are included. The agreement between the two data sets is good. The agreement with the VDM-quark model predictions given by the solid line is good in respect to the t-dependence but there is an indication that the s-dependence is somewhat stronger in φ-production.

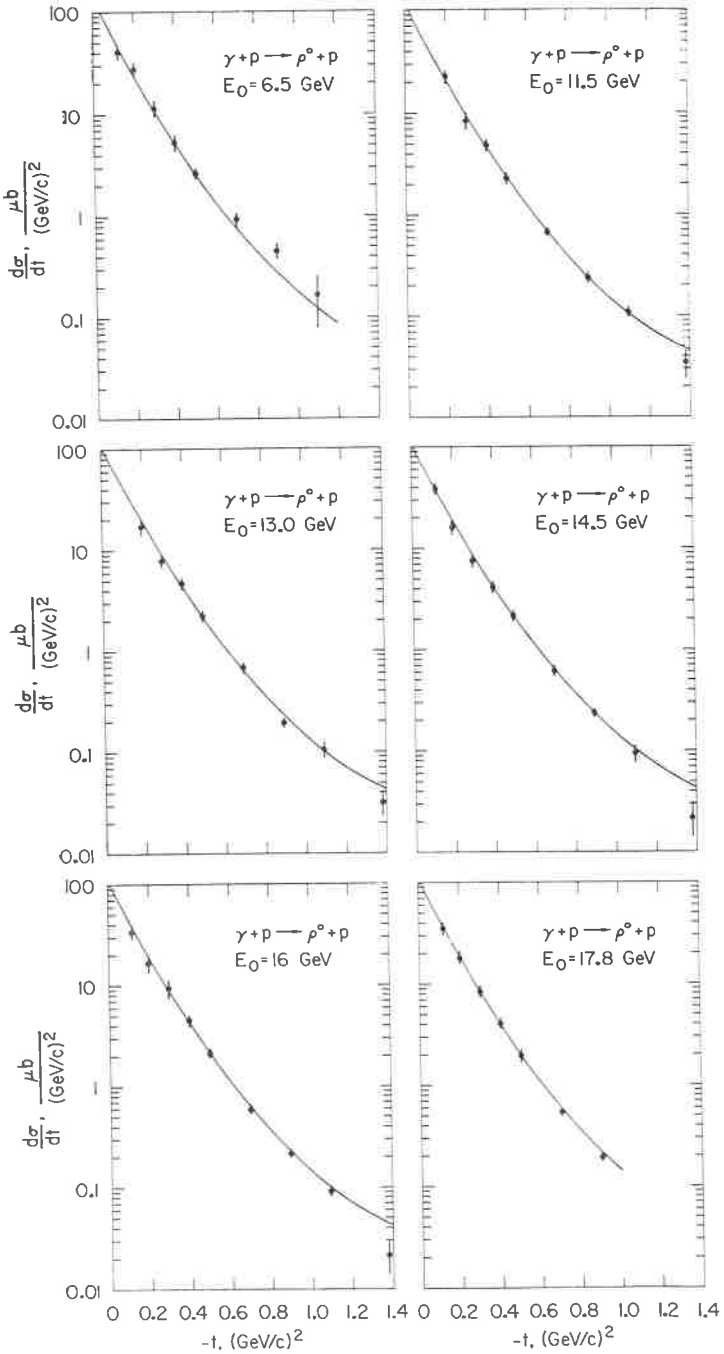

Fig. 3. – Differential cross-section of $\gamma p \to \rho^0 p$ [9]. Solid lines: combined VDM and quark model predictions, see text. Figure taken from ref. [9].

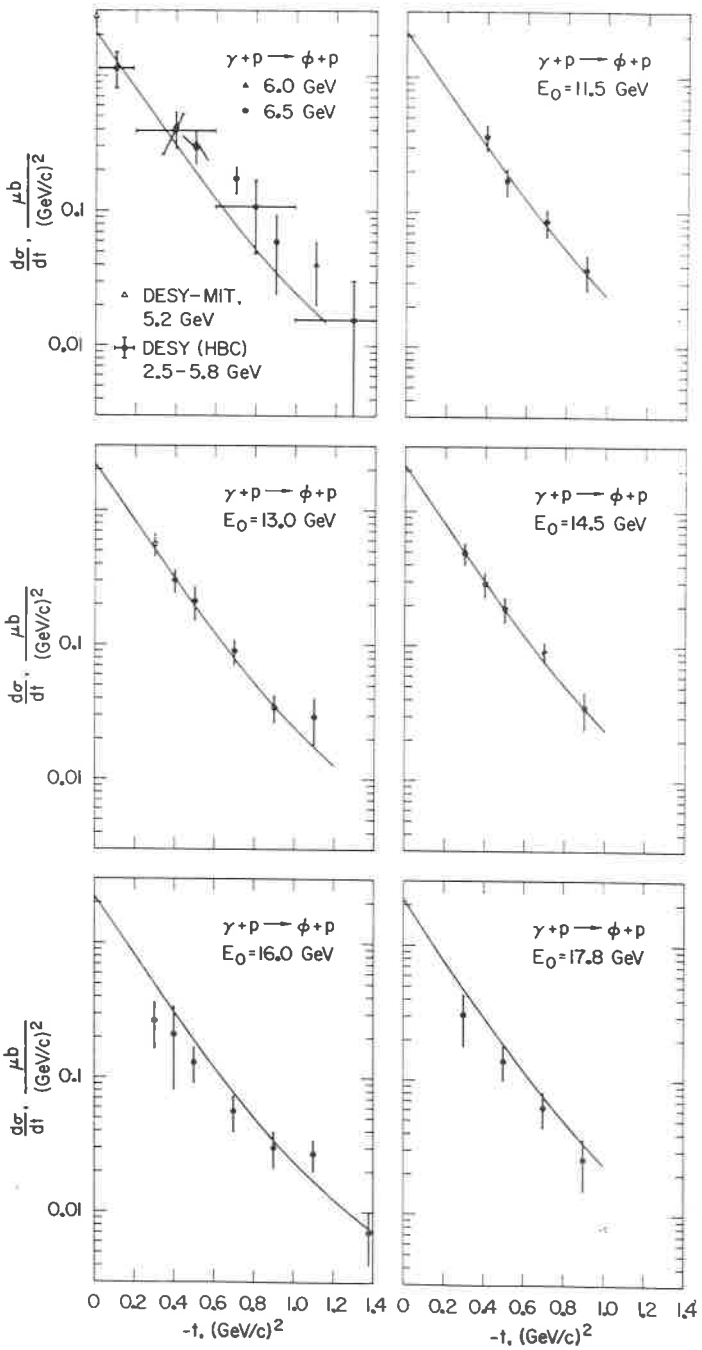

Fig. 4. – Differential cross-section of $\gamma p \to \varphi p$ [9-19]. Solid line: Combined VDM and quark model prediction. Figure taken from ref. [9].

For ρ production the production mechanism has been investigated in much more detail studying the decay angular distribution of ρ-mesons produced by linearly polarized photons. Such experiments have been done at DESY ([16]) and Cornell ([17]) using a polarized photon beam produced on a diamond

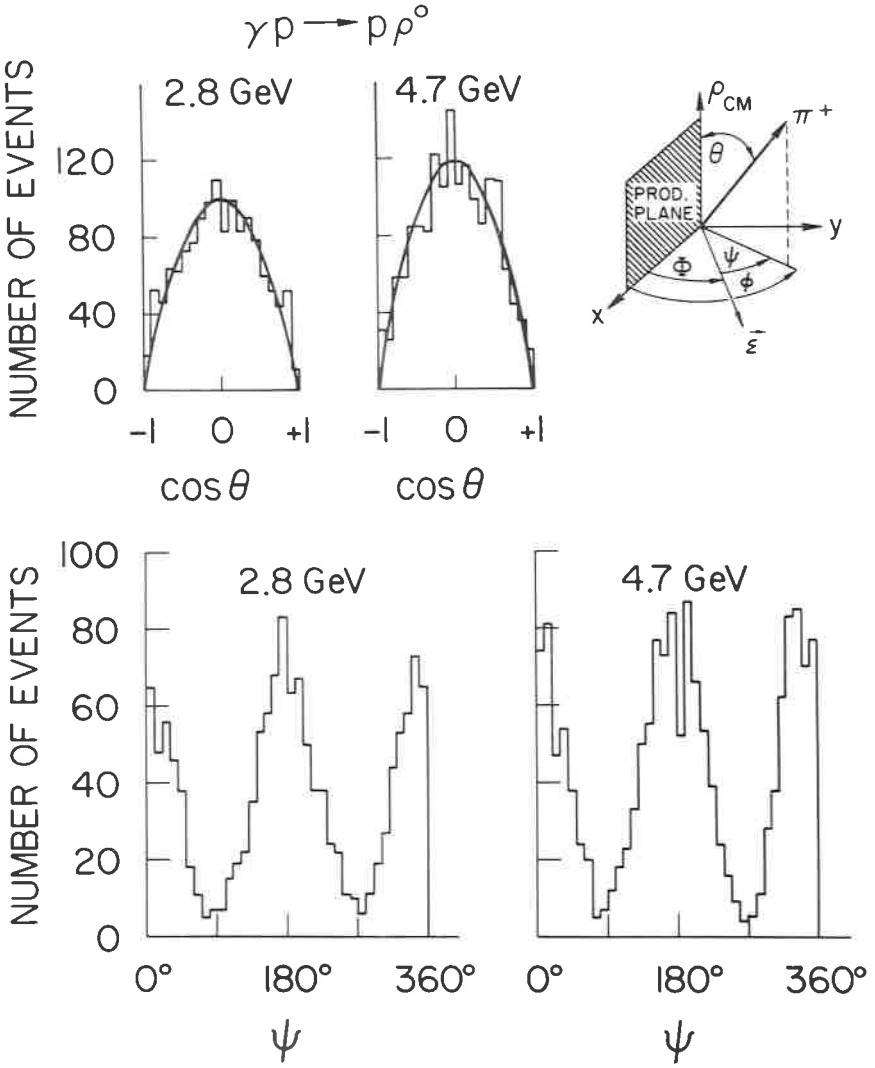

Fig. 5. – Reaction $\gamma p \to \rho^0 p$ ([18]). ρ^0 decay angular distributions in the helicity system for $|t| < 0.4\ \mathrm{GeV}^2$ and $0.6 < M_{\pi^+\pi^-} < 0.85\ \mathrm{GeV}$ without background subtraction The curves for the $\cos\vartheta$ distributions are proportional to $\sin^2\vartheta$. Figure taken from ref. ([22])

crystal. At SLAC ([18]) the photon beam is obtained by back scattering ruby laser light from the 20 GeV electron beam. By collimating both the electron and the backscattered photon beam to less than 10^{-5} radians the photon spectrum is nearly monoenergetic with a width of approximately 3% at 2.8 and 4.7 GeV. Furthermore the high energetic photons maintain the polarization of the incident visible light, resulting in 94% respectively 92% linear polarization for the two energies mentioned. The π's of the ρ decay and the recoil proton were detected in the 82″ SLAC bubble chamber, thus the total angular decay distribution could be measured. Fig. 5 shows the result. The frame of reference is the helicity system θ and φ being the polar and azimuthal angle of the π^+ in the ρ^0 rest frame, ψ is in the forward direction the angle between the electric polarization-vector $\boldsymbol{\varepsilon}$ of the photon and the ρ^0 decay plane.

The plots given for both energies show the θ and ψ distribution of events in the ρ mass region and for $|t| < 0.4$ GeV^2. The θ distribution are proportional to $\sin^2\theta$ which implies that the ρ mesons are produced with helicity ± 1 and since the incoming photons have the identic helicity one concludes that for ρ production helicity is conserved in the s-channel.

The ψ distributions are proportional to $\cos^2\psi$, showing that the ρ^0 is almost completely linearly polarized as the photon. Following the theorem of Stichel this tells us that ρ production is dominated by natural parity exchange in the t-channel. The contribution of unnatural parity exchange found is in the order of few percent.

Although the dynamics of ρ-production is understood it is not clear yet how to describe correctly the ρ mass shape and the non resonant $\pi^+\pi^-$ background in the ρ mass region. These difficulties not being discussed here reflect in an up to 30% uncertainty in the determination of ρ cross-section. This can be seen in Fig. 6 which gives the total cross-section for ρ, ω and φ photoproduction above 2 GeV.

Only some of the available ρ^0 data are included in the plot. They are selected in order to show

i) That the cross-section derived from the same measurements strongly depend on the mass formula used in the analysis.
ii) That the ρ cross-section stays nearly constant with energy being in the order of 13 μb at high energies.

Different from ρ-production the total ω cross-section drops off very quickly with energy between 2 and 5 GeV, although the t dependence of the ω cross-

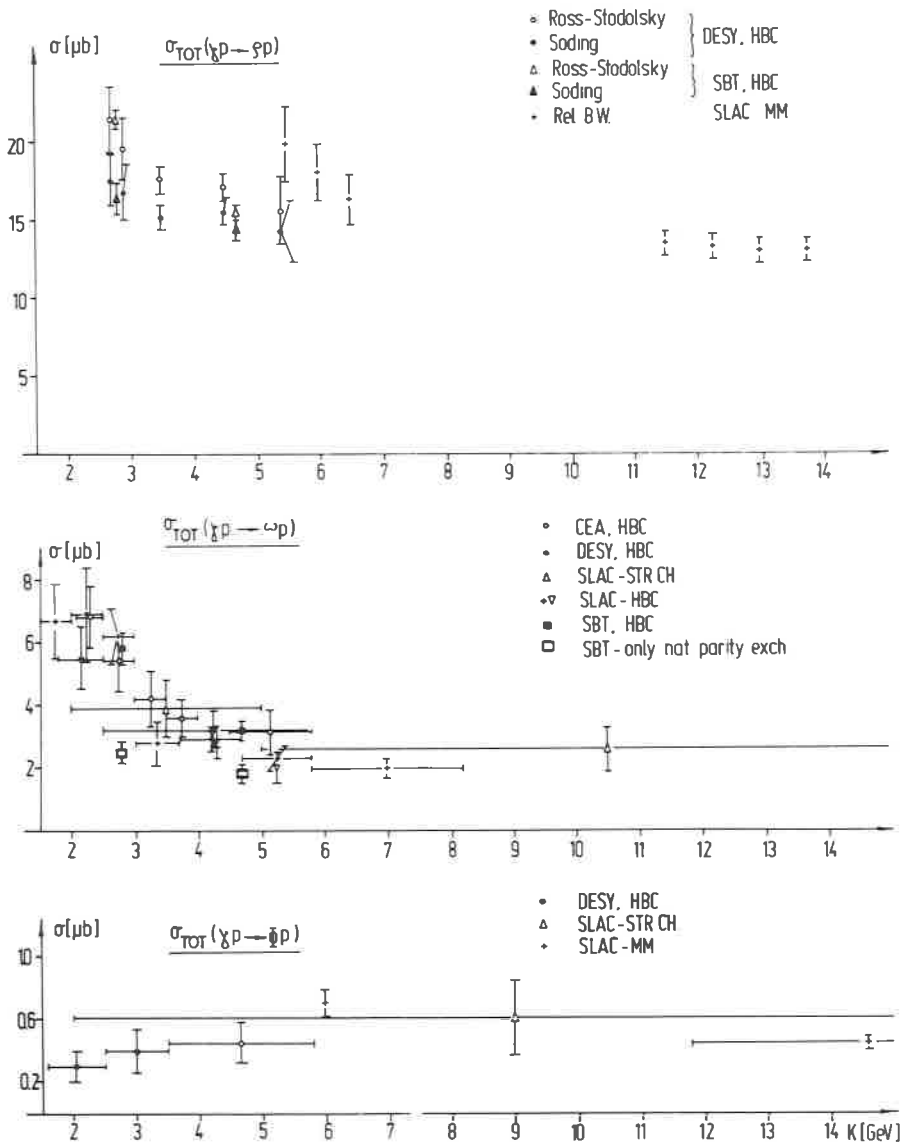

Fig. 6. – Total cross-sections for the reactions $\gamma p \to \rho^0 p$ [9,18,19], $\gamma p \to \omega p$ [18,19,25,26,27,28] and $\gamma p \to \varphi p$ [9,19,25].

section is close to that found in ρ production. The most likely explanation of the energy dependence of σ_ω is that two production mechanism contribute,

namely one pion exchange (OPE) and diffractive production. The first dominates the low energy region and the second takes over at higher energies. This is supported by the SBT experiment performed with linearly polarized photons. This way they could separate the contribution from unnatural and natural parity exchange corresponding to π and Pomeron exchange. In the plot are shown the contributions of the natural parity exchange at 2.8 and 4.7 GeV. This part does not show a significant energy dependence, whereas the total cross-section decreases by a factor two in this energy interval. The cross-section at high energies should be mainly diffractive and is in the order of 2 μb.

The data on φ total photoproduction cross-section are rather scarce. The cross-section is possibly energy independent and of the order of 0.5 μb.

The ratio of the cross-sections for the photoproduction of the three different vector-mesons is normally compared by using the forward differential cross-sections. Using VDM and the optical theorem one gets:

$$\frac{d\sigma}{dt}(\gamma p \to vp)_{t=0} = \frac{\alpha}{64\pi}\frac{1}{\gamma_v^2/4\pi}\sigma_{vp}^2(1+\beta_v) \tag{14}$$

$$\sim \frac{\alpha}{64\pi}\frac{1}{\gamma_v^2/4\pi}\sigma_{vp}^2$$

where β_v the ratio of the real to imaginary part of the forward scattering amplitude is approximately 0.2. From (14) one gets at $t=0$:

$$\frac{d\sigma^\varrho}{dt}:\frac{d\sigma^\omega}{dt}:\frac{d\sigma^\varphi}{dt} = \frac{\sigma_{\varrho p}^2}{\gamma_\varrho^2}:\frac{\sigma_{\omega p}^2}{\gamma_\omega^2}:\frac{\sigma_{\varphi p}^2}{\gamma_\varphi^2}. \tag{15}$$

Using as inputs the quark model predictions for the vector meson total cross-section

$$\sigma_{\varrho p} = \sigma_{\omega p} = \tfrac{1}{2}(\sigma_{\pi^+ p} + \sigma_{\pi^- p}) \qquad \sim 28 \text{ mb at } 5 \text{ GeV } ([20]) \tag{16}$$

$$\sigma_{\varphi p} = \sigma_{K^+ p} + \sigma_{K^- p} - \sigma_{\pi^+ p} \qquad \sim 13 \text{ mb at } 5 \text{ GeV } ([21]) \tag{17}$$

and for the coupling constants the ratio determined by storage ring

$$\frac{1}{\gamma_\varrho^2}:\frac{1}{\gamma_\omega^2}:\frac{1}{\gamma_\varphi^2} = 9:1.28:1.78\ ([15]) \tag{18}$$

one gets

$$\frac{d\sigma^{\varrho}}{dt}:\frac{d\sigma^{\omega}}{dt}:\frac{d\sigma^{\varphi}}{dt} = 9:1.28:0.37\,. \tag{19}$$

The vector meson photoproduction gives for this ratio either

$$9:1.2:0.25 \quad \text{or} \quad 9:1.7:0.34 \tag{20}$$

depending on the ϱ cross-section used. The data were taken from the SBT experiment at 4.7 GeV, where for $\frac{d\sigma^{\omega}}{dt}$ only the natural parity exchange contribution was used. For $\frac{d\sigma^{\varphi}}{dt}$ the value of 3 μb quoted by E. Lohrmann ([24]) was used.

The agreement between the combined VDM and quark model predictions with these data is reasonable supporting that the VDM gives a good qualitative understanding of photoproduction.

On the other hand the quantitative analysis of different processes as total cross-section, Compton scattering, charged π production and photoproduction on complex nuclei in the framework of VDM result in coupling constants $\gamma_{\varrho}^2/4\pi$ reaching from 0.3 to 0.8. Partially these differences are due to the mentioned difficulties in determining the ϱ cross-section.

Possible modifications of VDM have been proposed in two respects ([22]):

i) There exist a mass dependence either in the coupling constants or in the scattering amplitudes. Further informations to this point should come from electroproduction experiments, in which the photoproduction can be studied with space like photons of variable mass.
ii) There exist additional vector mesons which couple to the photon. But no such state has been observed yet. Although there are indications for a broad enhancement in the mass region from 1.3 to 2 GeV in 2π and 4π final states ([23]).

Acknowledgement.

I thank Prof. K. Lübelsmeyer for useful discussions.

REFERENCES

1) E. D. Bloom *et al.*: SLAC-PUB 653 (1969).
2) M. L. Perl *et al*: *Phys. Rev. Lett.*, **23**, 1191 (1969).
3) D. O. Caldwell *et al.*: *Phys. Rev. Lett.*, **25**, 609 (1970); W. P Hesse *et al.*: *Phys-Rev. Lett.*, **25**, 613 (1970).
4) H. Meyer *et al.*: *Phys. Lett.*, **33** B, 189 (1970).
5) T. A. Armstrong *et al.*: DNPL/P 62 (1971).
6) M. N. Focacci *et al.*: CERN Report 66-18.
7) B. Naroska: *Thesis* DESY F 1-70/3 (1970).
8) H. G. Hilpert *et al*: *Nucl. Phys.*, B **21**, 93 (1970).
9) R. L. Anderson *et al.*: *Phys. Rev. D*, **1**, 27 (1970).
10) M. Braunschweig *et al.*: *Nucl. Phys.*, B **20**, 191 (1970).
11) J. R. Johnson: SLAC-Report 124 (Sept. 1970).
12) W. Braunschweig *et al.*: *Phys. Lett.*, **33** B, 236 (1970).
13) P. Sonderegger *et al.*: *Phys. Lett.*, **20**, 75 (1966).
14) O. Guisan *et al.*: *Phys. Lett.*, **18**, 200 (1965).
15) J. E. Augustin *et al.*: *Phys. Lett.*, **28** B, 503 (1969).
16) L. Criegee *et al.*: *Phys. Rev. Lett.*, **25**, 1306 (1970).
17) G. Diambrini Palazzi *et al.*: *Phys. Rev. Lett.*, **25**, 478 (1970).
18) SLAC-Berkeley-Tufts Collaboration: *Phys. Rev. Lett.*, **24**, 955, 960 (1970).
19) Aachen - Berlin - Bonn - Hamburg - Heidelberg - München Collaboration: *Phys. Rev.*, **175**, 1669 (1968).
20) G. Giacomelli: CERN-Hera 69-3 (1969).
21) W. Gailbraith *et al.*: *Phys. Rev.*, B **138**, 913 (1965).
22) See *e.g.* G. Wolf: DESY 70/64 (1970).
23) See *e.g.* K. Lübelsmeyer: Kiev Conference 1970 and Bonn Rep. PIB 1-126.
24) E. Lohrmann: Lund Conference 1969 and DESY 69/21 (1969).
25) M. Davier *et al.*: *Phys. Rev. D*, **1**, 790 (1970).
26) J. Ballam *et al.*: *Phys. Lett.*, **30** B, 421 (1969).
27) Y. Eisenberg *et al.*: *Phys. Lett* , **34** B, 439 (1971).
28) CEA Bubble Chamber Group: *Phys. Rev.*, **155**, 1468 (1967).

Dipion photoproduction (*)

P. H. FRAMPTON
CERN - Geneva

1. General considerations.

1.*a*. – The subject of this talk (**) is the photoproduction of two pions in the process

$$\gamma + X \to \pi^+ + \pi^- + X\,, \tag{1.1}$$

where X is a proton or a complex nucleus. In particular the suppression of dipion production for high dipion mass, $m_{\pi\pi} = (1 \sim 2)$ GeV, will be discussed.

We shall use the symbol ϱ' to signify a p wave dipion system with mass $m_{\pi\pi} \simeq 1.5$ GeV, but this will not necessarily imply that the p wave is resonant there. The purpose will be to explain the experimentally observed small ratio for the Pomeron (P) couplings $g_{\gamma P\varrho'}/g_{\gamma P\varrho}$ in terms of a multiperipheral (Drell) production mechanism, and further to point out that this result has no implication for the ratio $g_{\gamma\varrho'}/g_{\gamma\varrho}$:

1.*b*. – The prediction of higher mass vector mesons is made both by the Veneziano model [1] and by the related models for the electromagnetic form factors [2,3]. The best measured electromagnetic form factor is the magnetic form factor $G_M^p(t)$ of the proton, for the range of momentum transfer $0 > t > -25$ GeV^2. This form factor is defined by writing the matrix element of the electromagnetic current operator between proton states

$$\sqrt{4k_0 k_0'}\,\langle p(k')|J_\mu(0)|p(k)\rangle = e\bar{u}(k')[F_1^p(t)\gamma_\mu + F_2^p(t)(\mu_p - 1)(2M)^{-1} i\,\sigma_{\mu\nu} q_\nu]u(k), \tag{1.2}$$

$$\mu_p\, G_M^p(t) = F_1(t) + (\mu_p - 1) F_2^p(t)\,, \tag{1.3}$$

(*) Invited paper

(**) The work described here was done in collaboration with K. Schilling and C. Schmid

with conventional notations (see ref. ([2])). We can take into account all vector states of the Veneziano model arising from the degenerate ϱ and ω parent trajectories $\alpha(t) = \frac{1}{2} + t$ by writing ([2])

$$G_M^p(t) = \frac{\Gamma(1-\alpha(t))\,\Gamma(r+1-\alpha(0))}{\Gamma(1-\alpha(0))\,\Gamma(r+1-\alpha(t))} \tag{1.4}$$

and then the best fit $r = 9/4$ gives a better one-parameter fit to the experimental data in the spacelike region than the dipole formula.

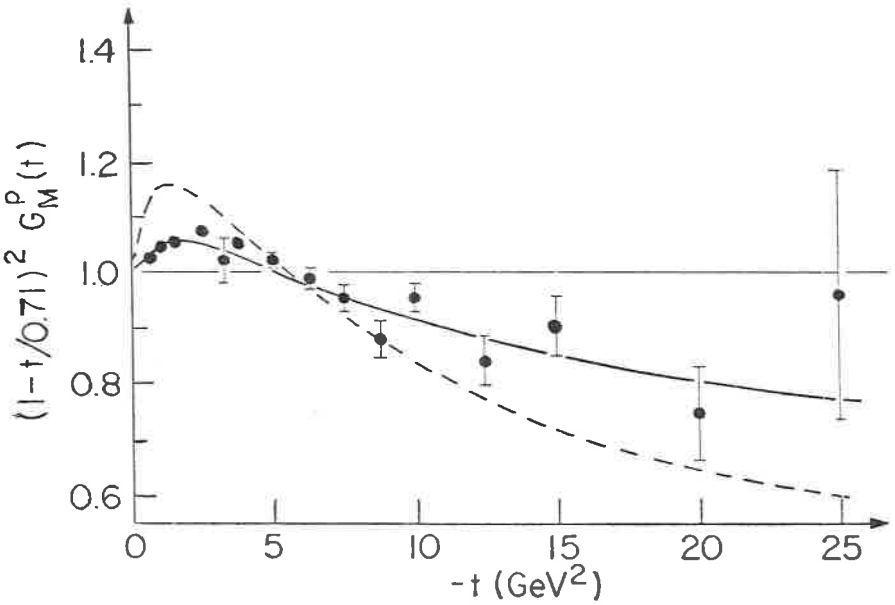

Fig. 1. – Comparison of formula (1.4) for $G_M^p(t)$ with the experimental data for $0 > t > -25$ GeV^2, and with the dipole fit $G_M^p(t) = (1 - t/(0.71\ \text{GeV}^2))^{-2}$ (solid line). The dashed curve is a fit of Di Vecchia and Drago (ref. ([3])) who take $\alpha(t) = \frac{1}{2} + 0.86t$ and $r = \frac{5}{2}$:

Expanding into poles gives (for $r = 9/4$)

$$G_M^p(t) = \frac{0.9}{\frac{1}{2} - t} - \frac{1.0}{\frac{3}{2} - t} + \frac{0.25}{\frac{5}{2} - t} + \ldots, \tag{1.5}$$

and hence, if we assume that the ϱ' is coupled normally to hadrons

($g_{\rho' NN} \sim g_{\rho NN}$), we see that it should also be coupled normally to the photon ($g_{\gamma\rho'} \sim g_{\gamma\rho}$).

More generally we note that a strong ρ' (or a strong nonresonating p wave of opposite sign to the ρ) is needed in order to satisfy the superconvergence relation required by the rapid decrease of the form factor in the spacelike region (at least t^{-2}).

1.*c.* – In the simplest Veneziano formula for $\pi\pi$ scattering ([1]) the ρ' occurs with elastic width approximately equal to that of the ρ (*i.e.*, about 120 MeV), but then one finds from simple models for $\pi\pi \to \pi A_1$ that a large width into the (πA_1) channel is also expected, giving a total width somewhat larger ([4]) ($\gtrsim$300 MeV).

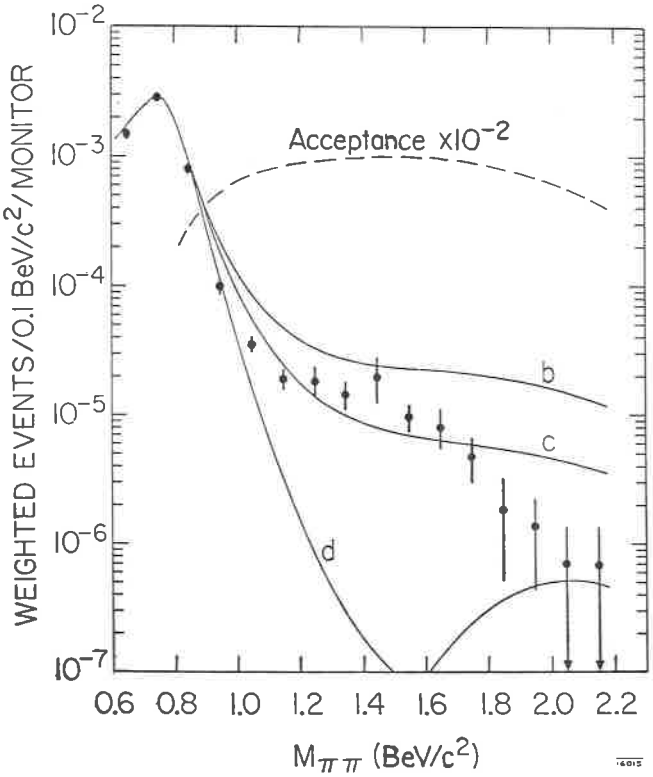

Fig. 2. – Data for photon energy $E_\gamma = 15$ GeV on beryllium (taken from F. BULOS *et al.*: *Phys. Rev. Lett.*, **26**, 149 (1971)).

1.*d*. – These predictions of a ρ' resonance have led to a succession of experiments on the photoproduction of high mass dipions off nuclear targets. The experiments characteristically measure symmetric pair production in the forward direction. Specifically we consider here the results of the

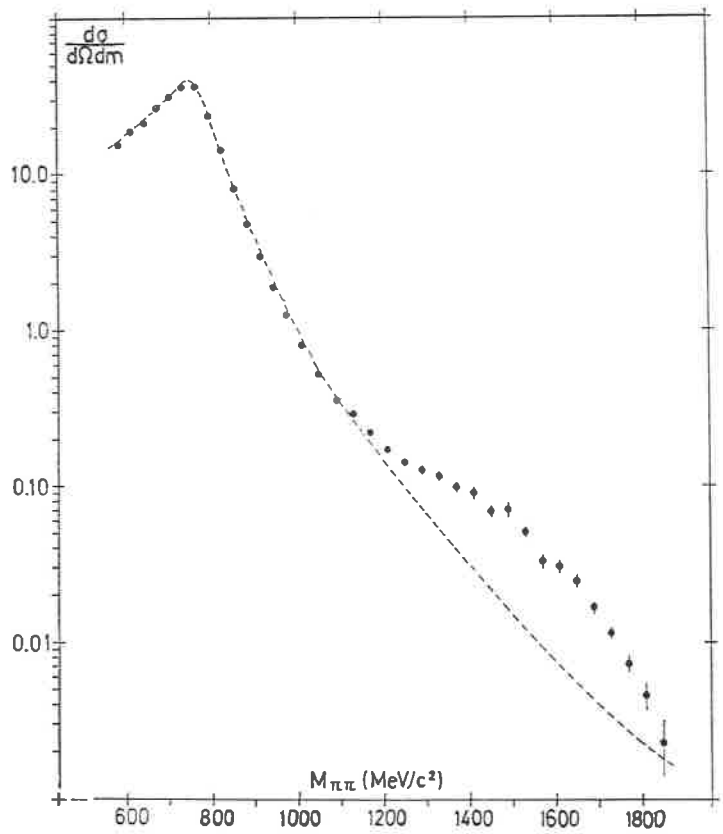

Fig. 3. – Data for photon energy $E_\gamma = 7$ GeV on carbon (taken from H. ALVENSLEBEN *et al.*: *Phys. Rev. Lett.*, **26**, 273 (1971)).

SLAC experiment ([5]) at 15 GeV incident photon momentum on Beryllium (Fig. 2) and of the DESY-MIT experiment ([6]) at 7 GeV on Carbon (Fig. 3).

The main feature of the data is the rapid fall-off in the cross-section by more than two orders of magnitude between the ρ peak and the point $m_{\pi\pi} = 1.5$ GeV. This is the fall-off which will be our main concern here.

In addition, it is worth mentioning that both sets of data, Figs. 2 and 3, show a broad shoulder between $m_{\pi\pi} = 1.3$ GeV and $m_{\pi\pi} = 1.8$ GeV. Whether or not this is the ρ' meson can only be answered by a careful study of the angular distribution.

1.*e*. – These data then show that the ratio of the Pomeron (P) couplings $g_{\gamma P\rho'}/g_{\gamma P\rho}$ is very small (Fig. 4*a*). We shall be able to understand this in terms of the multiperipheral (Drell) production mechanism ([7]) of Fig. 4*b*. This diagram is dominant in the double Regge limit E_γ very large and $m_{\pi\pi}$ high. Applying the idea of duality, we expect the magnitude of the photoproduced p wave dipion as a function of $m_{\pi\pi}$ to be governed by the p wave content of this diagram.

In the rho region a model has been proposed by Kramer and Uretsky ([8]) to justify the phenomenologically successful Ross-Stodolsky modification ([9]) of the ρ Breit-Wigner shape by relating it to the $(m_{\pi\pi})^{-2}$ structure of the p wave projection of the Drell term. We shall show that taking into account the off-shell character of the exchanged pion, one is led to a suppression factor which behaves asymptotically as $1/m_{\pi\pi}^6$ in the forward production amplitude, or, more specifically, in the three-point coupling $g_{\gamma P\rho'}$.

It is noted that a phenomenological use ([10]) of the beta function in describing diffractive dipion photoproduction does not give the observed suppression of ρ' without the addition of satellite terms.

1.*f*. – The coupling $g_{\gamma P\rho'}$ involves the diffractive production mechanism in an essential way, and is *not* simply related to the two-point coupling $g_{\gamma\rho}$, *i.e.*, a suppression of $g_{\gamma P\rho'}$ does not necessarily imply that $g_{\gamma\rho'}$ is suppressed. When one attempts to set up a generalized vector dominance model (Fig. 4*c*), however, the suppression effect should somehow be included. On can incorporate the suppression in either (i) an off-shell form factor for $g_{\gamma\rho'}$ between $k^2 = m_\rho^2$, and $k^2 = 0$, or (ii) a suppression of the coupling $g_{\rho' P\rho'}$, or (iii) inclusion of off-diagonal terms ($i \neq j$ in Fig. 4*c*).

Because there is no natural place to include this suppression, however, the generalized vector dominance model has little or no predictive power in relating the photoproduction process to the electromagnetic form factor.

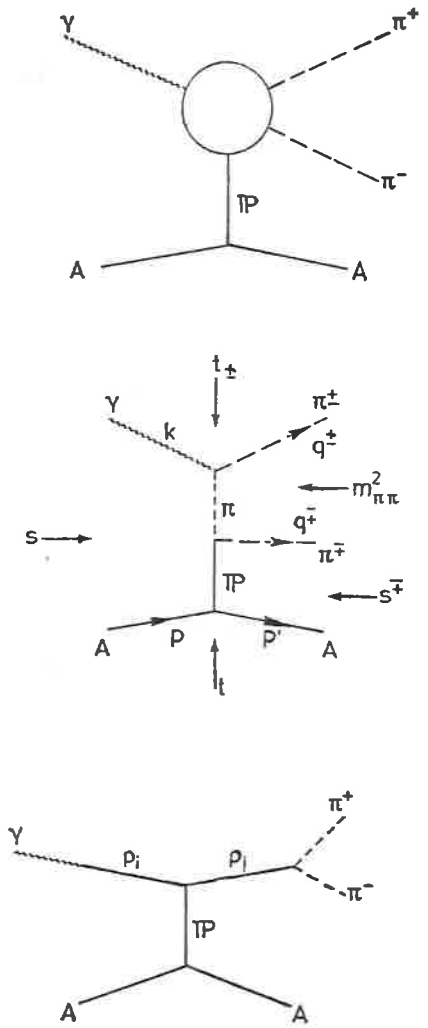

Fig. 4. – *a*) Diffractive dipion photoproduction. *b*) Multiperipheral (Drell) production me-mechanism and kinematics. *c*) Generalized vector meson dominance.

2. Diffraction dissociation model.

2.*a.* – The attitude adopted here is that the (Reggeized) Drell term is a good approximation at high $m_{\pi\pi}$ and still qualitatively good at $m_{\pi\pi} = 1.5$ GeV and Jackson angle $\theta = 90°$. Since the conclusions are independent of the target we take the simplest case of a proton (A = proton in Fig. 4). The amplitude for the Drell graph shown in Fig. 4*b* now is

$$T = e\left\{\frac{\varepsilon\cdot q^+}{k\cdot q^+} f_- T_+ - \frac{\varepsilon\cdot q^-}{k\cdot q^-} f_+ T_-\right\}, \tag{2.1}$$

where for simplicity we do not include the phase of the Reggeized π exchange but only a form factor which is equivalent to the Regge shrinkage factor:

$$f_\pm = \exp\left[A(m_{\pi\pi})(t_\pm - \mu^2)\right] = \left(\frac{m_{\pi\pi}^2}{s_0}\right)^{\alpha_\pi(t)} \tag{2.2}$$

and where $T_\pm$ is the $\pi^\pm$p elastic amplitude

$$T_\pm = is_\pm \exp\left[Bt\right]\sigma^{\text{tot}}_{\pi^\pm \text{p}} . \tag{2.3}$$

The following notations are used: ε_μ = photon polarization vector, $s_\pm = (q_\pm + p')^2$, $t_\pm = (q_\pm - k)^2$, $t = (p - p')^2$, $q = \frac{1}{2}(m_{\pi\pi}^2 - 4\mu^2)^{\frac{1}{2}}$.

We consider only forward production where $|t|$ is at its minimum value. Then, in the Coulomb gauge either in the over-all centre-of-mass or in the (2π) rest system expression (2.1) corresponds exactly to the gauge invariant amplitude of Kramer *et al.* [9], except for the form factors $f_\pm$. These form factors become important for symmetric pair production at high dipion mass. In an unmodified Soeding interference model calculation [5,11], both the Drell term and the diffractive production term are an order of magnitude too high at $m_{\pi\pi} = 1.5$ GeV and only by a delicate cancellation is the correct magnitude regained.

2.*b.* – For symmetric pair production ($\theta = 90°$) the fall-off in $m_{\pi\pi}$ of the Reggeized Drell term is given asymptotically by

$$\frac{\mathrm{d}\sigma}{\mathrm{d}t\,\mathrm{d}m_{\pi\pi}\,\mathrm{d}\Omega}(90°) \sim \frac{1}{m_{\pi\pi}} \exp\left[-Am_{\pi\pi}^2\right], \tag{2.4}$$

where we have used the formula for the cross-section in terms of T which reads

$$\frac{\mathrm{d}\sigma}{\mathrm{d}t\,\mathrm{d}m_{\pi\pi}\,\mathrm{d}\Omega} = \frac{q}{256\pi^4(s-M_\rho^2)^2}|T|^2 \tag{2.5}$$

in which $s = (k+p)^2$.

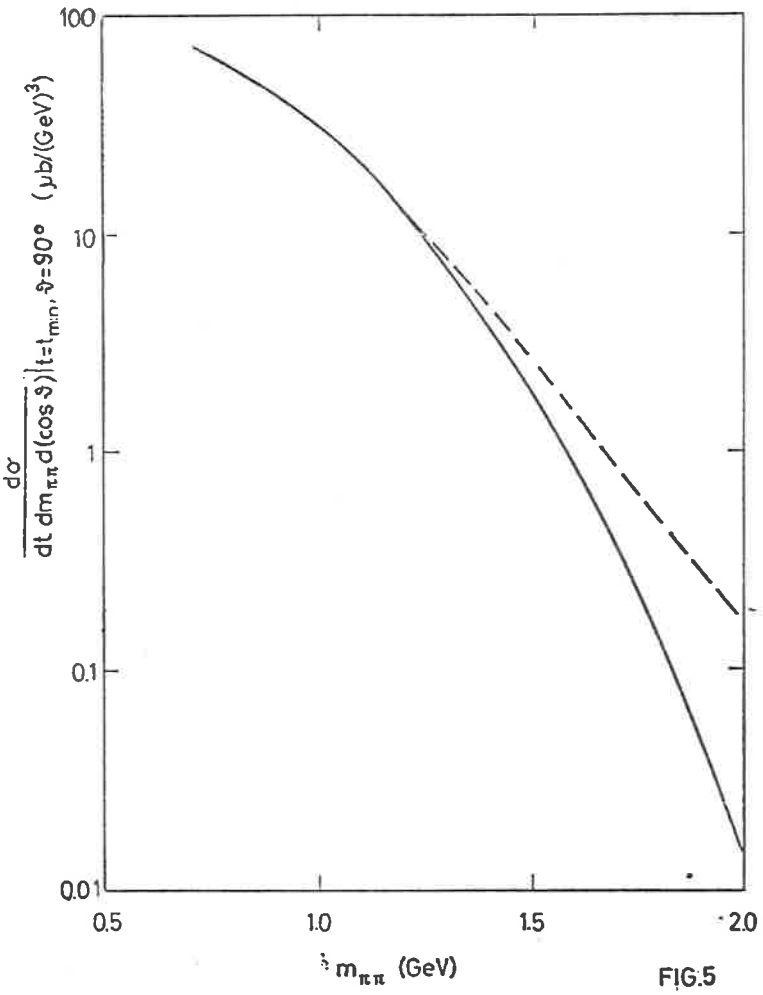

Fig. 5. – The differential cross-section $\mathrm{d}\sigma/(\mathrm{d}t\,\mathrm{d}m_{\pi\pi}\,\mathrm{d}\cos\theta)$ for the Drell term with Regge shrinkage factor (solid curve), and its p wave content (dashed curve), as explained in the text. The results are calculated for $E_\gamma = 15$ GeV on a proton target with form factor $\exp[2Bt] = \exp[9t]$, and the parameter $s_0 = m_\rho^2$

If we take $s_0 = m_\rho^2$ in eq. (2.2), then there is no form factor modification to the Drell term at $m_{\pi\pi} = m_\rho$, *i.e.*, $A(m_\rho) = 0$. At $m_{\pi\pi} = 1.5$ GeV (using $\alpha'_\pi = 1\ \text{GeV}^{-2}$) we obtain $A(m_{\pi\pi} = 1.5\ \text{GeV}) = 1.4$, and hence the 90° fall-off of the cross-section becomes

$$\frac{\sigma(90°, 1.5\ \text{GeV})}{\sigma(90°, m_\rho)} \approx \frac{1}{35} \tag{2.6}$$

The contribution of the Reggeized Drell term is plotted in the solid curve of Fig. 5. At $m_{\pi\pi} = m_\rho$ the Drell term yields a cross-section ~ 11 times smaller than the experimental cross-section at the peak ([11,12]). Therefore a fall-off of the data between $m_{\pi\pi} = m_\rho$ and $m_{\pi\pi} = 1.5$ GeV by a factor $11 \times 35 \approx 400$ can be easily explained. This agrees qualitatively with the fall-off observed in the SLAC experiment [5].

2.*c.* – Another suppression factor, which becomes more important the lower the photon energy and the heavier the nucleus, is the well known $t_{\min}$ effect in the nuclear form factor.

The nuclear form factor is $\exp[4\tilde{A}^2 t_{\min}]$ with $\tilde{A} =$ atomic weight and with $t_{\min} = -(m_{\pi\pi}^2/2E_\gamma)^2$. Between $m_{\pi\pi} = m_\rho$ and $m_{\pi\pi} = 1.5$ GeV this gives a suppression factor of 3 for $E_\gamma = 7$ GeV on a carbon target, and a factor 1.2 for $E_\gamma = 15$ GeV on a beryllium target. This explains the faster fall-off seen in the 7 GeV experiment ([6]).

3. Final state enhancement factor.

3.*a.* – For a description of the ρ region we use a model of a final state enhancement factor E in the p wave dipion syste mof the Drell amplitude, analogous to that of Kramer and Uretsky

$$T_{\mathrm{p}}^{(\mathrm{Drell})} \to T_{\mathrm{p}}^{(\mathrm{Drell})} \cdot E_\rho\ , \tag{3.1}$$

where

$$E_\rho = \frac{1/\pi}{m_\rho^2 - m_{\pi\pi}^2 - i m_\rho \Gamma_\rho}\ . \tag{3.2}$$

The average of E over a typical resonance spacing, $1/\alpha' \approx 1\ \text{GeV}^2$ is required to be 1 by duality-like arguments

$$\frac{1}{(1\ \text{GeV}^2)} \int_{m^2\rho - \frac{1}{2}\text{GeV}^2}^{m^2\rho + \frac{1}{2}\text{GeV}^2} \mathrm{d}m_{\pi\pi}^2 E(m_{\pi\pi}) = 1\ . \tag{3.3}$$

This fixes the normalization in eq. (3.2) in the case of narrow resonance $m\Gamma \ll 1$ GeV^2 (Kramer and Quinn [8]), consider the normalization of the enhancement factor a free parameter).

3.*b*. – At $m_{\pi\pi} = m_\rho$ the value of the enhancement factor is

$$|E_\rho|^2 = (\pi M_\rho \Gamma_\rho)^{-2} = 11.3\,, \tag{3.4}$$

in good agreement with the experimental enhancement of 11 over the Drell terms.

Here we have used the fact that the Drell term is mostly p wave in the ρ region.

3.*c*. – We now turn again to the ρ' region. Up to now we have assumed that the Drell term describes the gross features of the data for $m_{\pi\pi} \approx 1.5$ GeV (and $\theta = 90°$) and have shown that this picture works qualitatively well. Now we wish to estimate the ρ' production rate on the basis of our final state enhancement picture. In the ρ' region the non p wave contribution will be appreciable in the Drell term T. The p wave content, T_p, of the Drell term can be written

$$T_p = c(\boldsymbol{\varepsilon}\cdot\boldsymbol{q})\varphi_A(m_{\pi\pi})\,, \tag{3.5}$$

where $c = \left(-\frac{3}{2} i s e^{Bt} \sigma_{\pi p}^{\mathrm{tot}}\right)$ is independent of $m_{\pi\pi}$ and

$$\varphi_A = \frac{1}{s}\int_{-1}^{+1} \mathrm{d}z(1-z^2)\left[\frac{f_+ s_-}{t_+ - \mu^2} + \frac{f_- s_+}{t_- - \mu^2}\right], \tag{3.6}$$

where $z = \cos\theta$.

The full analytic expression for φ_A is given by

$$\varphi(m_{\pi\pi}) = \frac{4d\exp[Aba]}{Ab^2}\left[\left(\frac{2}{Ab} + a - c\right)\mathrm{ch}\,Ab - \right.$$

$$\left. - \left(\frac{2}{A^2 b^2} + (a-c)\left(\frac{1}{Ab} + a\right)\right)\mathrm{sh}\,Ab\right] +$$

$$+ (c-a)(1-a^2)\,\mathrm{d}b^{-1}\left[E_i(Ab(a+1)) - E_i(Ab(a-1))\right], \tag{3.7}$$

where the functions $a(m_{\pi\pi})$, $b(m_{\pi\pi})$, $c(m_{\pi\pi})$, $d(m_{\pi\pi})$ are defined by $(t_{\pm} - \mu^2) = b(a \pm z)$ and $(s_{\pm}/s) = \mathrm{d}(c \mp z)$. $E_i(x)$ is the exponential integral function ([13]).

The asymptotic behaviour when $s \to \infty$, $m_{\pi\pi}^2 \to \infty$ with $m_{\pi\pi}^2/s \to 0$ is given by

$$\varphi_A(m_{\pi\pi}) \sim -\frac{24}{A^2} \frac{\exp[-A\mu^2]}{m_{\pi\pi}^b} \quad (A \neq 0) \tag{3.8}$$

as mentioned already in the Introduction. If one takes $A = 0$ the corresponding limit is

$$\varphi_0(m_{\pi\pi}) \sim -\frac{2}{m_{\pi\pi}^2} \tag{3.9}$$

In the dashed curve of Fig. 5, we plot the contribution to differential cross-section $(\mathrm{d}\sigma/\mathrm{d}t\,\mathrm{d}m_{\pi\pi}\,\mathrm{d}\cos\theta)$ from the p wave content of our Drell term. At a ρ' resonance there would be an enhancement factor which we calculate, using eq. (3.3) as

$$|E_{\rho'}|^2 \approx 1.7\,, \tag{3.10}$$

taking $\Gamma_{\rho'} \sim 2\Gamma_{\rho}$. Due to the effects of inelasticity this enhancement factor can only be considered as an upper limit.

The p wave production in the $m_{\pi\pi} \approx 1.5$ GeV region thus does not differ much from the Drell p wave. From the dashed curve of Fig. 5, we see that the observed suppression of ρ' production is easily understood in this way.

3.*d*. – Expressed in terms of the three-point couplings of the Pomeron (P) the experimental data, and the multiperipheral production mechanism, both yield a small value of the ratio $(g_{\gamma P\rho'}/g_{\gamma P\rho})$.

4. Generalized vector dominance model.

4.*a*. – The inference from the experimental fact $g_{\gamma P\rho'}/g_{\gamma P\rho} \leqslant 1/10$ that the photon-vector meson couplings satisfy $g_{\gamma\rho'}/g_{\gamma\rho} \leqslant 1/10$ cannot be made, since there is no simple relation between these ratios. The former involves the Pomeron and the details of the production mechanism in photoproduction while the latter does not. Similarly the corresponding inference cannot be

made from data on photoproduction of muon pairs ([14]) for the same reasons.

4.*b*. – Within the generalized vector dominance graph of Fig. 4*c*, there is no natural place for the suppression by the production mechanism. Let us assume for the discussion that ρ_i is coupled normally to 2π. Then there are three possibilities, all of which lead to a complete loss of predictive power:

(i) $g_{\gamma\rho_i}$, which is defined for $k^2 = m^2_{\rho_i}$, might be strongly k^2 dependent so that extrapolation to $k^2 = 0$ introduces a suppression;

(ii) we might say that $\sigma^{el}_{\rho' p}$ is down by two orders of magnitude relative to $\sigma^{el}_{\rho p}$ (*i.e.*, $g_{\rho' P\rho'}/g_{\rho P\rho} \leqslant 1/10$);

(iii) off-diagonal terms might be included so that diffractive transitions between the various vector mesons become significant. To illustrate this point, consider the generalized vector dominance equations

$$g_{\gamma P\rho_i} = \sum_j g_{\gamma\rho_j}\ g_{\rho_j P\rho_i} \tag{4.1}$$

To solve for $g_{\gamma\rho_i}$ we must invert the matrix $g_{\rho_i P\rho_j}$ In general this is undetermined and there are always sets of solutions where the $g_{\gamma\rho_i}$ and $g_{\rho_j P\rho_i}$ are of normal strength, while some $g_{\gamma P\rho_i}$ may be suppressed. One trivial illustrative example: for only two vector mesons ρ_1 and ρ_2, put $g_{\gamma\rho_1} = 2g_{\gamma\rho_2}$, $g_{\rho_1 P\rho_1} = 2g_{\rho_2 P\rho_2} = -3g_{\rho_1 P\rho_2}$ and solve eq. (4.1) to find $g_{\gamma P\rho_2}/g_{\gamma P\rho_1} = 1/10$.

4.*c*. – To summarize, the experimentally observed small value for $(g_{\gamma P\rho'}/g_{\gamma P\rho})$ which is readily understood in terms of the Drell production mechanism has no implication for the ratio $(g_{\gamma\rho'}/g_{\gamma\rho})$. In generalized vector meson dominance there is no natural place to include this suppression; this model then looses almost all its teeth when higher mass vector mesons are included.

5. Concluding remarks.

5.*a*. – It was demonstrated that the Drell term (full curve of Fig. 5) describes the gross behaviour of the cross-section, for $m_{\pi\pi} \sim 1.5$ GeV and $\theta = 90°$. A detailed fit to the data is out of place in this report, since we need to know how significant are the non p wave resonant contributions, and to put in the appropriate parameters for the p wave, f wave, and so on. When

an angular correlation analysis is available, however, such a fit on the basis of the model presented here could be made to extract resonance parameters.

5.*b*. – To measure $g_{\gamma\rho'}$ directly, the colliding beam e^+e^- experiments clearly avoid the difficulties discussed in Section 4. The experimental situation here is not yet clarified in the ρ' region of the pion form factor ([15]). We must bear in mind that the ρ' signal need not be as strongly peaked as suggested by the residue in eqs. (1.4)-(1.5) since as pointed out recently by Antoniou and Baier ([16]), the unitarity corrections may be considerable.

REFERENCES

1) G. Veneziano: *Nuovo Cimento*, **57**, 190 (1968); C. Lovelace: *Phys. Lett.*, **28 B**, 264 (1968); J. Shapiro: *Phys. Rev.*, **129**, 1345 (1969).
2) P. H. Frampton: *Phys. Rev.*, **186**, 1419 (1969).
3) P. Di Vecchia and F. Drago: *Lett. Nuovo Cimento*, **1**, 917 (1969).
4) J. L. Rosner and H. Suura: *Phys. Rev.*, **187**, 1905 (1969).
5) F. Bulos *et al.*: *Phys. Rev. Lett.*, **26**, 149 (1971).
6) H. Alvensleben *et al.*: *Phys. Rev. Lett.*, **26**, 273 (1971).
7) S. D. Drell: *Phys. Rev. Lett.*, **5**, 278 (1960).
8) G. Kramer and J. Uretsky: *Phys Rev.*, **181**, 1918 (1969); G. Kramer and H. R. Quinn: *Nucl. Phys.*, B **27**, 77 (1971); J. Pumplin: *Phys. Rev.*, D **2**, 1859 (1970).
9) M. Ross and L. Stodolsky: *Phys. Rev.*, **149**, 1172 (1966).
10) H. Satz and K. Schilling: *Nuovo Cimento*, **67 A**, 511 (1970).
11) P. Soeding: *Phys. Lett.*, **19**, 702 (1966).
12) H. H. Bingham *et al.*: *Phys. Rev. Lett.*, **24**, 955 (1970).
13) A. Erdelyi *et al.*: *Higher Transcendental Functions*, eq. (9.7-1).
14) G. Mcclellan *et al.*: *Phys. Rev. Lett.*, **23**, 718 (1969); S. Hayes *et al.*: *Phys. Rev. Lett.*, **24**, 1369 (1970).
15) See Session III-A, these proceedings.
16) N. Antoniou and R. Baier: CERN Preprint TH. 1276 (1917).

A model for hadron production in e^+e^- collisions

V. WATAGHIN

Istituto di Fisica Teorica dell'Università - Torino
Istituto Nazionale di Fisica Nucleare - Sezione di Torino

Since its proposal, about ten years ago (1), the hypothesis of vector meson dominance (VMD) has been applied to several high-energy electromagnetic reactions involving hadrons (2). In particular, its validity has been tested in the case of the nucleon electromagnetic form factors (FF). However, a phenomenological, conventional parametrization in terms of simple poles corresponding to the three well known VM resonances ϱ^0, ω, φ, has not yielded a theoretically and experimentally satisfactory expression (3). On the other hand, a specific parametrization in terms of second order poles describing the contribution of these resonances to the FF has been shown in this case to be both in agreement with the experimental results and theoretically acceptable since it has the property of crossing symmetry and satisfies a dispersion relation (4). A characteristic and important property of this solution was that the application of SU_3 symmetry to the determination of the parameters fixed the asymptotic behaviour of the magnetic proton FF.

In a subsequent paper (5) the model was generalized in order to describe inelastic e-p scattering, aiming to determine in particular the structure functions W_1, W_2, whose behaviour was determined experimentally in the past few years at SLAC. Although some qualitative results and some predictions that can be tested by experiments were made (6), the functional structure of W_1, W_2 is not yet fully determined, in particular the s-dependence is unknown (7).

The aim of this paper is to show that in this model crossing symmetry and a simple assumption for the asymptotic s-dependence of W_1, W_2 lead to

a definite prediction for the q^2-dependence of σ_{tot} for the reaction $e^+ + e^- \to \bar{p} +$ anything. In view of the colliding beam experiments being done with Adone at Frascati, we also present the model's prediction for σ_{tot} for the reaction $e^+ + e^- \to \bar{p} + p$ as a function of $q^2 = 4E^2$, E being the c.m. energy of each beam.

1. The q^2-dependence of σ_{tot} for the reaction $e^+ + e^- \to \bar{p} +$ anything.

We start from the formula ([8]):

$$\frac{d^2\sigma}{dE\, d\cos\theta} = \frac{4\pi\alpha^2}{q^4}\frac{M^2\nu}{\sqrt{\bar{q}^2}}\left(1-\frac{q^2}{\nu^2}\right)^{\frac{1}{2}}\left[2\overline{W}_1 + \frac{2M\nu}{q^2}\left(1-\frac{q^2}{\nu^2}\right)\frac{\nu\overline{W}_2}{2M}\sin^2\theta\right], \qquad (1)$$

where $E =$ energy of the detected proton; $\theta =$ angle of the proton momentum in the c.m. system; $\overline{W}_1(q^2, \nu) = -W_1(q^2, -\nu)$; $\overline{W}_2(q^2, \nu) = -W_2(q^2, -\nu)$; $\nu = (p\cdot q)/M$ and $s = M^2 + 2M\nu + q^2$ are the usual kinematic variables.

We then introduce for W_1, W_2 the expression (4) of ref. (5), *i.e.*

$$\left.\begin{aligned} W_j(q^2, s) &= [G_j(q^2, s)]^2\,, \\ G_j(q^2, s) &= \sum_{k=1}^{3}\frac{a_{k,j}(s, \omega')q^2 + b_{k,j}(s, \omega')}{[q^2 - m_k^2 - \gamma_k(q_k^2 - q^2)^{\frac{1}{2}}]^2}\,, \end{aligned}\right\} \qquad (2)$$

with

$$a_{k,j}(s, \omega') = a^0_{k,j} + \left(\frac{s-M^2}{\omega'^2}\right)^{\frac{1}{2}} a^{(i)}_{k,j}(s, \omega')\,, \qquad (j = 1, 2)\,.$$

We must integrate (1) over $dE\, d\cos\theta$ with q^2 fixed; we change variables of integration by the relation $E = M\nu/\sqrt{\bar{q}^2}$ and integrate between the limits: $-1 \leqslant \cos\theta \leqslant 1$; $\sqrt{\bar{q}^2} \leqslant \nu \leqslant q^2/2M$. The result for large q^2 will depend on the asymptotic behaviour of $\sum_k a_{k,j}(s, \omega')$ for large s. We shall assume that $\lim_{\substack{s\to\infty \\ q^2 \text{ fixed}}} \sum_k a^{(i)}_{k,j}(s, \omega') = \text{const}$. One finds then:

$$\sigma_{\text{tot}} \sim \frac{\text{const}}{q^2}\,, \quad \text{for large } q^2.$$

2. The $e^+ + e^- \to \bar{p} + p$ **total cross-section.**

The calculation is straightforward. One can start for instance from formula (51) of ref. (9), which after integration and some transformations yields:

$$\sigma_{tot} = \frac{2\pi\alpha^2}{3q^2}\left(1 - \frac{4M^2}{q^2}\right)^{\frac{1}{2}}\left[2|G_{MP}|^2 + \frac{4M^2}{q^2}|G_{EP}|^2\right]. \tag{4}$$

Two different solutions of the model for G_{MP}, G_{EP} were inserted in formula (4), one from ref. (4), the other obtained as follows (10). The VM resonances were parametrized with second order pole expressions, in the sense

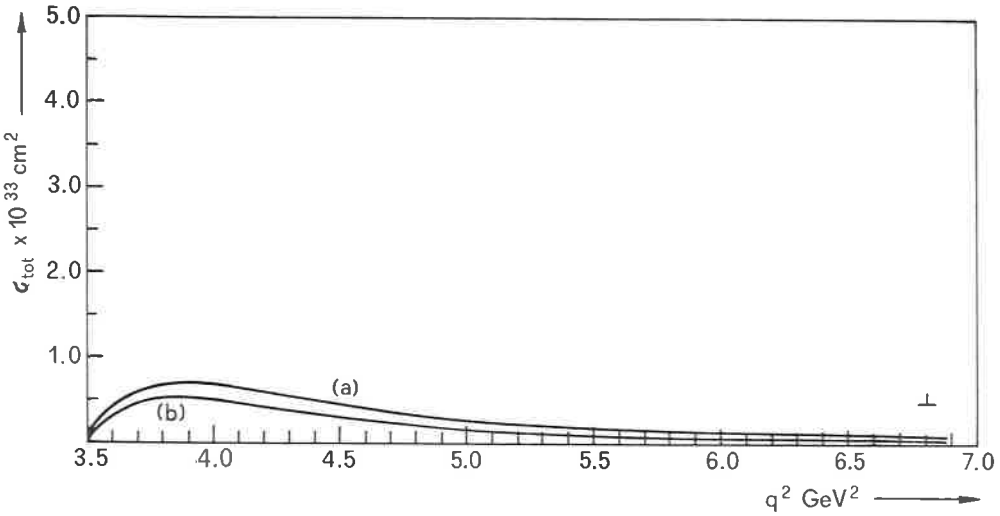

Fig. 1. – The total cross-section for the reaction $e^+ + e^- \to \bar{p} + p$ as a function of the square of the total c.m. energy, q^2, according to the second order pole model. Curve (*a*) was obtained assuming the VM resonances to be represented by second order poles (10), while curve (*b*) was deduced with a first order pole representation of these resonances (4).

of a Laurent expansion, and the parameters m_k^2 and γ_k were determined by fitting the experimental data from colliding beam experiments. With these values of m_k^2 and γ_k the calculation of ref. (4) was repeated and a new solution for G_{MP} and G_{EP} obtained. This solution, substituted in (4) leads to the result shown in curve (*a*) of Fig. 1; the solution of ref. (4) when introduced in (4) gives rise to curve (*b*) in the same Fig. 1. We note that the approximation $G_{MP} \mathbf{W} G_{EP}$ made in a preliminary estimate (11) based on the

relation $G_E = G_M$ valid at $q^2 = 4M^2$ is quite good, the difference in the region considered being at most about 10%: In Fig. 1, of course, is shown the exact result.

3. Discussions of the results.

There are at present no experimental data with which to check the prediction (3) for the total σ of the inclusive reaction $e^+ + e^- \to \bar{p}$+anything. We remark that the q^{-2} behaviour of $\sigma_{t\ t}$ was obtained as a result of summing over all final hadronic, states (s-integration) with only a specific asymptotic assumption and that this procedure corresponds to taking into account to some degree the unitarity condition. We con'ecture therefore that the recent colliding beam Frascati results on multiple hadron production which seem to indicate such a q^2 dependence, may admit of a similar explanation ([12,13]).

About the result (4) we remark that the only experimental data available at present is the upper limit σ ffl $0.48 \cdot 10^{-33}$ cm^2 of Conversi *et al.* at $q^2 = = 6.8$ GeV^2 ([14]). The experimental data being gathered however are unlikely to allow to discriminate between the two solutions, since the relative difference between the two curves is small.

REFERENCES

1) J. J. SAKURAI: *Ann. of Phys.*, **aa**, 1 (1960); M. GELL-MANN and F. ZACHARIASEU: *Phys. Rev.*, **ayo**, 953 (1961).
2) *Proceedings of the Lund International Conference on Elementary Particles* (1969), review talk by E. LOHRMANN.
3) T. MASSAM and A. ZICHICHI: *Nuovo Cimento*, **ou** A, 1137 (1966); V. WATAGHIN: *Nuovo Cimento*, **po** A, 805-840 (1968); K. Y. NG: *Phys. Rev.*, **adb**, 1436 (1968).
4) V. WATAGHIN: *Nucl. Phys.*, B **ab**, 107 (1969).
5) V. WATAGHIN: *Proceedings of the VIII Coral Gables International Conference* (Jan. 1971).
6) More specific experimental tests will be discussed in a subsequent paper.
7) Here s is the square of the four momentum of the final hadronic state.
8) S. D. DRELL, D. J. LEVY and T. M. YAN: *Phys. Rev.*, D **a**, 1617 (1970).
9) N. CABIBBO and R. GATTO: *Phys. Rev.*, **ayo**, 1577 (1961).
10) D. TRIGIANTE and V. WATAGHIN: to be published.
11) Only the approximate result was reported at the Conference.
12) For a specific model for such processes see: J. LAYSSAC and F. M. RENARD: preprint PM/71/2, University of Montpellier; also report by F. M. RENARD to this Conference.
13) We will elaborate on this remark elsewhere.
14) M. CONVERSI *et al.*: *Nuovo Cimento*, **ob**, 690 (1965).

SESSION III - C

Friday, 16 April 1971

Theoretical predictions on meson classification and their decay properties. The problem of exotics and their relations to duality. The narrow widths problem of high-mass resonances

Chairman: L. RADICATI

Secretaries: V. GRECCHI
J. L. PETERSEN

$\pi\pi$ scattering, non linear realizations of chiral $SU_2 \otimes SU_2$ and the $m_\sigma \to \infty$ limit

W. ALLES, P. MAZZANTI and M. SALVINI (*)
Istituto di Fisica dell'Università - Bologna
Istituto Nazionale di Fisica Nucleare - Sezione di Bologna

This communication deals on the $\pi\pi$ scattering lengths in a Lagrangian model theory.

When working with linear representations of the chiral $SU_2 \otimes SU_2$ symmetry introduced by Gell-Mann and Levy (2), one obtains from their $\pi\sigma$ Lagrangian in the limit $m_2^2 \to \infty$ of the σ-meson mass a nonlinear realization of $SU_2 \otimes SU_2$ (3) that reproduces, in the tree approximation, the Weinberg (4) $\pi\pi$ scattering lengths. In general, nonlinear realizations of $SU_2 \otimes SU_2$ are introduced (5) for reproducing when used as effective Lagrangians in the tree approximation low energy theorems derived from current algebra and PCAC. The Gell-Mann and Levy Lagrangian is uniquely determined when PCAC and renormalizability are required. Nevertheless, when these Lagrangians are used as effective Lagrangians in the tree approximation, the renormalizability requirement seems too restrictive. Furthermore, the nonlinear realization obtained in the $m_\sigma \to \infty$ limit from the Gell-Mann and Levy Lagrangian leads to a nonrenormalizable theory. Thus, we shall study the consequences in the tree approximation of the most general $SU_2 \otimes SU_2$ invariant Lagrangian broken by a σ term leading to PCAC, when the renormalizability condition is dropped from the beginning.

Let us consider first the simplest Lagrangian for the π and σ system, containing up to four fields and two derivatives that leads to all the features we want to discuss:

$$\mathscr{L} = -\frac{1}{2}(\partial\boldsymbol{\varphi})^2 - \frac{1}{2}(\partial\sigma)^2 - \frac{1}{2}\mu^2(\boldsymbol{\varphi}^2 + \sigma^2) + \frac{\lambda}{4}(\boldsymbol{\varphi}^2 + \sigma^2)^2 + \\ + b(\boldsymbol{\varphi}\cdot\partial_\mu\boldsymbol{\varphi} + \sigma\partial_\mu\sigma)^2 + f_\pi m_\pi^2 \sigma\,, \qquad (1)$$

(*) Invited paper presented by W. Alles.

and that leads to $\partial_\mu A_\mu = f_\pi m_\pi^2 \varphi$ with $f\varsigma = 94.5$ MeV. The pion φ field and the σ field transforming as the members of the (2, 2) representation of the chiral $SU_2 \otimes SU_2$ group. The term proportional to b leads to a non-renormalizable theory ([6]). When $b = 0$ (1) reduces to the Gell-Mann and Levy Lagrangian for the $\pi\sigma$ system.

The term linear in σ in (1) leads to a nonvanishing vacuum expectation value of σ, $\langle 0|\sigma|0\rangle = f_\pi$ and the convenience of introducing a new field $\sigma' = \sigma - \langle 0|\sigma|0\rangle$ for which $\langle 0|\sigma'|0\rangle = 0$ holds. The presence of the term proportional to b in (1) requires then a redefinition of σ', $\sigma_r = \sigma'/\sqrt{Z}$ to obtain the σ kinetic energy with the standard $-\frac{1}{2}$ coefficient. One obtains, for the σ renormalization constant:

$$Z = \frac{1}{1 - 2f_\pi^2 b}, \tag{2}$$

and of the Lagrangian (1) rewritten as a function of the fields φ and σ_n:

$$\mathscr{L} = -\tfrac{1}{2}(\partial_\mu \boldsymbol{\varphi})^2 - \tfrac{1}{2}(\partial_\mu \sigma)^2 - \tfrac{1}{2} m_\pi^2 \boldsymbol{\varphi}^2 - \tfrac{1}{2} m_\sigma^2 \sigma_r^2 -$$

$$- \frac{1}{8 f_\sigma^2}\left(\frac{m_\sigma^2}{Z} - m_\pi^2\right)(\mathbf{V}^2 + Z\sigma_r^2)^2 - \frac{\sqrt{Z}}{2f_\pi}\left(\frac{m_\sigma^2}{Z} - m_\pi^2\right)\sigma_r(\mathbf{V}^2 + Z\sigma_r^2) + \tag{3}$$

$$+ \frac{1}{2f_\pi^2}\left(1 - \frac{1}{Z}\right)(\boldsymbol{\varphi}\cdot\partial_\mu\boldsymbol{\varphi} + Z\sigma_r\partial_\mu\sigma_r)^2 + \frac{\sqrt{Z}}{f_\pi}\left(1 - \frac{1}{Z}\right)\partial_\mu\sigma_r(\boldsymbol{\varphi}\cdot\partial_\mu\boldsymbol{\varphi} + \sigma Z_r \partial^\mu \sigma_r)$$

and for the π and σ-meson masses:

$$m_\sigma^2 = Z(m_\pi^2 - 2\lambda f_\pi^2), \tag{4}$$

$$m_\pi^2 = \mu^2 - \lambda f_\pi^2. \tag{5}$$

It is now clear from (4) that there are two possibile and different ways of sending the mass of the σ field to infinity. In the first, and only way for the Lagrangian without the b term, this is obtained by taking $\lambda \to -\infty$; the ratio Z/m_σ^2 will in this case tend to 0, $Z/m_\sigma^2 \to 0$. On the other hand, one can keep λ finite and obtain $m_\sigma^2 \to \infty$ by making $Z \to \infty$ (that is $b \to 1/2f_\pi^2$) and in this case Z/m_σ^2 will be a parameter of the problem.

One can check easily that as expected for any model satisfying PCAC, when anyone of the pion four-moments goes to zero and the other three are on the mass shell the T-matrix goes to zero (Adler's self consistency

condition) (7). When the limit $m_\sigma \to \infty$ has been taken, the $\pi\pi$ scattering lengths *al;* a_2 and a_1 are given by

$$al = \frac{7}{32\pi} \cdot \frac{m_\pi}{f_\pi^2} \left\{ 1 + \frac{29}{7} \cdot \frac{m_\pi^2 Z}{m_\sigma^2} \right\}, \tag{6}$$

$$a_2 = -\frac{1}{16\pi} \cdot \frac{m_\pi}{f_\pi^2} \left\{ 1 - \frac{m_\pi^2 Z}{m_\sigma^2} \right\}, \tag{7}$$

$$a_1 = \frac{1}{24\pi} \cdot \frac{m_\pi^2}{f_\pi^2} \cdot \frac{1}{m_\pi^3} \left\{ 1 - \frac{2m_\pi^2 Z}{m_\sigma^2} \right\}. \tag{8}$$

It can be seen from these expressions that the $\pi\pi$ scattering lengths depend in a crucial way, even when m_σ^2 has been sent to infinity, on the ratio Z/m_σ^2: Only when $Z/m_\sigma^2 = 0$ one re-obtains the Weinberg scattering lengths. Let us at his point remark that we have in our model all the commutation relations (current-current and current-divergence) assumed by Weinberg, but that as evident from the expressions for a_1; a_2 and a_1 we have corrections to the Weinberg scattering lengths that are proportional to m_π^2/m_σ^2 and that in his approach would be neglected. In our model, because of the appearance of the factor Z, we cannot neglect these, even when $m_\sigma^2 \to \infty$; m_σ^2/Z can be of order m_π^2.

Let us further consider this point by studying the equations of motion of the σ and φ fields as derived from our Lagrangian (1).

$$\partial_\mu \left(\frac{\partial \mathscr{L}}{\partial(\partial_\mu \sigma)} \right) - \frac{\partial \mathscr{L}}{\partial \sigma} = 0 = -\Box\sigma + b\sigma\Box(\boldsymbol{\varphi}^2 + \sigma^2) + \mu^2\sigma - \lambda(\boldsymbol{\varphi}^2 + \sigma^2)\sigma - f_\pi m_\pi^2 \tag{9}$$

$$\partial_\mu \left(\frac{\partial \mathscr{L}}{\partial(\partial_\mu \boldsymbol{\varphi})} \right) - \frac{\partial \mathscr{L}}{\partial \boldsymbol{\varphi}} = 0 = -\Box\boldsymbol{\varphi} + b\boldsymbol{\varphi}\Box(\boldsymbol{\varphi}^2 + \sigma^2) + \mu^2\boldsymbol{\varphi} - \lambda\boldsymbol{\varphi}(\boldsymbol{\varphi}^2 + \sigma^2), \tag{10}$$

when $m_\sigma^2 = \infty$ is obtained by letting $\lambda \to \infty$ and $m_\pi^2 = \mu^2 - \lambda f_\pi^2$; eqs. (9) and (10) after dividing by λ and neglecting the $\Box/\lambda$ terms reduces to the usual nonlinear realization of $SU_2 \otimes SU_2$ (2), $\mathbf{V}^2 + \sigma^2 = f_\pi$: Our Lagrangian (1) reduces then to the standard Lagrangian of the nonlinear theory that is:

$$\mathscr{L} = -\tfrac{1}{2}(\partial_\mu \boldsymbol{\varphi})^2 - \tfrac{1}{2}(\partial_\mu \sigma)^2 + f_\pi m_\pi^2 \sigma \tag{11}$$

and it is not surprising that

$$a_0 = \frac{7}{32\pi}\frac{m_\pi}{f_\pi^2},$$

$$a_2 = -\frac{1}{16\pi}\frac{m_\pi}{f_\pi^2} \quad \text{and} \quad a_1 = \frac{1}{24\pi}\cdot\frac{m_\pi^2}{f_\pi^2}\cdot\frac{1}{m_\pi^2} \tag{11}$$

are obtained.

On the contrary, when $m_\sigma \to \infty$ as $Z \to \infty$ (that is, as $b \to 1/2f_\pi^2$), eqs. (9) and (10) tend to:

$$-\Box\sigma + \frac{1}{2f_\pi^2}\sigma\Box(\boldsymbol{\varphi}^2+\sigma^2) + \mu^2\sigma - \lambda(\boldsymbol{\varphi}^2+\sigma^2)\sigma - f_\pi m_\pi^2 = 0\,, \tag{12}$$

and

$$-\Box\boldsymbol{\varphi} + \frac{1}{2f_\pi^2}\boldsymbol{\varphi}\Box(\boldsymbol{\varphi}^2+\sigma^2) + \mu^2\boldsymbol{\varphi} - \lambda(\boldsymbol{\varphi}^2+\sigma^2)\boldsymbol{\varphi} = 0 \tag{13}$$

that lead to no solution of the form $\sigma = f(\boldsymbol{\varphi}^2)$. In this case, no nonlinear realization of $SU_2 \otimes SU_2$ arises although the σ-field mass has been shifted to infinity. That one does not obtain the Weinberg ππ scattering lengths is then compatible with the fact that (11) is the most general nonlinear Lagrangian and that all nonlinear realizations obtained from $\sigma = \sqrt{f_\pi^2 - \boldsymbol{\varphi}^2}$ by canonical transformations should lead to the same on-shell results [5].

The features of the above results do not depend on the particular Lagrangian we have introduced in (1). Taking for the system the most general $SU_2 \otimes SU_2$ invariant Lagrangian containing any number of fields and up to two derivatives, plus the term leading to PCAC:

$$\mathscr{L} = -\tfrac{1}{2}[(\partial_\mu\boldsymbol{\varphi})^2 + (\partial_\mu\sigma)^2]\sum_{n=0}^{\infty} a_n(\boldsymbol{\varphi}^2+\sigma^2)^n + \sum_{n=1}^{\infty} c_n(\boldsymbol{\varphi}^2+\sigma^2)^n +$$

$$+ (\boldsymbol{\varphi}\cdot\partial_\mu\boldsymbol{\varphi} + \sigma\cdot\partial_\mu\sigma)^2\sum_{n=0}^{\infty} b_n(\boldsymbol{\varphi}^2+\sigma^2)^n + f_\pi m_\pi^2\sigma\,, \tag{14}$$

with the restriction $\sum_{n=0}^{\infty} a_n f_\pi^{2n} = 1$ that does not limit the generality of (14) and that leads to no need of re-definition of the pion field. As above $\langle 0|\sigma|0\rangle = f_\pi$ and the σ field has to be re-defined by $\sigma_r = (\sigma - f_\pi)/\sqrt{Z}$ with the renormalization constant Z given by:

$$Z = \frac{1}{1 - 2\sum_{n=0}^{\infty} b_n f_\pi^{2(n+1)}}\,. \tag{15}$$

One can calculate from (14) the $\pi\pi$ scattering lengths that, when $m_\sigma^2 \to \infty$ are:

$$a_0 = \frac{7}{32\pi} \cdot \frac{m_\pi}{f_\pi^2} \left\{ 1 + \frac{Z m_\pi^2}{7 m_\sigma^2} [3(2a+3)^2 + 2(2a+1)^2] \right\} \tag{16}$$

$$a_2 = -\frac{1}{16\pi} \cdot \frac{m_\pi}{f_\pi^2} \cdot \left\{ 1 - \frac{Z m_\pi^2}{m_\sigma^2} (2a+1)^2 , \right\} \tag{17}$$

$$a_1 = \frac{1}{24\pi} \cdot \frac{m_\pi^2}{f_\pi^2} \cdot \frac{1}{m_\pi^2} \cdot \left\{ 1 - 2(1+a)(1+2a) \frac{Z m_\pi^2}{m_\sigma^2} \right\} , \tag{18}$$

where a is $a = \sum_{n=1}^{\infty} n a_n f_\pi^{2n}$. Again one can distinguish two cases. Let us assume the parameter a finite. When $m_\sigma^2 \to \infty$ and Z is finite (or tends to infinity less strongly than m_σ^2), $Z/m_\sigma^2 \to 0$ and (16) to (18) give the Weinberg values for a_0, a_2 and a_1: When, on the other hand, $m_\sigma^2 \to \infty$ by letting, $Z \to \infty$, a_0, a_2 and a_1 given by (16) to (18) are explicitly dependent on the limit of Z/m_σ^2 and the parameter a. From (16) to (18) one sees immediately since $Z/m_\sigma^2 \geqslant 0$, that for any value of Z/m_σ^2 and a,

$$a_0 \geqslant \frac{7}{32\pi} \frac{m_\pi}{f_\pi^2} , \qquad a_2 \geqslant -\frac{1}{16\pi} \frac{m_\pi}{f_\pi^2} , \qquad 2a_0 + a_2 \geqslant \frac{3}{8\pi} \frac{m_\pi}{f_\pi^2} ,$$

(the right-hand side of the inequalities being always the Weinberg values) and that the ratio a_0/a_2 is either $a_0/a_2 \leqslant -7/2$ or $+1 \leqslant a_0/a_2$: It is also evident that in the present model [Lagrangian (14)] no nonlinear realization arises for σ when $m_\sigma^2 \to \infty$ and $Z/m_\sigma^2 \nrightarrow 0$.

Let us further notice that a modification of the $SU_2 \otimes SU_2$ symmetry breaking term in (14), but letting it still transform like a member of the (2, 2) representation, of the form

$$\mathscr{L}_{\mathrm{SB}} = f_\pi m_\pi^2 \sigma f(\boldsymbol{\varphi}^2 + \sigma^2) ,$$

with $f(\sigma_0^2) = 1$, would lead to no new results. In fact, choosing for the new σ and $\boldsymbol{\varphi}$ fields, $S = \sigma f(\boldsymbol{\varphi}^2 + \sigma^2)$ and $\boldsymbol{F} = \boldsymbol{\varphi} f(\boldsymbol{\varphi}^2 + \sigma^2)$ would lead to the same on-mass-shell results and a Lagrangian of the form (14) for the S and $\boldsymbol{F}$ fields.

REFERENCES

1) W. Alles, P. Mazzanti and M. Salvini: *Lett. Nuovo Cimento*, **1**, 277 (1971).
2) M. Gell-Mann and M. Levy: *Nuovo Cimento*, **16**, 705 (1960); J. Schwinger: *Ann. Phys.*, **2**, 407 (1957).
3) W. A. Bardeen and B. W. Lee: *Phys. Rev.*, **177**, 2389 (1969).
4) S. Weinberg: *Phys. Rev. Lett.*, **7**, 616 (1966).
5) S. Weinberg: *Phys. Rev.*, **166**, 1568 (1968).
6) K. Symanzik: *Renormalization of models with broken symmetry*, presented at the *Second Coral Gables Conference on Fundamental Interactions at High-Energy* (1970), or DESY Report T-70/2.
7) S. L. Adler: *Phys. Rev.*, **139** B, 1638 (1965).

Harmonic oscillator pattern arising from an algebraic approach to chiral symmetry (*)

F. BUCCELLA
CERN Geneva

What I am saying is taken from a programme which involves E. Celeghini and E. Sorace in Florence, F. Nicoló and A. Pugliese in Roma and C. A. Savoy and myself at CERN.

The main tool is the use of the $SU_4 \times 0_3$ quantum numbers, which arise from the fact that the lowest meson states may be classified in the $15 + 1L = 0$ and $15 + 1L = 1$ representations, to build up axial charges satisfying the AW sum rules and the superconvergence relation following from the vanishing at infinite energy of the amplitudes with exotic t channel internal quantum numers.

One has the two algebraic conditions:

$$[X^a, X^b] = i\varepsilon^{abc} T^c, \tag{1}$$

$$[X^+, [X^+, m^2] = 0\,. \tag{2}$$

It has been known for a long time that the identification (in the $P_z = \infty$ frame)

$$T^a = A\left(\frac{\tau_a}{2}\right), \qquad X^a = A\left(\sigma_z \frac{\tau_a}{2}\right), \tag{3}$$

obeys the chiral algebra eq. (1) and satisfies the angular conditions required from Lorentz invariance. Since the $g_{\varrho\pi\pi}$ and $g_{\varrho\omega\pi}$ couplings from (3) come out larger but not very far from the experimental values, it is reasonable to think that the axial charge can be obtained through a suitable mixing procedure with simple transformation properties with respect to $SU_4 \times 0_3$:

The presence of rather strong decays $B \to \omega\pi$, $\sigma \to \pi\pi$, $f \to \pi\pi$, $A_1 \to \rho\pi$ and $A_2 \to \rho\pi$ suggests that the mixing operator at first order should transform

(*) Invited paper

as a 15 under SU_4 and a vector under 0_3. The requirement that it has $I = 0$ positive normality and $\Delta J_z = 0$ brings to the form

$$Z = (W \wedge M)_z \,, \tag{4}$$

where W is the isospin singlet spin 1 object of the 15 and M is a vector under 0_3.

With the charge defined as

$$X^a = U(\theta Z) A \left(\sigma_z \frac{\tau_a}{2}\right) U_+(\theta Z) \,,$$

where θ is a real parameter and

$$U(\theta Z) U^+(\theta Z) = 1 \,,$$

one gets several selection rules and branching ratios for the axial charge. Predictions typical of this approach are:

i) transverse decay for $\mathrm{B} \to \omega\pi$;

ii) forbidden π (1640) $\nleftrightarrow \mathrm{B}\pi$;

iii) longitudinal decay for $\pi(1640) \to \rho + \pi$.

Moreover, at first order in θ the ratio g_1/g_0 for $\mathrm{A}_1 \to \rho\pi$ is $\frac{1}{2}$ (pure d wave should give $-\frac{1}{2}$). The determination of Z is done starting from eq. (2) rotated with the tilt operator $U^+(\theta Z)$:

$$\left[A\left(\sigma_z \frac{\tau^+}{2}\right), \left[A\left(\sigma_z \frac{\tau^+}{2}\right), U^+(\theta Z) m^2 U(\theta Z)\right]\right] = 0 \,. \tag{2'}$$

Equation (2′) simply means that $U^+(\theta Z) m^2 U(\theta Z)$ behaves as a $(0,0) + (\frac{1}{2}, \frac{1}{2})^0$ under the $SU_2 \times SU_2$ algebra spanned by $A(1 \pm \sigma_z)(\tau_a/2)$.

If one expands m^2 in even powers of θ:

$$m^2 = m_0^2 + \theta^2 m_2^2 + \ldots \,,$$

and (2′) is required for the coefficients of all the powers in θ, three results show up:

i) $W_\pm$ is exactly the W spin operator: in fact it acts in the same way on $I = 0$ and $I = 1$ states;

ii) $M_+ = a^{\uparrow} + a_+^{\downarrow}$ where $L_3 = a^{\uparrow}a_+^{\uparrow} - a^{\downarrow}a_+^{\downarrow}$, $L_+ = a^{\uparrow}a_+^{0} + a^{0}a_+^{\downarrow}$:
$\boldsymbol{M}$ and $\boldsymbol{L}$ both act on the vector space defined by three quantum numbers:

$n_1 = a^{\uparrow}a_+^{\uparrow}$ = number of spin up

$n_2 = a^{0}a_+^{0}$ = number of neutral spin

$n_3 = a^{\downarrow}a_+^{\downarrow}$ = number of spin down.

Besides the angular momentum and its z component one has a third quantum number: $n = n_1 + n_2 + n_3$.

iii) $m_0^2 = A + \Delta n + B(\boldsymbol{L}\cdot\boldsymbol{S} + \frac{1}{2})(-1)^L$.
m_0^2 shows complete degeneracy between $I = 0$ and 1 states.

$m_0^2(J)$	Values of J allowed	C	Normality
$A - B/2 + \Delta J + 2\Delta K$	all	+	−
$A + B/2 + \Delta J + 2\Delta K$	all except 0	−	−
$A - B/2 - \Delta + (\Delta + B)J + 2\Delta K$	all even except 0	+	+
$A - \frac{3}{2}B + \Delta + (\Delta - B)J + 2\Delta K$	all even	+	+
$A + B/2 - \Delta + (\Delta - B)J + 2\Delta K$	all odd	−	+
$A + \frac{3}{2}B + \Delta + (\Delta + B)J + 2\Delta K$	all odd	−	+

There are six families of parallel equispaced trajectories where K gives the order of the daughter and is 0 for the parent trajectory.

It is worth stressing that while $\boldsymbol{M}$ is just the position operator in the non-relativistic three-dimensional harmonic oscillator, the term Δn is the energy of the same quantum system. One has to go deeper in this connection: now, one is brought to think of a q-$\bar{\text{q}}$ system bound by a harmonic potential.

Adler zero in the Chew-Low extrapolation of $\pi\pi$ and $\pi\mathcal{N}$ in OPE reactions (*)

J. BENECKE and F. WAGNER

Max-Planck-Institut für Physik und Astrophysik - München

1. Introduction.

Usually reactions like

$$\pi^+ p \to \pi^+ \pi^- \Delta^{++}, \qquad \pi^- p \to \pi^+ \pi^- n, \tag{1.1}$$

or

$$pp \to \pi^+ p \Delta^0, \qquad K^+ p \to \pi^+ p K^{*0}, \tag{1.2}$$

are assumed to be dominated by the exchange of a pion (OPE). Most information on $\pi\pi$ scattering comes from (1.1) by extrapolating in the mass, whereas (1.2) serves as a check, since $\pi\mathcal{N}$ amplitudes are known. We want to show that for low masses the way the on shell values are approached depends on the scattering lengths. Again (1.1) is used as a measurement, and the results of (1.2) provide a cross check.

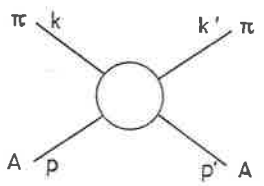

$k = (k_0, \vec{k}_{\pi})$, $k' = (k'_0, \vec{k}_{\pi'})$

$s = (k+p)^2 = (k'+p')^2$

$t = (k-k')^2$

$u = (k-p')^2$

Fig. 1. – Kinematics and notation.

All calculations are made under two assumptions: (for details see [1]) (A) Adler selfconsistency condition.

Provided there are no Born terms the amplitude $F(\pi A \to \pi A)$ vanishes if one of the π four momenta (*i.e.* k_μ, all kinematics are explained in Fig. 1)

(*) Invited paper presented by F. Wagner

vanishes (2).

$$F(s, t, u) = 0 \qquad \text{if } s = u = m_A^2\,,\ t = m_\pi^2\,,\ k^2 = -\Delta^2 = 0\,,$$

(M) Minimal dependence of F on Δ^2.

F depends on Δ^2 due to the mass dependence of t, u

$$t = -2\boldsymbol{k}_{\text{on}}^2 - \frac{\Delta^2 + m_\pi^2}{2s}(s + m_A^2 - m_\pi^2) - 2|\boldsymbol{k}_{\text{on}}||\boldsymbol{k}_{\text{off}}|\cos\theta\,, \tag{1.3}$$

$$u = 2m_A^2 + m_\pi^2 - \Delta^2 - s - t\,. \tag{1.4}$$

Any further strong Δ^2-dependence is neglected. This is reasonable if the 3π-spectrum becomes important not before the $A_{1,2}$ mass region. A non-trivial model satisfying (M) is the Lovelace-Veneziano model (3). Experimentally (M) can be tested in the Coulomb interference of $\pi^+\pi^-$ which should disappear off shell. In Sect. 2 (3) we apply (A) and (M) to $\pi\pi$ ($\pi\mathcal{N}$) scattering and in Sect. 4 possible influence of absorption is discussed.

2. $\pi\pi$ off shell scattering.

We expand the $\pi\pi$ amplitudes up to linear terms in s, t, u. Then crossing symmetry, (A) and (M) lead to the following S-wave amplitudes for $\pi^+\pi^\mp$ (4):

$$F_0(\pi^+\pi^-) = \frac{a^-}{2m_\pi^2}\left(s - m_\pi^2 - \left(1 + \frac{4a^+}{a^-}\right)\Delta^2\right), \tag{2.1}$$

$$F_0(\pi^+\pi^+) = -\frac{a^-}{2m_\pi^2}\left(s - m_\pi^2 + \left(1 + \frac{2a^+}{a^-}\right)\Delta^2\right), \tag{2.2}$$

a^+ (a^-) is the crossing even (odd) scattering length related to the usual isospin scattering lengths a_0, a_2 by

$$a^+ = \frac{1}{12}(2a_0 + 7a_2)\,, \qquad a^- = \frac{1}{12}(-2a_0 + 5a_2)\,,$$

a^+/a^- is predicted to be zero if there are no $I = 2$ σ terms (5) and in the Lovelace-Veneziano model (3). (2.1) vanishes along the line

$$\Delta_0^2(s) = (s - m_\pi^2)/\left(1 + \frac{4a^+}{a^-}\right). \tag{2.3}$$

This zero has been observed by Gutay *et al.* (6) in the *S-P* wave interference term (Fig. 2).

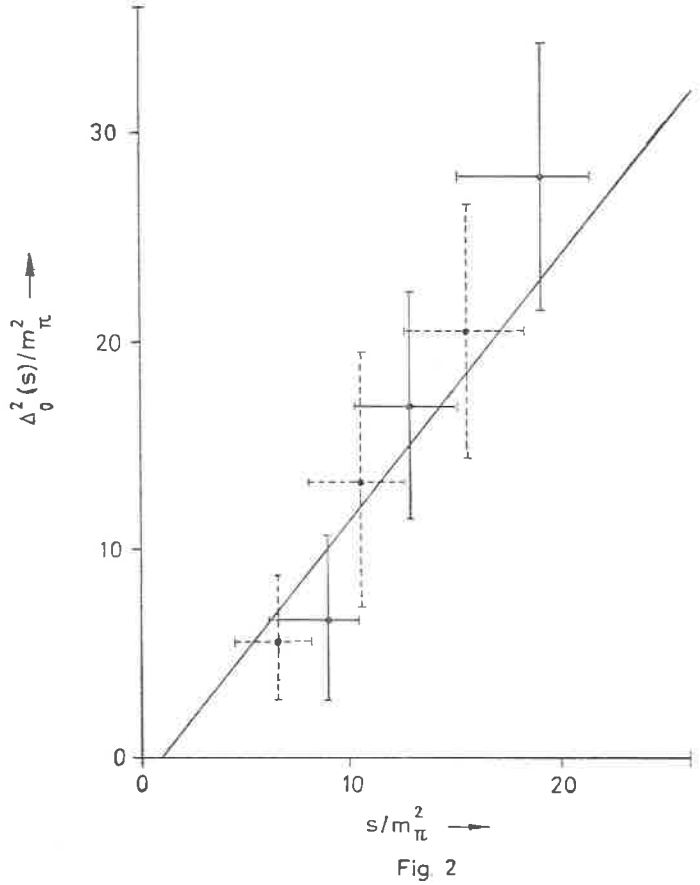

Fig. 2. – Comparison of the off shell zero in $\langle Y_1^0 \rangle$ (2.3) with experiment (from ref. (6)).

The deviation of slope from 1. in $\Delta_0^2(S)$ gives a value for a^+/a^-

$$a^+/a^- = 0.05 \pm 0.01 .$$

In contrast to $\pi^+\pi^-$ (2.2) predicts an *increase* of F^0 for $\pi^+\pi^+$. Available data on $\pi^+\pi^+$ confirm this behaviour (7). This difference is quite general: The Adler zero is outside the physical region for on shell scattering. Crossing symmetry moves it in some reactions into the physical region (like $\pi^+\pi^-$)

and in some away from it (like $\pi^+\pi^+$). A similar calculation can be done for πK and will be done for $\pi\mathcal{N}$ in the next section. We list reactions with off shell zero and with none in the following table

zero in	no zero
$\pi^+\pi^- \to \pi^+\pi^-$	$\pi^+\pi^+ \to \pi^+\pi^+$ $\pi^0\pi^- \to \pi^0\pi^-$ $\pi^+\pi^- \to \pi^0\pi^0$
$K^+\pi^- \to K^+\pi^-$	$K^+\pi^+ \to K^+\pi^+$ $K^+\pi^- \to K^0\pi^0$
$\pi^+p \to \pi^+p$	$\pi^-p \to \pi^-p$

Note that this predictions are derived from the assumption of small crossing even scattering lengths.

3. $\pi\mathcal{N}$ off shell scattering.

Due to the spin $\frac{1}{2}$ there are two invariant amplitudes $A^\pm$, $B^\pm$ for the crossing even (odd) amplitude $F^\pm$ in standard notation ([8])

$$F^\pm = \bar{u}\left(A^\pm + \tfrac{1}{2}\gamma(k+k')B^\pm\right) u. \tag{3.1}$$

The partial waves F_{lj} for total (orbital) angular momentum $j(l)$ satisfy the linearized unitarity relation for off shell scattering ([4])

$$\mathrm{Im}F^{\mathrm{off}}_{lj} = |k_{\mathrm{on}}| F^{\mathrm{on}*}_{lj} F^{\mathrm{off}}_{lj}, \tag{3.2}$$

(3.2) is solved by using a real Born term model

$$F^{\mathrm{off}}_{lj} = \frac{F^{\mathrm{off}}_{lj,B}}{F^{\mathrm{on}}_{lj,B}} \cdot F^{\mathrm{on}}_{lj}. \tag{3.3}$$

If F_B has the right S-wave scattering length, (3.3) reduces at threshold to

$$F^{\mathrm{off}}_{0j-\frac{1}{2}} = F^{\mathrm{off}}_{0\frac{1}{2},B} \tag{3.4}$$

The simplest choice for F_B with approximate right scattering length and the nucleon pole is

$$\left.\begin{aligned} A^+ &= \frac{g^2}{m}, \qquad A^- = 0, \\ B^- &= \frac{g^2}{m_N^2 - s} + \frac{g^2}{m_N^2 - u} + B_0^-, \qquad B^+ = \frac{g^2}{m^2 - s} - \frac{g^2}{m^2 - u}. \end{aligned}\right\} \tag{3.5}$$

If the constant B_0^- is absorbed in the scattering lengths we find for π^+p, from (3.5) at $s = (m + m_\pi)^2$

$$F_{0\frac{1}{2}}(\pi^+\mathrm{p}) = a_{\pi^+\mathrm{p}} + \frac{m_N}{(m_N + m_\pi)^2} \frac{g^2/4\pi}{(2m_N - m_\pi)^2} \frac{\Delta^2 + m_\pi^2}{1 + \dfrac{\Delta^2 + m_\pi^2}{2m_N^2 + m_\pi m_N - m_\pi^2}}, \tag{3.6}$$

$$F_{0\frac{1}{2}}(\pi^-\mathrm{p}) = a_{\pi^-\mathrm{p}}, \tag{3.7}$$

(3.6) predicts a zero around $\Delta^2 = 5m_\pi^2$, since $a_{\pi^+\mathrm{p}}$ is negative experimentally ($a_{\pi^+\mathrm{p}} = -0.103 m_\pi^{-1}$ from [10]), whereas no effect should be seen in π^-p. At higher energies we use (3.3) to calculate the off shell amplitude from phase shifts [9]. Replacing the Born model (3.5) by more refined models we found only corrections to (3.6) of the order m_π^2/m_ϱ^2, m_π^2/m_N^2: We investigated the following models:

1) G. Höhler *et al.* have given corrections to the nucleon pole in terms of a power series in $s - u$, t [10].
2) A^- and B^- can be described by adding the nucleon and the ϱ Born term [11]. A^+, B^+ we parametrize by σ and $\mathcal{N}$ poles constrained by (A).
3) A Veneziano model using
   t singularities exchange degenerate ϱ, f.
   s, u singularities exchange degenerate $\mathcal{N}$, Δ.

Free constants in (2) and (3) have been adjusted to give the same scattering length as (1). All these models assume that σ-terms are small which has come recently into question [12]. For zero S-wave also the $\langle Y_1^0 \rangle$ moment vanishes at low energy. For higher energies this zero moves to higher Δ^2, similar to the $\pi^+\pi^-$-case. Since none of the models for F_B describe the Δ resonance correctly, we expect that our calculations are valid only below $\sqrt{s} = 1236$.

Figure 3 shows the similar plot for π^+p as Fig. 2 for $\pi^+\pi^-$, using the Born term model (1). At this conference data on $K^+p \to K^\circ\pi^+p$ have been pre-

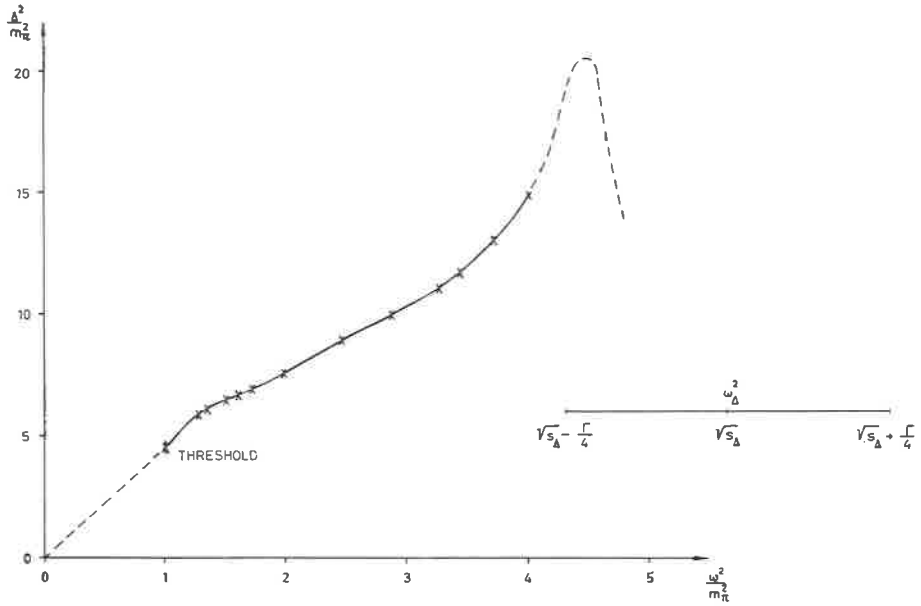

Fig. 3. – Same prediction for π^+p ($\omega = (1/2m_N)(s - m_N^2 - m_\pi^2)$). On the right $\sqrt{s_\Delta} = 1236$ and $\sqrt{s_\Delta} \pm \frac{\Gamma}{4}$ is indicated.

sented ([12]). Fig. 4 shows $\langle Y_1^0 \rangle$ as function of Δ^2 for three masses. The scattering length of ([10]) are in good agreement with Chew Low extrapolation of $\langle Y_1^0 \rangle$. If $\langle Y_1^0 \rangle$ is integrated over Δ^2, it should be small below 1236 MeV. This has been found earlier by Colton *et al.* ([14,15]), whereas no effect in π^-p is seen in agreement with our model.

4. Possible influence of absorption and conclusion.

As pointed out by Schlein ([15]), the similarity of $\langle Y_1^0 \rangle$ for π^+p in three reactions $\pi^+p \to \varrho^0\pi^+p$, $K^+p \to K^\circ\pi^+p$ and $pp \to \Delta^0\pi^+p$ makes it plausible that the zero in $\langle Y_1^0 \rangle$ is due to an off shell effect and not caused for example by absorption. For one reaction like $\pi^+\pi^-$ it is always possible to produce a mass dependent zero in $\langle Y_1^0 \rangle$ by assuming a strong mass dependent absorption constant $C(S_{\pi\pi})$. People willing to accept this are faced with the

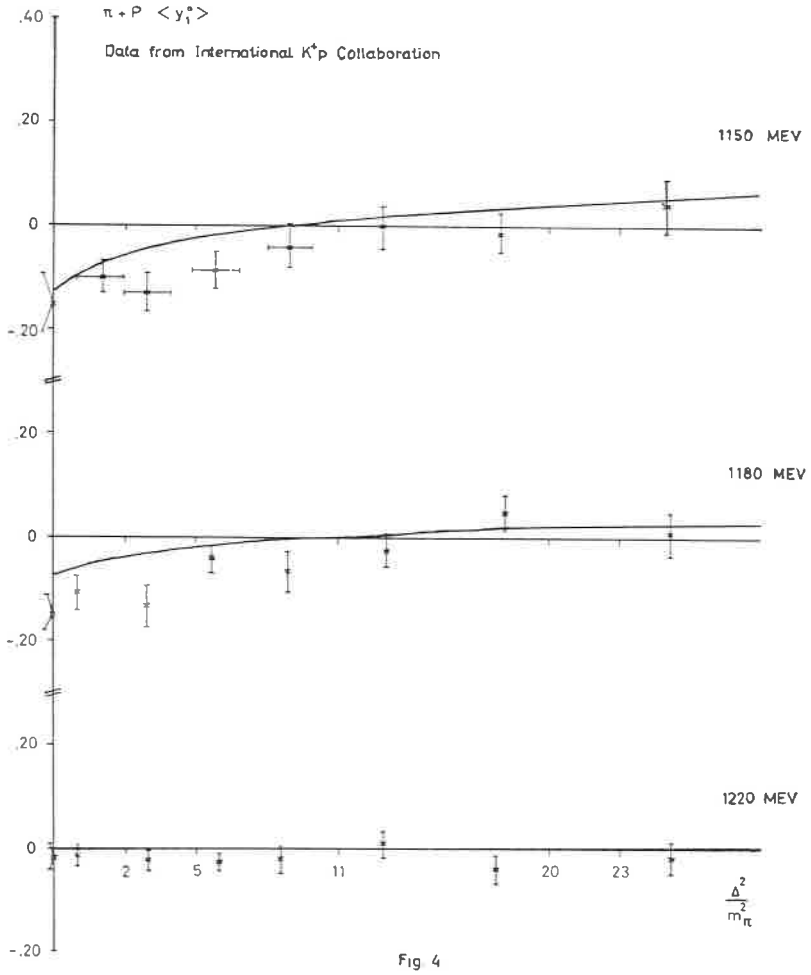

Fig. 4. – $\langle Y_1^0 \rangle$ fr $\pi^+ p$ as function of Δ^2 for three energies below 1200 MeV.

difficulty that $\pi^-\pi^0$ behaves different from $\pi^+\pi^-$ (no zero in $\langle Y_1^0 \rangle$ for $\pi^0\pi^-$). However, the assumption that the exotic $I=2$ part can be approximated by an effective single particle state (as usual in absorption calculations) may be wrong. This argument doesn't apply to the pair $pp \to \Delta^0\pi^+ p$ and $pp \to$ $\to \Delta^{++}\pi^- p$. There should be no difference in the absorption calculation. This qualitative argument leads us to believe that the observed zero's in $\pi^+\pi^-$, $\pi^+ p$ are due to an off shell effect and can be affected slightly by an absorption effect. Under the assumptions (*A*) and (*M*) the position of the

zero in π^+p are in agreement with the a_{π^+p} scattering length and small σ-terms. Therefore one concludes that the observed moving zero of $\langle Y_1^0 \rangle$ for $\pi^+\pi^-$ is in fact a measurement of the ratio of scattering length.

Acknowledgements.

We thank the members of ([13]) for permission to use their data. We are grateful to Professor P. E. Schlein for drawing our attention to this problem and for discussions.

REFERENCES

1) J. Benecke and F. Wagner: to be published.
2) S. L. Adler: *Phys. Rev.*, **137** B, 1022 (1965).
3) C. Lovelace: *Phys. Lett.*, **28** B, 264 (1968).
4) F. Wagner: *Nuovo Cimento*, **64** A, 189 (1969).
5) S. Weinberg: *Phys. Rev. Lett.*, **17**, 616 (1966).
6) L. J. Gutay, F. T. Meiere and J. H. Scharenguivel: *Phys. Rev. Lett.*, **23**, 431 (1969).
7) J. P. Baton, G. Laurens and J. Reignier: *Phys. Lett.*, **25** B, 419 (1967) and ([4]).
8) G. F. Chew, M. L. Goldberger, F. E. Low and Y. Nambu: *Phys. Rev.*, **106**, 1337 (1957).
9) C. Lovelace: *Irvine Conference* (1967). We thank Prof. C. Lovelace for private communication of numbers.
10) G. Höhler, H. Schlaile and R. Strauss: *Veits. Phys.*, **229**, 217 (1969).
11) G. Höhler, J. Baacke and F. Steiner: *Zeits. Phys.*, **214**, 381 (1968).
12) T. P. Cheng and R. Dashen: *Phys. Rev. Lett.*, **26**, 594 (1971). The result has been called in question by G. Höhler *et al.*: Karlsruhe preprint (March 1971).
13) V. Henri: *Introductory talk on* $K\pi$ *at this Conference* (1971); International K^+p Collaboration: *Phys. Lett.* (1971).
14) E. Colton, P. E. Schlein, E. Gellert and G. A. Smith: *Phys. Rev.*, D 1971, 1063 (1971).
15) P. E. Schlein: Review talk at *Argonne Conference* (1969), p. 1.

SU_3 symmetry breaking in radiative meson decays (*)

P. SINGER

Department of Physics, Technion-Israel Institute of Technology - Haifa

During recent years, quite a few models have been proposed in order to describe the radiative decays of vector and pseudoscalar mesons. One of the most successful is the vector-meson-dominance model of Gell-Mann-Sharp and Wagner [1], (G.S.W.), which gives a fairly reliable qualitative picture of both strong and electromagnetic decays. However, recent measurements on π, η, ω and φ radiative decays show that the SU_3 unbroken version of this approach is unable to account for the experimental values by factors ranging from 2 to 5. Moreover, inclusion of SU_3 breaking through ω-φ and η-X^0 mixing only, although improving the situation [2-4], does not seem to suffice for obtaining satisfactory agreement with all the data.

In this talk we review the vector-meson-dominance approach to this problem of Brown, Munczek and Singer [5,6] (B.M.S.), who use an effective Lagrangian with vector gauge fields and current mixing, and allow for the most general form consistent with octet-broken SU_3 for the VVP interaction term of the Lagrangian [7]. In presenting the formalism and calculations, we update the results of B.M.S. by using recent experimental data and furthermore extend their range of predictions by considering the new information available from the measurements on the $\varphi \to \eta\gamma$ and $X^0 \to 2\gamma$ decay modes.

Our underlying phenomenological Lagrangian responsible for PVV and PPV interactions is

$$\mathscr{L} = \mathscr{L}_{\mathrm{V}} + \mathscr{L}_{\mathrm{P}} + \mathscr{L}_{\mathrm{PVV}} , \tag{1}$$

where

$$\mathscr{L}_{\mathrm{P}} = \tfrac{1}{2} D_\mu P^a D_\mu P^a - \tfrac{1}{2} \mu^2_{ab} P^a P^b , \tag{2}$$

(*) Invited paper

with the covariant derivative

$$D_\mu F^a \equiv \partial_\mu F^a - g f^{abc} V_\mu^b F^c, \tag{3}$$

inducing the V → PP decays, and $a, b = 1, \ldots, 8$.

The Lagrangian for the nine vector fields, assumed to be of Yang-Mills type, is

$$\begin{aligned}\mathscr{L}_{\mathrm{V}} = &-\tfrac{1}{4} K^{ab} V^a_{\mu\nu} V^b_{\mu\nu} + \tfrac{1}{2} m^2 V^a_\mu V^b_\mu - \tfrac{1}{4} K^{00} V^0_{\mu\nu} V^0_{\mu\nu} + \\ &+ \tfrac{1}{2} m^2 V^0_\mu V^0_\mu - \tfrac{1}{2} K^{80} V^8_{\mu\nu} V^0_{\mu\nu}\,,\end{aligned} \tag{4}$$

where

$$V^a_{\mu\nu} = \partial_\mu V^a_\nu - \partial_\nu V^a_\mu - g f^{abc} V^b_\mu V^c_\nu\,, \tag{5}$$

while $K^{ab} = \delta^{ab} + \sqrt{3}\zeta d^{ab8}$ are the symmetry-breaking factors causing also the mass differences among the vector mesons. For the interacting VVP term we take

$$\begin{aligned}\mathscr{L}_{\mathrm{PVV}} = &\tfrac{1}{4}\,\varepsilon_{\alpha\beta\mu\nu}(h D^{abc} V^a_{\alpha\beta} V^b_{\mu\nu} P^c + \\ &+ \lambda D^{ab} V^a_{\alpha\beta} V^0_{\mu\nu} P^b + h_0 \Delta^{ab} V^a_{\alpha\beta} V^b_{\mu\nu} P_0)\,.\end{aligned} \tag{6}$$

In (6) we allow for the most general form consistent with octet-broken SU_3 for the coupling parameters, hence

$$\begin{aligned}D^{abc} = &\, d^{abc} + \sqrt{3}\;\varepsilon_1 d^{abd} d^{d8c} + \tfrac{1}{2}\sqrt{3}\varepsilon_2 (d^{acd} d^{d8b} + \\ &+ d^{bcd} d^{d8a}) + (\varepsilon_3/\sqrt{3})\,\delta^{ab}\delta^{c8},\end{aligned} \tag{7}$$

$$D^{ab} = \delta^{ab} + \sqrt{3}\,\varepsilon_4 d^{ab8}, \tag{8}$$

$$\Delta^{ab} = \delta^{ab} + \sqrt{3}\,\beta d^{ab8}. \tag{9}$$

Diagonalizing (5) in terms of the physical particle fields one obtains

$$\left.\begin{aligned}&V^{1,2,3}_\mu = (1/\sqrt{K_\varrho})\,\varrho^{1,2,3}_\mu\,; \qquad V^{4,5,6,7}_\mu = (1/\sqrt{K_{K^*}})K^{4,5,6,7}_\mu \\ &V^8_\mu = \frac{\sin\theta}{\sqrt{K_\omega}}\,\omega_\mu - \frac{\cos\theta}{\sqrt{K_\varphi}}\,\varphi_\mu\,; \\ &V^0_\mu = \frac{\cos\theta}{\sqrt{K_\omega}}\,\omega_\mu + \frac{\sin\theta}{\sqrt{K_\varphi}}\,\varphi_\mu\,,\end{aligned}\right\} \tag{10}$$

where $K_i = m^2/m_i^2$ and $m = 847$ MeV, $\theta = 27.5°$. Finally, the effective electromagnetic interaction is added in the vector-dominance formalism ([13,14]) as

$$\mathscr{L}_{\text{em}} = \frac{em^2}{g} [K_\varrho^{-\frac{1}{2}} \varrho_\mu^3 + (3K_\omega)^{-\frac{1}{2}} \omega_\mu \sin\theta - (3K_\varphi)^{-\frac{1}{2}} \varphi_\mu \cos\theta] A_\mu \,. \tag{11}$$

The Lagrangian (1)+(11) used in the tree approximation, accounts for the various strong and electromagnetic decays of the types $V \to P + P$, $V \to$ $\to (V) + P \to P + P + P$, $V \to P + \gamma$, $P \to V + \gamma$ as well as for additional 3-body decays like $V \to P + \gamma + \gamma$ and $V \to P + P + \gamma$ not discussed here. The « unbroken » form has the coupling constants h, λ and h^0 of (6), as well as g of (3). The symmetry breaking appears in our treatment in two different forms: firstly, the diagonalization of (4) in terms of the physical fields, introduces the mixing angle as well as mass factors (K_i) into the various vertices. Secondly, we allow for SU_3 breaking in the VVP coupling constants, introducing the parameters β, ε_1-ε_4 defined in eqs. (7)-(9). The two types of breaking are obviously unrelated, and one could try various other types of mixing for the vector meson Lagrangian, which would then correct by different mass-factors ([15]) the VVP or VPP vertices. In addition to the known theoretical preference for current mixing, it is well known that it improves markedly the agreement with experiment for the $V \to P + P$ decays ([16]). We shall show that the same is true for the decays related to the VVP vertices.

Let us now proceed with the actual calculation. For simplification and based on the recent Orsay experiment ([17]) giving $\Gamma(\varphi \to \pi\gamma) = (7.6 \pm 3)$ keV (compare to $\Gamma(\omega \to \pi\gamma) \simeq 1$ MeV!), we take $\Gamma(\varphi \to \pi\gamma) = 0$ which then gives the relation

$$\lambda = 2h(1 + \varepsilon_1)(\cot\theta)/\sqrt{3}(1 + \varepsilon_4) \,. \tag{12}$$

The SU_3 breaking corrections we mentioned modify the amplitudes for the various decays by factors containing the masses of the vector mesons, the vector-mesons mixing angle and the parameters β, ε_1-ε_4 (See *e.g.* Table I of Ref. ([5])). We first consider three decays $\omega \to 3\pi$, $\omega \to \pi\gamma$, $\pi^0 \to 2\gamma$ which have the same ε-type breaking. The factors multiplying the invariant Feynman amplitude are in these cases:

$$\omega \to 3\pi: \quad -4hg\{(1 + \varepsilon_1)/K_\varrho\sqrt{3K_\omega} \sin\theta\} \,,$$

$$\omega \to \pi\gamma: \quad -\frac{2he}{g}\{(1 + \varepsilon_1)/\sqrt{3K_\omega} \sin\theta\} \,,$$

$$\pi \to 2\gamma: \quad -\frac{4he^2}{3g^2}\{1 + \varepsilon_1\} \,.$$

The factors displayed in curly brackets approach unity in the SU_6 - symmetric limit (*i.e.* $\beta, \varepsilon_1 - \varepsilon_4 = 0, K_i = 1, \sin\theta = 1/\sqrt{3}$). Now considering these decays, which all depend on $h(1+\varepsilon_1)$ but on different powers of g, we have a consistency test for our current-mixing hypothesis if we can find values for $h(1+\varepsilon_1)$ and g to account for all three decays. Using

$$g^2/4\pi = 3.20\,, \qquad (m_\pi^2 h^2/4\pi)(1+\varepsilon_1)^2 = 0.10\,, \tag{13}$$

we obtain the following decay rates, to be compared with the experimental values ([18]):

$$\Gamma_{\text{th}}(\omega \to 3\pi) = 10.3 \text{ MeV}\,; \qquad \Gamma_{\text{exp}}(\omega \to 3\pi) = (10.3 \pm 1.1) \text{ MeV}\,,$$

$$\Gamma_{\text{th}}(\omega \to \pi\gamma) = 1.20 \text{ MeV}\,; \qquad \Gamma_{\text{exp}}(\omega \to \pi\gamma) = (1.06 \pm 0.21) \text{ MeV}\,,$$

$$\Gamma_{\text{th}}(\pi_0 \to 2\gamma) = 7.9 \text{ eV}\,; \qquad \Gamma_{\text{exp}}(\pi_0 \to 2\gamma) = (7.8 \pm 1.0) \text{ eV}\,.$$

While the uncorrected G.S.W. model gives discrepancies of 2 or more in comparing these decays with each other, the remarkable agreement shown above gives one confidence in the current-mixing treatment for the vector-mesons Lagrangian. Furthermore, from g one obtains also the $\rho\pi\pi$ coupling constant, as $g^2_{\varrho\pi\pi}(0) = g/\sqrt{K_\varrho}$. With the value from (13) one has $g^2_{\varrho\pi\pi}(0)/4\pi = 2.63$, so that we get the gratifying result

$$\Gamma_{\varrho\to\pi\pi} = 137 \text{ MeV}\,, \qquad \text{if} \qquad g_{\varrho\pi\pi}(0) \simeq g_{\varrho\pi\pi}(m_\varrho^2)\,.$$

Turning to the η decays, we now consider the decays $\eta \to \gamma\gamma$, $\eta \to \pi\pi\gamma$ and $\pi \to 2\gamma$. The first two have the following coupling parameters:

$$\eta \to 2\gamma: \qquad \frac{4he^2}{3\sqrt{3}g^2}\{1 - \varepsilon_1 + 2\varepsilon'\} \qquad ; \ \varepsilon' = \varepsilon_2 + \varepsilon_3\,.$$

$$\eta \to \pi\pi\gamma: \qquad \frac{4he}{\sqrt{3}}\left\{\frac{1}{K_\varrho}(1 - \varepsilon_1 + \varepsilon')\right\}.$$

The calculation of these rates with $\varepsilon_i = 0$ gives fairly large discrepancies when compared to experiments, as the mass-factors are insufficient to correct for discrepancies of factors as large as six. Using the experimental values ([18]) $\Gamma(\eta \to 2\gamma) = 1.02$ keV, $\Gamma(\eta \to \pi\pi\gamma) = 124$ keV, $\Gamma(\pi^0 \to 2\gamma) = 7.8$ eV, we

obtain, when comparing with the theoretical rates calculated from (1) and (11), two equations:

$$(1-\varepsilon_1+2\varepsilon')^2 = 5.86(1+\varepsilon_1)^2\,;$$

$$(1-\varepsilon_1+\varepsilon')^2 = 1.56(1+\varepsilon_1)^2\,. \tag{14}$$

These equations give four sets of solutions for ε_1 and ε', two of which can be excluded as they lead later on ([5]) to absurdly large rates for $\varphi, \omega \to \eta + \gamma$. The two admissible solutions are

$$\left.\begin{array}{lll} \varepsilon_1 = 0.85\,; & \varepsilon' = \quad 2.16 & \text{(A)} \\ \varepsilon_1 = 1.18\,; & \varepsilon' = -2.54 & \text{(B)} \end{array}\right\} \tag{15}$$

These solutions enable us to calculate the rates for $K^{*0} \to K^0\gamma$, $\rho \to \pi\gamma$ and $\rho \to \eta\gamma$ whose matrix elements have factors

$$K^{*0} \to K^0\gamma: \quad -\frac{4he}{3g}\left\{\frac{1}{\sqrt{K_{K^*}}}\left(1-\frac{\varepsilon_1}{2}\right)\right\}$$

$$\rho \quad \to \pi\gamma: \quad -\frac{2he}{3g}\left\{\frac{1+\varepsilon_1}{\sqrt{K_\rho}}\right\}$$

$$\rho \quad \to \eta\gamma: \quad \frac{2he}{\sqrt{3}g}\left\{\frac{1}{\sqrt{K_\rho}}(1-\varepsilon_1+\varepsilon')\right\}.$$

Our predictions for these decays are then

$$\Gamma_{\text{th}}(K^{*0} \to K^0\gamma) = \left\{\begin{array}{ll} 24 \text{ keV} & \text{(Sol A)} \\ 13 \text{ keV} & \text{(Sol B)} \end{array}\right\} \tag{16a}$$

$$\Gamma_{\text{th}}(\rho \to \pi\gamma) = 79 \text{ keV}\,; \quad \Gamma_{\text{th}}(\rho \to \eta\gamma) = 48 \text{ keV}\,. \tag{16b}$$

The results in (16*b*) obtain for both solutions A and B.

Equation (16*a*) is the most striking prediction of this model, implying that $K^{*0} \to K^0\gamma$ should be one order of magnitude smaller than the symmetry value. At this point, we should like to stress that due to the experimental uncertainty in the values of the various decay rates (mainly those related to

η-meson), which go as high as 20÷30%, our results should be considered mainly in regard to their qualitative value, and more firm predictions can be made only when these will reduce to 5÷10% ([19]).

So far, there is no experimental measurement for this decay, but photoproduction experiments ([20]) on $\gamma + p \to \Sigma^+ + K^0$ (in which a K^{*0} is exchanged) seem to confirm the effect predicted here.

For the $K^{*+} \to K^+\gamma$ decay, the coupling-factor is

$$K^{*+} \to K^+\gamma: \quad \frac{2he}{3g}\left\{\frac{1}{\sqrt{K_{K^*}}}\left(1-\frac{\varepsilon_1}{2}+\frac{3\varepsilon_2}{4}\right)\right\}.$$

Hence, unless $\varepsilon_2 = 0$, the ratio between the rates for the charged and neutral K* radiative decays is no longer $\frac{1}{4}$. From considerations of the electromagnetic mass-differences of pseudoscalar mesons, it has been suggested ([21]) that ε_2 is large and would induce a rate for $K^{*+} \to K^+ + \gamma$ of the order of 1 MeV (an order of magnitude larger than the symmetry value). So far there is no other evidence on its magnitude, but more information can be obtained from an analysis of weak radiative decays of K-mesons ([22]).

From the above considerations, it is clear that a measurement of $K^* \to K\gamma$ decays is highly desirable, as it provides a sensitive test for the type of model described here.

The decays $\varphi \to \eta\gamma$ and $\omega \to \eta\gamma$ have the factors:

$$\varphi \to \eta\gamma: \quad \frac{4\sqrt{2}he}{3\sqrt{3}g}\left\{\frac{\sqrt{\frac{3}{2}}\cos\theta}{2\sqrt{K_\varphi}}\left[1-\varepsilon_1-\varepsilon'+\frac{1+\varepsilon_1}{1+\varepsilon_4}(1-\varepsilon_4)\right]\right\},$$

$$\omega \to \eta\gamma: \quad \frac{2he}{3\sqrt{3}g}\left\{\frac{\sqrt{3}}{\sqrt{K_\omega}\sin\theta}\left[-\sin^2\theta(1-\varepsilon_1-\varepsilon')+\cos^2\theta\,\frac{(1+\varepsilon_1)(1-\varepsilon_4)}{1+\varepsilon_4}\right]\right\}.$$

From the recent measurement ([17]) $\Gamma_{\text{exp}}(\varphi \to \eta\gamma) = 77 \pm 23$ keV we can calculate the value of ε_4 for solutions *A* and *B* and then predict the rate for $\Gamma(\omega \to \eta\gamma)$ in our model. For each of solutions *A* and *B* one gets two values for ε_4, as follows:

$$\varepsilon_4 = -0.32 \quad \text{or} \quad 0.65 \qquad \text{(Sol A)}, \tag{17a}$$

$$\varepsilon_4 = \quad 1.53 \quad \text{or} \quad -3.12 \qquad \text{(Sol B)}. \tag{17b}$$

From either (17*a*) or (17*b*) one obtains the same two alternative predictions,

namely

$$\Gamma_{\text{th}}(\omega \to \eta\gamma) = 188\,\text{keV} \qquad \text{or } 9.5\,\text{keV}\,. \tag{18}$$

The first of the two possible values should soon be verifiable as it is some 2% of the total ω-decay rate.

Turning now to decays involving X^0, we write down the coupling factors ([6]) entering the four possible modes:

$$X^0 \to \rho\gamma: \qquad (2h_0 e/g)\{(1+\beta)/\sqrt{K_\rho}\}\,,$$

$$X^0 \to \omega\gamma: \qquad (2h_0 e/3g)\{(1-\beta)\sqrt{3}\,(\sin\theta)/\sqrt{K_\omega}\}\,,$$

$$X^0 \to 2\gamma: \qquad (8h_0 e^2/3g^2)\{\tfrac{1}{2}(2+\beta)\}\,,$$

$$\varphi \to X^0\gamma: \qquad -(2\sqrt{2}\,h_0 e/3g)\{(1-\beta)\sqrt{\tfrac{3}{2}}\,(\cos\theta)/\sqrt{K_\varphi}\}\,.$$

So far, we have no information on absolute decay rates for the X^0-meson, but we know $\Gamma^{X^0}_{\text{tot}} < 4$ MeV, and as $X^0 \to \rho\gamma$ accounts for approx. 30% of the total rate ([18]), one has $\Gamma(X^0 \to \rho\gamma) < 1.2$ MeV. The measurement of the ratio of two of the decays involving X^0 would enable us to determine the symmetry-breaking parameter β. An exception to this is the ratio of the decay $\varphi \to X^0\gamma$ and $X^0 \to \omega\gamma$, which is independent of β and is predicted in our model to be

$$\Gamma(\varphi \to X^0\gamma)/\Gamma(X^0 \to \omega\gamma) = 0.11\,. \tag{19}$$

At this point it is worthwhile to point out some differences and similarities between our treatment and the model of Dalitz and Sutherland (D.S.), who use η-X^0 mixing as the SU_3-breaking mechanism. In our model the rate $\Gamma(X^0 \to \omega\gamma)/\Gamma(X^0 \to \rho\gamma)$ depends on the symmetry-breaking parameter β, while the same ratio is unaffected by the η-X^0 mixing angle in the D.S. model and turns out to be $0.057 \div 0.084$ for an ω-φ mixing angle ranging between $(27.5 \div 35)^0$. On the other hand, the ratio $\Gamma(X^0 \to 2\gamma)/\Gamma(X^0 \to \rho\gamma)$ depends on the symmetry-breaking parameter in both models and formally in a similar way, while the ratio given in (19) depends on the symmetry-breaking parameter only in the D.S. model.

The numerical values for the various ratios are in our model

$$\Gamma(X^0 \to \omega\gamma) / \Gamma(X^0 \to \rho\gamma) = 5.7 \cdot 10^{-2}(1-\beta)^2/(1+\beta)^2 , \tag{20}$$

$$\Gamma(X^0 \to 2\gamma) / \Gamma(X^0 \to \rho\gamma) = 5.2 \cdot 10^{-2}(1+\tfrac{1}{2}\beta)^2/(1+\beta)^2 , \tag{21}$$

$$\Gamma(\varphi \to X^0\gamma)/\Gamma(X^0 \to \rho\gamma) = 6.2 \cdot 10^{-3}(1-\beta)^2/(1+\beta)^2 . \tag{22}$$

Recently, there have been several reports on the detection of the $X^0 \to 2\gamma$ mode. A comparison of the experimental $X^0 \to 2\gamma/X^0 \to \rho\gamma$ ratio would enable us to determine β and consequently predict the percentage of the $X^0 \to \omega\gamma$ partial decay rate. Unfortunately, the various experimental data available at present for $X^0 \to 2\gamma$ differ widely, ranging ([18,24]) between 1.85% to 6.5%, with fairly large uncertainties. We present our predictions for the $X^0 \to \omega\gamma/X^0 \to \rho\gamma$ ratio for several possible values of the parameter β, determined from eq. (21) by taking for $X^0 \to 2\gamma/X^0 \to \rho\gamma$ several values within the existing experimental range.

TABLE I.

$X^0 \to 2\gamma$ (% of $\Gamma^{X^0}_{\text{tot}}$)	1.56%	1.8%	2.5%	4.2%	5.1%	6.6%
$(X^0 \to 2\gamma)/(X^0 \to \rho\gamma)$ (using $\Gamma(X^0 \to \rho\gamma) = 0.3\Gamma^{X^0}_{\text{tot}}$)	0.052	0.06	0.083	0.14	0.17	0.22
β	0	−0.12	−0.34	−0.56	−0.62	−0.68
$(X^0 \to \omega\gamma)/(X^0 \to \rho\gamma)$	0·057	0.092	0.23	0.71	1.0	1.57

The relation displayed in this table between $X^0 \to 2\gamma/X^0 \to \rho\gamma$ and $X^0 \to \gamma\omega/X^0 \to \rho\gamma$, is another specific prediction of our model. As opposed to other models ([2-4,23]), our approach can accommodate any ratio for $X^0 \to 2\gamma/X^0 \to \rho\gamma$; however, by determining β from it, we then get a definite prediction for $X^0 \to \omega\gamma/X^0 \to \rho\gamma$ and we have thus another sensitive test of the model. The measurement of this ratio therefore becomes of great interest.

Recently, Brown and Munczek discussed ([25]) the VVP interactions in the context of chiral $SU_3 \otimes SU_3$ symmetry. Assuming that it transforms like a combination of zeroth and eighth components of a $(3,3^*) \oplus (3^*,3)$ representation, they found in a Lagrangian treatment that they reproduce exactly the parametrization discussed here of refs. ([5]) and ([6]), with one constraint relating β, h_0 to h, ε_1 . As this formulation has one less parameter, one can

use the value of β determined in Table I, as well as the values of h and ε_1 determined from eqs. (13) and (15), to calculate h_0, and hence the absolute rates for the X^0 partial modes.

The constraint obtained in ref. ([25]) is ([26])

$$h_0 = \sqrt{\frac{2}{3}}\,\frac{h}{\beta}\,\varepsilon_1 . \tag{23}$$

As for both solutions (*A*) and (*B*) of eq. (15) ε_1 is quite close to 1, we approximate here $\varepsilon_1 = 1$ and then from (13) we get

$$\frac{m_\pi^2 h_0^2}{4\pi} = \frac{2}{3}\,\frac{0.1\varepsilon_1^2}{(1+\varepsilon_1)^2\beta^2} = \frac{0.017}{\beta^2} . \tag{24}$$

The decay rate for $X^0 \to \rho\gamma$ is given in our model by

$$\Gamma(X_0 \to \rho\gamma) = \frac{(m_\pi^2 h_0^2/4\pi)\alpha(M_X^2 - M_\varrho^2)^3(1+\beta)^2}{M_X^3 m_\pi^2 K_\varrho (g^2/4\pi)} . \tag{25}$$

Using (24) one obtains $(X^0 \to \rho\gamma) = 3.44 \times 10^{-2}\ (1+\beta)^2/\beta^2$ MeV.

Considering the values $\beta = -0.12, -0.34, -0.56$ which seem to cover the most probable range for the $X^0 \to 2\gamma$ percentage, one predicts from the relation (23) of Brown and Munczek:

TABLE II.

β	$\Gamma(X^0 \to \rho\gamma)$ (MeV)
−0.12	1.85
−0.34	0.13
−0.56	0.02

To summarize, we emphasize that in our approach the large discrepancies from the SU_3-symmetry observed in η-decays are related to similar departures in $K^* \to K\gamma$ decays, unlike the models which try to account for this by η-X^0 mixing only. The most decisive tests for the model are summarized in eqs. (16*a*), (16*b*), (18), (19) and Table I. However, the numerical predictions should all be considered with the reservation of the still existing experimental uncertainties in the various imput numbers used.

REFERENCES

1) M. GELL-MANN, D. SHARP and W. G. WAGNER: *Phys. Rev. Lett.*, **8**, 261 (1962).
2) E. CREMMER: *Nucl. Phys.*, B **14**, 52 (1969).
3) A. BARACCA and A. BRAMON: *Nuovo Cimento*, **69** A, 613 (1970).
4) M. GOURDIN: *Radiative decays of mesons* (Proceedings of this Conference).
5) L. M. BROWN, H. MUNCZEK and P. SINGER: *Phys. Rev. Lett.*, **21**, 707 (1968).
6) P. SINGER: *Phys. Rev.*, D **1**, 86 (1970).
7) Recently several other authors have suggested models for radiative decays which include SU_3-breaking, a very incomplete list being given by refs. ([8-12]). These models have some features in common with the approach discussed by us, but time limitation prevents me from mentioning any details specific to them.
8) RIAZUDDIN and A. Q. SARKER: *Phys. Rev. Lett.*, **20**, 1455 (1968).
9) G. J. GOUNARIS: *Nuovo Cimento*, **53** A, 565 (1968); *Phys. Rev.*, D **1**, 1426 (1970); D **2**, 2734 (1970).
10) S. L. GLASHOW, R. JACKIW and S. S. SHEI: *Phys. Rev.*, **187**, 1916 (1969).
11) W. ALLES: *Lett. Nuovo Cimento*, **3**, 163 (1970); **4**, 137 (1970).
12) A. ESTEVE, J. LEON and A. TIEMBLO: *Lett. Nuovo Cimento*, **1**, 30 (1971).
13) N. M. KROLL, T. D. LEE and B. ZUMINO: *Phys. Rev.*, **157**, 1376 (1967).
14) T. D. LEE and B. ZUMINO: *Phys. Rev.*, **163**, 1667 (1967).
15) L. H. CHAN, L. CLAVELLI and R. TORGERSON: *Phys. Rev.*, **185**, 1754 (1969).
16) J. J. SAKURAI: *Phys. Rev. Lett.*, **19**, 803 (1967).
17) G. COSME: Proceedings of this Conference.
18) N. BARASH-SCHMIDT *et al.*: *Particle Properties Tables* (April 1971).
19) For instance, our values for ε_1 and ε' (eq. (15)) differ by (10÷20)% from those in ref. ([5]), due to the appropriate changes which occurred lately in the experimental values. This obviously propagates into the predictions for $K^{*0} \to K^0\gamma$. However, the main qualitative feature of a large symmetry breaking is retained.
20) M. G. ALBROW *et al.*: *Phys. Lett.*, **29** B, 54 (1969); *Nucl. Phys.*, B **23**, 509 (1970).
21) L. M. BROWN, H. MUNCZEK and P. SINGER: *Phys. Rev.*, **180**, 1474 (1969).
22) M. MOSHE and P. SINGER: Phys, Rev., D **5**, (1972).
23) R. H. DALITZ and D. G. SUTHERLAND: *Nuovo Cimento*, **37**, 1777 (1965); **38**, 1945 (E) (1965).
24) M. BASILE *et al.*: Proceedings of this Conference; M. N. KREISLER: ibidem.
25) L. M. BROWN and H. MUNCZEK: *Phys. Rev.*, D **1**, 2595 (1970). See also ref. ([11]).
26) This relation implies that if $\varepsilon_1 \neq 0$, then there must be breaking of SU_3 also in the $V^aV^bP^0$ vertex (*i.e.* $\beta \neq 0$).

SESSION III - D

Friday, 16 April 1971

Outstanding problems

Chairman: G. PUPPI

Secretaries: G. VENTURI
P. FRAMPTON

New instruments for the high-energy physicist (*)

G. CHARPAK
CERN - Geneva

In such a field as high-energy physics the progress in our knowledge is closely tied to the instrumentation available to produce high-energy particles and to study them.

A steady improvement in the detection equipment is produced by the daily effort of the experimenting groups. I am going to give a biased selection of some particular recent developments with which I am more familiar, with the hope that their presentation may stir some new ideas as to their use.

1. Progress in the visual detectors.

Streamer chambers are progressively being introduced in some experiments. Let me mention a recent development of a mixed streamer and cloud chamber by the Tiflis group [1] (Fig. 1*b*). The electrons are just amplified by a pulse, then the chamber is expanded in such a way that only the avalanches give rise to condensed droplets.

The principle of such a chamber was used a long time ago to visualize β-rays [2], but the Tiflis group brought it to a beautiful operational stage illustrated in Fig. 1. The advantage of such a chamber is that it can be operated in many gases. There are no limitations of light output. It has the disadvantage of a long recovery time, like Wilson chambers. However, one can imagine that for the study of very complex events, with a large multiplicity, this is not a limitation.

It is worth noting that such a development has not stirred a great deal of excitement in the laboratories. It would have done so decades ago. Is it that high-energy physics is now an old science? Twenty years ago it was sufficient to see a new pattern in any visual detector to suspect the existence

(*) Invited paper

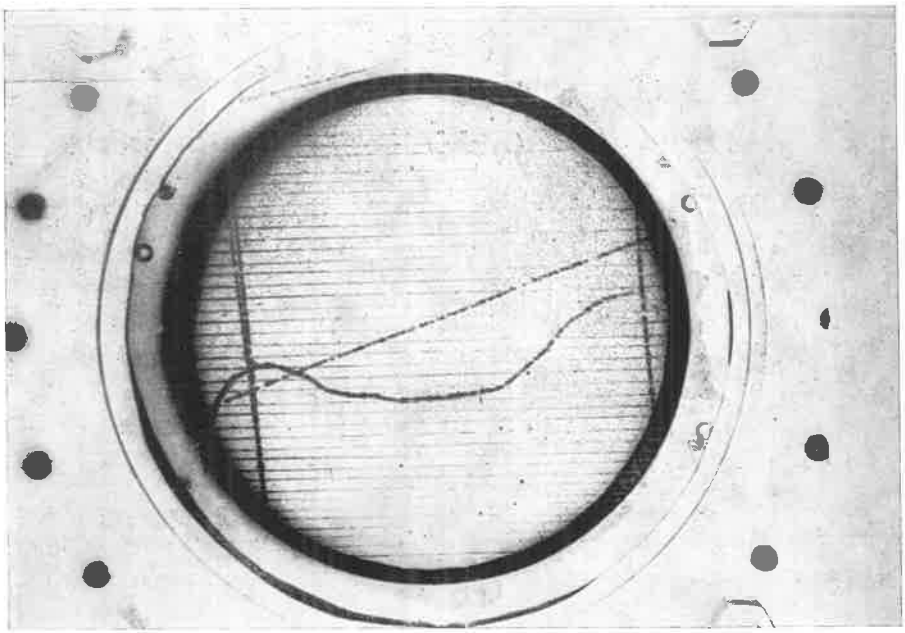

Fig. 1. – *a*) Tracks in a hybrid avalanche and Wilson chamber (1). The expansion is adjusted to detect the head of the avalanches.

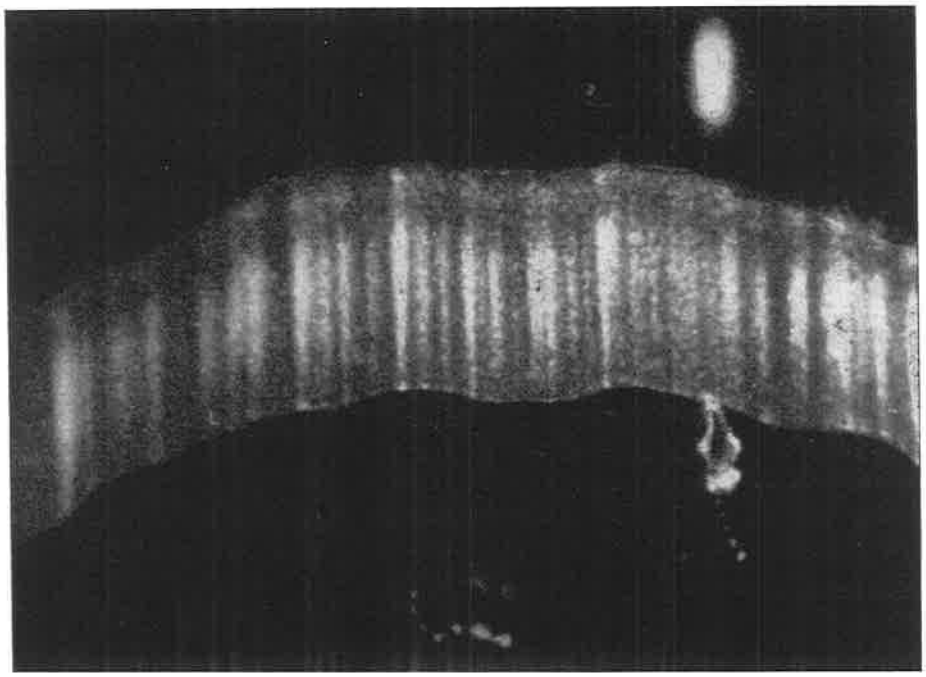

Fig. 1. – *b*) β-rays in a Wilson chamber with avalanches produced by an electric field (2). The expansion is adjusted to detect the primary track also.

of a new particle. The discovery of the $\pi\mu e$ decay in the emulsion or the discovery of the V-particles illustrate this fact. Now we have a well-accepted scheme of particle classification and if we would observe an anomalous decay we would rather regard it as an accident. This does not mean that we do not look for new particles, but the ones we look for are the ones authorized by the theoretical establishment, like quarks or monopoles, with rather well-defined properties. What we are looking for is methods to obtain much higher accuracy in the measurement of well-known objects. This is why a faster expansion is observed in the field of the high-counting-rate instruments, or in the field of high spatial accuracy, which is of prime importance with the advent of machines in the 1000 GeV range.

2. Progress in the fast counting techniques: the multiwire proportional chamber.

The multiwire chambers are the revival of the old technique of proportional counters. It is a structure made of a plane of wires between two flat electrodes, immersed in a proper gas. Figure 2 shows the electric field surrounding a wire when a potential, positive with respect to the outer electrodes, is applied to the central wires.

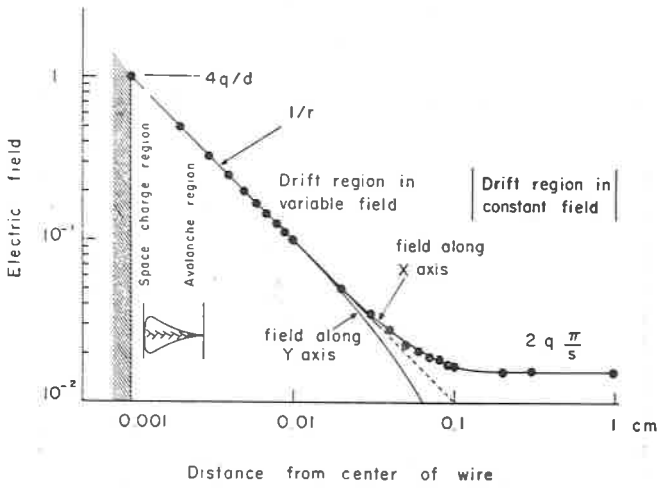

Fig. 2. – Variation of the field around a wire as a function of the azimuth. Logarithmic scales. Fields along X and Y axes. At short distance from the wire, $E = 1/r$ irrespective of azimuth ([3]).

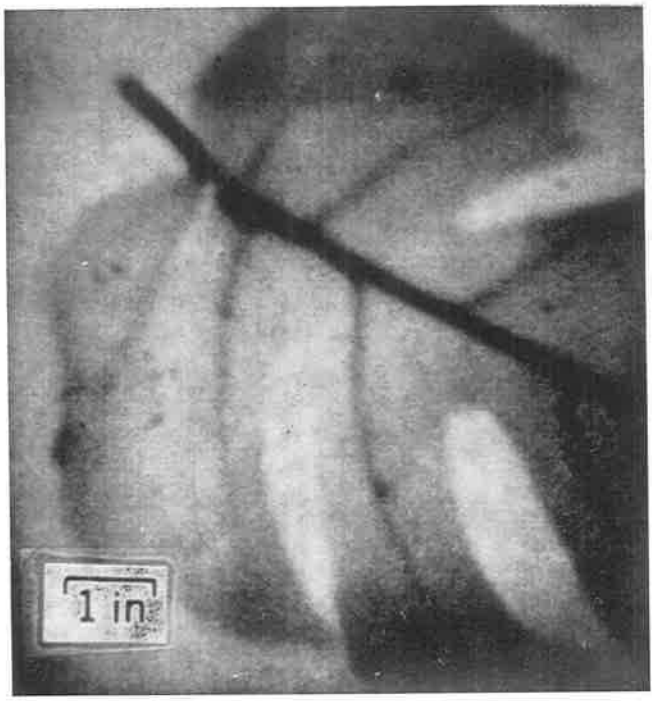

Fig. 3*a*. – X-ray radiography of a philodendron leaf taken with a 0.3 mR exposure at 5.9 keV ([4]).

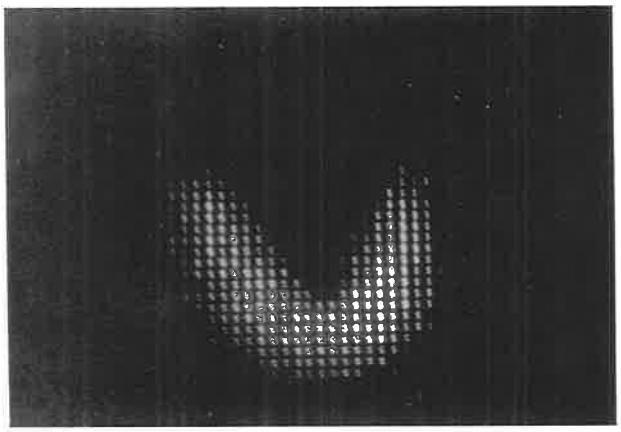

Fig. 3*b*. – Spatial distribution of γ-ray from iodine-131 in a human thyroid (R. ALLEMAND *et al.*: Centre d'études nucléaires de Grenoble, private communication).

Such a structure is characterized by the following properties ([3])

a) Every wire can amplify electrons liberated in the gas by a charged particle. The avalanche produces a negative pulse on the wire.

b) An avalanche on a wire gives rise to positive pulses on the neighbouring wires, making it very easy to localize the wire on which the avalanche is developed.

c) An avalanche on a wire gives rise to positive pulses on the high-voltage electrodes. If these electrodes are made of wires orthogonal to the central wires, it is possible to localize the position of an avalanche along the wire with an accuracy of 0.15 mm. This is important for the mapping of the spatial distribution of soft X-rays. Figure 3 shows a radiography obtained in a multiwire chamber by Perez-Mendez *et al.* at the Lawrence Radiation Laboratory ([4]), and the spatial distribution of an X-ray emitting isotopes, in a human thyroid gland, as obtained in CENG at Grenoble by R. Allemand *et al.* (*).

d) The delay between the detection of a pulse and the passage of a particle is strictly correlated to the distance between the trajectory and the closest wire. With 2 mm wire spacing the maximum spread of this delay is 24 ns. By measuring this delay, in special chambers, with a wire spacing of 1 cm, a Heidelberg group ([5]) was able to obtain resolutions of 0.5 mm.

By adding to the gas electronegative components which restrict the sensitive region in the chamber to narrow cylinders around the wires, time resolutions of 2.5 ns could be obtained (Fig. 4). It is worth observing that this is a rather unique massless collimator. It is possible, by making coincidences between wire planes placed at large distance, to select a beam within angular spreads of say, 10^{-5} radians, corresponding to what is necessary to study scattering effects in crystals. By staggering successive planes with CF_3Br limiting the sensitivity to narrow cylinders around the wires, Merkel, at the Orsay Linear Accelerator obtains accuracies of 0.15 mm.

e) The counting rate per wire can exceed 10^6 particles/s. Let us mention, among the first large-scale experiments making use of MWPC, the study of the K^0 parameter by the CERN-Heidelberg Goup. Instant rates of 10^6 counts per machine burst are accepted by the chambers. About 1000 good events are accepted at every machine burst, a rate at least one order of magnitude greater than was possible in the previous experiments on the same subject.

f) New gases have been developed at CERN ([7]) which give rise to an amplification factor of 10^8. One single electron gives rise to pulses of about

---

(*) Private communication.

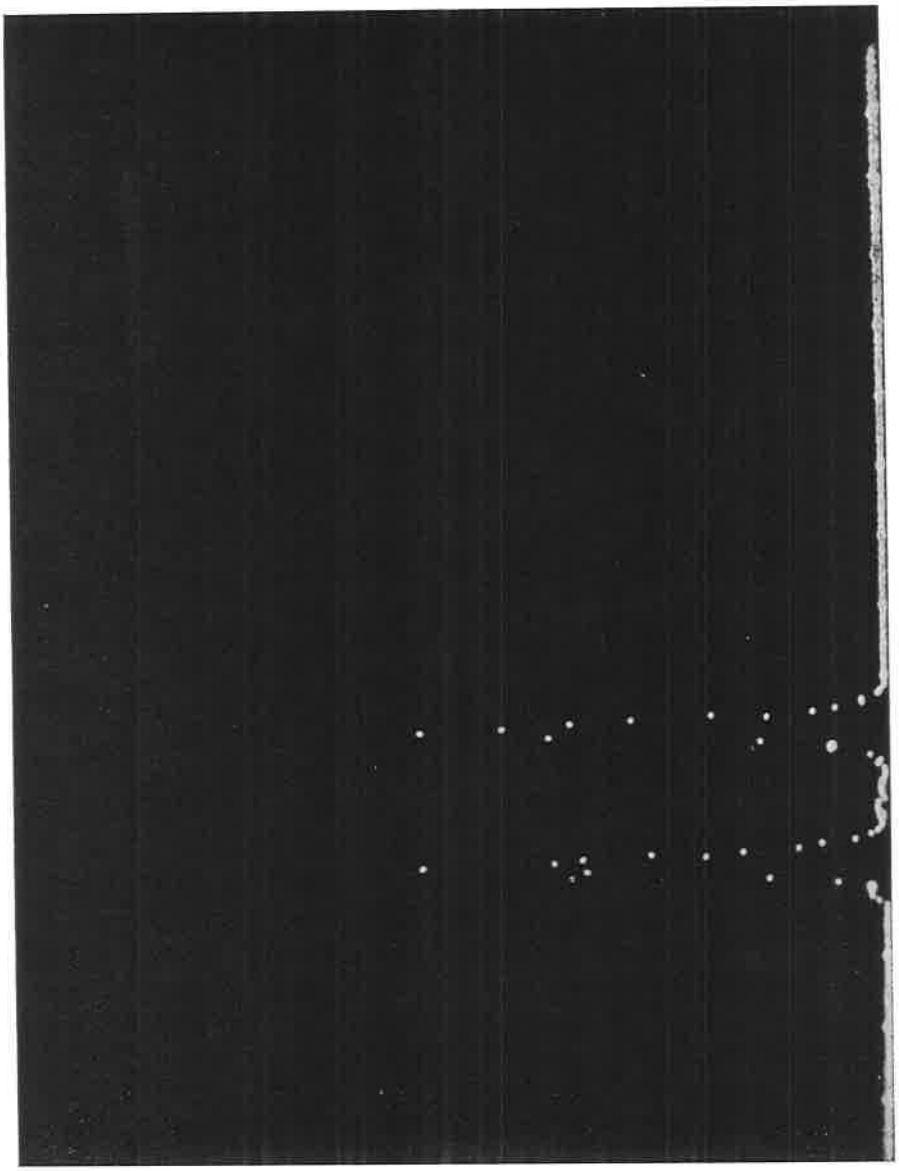

Fig. 4. – Time jitter with electronegative additives Helium + CF_3Br (92/8), wire spacing 2 mm, gap of 8 mm, high voltage = 7100 V, efficiency 20%, calibration peak at 16 ns, FWHM $\sim$ 2.5 ns.

100 mV, of a size limited by space charge saturation. This has simplified the electronic circuits associated with every wire.

g) The use of the proportionality between the pulse height and the energy lost in the gas can also find nice applications. The relativistic rise of

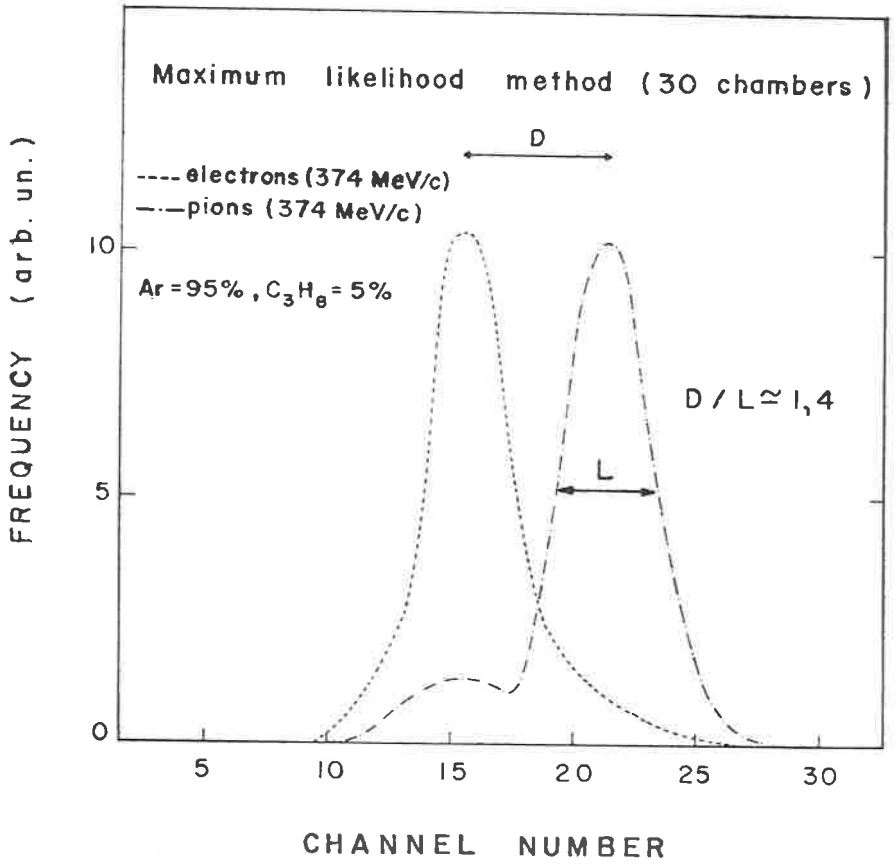

Fig. 5. – Electron-pion separation by the maximum likelihood method: the contamination of 5% of electrons in the pion beam is clearly visible (Argon-propane, 347 MeV/c).

charged particles in gases has been investigated by a cascade of 30 proportional chambers, by Dimčovski *et al.* ([12]), and shows promising prospects for particle separation at ultrarelativistic energies (Fig. 5).

Parker *et al.* studied electron induced showers in six successive planes. At 9 GeV they obtain an accuracy $(\delta E/E)_{\mathrm{rms}} = 0.10 \pm 0.01$.

h) By reducing the pressure to values of about 3 mm of organic vapours,

the time resolution of the chambers improves to 2.5 ns (FWHM). While the interest for this type of detector is limited to high ionization, it may be interesting for low energy nuclear physics [14].

Several chambers of several metres are under operation. Many practical problems have had to be solved by the different groups. I refer you to their publications [3,10]. Let me mention that to equip the splitfield magnet which is going to analyse the particles at one intersecting region of the CERN storage rings, a group at CERN [11] is building a detector with chambers of about (2×1) m, with about 50000 wires.

Enough confidence has been gained in the practical operation of the chamber to encourage rather large-scale adventures.

3. Progress in high spatial accuracy detectors.

With narrow gap spark chambers at atmospheric pressure, the accuracy in the determination of the trajectory position is, in the best cases, of the order of $\sigma = 0.3$ mm. With large gap chambers, for tracks orthogonal to the plates it can reach $\sigma = 0.1$ mm. With the advent of very high energy machines a considerable interest is attached in an improvement of these figures. Any progress in this direction is connected to a proportional reduction in the magnetic strength required for achieving a given analysing power in spectrometers. In 1968 L. Alvarez [15] had discussed the potentialities of spark chambers in liquid noble gases, then of proportional chambers in these liquids. The advantage of using a liquid is to open the possibility of narrow gaps, of the order of 50 μm, with 100% efficiency for minimum ionizing tracks. A serious amount of research has been devoted to exploring the possibility of liquid chambers [16,17]. It has resulted in a fine discovery made by the Alvarez Group. While they observed amplification in liquid argon, with rather poor efficiency, they discovered that liquid xenon behaves in quite a different way. Pulses with 6 ns rise-time can be observed, three orders of magnitude faster than in argon. Since these pulses are due to the motion of the positive charges, just like in a normal proportional chamber, their results show that positive charges move in liquid xenon by a mechanism of hole conduction, which is a phenomenon so far unknown in liquids. Although the discovery of the amplification in xenon is by itself a big step, there remains the formidable problem of having wires or points every 20 μm and to retrieve the data from every sensing element, at a reasonable cost. This group has tackled this problem with many new ideas and confidence in their success.

In a more conservative way, several groups have attempted to improve the accuracy in spark or proportional chambers by using high pressure gas filling and scaling down the gap thickness in proportion. Very encouraging results have been obtained and accuracies of the order of 60 μm have been reported by several groups.

It is a field where more investment of research effort would certainly be rewarding.

REFERENCES

1) Z. SH. MANJAVIDZE and V. N. ROINISHVILI: *Phys. Lett.*, **24**, 392 (1967).
2) F. REIMAN: *Zeits. Phys.*, **122**, 262 (1944).
3) G. CHARPAK: *Evolution of the automatic spark chambers*, in *Ann. Rev. Nucl.Sci.*, **20** (1970).
4) L. KAUFMAN, V. PEREZ-MENDEZ, J. SPERNIDE and G. STOKER, UCRL 20653, April 1971.
5) A. M. WALENTA, J. HEINTZE and B. SCHÜLEIN: *Nucl. Instrum. Methods*, **92**, 373 (1971).
6) B. MERKEL: *A high resolution beam hodoscope using multiwire proportional chambers*, Orsay Linear Accelerator Laboratory, Report LAL 1246, March 1971.
7) R. BOUCLIER, G. CHARPAK, Z. DIMČOVSKI, G. FISCHER and F. SAULI: *Nucl. Instrum. Methods*, **88**, 149 (1970).
8) P. SCHILLY, P. STEFFEN, J. STEINBERGER, T. TRIPPE, F. VANNUCCI, H. WAHL, K. KLEINKNECHT and V. LÜTH: *Nucl. Instrum. Methods*, **91**, 221 (1971).
9) G. CHARPAK, H. G. FISCHER, A. MINTEN, L. NAUMANN, F. SAULI, G. FLÜGGE, C. H. GOTTFRIED and R. TIRLER: *Some features of large multiwire proportional chambers*, submitted to *Nucl. Instrum. Methods*, May 1971.
10) G. CHARPAK, H. G. FISCHER, C. R. GRUHN, A. MINTEN, G. PLCH and G. FLÜGGE: *Time degeneracy of MWPC*, submitted to *Nucl. Instrum. Methods*, May, 1971.
11) *The split-field magnet facility* (A. MINTEN ed.), CERN SFMD-4 Note, April 1971.
12) Z. DIMČOVSKI, J. FAVIER, G. CHARPAK and G. AMATO: *High-energy charged particles separation by means of a cascade of MWPC*, *Nucl. Instrum. Methods*, 94, 151, 1971.
13) S. PARKER, R. JONES, J. RADYK, L. STEVENSON, T. KATSURA, V. PETERSON and D. YOUNT: *Measurement of the position and energy of* (4÷5) GeV *and* 9 GeV *electron induced showers using multiwire proportional chambers*, UCRL 20284.
14) F. BINON, V. V. BOBYR, G. DUTEIL, M. GOUANÈRE, L. HUGON, M. SPIGHEL and J. P. STROOT: *Low pressure multiwire proportional chambers with high time resolution for strongly ionizing particles*, *Nucl. Instrum. Methods*, 94, 27, 1971,
15) L. W. ALVAREZ: *The use of liquid noble gases in particle detectors*, LRL Group A Physics Note 672 (1968).
16) S. DERENZO *et al.*: *The prospect of high spatial resolution for counter experiments: a new particle detector using electron multiplication in liquid argon*, UCRL 19254.
17) R. A. MÜLLER, R. RICHARD and A. MÜLLER *et al.*: *Particle detectors based on noble liquids*, UCRL 20125.

A remark by M. Conversi

I wish first of all to express my admiration for the beautiful technique of the proportional wire chamber developed so successfully by George Charpak. I think it is a powerful tool for experiments with particle accelerators, which will become more and more important in the future. The purpose of my « remark » (I apologize if it will be a remark unusually long) is to mention some other prospects for instrumentation for particle physics, which are suggested by the preliminary results of work being carried out at Frascati on flash-tubes. As I shall explain, this type of instrumentation appears as complementary to that, considerably more refined but somewhat less flexible and certainly much more expensive, illustrated by Charpak in his excellent review talk.

But let me first recall the working principle of the flash-tube « hodoscope chamber » ([1]), since this instrument is not familiar to particle physicists, even though rather widely used in cosmic ray research ([2]). With the help of the following drawing one sees that the working principle is just the same as that of the familiar spark chamber, (the type of gas discharge being different, however, in the two cases). And, in fact, the two important steps which led to the final version of the spark chamber (the « triggered spark counter » developed independently at Pisa ([3]) and at Harwell ([4]), and the « discharge chamber » of Fukui and Miyamoto ([5])) were both originated ([6]) by the 1955 work on the flash-tube chamber.

There is now an entire family of track detectors which may be called « electrically pulsed track chambers ». All members of this family (various types of spark chambers, streamer chambers, etc.) use the same basic principle. The principle, as you know and as it appears from the drawing, uses the idea ([7]) of making the detector sensitive only for a short time, soon after the occurrence of a physical event selected by counters with some suitable « logic circuit ». This allows one to achieve great stability of operation and, most important, to combine the space resolution inherent in the track detector with a time resolution which is determined by the « memory » of its « sensitive material » (flash-tubes, or gas...). Clearly the new family of electrically pulsed track detectors does not include the multiwire chambers developed by Charpak, which are sensitive continuously. Thus, to a high space-time resolution these chambers add the advantage of being themselves able to detect the desired events with the help of suitable electronics. The drawback of these remarkable qualities is in my opinion the complexity of the mechanics and electronics

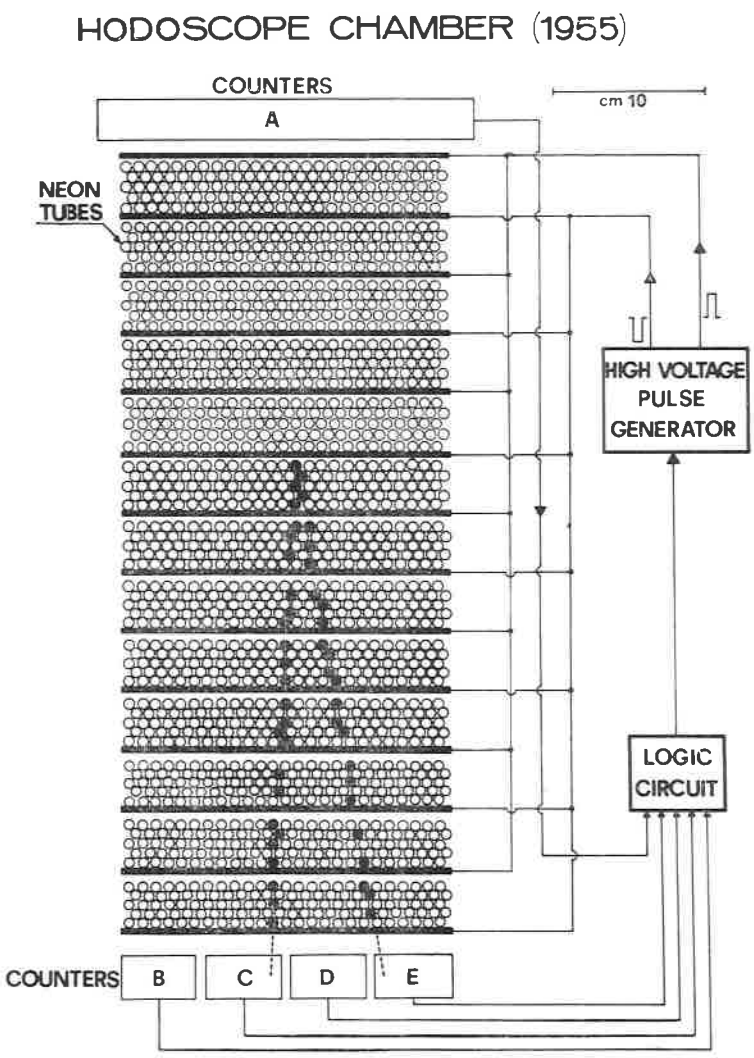

Fig. 1. – Representation to scale of the first flash-tube chamber, with a two-track event superimposed. Counters A, B, C, D, E and the « logic circuit » (not to scale) were used to select the desired events. On the occurrence of these events the chamber was triggered by applying to its plates high voltage pulses, just as in the familiar spark chamber developed five years later (*). Only neon-tubes crossed by ionizing particles flash when the high voltage pulses are applied. Space reconstruction of the events is obtained by alternating layers of tubes perpendicular to each other and by taking two photographs at right angles.

(*) In his « historical talk » to the first Spark Chamber Symposium (Argonne, 1960), A. Roberts preferred, however, to define the 1955 hodoscope chamber as «a modification of the spark chamber » (see *Rev. Sci.*e *Instr.*, **32**, 483 (1961)).

involved, and the « cost per wire » which is consequently still relevant, even if decreasing quickly in time as pointed out by Charpak.

Now there are types of experiments—and more there will be presumably in the future—in which the high performances of the multiwire proportional chambers are fully exploited to justify their relevant cost. But there are also other types of experiments, in which the space-time resolution required is more limited, no fast recording of the events is needed and a 4π geometry is desired; in these cases the technique of the flash-tubes, with the recent improvements outlined below, appears quite promising.

For example, in our present experiments with «Adone» we have found it convenient to replace some of the large spark chambers used to stop muons, with bigap hodoscope chambers with a surface of several square meters. They contain flash-tubes, 1.5 m long and 2 cm in diameter, filled with « henogal » at 350 torr. These chambers are very cheap, the cost being determined essentially by that of the flash-tubes ($\sim$ 1 dollar/tube «if home made»). They are easy to construct and operate and, more important, they allow one to save many millions of lire per year for gas needed in ordinary spark chambers of similar size. Hodoscope chambers of this type could well be used also in neutrino experiments with accelerators, in spite of the relatively long sensitive time (a few tens of μsec) of the large flash-tubes employed. Smaller tubes can be operated under conditions of more severe background; we plan to use now at Adone chambers filled with thinner tubes, in order to observe multitrack events with better efficiency than in the case of ordinary spark chambers. In fact the flashing of one tube does not prevent the other tubes from flashing as well, whereas sparks between the same plates influence one another, making the recording of a many-track event by the same spark chamber inefficient. Furthermore, tracks of any angular inclination can be observed efficiently in hodoscope chambers but not in spark chambers.

The technique is particulary flexible. In principle one can give the glass tubes any shape apt to fullfil particular geometrical requirements. But also ordinary linear tubes can be employed efficiently in experiments requiring a 4π geometry. Layers of tubes with appropriate orientations must be alternated, of course, for space reconstruction of complex events. The tracks can be recorded either on film (from distances as large as 20 m) or by means of vidicon methods, or exploiting the individuality of the tubes, which allows one to digitize easily the information with the help of light sensors([8]) or of simple pick–up probes([9]) placed outside the electrodeless tubes.

We obtained recently flash tubes with a memory in the microsecond

region, suitable for experiments with particle accelerators. Wider use of digitized hodoscope chambers at particle accelerators is linked, however, to the possibility of reducing the flash-tube recovery times, which are at present no less that 80 msec.([10])

We wish finally to point out that the unique feature of this technique, to give both electric and optical signals, leaves open to the future the possibility of recording on film only very complex and presumably rare events, which cannot be unambiguosly interpreted by elaborating the information electronically.

REFERENCES

1) This technique, started in 1954-55 (see M. CONVERSI and A. GOZZINI: *Nuovo Cimento*, **2**, 189 (1955)) was soon afterwards developed further by groups in Pisa, Osaka and at Durham, where A. W. Wolfendale and his collaborators also applied it to a variety of interesting experiments on cosmic rays.
2) Large flash-tube chambers have been developed for and/or used in cosmic ray research, by groups from England, Germany, Hong Kong, India, Japan, Poland, South Africa, West Africa and U.S.A.
3) S. FOCARDI, C. RUBBIA, G. TORELLI and F. BELLA: *Nuovo Cimento*, **5**, 275 (1957). Probably because published in Italian, this work has never been quoted in the publications concerning the development of the spark chamber.
4) T. E. CRANSHAW and J. D. DEBEER: *Nuovo Cimento*, **5**, 1107 (1957).
5) S. FUKUI and S. MIYAMOTO: *Nuovo Cimento*, **11**, 113 (1959).
6) SEE S. FUYUI and S. MIYAMOTO: « A Study of the Hodoscope Chamber » INS-TCA **10** (1957) (Institute for Nuclear Study Tecnical Report, University of Tokyo).
7) This idea was independently applied by A. A. Tyapkin to impulse hodoscopes of G.M. counters for use in experiments with particle accelerators (A. A. TYAPKIN: *Prib. e Techn. Exper.*, **3**, 51 (1956); V. V. VISHNIAKOV and A. A. TYAPKIN: *Atomnaya Energyia*, **3**, no. 10 (1957)).
8) F. REINES: Proc. Roy. Soc. A**301**, 124 (1967).
9) C. A. AYRE and G. M. THOMPSON, Nucl. Instr. Meth. **69**, 106 (1969).
10) W. M. EVANS and J. C. BAXER, Internal Report RHEL/M/H/4 (March 1971).

List of participants

ADAMS, J. B.	CERN, Geneva, Switzerland.
ALEXANDER, G.	Tel-Aviv University, Dept. of Physics and Astronomy, Ramat-Aviv, Tel-Aviv, Israel.
ALITTI, J.	CEA Saclay, BP 2, 91 Gif-sur-Yvette, France.
ALLES, W.	Istituto di Fisica dell'Università, Via Irnerio 46, Bologna, Italy.
ALTARELLI, G.	Istituto di Fisica dell'Università, Piazzale delle Scienze 5, Rome, Italy.
AMALDI, E.	Istituto di Fisica dell'Università, Piazzale delle Scienze 5, Rome, Italy.
ARMENTEROS, R.	TC Division, CERN, Geneva, Switzerland.
ASCOLI, G.	University of Illinois, Dept. of Physics, Urbana, Ill. 61801, U.S.A.
ASHMORE, A.	Daresbury Nuclear Physics Lab., Daresbury, Nr. Warrington, Lancs., England.
ASTBURY, A.	Rutherford High Energy Laboratory, Building R1, Chilton, Didcot, Berks., England.
BACCI, C.	Laboratori Nazionali di Frascati, CP 70, Frascati (Rome), Italy.
BACON, T. C.	Rutherford High Energy Laboratory, Building R1, Chilton, Didcot, Berks., England.
BAKKER, A. M.	Zeemanlab. der Univ. van Amsterdam, Plantage Muidergracht 4, Amsterdam, Holland.

BALDO-CEOLIN, M.	Istituto di Fisica Nucleare, Via Marzolo 8, Padova, Italy.
BARACCA, A.	C.E.N./Saclay, Dep. de Physique Theorique, Centre d'Études Nucléaires, Saclay, France.
BARBIELLINI, G.	N.P. Division, C.E.R.N., Geneva, Switzerland.
BARTOLI, L.	Laboratori Nazionali di Frascati, C.P. 70, Frascati (Rome), Italy.
BASILE, M.	Istituto di Fisica dell'Università, Via Irnerio 46, Bologna, Italy.
BASSLER, E.	D.E.S.Y., Notkestieg 1, Hamburg 52, Germany.
BATON, J. P.	Dép. de Physique des Particules Elémentaires, C.E.A. Saclay, B.P. 2, 91 Gif-sur-Yvette, France.
BEHR, L.	Laboratoire Leprince Ringuet, École Polytechnique, 17 rue Descartes, Paris V^{e}, France.
BEHREND, H. J.	D.E.S.Y., Notkestieg 1, Hamburg 52, Germany.
BELL, J. S.	T.H. Division, C.E.R.N, Geneva, Switzerland.
BELLAMY, E.	Physics Dept., Westfield College, Hampstead, London N.W. 3, England.
BELLETTINI, G.	N.P. Division, C.E.R.N., Geneva, Switzerland.
BENAKSAS, D.	Accelérateur Linéaire, Faculté des Sciences, Bâtiment 200, 91 Orsay, France.
BENDER, I.	Inst. für Theor. Physik, Philosophenweg 16, Heidelberg, Germany.
BERGE, J. P.	T.C. Division, C.E.R.N., Geneva, Switzerland.

BERGIA, S. — Istituto di Fisica dell'Università, Via Irnerio 46, Bologna, Italy.

BERTHELOT, A. — Dép. de Physique des Particules Elémentaires, C.E.A. Saclay, B.P. 2, 91 Gif-sur-Yvette, France.

BETTINI, A. — Istituto di Fisica Nucleare, Via Marzolo 8, Padova, Italy.

BEUSCH, W. — N.P. Division, C.E.R.N., Geneva, Switzerland.

BIETTI, A. — Istituto di Fisica dell'Università, Piazzale delle Scienze 5, Rome, Italy.

BIZZARRI, R. — Istituto di Fisica dell'Università, Piazzale delle Scienze 5, Rome, Italy.

BLUM, W. — Max-Planck Inst. für Phys. und Astrophys., Fohringer Ring 6, Munich, Germany.

BÖCKMANN, K. — T.C. Division, C.E.R.N., Geneva, Switzerland.

BOLLINI, D. — Istituto di Fisica dell'Università, Via Irnerio 46, Bologna, Italy.

BORGIA, B. — Istituto di Fisica dell'Università, Piazzale delle Scienze 5, Rome, Italy.

BOWLER, M. — Nuclear Physics Lab., Oxford University, Keble Road, Oxford, England.

BRODY, A. — T.C. Division, C.E.R.N., Geneva, Switzerland.

BRUNINI, P. — Istituto di Fisica dell'Università, Via Irnerio 46, Bologna, Italy.

BUCCELLA, F. — T.H. Division, C.E.R.N., Geneva, Switzerland.

BUDINI, P.	International Centre for Theoretical Physics, Miramare-Grignano, P.O. Box 586, 34100 Trieste, Italy.
BURKHARDT, E.	Physikalisches Inst. der Univ., Albert-Ueberle-Strasse 2, Heidelberg, Germany.
BUTTERWORTH, I.	Rutherford High Energy Laboratory, Building R1, Chilton, Didcot, Berks., England.
CABIBBO, N.	Istituto di Fisica dell'Università, Piazzale delle Scienze 5, Rome, Italy.
CAPON, G.	Laboratori Nazionali di Frascati, C.P. 70, Frascati (Rome), Italy.
CAPRASSE, H.	Faculté des Sciences, Université de Liège, Liège, Belgium.
CHARPAK, G.	N.P. Division, C.E.R.N., Geneva, Switzerland.
CONFORTO, G.	Rutherford High Energy Lab., Building R1, Chilton, Didcot, Berks., England.
CONVERSI, M.	Istituto di Fisica dell'Università, Piazzale delle Scienze 5, Rome, Italy.
CORBETT, I.	Rutherford High Energy Laboratory, Building R1, Chilton, Didcot, Berks., England.
COSME, G.	Accélérateur Linéaire, Faculté des Sciences, Bâtiment 200, 91 Orsay, France.
COSTA, G.	Istituto di Fisica dell'Università, Via Amendola 173, Bari, Italy.
CREMMER, E.	Lab. de Physique Théorique et Hautes Energies, Bâtiment 211, Faculté des Sciences, 91 Orsay, France.
CRESTI, M.	Istituto di Fisica Nucleare, Via Marzolo 8, Padova, Italy.
CROZON, M.	Lab. de Physique Nucléaire, Collège de France, place Marcelin-Bethelot, Paris V^{e}, France.

CSONKA, P.	Physics Dept., University of Oregon, Eugene O.R. 97043, U.S.A.
DALITZ, R. H	University of Oxford, Dept of Theoretical Physics, 12 Parks Road, Oxford, England.
DALPIAZ, P.	N.P. Division, C.E.R.N., Geneva, Switzerland.
DEFOIX, CH.	Lab. de Physique Nucléaire, Collège de France, place Marcelin-Berthelot, Paris Ve, France.
DEGRANGE, E.	Laboratoire Leprince-Ringuet, École Polytechnique, 17 rue Descartes, Paris Ve, France.
DETHLEFSEN, I. M.	Niels Bohr Institute, Blegdamsvej 17, Copenhagen, Denmark.
DEVLIN, TH.	Rutgers University, Dept. of Physics, New Brunswick, N.J. 08903, U.S.A.
DIAMBRINI PALAZZI, G.	Istituto di Fisica dell'Università, Viale Benedetto 15, Genova, Italy.
DI CORATO, M.	Istituto di Fisica dell'Università, Via Celoria 16, Milano, Italy.
DIETL, H.	Max-Planck-Inst. für Phys. und Astrophys., Fohringer Ring 6, Munich, Germany.
DIETZ, K.	Inst. of Physics, Univ. of Bonn, Nussallee 12, Bonn, Germany.
DÌ GIACOMO, A.	Istituto di Fisica dell'Università, Piazza Torricelli 2, Pisa, Italy.
DORNAN, P. J.	Physics Dept., Imperial College, Prince Consort Road, London S.W. 7, England.
DRECHSLER, W.	Max-Planck-Inst. für Phys. und Astrophys., Fohringer Ring 6, Munich 23, Germany.

DUIMIO, F.	Istituto di Fisica dell'Università, Via Celoria 16, Milano, Italy.
EDWARDS, D. N.	Physics Dept., University of Liverpool, P.O. Box 147, Liverpool, England.
ELLIS R.	Istituto di Fisica dell'Università, Via Irnerio 46, Bologna, Italy.
ENGELS, J. F.	D.E.S.Y., Notkestieg 1, Hamburg 52, Germany.
ENGLER, A.	Carnegie Mellon University, 5000 Forbes Ave., Pittsburgh, Pennsylvania 15213, U.S A.
EKSPONG, G.	Physics Dept., University of Stockholm, Vanadisvägen 9, Stockholm, Sweden.
FELD, B.	Physics Dept., M.I.T., Laboratory for Nuclear Science, Cambridge, M.A. 02139, U.S.A.
FELTESS, E. J.	Dép. de Physique des Particules Elémentaires, C.E.A. Saclay, B.P. 2, 91 Gif-sur-Yvette, France.
FERRARI, E.	Istituto di Fisica dell'Università, Piazzale delle Scienze 5, Rome, Italy.
FIDECARO G.	N.P. Division, C.E.R.N., Geneva, Switzerland.
FIELDS, T. H.	H.E.P. Division, Argonne Nat'l Lab. Argonne, Illinois 60439, U.S.A.
FLATTÉ, S.	Lawrence Berkeley Laboratory, University of California, Berkeley, C.A. 94720, U.S.A.
FOÀ, L.	Scuola Normale Superiore, Piazza dei Cavalieri, Pisa, Italy.
FOCARDI, S.	Istituto di Fisica dell'Università, Via Irnerio 46, Bologna, Italy.

FORINO, A.	Istituto di Fisica dell'Università, Via Irnerio 46, Bologna, Italy.
FOURNIER, T.	Accélérateur Linéaire, Faculté des Sciences, Bâtiment 200, 91 Orsay, France.
FRABETTI, P. L.	Istituto di Fisica dell'Università, Via Irnerio 46, Bologna, Italy.
FRAMPTON, P.	T.H. Division, C.E.R.N., Geneva, Switzerland.
FRANK, S.	University of Southampton, Physics Dept. Highfield. Southampton, England.
FRENCH, B.	T.C. Division, C.E.R.N., Geneva, Switzerland.
FROGGATT, C.	Niels Bohr Institute, Blegdamsvej 17, Copenhagen, Denmark.
FROISSART, M.	Dép. de Physique des Particules Elémentaires, C.E.N. Saclay, B.P. 2, 91 Gif-sur-Yvette, France.
GABATHULER, E.	Daresbury Nuclear Physics Laboratory, Daresbury Nr. Warrington, Lancs., England.
GANSSANGE, E.	DESY, Notkestieg 1, Hamburg 52, Germany.
GARBUTT, D.	Physics Dept., Imperial College, Prince Consort Road, London S.W.7, England.
GENSINI, P.	Istituto di Fisica dell'Università, Via Anesano, Lecce, Italy.
GHIDINI, B.	TC Division, CERN, Geneva, Switzerland.
GLASHOW, S.	The Physics Laboratory, Harvard University, Cambridge, MA 02138, U.S.A.
GIACOMELLI, G.	Istituto di Fisica dell'Università, Via Irnerio 46, Bologna, Italy.
GOLDSCHMIDT-CLERMONT, Y.	TC Division, CERN Geneva, Switzerland.

GOLDZAHL, L.	CEA Saclay, Groupe Deutéron, « Saturne », BP 2, 91 Gif-sur-Yvette, France.
GOOD, M. L.	Physics Dept., State University of New York, Stony Brook, N.Y. 11790, U.S.A.
GOURDIN, M.	TH Division, CERN, Geneva, Switzerland.
GRAFFI, S.	Istituto di Fisica dell'Università, Via Irnerio 46, Bologna, Italy.
GRANT, A.	TC Division, CERN, Geneva, Switzerland.
GRARD, F.	Laboratory, University Belge des Hautes Energies 4 rue Hobbema, Brussels 4, Belgium.
GRECCHI, V.	Istituto di Fisica dell'Università, Via Irnerio 46, Bologna, Italy.
GRECO, M.	Laboratori Nazionali di Frascati, CP 70, Frascati (Rome), Italy.
GREEN, M.	Physics Dept., Westfield College, Hampstead, London, England.
GRIVAZ, J.	Accélérateur Linéaire, Faculté des Sciences, Bâtiment 200, 91 Orsay, France.
GUIDONI, P.	Istituto di Fisica dell'Università, Piazzale delle Scienze 5, Rome, Italy.
GUSTAFSON, G.	NORDITA, Blegdamsvej 17, Copenhagen, Denmark.
HALZEN, F.	F.N.R.S., Egmonstraat 11, Brussels, Belgium.
HANNA, R.	Rutherford High Energy Laboratory, Building R1, Chilton, Didcot, Berks., England.
HENRI, V. P.	TC Division, CERN, Geneva, Switzerland.
HERQUET, P.	Lab. Univ. Belge des Hautes Energies, 4 rue Hobbema, Brussels 4, Belgium.

HONECKER, R.	Institute of Physics, Charlottenstrasse 14, Aachen, Germany.
HUGHES, I. S.	Dept. of Natural Philosophy, Glasgow University, Glasgow W 2, Scotland.
HYAMS, B. D.	NP Division, CERN, Geneva, Switzerland.
IDSCOK, U.	Institute of Physics, University of Bonn, Nussallee 12, Bonn, Germany.
JACOB, M.	TH Division, CERN, Geneva, Switzerland.
JEAN MARIE, B.	Accélérateur Linéaire, Faculté des Sciences, Bâtiment 200, 91 Orsay, France.
JEANNET, E.	Université de Neuchâtel, Institut de Physique, rue L. Breguet 1, Neuchâtel, Switzerland.
JENTSCHKE, W.	DI Division, CERN, Geneva, Switzerland.
JOBES, M.	Physics, Dept., University of Birmingham, PO Box 373, Birmingham, England.
JOHNSSEN, W.	Institute of Physics, University of Bonn, Nussallee 12, Bonn, Germany.
KALMUS, P.	Queen Mary College, Dept. of Physics Mile End Road, London, E1 England.
KEMP, A.	Daresbury Nuclear Physics Laboratory, Daresbury, Nr. Warrington, Lancs., England.
KESSLER, P.	Collège de France, Laboratoire de Physique atomique et moléculaire, 11 place Marcelin-Berthelot, Paris V^{e}, France.
KITTEL, E. W.	TC Division, CERN, Geneva, Switzerland.
KLANNER, R.	University of Munich, Schellingstrasse 2-8, Munich 13, Germany.

KORTHALS-ALTES, A.	Inst. voor Theor. Fysica, Valckeniersstraat 65, Amsterdam, Holland.
KOSE, R.	Institute of Physics, University of Bonn, Nussallee 12, Bonn, Germany.
KREISLER, M. N.	Princeton University, Dept. of Physics, Joseph Henry Laboratories, Jadwin Hall, PO, Box 708 Princeton, N.J. 08540, U.S.A.
KUHNELT, H.	Institut für Theoretische Physik, Universität Karlsruhe, 75 Karlsruhe, Germany.
LAI K. W.	Physics Dept., Brookhaven National Laboratory, Upton, New York 11973, U.S.A.
LAURENS, A. G.	Dépt. de Physique des Particules Élémentaires, CEA Saclay, BP 2, 91 Gif-sur-Yvette, France.
LECHANOINE, C.	NP Division, CERN, Geneva, Switzerland.
LEFRANCOIS, J.	Lab. de Phys. Theor. et Hautes Energies, Bâtiment 211, Faculté des Sciences, 91 Orsay, France.
LE GUILLOU, J.	TH Division, CERN, Geneva, Switzerland.
LERAY, TH.	Lab. de Physique Nucléaire, Collège de France, 11 place Marcelin-Berthelot, Paris V^{e}, France.
LESTIENNE, R.	Laboratoire Leprince-Ringuet, École Polytechnique, 17 rue Descartes, Paris V^{e}, France.
LEVY, F.	Institut de Physique Nucléaire, Hall aux Vins, 9 quai St. Bernard, Paris V^{e}, France.
LEVY, N.	DESY, Gruppe Theorie, Notkestieg 1, 2000 Hamburg 52, Germany.
LILLESTØL, E.	Fysisk Inst., University of Bergen, Allegaten 53-55, Bergen, Norway.

LIPMAN, N. H.	Rutherford High Energy Laboratory, Building RI Chilton, Didcot, Berks, England.
LOHRMANN, E.	DESY, Notkestieg 1, Hamburg 52, Germany.
LUTZ, G.	Physics Dept., Northeastern University, 360 Huntingdon Ave., Boston, MA 02215, U.S.A.
MAIANI, L.	Laboratorio di Fisica, Istituto Superiore di Sanità, Viale Regina Elena 29, Rome, Italy.
MAKOWSKI, B.	ITN Calculatrice, 9 quai St. Bernard, Paris V^{e}, France.
MANDELLI, L.	TC Division, CERN, Geneva, Switzerland.
MANNELLI, I.	Istituto di Fisica dell'Università, Piazza Torricelli 2, Pisa, Italy.
MARECHAL, B.	TC Division, CERN, Geneva, Switzerland.
MARSHALL, R.	Daresbury Nuclear Physics Lab., Daresbury, Nr. Warrington, Lancs., England.
MARTINIS, M.	Inst. Rudjer Boskovic, Bijenicka Cesta 54, Zagreb, Yugoslavia.
MARTINSKA, G.	JINR, Dubna, Moscow, U.S.S.R.
MASON, P.	Physics Dept., University of Liverpool, P.O. Box 147, Liverpool, England.
MASSAM, T.	Istituto di Fisica dell'Università, Via Irnerio 46, Bologna, Italy.
MAZZANTI P.	Istituto di Fisica dell'Università, Via Irnerio 46, Bologna, Italy.
MENCUCCINI, C.	Laboratori Nazionali di Frascati, CP 70, Frascati (Rome), Italy.

MERKEL, B.	Laboratoire de l'Accélérateur Linéaire, Bâtiment 200, Faculté des Sciences, Orsay, France.
MEYER BERKHOUT, U.	Sektion Physik der Universität, Amalienstrasse 54, 8 Munich 13, Germany.
METTEL, D.	ITN Calculatrice, 9 quai St. Bernard, Paris V^{e}, France.
MILLER, D. H.	Physics Dept., Purdue University, Lafayette, Indiana 47907, U.S.A.
MINGUZZI-RANZI, A.	Istituto di Fisica dell'Università, Via Irnerio 46, Bologna, Italy.
MINTEN, A.	TC Division, CERN, Geneva, Switzerland.
MOEBES, J. P.	TC Division, CERN, Geneva, Switzerland.
MONARI, L.	Istituto di Fisica dell'Università, Via Irnerio 46, Bologna, Italy.
MONETI, G.	Physics Dept., Syracuse University, Syracuse, N.Y. 13210, U.S.A.
MOREL, A.	Lab. de Physique Théorique, CEA Saclay, BP 2, 91 Gif-sur-Yvette, France.
MORGAN, D.	Rutherford High Energy Laboratory, Chilton, Didcot, Berks., England.
MORITZ, J.	Inst. für Exp. Kernphysik, Univ. Karlsruhe, Postfach 3640, Karlsruhe, Germany.
MORPURGO, G.	Istituto di Fisica dell'Università, Viale Benedetto XV, Genova, Italy.
MUIRHEAD, H.	Physics Dept., University of Liverpool, P.O. Box 147, Liverpool, England.
MURTAS, G. P.	Laboratori Nazionali di Frascati, CP 70, Frascati (Rome), Italy.
NAISSE, J.	Faculté des Sciences, Université Libre de Bruxelles, 50 avenue F. D. Roosevelt, B-1050 Brussels, Belgium.

NAVACH, F.	TC Division, CERN, Geneva, Switzerland.
NAVARRIA, F.	Istituto di Fisica dell'Università, Via Irnerio 46, Bologna, Italy
NE'EMAN, Y.	Tel-Aviv University, Dept. of Physics, Ramat-Aviv, Tel-Aviv, Israel.
NIGRO, M.	Istituto di Fisica Nucleare, Via Marzolo 8, Padova, Italy.
NOREM, J.	Rutgers University, Physics Department, New Brunswick, N.J. 08903, U.S.A.
OCHS, W.	Max-Planck-Institute für Physics und Astrophysics, Föhringer Ring 6, Munich 23, Germany.
O'NEALL, J.	Laboratoire Leprince Ringuet, École Polytechnique, 17 rue Descartes, Paris V^{e}, France.
PALMONARI, F.	Istituto di Fisica dell'Università, Via Irnerio 46, Bologna, Italy.
PARISI, G. R.	Collège de France, Laboratoire de Physique atomique et moléculaire, 11 Place Marcelin-Berthelot, Paris V^{e}, France.
PARROUR, G.	Accélérateur Linéaire, Faculté des Sciences, Bâtiment 200, 91 Orsay, France.
PASQUIER, R.	Laboratoire de Physique Nucléaire, Bâtiment 100, Faculté des Sciences, 91 Orsay, France.
PASQUIER, J.	Laboratoire de Physique Nucléaire, Bâtiment 100, Faculté des Sciences, 91 Orsay, France.
PAUL, W.	Physikalisches Institut, University of Bonn, Nussallee 12, Bonn, Germany.
PETERSEN, J. L.	Niels Bohr Institute, Blegdamsvej 17, Copenhagen Denmark.
PEVSNER, A.	Johns Hopkins University, Physics Dept., Baltimore, MD 212 18, U.S.A.

PEYROU, CH.	T.C. Division, C.E.R.N., Geneva, Switzerland.
PHELAN, J. J.	Rutherford High Energy Laboratory, Building R1, Chilton, Didcot, Berks., England.
PHILLIPS, P. R.	Washington University, Dept. of Phys., St. Louis, Missouri 63130, U.S.A.
PICKAVANCE, T. G.	Science Research Council, State House, High Holborn, London W.C. 1.
PIETSCHMANN, H.	Institut für Theoretische Physik der Universität Wien, Boltzmangasse 5, A-1090 Vienna, Austria.
PISTILLI, P.	Istituto di Fisica dell'Università, Piazzale delle Scienze 5, Rome, Italy.
PIŠUT, J.	Fysikalni Ustav Csav, Na Slovance 2, Prague 8, Czechoslovakia.
POELZ, G.	D.E.S.Y., Notkestieg 1, Hamburg 52, Germany.
POLLMANN, P.	Inst. für Theoretische Physik der Univ., Philosophenweg 12, 69 Heidelberg, Germany.
PREISWERK, P.	N.P. Division, C.E.R.N., Geneva, Switzerland.
PUPPI, G.	Istituto di Fisica dell'Università, Via Irnerio 46, Bologna, Italy.
QUARENI-VIGNUDELLI, A.	Istituto di Fisica dell'Università, Via Irnerio 46, Bologna, Italy.
QUERZOLI, R.	Istituto di Fisica Teorica, Università di Firenze, Enrico Fermi 2, Firenze, Italy.
RADICATI, L.	Scuola Normale Superiore, Piazza dei Cavalieri 5, Pisa, Italy.
RATTI, S.	Istituto di Fisica dell'Università, Via Celoria 16, Milano, Italy.

REIFF, J.	Inst. voor Theor. Fysica, Maliesingel 23, Utrecht, Holland.
REMIDDI E.	Istituto di Fisica dell'Università, Via Irnerio, 46 Bologna, Italy.
RENARD, F.	Dep. de Physique Matematique, Faculté des Sciences, 34 Montpéllier, France.
RINAUDO, G.	Istituto di Fisica dell'Università, Via Pietro Giuria 1, Torino, Italy.
ROBASCHIK, D.	J.I.N.R., Dubna, Moscow, U.S.S.R.
ROMER, H.	Institute of Physics, Univ. of Bonn, Nussallee 12, Bonn, Germany.
ROOS, M.	D.D. Division, C.E.R.N., Geneva, Switzerland.
ROSS, M.	Physics Dept., Univ. of Michigan, Ann Arbor, M.I. 48104, U.S.A.
ROST, M.	Institute of Physics, Univ. of Bonn, Nussallee 12, Bonn, Germany.
ROTELLI P.	Imperial College, Physics Dept., London SW 7, England.
ROUGÉ, A.	Laboratoire de Physique Nucléaire, Collège de France 11 place Marcelin-Berthelot, Paris V^{e}, France.
RUUSKANEN, V.	TH. Division, C.E.R.N., Geneva, Switzerland.
SABAU, M.	J.I.N.R., Dubna, Moscow, U.S.S.R.
SALAM, A.	International Centre for Theoretical Physics, Miramare-Grignano, P.O. Box 586, 34100 Trieste, Italy.
SALMERON, R. A.	École Polytechnique, 17 rue Descartes, Paris V^{e}, France.
SALVINI, G.	Istituto di Fisica dell'Università, Piazzale delle Scienze 5, Rome, Italy.

SALVINI, M.	Istituto di Fisica dell'Università, Via Irnerio 46, Bologna, Italy.
SANDHAS, W.	University of Mainz, Int. für Theoretical Physik, Mainz, Germany.
SCARROT, S. M.	Science Laboratories, Univ. of Durham, South Road, Durham City, England.
SCHIERHOLZ, G.	D.E.S.Y., Notkestieg 1, Hamburg 52, Germany.
SCHMID, C.	T.H. Division C.E.R.N., Geneva, Switzerland.
SCHMITZ, D.	Institute of Physics, Univ. of Bonn, Nussallee 12, Bonn, Germany.
SCHNEIDER, H.	Institute Physikalisches, Albert-Ueberle-Strasse 2, Heiderlberg, Germany.
SCHOENFELTER, J. L.	Dept. of Mathematical Physics, University of Birmingham, Birmingham, England.
SEKERA, Z.	T.C. Division, C.E.R.N., Geneva, Switzerland.
SENE, M.	Institut de Physique Nucléaire, Faculté de Sciences, Bâtiment 100, 91 Orsay, France.
SILVERSTRINI, V.	Laboratori Nazionali di Frascati, C.P. 70, Frascati (Rome), Italy.
SINGER, P.	Department of Physics, Technion, Israel Institute of Technology, Haifa, Israel.
SÖDING, P.	D.E.S.Y., Notkestieg 1, Hamburg 52, Germany.
SOLIANI, G.	Istituto di Fisica dell'Università, Via Anesano, Lecce, Italy.
STAFFORD, G.	Rutherford High Energy Laboratory, Building R1, Chilton, Didcot, Berks., England.
STAUDENMAIER, H. M.	Institut für Experimentelle Kernphysik, Univ. Karlsruhe, Postfach 366, Karlsruhe, Germany.

STRAUSS, R.	Inst. für Theor. Kernphysik, Kaiserstrasse 12, Karlsruhe, Germany.
STRUCZINSKI, W.	D.E.S.Y., Notkestieg 1, Hamburg 52, Germany.
TAVERNIER, S.	Lab. Univ. Belge des Hautes Energies, 4 rue Hobbema, Brussels, Belgium.
TOMASINI, G.	Istituto di Fisica dell'Università, Viale Benedetto 15, Genova, Italy.
TRASATTI, L.	Lab. Nazionali di Frascati, Frascati (Rome) Italy.
TURCHETTI, G.	Istituto di Fisica dell'Università, Via Irnerio 46, Bologna Italy.
TURNBULL, R. M.	Dept. of Natural Philosophy, Glasgow University, Glasgow W2, Scotland.
VAN DE WALLE, R.	Institut voor Fysica, Driehuizerweg, Nijmegen, Holland.
VEGNI, G.	Istituto di Fisica dell'Università, Via Celoria 16, Milano, Italy.
VENTURI, G.	Istituto di Fisica dell'Università, Via Irnerio 46, Bologna, Italy.
VEILLET, J.	Accélérateur Linéaire, Faculté des Sciences, Bâtiment 200, 91 Orsay, France.
VIDEAU, H.	Laboratoire Leprince Ringuet, École Polytechnique 17 rue Descartes, Paris V^{e}, France.
WAGNER, F.	Max-Planck-Inst. für Phys. und Astrophys., Föhringer Ring 6, Munich, Germany.
WALOSCHEK, P.	D.E.S.Y., Notkestieg 1, Hamburg 52, Germany.
WALTERS, J.	Dept. of Physics, Carleton University, Ottawa, Canada.

WAMBACH, U.	Institute für Theor. Physik, Ruhr-Universität Bochum, Bascheystrasse, D-4630 Bochum-Querenburg, Germany.
WATAGHIN, V.	Istituto di Fisica dell'Università, Via P. Giuria 1, 10125 Torino, Italy.
WEITSCH, A.	Institute für Theor. Physik, Univ. of Munich, Schellingstrasse 2-8, 8000 Munich 13, Germany.
WERBROUCK, A.	Istituto di Fisica dell'Università, Via Pietro Giuria 1, 10125 Torino, Italy.
WHITTAKER, J.	T.C. Division, C.E.R.N., Geneva, Switzerland.
WINDMOLDERS, R.	Lab. Univ. Belge des Hautes Energies, 4 Rue Hobbema, Brussels, Belgium.
WINZELER, H.	Instituut voor Fysica, Dreihuizerweg, Nijmegen, Holland.
WOLF, G.	Max-Planck-Inst. für Phys. und Astrophys., Föhringer Ring 6, Munich, Germany.
YAMDAGNI, N.	Physics Dept., Univ. of Stockholm, Vanadisvägen 9, Stockholm 46, Sweden.
ZACHARIASEN, F.	California Institute of Technology, Pasadena, California 91109, U.S.A.
ZAVATTINI, E.	N.P. Division, C.E.R.N., Geneva, Switzerland.
ZICHICHI, A.	N.P. Division, C.E.R.N., Geneva, Switzerland.
ZORN, G.	Physics Dept., Univ. of Maryland, College Park, M.D. 20742, U.S.A.